

Evaluation of underground environment effects on  
hydraulic properties and swelling pressure of bentonites  
in HLW disposal

高レベル放射性廃棄物処分におけるベントナイトの  
浸透特性と膨潤圧に及ぼす地下環境の影響評価

December 2022

Kunlin RUAN

阮 坤林



Evaluation of underground environment effects on  
hydraulic properties and swelling pressure of bentonites  
in HLW disposal

高レベル放射性廃棄物処分におけるベントナイトの  
浸透特性と膨潤圧に及ぼす地下環境の影響評価

December 2022

Waseda University

Graduate School of Creative Science and Engineering

Department of Civil and Environmental Engineering

Research on Geotechnical Engineering

Kunlin RUAN

阮 坤林

## Abstract

Bentonite was selected as the candidate buffer material in deep geological disposal project for dealing with high level radioactive waste from nuclear power industry. As two important factors for assessing the properties of bentonite, swelling pressure and hydraulic properties (hydraulic conductivity and water diffusivity) were studied.

Three bentonites, including MX80, KV1 and KB, were used to study swelling pressure and hydraulic properties under confined wetting. A newly designed swelling pressure apparatus and a developed multi-ring were applied to conduct swelling pressure, water distribution and X-ray diffraction (XRD) tests at the same time. The effects of dry density, salt solution concentration, salt type and temperature on swelling pressure and hydraulic properties of bentonites were researched. The results from this study can be summarized as the followings.

Swelling pressures during saturation of bentonites increase with the rise of dry density and reduce as the concentration increases. The liquid salt type has opposite impact on swelling pressures of different cation bentonites. For sodium bentonites (MX80 and KV1),  $\text{Ca}^{2+}$  saturated specimens have bigger swelling pressures during saturation than  $\text{Na}^+$  saturated ones. In case of calcium bentonite (KB), swelling pressure increases when saturation liquid changes from  $\text{Ca}^{2+}$  to  $\text{Na}^+$ . No matter the bentonite cation type, distilled water obtained larger swelling pressure than those from salt solutions. Temperature also has inconsistent influence on swelling pressure during saturation. Particle bentonite (MX80) has larger swelling pressure during saturation as the temperature reduces. For powder bentonites (KV1 and KB), swelling pressures are larger in higher temperature conditions. There are no effects from initial water content and specimen preparation method on equilibrium swelling pressure of KV1.

With the relation between volumetric water content and a new parameter  $\chi$ , the water diffusivity of bentonites during saturation was calculated. Hydraulic conductivity was obtained by the relation between hydraulic conductivity, water diffusivity and soil water retention curve. Hydraulic conductivity shows a  $\cap$  shape with the variation of volumetric water content and decreases as the dry density rises. Water diffusivity reduces with the increases of volumetric water content and degree of saturation. Water diffusivity rises as the increases of concentration and temperature. Similar with the swelling pressures, liquid cation type has opposite impact on the water diffusivity of different cation bentonites. Sodium bentonites saturated by  $\text{Ca}^{2+}$  have larger water diffusivities than those from  $\text{Na}^+$ . For calcium type bentonite,  $\text{Na}^+$  saturated specimens had larger water diffusivities than saturated  $\text{Ca}^{2+}$  ones. No matter bentonite type, water diffusivities saturated by distilled water were lower than those saturated by  $\text{Ca}^{2+}$  and  $\text{Na}^+$ .

Basal spacing was achieved by the results of XRD tests for slices from multi-ring. Basal spacing under wetting process grows with the rise of volumetric water content and degree of saturation. The dry density and concentration have negative influence on the basal spacing during wetting. Basal spacing decreases when saturation liquid changes from distilled water to salt solutions. For sodium bentonites, basal spacing saturated by  $\text{Ca}^{2+}$  is greater than that by  $\text{Na}^+$ . Regarding calcium bentonite, basal spacing is larger when saturation liquid is  $\text{Na}^+$  instead of  $\text{Ca}^{2+}$ . Initial water content has no effect on the basal spacing of distilled water saturated bentonite.

Key words: Bentonites, swelling pressure, hydraulic properties, X-ray diffraction

# Content

INTRODUCTION.....	1
1.1    Background.....	2
1.2    Deep Geological Disposal for High Level Radioactive Waste.....	4
1.3    Hydraulic properties and swelling pressure of bentonites .....	6
1.3.1    Hydraulic properties.....	10
1.3.2    Swelling pressure .....	19
1.3.3    X-ray diffraction .....	22
1.4    Research objectives .....	26
1.5    The innovations of this study.....	26
1.6    Construction of the thesis .....	27
Reference.....	30
MATERIALS AND PHYSICAL PARAMETERS.....	39
2.1 Materials.....	40
2.2 Physical parameters .....	40
2.2.1 Grain size distribution .....	41
2.2.2 Soil particle density .....	42
2.2.3 Liquid limit and plastic limit .....	43
2.2.4 Montmorillonite content.....	45
2.2.5 Cation exchangeable capacity .....	46
Reference.....	48
DEVICES AND TESTING METHODOLOGY .....	50
3.1 Devices .....	51
3.1.1 Swelling pressure apparatus .....	51
3.1.2 Multi-ring .....	60
3.2 Testing Methodology.....	61
Reference.....	64
HYDRAULIC PROPERTIES AND SWELLING PRESSURE OF BENTONITES WITH XRD.....	66
4.1 Testing overview .....	67
4.2 Results .....	67
4.2.1 Swelling pressure.....	67
4.2.2 Hydraulic properties .....	70

4.2.3 XRD results .....	78
4.3 Discussion .....	89
4.3.1 The developing pattern difference for hydraulic conductivity during saturation between bentonite and normal soil .....	89
Conclusion.....	93
Reference.....	94
<b>THE EFFECT OF DRY DENSITY ON HYDRAULIC PROPERTIES AND SWELLING PRESSURE OF BENTONITES WITH XRD.....</b>	
5.1 Testing overview .....	97
5.2 Results .....	97
5.2.1 Swelling pressure.....	97
5.2.2 Hydraulic properties .....	104
5.2.3 XRD results .....	114
5.3 Discussion .....	127
Conclusion.....	134
Reference.....	135
<b>THE EFFECT OF NA<sup>+</sup> CONCENTRATION ON HYDRAULIC PROPERTIES AND SWELLING PRESSURE OF BENTONITE WITH XRD.....</b>	
6.1 Testing overview .....	138
6.2 Results .....	139
6.2.1 Swelling pressure.....	139
6.2.2 Water diffusivity.....	142
6.2.3 XRD results .....	147
6.2.4 Osmotic suction .....	150
6.3 Discussion .....	152
6.3.1 Relation between osmotic suctions and swelling pressures.....	152
Conclusions .....	156
Reference.....	157
<b>THE EFFECT OF NA<sup>+</sup> CONCENTRATION ON MOVEMENT OF WATER AND SALTS IN BENTONITES WITH XRD .....</b>	
7.1 Testing overview .....	159
7.2 Results .....	161
7.2.1 Movement of water.....	161
7.2.2 Movement of Na <sup>+</sup> .....	171

7.2.3 XRD results .....	176
7.3 Discussion .....	178
7.3.1 Mechanism for the movement of water and Na <sup>+</sup> in high dry density bentonite basing on pores distribution.....	178
Conclusion.....	183
Reference.....	184
<b>THE EFFECT OF SALT TYPES ON HYDROLOGICAL PROPERTIES ANS SWELLING PRESSURE OF BENTONITES WITH XRD.....</b>	
8.1 Testing overview .....	186
8.2 Results .....	187
8.2.1 Swelling pressure.....	187
8.2.2 Water diffusivity.....	193
8.2.3 XRD.....	201
8.2.4 Mineral detection, CECs and EXCs .....	216
8.3 Discussion .....	219
8.3.1 The effect of solutions on water diffusivity.....	220
8.3.2 Equilibrium swelling pressure of different type bentonites saturated by different salt solutions .....	222
Conclusions .....	225
References .....	226
<b>THE EFFECT OF TEMPERATURE ON HYDRAULIC PROPERTIES AND SWELLING PRESSURE OF BENTONITES.....</b>	
9.1 Testing overview .....	229
9.2 Results .....	231
9.2.1 Swelling pressures .....	231
9.2.2 Water diffusivity.....	240
9.3 Discussion .....	258
9.3.1 Equilibrium swelling pressure at different temperatures for bentonite with different grain sizes .....	258
9.3.2 Water diffusivity at different temperatures.....	261
Reference.....	264
<b>THE EFFECTS OF INITIAL WATER CONTENT AND SPECIMEN PREPARATION METHOD ON SWELLING PRESSURES OF BENTONITE WITH XRD.....</b>	
10.1 Testing overview .....	267
10.2 Results .....	270

10.2.1 Swelling pressures and XRD results from water spray method .....	271
10.2.2 Swelling pressures and XRD results from humidity control method .....	284
10.3 Discussion.....	294
10.3.1 Effects of specimen preparation method and initial water content on basal spacing of specimens in initial and saturated states.....	294
10.3.2 Effects of specimen preparation and initial water contents on equilibrium swelling pressure .....	298
Conclusion.....	300
Reference.....	301
APPLICATION IN PRACTICAL FIELD AND CONCLUSIONS.....	302
11. 1 Overview .....	303
11. 2 The choice of dry density .....	307
11. 3 The choice of bentonite cation type.....	308
11. 4 The choice of bentonite grain size.....	312
11. 5 The choice of Initial water content and specimen preparation method .....	315
11. 6 Future plan.....	317
Reference.....	318
References .....	320
Acknowledgement.....	321
Figure list.....	323
Table list.....	333

# Chapter 1

## **INTRODUCTION**

## 1.1 Background

With the progress of urbanization and industrialization, the global electricity demand grew quickly in the past decades. Figure 1-1 shows the global change in electricity demand from International Energy Agency (IEA). As we can easily found from Fig. 1-1, from 2015 to 2018, the demand of electricity increased rapidly. Even though the demand decreased to some degree due to the Covid-19 pandemic virus in 2019 and 2020, the demand recovered very fast in 2021. It can be seen as Fig. 1-1, electricity demand in subsequent years has stabilized annually at approximately 800 TWh, which is a pretty big number.

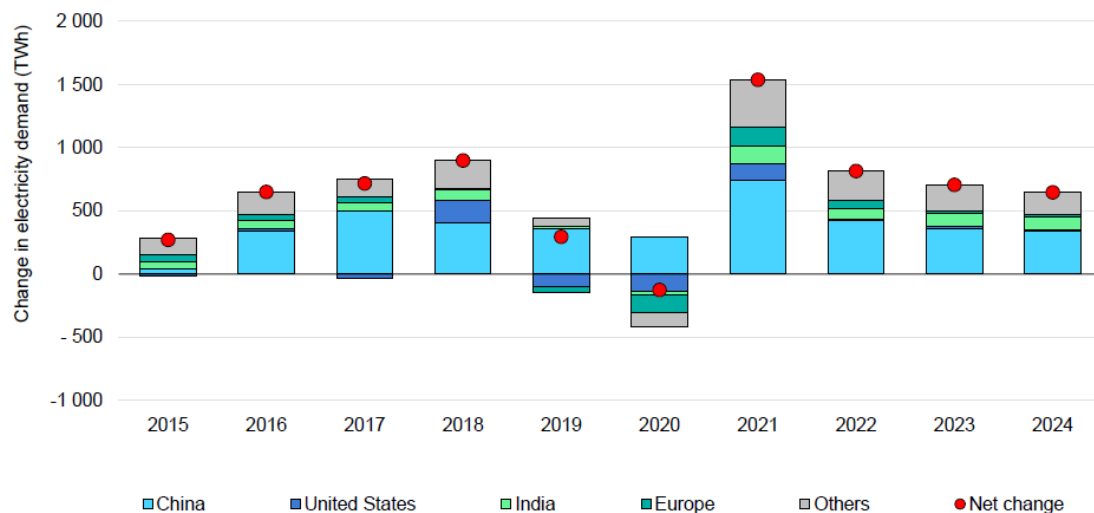


**Figure 1-1 Global change in electricity demand (IEA 2022)**

For offering such a huge amount of electricity demand, various electricity generation methods had been accepted by countries, such as coal, gas and renewables. The survey for the electricity generation methods is presented in Fig. 1-2 from IEA. It is a generally truth from Fig. 1-2 that, the coal and gas still occupied the vast majority. The percent of renewables and nuclear generations was just a small part. However, the production of electricity from coal and gas would generate a great amount of greenhouse gases, such as carbon dioxide (CO<sub>2</sub>).

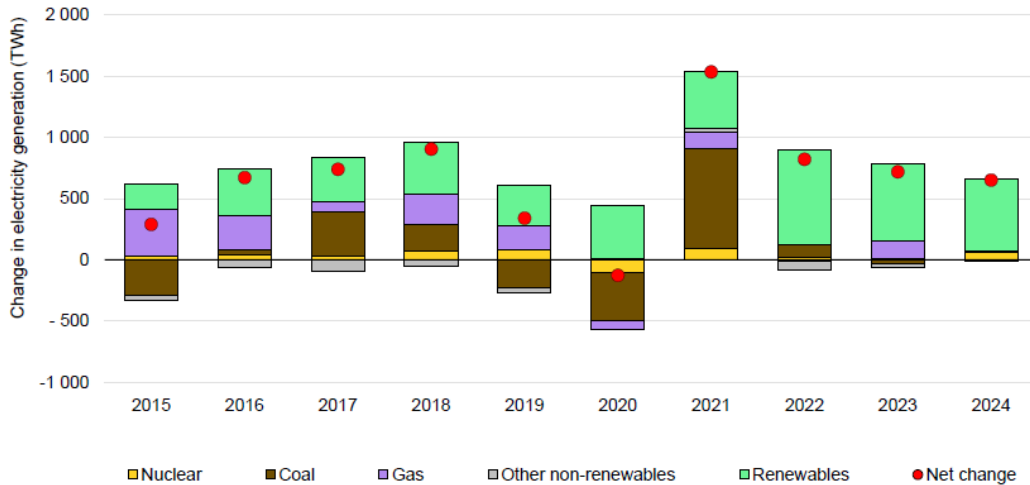


**Figure 1-2 Global change in electricity generation (IEA 2022)**

The over emission of carbon dioxide has been an emergent issue world-widely. Figure 1-3 reveals the regional evaluation of CO<sub>2</sub> intensity (IEA 2022). It is apparently from Fig. 1-3 that, the average of CO<sub>2</sub> intensity for the world in 2020 was about 500 g CO<sub>2</sub>/kWh. The CO<sub>2</sub> over-emission induced the temperature rise of the earth, which is generally designated as global warming, leading the frequent occurrence of unforeseen disasters. Due to this situation, efforts were made by the societies to changing coal and gas methods to renewables and nuclear ways.

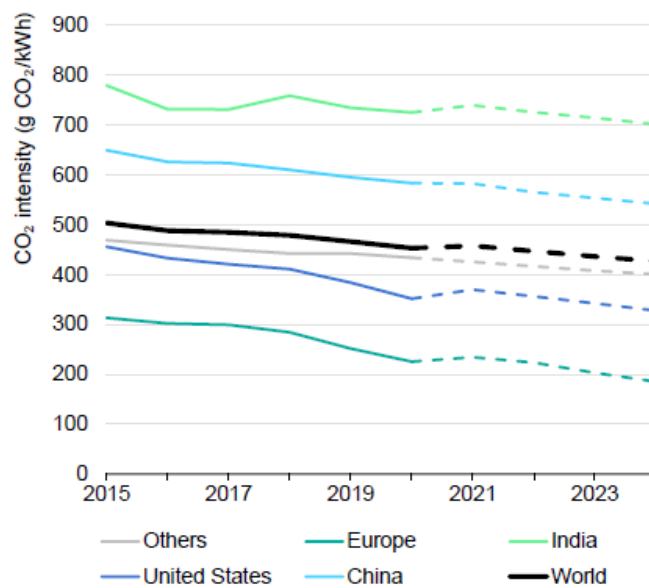


**Figure 1-3 Regional evaluation of CO<sub>2</sub> intensity (IEA 2022)**

## 1.2 Deep Geological Disposal for High Level Radioactive Waste

As one of clean powers, nuclear power was paid more and more attention by massive countries in the world. However, as presented in Fig. 1-2, the percent of nuclear power in total electricity generation is still very limited. Japanese government has decided to progress the nuclear power industry widely in Japan (METI 2020). Thus, the disposal of high level radioactive waste (HLW) from nuclear power industry is a very significant issue for utilizing nuclear power.

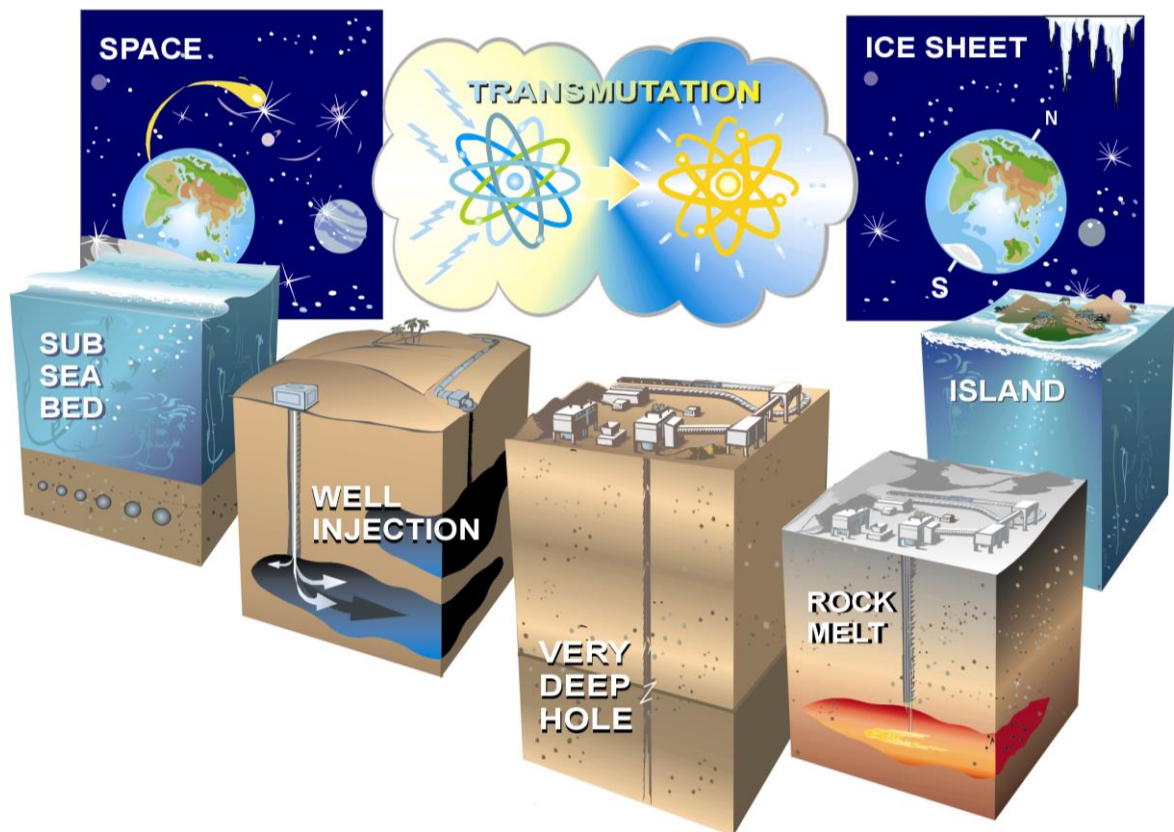


**Figure 1-4 Disposal methods for high level radioactive waste (WNA 2022)**

Several methods were proposed for dealing with HLW as revealed in Fig. 1-4, including space, ice sheet, island, sub seabed. Among these methods, many countries planned to seal HLW in very deeply underground, which is designated as deep geological disposal method. Comparing to other methods, the reasons why deep geological disposal method

was widely selected are the feasibility and economy.

Table 1-1 shows the details for deep geological disposal method of some countries in the world from Chen 2022. As we can see from Table 1-1, a multi-barrier system would be employed for the deep geological disposal project by massive countries all over the world. The multi-barrier system usually consists of waste container, surround rock, buffer material as indicated in Table 1-1 and Fig. 1-5. For some ingredients of multi-barrier system, different country has different choices. For example, the depths for constructing the multi-barrier system.

**Table 1-1 Details for deep geological disposal world widely (from Chen 2022)**

Nation	Waste canister	Surround rock	Buffer material	Depth (m)
Canada	Copper shell, carbon steel inner tank	Crystalline rock	Bentonite sand mixture (50:50)	500-1000
Finland	Copper - steel	Crystalline rock	Pure bentonite	500
French	Concrete	Crystalline Rock	Pure bentonite	400-1000
	Copper shell, stainless steel inner tank	Crystalline rock	Bentonite sand mixture (30:70)	400-1000
	Carbon steel inner tank	Clay rock	Pure bentonite	500
Sweden	Copper - steel	Crystalline rock	Pure bentonite	400-700
	Copper – steel Stainless steel shell	Crystalline rock		400-700
China		Granite	Pure bentonite	800-1000

A multi-barrier would be employed in the deep geological disposal project for Japan as well, including Engineering barriers and Natural barriers as presented in Fig. 1-5. In a Japanese deep geological project, the multi-barrier system would be constructed in more than 300m underground to prevent the leakage of nuclide waste (JNC 1999; METI 2020; NUMO 2022). For the engineering barriers, there are solidified body, packing

container and buffer/backfill material. The natural barriers consist of rocks and surrounding soils. Meanwhile, the Japanese deep geological disposal planned to cite in coastal area for the feasibility of transportation (JNC 1999; METI 2020; NUMO 2022).

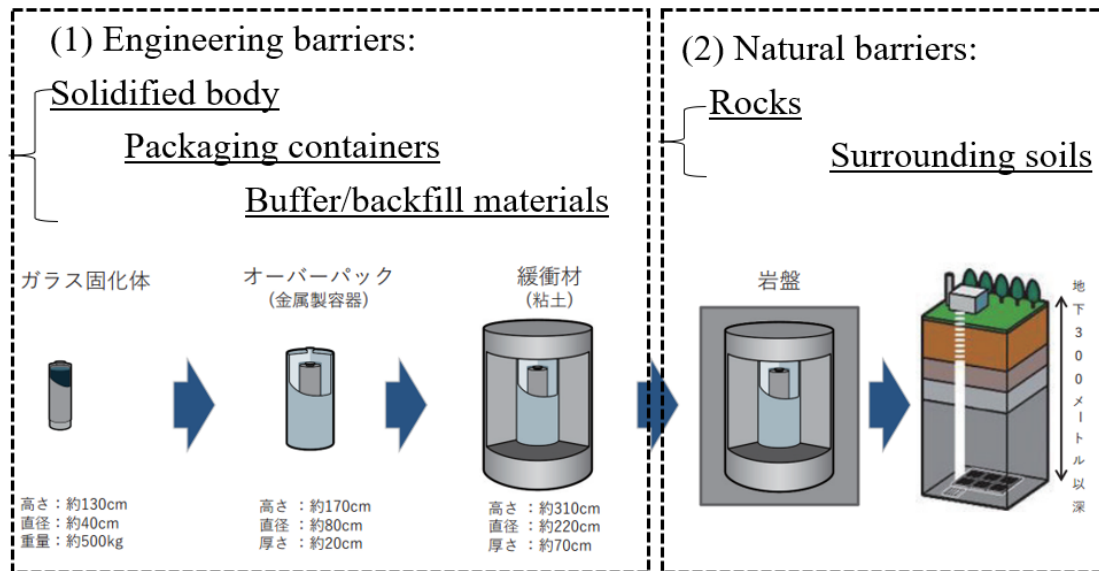


**Figure 1-5 Deep geological disposal method in Japan (modified from NUMO 2022)**

### 1.3 Hydraulic properties and swelling pressure of bentonites

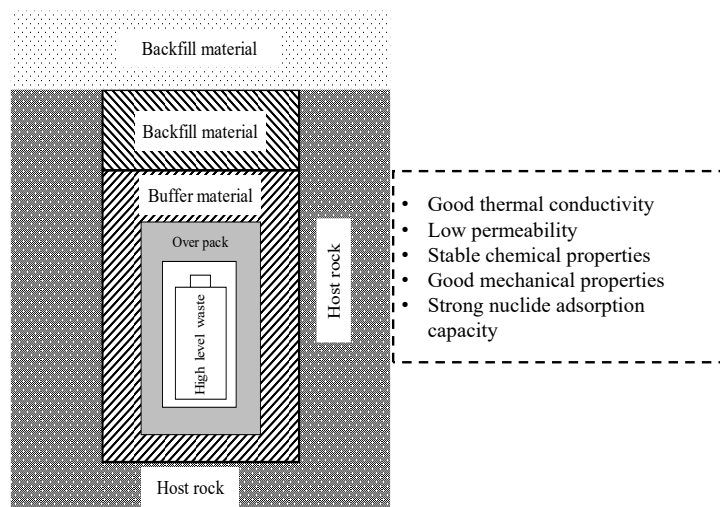


**Figure 1-6 Host rock, buffer material and over packer**

As one of the most crucial ingredients of multi-barrier system, buffer material requires selected mechanical characteristics as (Fig. 1-6): good thermal conductivity, low permeability, stable chemical properties, good mechanical properties and strong nuclide adsorption capacity. Bentonites were chosen as candidate buffer materials by numerous countries all over the world, such as China (Wang et al. 2018), Japan (METI 2020), Sweden (SKB 2011), Finland (Posiva 2012) etc. Different bentonites were chosen by different countries for the buffer materials, as: MX-80, USA; GMZ, China; Kunigel-V1, Japan; and FEBEX, Spanish.

**Table 1-2 Bentonites selected by different countries as buffer material**

Nation	Bentonite	Location
USA	MX-80	Wyoming
China	Gaomiaozi (GMZ)	Inner Mongolia
Japan	Kunigel-V1	Yamagata
Spanish	FEBEX	Cortijo de Archidona deposit, Almería

Comparing to other soils, the thermal conductivity of bentonite is much better. As the experimental observations by Xu et al. (2019a) and Xu et al. (2019b) for GMZ and MX-80 bentonites, the thermal conductivity of GMZ and MX-80 are approximate 0.3-1.5 W/mK. Low permeability is very important for avoiding the outflow of HLW in multi-barrier system. The saturated hydraulic conductivities of bentonites are approximate  $10^{-15}$  -  $10^{-12}$  m/s by the testing studies from Komine (2008). Meanwhile, as reported by Liu et al. (2006), bentonites have pretty good physical and chemical stabilities. Meanwhile, according to Kubota et al. (2013), bentonite has strong adsorption capacity for nuclide molecules as cesium, strontium and iodine. As discussed above, bentonites

are suitable candidate buffer materials.

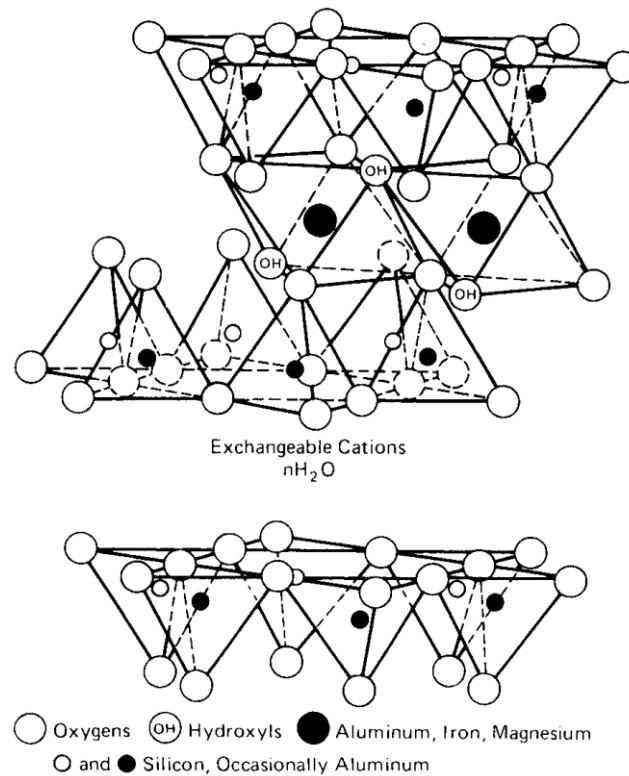


**Figure 1-7 Mineral structure of montmorillonite (Mitchell and Soga 2005)**

Bentonite is generally considered as the soil consists of swelling minerals and non-swelling minerals. Montmorillonite is generally accepted as the only swelling mineral in bentonites by some scholars (e.g., Komine and Ogata 1996; Komine and Ogata 2004). Montmorillonite is also designated as smectite for soil science researchers. As well known in geotechnical area, montmorillonite has a special 2:1 mineral structure, which includes an alumina octahedral sheet and two silica tetrahedral sheets as indicated in Fig. 1-7 from Mitchell and Soga (2005).

Figure 1-8 shows the traditional microstructure of montmorillonite from Ruan et al. (2021). The fabric units, pores and their evolution were concluded in Ruan et al. (2022). As we can see from Fig. 1-8, unit layers are often stacked one above another in a face-to-face orientation, further composing particles (Yong 1999). The number of unit layers required to form a particle varies. Reportedly, it decreases as the degree of saturation

increases (Saiyouri et al. 2004; Chen et al. 2021), meaning that, through the evolution of hydration, a “big particle” would change to a “small particle” (Laird 1996; Laird 2006). Aside from that point, aggregates comprising several particles are configured. The aggregate structure is also flexible as wetting proceeds. With an increasing degree of saturation, “big aggregates” are expected to divide to “small aggregates” and particles (Suzuki et al. 2005; Musso et al. 2013; Chen et al. 2021). Fabric units are often divided into three aspects according to their sizes (Fig. 1-8): 1) micro-level, unit layer, 2) meso-level, particle, and 3) macro-level, aggregate. Additionally, pores can be classified into three types by their respective positions: 1) Micro-pores, inter-layer-pores; 2) Meso-pores, inter-particle pores; and 3) Macro-pores, inter-aggregate pores.

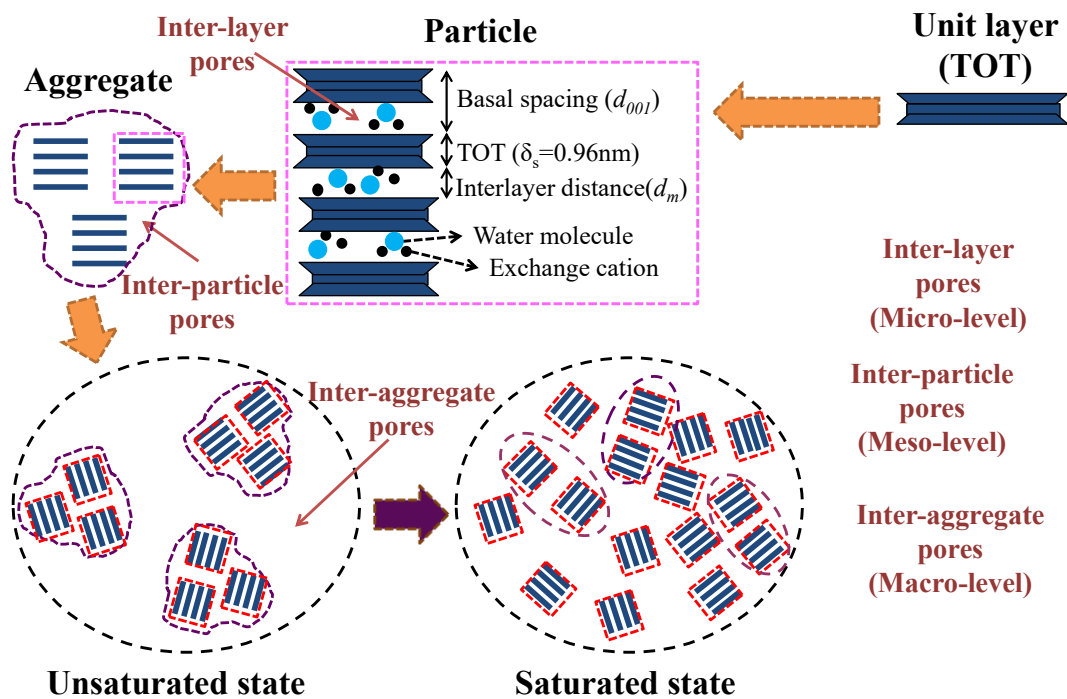


**Figure 1-8 Microstructure of montmorillonite (Ruan et al. 2022)**

The hydrological properties and swelling pressure of bentonites are very important for the disposal of HLW. Many scholars paid attention and made effort to the hydrological properties and swelling pressure of bentonites by experiments (e.g., Samper et al. 2008; Zheng et al. 2011) and simulations (e.g., Zheng et al. 2017). However, there is still

lacking microstructural investigations for hydrological properties and swelling pressure of bentonites due to the technological shortages of testing methodology.

### 1.3.1 Hydraulic properties

The hydrological properties, including water diffusivity and hydraulic conductivity, of bentonites is very crucial for the deep geological disposal project. As reported by Posiva (2012) and SKB (2011), thousands or even millions of years are needed for the HLW to decay fully. In this extremely long term, the ground water would intrude consistently into buffer material, thereby inducing the movement of ground water into buffer material. Hydrological properties, which are adopted to assess the movement of water, are significant for the application of bentonite as buffer material.

Water diffusivities ( $D$ ) of bentonites were studied by scholars with experimental investigations (Takeuchi et al. 1995; Komine et al. 2018; Wang et al. 2020) and simulations (e.g., Chijimatsu et al. 2000). From the aspect of tests, there were generally two methods (Ruan 2022): 1) instantaneous profile method (Fredlund and Rahardjo 1993; Lu and Likos 2004); and 2) reading the reduction of the water in water tube (Komine et al. 2018; Shirakawabe 2021).

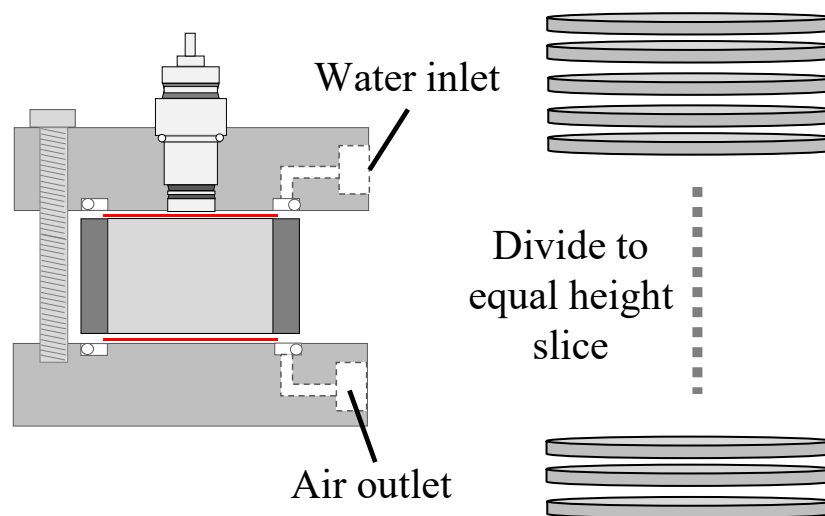


**Figure 1-9 Instantaneous profile method by cutting evenly height slices (Modified from Cho 2022)**

Firstly, instantaneous profile method. Normally, scholars studied water diffusivity of soils by cutting evenly height slices from unsaturated specimens wetted by different durations (Fig. 1-9). And then, by the relation between water contents (gravimetric water content,  $w$ ; volumetric water content,  $\theta$ ), wetting time ( $t$ ) and distance from the bottom of specimen ( $z$ ). Takeuchi et al. (1995) studied the water diffusivity of Kunigel-V1 bentonite with instantaneous profile method by using the following equation:

$$D(\theta) = \frac{\frac{1}{t_2 - t_1} \times \int_{z_i}^l (\theta_{t=t_2} - \theta_{t=t_1}) dz}{\frac{1}{2} \left\{ \left( \frac{\partial \theta}{\partial z} \right)_{t=t_2} + \left( \frac{\partial \theta}{\partial z} \right)_{t=t_1} \right\}} \quad (1-1)$$

Figure 1-10 reveals the water diffusivity changing with degree of saturation for  $1.6\text{g/cm}^3$  Kunigel-V1 bentonite from Takeuchi et al. (1995) by using equation (1-1). It is apparent from Fig. 1-10 that, the water diffusivity exhibits a “U” shape with the changing degree of saturation. Changing another word, water diffusivity decreases with increasing degree of saturation, when degree of saturation is low. And, water diffusivity rises as degree of saturation increase, when degree of saturation is high. Different phenomenon was found in different degree of saturation levels in Takeuchi et al. (1995).

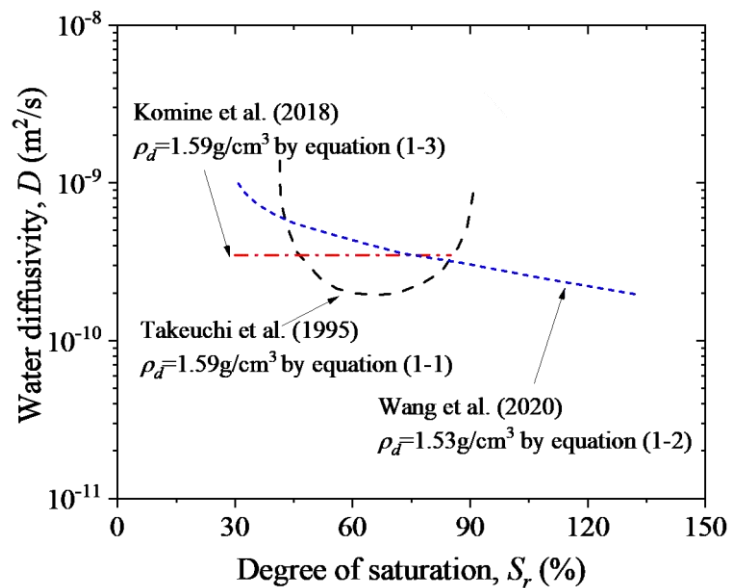


**Figure 1-10 Water diffusivity changing with degree of saturation by using different equations**

Additionally, other investigators tried to find a mathematic relation between water diffusivity and volumetric water content. An exponential function was found by Wang et al. (2020) between volumetric water content and a parameter  $\chi=z/t$ . And then, by bringing that exponential function into Darcy equation, an easy equation for obtaining the water diffusivity during wetting was obtained, as:

$$D(\theta) = \frac{AB}{2} - \frac{B^2}{2} (\ln(\theta - C) - 1) \quad (1-2)$$

where  $A$  and  $B$  in equation (1-2) are fitting parameters between volumetric water content and new parameter  $\chi$ . Figure 1-10 reveals the relation between water diffusivity and degree of saturation by equation (1-2) from Wang et al. (2020) when the dry density is  $1.53\text{g/cm}^3$ . It is a generally truth from Fig. 1-10 that, water diffusivity decreases consistently with the increase of degree of saturation.

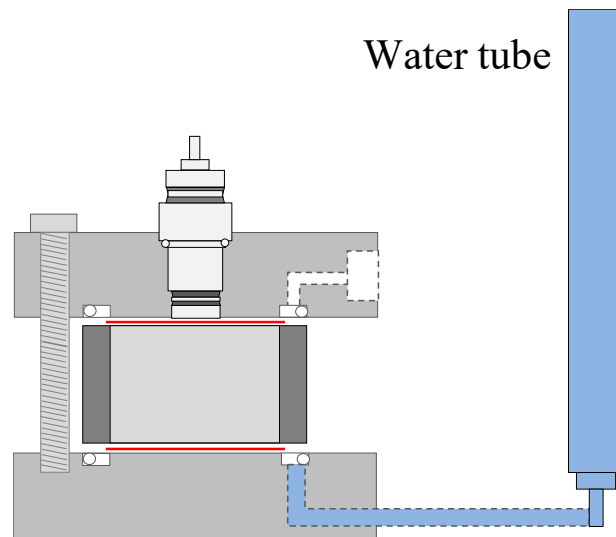


**Figure 1-11 Water diffusivity by reading the reduction of the water in tube**

Secondly, water diffusivity by reading the reduction of water in water tube (Fig. 1-11). A linear relation was found between amount of adsorbed water ( $Q$ ) and  $\sqrt{t}$  by Komine et al. (2018), and the water diffusivity calculating equation was proposed as:

$$Q = 2A'n_e' \sqrt{\frac{D}{\pi}} \sqrt{t} \quad (1-3)$$

where  $A'$  is the sectional area of the specimen;  $n_e$  is the effective porosity. And, the  $D$  in equation (1-3) can be viewed as an average  $D$  during saturation as shown in Fig. 1-10 for  $1.59\text{g/cm}^3$  Kunigel-V1 bentonite. As it is clearly from Fig. 1-10, different calculation equation brings different water diffusivity patterns. However, at the similar dry density, the difference in the water diffusivity is somewhat small.

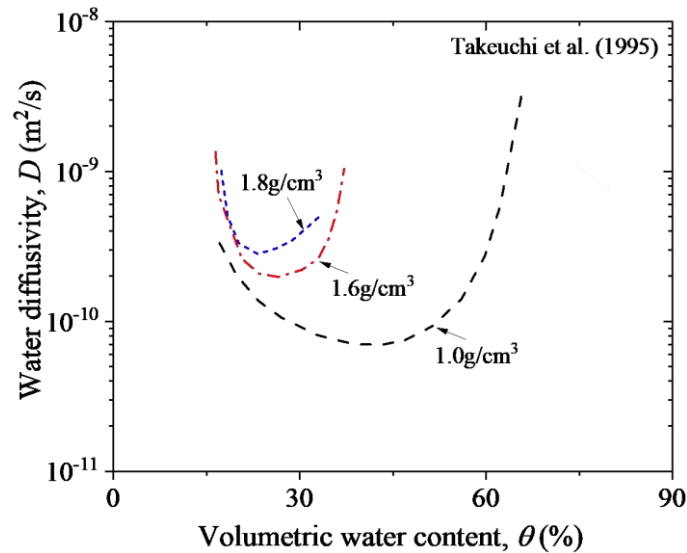


**Figure 1-12 Effect of dry density on water diffusivity by instantaneous profile method**

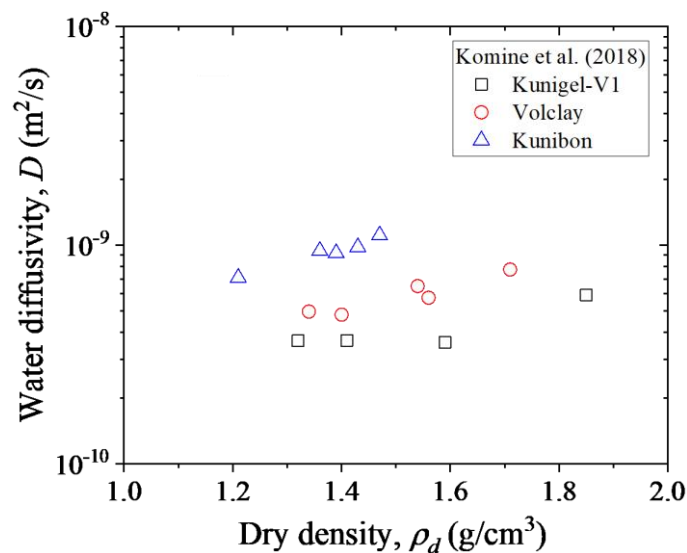


**Figure 1-13 Effect of dry density on water diffusivity by reading water reduction in water tube**

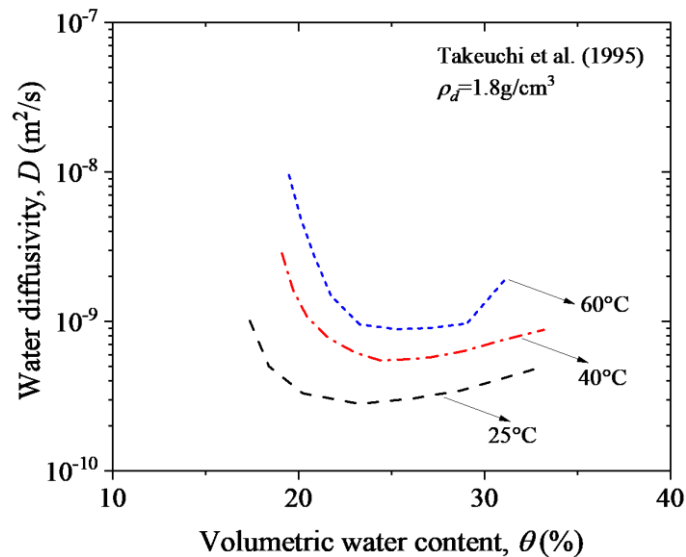


**Figure 1-14 Effect of temperature on water diffusivity by instantaneous profile method**

As a significant parameter to evaluate the movement of water in soil, water diffusivity was generally accepted being affected by tremendous ingredients. Figure 1-12 reveals the effect of dry density on water diffusivity by instantaneous profile method from Takeuchi et al. (1995). Figure 1-13 indicates the effect of dry density on water diffusivity by reading the water reduction in water tube from Komine et al. (2018). It can be easily concluded from Fig. 1-12 and Fig. 1-13 that, water diffusivity increases with the increase of dry density. Takeuchi et al. (1995) also conducted the effect of temperature on water diffusivity of Kunigel-V1 bentonite during saturation, which is presented in Fig. 1-14. As can be seen from Fig. 1-14, water diffusivity increases as the temperature rises. Shirakawabe (2019) and Shirakawabe et al. (2021) putted powder bentonites into different temperature for different durations and detected the water diffusivity of compacted bentonite by reading the water reduction in water tube. The results from Shirakawabe et al. (2021) are that: thermal history has no effect on the water diffusivity of bentonites. As described above, there is still lacking the research concerning the effect of salt solutions on water diffusivity of bentonites.

Measuring hydraulic conductivity ( $k$ ), including saturated hydraulic conductivity and unsaturated hydraulic conductivity, of bentonite is pretty hard from the aspect of the technology. Firstly, the saturated hydraulic conductivity of bentonite is extremely low at approximately  $10^{-12}$  -  $10^{-15}$  m/s as indicated in Fig. 1-15. Traditional falling head

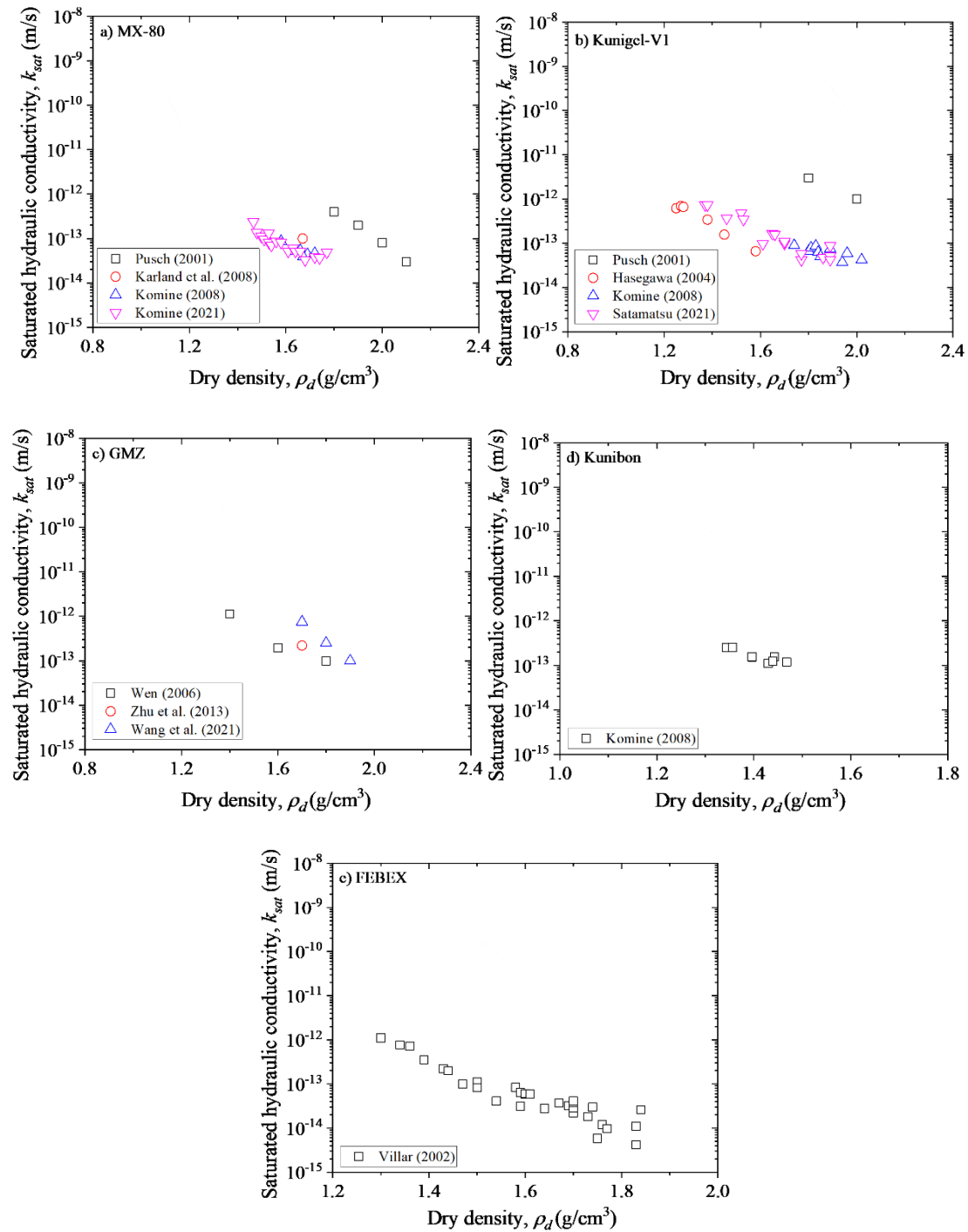


**Figure 1-15 Saturated hydraulic conductivity changing with the dry density of some bentonites**

and constant head tests are too hard for getting the testing database of such low saturated hydraulic conductivity material. Secondly, among the hydraulic conductivity testing duration, the hydration of montmorillonite in bentonite would bring extra volume deformation, thereby inducing unprecise results.

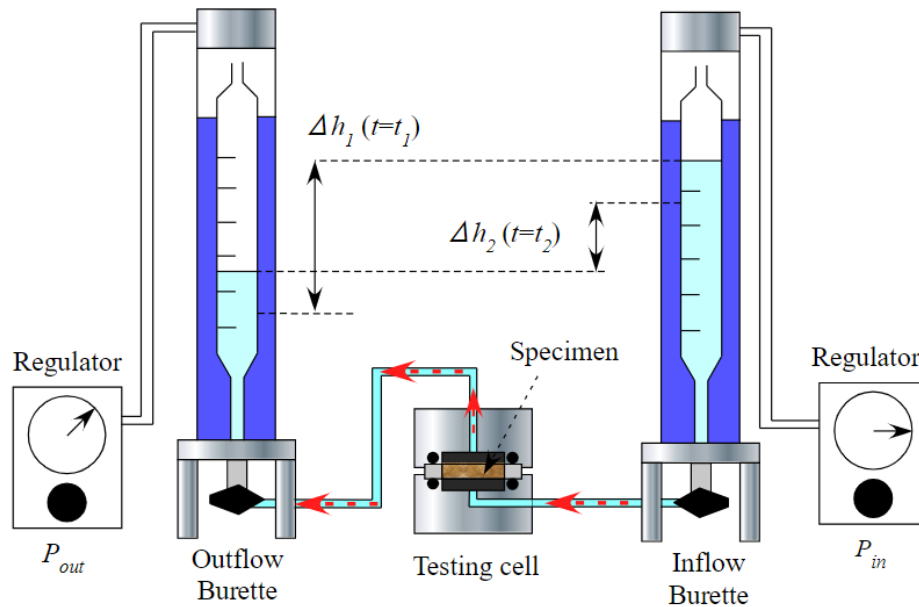


**Figure 1-16 Hydraulic conductivity test device for bentonite by adding air pressure (from Ito 2022)**



**Figure 1-17 Hydraulic conductivity for bentonite by compression apparatus (from Butsuda 2006)**

Efforts were made by investigators to progress the testing device in order to measure hydraulic conductivities of bentonites. Now, there are generally two methods adopting by scholars. Firstly, adding air pressure in traditional falling head tests (Fig. 1-16 from Ito 2022) to accelerate the flow of water in compacted bentonite. Secondly, transferring the compression index from compression test to hydraulic conductivity (Fig. 1-17 from Butsuda et al. 2006). Both these two experimental methodologies can obtain relative precise saturated hydraulic conductivity of bentonite.

As well known, saturated hydraulic conductivity of bentonite is greatly affected by many factors, such as dry density, temperature, saturation liquid and testing methodology. Figure 1-15 presents saturated hydraulic conductivities of MX-80, Kunigel-V1, GMZ, Kunibon and FEBEX bentonites from literatures. It is a generally truth from Fig. 1-15 that, for all bentonites, saturated hydraulic conductivity decreases with the increase of dry density. Attention was paid to the effect of temperature on saturated hydraulic conductivity of bentonites by scholars. The results from Cho et al. (1999) showed that, saturated hydraulic conductivity increases with growing experimental temperature. Some researchers concluded that, saturated hydraulic conductivity rises when saturation liquid changed from distilled water to salt solutions (e.g., Komine 2020). Besides that, it was reported that, the saturated hydraulic conductivities from above mentioned two methods have somewhat difference (Ruan et al. 2020).

In addition to saturated hydraulic conductivity, unsaturated hydraulic conductivity of bentonite testing technology was also proceeded recent years. Cui et al. (2008), Ye et al. (2009) and Wang et al. (2013) installed relative humidity sensors in a column permeability-meter (Fig. 1-18) to achieve hydraulic conductivities of bentonites during saturation. By instantaneous profiling method, Takeuchi et al. (1995) transferred water

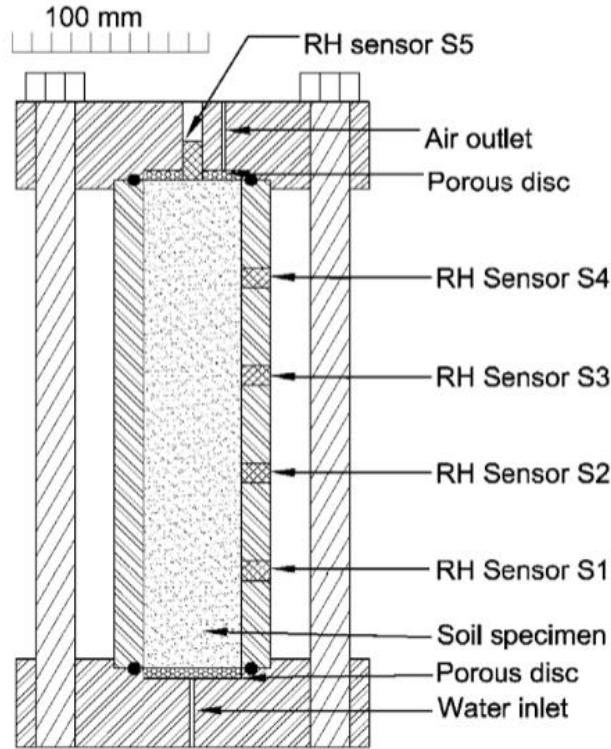


**Figure 1-18 An apparatus for measuring hydraulic conductivity of unsaturated bentonite (from Cui et al. 2008)**

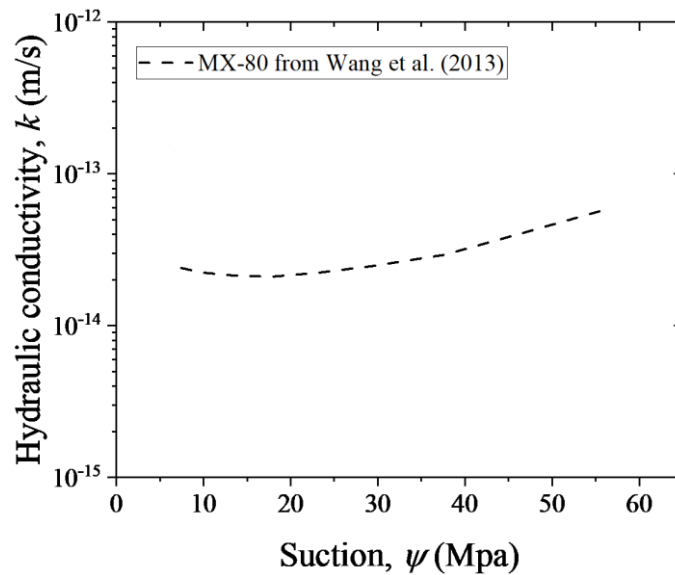


**Figure 1-19 Hydraulic conductivity changing with suction for MX-80 bentonite diffusivity to unsaturated hydraulic conductivity by Darcy equation. A “U” shape was reported by Cui et al. (2008), Ye et al. (2009) and Wang et al. (2013) for the relation between hydraulic conductivity and suction as revealed in Fig. 1-19. But, there is still**

not so many experimental databases for the effect of dry density, temperature and salt solutions on unsaturated hydraulic conductivity of bentonites.

### 1.3.2 Swelling pressure

In addition to low hydraulic conductivity, another important characteristic of bentonite is its high self-healing ability. As interpreted above, during the decay period of HLW decaying, ground water would intrude into buffer material. After bentonite contacts water, its volume will expand, thereby filling the possible voids in multi-barrier system, which is designated as self-healing capability. As important ingredients to evaluate self-healing ability, swelling pressures ( $p_s$ ) during saturation, including pressures at peak ( $p_{peak}$ ), valley ( $p_{valley}$ ), re-peak ( $p_{re-peak}$ ) and equilibrium ( $p_{eq}$ ) points of swelling curve (Fig. 1-20) had been studied by experiments (e.g., Wang et al. 2021; Wang et al. 2022). As Wang et al. (2022) reported that, pressures at peak, valley, re-peak points increase with the increase of dry density (Fig. 1-21). However, among those swelling pressures, most scholars specifically examined equilibrium swelling pressure instead of peak, valley, re-peak swelling pressures.

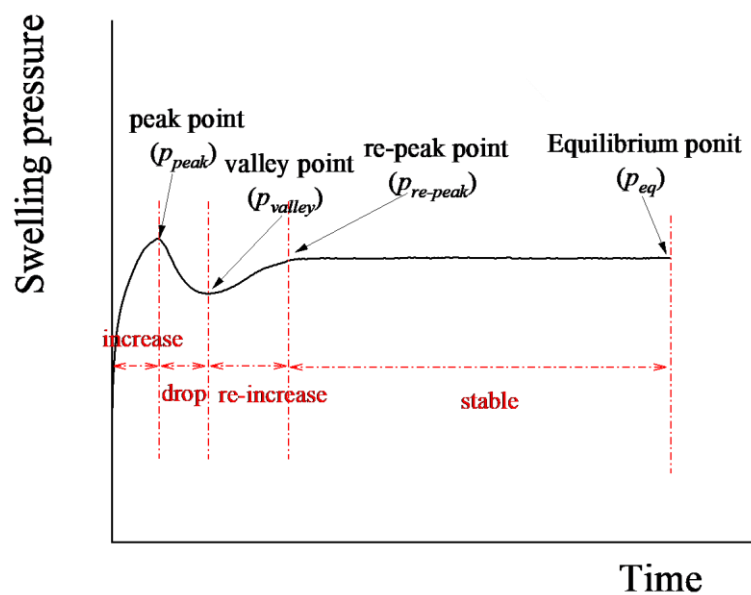


**Figure 1-20 Traditional swelling pressure evolution curve and definition of swelling pressures**

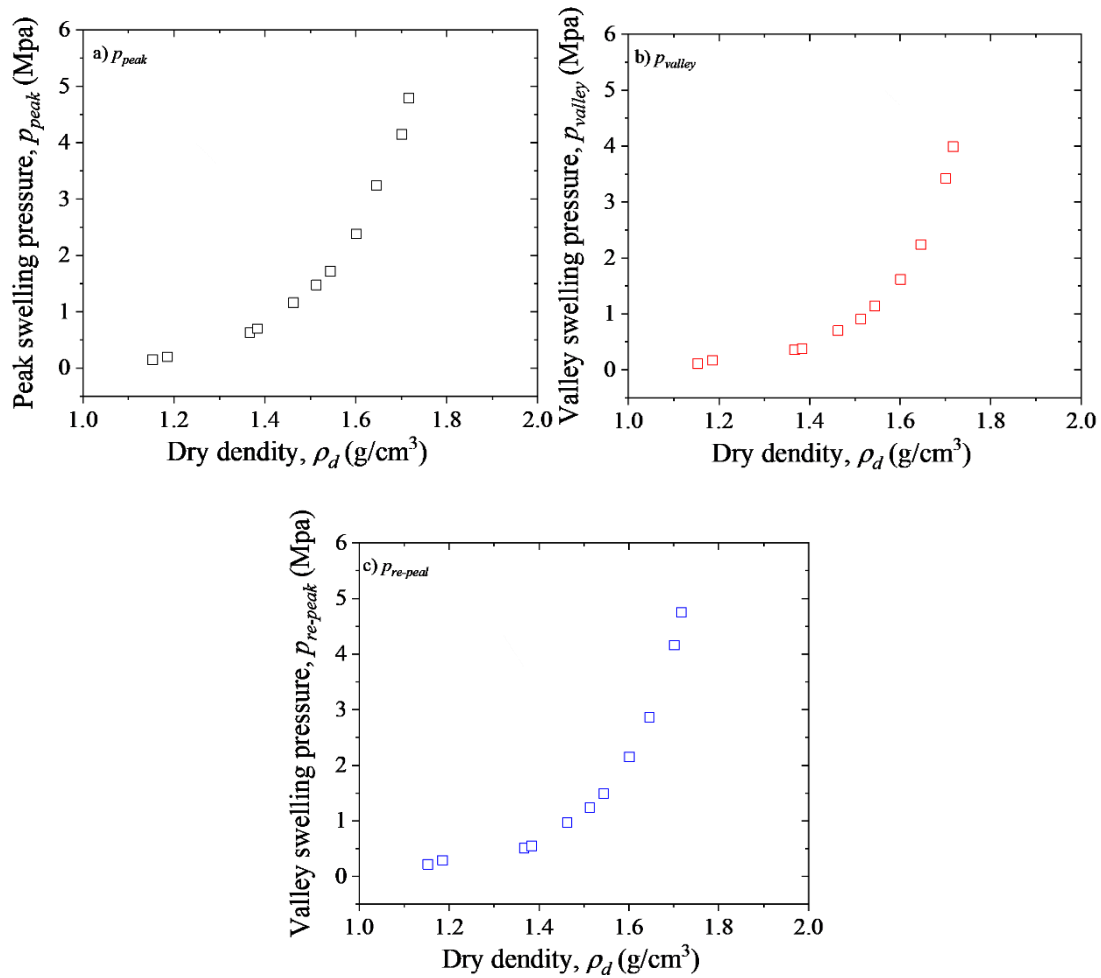


**Figure 1-21 Peak, valley and re-peak swelling pressures changing with dry density from 5mm thickness specimen (Wang et al. 2022)**

There are generally four methods adopting to obtain equilibrium swelling pressure of compacted bentonite (Sun et al., 2009; Tang et al., 2011): 1) stepwise consolidation method, 2) one step consolidation method, 3) constant volume method and 4) zero swelling method. With those methods, equilibrium swelling pressures of bentonites were greatly investigated. Equilibrium swelling pressure is sensitive to many factors such as dry density and saturation liquid. A literature survey is revealed in Fig. 1-22 for indicating the trend of equilibrium swelling pressure with changing dry density. It is a general truth from Fig. 1-22 that, for all these bentonites, equilibrium swelling pressure increases with the increase of dry density. Besides that, equilibrium swelling pressure was reported decreasing when the saturation liquid changed from distilled water to salt

solutions (Zhu et al. 2013; Sun et al. 2015; Chen et al. 2019). And, equilibrium swelling pressure reduces as increasing concentration of salt solution (e.g., Lee et al. 2012; Sun et al. 2015).

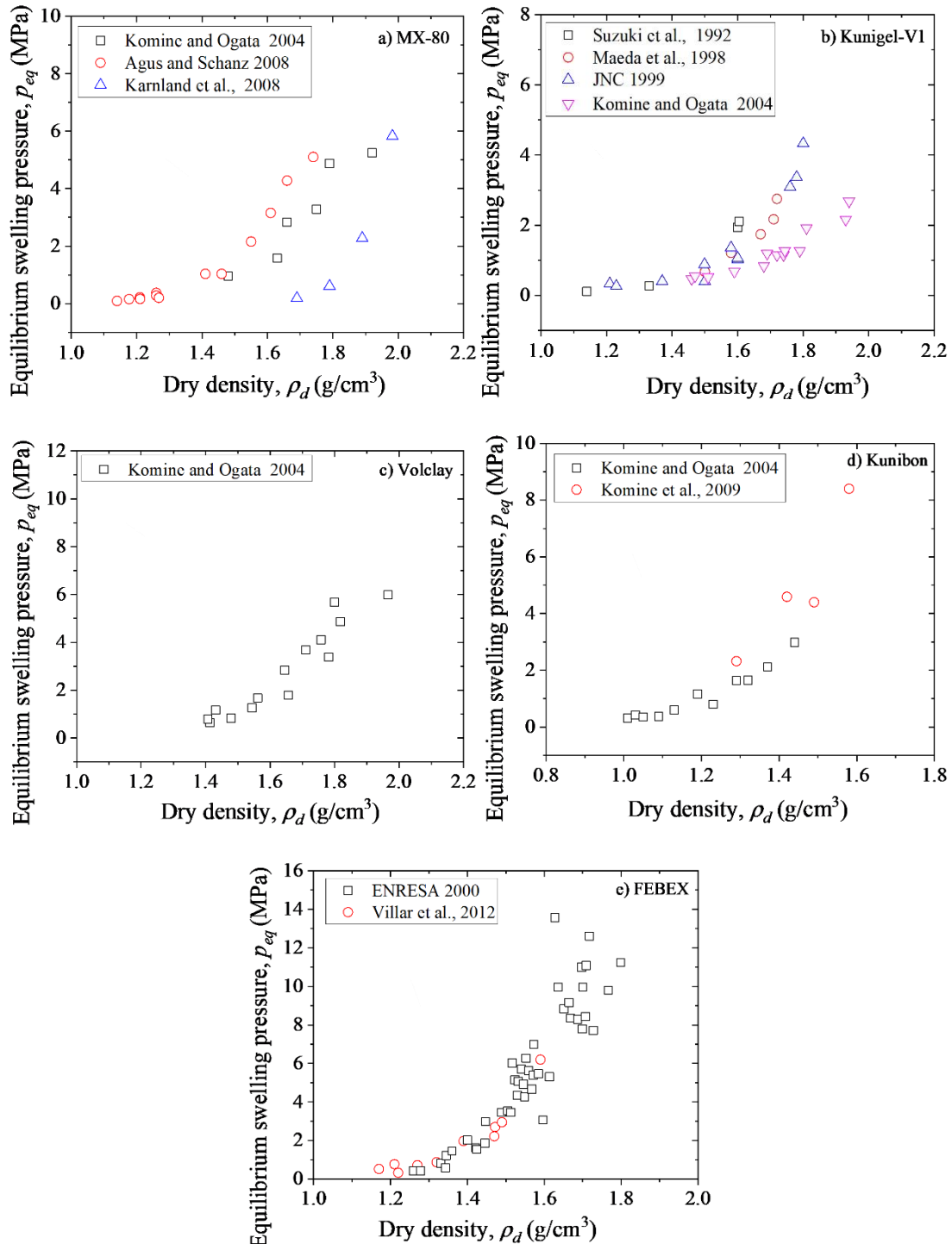


**Figure 1-22 Equilibrium swelling pressure of some bentonites changing with dry density from literatures**

Different from above ingredients, temperature effects on equilibrium swelling pressure were inconsistent based on the results of a literature survey presented in Table 1-3. As one might be noted from Table 1-3, equilibrium swelling pressure of Kunigel-V1 bentonite (Kodama et al. 2004; Kanazawa et al. 2020) and Bikaner bentonite (Bag and Rabbani 2017) increased with increasing temperature. Equilibrium swelling pressure of MX-80 (Pusch et al. 1990; Bag 2011; Tripathy et al. 2015), FEBEX (Villar and Lloret 2004; Villar et al. 2010), GMZ01 (Ye et al. 2014; Chen et al. 2018; Chen et al. 2019), and B bentonite from India (Jadda and Bag 2020) decreased as the increase of temperatures.

**Table 1-3 Temperature effect on equilibrium swelling pressure of bentonites from Literatures**

Bentonite	<sup>1</sup> Kunigel-V1	<sup>2</sup> MX-80	<sup>3</sup> FEBEX	<sup>4</sup> GMZ01	<sup>5</sup> Bikaner	<sup>6</sup> B
Type	Na	Na	Ca-Mg	Na	Ca	Na
Temperature (°C)	20–90	20–90	20–80	20–80	25–90	25–95
Dry density (g/cm <sup>3</sup> )	1.6 and 1.8	1.2–2.0	1.5–1.8	1.7	1.6	1.6
Effect	Increase	Decrease	Decrease	Decrease	Increase	Decrease

**Notes:** Increase, increase with rising temperature; Decrease, decrease with rising temperature.

<sup>1</sup> Kodama et al. 2004, Kanazawa et al. 2020; <sup>2</sup> Pusch et al. 1990, Bag 2011, Tripathy et al. 2015;

<sup>3</sup> Villar and Lloret 2004, Villar et al. 2010; <sup>4</sup> Chen et al. 2018, Chen et al. 2019;

<sup>5</sup> Bag and Rabbani 2017; <sup>6</sup> Jadda and Bag 2020.

### 1.3.3 X-ray diffraction

X-ray diffraction (XRD) technology was employed to make sense of soil characteristics in geotechnical area. Normally, the XRD was used to analysis the mineral composition in the soils. A specific XRD diffraction angle degree ( $\varphi$ ) is considered to correspond to

a specific mineral. An example is presented in Fig. 1-23 as the XRD profile of Kunigel-V1 bentonite in this study. It can be seen from Fig. 1-23, for the detection of mineral in bentonite, the diffraction angle is corresponding to approximate.  $6^\circ$  and  $29^\circ$ . However, it is pretty hard to obtain the percent of specific mineral in a soil by the intensity of a specific diffraction angle. Thus, a great amount of scholars just made use of the diffraction angle instead of intensity.

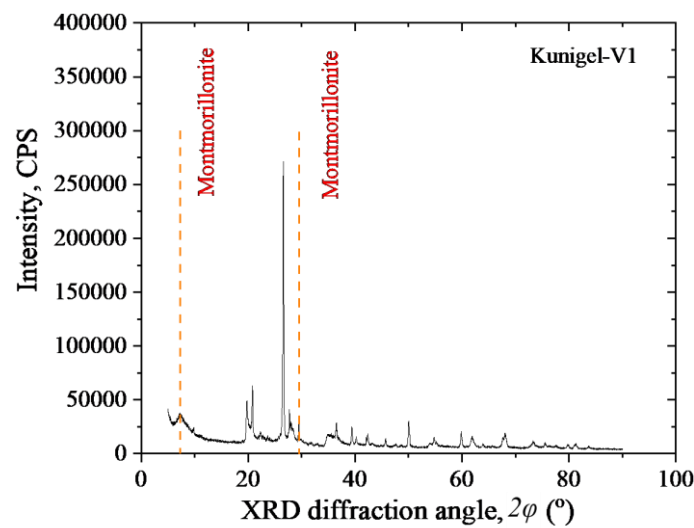


**Figure 1-23 XRD profile of Kunigel-V1 bentonite used in this study**

Recently, for bentonite researchers, XRD was used to detect the difference in interlayer distance (basal spacing,  $d_{001}$ ) of liquid-saturated bentonite specimens (Suzuki et al. 2005; Lee et al. 2012; Villar et al. 2012), furthermore explaining the difference in equilibrium swelling pressure. When bentonite absorbs water, the montmorillonite crystal layers undergo a hydration reaction, causing swelling in the c direction (001). Along with the increase of adsorbed water molecules, the swelling of montmorillonite proceeds and the distance between montmorillonite (basal spacing,  $d_{001}$ ) crystal layers increases. This distance can be detected using XRD tests results (e.g., Holmboe et al. 2012; Villar et al. 2012). As Villar et al. (2012) reported, the basal spacing can be calculated from the peak position when  $2\phi$  = approx.  $4$ - $8^\circ$  using Bragg's law as:

$$d_{001} = \frac{\mu\lambda}{2 \sin \varphi_{peak}} \quad (1-4)$$

where  $\lambda$  denotes the wavelength of incident wave ( $=1.5418 \text{ \AA}$ ),  $n$  expresses the position integer ( $=1$ ), and  $\varphi_{peak}$  signifies  $\varphi$  at the peak ( $^\circ$ ). About the unsaturated state, water vapor with a certain humidity was often used to obtain unsaturated specimen for XRD detection instead of liquid water (Saiyouri et al. 2004; Likos and Lu 2006). Meanwhile, for unsaturated bentonite XRD tests, powder specimen rather than compacted one was adopted (Moore and Hower 1986; Morodome and Kawamura 2009). Another important parameter can be observed from basal spacing is the state of water molecule arrangement in inter-layer space ( $L$ , Fig. 1-24). As Wang et al. (2020) reported,  $d_{001}=1.01 \text{ nm}$ ,  $1.25 \text{ nm}$ ,  $1.55 \text{ nm}$  and  $1.90 \text{ nm}$  are viewed as the dividing values for  $L=0w$ ,  $1w$ ,  $2w$  and  $3w$ , respectively.

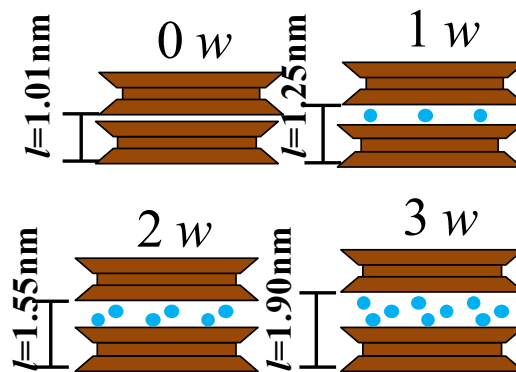


**Figure 1-24 Schematic showing state of water molecule arrangement between montmorillonite layers ( $L$ )**

Regarding the basal spacing of saturated specimen, it was reported by experimental investigations that being affected by many factors. It was found that basal spacing of saturated specimen decreases with the increase of dry density as revealed in Fig. 1-25 for MX-80 bentonite from Holmboe et al. (2012) and Villar et al. (2012). And, it was discovered that basal spacing of saturated specimen reduces as concentration of salt solution rises (Lee et al. 2012). In case of basal spacing of specimen during saturation.

Wang et al. (2020) saturated Kunigel-V1 bentonite with distilled water. The results indicated that basal spacing increases step wisely with rising water content as presented in Fig. 1-26. But there is lacking the testing database for basal spacing of bentonite saturated by salt solutions.

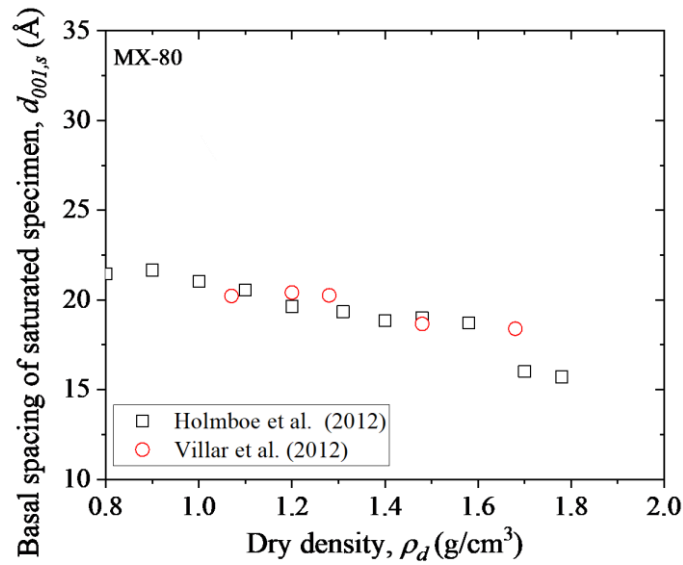


**Figure 1-25 Basal spacing of saturated specimen changing with dry density for MX-80 bentonite from literatures**

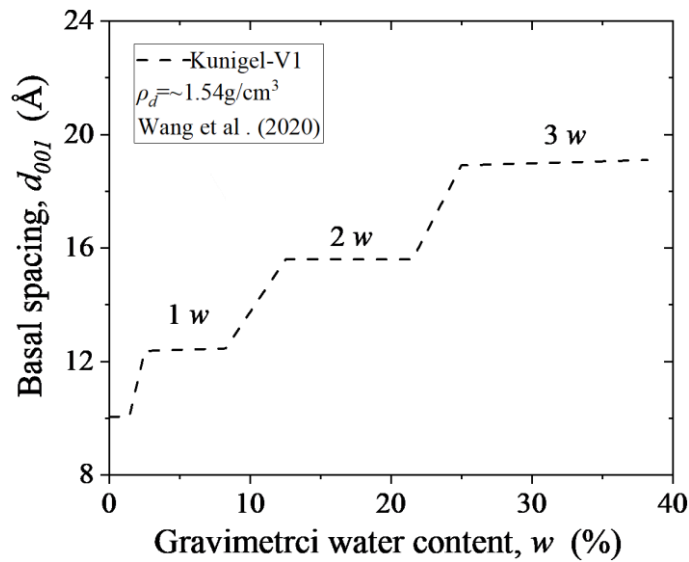


**Figure 1-26 Relation between water content, basal spacing and interlayer water molecule state**

#### 1.4 Research objectives

In this thesis, a newly developed multi-ring was applied in a newly designed swelling pressure apparatus to evaluate the hydraulic properties and swelling pressure of three bentonites (two sodium bentonites: MX-80 and Kunigel-V1; one calcium bentonite: Kunibond) during saturation. At the same time, slices from the multi-ring were sent to X-ray diffraction tests to observe the basal spacing. The effects of dry density, salt solution, concentration, temperature and initial water content on hydrological properties and swelling pressure of bentonites were researched. Basal spacings from X-ray diffraction tests were used to explain the effects of dry density, salt solution, concentration, temperature and initial water content on hydraulic properties and swelling pressure of these bentonites.

#### 1.5 The innovations of this study

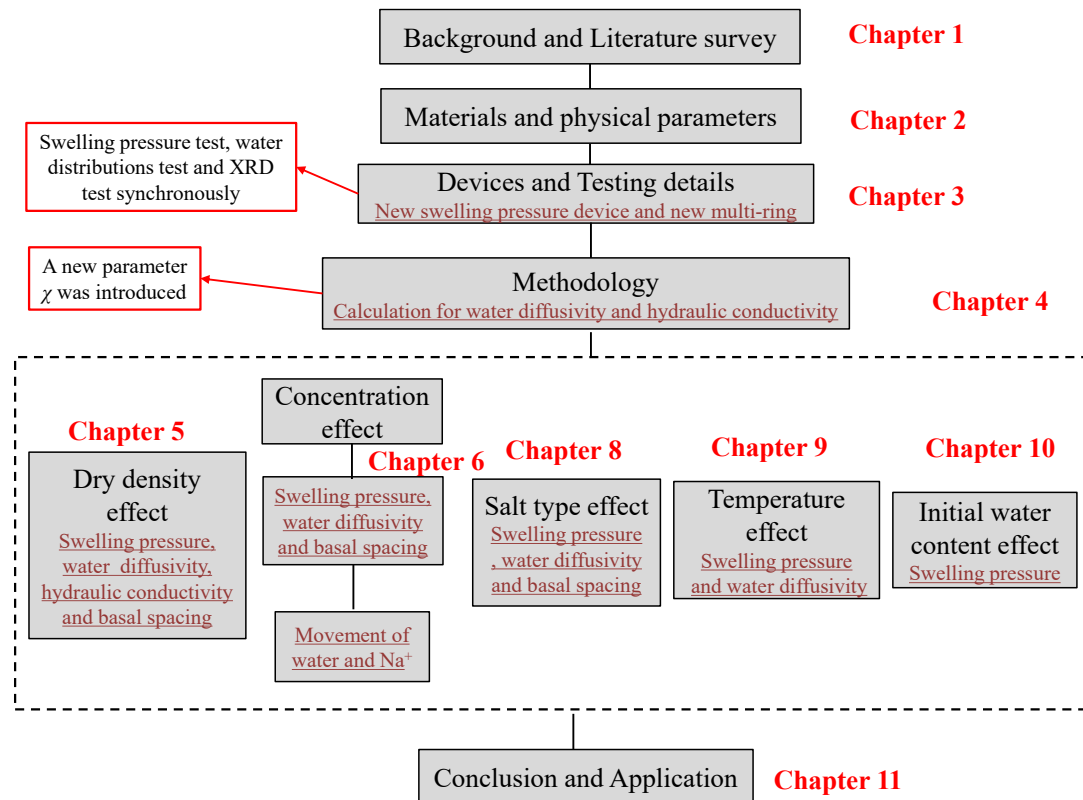
Firstly, this study used a newly developed swelling pressure apparatus. Comparing to other traditional swelling apparatus, this new swelling pressure apparatus can obtain repeatable swelling pressures of bentonites during saturation process.

Secondly, this study used a new multi-ring. By applying this new multi-ring in the newly developed swelling pressure apparatus, swelling pressure, hydraulic properties and XRD information can be obtained at the same time.

Thirdly, a new dual pore system was proposed basing on the microstructure of bentonite. Meanwhile, basing on the assumption that montmorillonite unit layers uniformly distributed in the compacted specimen during saturation, new equations for quantifying the dual pore system were proposed. Additionally, the new dual pore system was

adopted to evaluate the swelling pressure and hydraulic properties of bentonites during hydration.

### 1.6 Construction of the thesis



### 1-27 Research flow

This thesis is divided into 11 chapters and can be seen as the following flow chart in Fig. 1-27. The details were presented as followings:

Chapter 1: Introduction. In this chapter, the background and literature survey were carefully interpreted.

Chapter 2: Materials and physical parameters. Three bentonites used in this study were introduced. The testing methodologies for physical parameters and their values were introduced.

Chapter 3: Devices and testing methodology. The newly developed swelling pressure

apparatus and the new multi-ring were introduced.

Chapter 4: Hydraulic properties and swelling pressure of bentonites with XRD. The results, including swelling pressure, water distribution and XRD profiles, from new devices were displayed. By introducing a new parameter  $\chi$ , a simple equation for calculating the water diffusivity was proposed. Furthermore, by water diffusivity and soil water retention curve, the hydraulic conductivity during saturation was achieved. Basing on the XRD profiles, the basal spacing was calculated with Braag law.

Chapter 5: The effect of dry density on hydraulic properties and swelling pressures of bentonites with XRD. Swelling pressure, water diffusivity and hydraulic conductivity during saturation of different dry densities bentonites were displayed. The basal spacings from different dry densities bentonites were used to make sense the dry density effect on swelling pressure and hydraulic properties.

Chapter 6: The effect of  $\text{Na}^+$  concentration on hydraulic properties and swelling pressure of bentonite with XRD. In this chapter, NaCl solutions with different concentrations were used as saturation liquids to investigate the concentration effect of swelling pressure and water diffusivity of bentonite under wetting process. Additionally, by the XRD results, the concentration effects were discussed.

Chapter 7: The effect of  $\text{Na}^+$  concentration on movement of water and salt in bentonites with XRD. By using a simple wetting apparatus and multi-ring, infiltration tests wetted by NaCl solutions with different concentrations were conducted. The movements of water and salt were assessed by the water content and soil water concentration, respectively.

Chapter 8: The effect of salt types on hydraulic properties and swelling pressure of bentonites with XRD. In this chapter, distilled water, 0.5mol/l NaCl solution and 0.5mol/l  $\text{CaCl}_2$  solution were used as saturation liquids. Combining XRD results,

swelling pressure and water diffusivity of different cation bentonites saturated by different solutions were discussed.

Chapter 9: The effect of temperature on hydraulic properties and swelling pressure of bentonites. In this chapter, swelling pressures and water diffusivity tests of bentonites were carried out at different temperature. By the grain size of bentonite, the swelling pressure and water diffusivity phenomenon were explained.

Chapter 10: The effects of initial water content and specimen preparation method on swelling pressures of bentonite with XRD. In this chapter, the swelling pressure evolution curve pattern of specimen with different initial water contents was discussed. The effects of specimen preparation method and initial water content on equilibrium swelling pressure were interpreted. Basal spacing of specimen before and after wetting test was used for discovering the mechanism.

Chapter 11: Conclusion and Application. The conclusions from this thesis were concluded in this chapter. Besides that, how this thesis can progress the application of bentonite in deep geological disposal project was interpreted.

## Reference

- Agus, S. S., and Schanz, T., 2008. A method for predicting swelling pressure of compacted bentonites. *Acta Geotechnica*, **3**: 125-137.
- Bag, R. 2011. Coupled thermo-hydro-mechanical-Chemical behaviour of MX80 bentonite in geotechnical applications. Doctor thesis, Cardiff University.
- Bag, R., and Rabbani, A. 2017. Effect of temperature on swelling pressure and compressibility characteristics of soil. *Applied Clay Science*, **136**: 1–7.
- Butsuda, R., Komine, H., Yasuhara, K., Murakami, S., 2006. Advancement of experimentation for measuring hydraulic conductivity of bentonite using high-pressure consolidation test apparatus. *JSCE (C)*, **62 (3)**: 573-578.
- Chen, Q., 2022. Current Situation of Deep Geological Disposal for High-level Radioactive Waste in China and the Study on Prediction Swelling Pressure of Compacted Bentonite. Master Thesis, Waseda University.
- Chen, T., Sedighi, M., Jivkov, A.P., and Seetharam, S.C. 2021. A model for hydraulic conductivity of compacted bentonite – inclusion of microstructure effects under confined wetting. *Géotechnique*, **71(12)**: 1071–1084.
- Chen, Y.G., Dong, X.X., Zhang, X.D., Ye, W.M., and Cui, Y.J. 2018. Combined thermal and saline effects on the swelling pressure of densely compacted GMZ bentonite. *Applied Clay Science*, **166**: 318–326.
- Chen, Y.G., Dong, X.X., Zhang, X.D., Ye, W.M., and Cui, Y.J. 2019. Cyclic thermal and saline effects on the swelling pressure of densely compacted Gaomiaozhi bentonite. *Engineering Geology*, **255**: 37–47.
- Chijimatsu, M., Fujite, T., Kobayashi, A., and Nakano, M., 2000. Experiment and validation of numerical simulation of coupled thermal, hydraulic and mechanical behavior in the engineered buffer materials. *International Journal of Numerical and Analytical*

Methods in Geomechanics, **24**: 403-424.

Cho, K., 2022. Study on monitoring system of bentonite-based material in geological disposal project for high level radioactive waste. Undergraduate thesis, Waseda university.

Cho, W.J., Lee, J.O., and Chun, K.S., 1999. The temperature effects on hydraulic conductivity of compacted bentonite. *Applied Clay Science*, **14**: 47-58.

Cui, Y.J., Tang, A.M., Loiseau, C., and Delage, P., 2008. Determining the unsaturated hydraulic conductivity of a compacted sand–bentonite mixture under constant-volume and free-swell conditions. *Physics and Chemistry of the Earth, Parts A/B/C*, **33**: S462–S471.

ENRESA 2000. FEBEX project-full scale engineered barriers experiments for a deep geological repository for high level radioactive waste in crystalline host rock. Final report, Publicación técnica 1/2000, Empresa Nacional de Residuos Radiactivos SA (ENRESA), Madrid, Spain.

Fredlund, D.J., and Rahardjo, H., 1993. Soil mechanics for unsaturated soils. USA: John Wiley and Sons, Inc.

Hasegawa, T., 2004. Investigation on the effect of seawater to hydraulic property and wetting process of bentonite. Central Research Institute of Electric Power Industry, N04005 (In Japanese).

Holmboe, M., Wold, S., and Jonsson, M. 2012. Porosity investigation of compacted bentonite using XRD profile modeling. *Journal of Contaminant Hydrology*, **128**: 19–32.

IEA 2022. Electricity Market Report-January 2022, International Energy Agency. <https://www.iea.org/reports/electricity-market-report-january-2022>(Accessed 7 Feb. 2022).

- Ito, D., 2022. Study on the changes in swelling and permeability properties of bentonite materials by the chronological time scale cementation effects. Doctor thesis, Waseda university. (in Japanese)
- Jadda, T., and Bag, R. 2020. Effect of initial compacted pressure and elevated temperature on swelling pressure of two Indian bentonites. *Environmental Earth Science*, **79**: 197.
- JNC 1999. Technical reliability of the geological disposal for high-level radioactive waste in Japan - geological disposal research and development Second compiled – General report. Japan Nuclear Cycle Development Institute, JNC TN1400 99-020. (in Japanese) <https://www.jaea.go.jp/04/tisou/houkokusyo/dai2jitoimatome.html> (Accessed 8 Feb. 2022)
- Kanazawa, S., Kobayashi, S., Ichikawa, N., Yanai, M., and Ishiyama, K. 2020. The swelling behaviour of bentonite buffer material considering the effect of temperature. *International Journal of Geomate*, **19(74)**: 216–221.
- Karnland, O., Nilsson, U., Weber, H., Wersin, P., 2008. Sealing ability of Wyoming bentonite pellets foreseen as buffer material-laboratory results. *Physics and Chemistry of the Earth. Parts A/B/C*, **33**: S472–S475.
- Komada, J., Adachi, K., Tanabe, R., Suzuki, E., and Yamamoto, S. 2004. Swelling characteristics of bentonite–silica mixture under high temperature. *Journal of JSCE*, **764**: 319–328. (in Japanese)
- Komine, H., and Ogata, N., 1996. Prediction for swelling characteristics of compacted bentonite. *Canadian Geotechnical Journal*, **33**: 11–22.
- Komine, H., and Ogata, N. 2004. Prediction swelling characteristics of bentonites. *Journal of Geotechnical and Geoenvironmental Engineering*, **130(8)**: 818–829.
- Komine, H., 2008. Theoretical equations on hydraulic conductivities of bentonite-base

- d buffer and backfill for underground disposal of radioactive wastes. *Journal of Geotechnical and Geoenvironmental Engineering*, **134(4)**: 497–508.
- Komine, H., Yasuhara, K., and Murakami, S. 2009. Swelling characteristics of bentonites in artificial seawater. *Canadian Geotechnical Journal*, **46(2)**: 177-189.
- Komine, H., Oyamada, T., Ozaki, T., and Iso, S., 2018. Discussion on water migration and swelling of compacted powder bentonites. *Journal of JSCE(c)*, **74(1)**: 63–75. (in Japanese).
- Komine, H., 2020. Scale-model test for disposal pit of high-level radioactive waste and theoretical evaluation of self-sealing of bentonite-based buffers. *Canadian Geotechnical Journal*, **57(4)**: 608–615.
- Kubota, T., Fukutani, S., Ohta, T., and Mahara, Y., 2013. Removal of radioactive cesium, strontium, and iodine from natural water using bentonite, zeolite, and activated carbon. *Journal of Radioanalytical And Nuclear Chemistry*, **296 (2)**: 981-984.
- Laird, D.A. 1996. Model for crystalline swelling of 2:1 phyllosilicates. *Applied Clay Science*, **44(4)**: 553–559.
- Laird, D.A. 2006. Influence of layer charge on swelling of smectites. *Applied Clay Science*, **34(1-4)**: 74–87.
- Lee, O.L., Lim, J.G., Kang, I.M., and Kwon, S., 2012. Swelling pressures of compacted Ca-bentonite. *Engineering Geology*, **129-130**: 20-26.
- Likos, W.J., and Lu, N., 2006. Pore-scale analysis of bulk volume change from crystalline interlayer swelling in Na<sup>+</sup>-and Ca<sup>2+</sup>-smectite. *Clays and Clay Minerals*, **54(4)**: 515–528
- Liu, J., and Neretnieks, I., 2006. Physical and chemical stability of bentonite buffer. December 2006, SKB report, R-06-103.
- Lu, N., and Likos, W.J., 2004. *Unsaturated soil mechanics*. New York: Wiley.

Maeda, M., Tanai, K., Ito, M., Mihara, M. and Tanaka, M. 1998. Mechanical properties of the Ca exchanged and Ca bentonite: swelling pressure, hydraulic conductivity, compressive strength and elastic modulus. Technical Report, Japan Nuclear Cycle Development Institute, PNC-TN8410 98-021 (in Japanese). <https://jopss.jaea.go.jp/pdfdata/PNC-TN8410-98-021.pdf>

METI 2020. Learn from foreign experience in HLW management-2020 version. Agency for Natural Resources and Energy, Ministry of Economy, Trade and Industry (in Japanese). <http://www2.rwmc.or.jp/publications:hlwkj2020>

Mitchell, J.K., and Soga, K. 2005. Fundamentals of soil behavior, Third Edition. John Wiley & Sons, Inc., Hoboken, New Jersey.

Morodome, S., and Kawamura, K. 2009. Swelling behavior of Na- and Ca montmorillonite up to 150°C by in situ X-ray diffraction experiments. *Clays and Clay Minerals*, **57(2)**: 150–160.

Moore, D.M., and Hower, J., 1986. Ordered interstratification of dehydrated and hydrated Na-smectite. *Clays and Clay Minerals*, **34(4)**: 379–384.

Musso, G., Romero, E., and Della, V.G. 2013. Double-structure effects on the chemo-hydro-mechanical behaviour of a compacted active clay. *Géotechnique*, **63 (3)**: 206–220.

NUMO 2022. The Nuclear Waste Management Organization of Japan. <https://www.numo.or.jp/en/jigyuu/geological.html> (Accessed 8 Feb. 2022).

Pusch, R., Karnland, O., and Hokmark, H. 1990. GMM – a general microstructural model for qualitative and quantitative studies on smectite clays. SKB Technical Report 90-43.

Pusch, R. 2001. The microstructure of MX-80 clay with respect to its bulk physical properties under different environmental conditions. SKBF/KBS technical report. No.T

R01-08.

Posiva 2012. Safety Case for the Disposal of Spent Nuclear Fuel at Olkiluoto – Synthesis 2012. Posiva Oy, December 2012.

Ruan, K.L., Sun, D.A., and Fu, X. L., 2020. Swelling characteristics and hydraulic conductivities of bentonite and sand mixtures saturated with landfill leachate. *Journal of Shanghai University*, **26 (6)**: 989-1000. (in Chinese)

Ruan, K.L., and Fu, X. L., 2021. A modified Kozeny-Carman equation for predicting saturated hydraulic conductivity of compacted bentonite in confined condition. *Journal of Rock Mechanics and Geotechnical Engineering*, in press. <https://doi.org/10.1016/j.jrmge.2021.08.010>.

Ruan, K.L., Komine, H., Ito, D., Miyoshi, K., and Gotoh, T., 2022. Hydraulic conductivity and X-ray diffraction tests of unsaturated bentonites with a multi-ring and their predictions by pores distributions. *Engineering Geology*, **306 (5)**: 106738.

Saiyouri, N., Tessier, D., and Hicher, P.Y. 2004. Experimental study of swelling in unsaturated compacted clays. *Clay Minerals*, **39**: 469–479.

Samper, J., Zheng, L., Montenegro, L., Fernandez, A.M., Rivas, P., 2008. Coupled the thermo-hydro-chemical models of compacted bentonite after FEBEX in situ test. *Applied Geochemistry*, **23**: 1186-1201.

Sadamatsu, A., 2021. Measurement of hydraulic conductivity of compacted bentonite by the falling head test method. Master thesis, Waseda University. (In Japanese).

Saiyouri, N., Tessier, D., and Hicher, P.Y., 2004. Experimental study of swelling in unsaturated compacted clays. *Clay Minerals*, **39**: 469–479.

Shirakawabe, T., 2019. Evaluation of the effect of thermal history on swelling and water transfer characteristics of unsaturated bentonites. Master thesis, Waseda University. (in Japanese)

- Shirakawabe, T., Wang, H., Goto, S., Yamamoto, S., Koimne, H., 2021. Study of thermal history effect on water movement in unsaturated bentonite. *JSCE (C)*, **77 (2)**: 103-117. (in Japanese)
- SKB 2011. Long-term safety for the final repository for spent nuclear fuel at Forsmark -Main report of the SR-Site project, Volume 1, TR-11-01.
- Sun, D.A., Zhang, L., Li, J., and Zhang, B.C. 2015. Evolution and prediction of the swelling pressures of GMZ bentonites saturated with saline solution. *Applied Clay Science*, **105-106**: 207–216.
- Suzuki, H., Shibata, M., Yamagata, J., Hirose, I. and Terakado, K 1992. Mechanical experiments of buffer material. Technical Report, Japan Nuclear Cycle Development Institute, PNC-TN8410 92-057 (in Japanese). <https://jopss.jaea.go.jp/pdfdata/PNC-TN8410-92-057.pdf>
- Suzuki, S., Prayongphan, S., Ichikawa, Y., and Chae, B.G. 2005. In situ observations of the swelling of bentonite aggregates in NaCl solution. *Applied Clay Science*, **29 (2)**: 89–98.
- Takeuchi, S., Hara, K., and Nakano, M., 1995. Water retention curve, water diffusivity and water movement of compacted bentonite. *Soils and Foundations*, **35 (3)**: 129–137. (in Japanese).
- Tripathy, S., Bag, R., and Thomas, H.R., 2015. Enhanced isothermal effect on swelling pressure of compacted MX80 bentonite. *Engineering Geology for Society and Territory*, **6**: 537–539.
- Villar, M. V. 2002. Thermo-hydro-mechanical characterisation of a bentonite from Cabo de Gata. Ph.D. thesis, Universidad Complutense de Madrid, Madrid, Spain.
- Villar, M.V., and Lloret, A. 2004. Influence of temperature on the hydro-mechanical behaviour of a compacted bentonite. *Applied Clay Science*, **26**: 337–350.

- Villar, M.V., and Lloret, A. 2008. Influence of dry density and water content on the swelling of a compacted bentonite. *Applied Clay Science*, **39**: 38–49.
- Villar, M.V., Rgomez, E.R., and Lloret, A. 2010. Experimental investigation into temperature effect on Hydro mechanical behaviors of bentonite. *Journal of Rock Mechanics and Geotechnical Engineering*, **2(1)**: 71–78.
- Villar, M.V., Espina, R.G., and Nebot, L.G. 2012. Basal spacings of smectite in compacted bentonite. *Applied clay science*, **(65-66)**: 95-105.
- Wang, H.L., Shirakawabe, T., Komine, H., Ito, D., Gotoh, T., Ichikawa, Y., and Chen, Q., 2020. Movement of water in compacted bentonite and its relation with swelling pressure. *Canadian Geotechnical Journal*, **57(6)**: 921–932.
- Wang, H.L., Komine, H., and Gotoh, T. 2021. A swelling pressure cell for X-ray diffraction test. *Géotechnique*, in press. <https://doi.org/10.1680/jgeot.20.00005>
- Wang, H.L., Ruan, K.L., Harasaki, S., and Komine, H., 2022. Effects of specimen thickness on apparent swelling pressure evolution of compacted bentonite. *Soils and Foundations*, **62**: 101099.
- Wang, J., Chen, L., Su, R., and Zhao, X., 2018. The Beishan underground research laboratory for geological disposal of high-level radioactive waste in China: Planning, site selection, site characterization and in suit tests. *Journal of Rock Mechanics and Geotechnical Engineering*, **10**: 411-435.
- Wang. Q., Cui, Y.J., Tang, A.M., Barnichon, J.D., Saba, S., and Ye, W.M., 2013. Hydraulic conductivity and microstructure changes of compacted bentonite/sand mixture during saturation. *Engineering Geology*, **164**: 67-76.
- Wang, Y.P., Wang, Z., Zhao, Y., Yi, F.C., and Zhu, B.L., 2021. Swelling properties and permeability of GMZ bentonite-sand mixtures during different solutions infiltration. *Sustainability*, **13**: 1622.

Wen, Z. J. 2006. Physical property of China's buffer material for high level radioactive waste repositories. *Chinese Journal of Rock Mechanics and Engineering*, **25**: 794-800 (In Chinese).

World Nuclear Association. 2022. Storage and Disposal of Radioactive Waste. <https://world-nuclear.org/information-library/nuclear-fuel-cycle/nuclear-waste/storage-and-disposal-of-radioactive-waste>.

Xu, Y., Sun, D.A., Zeng, Z., and Lv, H., 2019a. Temperature dependence of apparent thermal conductivity of compacted bentonites as buffer material for high-level radioactive waste repository. *Applied Clay Science*, **174**: 10-14.

Xu, Y., Sun, D.A., Zeng, Z., and Lv, H., 2019b. Effect of aging on thermal conductivity of compacted bentonites. *Engineering Geology*, **253**: 55-63.

Ye, W.M., Cui, Y.J., Qian, L.X., and Chen, B., 2009. An experimental study of the water transfer through confined compacted GMZ bentonite. *Engineering Geology*, **108(3-4)**: 169–176.

Yong, R.N. 1999. Soil suction and soil–water potentials in swelling clays in engineered clay barriers. *Engineering Geology*, **54**: 3–13.

Zheng, L., Samper, J., and Montenegro, L., 2011. A coupled THC model of the FEBEX in situ test with bentonite swelling and chemical and thermal osmosis. *Journal of Contaminant Hydrology*, **126**: 45-60.

Zheng, L., Rutqvist, J., Xu, H., and Birkholzer, T., 2017. Coupled THMC models for bentonite in an argillite repository for nuclear waste: Illitization and its effect on swelling stress under high temperature. *Engineering Geology*, **230**: 118-129.

Zhu, C. M., Ye, W. M., Chen, Y. G., Chen, B., and Cui, Y. J. 2013. Influence of salt solutions on the swelling pressure and hydraulic conductivity of compacted GMZ01 bentonite. *Engineering Geology*, **166**: 74–80.

# Chapter 2

## **MATERIALS AND PHYSICAL PARAMETERS**

## 2.1 Materials

Three bentonites were used in this study: 1) a sodium type bentonite from Wyoming, USA: MX-80 (MX80). MX80 has been selected as candidate buffer material for many countries, such as USA; 2) a sodium type bentonite from Yamagata, Japan: Kunigel-V1 (KV1). KV1 was chosen as the candidate buffer material for Japanese deep geological disposal project; and 3) a calcium type bentonite from Miyagi, Japan: Kunibond (KB). Figure 2-1 shows the outlook of these three bentonites. As we can see from Fig. 2-1, MX80 has a brown particle appearance. KV1 is a grey powder and KB is a yellow powder.



**Figure 2-1 Outlook of bentonites**

## 2.2 Physical parameters

## 2.2.1 Grain size distribution

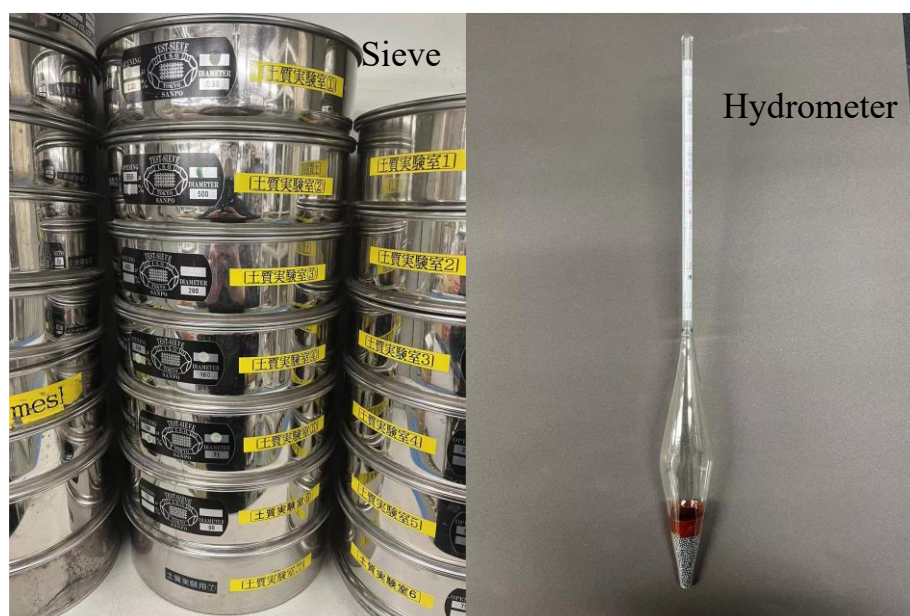


**Figure 2-2 Sieve and hydrometer for grainsize distribution test**

The grain size distributions of bentonites were tested generally following JIS A 1204-2020. Herein, grain size distributions of MX80 bentonites were tested with both sieve and hydrometer (Fig. 2-2). The grain size distributions of KV1, and KB were detected using only hydrometer (Fig. 2-2). Grain size distribution with the sieve was decided by weighing the soil mass. It is noteworthy that in JIS A 1204-2020, when using a hydrometer to obtain grain size distribution for clayey soil, an approx. 65 g soil mass is recommended for mixing with 1 L solution. However, Wang et al. (2020) tested the grain size distribution of KV1 bentonite with a hydrometer and recommended 15-30 g for hydrometer test can obtain better repeatable results. For this study, an approx. 20 g mass was adopted for hydrometer tests. Figure 2-3 indicates the grain size distributions of these three bentonites as the method introduce above. Mitchell and Soga (2005) divided soil grain sizes into two aspects: 1) fine (powder) soils, with grains of diameter less than 0.07 mm; and 2) particle soils, with grains of diameter greater than 0.07 mm. It is apparent from Fig. 2-3 that grains larger than 0.07 mm of MX80 are both over 50%, which shows that particle soils dominate the contents of MX80 bentonites. For this

study, MX80 was designated as particle bentonite. For KV1 and KB bentonites, 95% of grains were smaller than 0.07 mm, reflecting that powder soils account for most of the composition. Therefore, KV1 and KB are designated as powder bentonites.

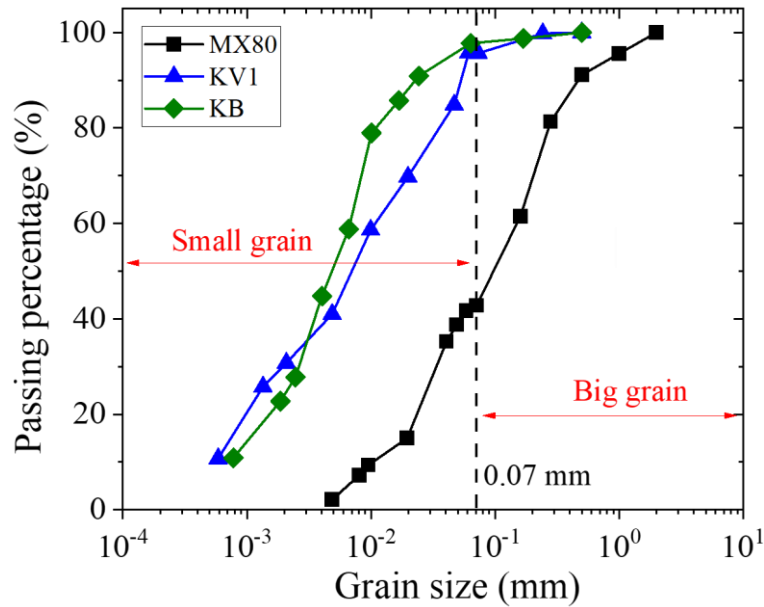


**Figure 2-3 Grain size distributions of bentonites**

### 2.2.2 Soil particle density

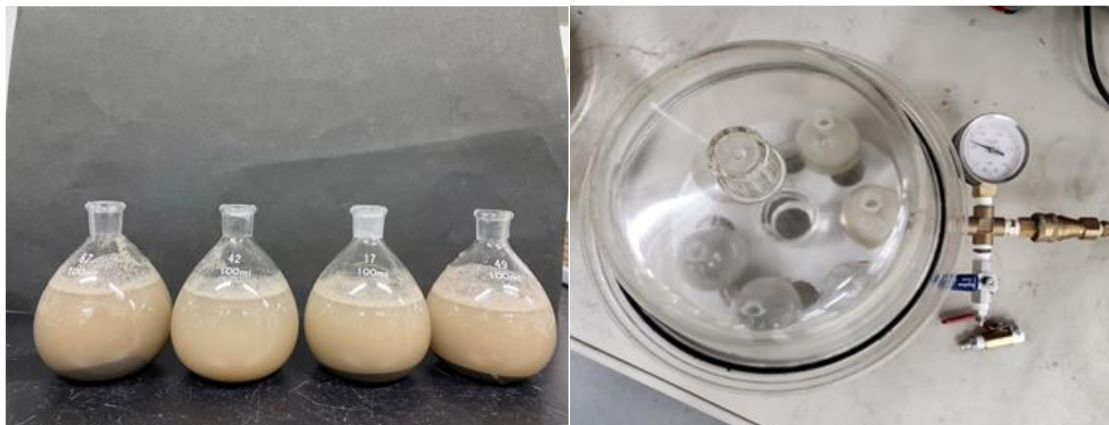


**Figure 2-4 Soil particle density testing details**

Soil particle density was measured by JIS A 1202:2020. It is noted that 5g powders was used for the soil particle density tests, even though ~10 g was recommended by JIS A 1202:2020. This is because of the fact that, as the experimental observation by Wang et al. (2021), ~10 g powder with 100 ml pycnometer (Fig. 2-4) is very hard for letting

all the air out when vacuuming the pycnometer (Fig. 2-4). The test apparatuses required are as followings:

- (1) Pycnometer
- (2) Thermometer
- (3) Ultrasonic disperser
- (4) Desiccator, decompression pump

Procedures for the test method are as follows:

- (1) Measure the mass of the pycnometer and the mass when the pycnometer is filled with pure water. Also, measure the temperature of distilled water.
- (2) Put 50 ml of pure water and ~ 5 g of powdered sample in a beaker and disperse the sample using an ultrasonic disperser.
- (3) Use a funnel to transfer the beaker contents to the pycnometer and add pure water to two-thirds of the total pycnometer.
- (4) Place the pycnometer in a desiccator decompressed by a pump and continue vacuum degassing for 1 week. In addition, shake the pycnometer once a day to promote degassing. Figure 2-5 shows the appearance of vacuum degassing.
- (5) Determine the density of soil particles.

Soil particle densities of bentonites are indicated in Table 2-1.

**Table 2-1 Soil particle densities of bentonites**

	MX80	KV1	KB
Soil particle density (g/cm <sup>3</sup> )	2.88	2.76	2.63

### 2.2.3 Liquid limit and plastic limit



**Figure 2-5 Liquid and plastic limits testing details**

The liquid limit and plastic limit tests were conducted to investigate the changes in the state of soil depending on its water content. If the liquid limit test is performed according to general method (JIS A 1205:2020) the sample swells every time as water is added. Hence, the sample need to be cured about one week (Fig. 2-5) so that to avoid the problem of thixotropy. In this study, the following method was performed to obtain reliable results. Following list presents the test apparatus.

- (1) Liquid limit measuring apparatus
- (2) Groove-cutting gauge
- (3) Glass plate
- (4) Spatula
- (5) Dryer
- (6) Evaporating dish
- (7) Constant temperature drying oven
- (8) Round bar of 3 mm in diameter

Outline of test method are as followings:

(1) For the plastic limit test, the above method is used because reliable results can be obtained by standard method (JIS A 1205:2020). For the liquid limit test, the following method is used.

(2) Prepare about 100 g of the sample and transfer it to a vat. Add pure water to the vat, cover with plastic wrap, and cure for one week. The amount of water added should be such that the number of blows would be about 10 times when using a liquid limit measuring device.

(3) Transfer an appropriate amount of the cured sample to a glass plate and knead it with a spatula. At the time, a dryer is utilized to reduce the water content, and moisture on the surface is blown off by the dryer, so the entire sample is kneaded evenly (Fig. 2-5).

(4) Measure the liquid limit of the sample after adjusting the water content ratio in the method described in 3) using the liquid limit measuring instrument.

Plastic and liquid limit of bentonites are indicated in Table 2-2.

**Table 2-2 Liquid and plastic limits of bentonites**

	MX80	KV1	KB
Liquid limit (%)	437.3	468.1	128.7
Plastic limit (%)	28.7	29.1	58.4
Plasticity index (%)	408.6	439	70.3

#### 2.2.4 Montmorillonite content

The swelling properties of bentonite are mainly attributed to montmorillonite. Therefore, the content of montmorillonite is a significant indicator to describe the property of bentonite. Montmorillonite content was determined by the methylene blue adsorption capacity test using the spot method (JIS Z 2451:2019). The final results are

revealed in Fig. 2-6. And, the montmorillonite contents of bentonites are listed in Table 2-3.

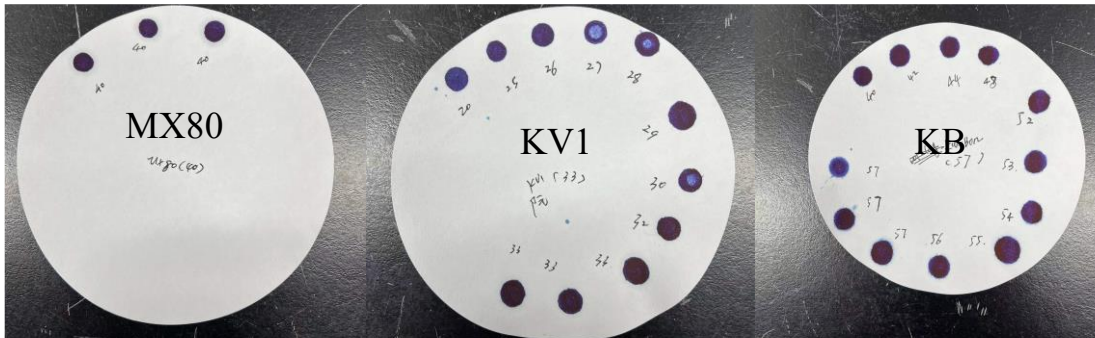


**Figure 2-6 Montmorillonite content testing details**

**Table 2-3 Montmorillonite contents of bentonites**

	MX80	KV1	KB
Montmorillonite content (%)	61	50	78

### 2.2.5 Cation exchangeable capacity



**Figure 2-7 CEC testing details**

**Table 2-4 CECs and EXCs of bentonites**

		MX80	KV1	KB
Bentonite type		Na	Na	Ca
CEC, Total cation exchangeable capacity (meq/100 g); EXC, amount of extractable cations (meq/100 g)	CEC	1.237	1.043	0.775
	EXC <sub>Na</sub>	0.727	0.613	0.114
	EXC <sub>Ca</sub>	0.408	0.404	0.570
	EXC <sub>Mg</sub>	0.091	0.02	0.07
	EXC <sub>K</sub>	0.011	0.01	0.02

As a very special soil, cation exchangeable exchange capacity (CEC) is crucial for understanding the physical properties of bentonite. In Komine and Ogata (2004), CEC was used to predict the swelling characteristics of several bentonites. And Komine (2008) used the CEC to estimate saturated hydraulic conductivity of bentonite. The CECs of these three bentonites were tested with JGS 0261-2020. In this method, in order to determine CEC of bentonite, bentonite samples are leached with BaCl<sub>2</sub> and MgSO<sub>4</sub> solution and the leached solutions are analyzed by inductively ICP-OES (Fig. 2-7). Because bentonite has relatively higher CEC than other soils, as reported by Yan (2021), only leaching one time by BaCl<sub>2</sub> and MgSO<sub>4</sub> is not enough. Thus, this study leached the powder bentonites 3 times before taking to concentration test by ICP-OES. Table 2-4 lists the CECs and EXCs of bentonites. As we can see from Table 2-4, Na<sup>+</sup> dominates the EXC of MX80 and KV1 and Ca<sup>2+</sup> dominates the EXC of KB.

## Reference

- JGS 2020. Determination of cation exchange capacity. JGS 0261-2020, Laboratory Testing Standards of Geomaterials, Japanese Geotechnical Society Standards.
- JIS 2019. Test method for methylene blue adsorption on bentonite and acid clay. JIS standard Z2451. Japanese Industrial Standard Committee.
- JIS 2020. Test method for density of soil particles. JIS A 1202-2020, Laboratory Testing Standards of Geomaterials, Japanese Geotechnical Society Standards.
- JIS 2020. Test method for particle size distribution of soils. JIS A 1204-2020, Laboratory Testing Standards of Geomaterials, Japanese Geotechnical Society Standards.
- JIS 2020. Test method for liquid and plastic limit of soils. JIS A 1205-2020, Laboratory Testing Standards of Geomaterials, Japanese Geotechnical Society Standards.
- Komine, H., and Ogata, N., 1996. Prediction for swelling characteristics of compacted bentonite. *Canadian Geotechnical Journal*, **33**: 11–22.
- Komine, H., and Ogata, N., 2004. Prediction swelling characteristics of bentonites. *Journal of Geotechnical and Geoenvironmental Engineering*, **130 (8)**: 818-829.
- Komine, H., 2008. Theoretical equations on hydraulic conductivities of bentonite-based buffer and backfill for underground disposal of radioactive wastes. *Journal of Geotechnical and Geoenvironmental Engineering*, **134(4)**: 497–508.
- Mitchell, J.K., and Soga, K. 2005. *Fundamentals of soil behavior*, Third Edition. John Wiley & Sons, Inc., Hoboken, New Jersey.
- Wang, H.L., Shirakawabe, T., Komine, H., Ito, D., Gotoh, T., Ichikawa, Y., and Chen, Q. 2020. Movement of water in compacted bentonite and its relationship with swelling pressure. *Canadian Geotechnical Journal*, **57**: 921–932.
- Wang, H.L., Komine, H., and Gotoh, T. 2021. A swelling pressure cell for X-ray

diffraction test. Géotechnique. <https://doi.org/10.1680/jgeot.20.00005>

Yan, X.F., 2021. Determination of cation exchange capacity of bentonite and the change in leached cations of bentonite in saline environment. Master thesis, Waseda University.

# Chapter 3

## **DEVICES AND TESTING METHODOLOGY**

### 3.1 Devices

#### 3.1.1 Swelling pressure apparatus

As significant ingredient to assess swelling ability, swelling pressures ( $p_s$ ) of bentonites had been greatly researched by different experimental methods. There are generally four methods adopting to obtain swelling pressure of compacted bentonite (Sun et al., 2009; Tang et al., 2011): 1) stepwise consolidation method, 2) one step

**Table 3-1 Physical parameters values of materials in literature survey**

Material	Mining location	Montmorillonite content	‡CEC or EXC (meq/100g)	Reference
KV1	Tsukinuno mine, Yamagata, Japan	50-55%	Na: 51.3, Ca: 41.7 Mg: 8.8 K: 0.89	Suzuki et al., 1992
	ditto	50%	Na: 53.9, Ca: 48.5 Mg: 7.4 K: 1.4	Maeda et al., 1998
	ditto	46-49%	Na: 54.6, Ca: 41.9 Mg: 6.6 K: 1.3	JNC 1999
	ditto	48%	CEC: 73.2 Na: 40.4, Ca: 28.7 Mg: 3.0 K: 0.9	Komine and Ogata 2004
FEBEX	Cortijo de Archidona deposit, Almería, Spain	92±3%	CEC: 102±4 Na: 27±1, Ca: 35±2 Mg: 31±3	Villar et al., 2012
	ditto	ditto	CEC: 102±4 Na: 25±2, Ca: 42±3 Mg: 32±2 K: 2.5±0.3	ENRESA 2000

‡ CEC: total cation exchangeable capacity; EXC: amount of extractable cations.

consolidation method, 3) constant volume method and 4) zero swelling method. Among these methods, zero swelling method is most often used because this method is most close to actual condition - deformation of buffer material is restricted by surrounding natural rock.

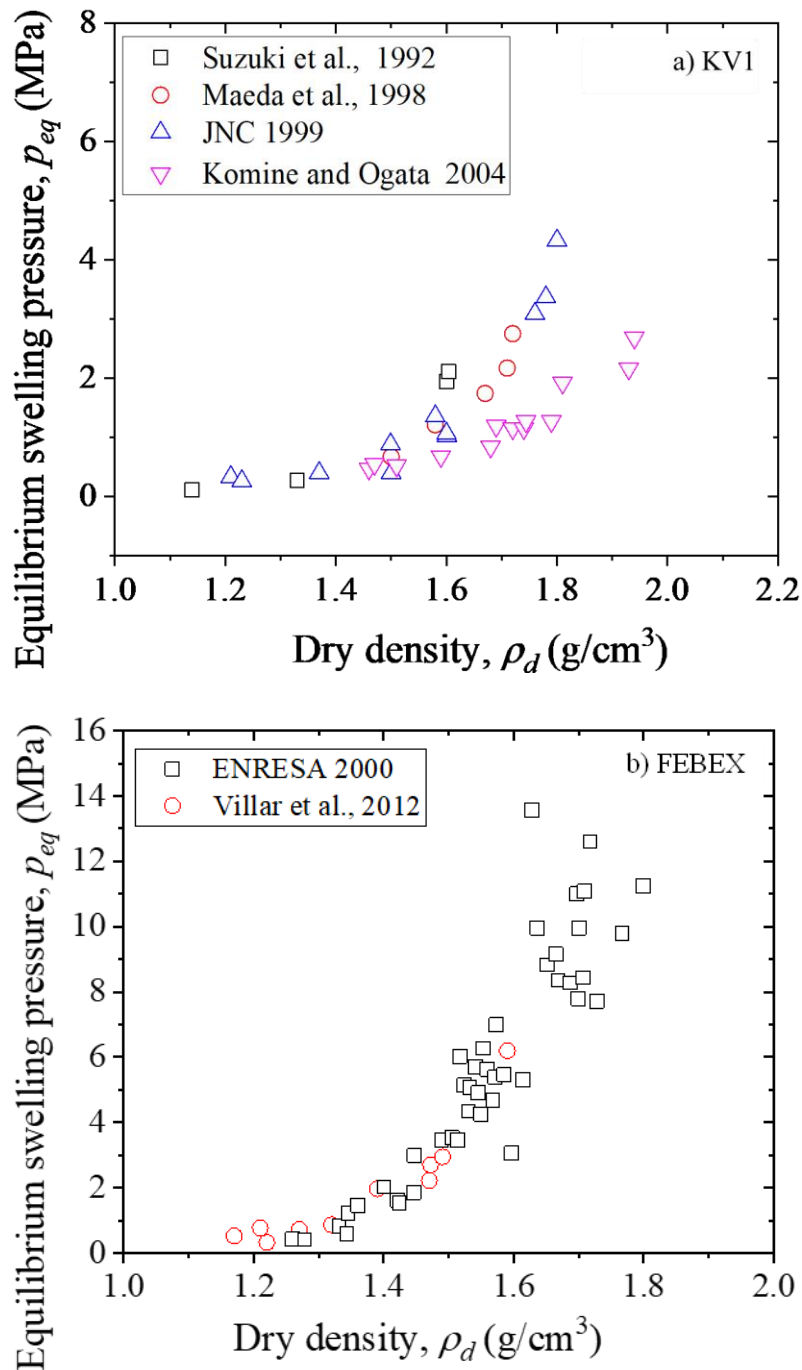
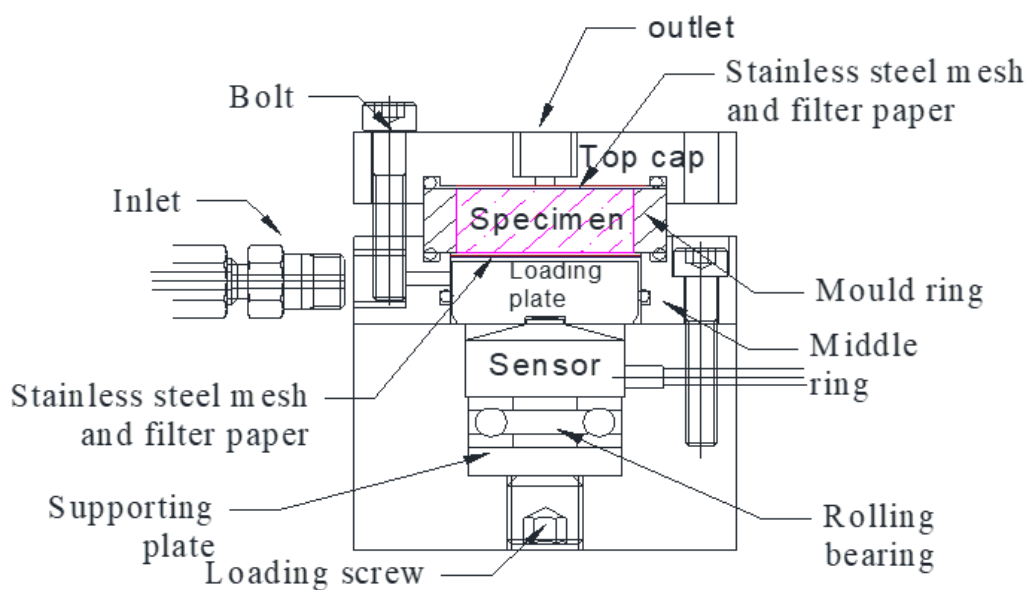


Figure 3-1 Equilibrium swelling pressures from literatures: a) KV1 and b)

FBBEX

Numerous investigations studied equilibrium swelling pressure ( $p_{eq}$ , swelling pressure in equilibrium state) of compacted bentonites, which has been proved sensitive to many factors, such as dry density (Villar and Lloret, 2008; Kaufhold et al., 2015; Wang et al., 2021). A literature survey was conducted to find the variation of equilibrium swelling pressure with dry density by utilizing zero swelling method. Testing results of KV1 (sodium type bentonite, candidate buffer material for Japanese project) and FEBEX (calcium-magnesium bentonite, buffer material for Spanish project) by some researchers are indicated in Fig. 3-1. Their materials physical parameters values are presented in Table 3-1. As easily found from Figure 3-1 that equilibrium swelling pressures of similar specimens under the same dry density might have several hundred kilopascals or even several megapascals difference. For example, as KV1 bentonite, the equilibrium swelling pressure from JNC (1999) and Komine and Ogata (1994) have somewhat difference, even though their physical parameters were similar. Reasons for this phenomenon can be explained from the experimental instrument issues (Tanaka 2011; Tanaka and Watanabe 2019). Therefore, it is needed to improve apparatus for getting consistent results.

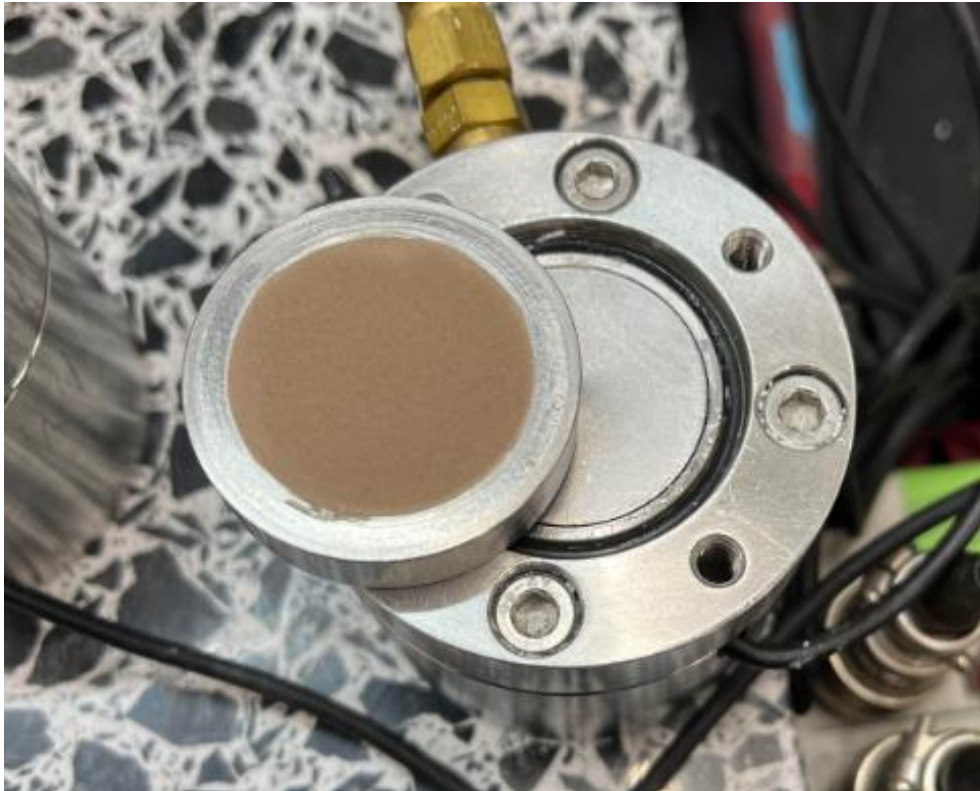


**Figure 3-2 New swelling pressures apparatus**

In this study, a developed apparatus (Wang et al. 2022) was used for measuring swelling pressure. The new swelling pressure apparatus overview is presented in Fig. 3-2. A 10mm-height ring is confined by the top cap and middle ring, the vertical deformation of specimen (10 mm-height, 28 mm-diameter) is restricted by the top cap and loading plate. Under the loading plate, there are sensor, rolling bearing, supporting plate and loading screw. Initial touch between specimen and loading plate can be achieved by rotating the loading screw. The loading plate diameter is designed to be greater than the ring inner diameter to avoid imparting stress on the specimen when rotating the loading screw for initial contact. Water is designed to be supplied from the opening of middle ring. After passing through an approximately 0.3 mm-wide gap between loading plate and middle ring, water flows into the specimen from around the loading plate. All the parts of swelling pressure apparatus were made by SUS303 stainless steel. Herein, several issues concerning the apparatus design are clarified as followings:

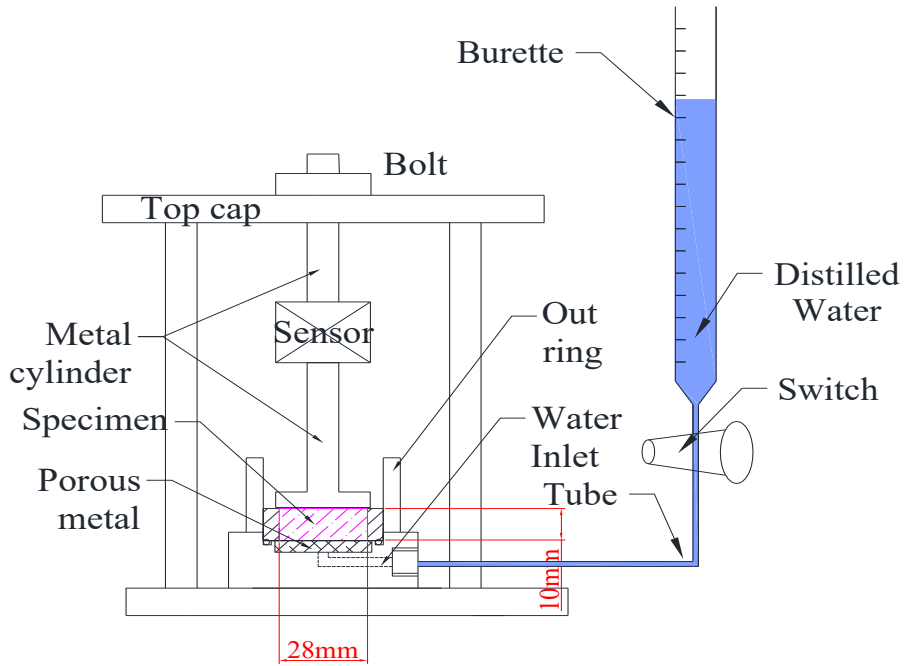
(1) The application of loading plate. A loading plate was used in the new swelling pressure apparatus instead of porous metal/stone for increasing system stiffness of swelling pressure apparatus. As reported by Tanaka and Watanabe (2019), slight volumetric strain of compacted bentonite caused by the finite apparatus stiffness may induce a reduction of measuring swelling pressure. The stiffness of loading plate is much greater than porous metal/stone, further increasing the system stiffness.

(2) Sensor vertical deformation. A strain-gauge type sensor (CLS-10KNB, Tokyo Measuring Instruments Lab.) was applied in the new swelling pressure. From the personal communication, the theoretical vertical deformation is approx.  $1.35 (\mu\text{m}/\text{MPa of } p_s)$ , which is very small. Meanwhile, no obvious deformation was found for specimen after swelling pressure test as Fig. 3-3.

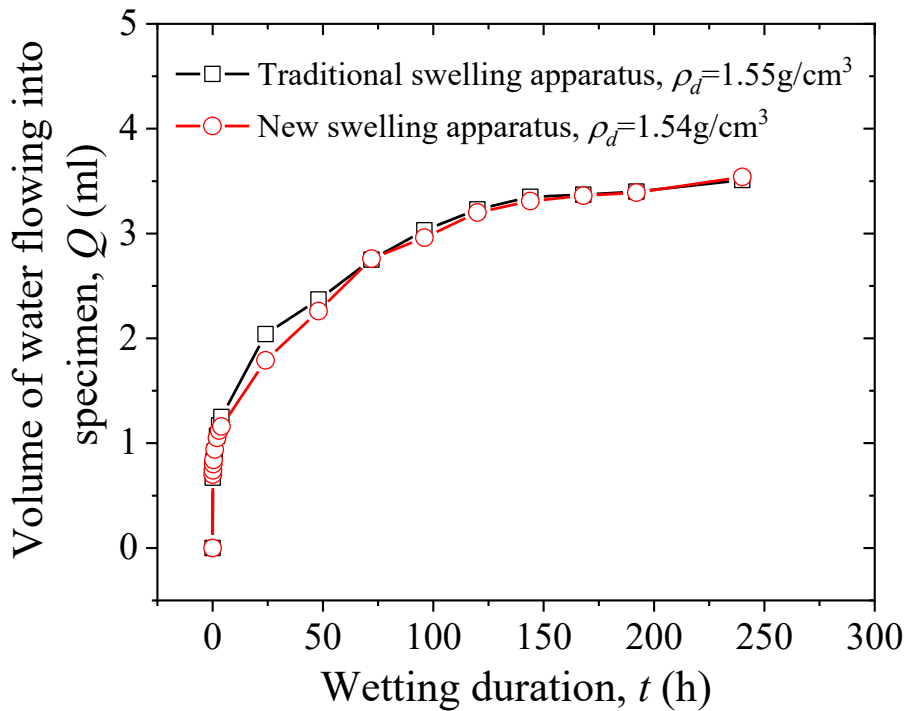


**Figure 3-3 Schematic diagram of specimen after swelling pressure test**

(3) Penetration issue. As described above, there is an only 0.3-mm gap for the testing liquid to flow into the specimen, it is reasonable to suspect whether the specimen can be supplied effectively. For checking whether the specimens were effectively saturated during wetting, another sets of infiltration tests by different swelling pressure apparatus were conducted. Figure 3-4 shows a traditional swelling pressure apparatus by applying a porous metal in the bottom of the specimen. The water volume flowing into the compacted bentonite with the change of wetting duration by traditional device as Fig. 3-4 and new swelling device as Fig. 3-2. In case of traditional swelling pressure apparatus, it is noted that the porous metal was pre-saturated before the infiltration test. It can be easily found from Fig. 3-5, the water volume flowing into the specimen at the similar dry density with two devices are somewhat close with each other, which may indicate that the specimen applied in the new swelling pressure device can be saturated effectively during hydration process.



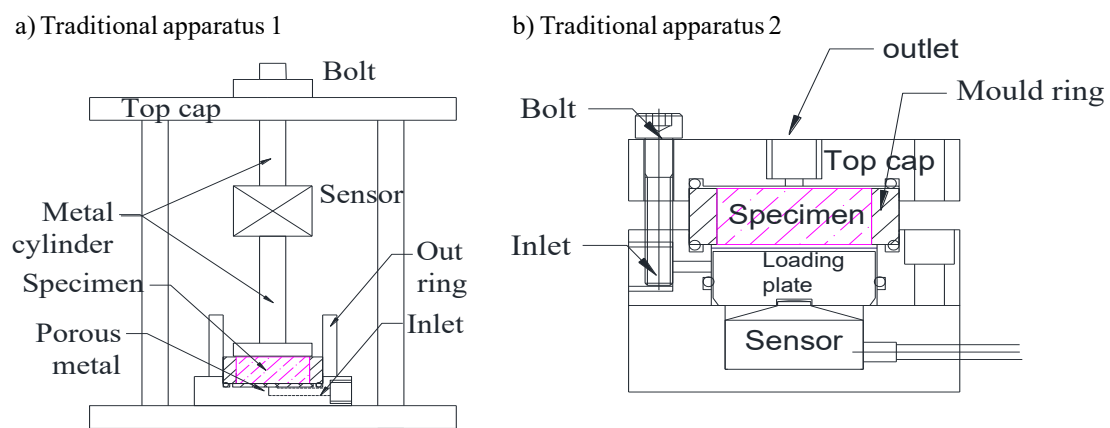
**Figure 3-4 Schematic diagram of swelling apparatus**



**Figure 3-5 Water flow histories conducted on new apparatus and traditional apparatus**

After that, it is necessary to check the repeatability of the newly designed swelling apparatus comparing to other swelling pressure apparatus. Figure 3-6 presents two

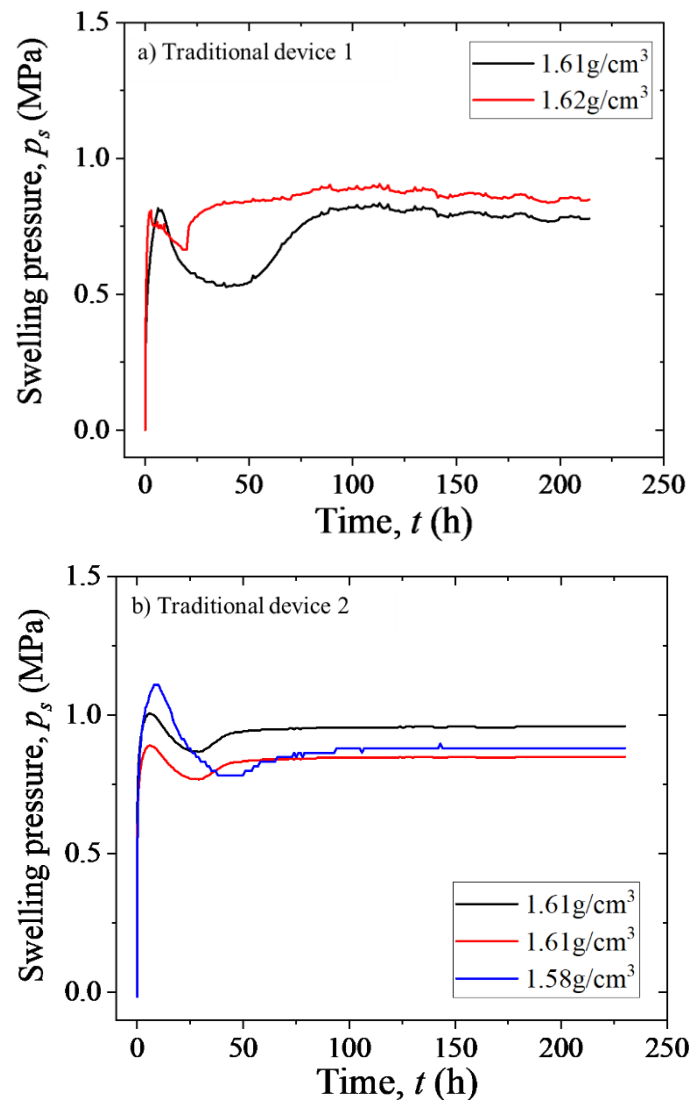
traditional swelling pressure apparatus from Komine Lab, Waseda university. These two devices are pretty different from the newly developed apparatus. For the traditional apparatus 1, the deformation of specimen was designed to be restricted by the bolt in the top cap. And, the sensor was installed between two metal cylinders. Regarding the traditional apparatus 2, the sensor was installed under the loading plate. However, there is no loading screw under the loading plate to ensure the initial touch of specimen and sensor.



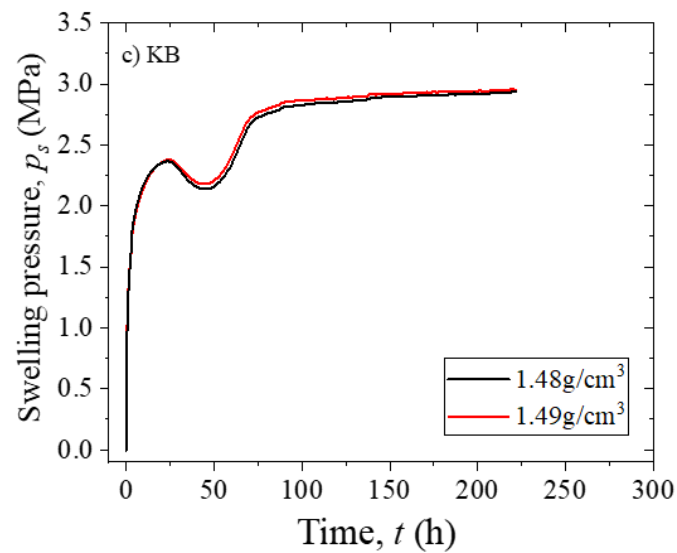
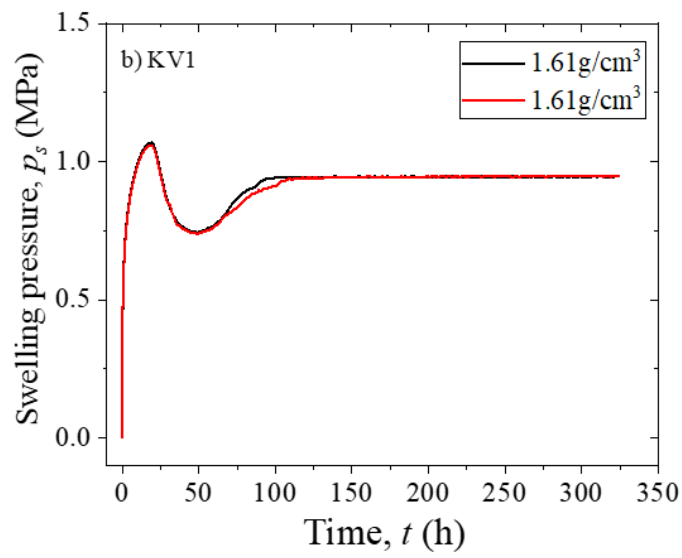
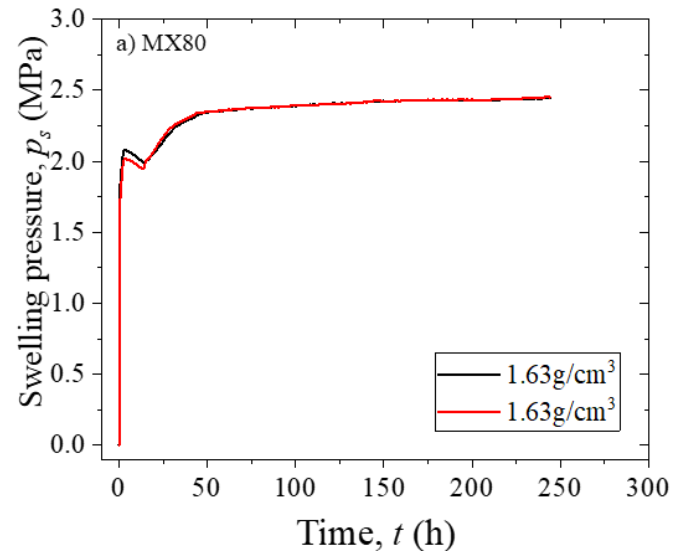
**Figure 3-6 Two traditional swelling pressure apparatuses**

Figure 3-7 reveals the swelling pressure evaluation curves of KV1 from two traditional swelling pressure apparatus when their dry densities are approximately  $1.6 \text{ g/cm}^3$ . It can be easily seen from Fig. 3-7 that, under the similar specimen dry density, neither the swelling pressure evolution curve and equilibrium swelling pressure have good repeatability. From Fig. 3-7 (a), for the traditional apparatus 1, the peak and valley points of swelling pressure evolution curves are pretty different. Meanwhile, the equilibrium swelling pressure have somewhat difference. Additionally, the swelling pressure evolution curves with traditional apparatus 2 are presented in Fig. 3-7 (b). Comparing to the traditional apparatus 1, the repeatability of swelling pressure evolution was greatly progressed. But, the equilibrium swelling pressure did not exhibit consistent results.

Figure 3-8 indicates some swelling pressure evolution curves of three bentonites used in the study by using the new swelling pressure apparatus. It can be easily concluded from Fig. 3-8, for all three bentonites (MX80, KV1 and KB), the swelling pressure evolution curves become very close when they have similar specimen initial conditions. Besides that, regarding equilibrium swelling pressures of these three bentonites. The equilibrium swelling pressures are very close when the dry densities are similar.



**Fig. 3-7 Swelling pressure evolution curve of KV1 bentonite by different traditional apparatus**



**Figure 3-8 Some swelling pressure evolution curves of bentonites by the new apparatus**

### 3.1.2 Multi-ring

In this study, for combining hydrological-mechanical tests with X-ray diffraction (XRD) test, a multi-ring was designed to apply in the swelling pressure apparatus, which is indicated in Fig. 3-9. By combining 5 approximately 2 mm mold rings (Fig. 3-10) and 4 approximately. 0.25 mm two-piece rings (Fig. 3-10), the multi-ring has the height of approximately. 11 mm and the inner diameter of 28 mm (Fig. 3-9).

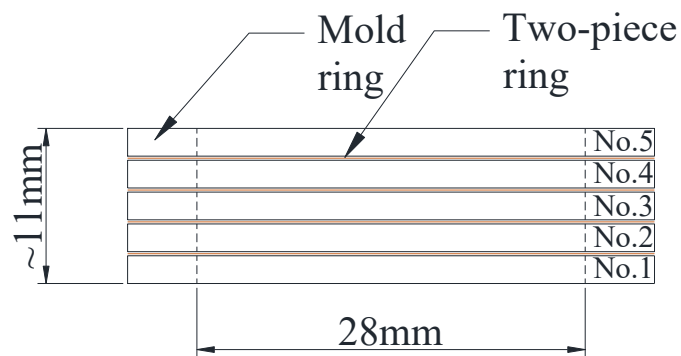


**Figure 3-9 Schematic of Multi-ring**

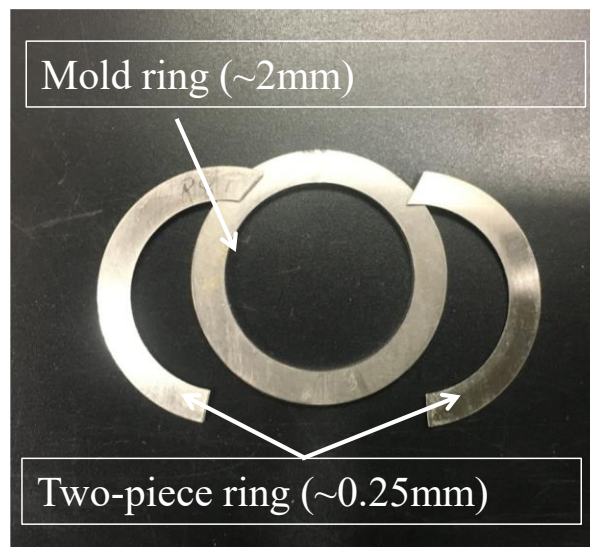


**Figure 3-10 Schematic of Mold ring and Two-piece ring**

### 3.2 Testing Methodology

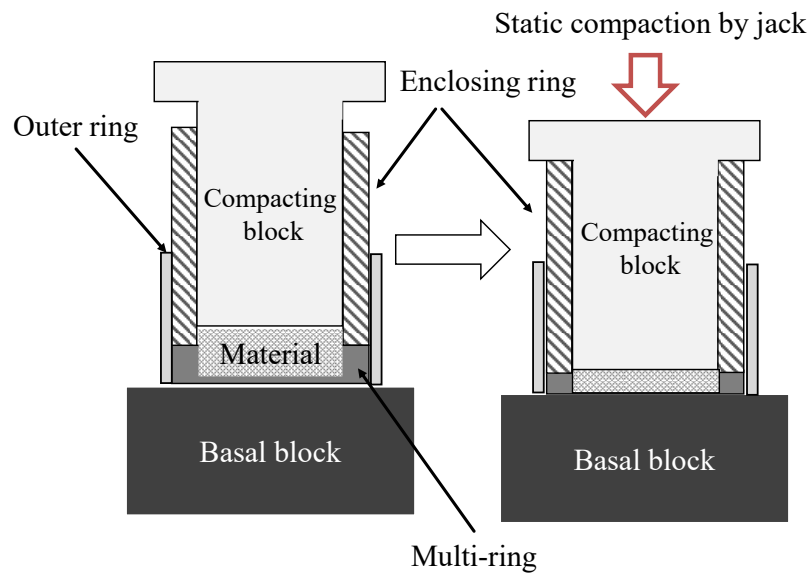


**Figure 3-11 Schematic of making compacted specimen**



**Figure 3-12 Static compression device**

Firstly, air dried powders were putted into the multi-ring (Fig. 3-11) and compressed in the static compaction device (Fig. 3-12). For each bentonite, several specimens were prepared for different wetting duration. After specimens were wetted for various

durations, multi-rings were taken out from swelling apparatus. Vertical deformation of the multi-ring was constrained by the clip immediately (Fig. 3-13). Later, two-piece rings were removed. The specimen was sliced carefully into five slices using a thin saw (0.20–0.25 mm thickness, Fig. 3-13). Then, each slice was sealed with Para film immediately. Slices were left in constrained condition (Fig. 3-13) at room temperature for at least 48 h to achieve a uniform water distribution inside the slice.

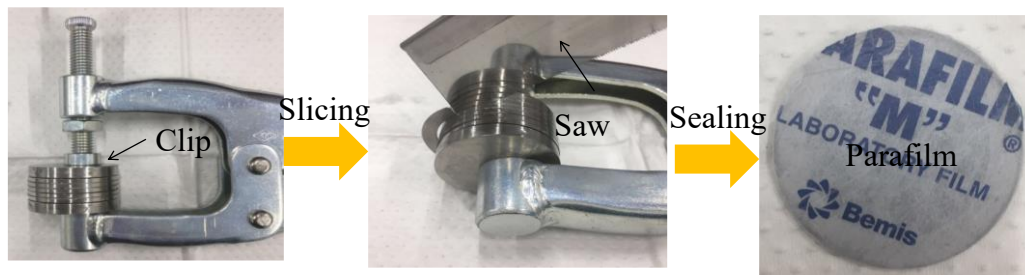


**Figure 3-13 Schematic for making slices from multi-ring**

Subsequently, slices were taken to XRD tests (Fig. 3-14). The XRD device is RINT-UltimaIII; Rigaku Corp., Japan (Fig. 3-15). The X-ray scan range was  $2.7^{\circ}$ - $10^{\circ}$  with scan speed of  $20^{\circ}/\text{min}$ . After swelling and XRD tests, the water content of each slice was measured.

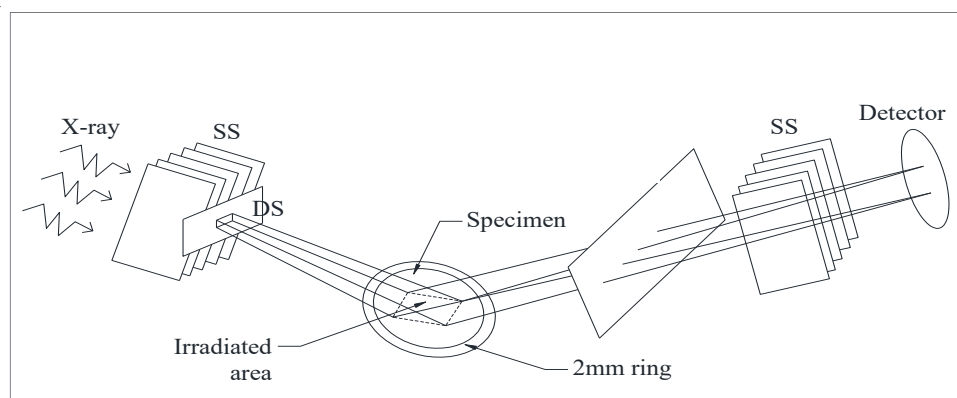


**Figure 3-14 Schematic for XRD test**



**Figure 3-15 XRD apparatus**

## Reference

ENRESA 2000. FEBEX project-full scale engineered barriers experiments for a deep geological repository for high level radioactive waste in crystalline host rock. Final report, Publicación técnica 1/2000, Empresa Nacional de Residuos Radiactivos SA (ENRESA), Madrid, Spain.

JNC 1999. Technical reliability of the geological disposal for high level radioactive waste in Japan geological disposal research and development. Second compiled General report. Japan Nuclear Cycle Development Institute, JNC TN1400 99-120. (in Japanese). <https://www.jaea.go.jp/04/tisou/houkokusyo/dai2jitoimatome.html>

Komine, H., and Ogata, N., 2004. Prediction swelling characteristics of bentonites. *Journal of Geotechnical and Geoenvironmental Engineering*, **130**(8): 818-829.

Maeda, M., Tanai, K., Ito, M., Mihara, M. and Tanaka, M. 1998. Mechanical properties of the Ca exchanged and Ca bentonite: swelling pressure, hydraulic conductivity, compressive strength and elastic modulus. Technical Report, Japan Nuclear Cycle Development Institute, PNC-TN8410 98-021 (in Japanese). <https://jopss.jaea.go.jp/pdfdata/PNC-TN8410-98-021.pdf>

Sun, D. A., Cui, H. B., and Sun, W. J., 2009. Swelling of compacted sand-bentonite mixture. *Applied Clay Science*, **43**: 485-492.

Suzuki, H., Shibata, M., Yamagata, J., Hirose, I. and Terakado, K 1992. Mechanical experiments of buffer material. Technical Report, Japan Nuclear Cycle Development Institute, PNC-TN8410 92-057 (in Japanese). <https://jopss.jaea.go.jp/pdfdata/PNC-TN8410-92-057.pdf>

Tanaka, Y., 2011. Numerical simulation on effects of test conditions on measured swelling pressure of compacted bentonite by swelling model. *Journal of JSCE (C)*, **67** (4): 513–531 (in Japanese). <https://doi.org/10.2208/jscejge.67.513>

Tanaka, Y., and Watanabe, Y., 2019. Modeling the effects of test conditions on the measured swelling pressure of compacted bentonite. *Soils and Foundations*, **59** (1): 136-150.

Tang, C. S., Tang, A. M., Cui, Y. J., Delage, P., Schroeder, C. and De Laure, E. 2011. Investigating the swelling pressure of compacted crushed-Callovo-Oxfordian claystone. *Physics and Chemistry of the Earth*, **36**: 1857-1866.

Villar, M. V., and Lloret, A., 2008. Influence of dry density and water content on the swelling of a compacted bentonite. *Applied Clay Science*, 39(1–2): 38–49.

Wang, H. L., Komine, H., and Gotoh, T., 2021. A swelling pressure cell for X-ray diffraction test. *Géotechnique*. Printed ahead online. <https://doi.org/10.1680/jgeot.20.00005>

Wang, H.L., Shirakawabe, T., and Ito, D. 2022. Apparatus design and measuring of apparent swelling pressure of compacted bentonite. Fifth International Conference on New Developments in Soil Mechanics and Geotechnical Engineering, Online, June 30-July 2, 2022.

# Chapter 4

**HYDRAULIC PROPERTIES AND SWELLING**

**PRESSURE OF BENTONITES WITH XRD**

## 4.1 Testing overview

In this chapter, MX80, KV1 and KB were used. For each bentonite, seven specimens were prepared for the wetting duration of 2-240 h. Specimen details are presented in Table 4-1. The swelling pressure apparatus used in chapter is shown as Fig.3-2. And the testing methodology was followed as interpreted in Chapter 3.

**Table 4-1 Specimen details**

Bentonite	Target dry density (g/cm <sup>3</sup> )	Initial water content (%)	Size (Height× Diameter)	Wetting duration (h)
MX80	1.6	8.92-8.99	~11mm×28mm	2, 4, 8, 24, 48, 120 and 240
KV1	1.6	8.27-8.46		
KB	1.3	13.63-14.02		

## 4.2 Results

### 4.2.1 Swelling pressure

Figure 4-1 presents the swelling pressure evolution curves for the bentonites: MX80, KV1, and KB. A curve with peaks and valleys were reported massively by scholars (Imbert and Villar 2006; Wang et al. 2020) for the swelling pressure changing with wetting duration. Additionally, this curve can be divided into 4 areas, as: 1) initial quick increase area, 2) drop area, 3) re-increase area, and 4) long-term stable area. As might be apparent from Fig. 4-1, swelling pressures increase quickly for all three bentonites during the first approx. 5 h. Swelling pressures subsequently dropped at approx. 20 h. Later, stable rising of swelling pressures occurred. Finally, swelling pressures remained at relative stable values for a long time. The swelling pressure developing patterns in this study are similar as Imbert and Villar (2006) and Wang et al. (2020).

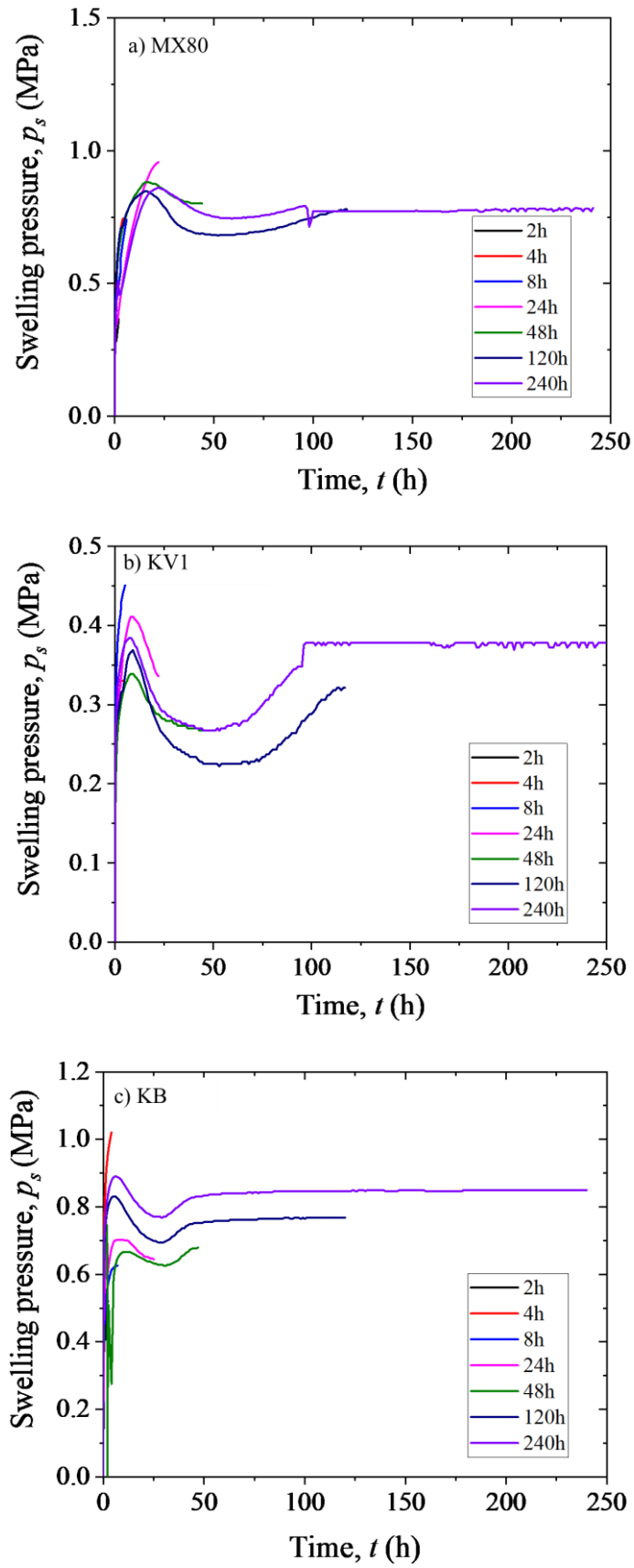
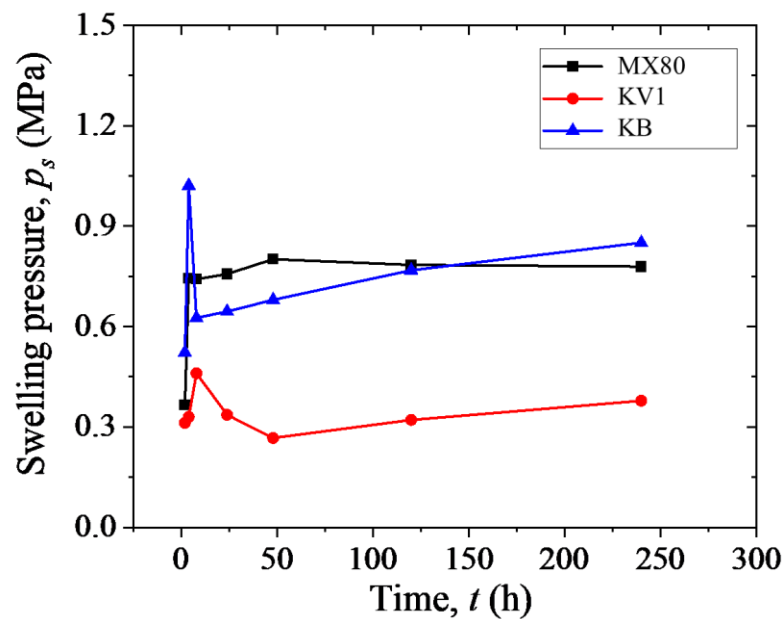


Figure 4-1 Swelling pressure evolution curves of bentonites

Swelling pressures of bentonites at different wetting durations is indicated in Fig. 4-2. Firstly, regarding MX80 and KV1 bentonites swelling pressure during saturation. MX80 and KV1 are both sodium bentonites. Meanwhile, the dry density of MX80 and KV1 are both  $1.6\text{g/cm}^3$ , respectively. As we can see from Fig. 4-2, swelling pressures during saturation of MX80 are bigger than KV1. Table 2-3 presents the montmorillonite contents of MX80 and KV1. The montmorillonite content of MX80 (61%) is greater than KV1 (50%). A ready conclusion might be made herein that, for the same cation type bentonite at same dry density, larger montmorillonite content has bigger swelling pressure along with the saturation. However, there is still no clear trend can be found from Fig-4-2 for the effect of bentonite cation type on swelling pressures during saturation. Because the dry density of KB adopted in this study is much lower than MX80 and KV1.



**Figure 4-2 Swelling pressures of bentonites at different wetting durations**

#### 4.2.2 Hydraulic properties

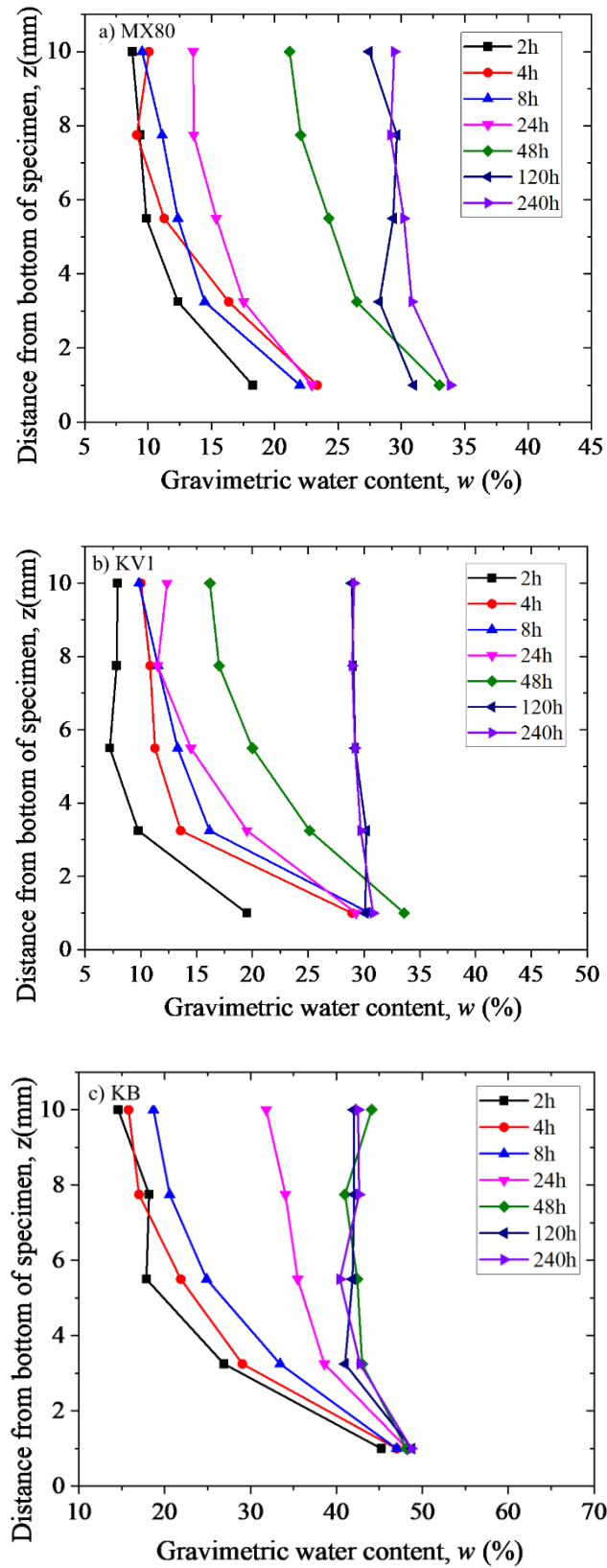


**Figure 4-3 Gravimetric water content of slice changing with distance from bottom of bentonites**

Gravimetric water contents in slices after water absorption are presented in Fig. 4-3. It is a general truth from Fig. 4-3, gravimetric water content generally decreases as increasing distance from bottom of specimen and increases with the rising wetting duration, when the wetting duration shorter than 120h. After 120h, gravimetric water contents stay in relative stable values. Bruce and Klute (1956) and Corey (2003) related water diffusivity ( $D$ ) of soil with volumetric water content ( $\theta$ ) and hydraulic conductivity ( $k$ ) by Darcy equation as:

$$\frac{\partial \theta}{\partial t} = \frac{\partial}{\partial z} \left( D(\theta) \frac{\partial \theta}{\partial z} \right) + \frac{\partial k}{\partial z} \quad (4-1)$$

When analyzing the results, the influence of gravity ( $\partial k / \partial z$ ) on water flow was often ignored. Therefore, equation (4-1) can be expressed as:

$$\frac{\partial \theta}{\partial t} = \frac{\partial}{\partial z} \left( D(\theta) \frac{\partial \theta}{\partial z} \right) \quad (4-2)$$

Klute and Dirksen (1986) brought a parameter  $\chi$  ( $=z/\sqrt{t}$ ) into equation (4-2), and used Boltzmann transformation changed that partial differential equation into an ordinary equation as:

$$D(\theta) = -\frac{1}{2} \left( \frac{d\chi(\theta)}{d\theta} \right) \int_{\theta_0}^{\theta_s} \chi(\theta) d\theta \quad (4-3)$$

where  $\theta_0$  signifies the initial volumetric water content, %. In this study, specimens were cut into slices of equal height to obtain water diffusivity. Clothier et al. (1983) and Wang et al. (2020) tried to use mathematical methods to fit the relation between  $\chi$  and  $\theta$ . As Wang et al. (2020) reported, the relation between  $\chi$  and  $\theta$  can be given as:

$$\chi(\theta) = A - B \ln(\theta - C) \quad (4-4)$$

where A, B and C are fitting parameters with testing data. Besides that, by bringing equation (4-4) into equation (4-3), an easy equation for the calculation of water diffusivity can be proposed:

$$D(\theta) = \frac{AB}{2} - \frac{B^2}{2} (\ln(\theta - C) - 1) \quad (4-5)$$

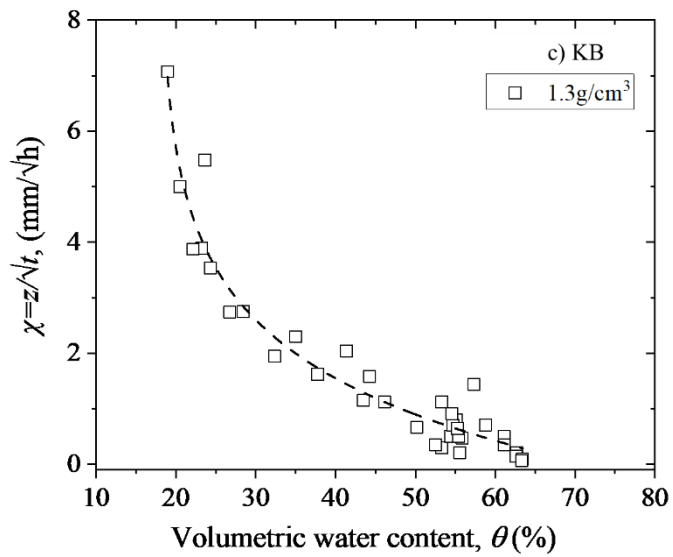
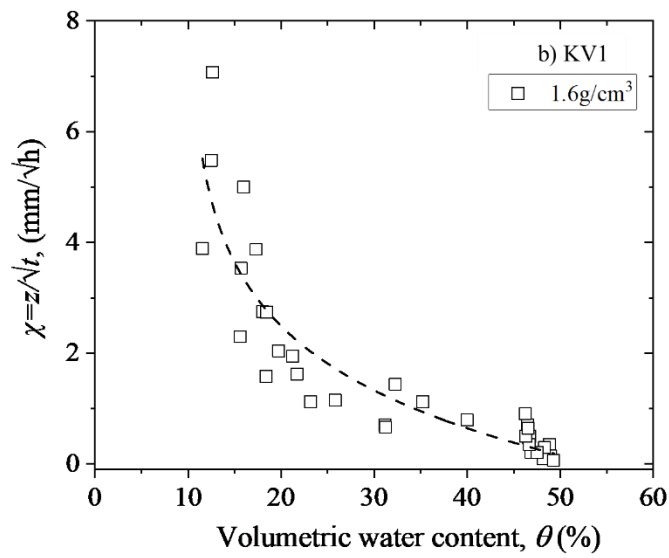
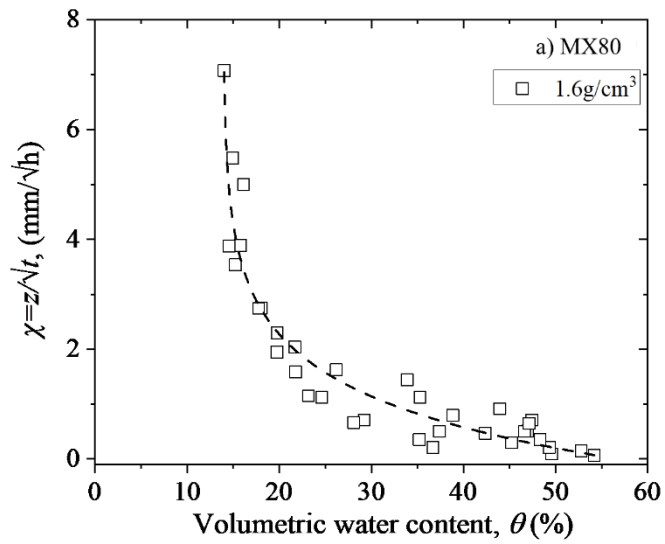
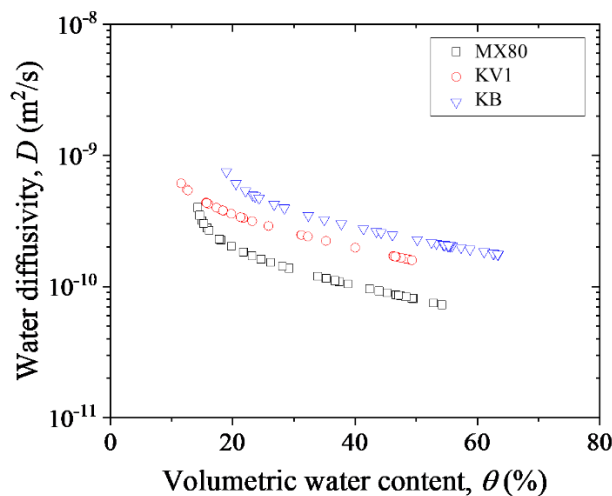


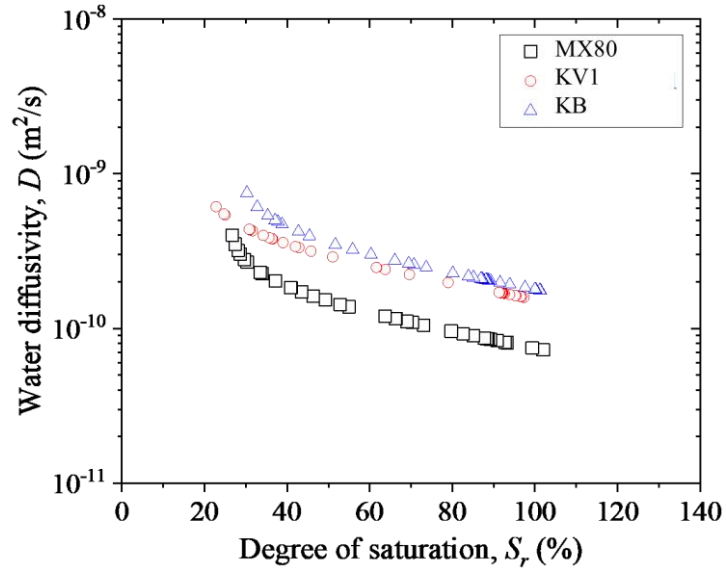
Figure 4-4 Relation between  $\theta$  and  $\chi$  of bentonites

Figure 4-4 presents the relation between  $\theta$  and  $\chi$  for MX80, KV1 and KB, respectively. It can be seen from Fig. 4-4, experimental database generally follows equation (4-4). Therefore, the determination for water diffusivity in this study can be calculated by using equation (4-5). Figure 4-5 depicts water diffusivity changing with the volumetric water content. It is apparent from 4-5, water diffusivity decreases with the increase of volumetric water content. Water diffusivity changing with the degree of saturation is revealed in Fig 4-6. As we can found from Fig. 4-6 that, water diffusivity reduces consistently with increasing degree of saturation. In Fig. 4-6, it can be observed that degrees of saturation of bentonites all over 100%, which was also revealed in Wang et al. (2020). This phenomenon may because of the fact that the water density in compacted bentonite  $> 1\text{g/cm}^3$  (Wang et al. 2020), which may result from the higher density for the water in inter-layer pores of bentonite.

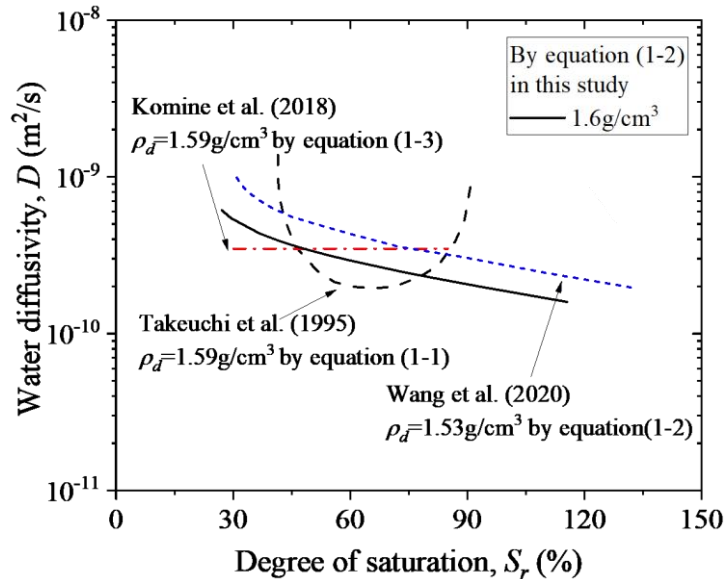
A U shape curve for the relation between water diffusivity and degree of saturation was reported by Takeuchi et al. (1995) by using the equation (1-1). And, a linear relation was informed by Komine et al. (2018). A continuous decreasing curve was reported by this chapter and Wang et al. (2020).



**Figure 4-5 Water diffusivity changing with volumetric water content of bentonites**



**Figure 4-6 Water diffusivity changing with degree of saturation for bentonites**



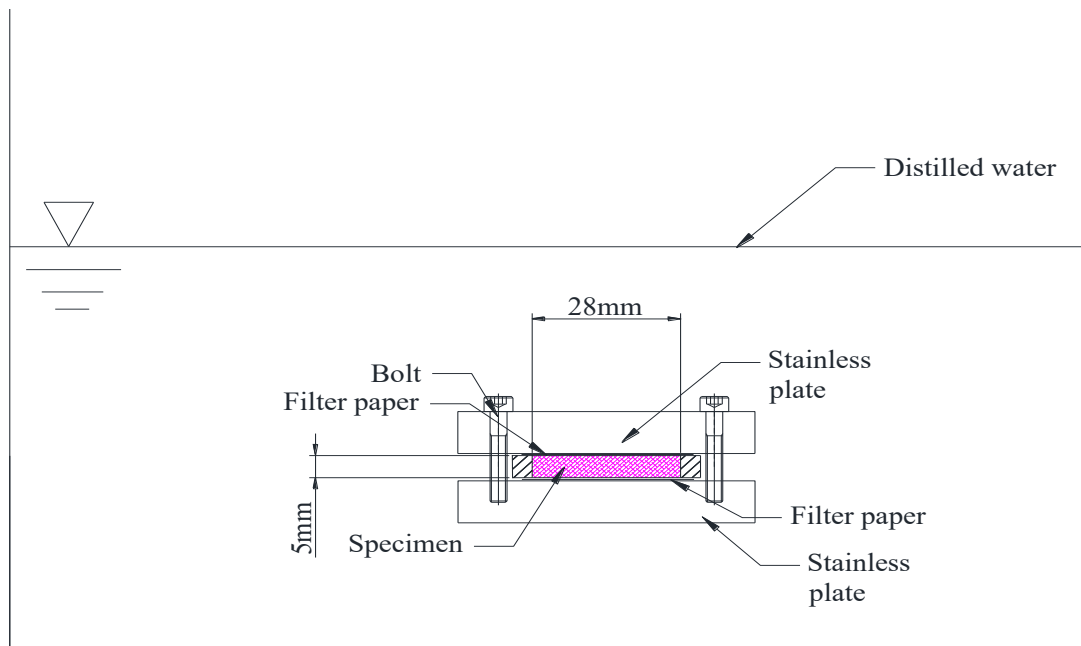
**Figure 4-7 Water diffusivity changing with degree of saturation for KV1 from literatures and this study**

Figure 4-7 shows the water diffusivity results of KV1 for dry density at approximate  $1.6\text{g/cm}^3$  from Takeuchi et al. (1995), Komine et al. (2018), Wang et al. (2020) and this study. As we can see from Fig. 4-7, even though different curves shape were obtained by different calculating equations, the differences between different equation are somewhat small.

Additionally, the relation between water diffusivity and hydraulic conductivity can be given as (Corey 2003; Lu and Likos 2004):

$$k(\theta) = D(\theta) \left( \frac{\partial(\theta)}{\partial(\psi)} \right) \quad (4-6)$$

where  $\partial(\psi)/\partial(\theta)$  can be obtainable from SWRC (Soil water retention curve). For obtaining the SWRC of bentonite, a set of simple wetting tests were carried out as Fig. 4-8. Herein, air dried bentonites were compressed into a 5mm-height and 28mm-diameter ring. Then, the vertical deformation of ring and specimen was restricted by two stainless plates, whose deformation was constricted by the bolts. After that, this wetting system was immersed into the distilled directly. The wetting system was taken out from the distilled water after different wetting durations. The ring and specimen were sealed by the para film and cured for at least 5 days for achieving the uniformly water distribution in the specimen. Hereafter, the specimens were sent to the suction detection by using WP4C dew-point potentiometer. Finally, the water content of specimen was measured.



**Figure 4-8 Schematic for showing the SWRC test**

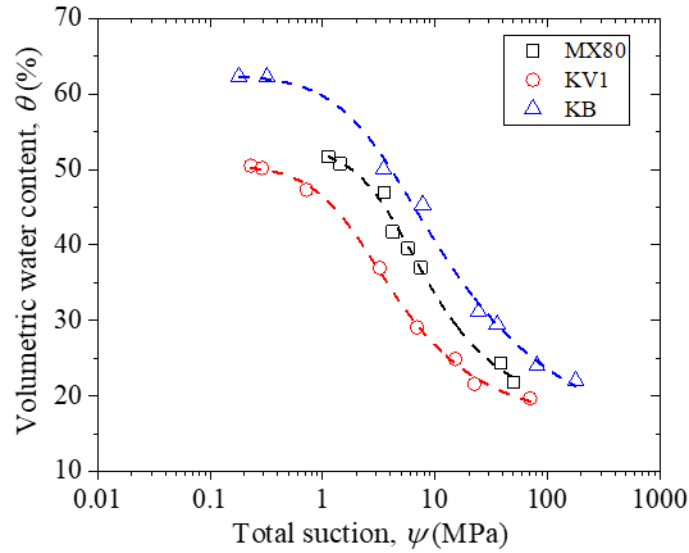


**Figure 4-9 Total suction changing with volumetric water content and their fitting by VG equation**

**Table 4-2 Fitting parameters values of SWRCs by Van Genuchten model**

Bentonite	MX-80	Kunigel-V1	Kunibon
$\rho_d$ (g/cm <sup>3</sup> )	1.6	1.6	1.3
$\alpha$	0.25	0.56	0.34
$n$	1.81	1.69	1.44
$\theta_s$	53.14	50.63	62.60
$\theta_r$	17.88	16.57	13.39

The SWRC of these three bentonites is presented in Fig. 4-9. Different equations were proposed for fitting and predicting the SWRC of soil. In this study, Van Genuchten (VG) (Van Genuchten 1980) equation was adopted. The relation between the volumetric water content and total suction from Van Genuchten 1980 can be expressed as:

$$\theta = \theta_r + \frac{\theta_s - \theta_r}{[1 + (\alpha\psi)^n]^{1 - \frac{1}{n}}} \quad (4-7)$$

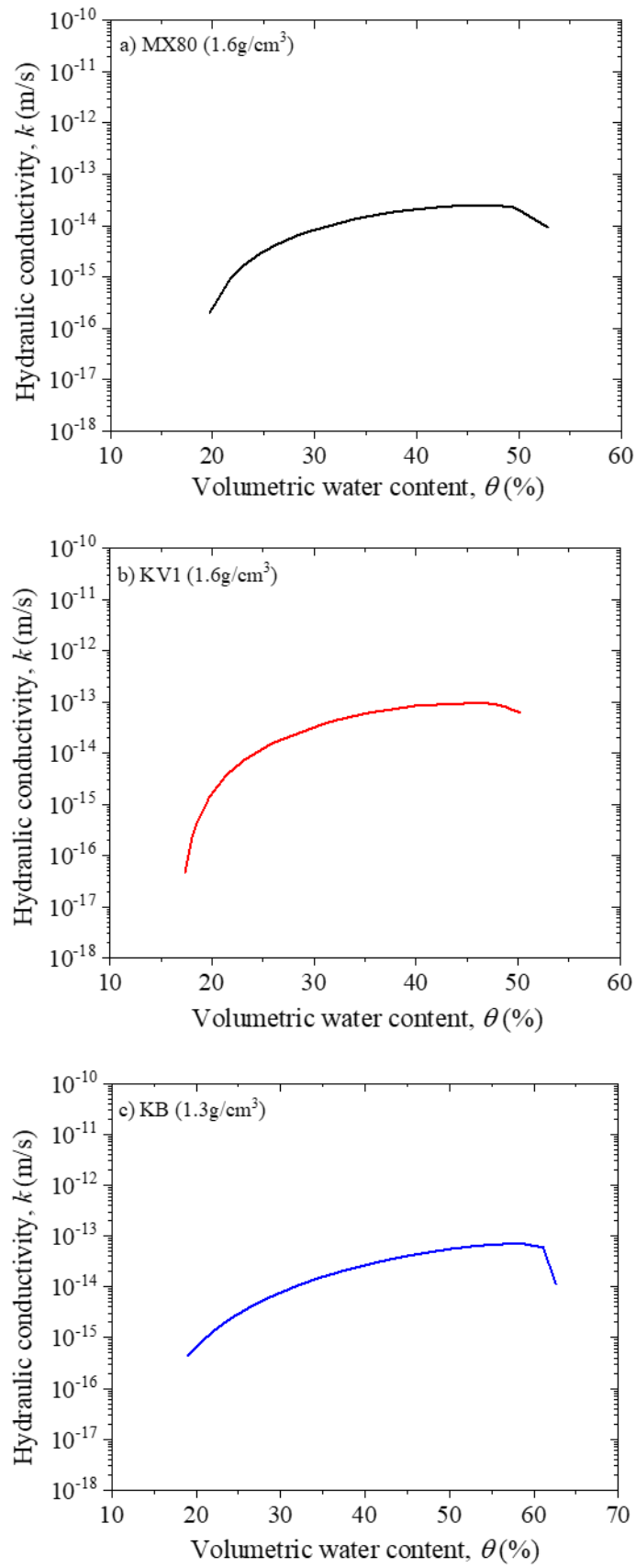


**Figure 4-10 Hydraulic conductivity changing with volumetric water content**

where  $\alpha$  and  $n$  are fitting parameters with testing database;  $\theta_s$  is volumetric water content of saturated specimen, %;  $\theta_r$  is residual volumetric water content, %. The fitting lines by VG equation are also presented as dash lines in Fig. 4-9. It is apparent from Fig. 4-9, the results in this study can be fitted by VG equation well. The fitting parameters and their values are presented in Table 4-2. By combining Fig. (4-5), Eq. (4-6) and Table 4-2, hydraulic conductivities during saturation can be achieved. Figure 4-10 shows hydraulic conductivity changing with volumetric water content of bentonites. It is apparently from Fig. 4-10 that, hydraulic conductivity exhibits a “ $\Omega$ ” shape with the change of volumetric water content. A “ $\Omega$ ” shape was also reported by Takeuchi et al. (1995) for  $k - \theta$  curve of KV1 bentonite.

#### 4.2.3 XRD results

Figure 4-11 and 4-12 and 4-13 show XRD profiles of slices in vertical direction at some wetting durations. It is noteworthy that the Y axis in Fig. 4-11, 4-12 and 4-13 are an arbitrary scale, not a specific scale. It can be easily found from Fig. 4-11, 4-12 and 4-13, for all three bentonites, water content generally decreases when slice changes from No. 1-No. 5, when  $t=4h$  and  $24h$ . And when  $t=240h$ , water contents are in relative stable values. Besides that, from Fig. 4-11, 4-12 and 4-13, one can readily inferred is the peaks exist in the XRD profiles. As we can see from Fig. 4-11, 4-12 and 4-13, for all three bentonites, when  $t=4h$  and  $24h$ , the peaks slowly move to the right when slice changes from No. 1-No. 5. When  $t=240h$ , peaks seem to occur in similar diffraction angles.

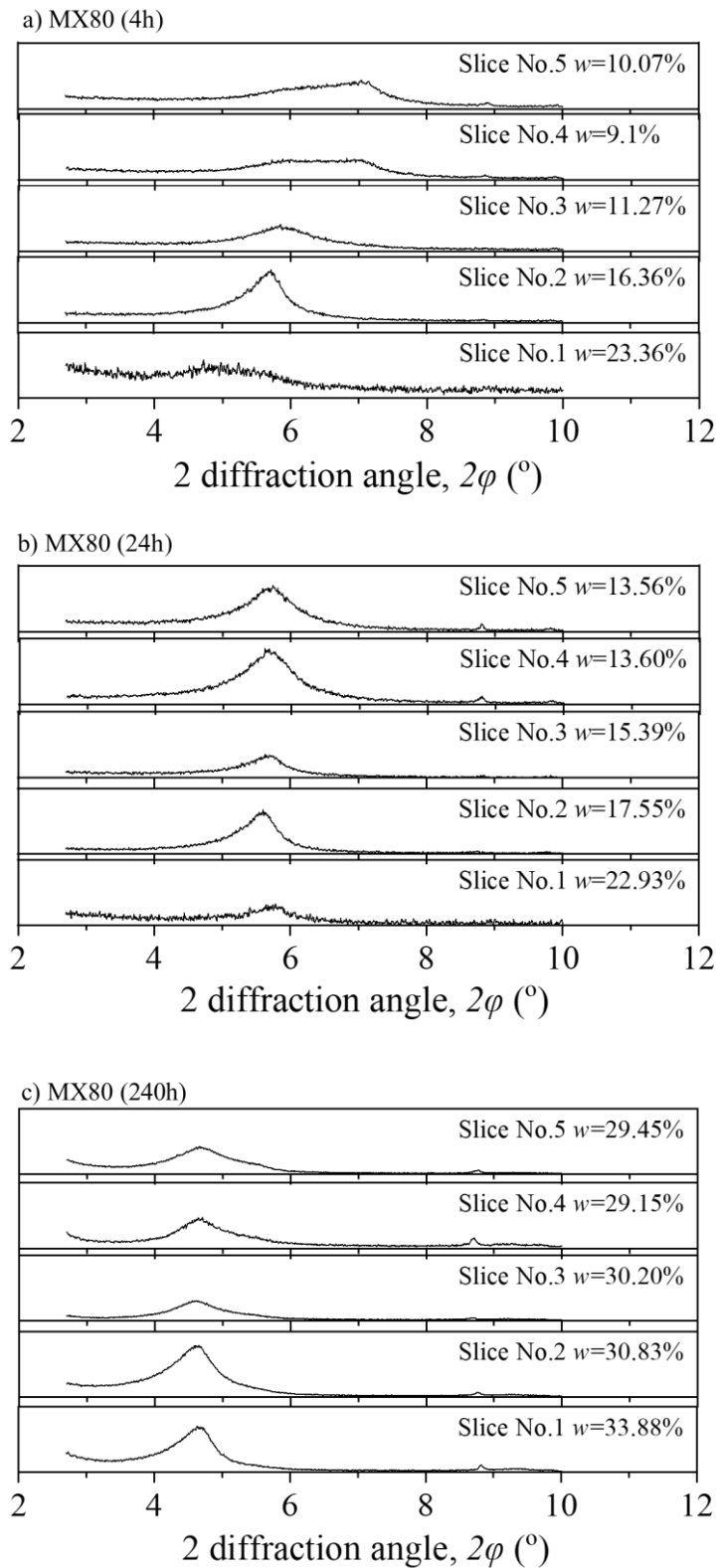


**Figure 4-11 XRD profiles of slices in vertical direction for MX80**

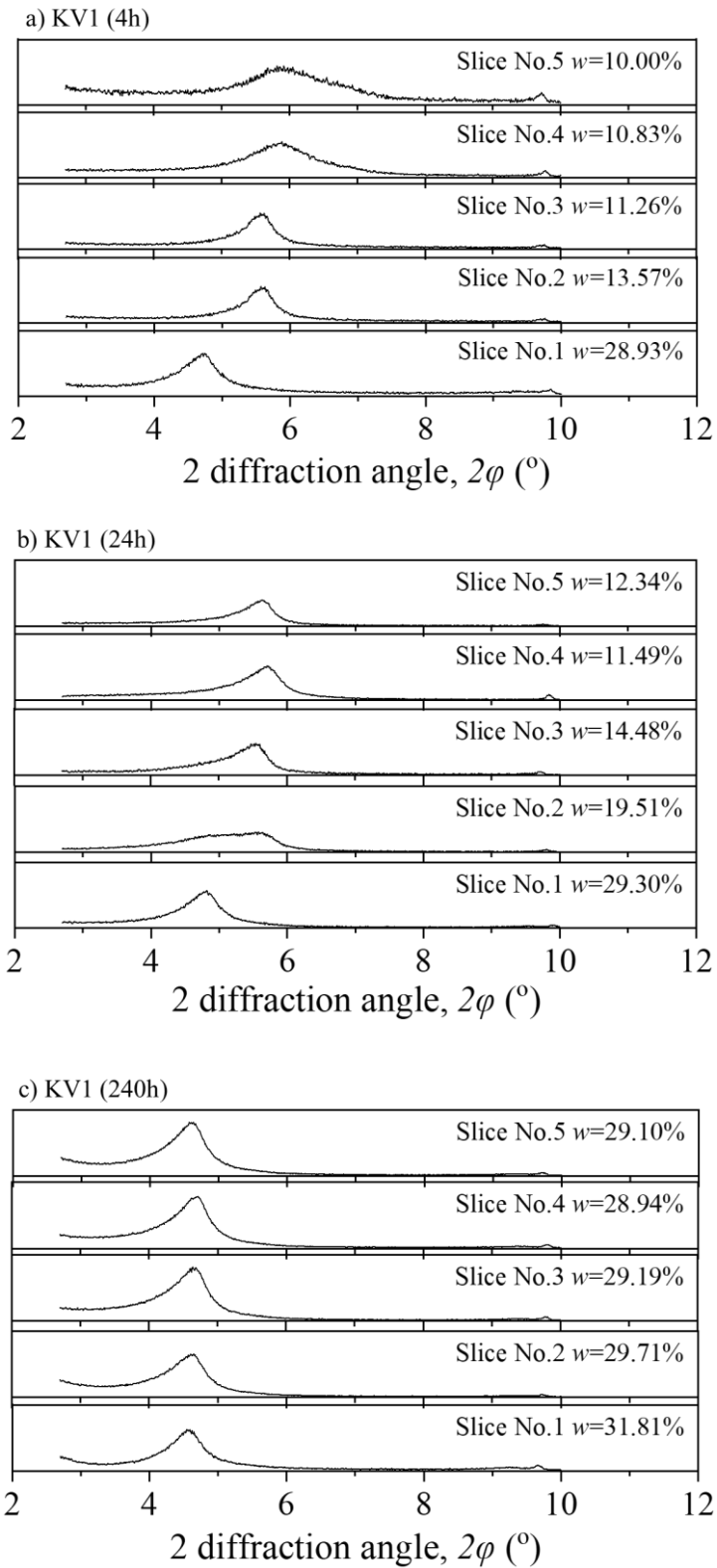


**Figure 4-12 XRD profiles of slices in vertical direction for KV1**

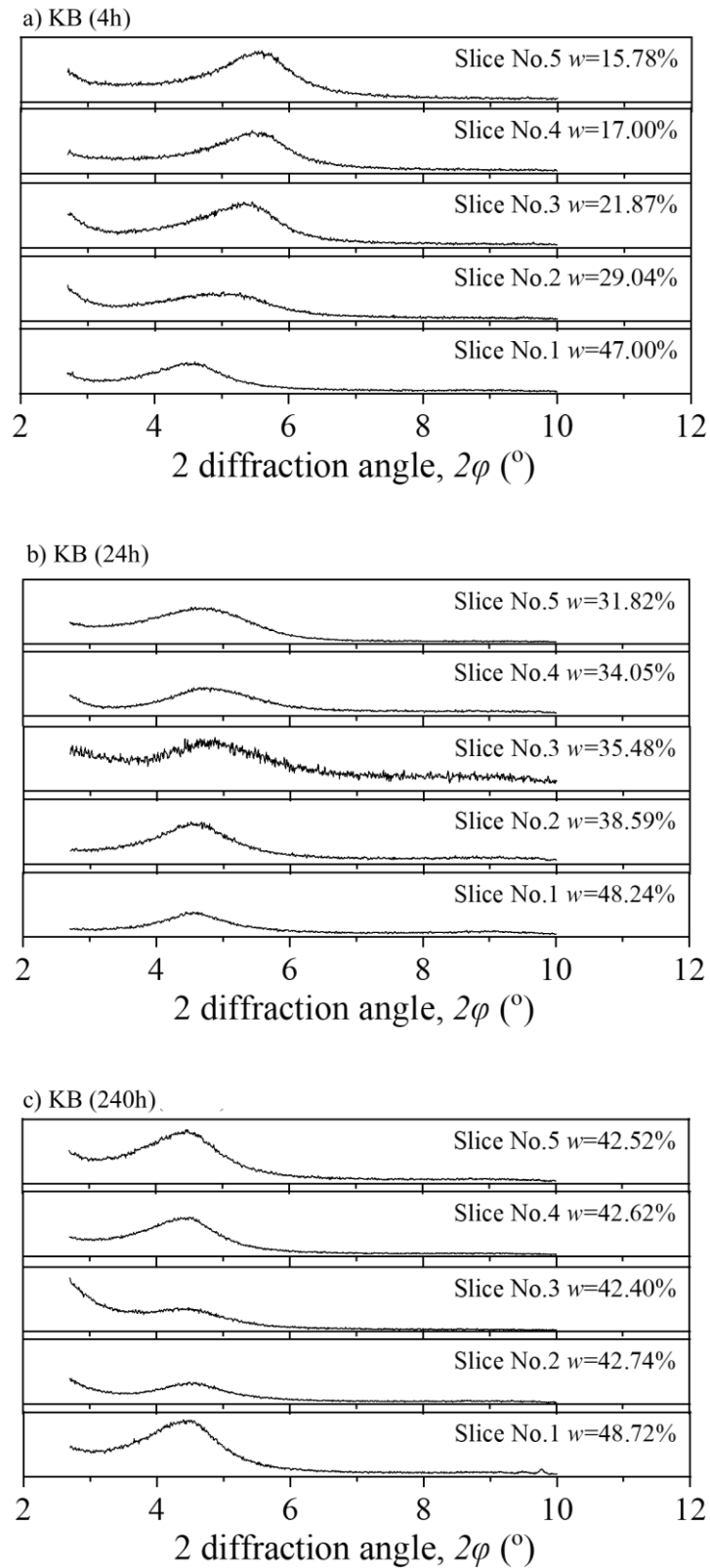
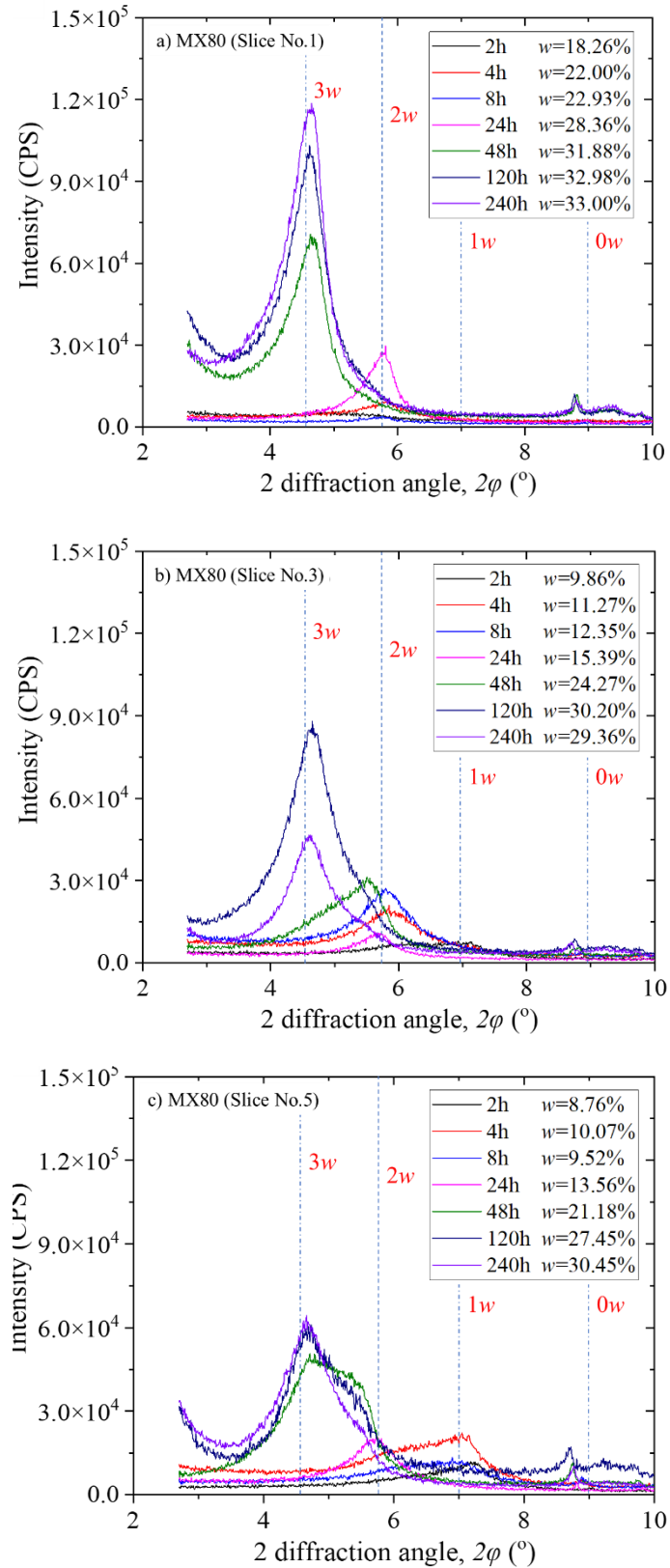


Figure 4-13 XRD profiles of slices in vertical direction for KB



**Figure 4-14 XRD profiles and *L* state of slices changing with wetting duration for**

**MX80**

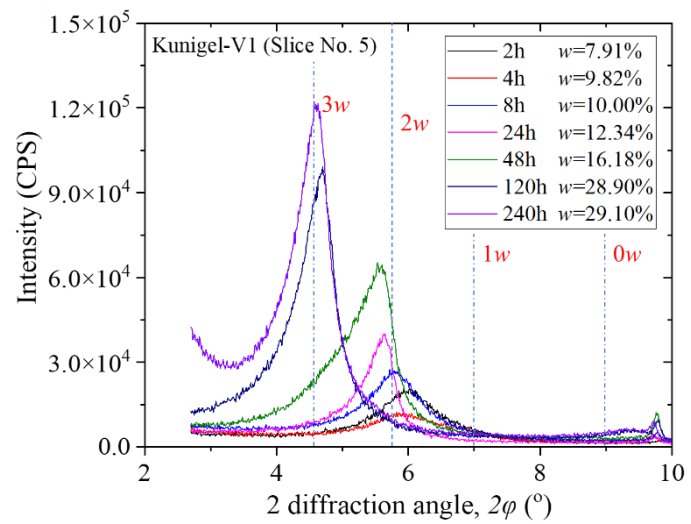
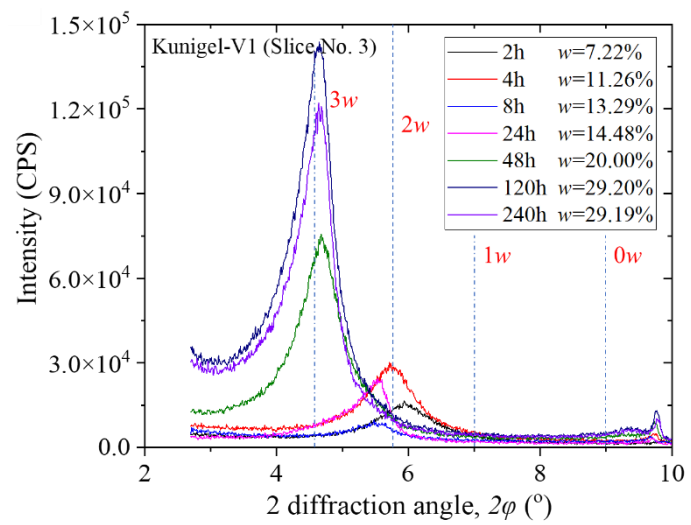
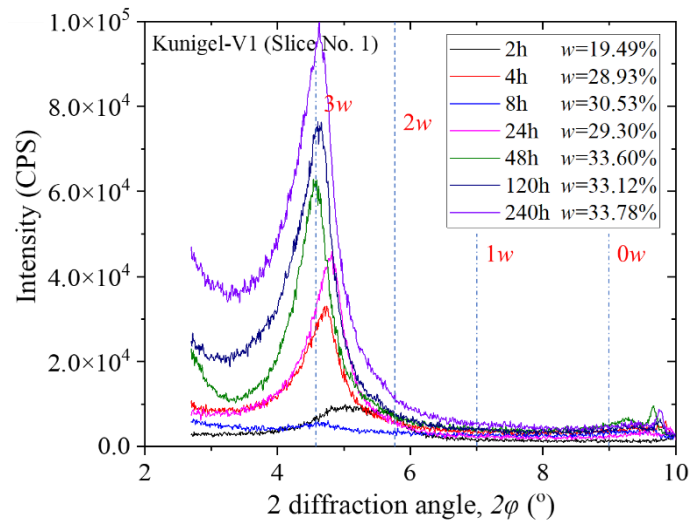


Figure 4-15 XRD profiles and *L* state of slices changing with wetting duration for

KV1

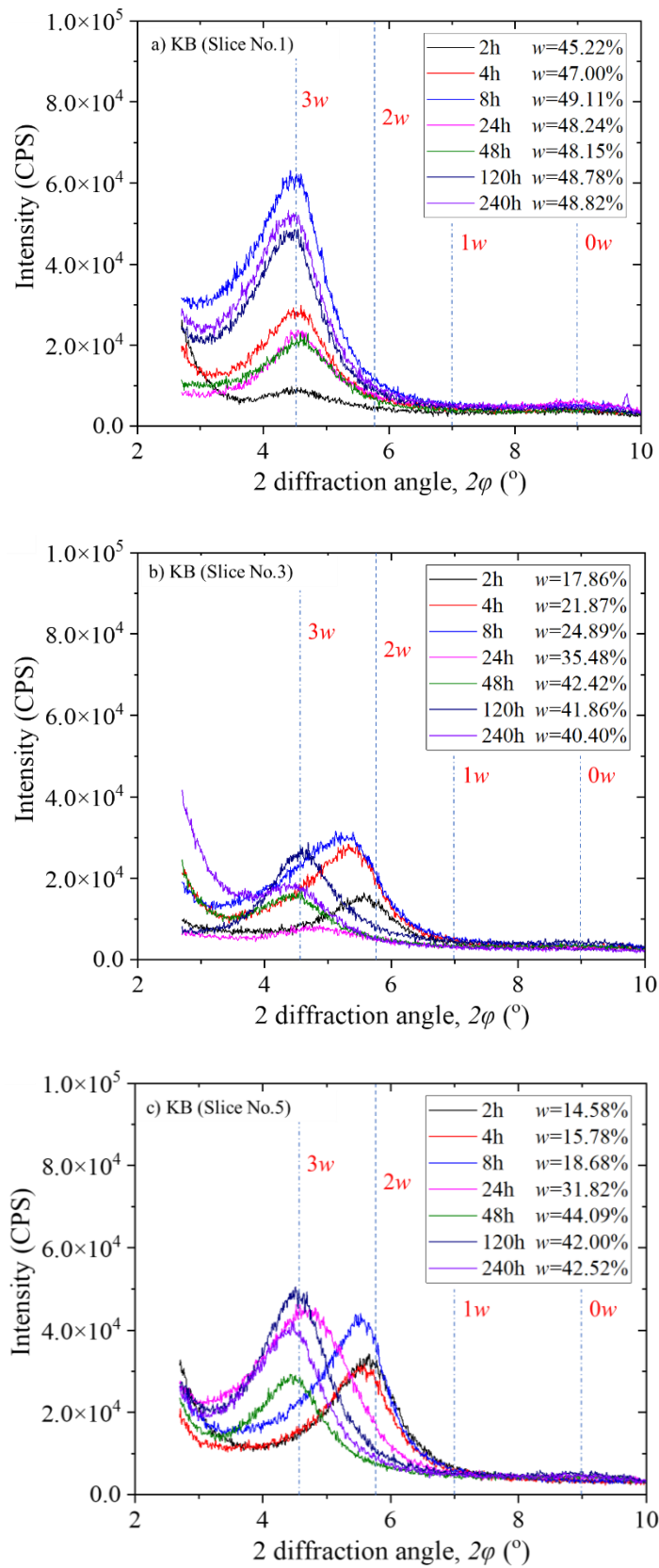


Figure 4-16 XRD profiles and L state of slices changing with wetting duration for

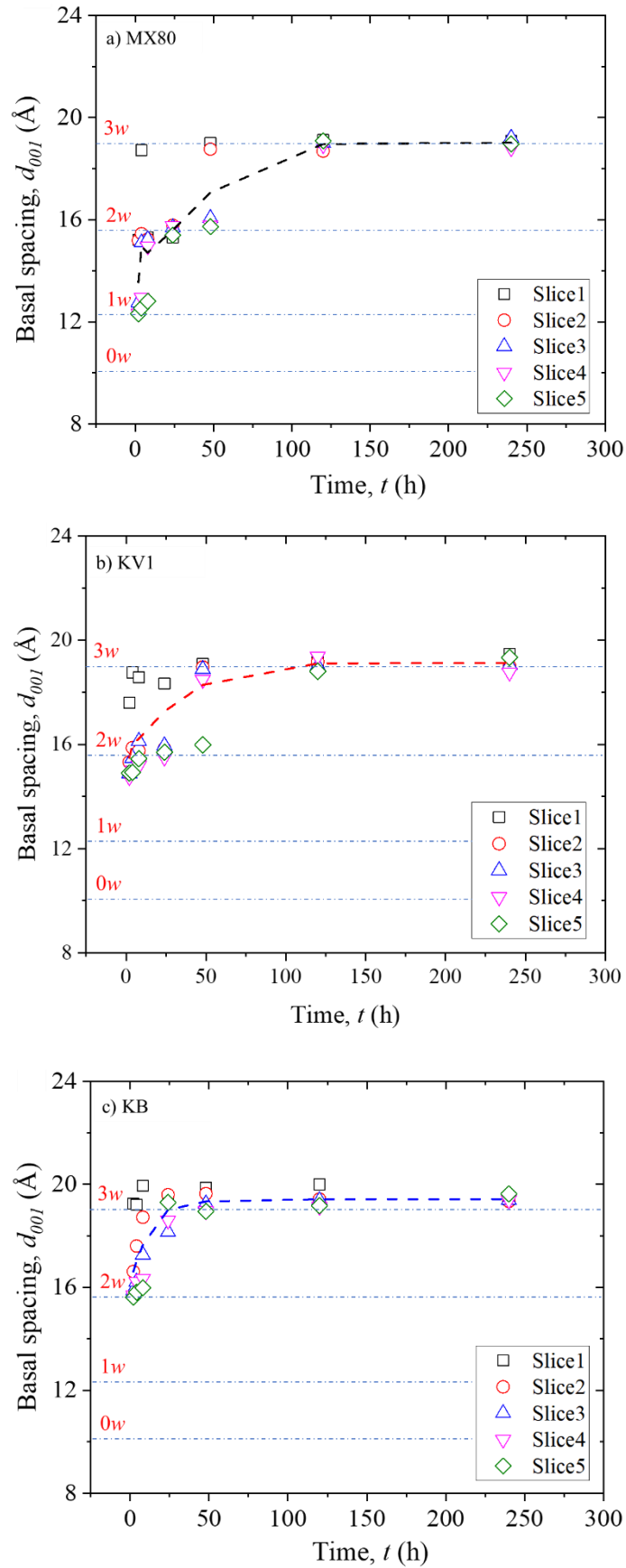
KB

Figure 4-14, 4-15 and 4-16 depicts XRD profiles of some slices changing with wetting duration. Unlike Fig. 4-11, 4-12 and 4-13, Y axis in Fig. 4-14, 4-15 and 4-16 is a specific scale. As indicated in Fig. 4-14, 4-15 and 4-16, water contents of slices generally increase as wetting duration rises.

Regarding the peak position, from Fig. 4-14, 4-15 and 4-16, peaks happen when  $2\varphi$  = approx.  $4-8^\circ$ . A generally trend from Fig. 4-14, 4-15 and 4-16 can be concluded that, peak moves from approx.  $8^\circ$  to approx.  $4^\circ$  as wetting duration rises.

Another phenomenon can be found from Fig. 4-14, 4-15 and 4-16 that, intensity of XRD profile seems grow as increasing wetting duration, which means that intensity of XRD profile might increase as the increase of water content.

Another important ingredient can be observed from Fig. 4-14, 4-15 and 4-16 is the state of water molecule arrangement in inter-layer space ( $L$ ). As Wang et al. (2020) reported,  $d_{001}=10.1 \text{ \AA}$ ,  $12.5 \text{ \AA}$ ,  $15.5 \text{ \AA}$  and  $19.0 \text{ \AA}$  are viewed as the dividing values for  $L=0w$ ,  $1w$ ,  $2w$  and  $3w$ , respectively. Meanwhile, from Wang et al. (2021), the dividing values for  $2\varphi_{\text{peak}}$  of different  $L$  states are  $2\varphi_{\text{peak}}= 9^\circ$  ( $0w$ ),  $2\varphi_{\text{peak}}= 7^\circ$  ( $1w$ ),  $2\varphi_{\text{peak}}= 5.6^\circ$  ( $2w$ ) and  $2\varphi_{\text{peak}}= 4.7^\circ$  ( $3w$ ), respectively. As we can see from Fig. 4-14, 4-15 and 4-16,  $L$  states slowly move to  $3w$  as wetting duration increases.



**Figure 4-17 Basal spacings of bentonites changing with saturation time**

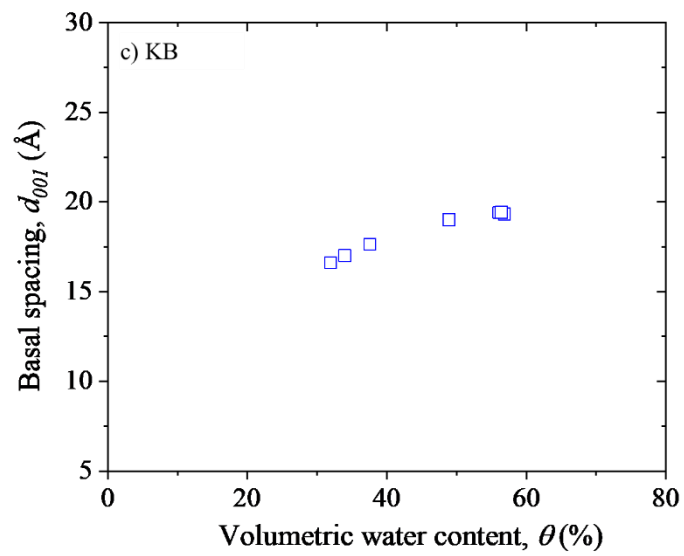
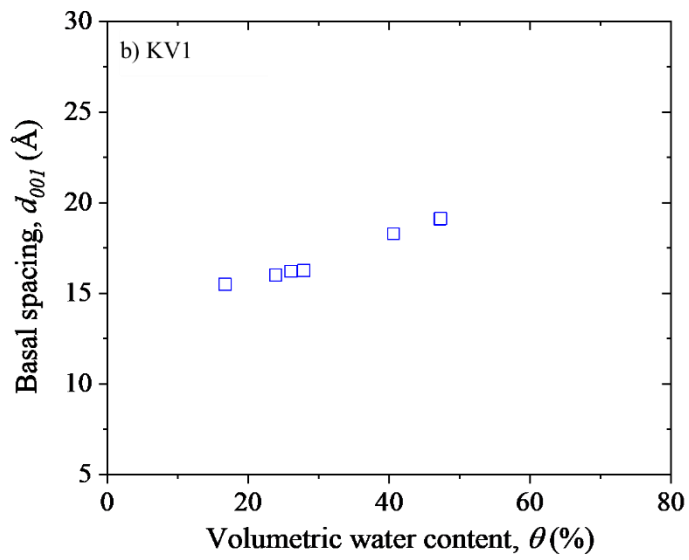
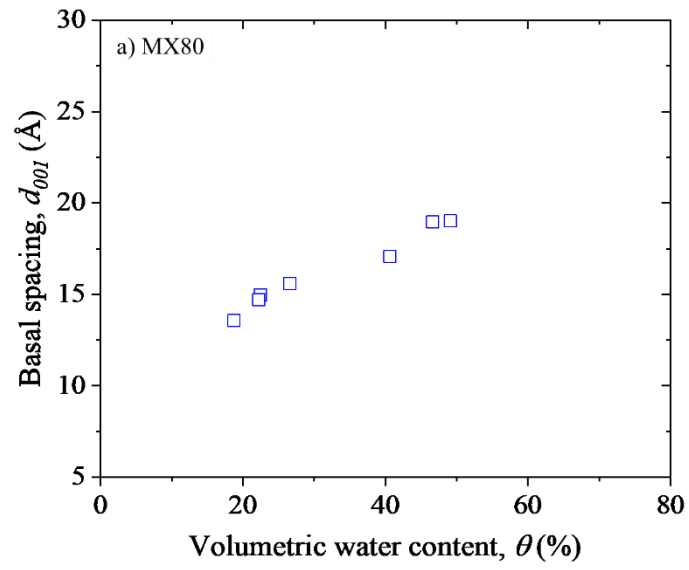


**Figure 4-18 Basal spacing changing with volumetric water content**

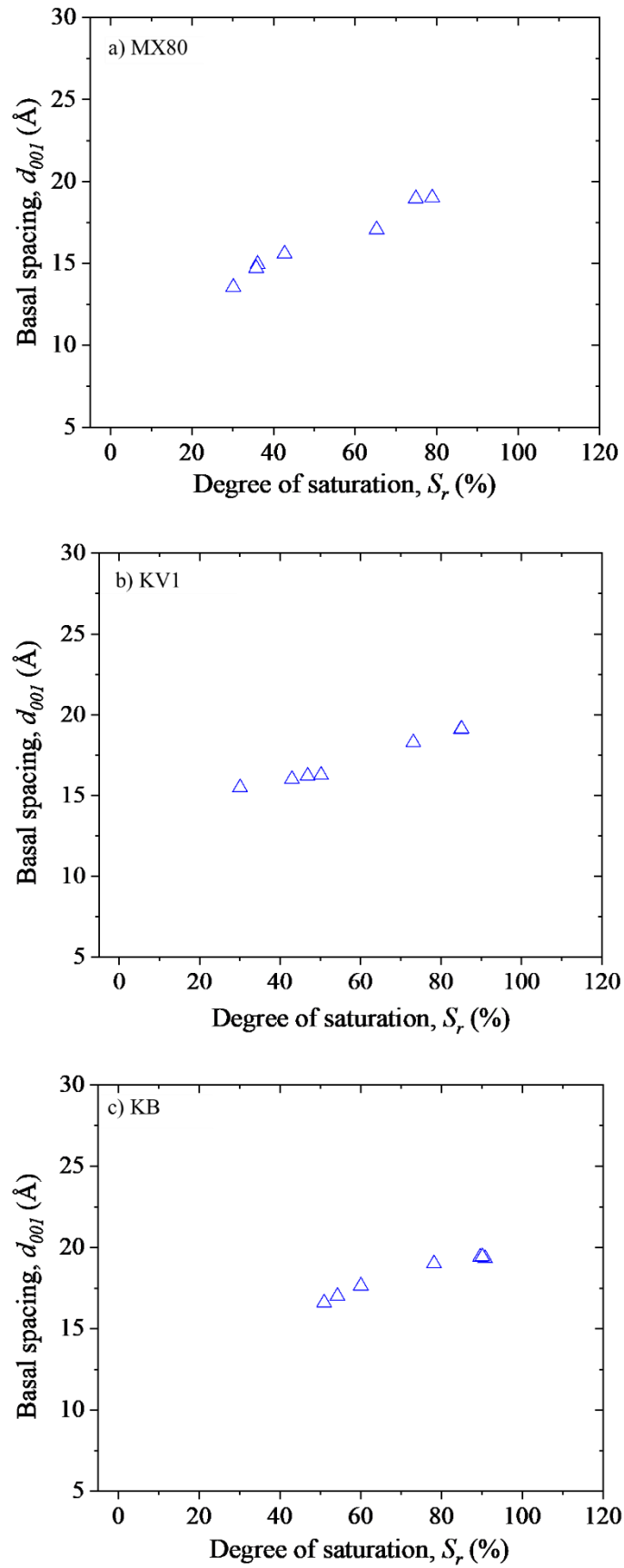


**Figure 4-19 Basal spacing changing with degree of saturation**

Figure 4-17 reveals the basal spacing of each slice for bentonites used in study. By connecting average values of five slices with the same saturation periods by dash lines in figure, the overall trend of specimens with the same dry density is indicated. It can be readily inferred from Fig. 4-17 that, for three bentonites in this study, basal spacings increase dramatically at the beginning of the wetting period. Then, basal spacings enter into stable state. Times for different bentonites to reach stable values are various: approx. 120 h for MX80, approx. 120 h for KV1, and approx. 50 h for KB. Figure 4-17 also reveals state of water molecule arrangement in inter-layer space ( $L$ ) for different bentonites during saturation. Following definition of the water molecule arrangement in inter-layer space indicated in Fig. 1-24. As we can see from Fig. 4-17, over time, all three bentonites eventually reach  $3w$  state (MX80:  $1w-3w$ ; KV1:  $1w-3w$ ; KB:  $2w-3w$ ). Basal spacing changing with volumetric is presented in Fig. 4-18. It is noted herein, the basal spacing and volumetric water content are the average of five slices. An easy conclusion can be made from Fig. 4-18 that, basal spacing rises with the increase of volumetric water content. Same conclusion was draw by the experimental observations from Saiyouri et al. (2003), Likos and Lu (2006) and the simulation from Sedighi and Thomas (2014). Basal spacing changing with degree of saturation is presented in Fig. 4-19. As Fig. 4-19 shown that, basal spacing rises with increasing degree of saturation.

### 4.3 Discussion

#### 4.3.1 The developing pattern difference for hydraulic conductivity during saturation between bentonite and normal soil

As introduced in Fig. 4-10, the hydraulic conductivity during saturation exhibits a “ $\cap$ ” pattern with the variation of the volumetric water content. Changing another word, the

hydraulic conductivity increases with the rising volumetric water content in the beginning wetting durations. After arriving the peak point, hydraulic conductivity decreases as the increase of volumetric water content. These results do not correspond to the observations made on non-expansive unsaturated soils, in which hydraulic conductivity increases in a continuous way upon wetting (Meerdink et al. 1996).

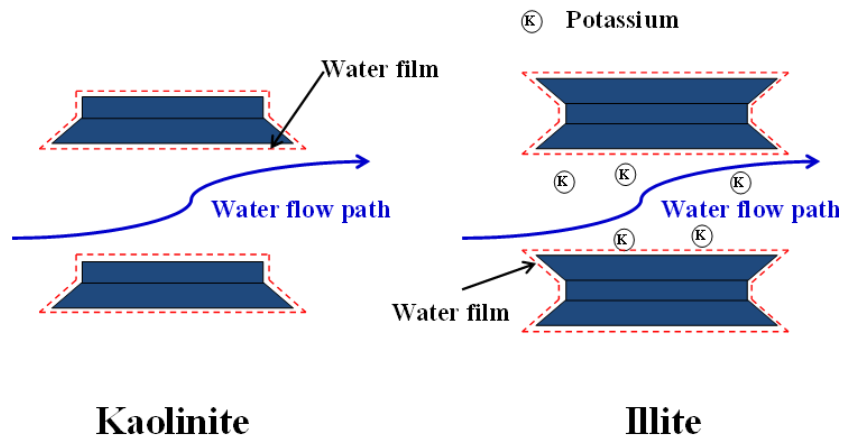


**Figure 4-20 Water flow path in Kaolinite and Illite**

This difference may be due to the fabric unit evolution difference during saturation for different soils. From Ruan et al. 2022(a) and Ruan et al. 2022(b), unlike Kaolinite and Illite that water can flow through inter-layer space (Fig. 4-20), the inter-layer pore is very hard for the moveable water in montmorillonite to flow through. At the same time, many other researchers also reported that the inter-layer pore is negligible for the movement of water in compacted bentonite (Ichikawa et al. 1999; Suzuki et al. 2005). Thus, in this study, the moveable water was assumed flow through the pores outside the inter-layer space (Fig. 4-21). In this study a new dual system was proposed (Fig. 4-22) as: 1) micropore (inter-layer pore) and 2) macropore (inter-particle and inter-aggregate pores). As the discussion above, the macropore was assumed as the water flowing path in bentonite.

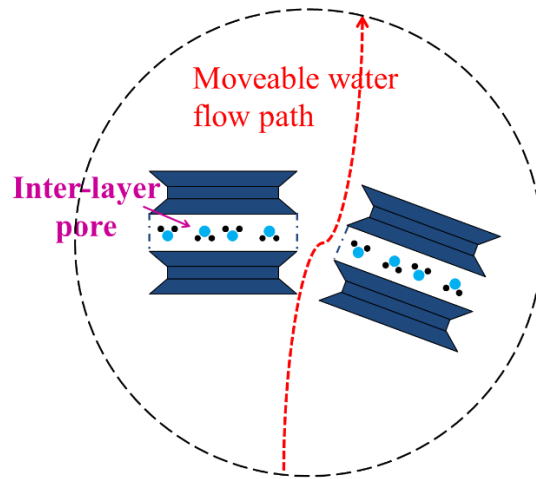


Figure 4-21 Water flow path in montmorillonite

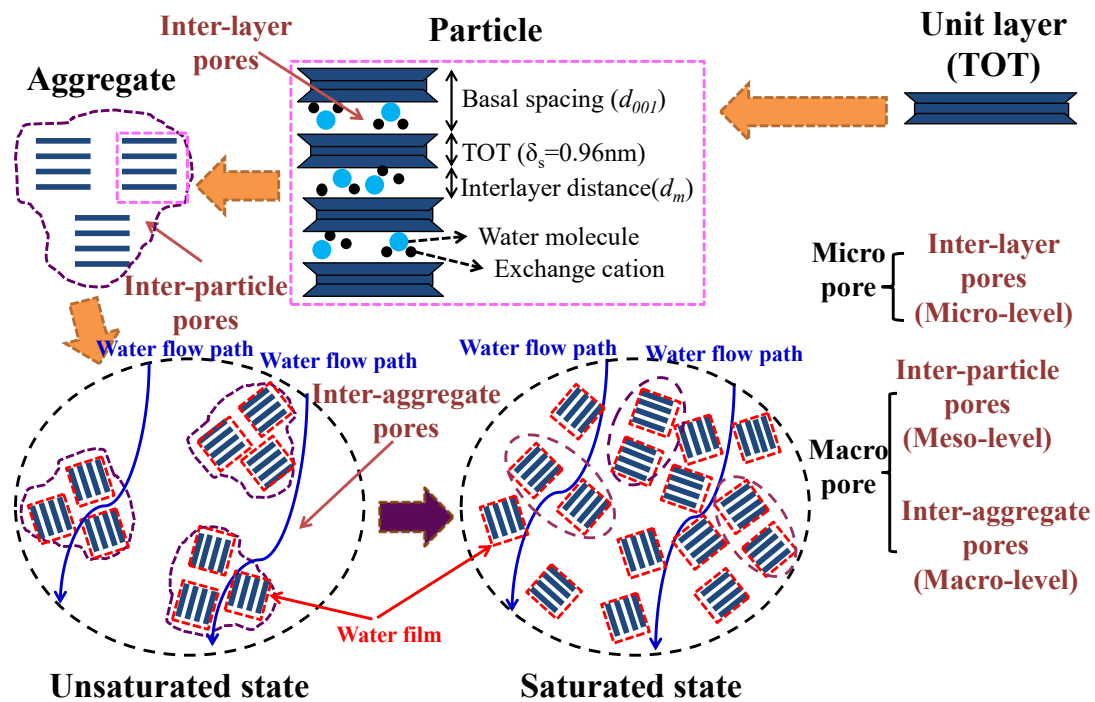


Figure 4-22 Fabric units of bentonite and their evolution during saturation

With MIP and SEM tests, Musso et al. (2013) and Romero (2013) indicated that the fabric units of bentonite is dynamic due to water adsorption. With increasing water content, aggregates are expected to become divisible into particles (e.g., Musso et al. 2013, Fig. 4-22). At the relatively dry stage, permeability was dominated by the suction gradient. As water infiltrates, the suction decreases with increasing water content and the permeability increases. As saturation approached, aggregates were expected to

break into particles. The permeability is converted to be controlled by the macropore. As saturation progresses, the volume of the particles expands, thereby compressing the macropore pores. As the inter-particle pores decrease, the permeation channels become smaller and the permeability decreases.

Another possible reason for the “ $\cap$ ” shape between volumetric water content and hydraulic conductivity is the calculation method in this study. In this study, the hydraulic conductivity was calculated by the water diffusivity and SWRC. The results from equation (4-5) shows a continuously decrease of water diffusivity with increasing volumetric water content.  $\partial(\psi)/\partial(\theta)$  was reported by Takeuchi et al. (1995) has a “ $\cap$ ” shape with the change of volumetric water. A decreasing curve multiplied by a “ $\cap$ ” shape as equation (4-6), leading a “ $\cap$ ” shape between volumetric water content and hydraulic conductivity.

## Conclusion

Swelling pressures and water content distributions of bentonites during saturation process were achieved with a developed swelling pressure device and a new multi-ring. Basal spacings were got by sending slices from multi-ring to X-ray diffraction tests. By bringing the relation between volumetric water content and new parameter  $\chi$  into traditional Darcy equation, an easy equation for calculating water diffusivity was proposed. With the relation between water diffusivity and hydraulic conductivity, hydraulic conductivity during saturation process was obtained. The results can be concluded as:

1. Swelling pressure evolution curves of bentonites show a pattern with obvious peaks and valleys;
2. Water diffusivity decreases with the increases of volumetric water content and reduces as degree of saturation rises. A  $\cap$  shape was discovered for the relation between hydraulic conductivity and volumetric water content;
3. Basal spacing during saturation rises with increasing volumetric water content and increases with the increase of degree of saturation.

## Reference

- Bruce, R., and Klute, A., 1956. The movement of soil moisture diffusivity. *Soil Science Society of America Proceedings*, **20**: 458–462.
- Corey, T., 2003. *Mechanics of immiscible fluids in porous media*. Water Resources Publication, LLC, Colorado, USA.
- Ichikawa, Y., Kawamura, K., Nakano, M., Kitayama, K., and Kawamura, H., 1999. Unified molecular dynamics and homogenization analysis for bentonite behavior: current results and future possibilities. *Engineering Geology*, **54**: 21-32.
- Imbert, C., and Villar, M.V. 2006. Hydro-mechanical response of a bentonite pellets/powder mixture upon infiltration. *Applied Clay Science*, **32**:197–209.
- Klute, A., and Dirksen, C., 1986. Hydraulic conductivity and diffusivity: laboratory methods. *Methods of Soil Analysis, Part 1. Physical and Mineralogical methods*, Soil Science Society of America, Monograph No. 9, Madison, WI, 687-734.
- Likos, W.J., and Lu, N., 2006. Pore-scale analysis of bulk volume change from crystalline interlayer swelling in Na<sup>+</sup>-and Ca<sup>2+</sup>-smectite. *Clays and Clay Minerals*, **54(4)**: 515–528
- Meerdink, J.S., Benson, C.H., and Khire, M.V., 1996. Unsaturated hydraulic conductivity of two compacted barrier soils. *Journal of Geotechnical Engineering*, **122(7)**: 565-576.
- Morodome, S., and Kawamura, K. 2009. Swelling behavior of Na- and Camontmorillonite up to 150°C by IN SITU X-ray diffraction experiments. *Clays and Clay Minerals*, **57 (2)**: 150-160.
- Musso, G., Romero, E., and Della, V.G. 2013. Double-structure effects on the chemo-hydro-mechanical behaviour of a compacted active clay. *Géotechnique*, 63(3): 206–220.

- Ruan, K., Komine, H., Ito, D., Miyoshi., and Gotoh, T., 2022a. Hydraulic conductivity and X-ray diffraction tests of unsaturated bentonites with a multi-ring and their predictions by pores distributions. *Engineering Geology*, **306** (5): 106738.
- Ruan, K., and Fu, X.L., 2022. A Modified Kozeny-Carman Equation for Predicting Saturated Hydraulic Conductivity of Compacted Bentonite in Confined Condition. *Journal of Rock Mechanics and Geotechnical Engineering*. **14** (3): 984-993.
- Romero, E., 2013. A microstructural insight into compacted clayey soils and their hydraulic properties. *Engineering Geology*, **165**: 3–19.
- Saiyouri, N., Tessier, D., and Hicher, P.Y., 2004. Experimental study of swelling in unsaturated compacted clays. *Clay Minerals*, **39**: 469–479.
- Sedighi, M., and Thomas, H.R., 2014. Microporosity evolution in compacted swelling clays—a chemical approach. *Applied Clay Science*, **101**: 608–618.
- Suzuki, S., Prayongphan, S., Ichikawa, Y., and Chae, B.G., 2005. In situ observations of the swelling of bentonite aggregates in NaCl solution. *Applied Clay Science*, **29** (2): 89-98.
- Takeuchi, S., Hara, K., and Nakano, M., 1995. Water retention curve, water diffusivity and water movement of compacted bentonite. *Soils and Foundations*, **35** (3): 129–137. (in Japanese).
- Villar, M.V., Espina, R.G., and Nebot, L.G. 2012. Basal spacings of smectite in compacted bentonite. *Applied clay science*, (65-66): 95-105.
- Wang, H.L., Shirakawabe, T., Komine, H., Ito, D., Gotoh, T., Ichikawa, Y., and Chen, Q., 2020. Movement of water in compacted bentonite and its relation with swelling pressure. *Canadian Geotechnical Journal*, **57**(6): 921–932.
- Wang, H.L., Komine, H., and Gotoh, T., 2021. A swelling pressure cell for X-ray diffraction test. *Géotechnique*. <https://doi.org/10.1680/jgeot.20.00005>

# Chapter 5

## **THE EFFECT OF DRY DENSITY ON HYDRAULIC PROPERTIES AND SWELLING PRESSURE OF BENTONITES WITH XRD**

## 5.1 Testing overview

In this chapter, three bentonites (MX80, KV1 and KB) were used to study the effect of dry density on hydraulic properties and swelling pressure. For each bentonite at different dry densities, seven specimens were prepared for the wetting duration of 2-240 h. Specimen details are presented in Table 5-1. The swelling pressure apparatus is shown as Fig.3-2. And, the testing methodology was followed as Chapter 3. In this chapter, MX80  $1.6\text{g/cm}^3$ , KV1  $1.6\text{g/cm}^3$  and KB  $1.3\text{g/cm}^3$  are the database from chapter 4. Herein, the effect of dry density on swelling pressures, water diffusivities, hydraulic conductivity and basal spacings of those three bentonites are researched, respectively. And comprehensive comparisons between testing database in this study and literatures are carried out. The effect of dry density on hydraulic properties and swelling pressure are explained by the basal spacing.

**Table 5-1 Specimen details**

Bentonite	Dry density ( $\text{g/cm}^3$ )	Initial water content (%)	Size (Hight× Diameter)	Wetting duration (h)
MX80	1.4, 1.5 and 1.6	8.92-8.99	~11mm×28mm	2, 4, 8, 24, 48, 120 and 240
KV1	1.4, 1.5 and 1.6	8.27-8.46		
KB	1.2 and 1.3	13.63-14.02		

## 5.2 Results

### 5.2.1 Swelling pressure

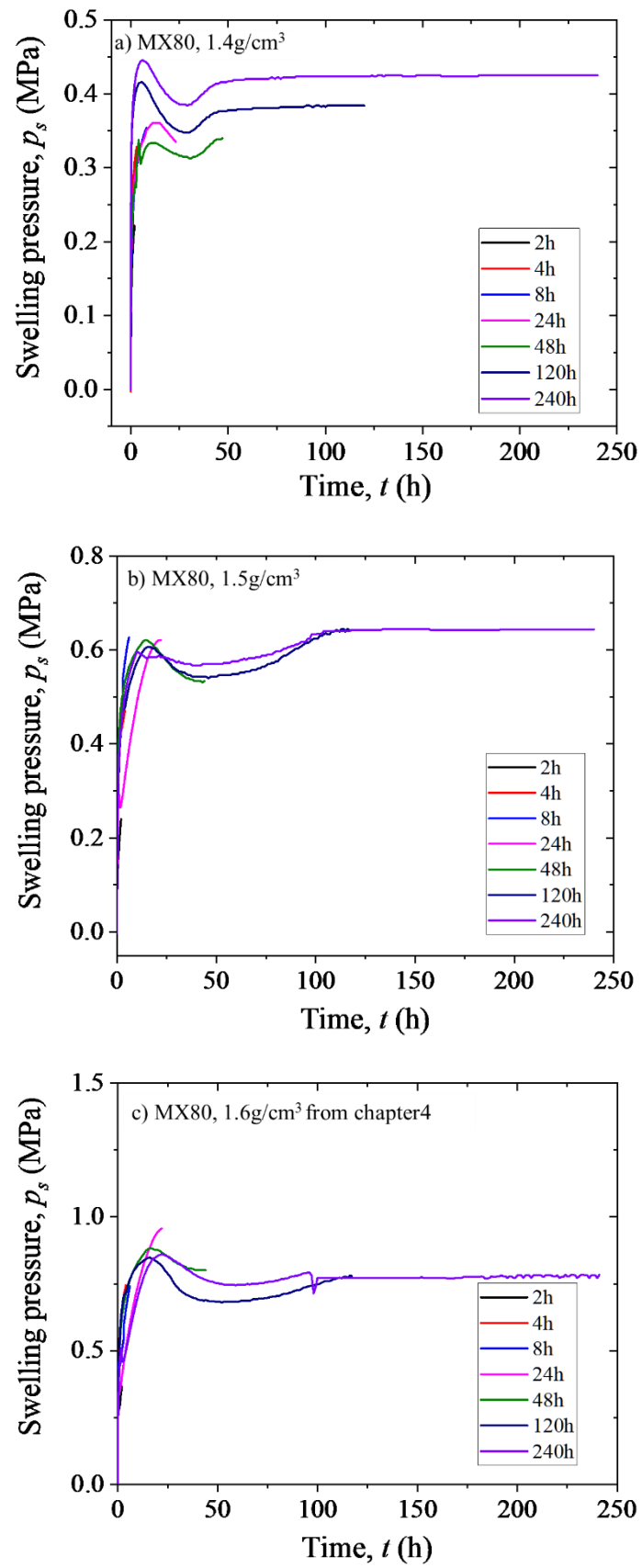


Figure 5-1 Swelling pressure evolution curves of MX80 at different dry densities

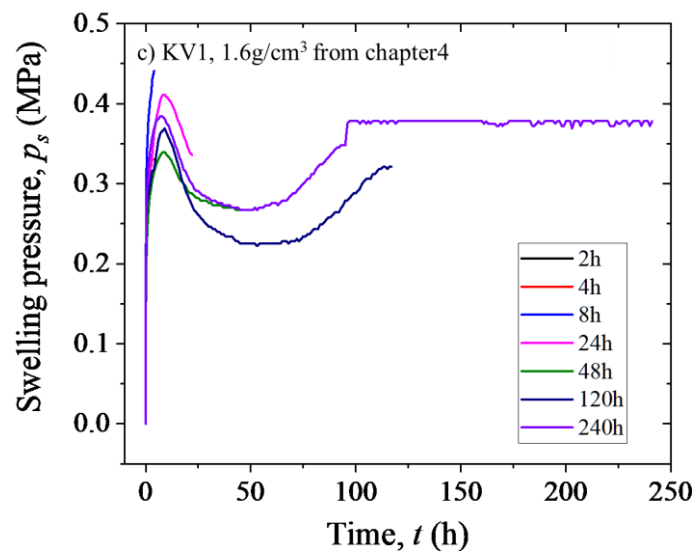
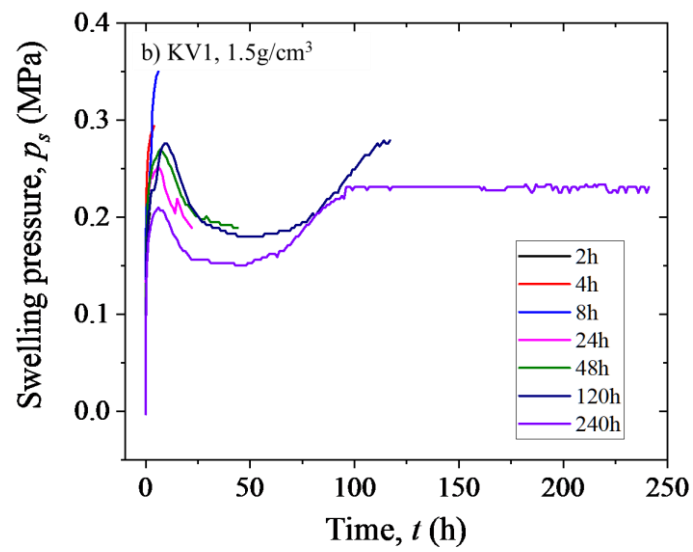
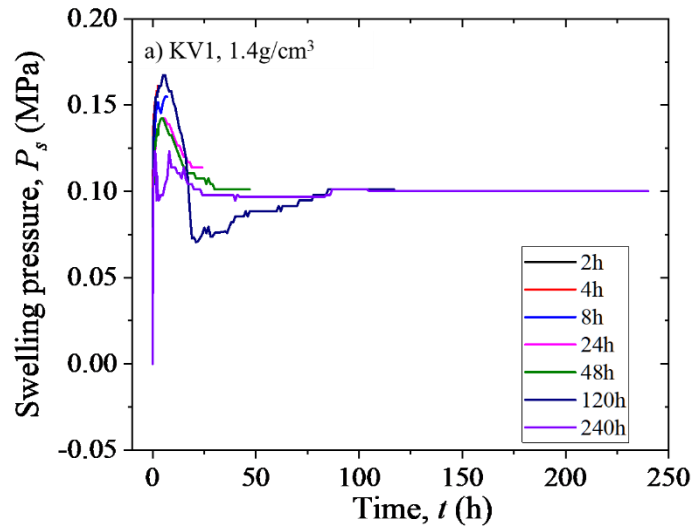
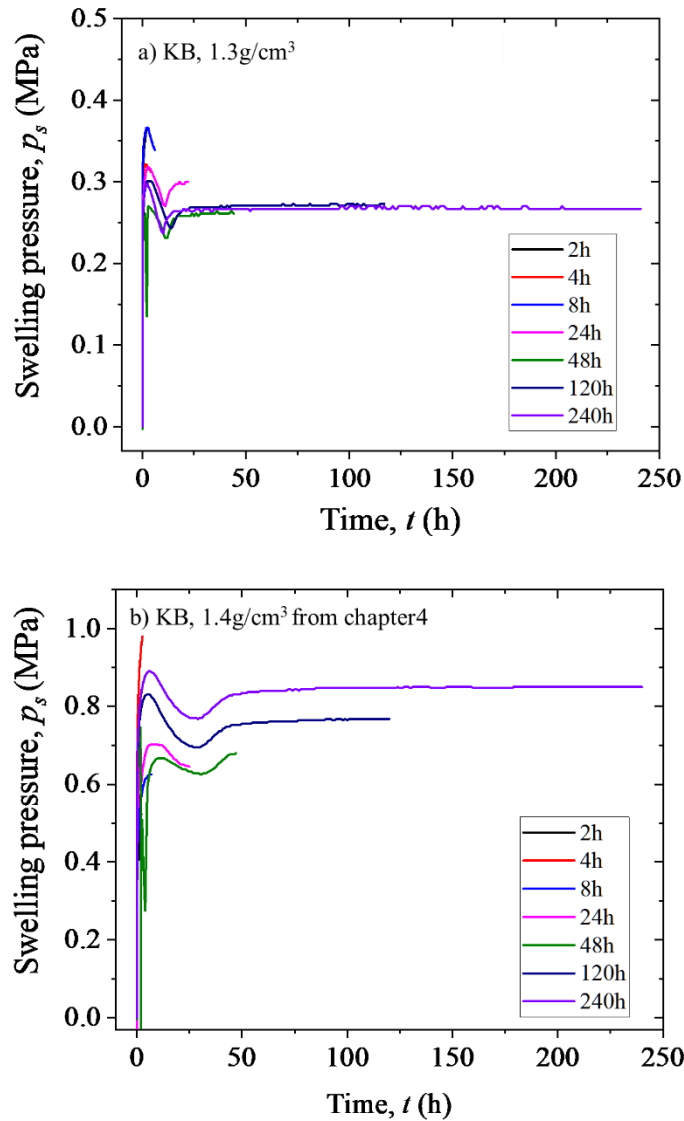


Figure 5-2 Swelling pressure evolution curves of KV1 at different dry densities



**Figure 5-3 Swelling pressure evolution curves of KB at different dry densities**

As interpreted in chapter 4, a well reported swelling pressure evolution curve of bentonite shows a pattern with obvious peak and valley. Swelling pressure evolution curves for bentonites at different dry densities are revealed in Fig. 5-1, 5-2 and 5-3, respectively. In this chapter, for all three bentonites at different dry densities, almost all swelling pressure evolution curves show clear peaks and valleys. Another interesting phenomenon can be found from Fig. 5-1, 5-2 and 5-3 that, for all three bentonites, the times for arriving peaks, valleys and re-peak points seems increase with the rise of dry density.

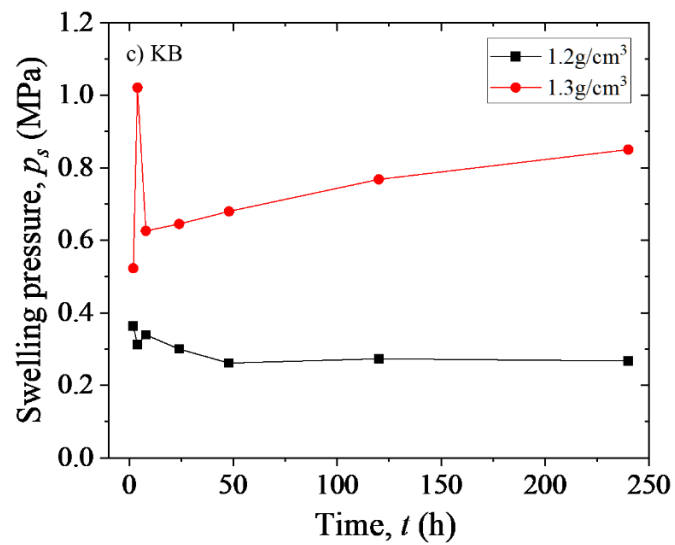
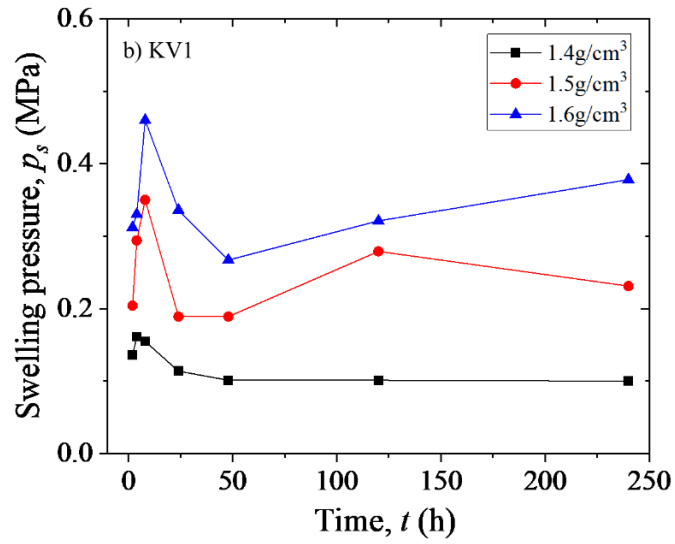
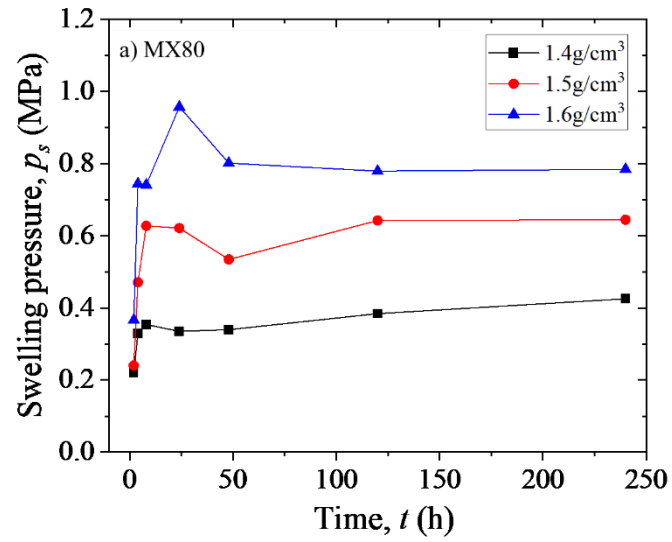
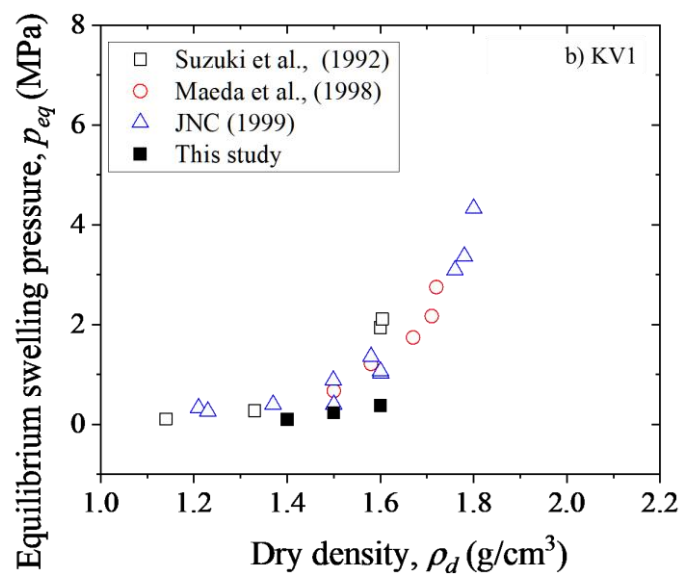
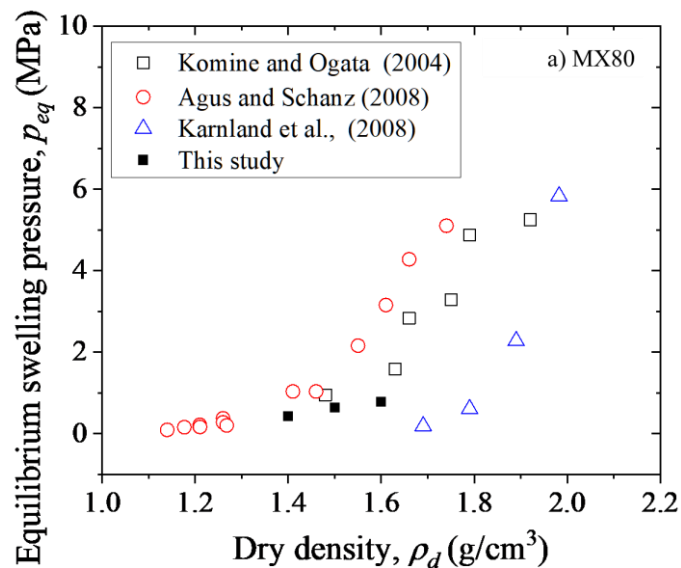
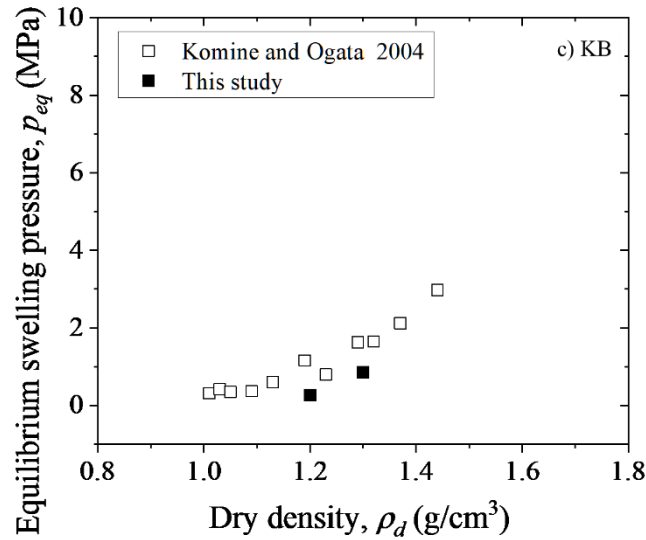


Figure 5-4 Swelling pressures at different wetting durations of different dry densities bentonites

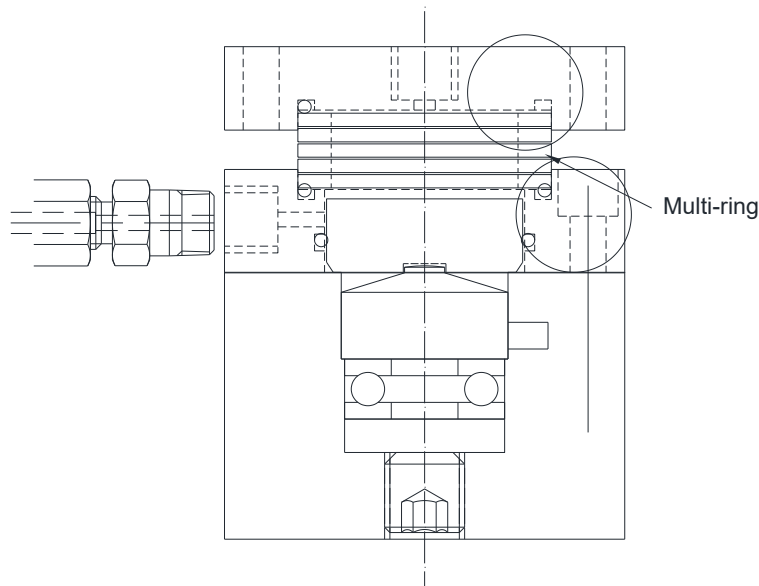
Figure 5-4 indicates the swelling pressure at different wetting durations for bentonites at different dry densities. It can be easily found from Fig. 5-4 that, along with the saturation, swelling pressure increases with the increase of dry density for all three bentonites. The swelling pressure evolution pattern with peak and valleys can also be seen from Fig. 5-4.

Figure 5-5 presents the equilibrium swelling pressure of MX80, KV1 and KB form literatures and this study, respectively. As we can easily conclude from Fig. 5-5, the equilibrium swelling pressure increase with rising dry density, no matter from literatures and this study.





**Figure 5-5 Equilibrium swelling pressure from literatures and this study**



**Figure 5-6 Swelling pressure apparatus with multi-ring**

Another finding can be easily seen from Fig. 5-5 that, for all three bentonites, among all the testing database, the database from this study is somewhat lower. This phenomenon may be due to the application of multi-ring in this study. As introduced in chapter 3, the multi-ring is consisting of 2mm ring and two-piece ring. After inserting the multi-ring into swelling apparatus, the two-piece ring may in touch with the swelling pressure apparatus (Fig. 5-6), thereby giving a friction between multi-ring and apparatus.

## 5.2.2 Hydraulic properties

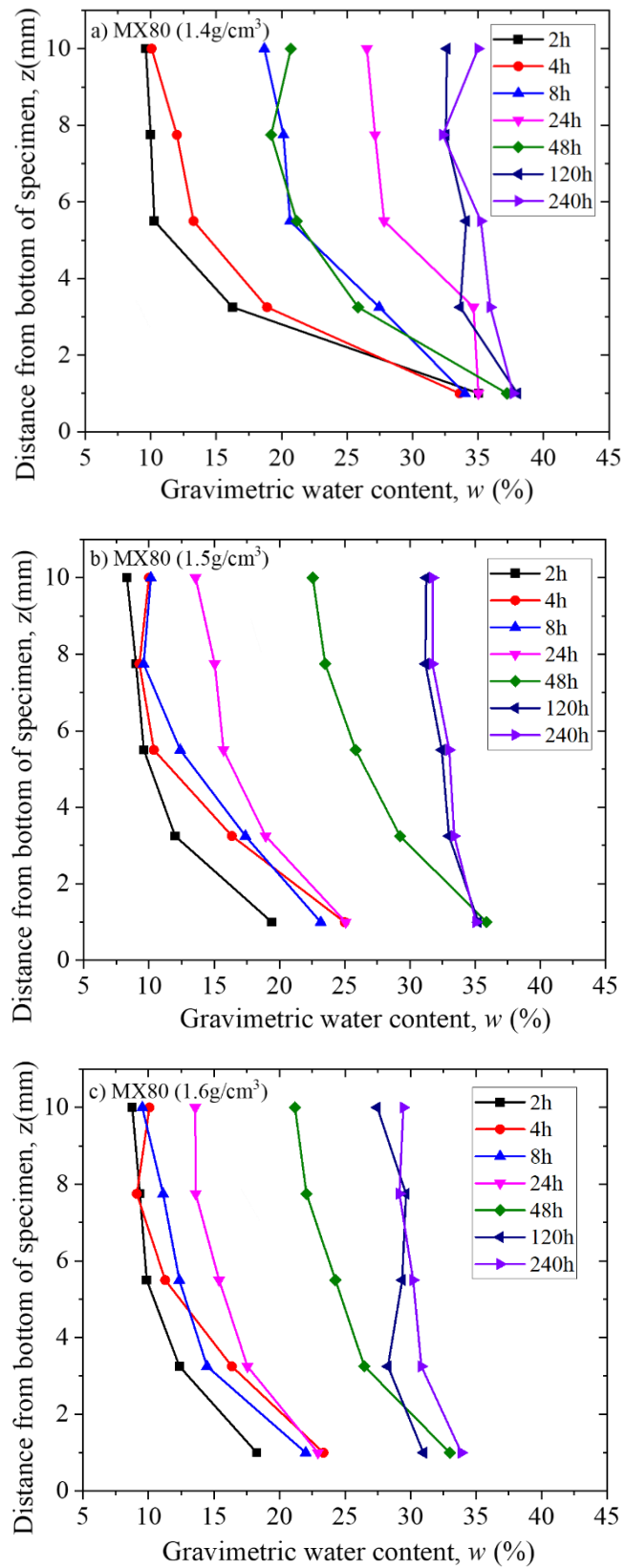


**Figure 5-7 Gravimetric water content of slices for MX80 at different dry densities**

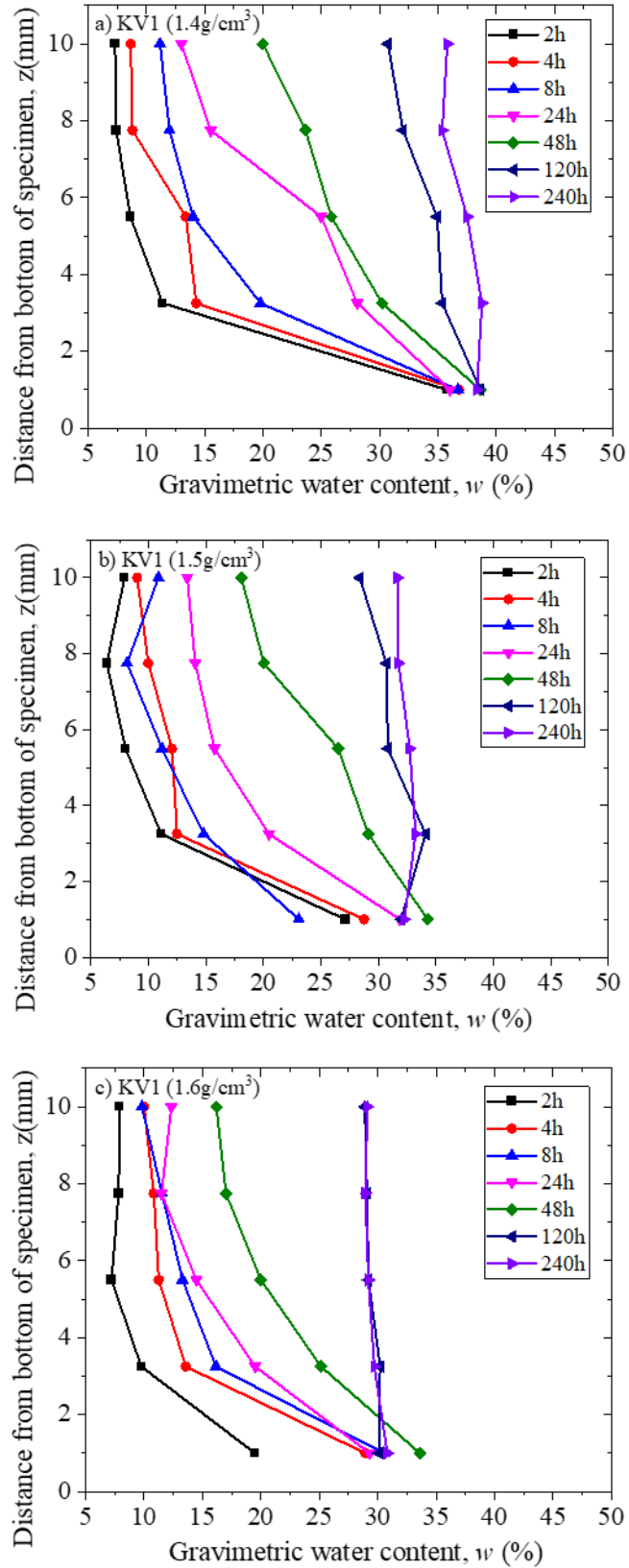
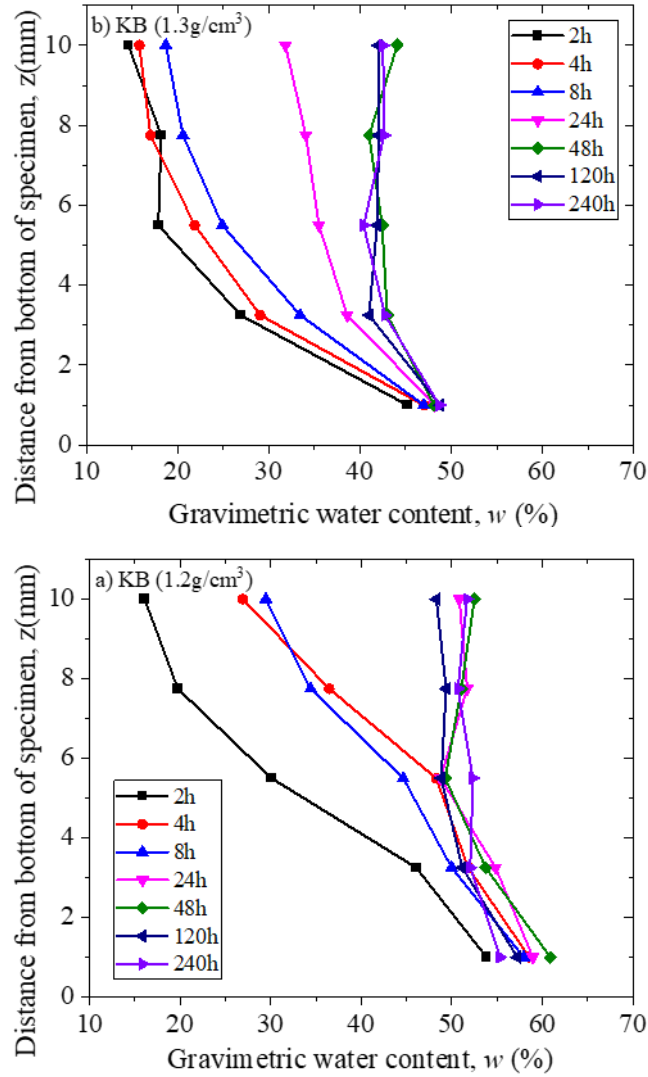


Figure 5-8 Gravimetric water content of slices for KV1 at different dry densities



**Figure 5-9 Gravimetric water content of slices for KB at different dry densities**

Gravimetric water contents in slices after water absorption for MX80, KV1 and KB are presented in Fig. 5-7, 5-8 and 5-9, respectively. It can be seen from Fig. 5-7, 5-8 and 5-9, gravimetric water contents of MX80, KV1 and KB generally decrease as increasing distance from bottom of specimen. Meanwhile, in shorter wetting durations (MX80 and KV1:  $t < 120$  h; KB:  $t < 24$  h), water content of slice increases with the rising wetting duration. In longer wetting durations, water contents of slices seem stay in relative stable values.

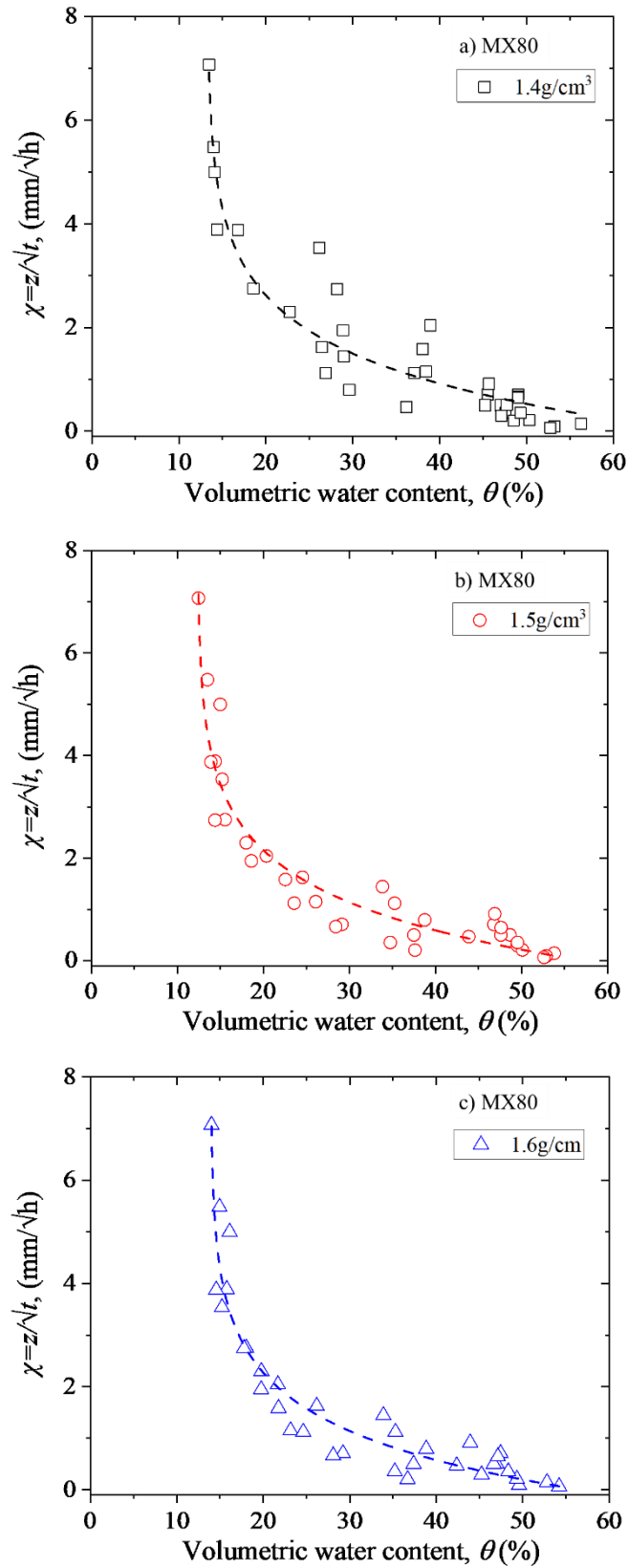


Figure 5-10 Relation between  $\theta$  and  $\chi$  of MX80 at different dry densities

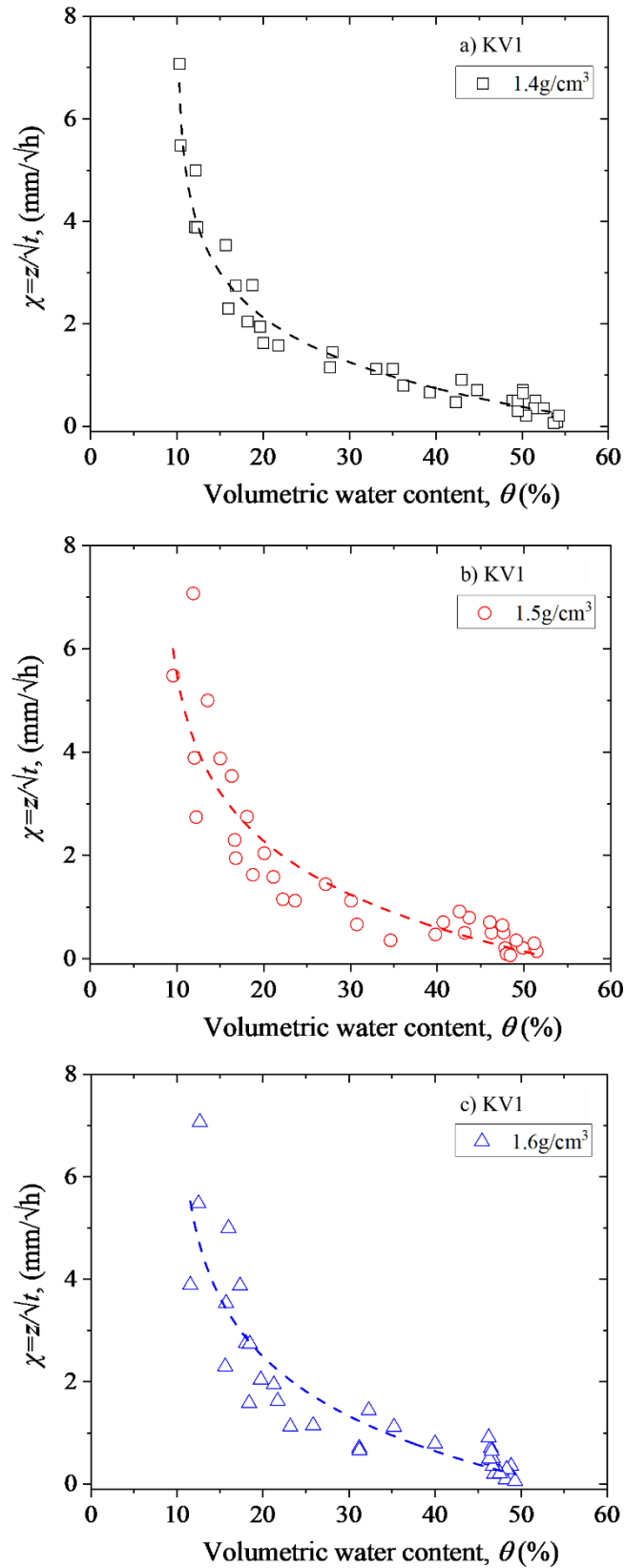
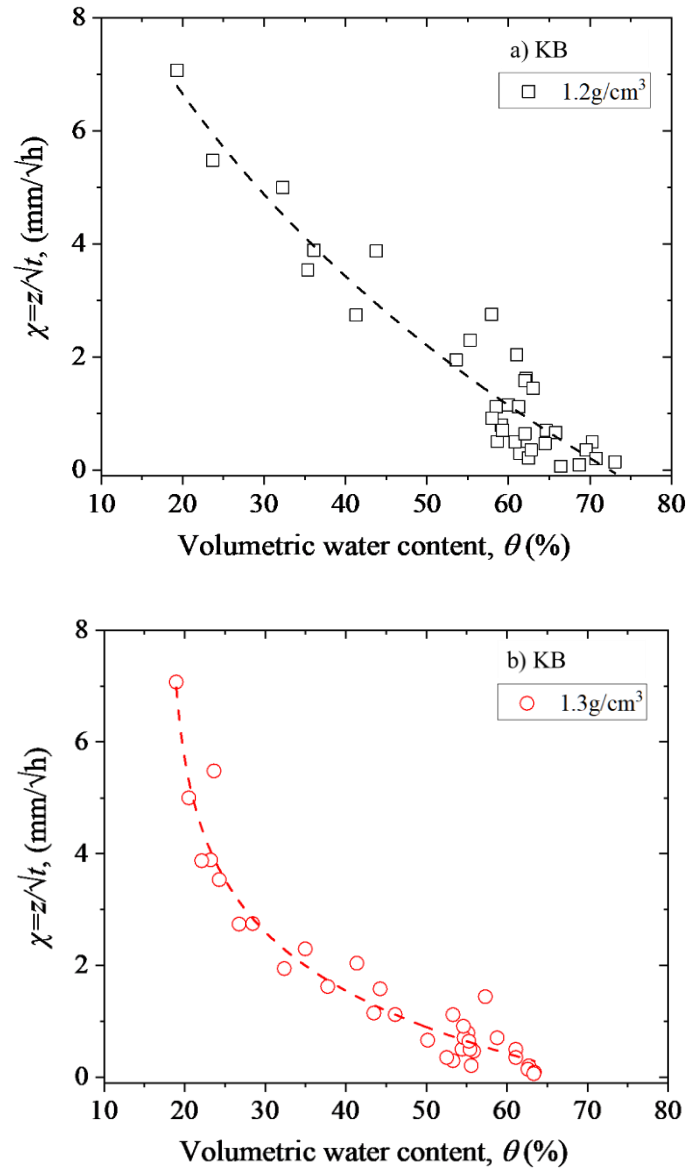
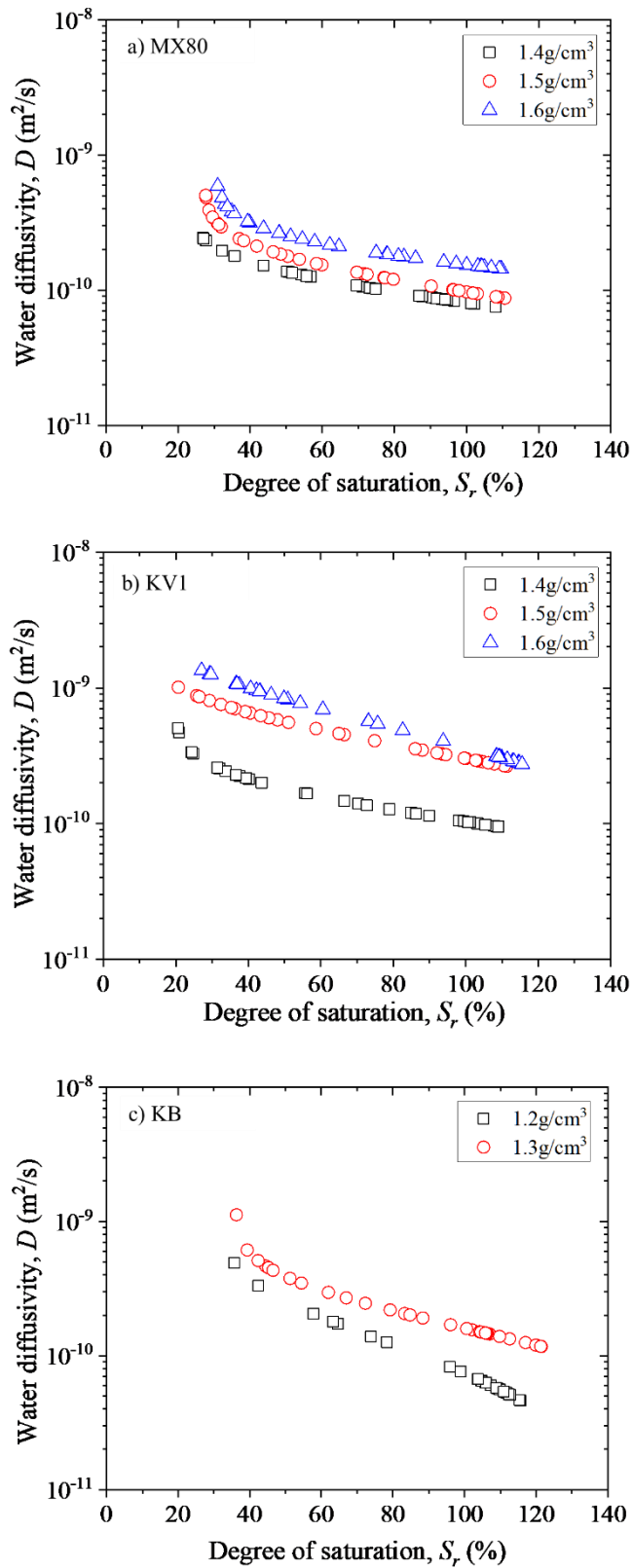


Figure 5-11 Relation between  $\theta$  and  $\chi$  of KV1 at different dry densities



**Figure 5-12 Relation between  $\theta$  and  $\chi$  of KB at different dry densities**

Meanwhile, from Fig. 5-7, 5-8 and 5-9, the times for gravimetric water content reaches relative stable values vary with the change of dry density. It can be concluded from Fig. 5-7, 5-8 and 5-9 that, those times decrease with the rising dry density, which means that more time are needed for higher dry density specimen to reach saturated state. Figure 5-10, 5-11 and 5-12 present the relations between  $\theta$  and  $\chi$  for MX80, KV1 and KB, respectively. It can be seen from Fig. 5-10, 5-11 and 5-12, experimental database generally follows equation (4-4). Therefore, the determination for water diffusivity in this study can be calculated by using equation (4-5).



**Figure 5-13 Water diffusivity changing with degree of saturation for bentonites at different dry densities**

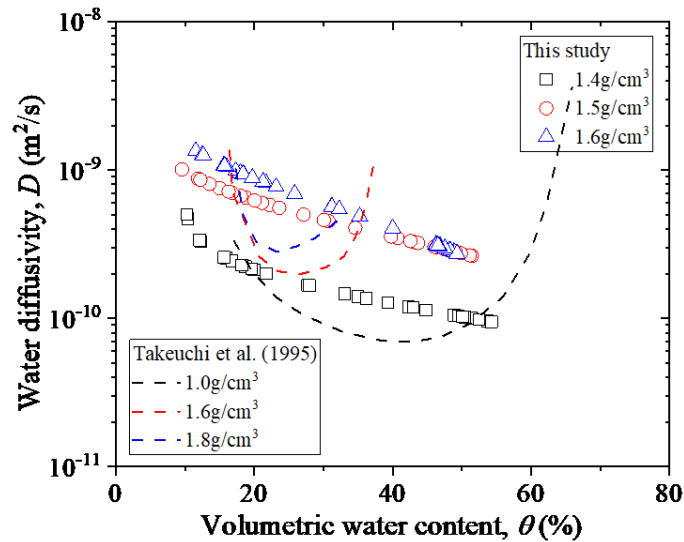


**Figure 5-14 Water diffusivity changing with volumetric water content of KV1 bentonite from Takeuchi et al. (1995) and this study**

Water diffusivity changing with degree of saturation of bentonites are indicated in Fig. 5-13. A clear trend from Fig. 5-13 can be easily concluded that, water diffusivity decreases with the increase of degree of saturation. Same phenomenon was reported in chapter 4. Meanwhile, when the degree of saturation is the same, water diffusivity rises with increasing dry density. Figure 5-14 shows water diffusivity changing with volumetric water content of KV1 bentonite from Takeuchi et al. (1995) and this study. It can be viewed from Fig. 5-14, different shapes were obtained from Takeuchi et al. (1995) and this study. This phenomenon was explained in chapter 1 and chapter 4.

Figure 5-15 shows the SWRCs of bentonites at different dry densities. Followed the method in Chapter 4, hydraulic conductivities changing with volumetric water content for different dry densities bentonites are revealed in Fig. 5-16. It is a generally truth from Fig 5-16 that, hydraulic conductivity decreases with the increasing dry density when their volumetric water contents are the same. Additionally, a  $\cap$  shape was found for the relation between volumetric water content and hydraulic conductivity, which is similar as the founding in Chapter 4.

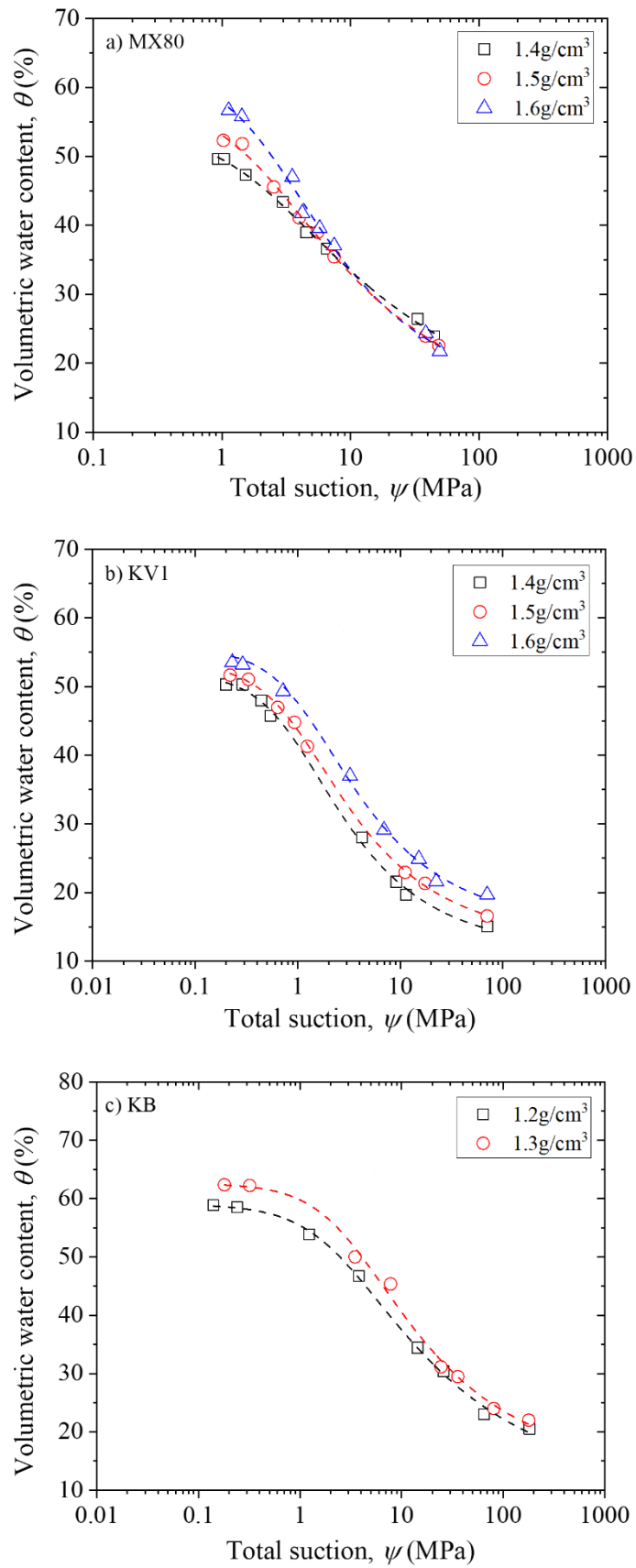


**Figure 5-15 Volumetric water content changing with total suction for different dry densities bentonites**

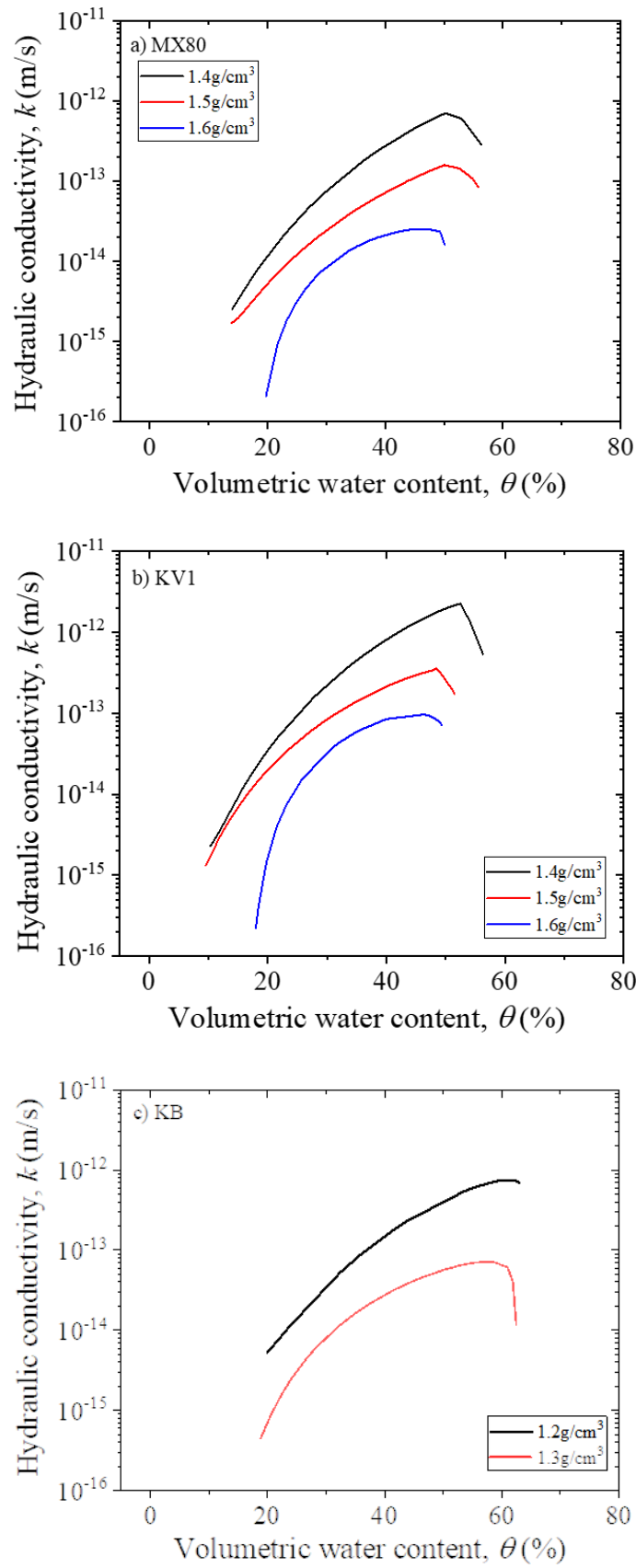


**Figure 5-16 Hydraulic conductivities changing with volumetric water content for bentonites at different dry densities**

### 5.2.3 XRD results

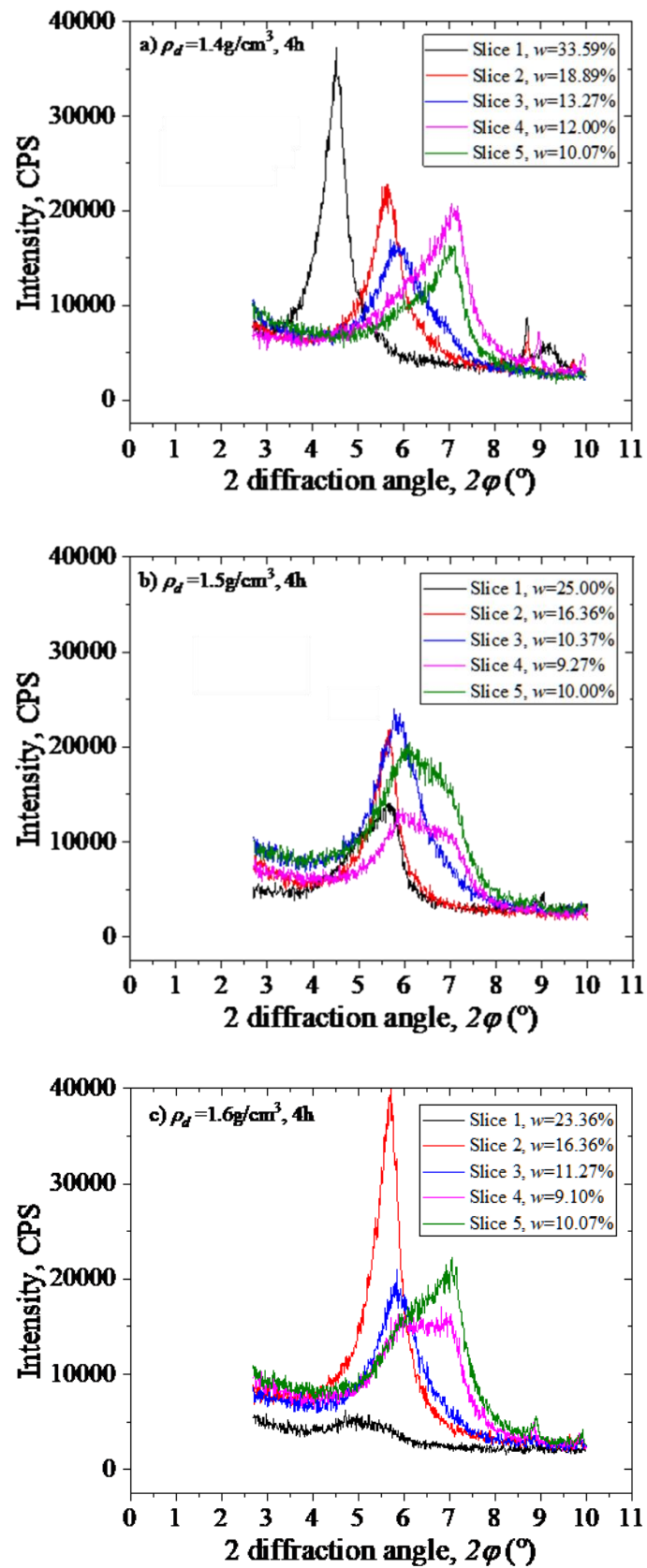


Figure 5-17 XRD profiles of different dry densities MX80 at 4h

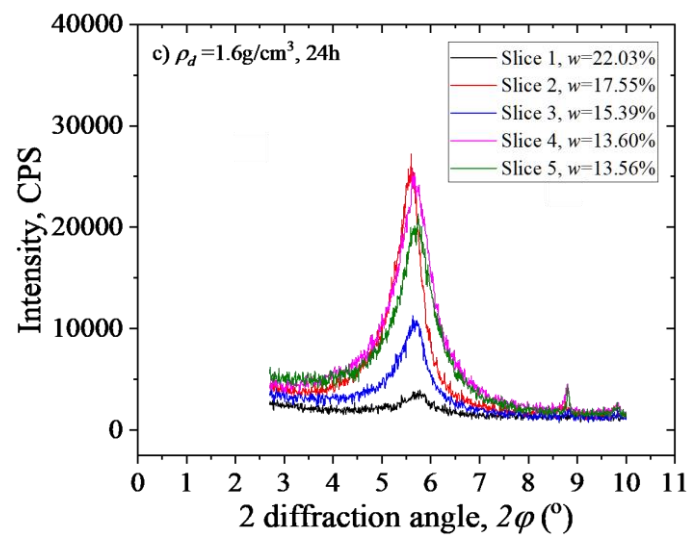
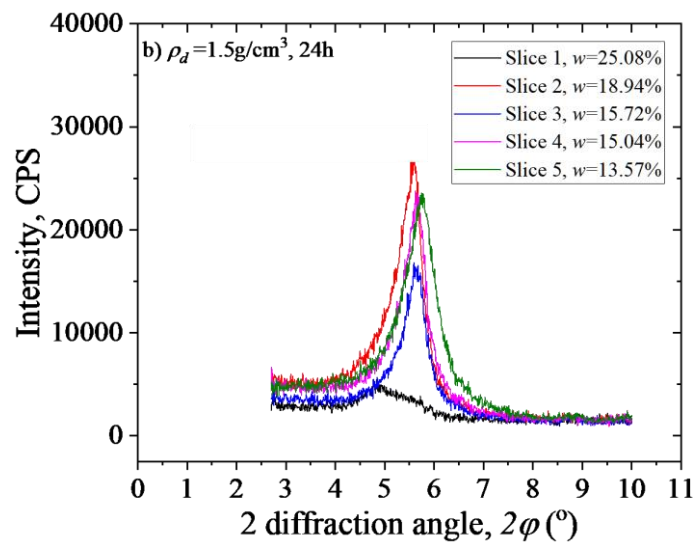
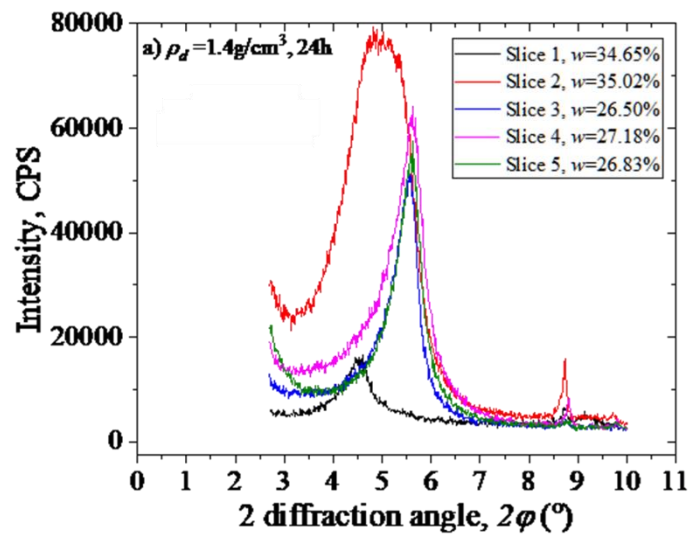


Figure 5-18 XRD profiles of different dry densities MX80 at 24h

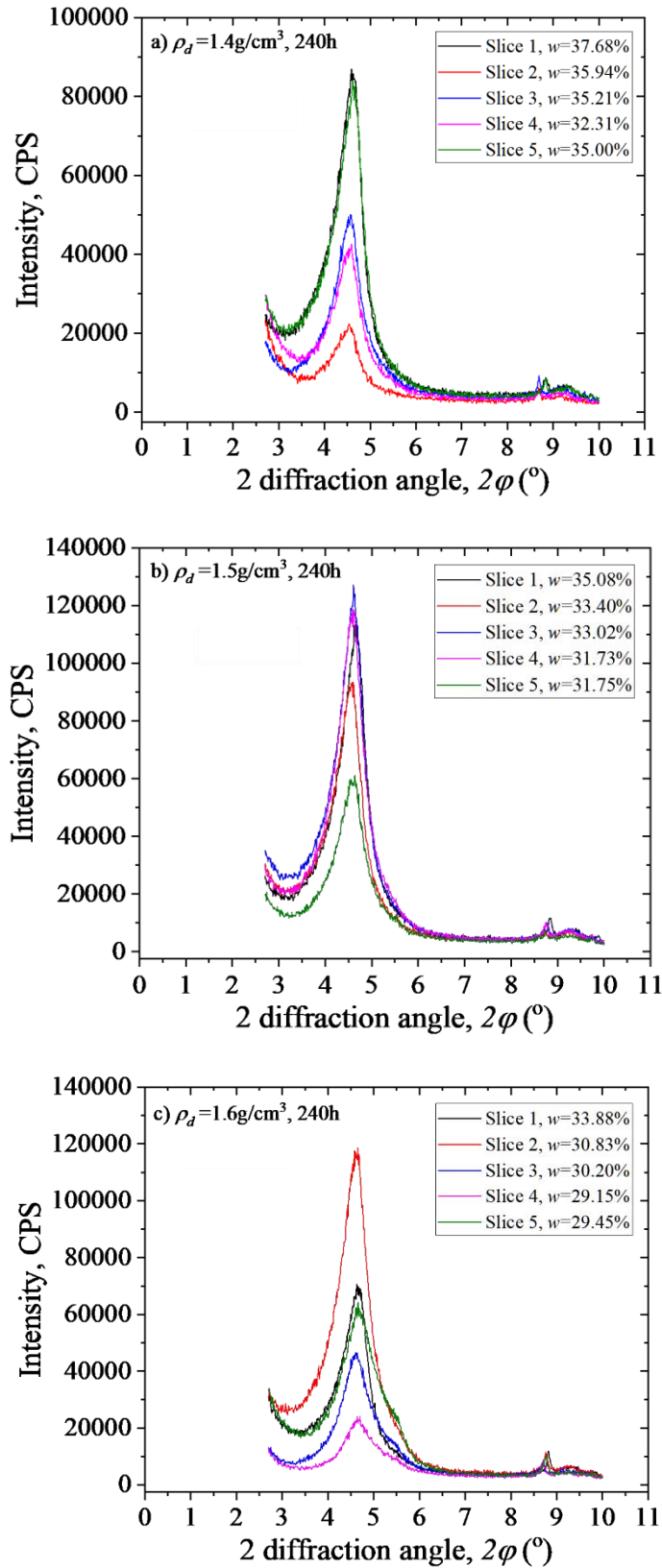


Figure 5-19 XRD profiles of different dry densities MX80 at 240h

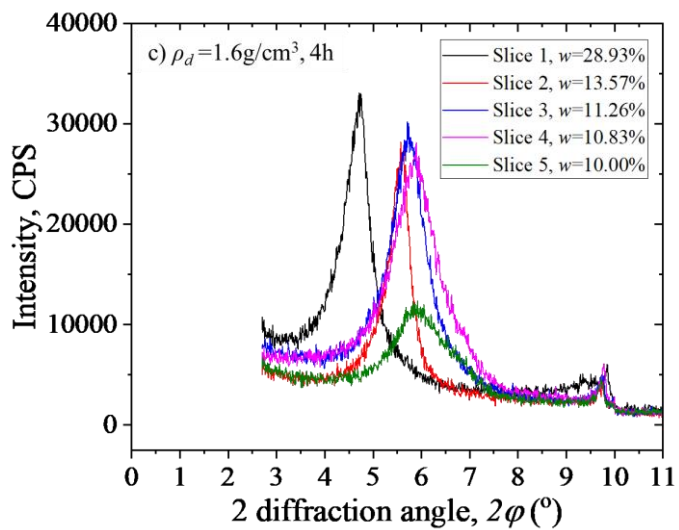
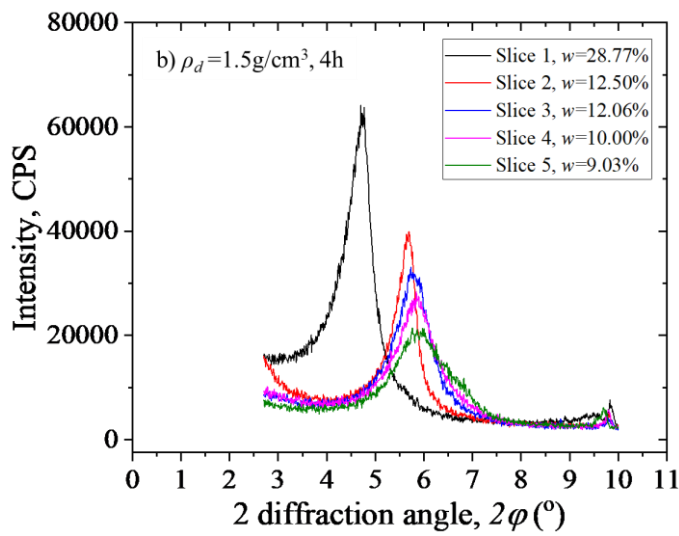
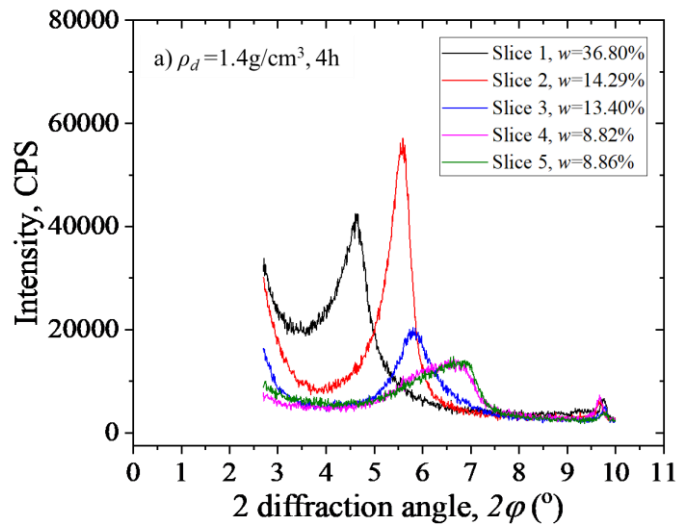


Figure 5-20 XRD profiles of different dry densities KV1 at 4h

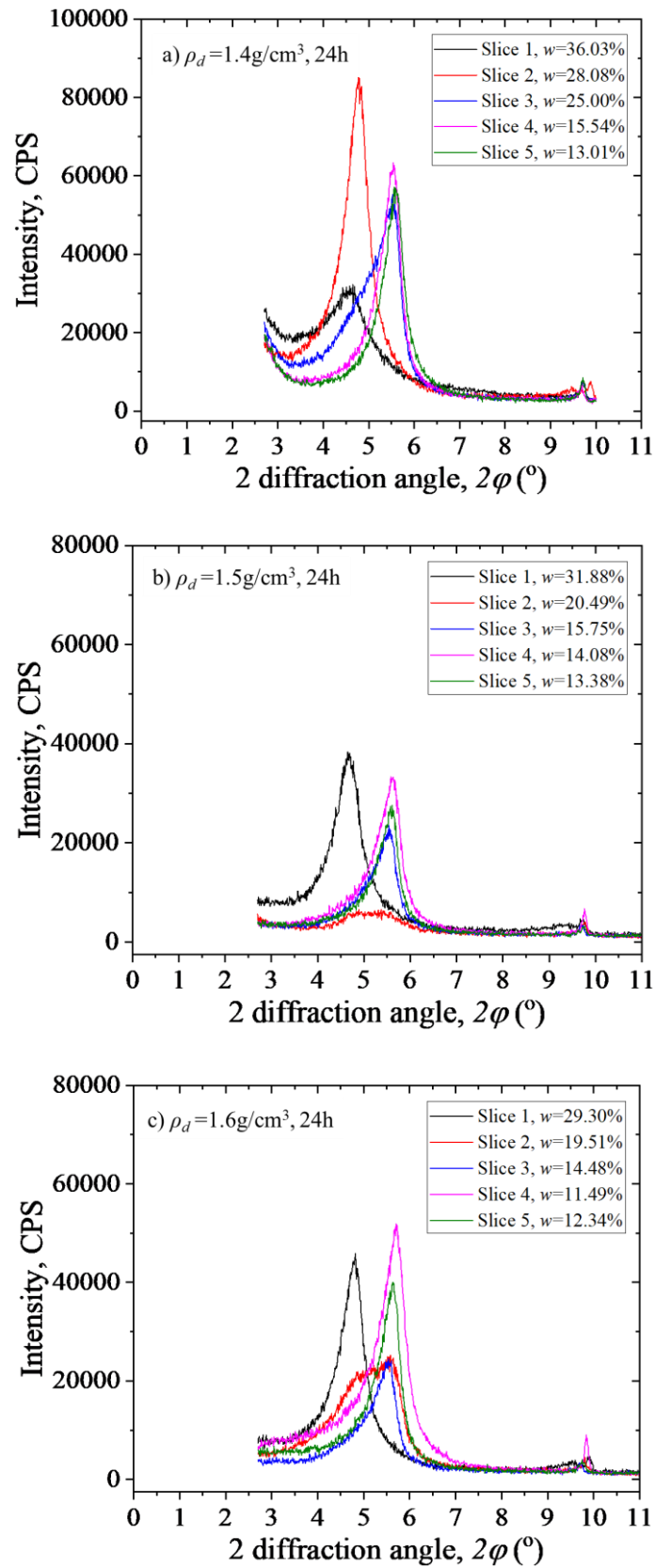


Figure 5-21 XRD profiles of different dry densities KV1 at 24h

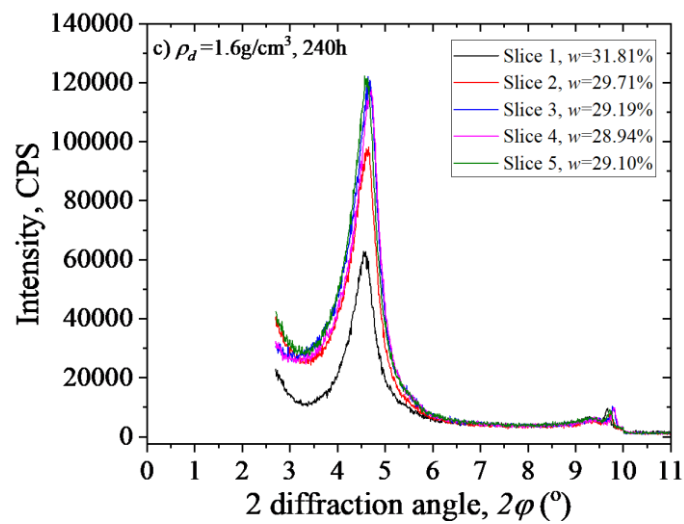
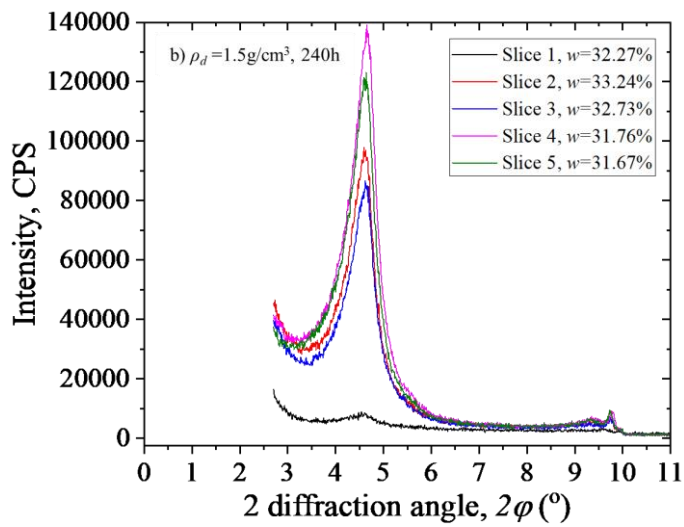
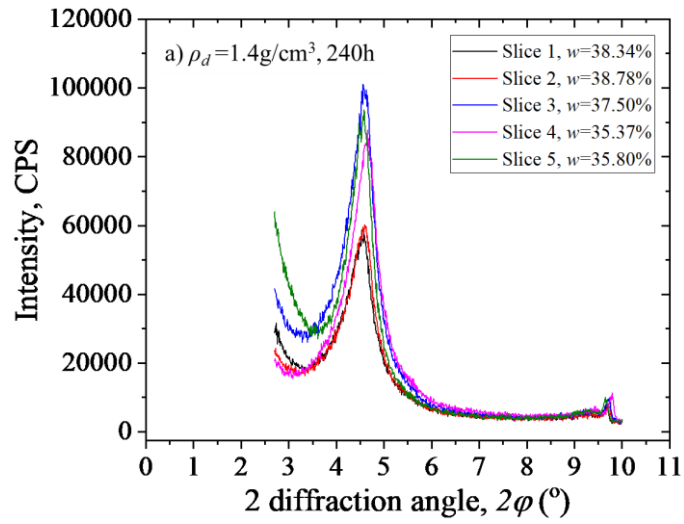


Figure 5-22 XRD profiles of different dry densities KV1 at 24h

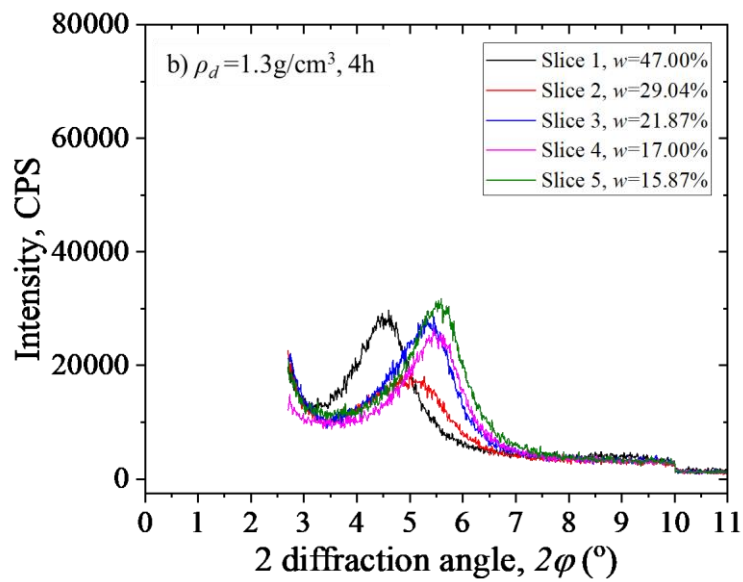
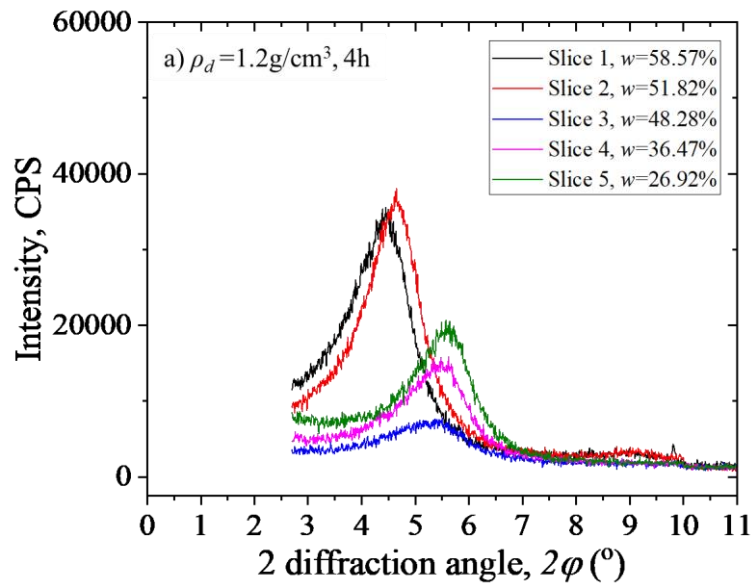


Figure 5-23 XRD profiles of different dry densities KB at 4h

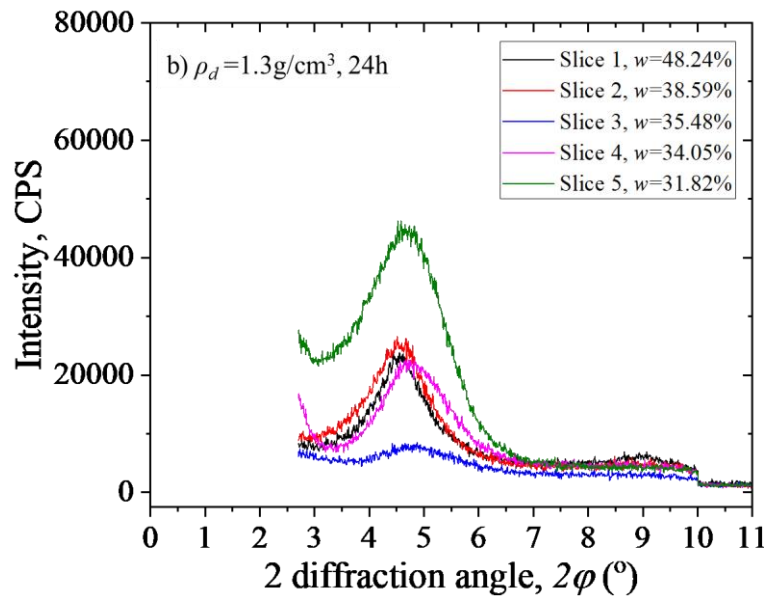
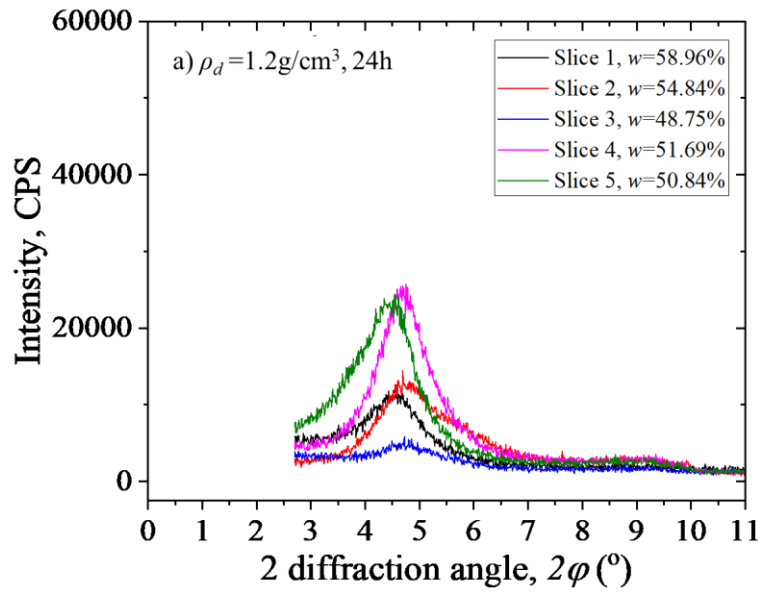
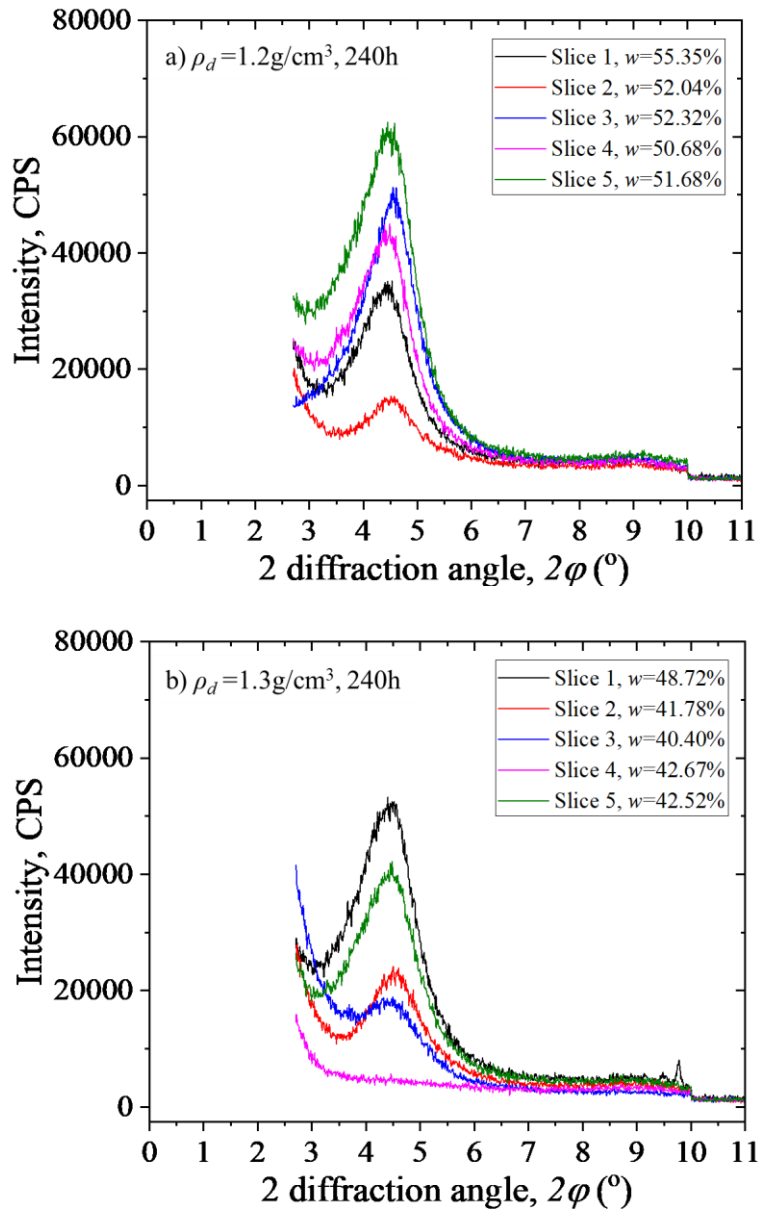
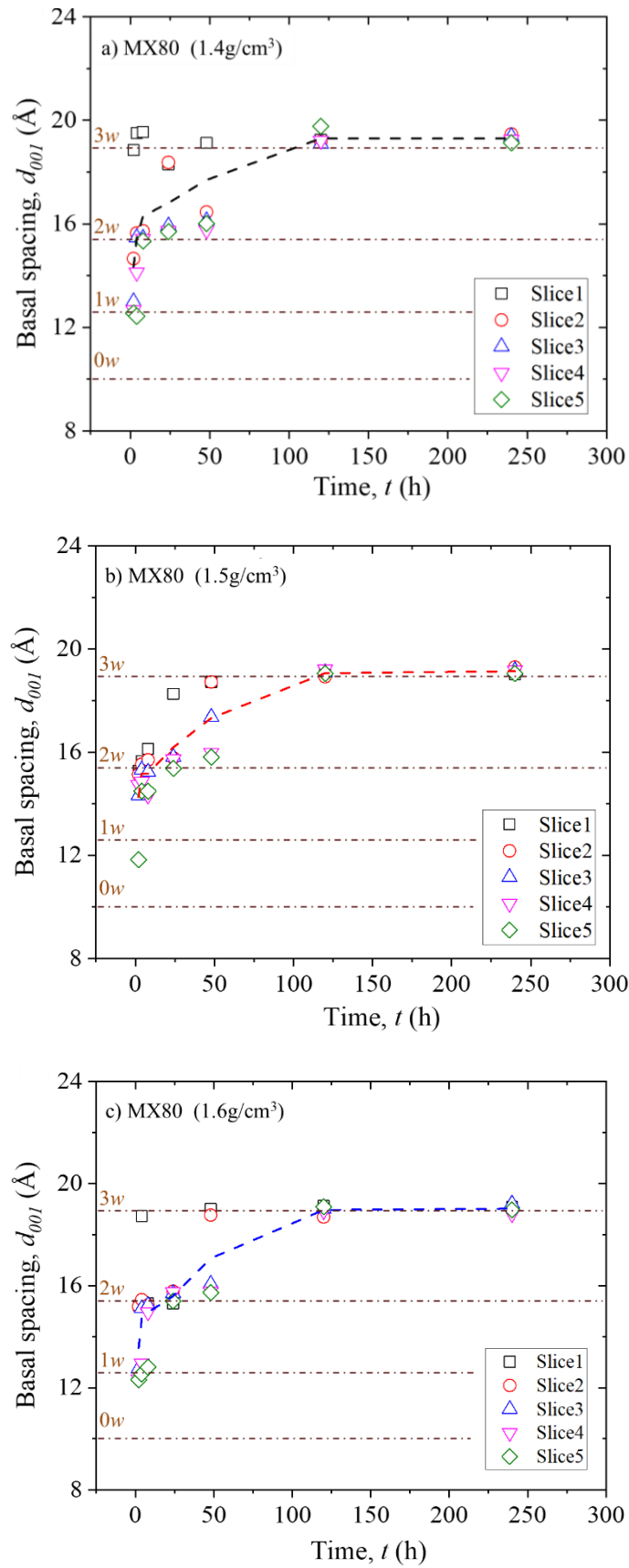


Figure 5-24 XRD profiles of different dry densities KB at 24h



**Figure 5-25 XRD profiles of different dry densities KB at 240h**

Figure 5-17, 5-18 and 5-19 show XRD profiles of different dry densities MX80 at 4h, 24h and 240h, respectively. Figure 5-20, 5-21 and 5-22 present XRD profiles of different dry densities KV1 at 4h, 24h and 240h, respectively. Figure 5-23, 5-24 and 5-25 indicate XRD profiles of different dry densities KB at 4h, 24h and 240h, respectively. Regarding the water content of slices at different wetting durations. As we can see, for MX80, KV1 and KB, when  $t=4h$  and  $24h$ , water content increases as slice number decreases. But, at  $240h$  wetting duration, the water contents



**Figure 5-26 Basal spacing changing with time of MX80 bentonite at different dry densities**

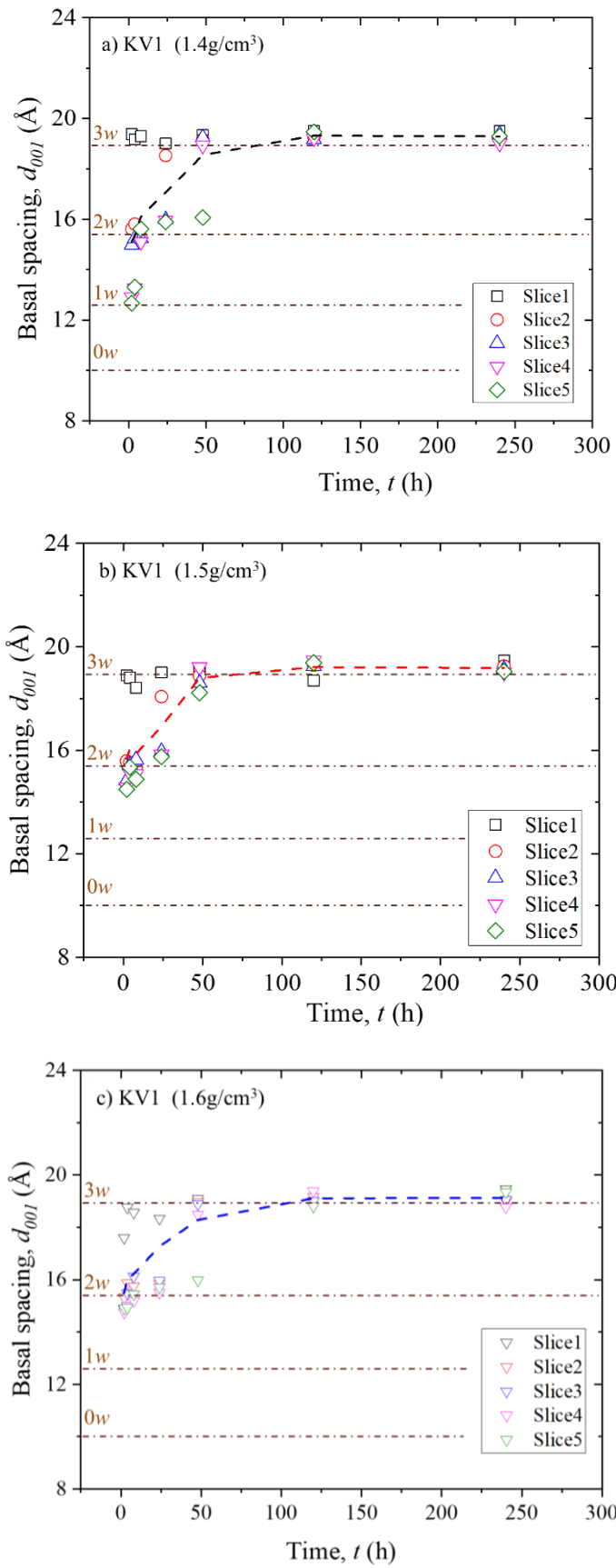


**Figure 5-27 Basal spacing changing with time of KV1 bentonite at different dry densities**

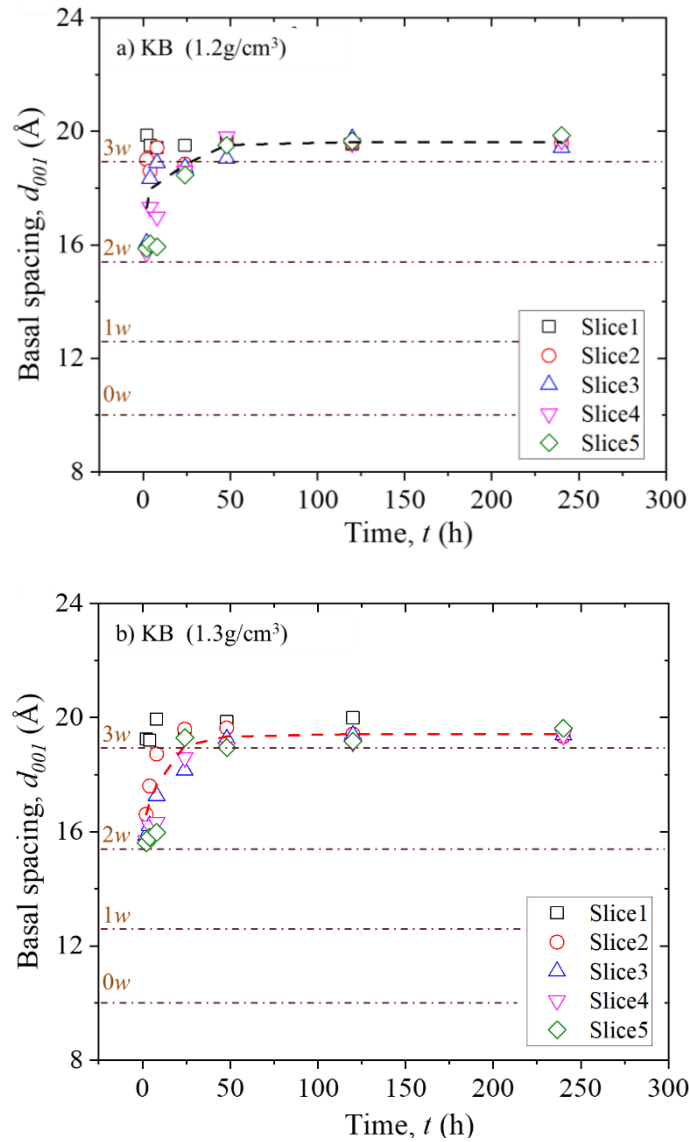


**Figure 5-28 Basal spacing changing with time of KB bentonite at different dry densities**

of slices remain stable for all bentonites at different dry densities. In case of peak position exists in the XRD profiles. When  $t=4\text{h}$  and  $24\text{h}$ , peak angle generally moves to right as the slice number rise. However, when  $t=240$ , peak angle has not so much difference with the change of slice number.

By connecting average values of five slices with the same saturation periods by dash lines in figure, the overall trend of bentonites specimens with the different dry densities are indicated in Fig. 5-26, 5-27 and 5-28. It can be readily inferred from Fig. 5-26, 5-27 and 5-28 that basal spacings increase dramatically at the beginning of the wetting period. Then, basal spacings enter into stable states. For those dry density conditions, all three bentonites gradually reach 3 *w* state. MX80 moves from 1-3 *w*, KV1 moves from 1-3 *w* and KB moves from 2-3 *w*.

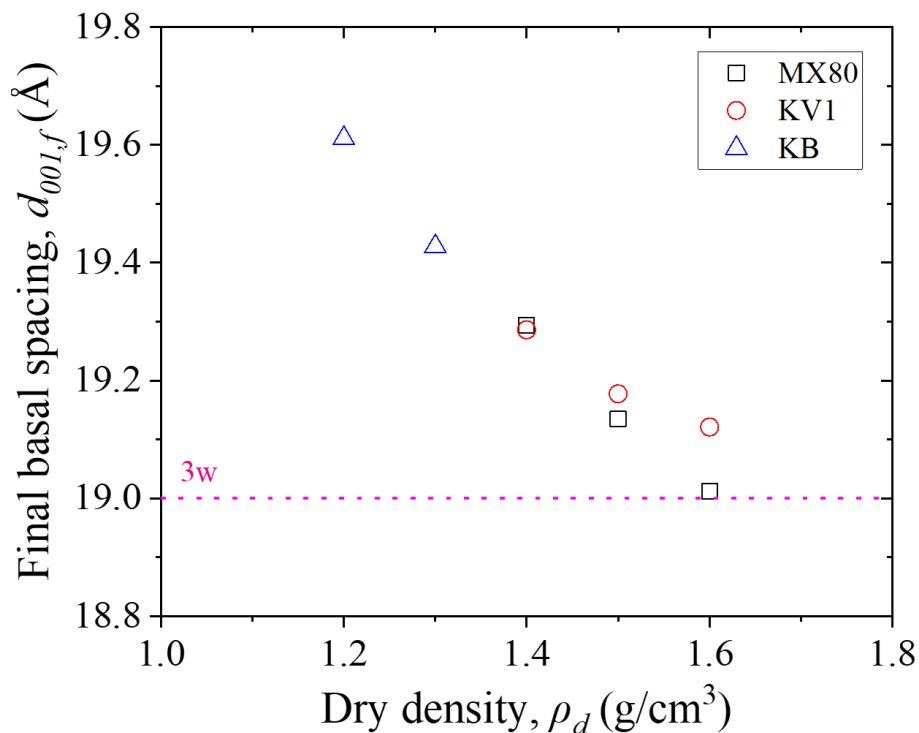


**Figure 5-29 Final basal spacing changing with dry density of bentonites**

Final basal spacing changing with dry density of MX80, KV1 and KB are presented in Fig. 5-29. An apparent conclusion can be made from Fig. 5-29, final basal spacing decreases with the increase of dry density. Figure 5-30 and 5-31 show final basal spacing for MX80 and KV1 from literatures and this study, respectively. Same founding can be easily seen from Holmboe et al. (2012) and Villar et al, (2012) for MX80 as this study that, final basal spacing reduces with increasing dry density. However, there is no clear trend for KV1 from Wang et al. (2021).

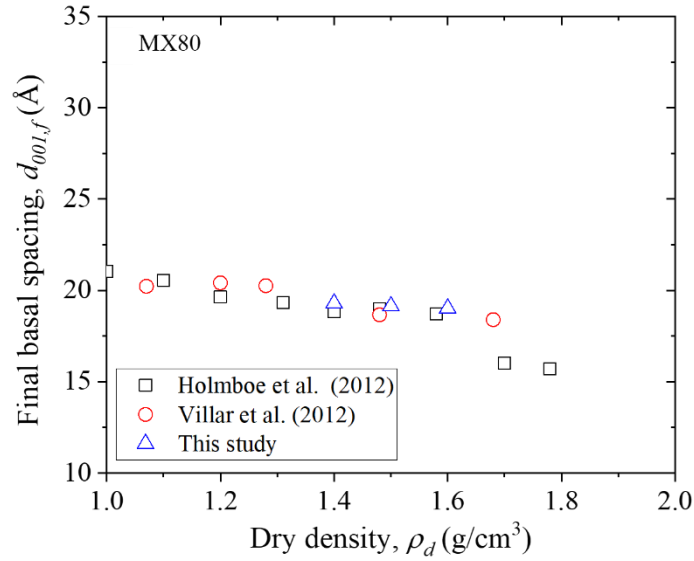


**Figure 5-30 Final basal spacing of MX80 from literatures and this study**

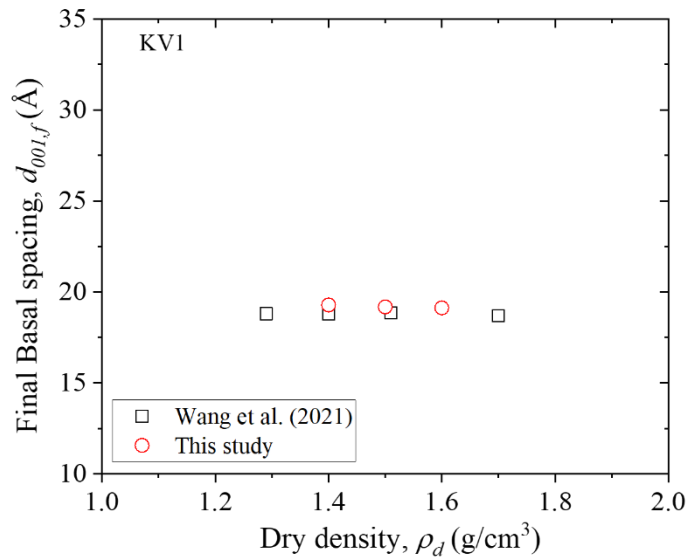


**Figure 5-31 Final basal spacing of KV1 from literatures and this study**

### 5.3 Discussion

Reports of numerous studies (Villar et al. 2012; Wang et al. 2020) had described that basal spacing has a marked effect on swelling pressure. Regarding specimen during saturation, it was reported that swelling pressure increases with growing basal spacing (Wang et al. 2020). Figure 5-32, 5-33 and 5-34 indicates basal spacing changing with

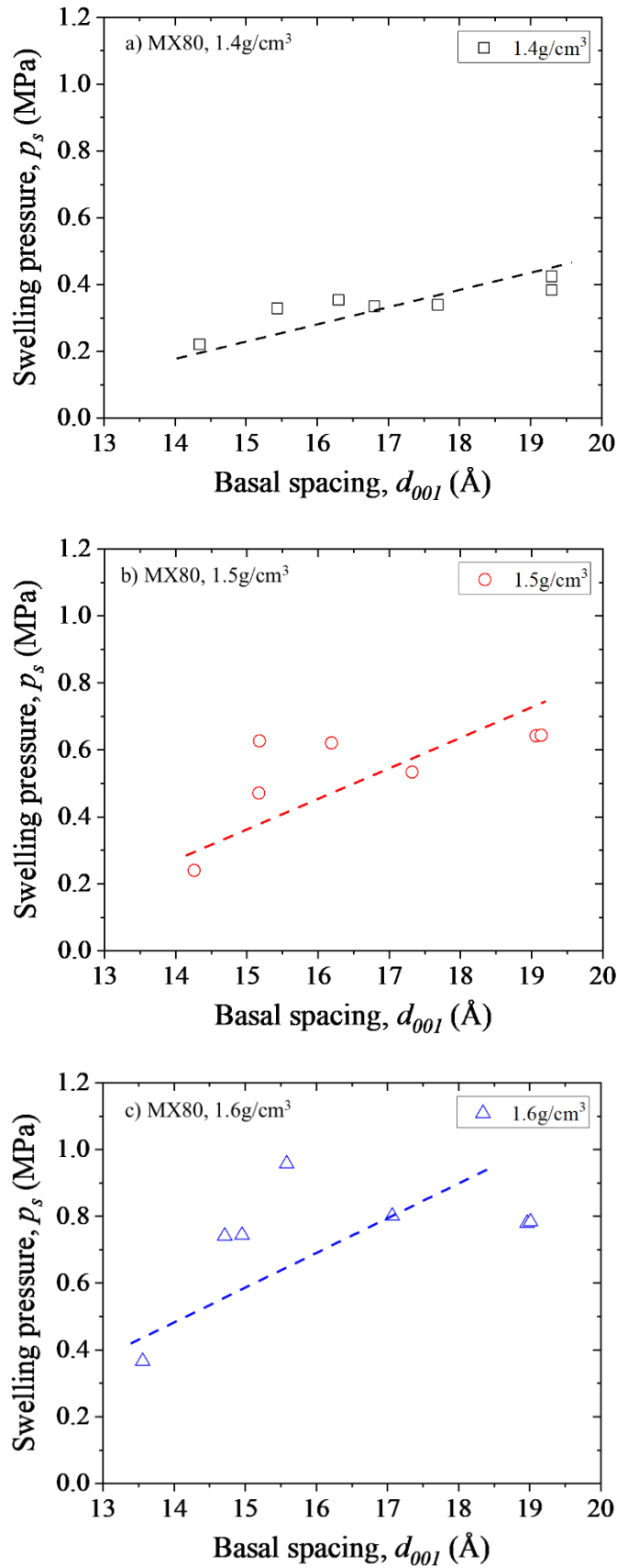


**Figure 5-32 Basal spacing changing with swelling pressure of different dry densities MX80**

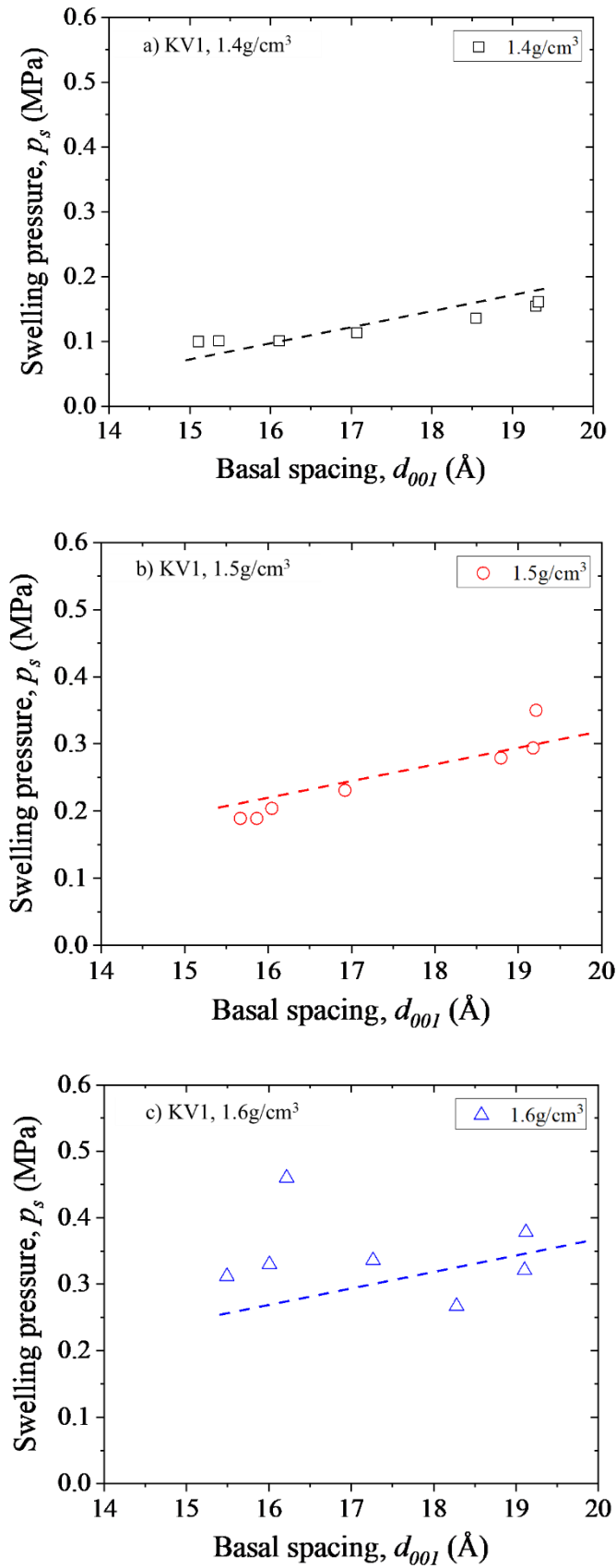


**Figure 5-33 Basal spacing changing with swelling pressure of different dry densities KV1**

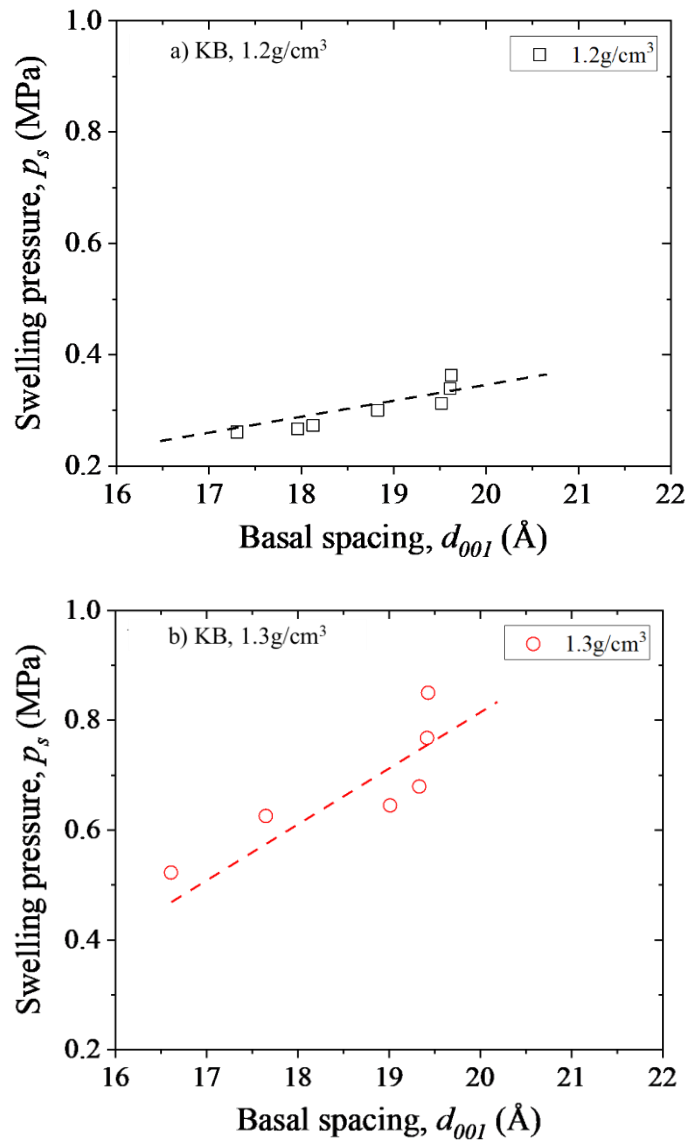


**Figure 5-34 Basal spacing changing with swelling pressure of different dry densities KB**

swelling pressure of different bentonites during saturation in this study. As we can see from Fig. 5-32, 5-33 and 5-34, for all three bentonites at different dry densities, swelling pressure generally increases with increasing basal spacing. Figure 5-35 shows the montmorillonite evolutions during saturation. As we can see from Fig. 5-35, the saturation process can be considered to a process of gradual differentiation of grains into aggregates and particles (Musso et al. 2013; Romero 2013). In the unsaturated stage, the back stress from the grains dominates the detection of swelling pressure (Fig. 5-35,

Stage 1). Growing basal spacing from the entering of water molecules into inter-layer space would give grains increasing back stress to each other. In the constant volume condition, bigger back stress from the grains gives greater measured swelling pressure. This may be the reason that swelling pressure increases with the rise of basal spacing during wetting process.

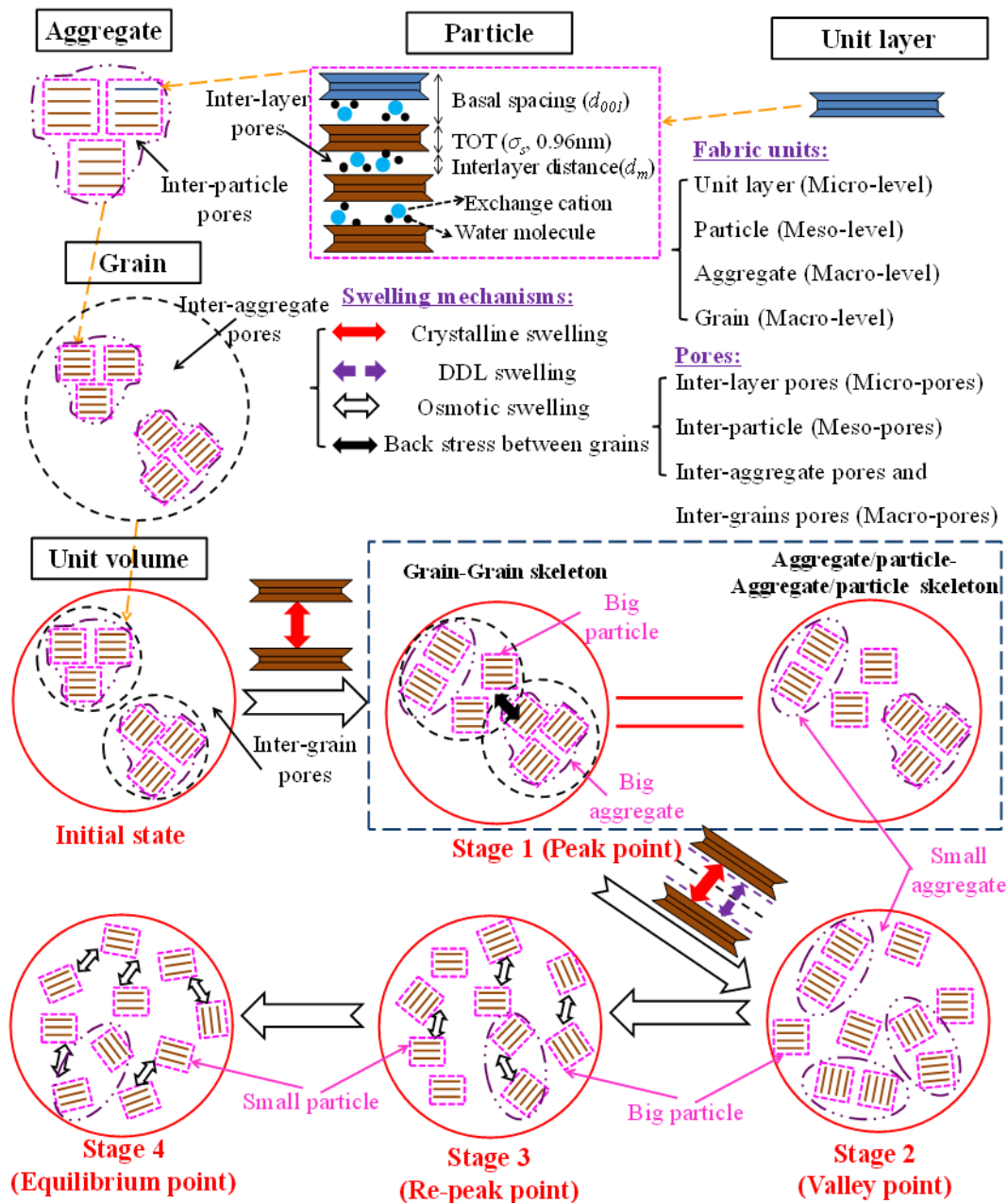
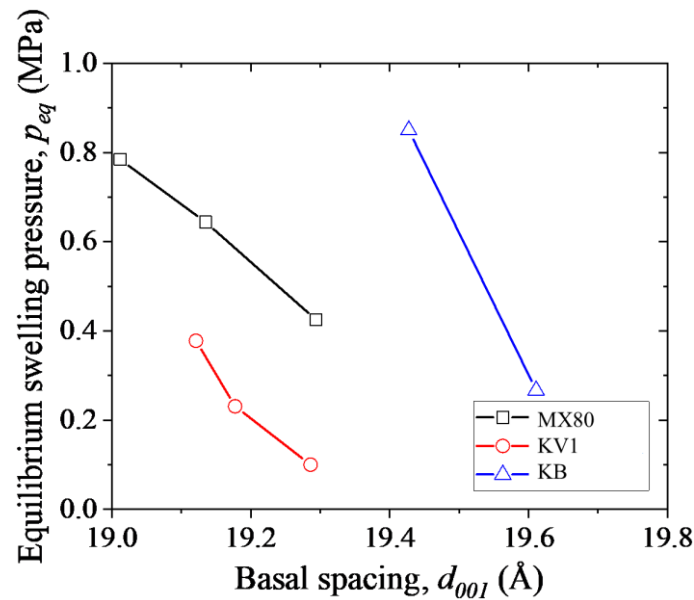
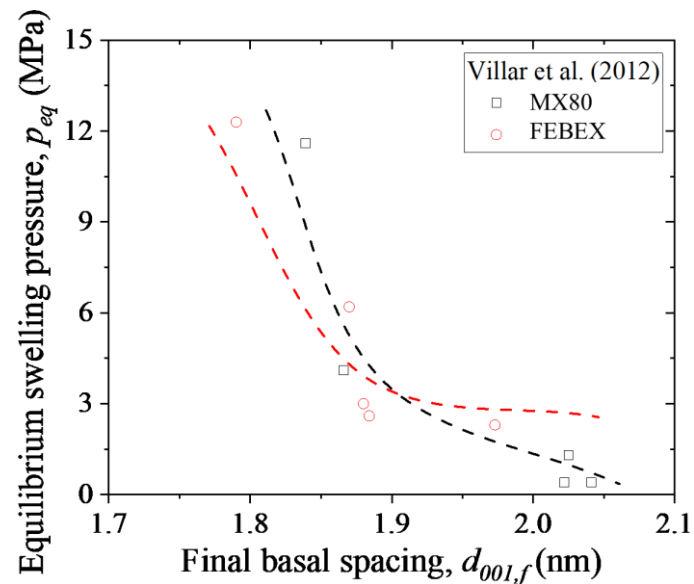


Figure 5-35 Schematic showing montmorillonite fabric units evolution during saturation

For saturated compacted bentonites, larger final basal spacing is generally assumed accompanying smaller equilibrium swelling pressure from testing studies (e.g., Villar et al. 2012). Figure 5-36 shows equilibrium swelling pressures changing with final basal spacings for MX80, KV1 and KB in this study, respectively. Figure 5-37



**Figure 5-36 Final Basal spacing changing with equilibrium swelling pressure of bentonites**



**Figure 5-37 Final basal spacing changing with equilibrium swelling pressure from Villar et al. (2012)**

presents testing equilibrium swelling pressures changing with final basal spacings for MX80 and FEBEX bentonites from Villar et al. (2012). It is apparently from Fig. 5-36 and 5-37, equilibrium swelling pressure decreases with the increase of final basal spacing. After specimen is fully saturated, it was assumed that the force between layers dominates the specimen instead of the force between the grains. Bigger basal spacing would lead to smaller repulsive between unit layers (Komine and Ogata 2004; Tripathy et al. 2004), thereby inducing decreasing measured swelling pressure.

As Fig. 5-17 presents, hydraulic conductivity during saturation decreases with the increase of dry density. It can be interpreted from the micropore and macropore as introduced before. As discussed in Chapter 4, the macropore was assumed as the water flowing path. Figure 5-38 shows the micropore and macropore for bentonite at different dry densities. Although the small basal spacing occupies the smaller micropore in the case of high dry density, the macropore actually becomes smaller due to the existences of more unit layers, furthermore leading smaller hydraulic conductivity.

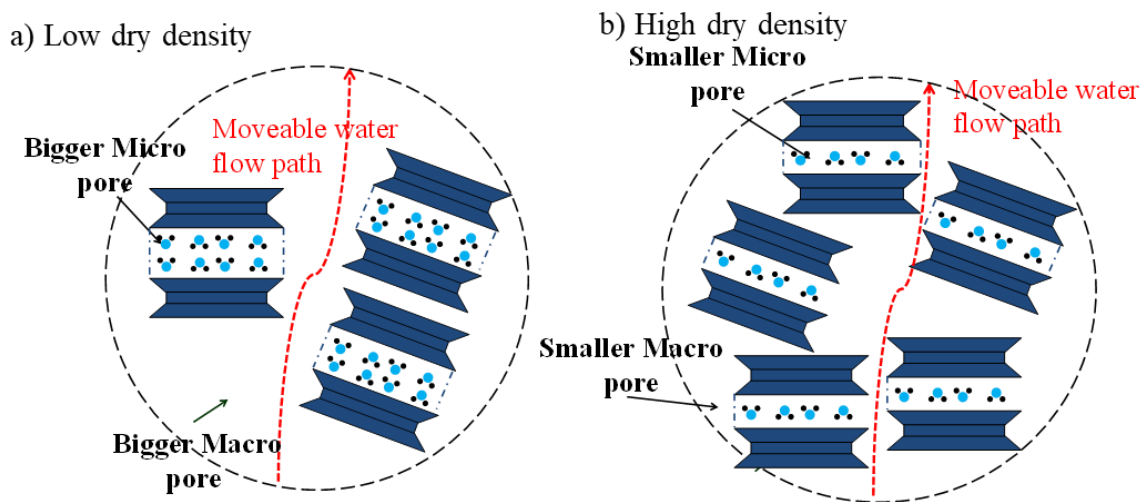


**Figure 5-38 Micropore and Macropore for bentonite at different dry densities**

## Conclusion

Three dry densities for bentonites were adopted to investigate the effect of dry density on swelling pressure, hydraulic properties and basal spacing during saturation. The results from the testing observations can be concluded as:

1. Swelling pressures of bentonites during saturation increases with the increase of dry density;
2. Water diffusivities of bentonites increase as dry density rises. Hydraulic conductivity decreases with the increasing dry density;
3. Final basal spacing decreases with increasing dry density.

## Reference

- Agus, S. S., and Schanz, T., 2008. A method for predicting swelling pressure of compacted bentonites. *Acta Geotechnica*, **3**: 125-137.
- Karnland, O., Nilsson, U., Weber, H., Wersin, P., 2008. Sealing ability of Wyoming bentonite pellets foreseen as buffer material-laboratory results. *Physics and Chemistry of the Earth. Parts A/B/C*, **33**: S472–S475.
- Maeda, M., Tanai, K., Ito, M., Mihara, M. and Tanaka, M. 1998. Mechanical properties of the Ca exchanged and Ca bentonite: swelling pressure, hydraulic conductivity, compressive strength and elastic modulus. Technical Report, Japan Nuclear Cycle Development Institute, PNC-TN8410 98-021 (in Japanese). <https://jopss.jaea.go.jp/pdfdata/PNC-TN8410-98-021.pdf>
- Musso, G., Romero, E., and Della, V.G. 2013. Double-structure effects on the chemo-hydro-mechanical behaviour of a compacted active clay. *Géotechnique*, **63**(3): 206–220.
- Holmboe, M., Wold, S., and Jonsson, M. 2012. Porosity investigation of compacted bentonite using XRD profile modeling. *Journal of Contaminant Hydrology*, **128**: 19–32.
- JNC 1999. Technical reliability of the geological disposal for high-level radioactive waste in Japan - geological disposal research and development Second compiled – General report. Japan Nuclear Cycle Development Institute, JNC TN1400 99-020. (in Japanese) <https://www.jaea.go.jp/04/tisou/houkokusyo/dai2jitoimatome.html>  
(Accessed 8 Feb. 2022)
- Komine, H., and Ogata, N. 2004. Prediction swelling characteristics of bentonites. *Journal of Geotechnical and Geoenvironmental Engineering*, **130**(8): 818–829.
- Romero, E., 2013. A microstructural insight into compacted clayey soils and their

hydraulic properties. *Engineering Geology*, **165**: 3–19.

Suzuki, H., Shibata, M., Yamagata, J., Hirose, I. and Terakado, K 1992. Mechanical experiments of buffer material. Technical Report, Japan Nuclear Cycle Development Institute, PNC-TN8410 92-057 (in Japanese). <https://jopss.jaea.go.jp/pdfdata/PNC-TN8410-92-057.pdf>

Takeuchi, S., Hara, K., and Nakano, M., 1995. Water retention curve, water diffusivity and water movement of compacted bentonite. *Soils and Foundations*, **35 (3)**: 129–137. (in Japanese).

Tripathy, S., Sridharan, A., and Schanz, T. 2004. Swelling pressures of compacted bentonites from diffuse double layer theory. *Canadian Geotechnical Journal*, **41**: 437–450.

Villar, M.V., Espina, R.G., and Nebot, L.G. 2012. Basal spacings of smectite in compacted bentonite. *Applied clay science*, **(65-66)**: 95-105.

Wang, H.L., Shirakawabe, T., Komine, H., Ito, D., Gotoh, T., Ichikawa, Y., and Chen, Q., 2020. Movement of water in compacted bentonite and its relation with swelling pressure. *Canadian Geotechnical Journal*, **57(6)**: 921–932.

Wang, H.L., Komine, H., and Gotoh, T. 2021. A swelling pressure cell for X-ray diffraction test. *Géotechnique*, in press. <https://doi.org/10.1680/jgeot.20.00005>

# Chapter 6

**THE EFFECT OF  $\text{Na}^+$  CONCENTRATION ON  
HYDRAULIC PROPERTIES AND SWELLING  
PRESSURE OF BENTONITE WITH XRD**

## 6.1 Testing overview

The device used in this chapter is shown in Fig. 6-1. As we can see from Fig. 6-1, this is a traditional swelling apparatus, in which the vertical and lateral displacement of compacted specimen in the metal mold was constrained.

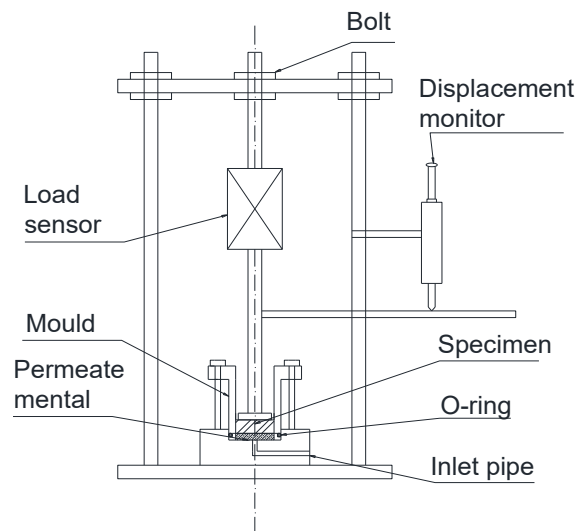


**Figure 6-1 Traditional swelling pressure apparatus**

During swelling pressure test, the stress from specimen was measured by the upper load sensor and recorded by the data logger. In this study, the metal mould was changed to the multi-ring as introduced above in chapter 3. Air dried bentonite powders were putted into the multi-ring mold and compressed in the static load device to achieve the height of  $\sim 11$ mm, the diameter of 28mm (Fig. 6-2) and the target dry density of  $1.65 \text{ g/cm}^3$ , respectively. The specimen details were listed in Table 6-1. And another outer O-ring was (Fig. 6-2) placed in the outer side of the multi-ring to avoid the evaporation of specimen and movement of multi-ring during tests. Additionally, another separate serial test (same conditions as swelling tests) was carried to measure the electrical conductivity (EC) of soil water. Their soil waters were extracted by the ASTM (D 4542-85). Electrical conductivities of soil waters were measured at once after the extraction of soil water.

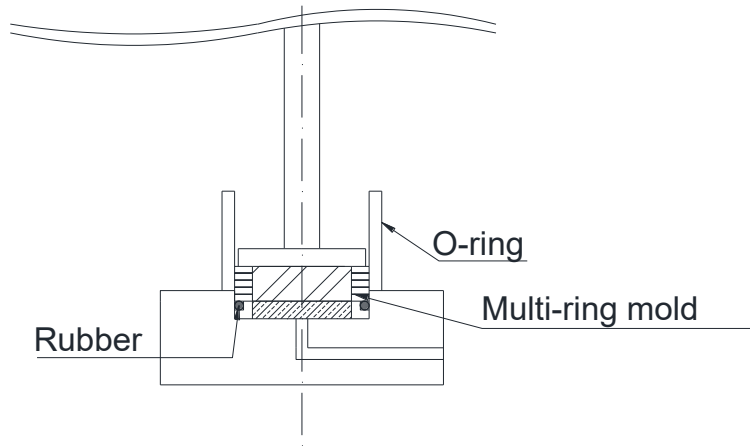


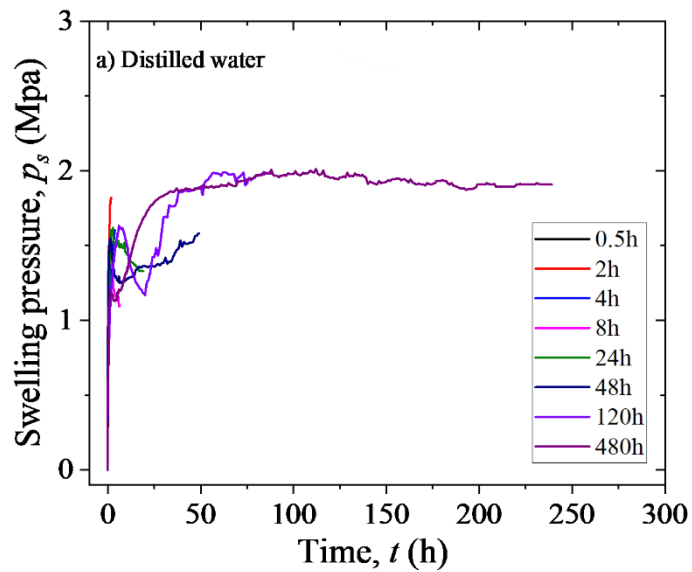
**Figure 6-2 Multi-ring mold applied in traditional swelling pressure apparatus**

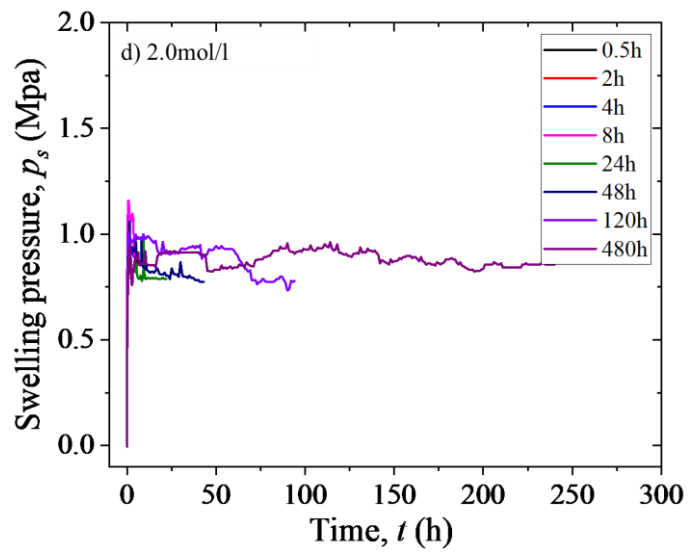
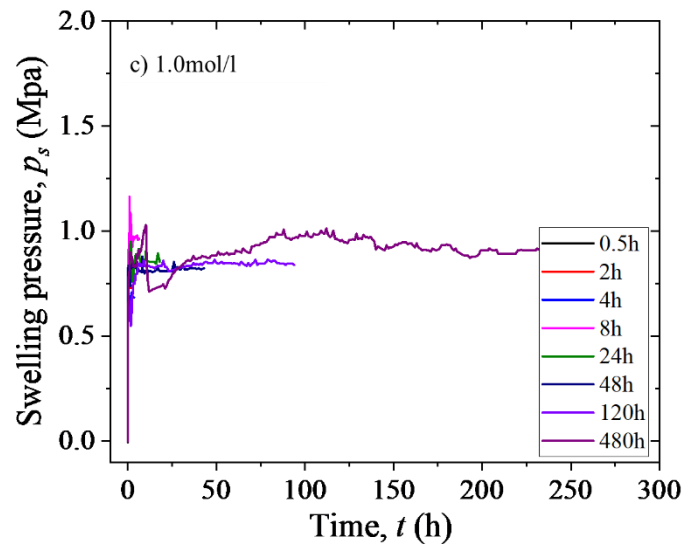
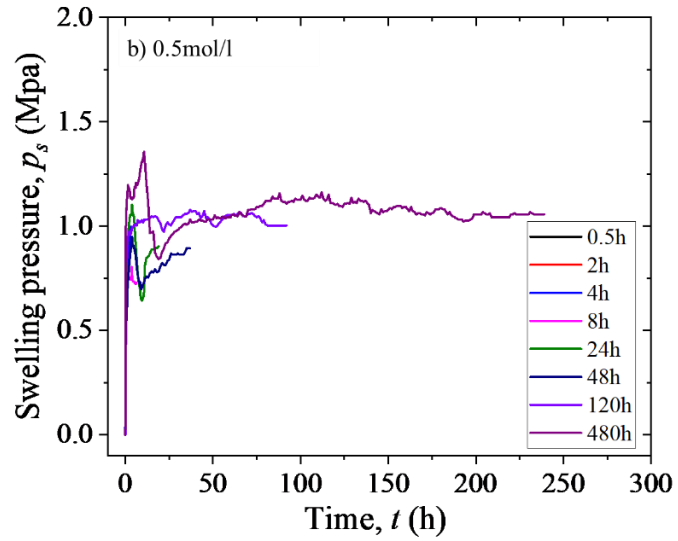
**Table 6-1 Specimen details**

Material	Dry density (g/cm <sup>3</sup> )	Saturation liquid
KV1	1.65	Distilled water, 0.5mol/l NaCl, 1.0 mol/l NaCl and 2.0 mol/l NaCl

## 6.2 Results

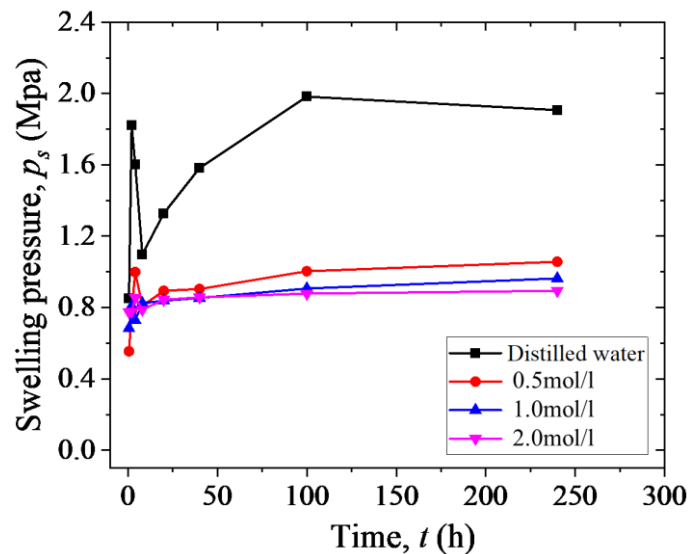
### 6.2.1 Swelling pressure





**Figure 6-3 Swelling pressure evolution curves for KV1 bentonite saturated by different concentrations NaCl solutions**

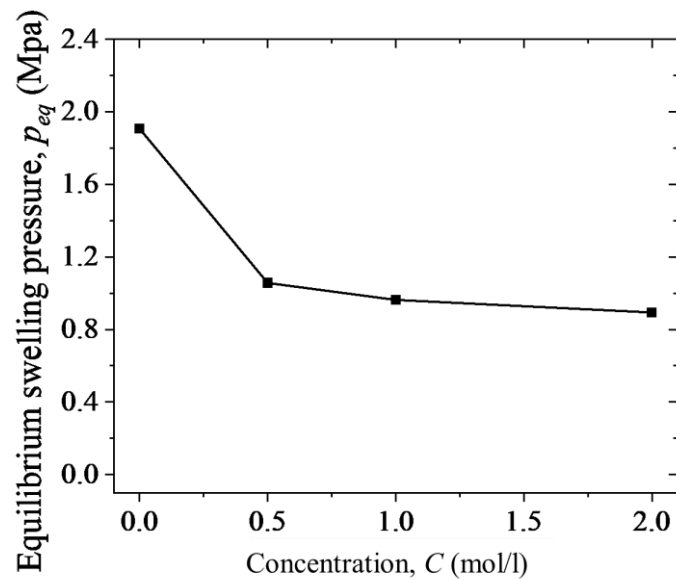
Figure 6-3 shows the developments of swelling pressures saturated by different solutions (distilled water, 0.5 mol/l NaCl, 1.0 mol/l NaCl and 2.0 mol/l NaCl). As can be seen from Fig. 6-3, for all the solutions, swelling pressures increase very rapidly at the beginning of swelling. After these fast developments, drops of swelling pressures happen. Then, drops of swelling pressures would recover in a several hours duration, and stable rises of swelling pressures follow. At last, swelling pressures stay in a relative constant value for a long time. This phenomenon is similar as the swelling pressure evolution pattern as distilled water introduced above in chapter 4. Figure 6-3 also reveals that, durations for the initial quick increase of swelling pressures vary with solutions. Distilled water for ~8 hours, 0.5 mol/l NaCl for ~5 hours, 1.0 mol/l NaCl for ~2.5 hours and 2.0 mol/l NaCl for ~1 hour. Thus, with the increase of concentration, the time needed for arriving the initial quick decreases.



**Figure 6-4 Swelling pressure changing with wetting duration saturated by different concentration NaCl solutions**

Figure 6-4 presents the swelling pressures saturated by different solutions at different wetting durations. It can be easily found from Fig. 6-4 that, swelling pressure reduces when saturation liquid changed from distilled water to NaCl solutions at same wetting

duration. Meanwhile, swelling pressure decreases as the increasing concentration when they were wetted for same durations.

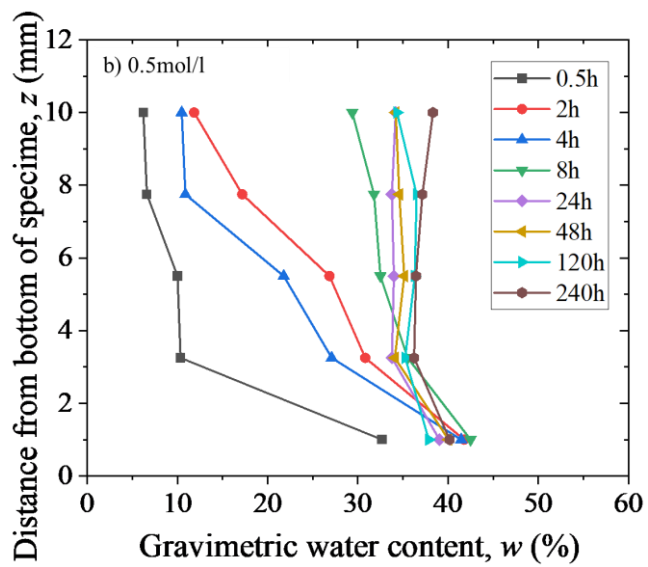
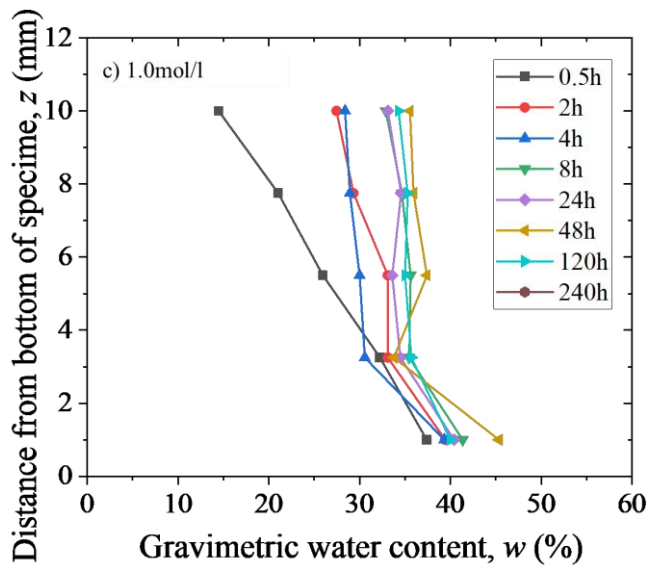
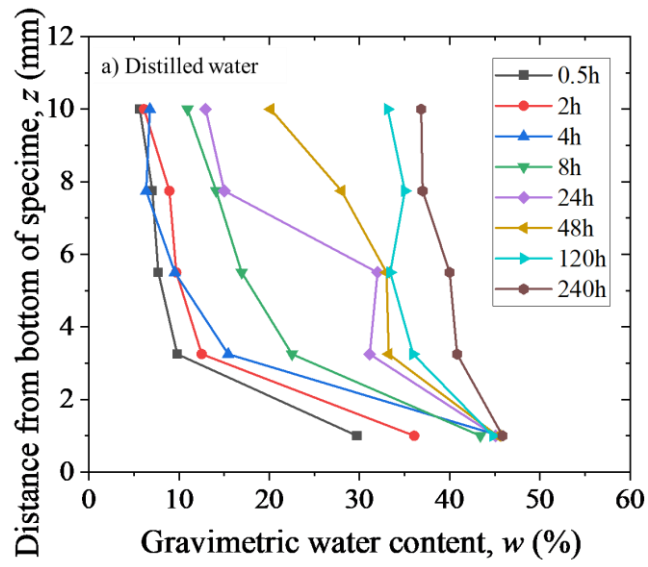


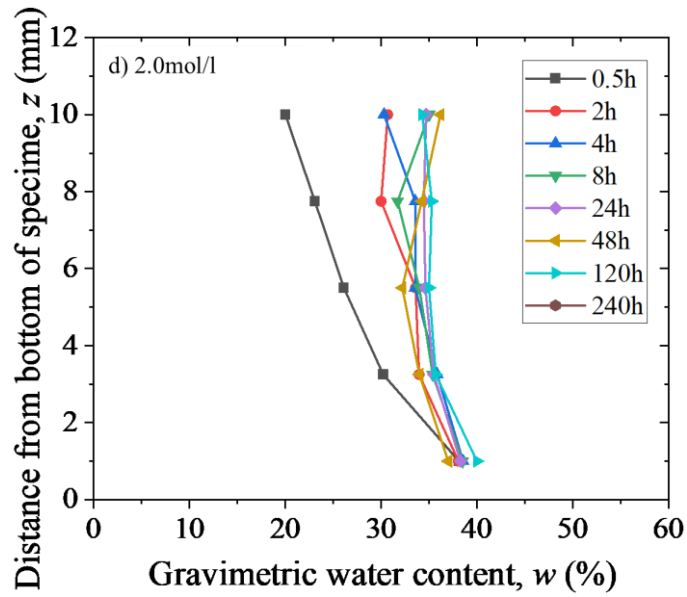
**Figure 6-5 Equilibrium swelling pressure changing with concentration of NaCl solution**

Figure 6-5 indicates equilibrium swelling pressure changing with the concentration of NaCl solution. It is apparent from Fig. 6-5, equilibrium swelling pressure reduces with the increase of concentration. Similar conclusion was draw by Lee et al. (2012), Zhu et al. (2013) and Sun et al. (2015).

### 6.2.2 Water diffusivity

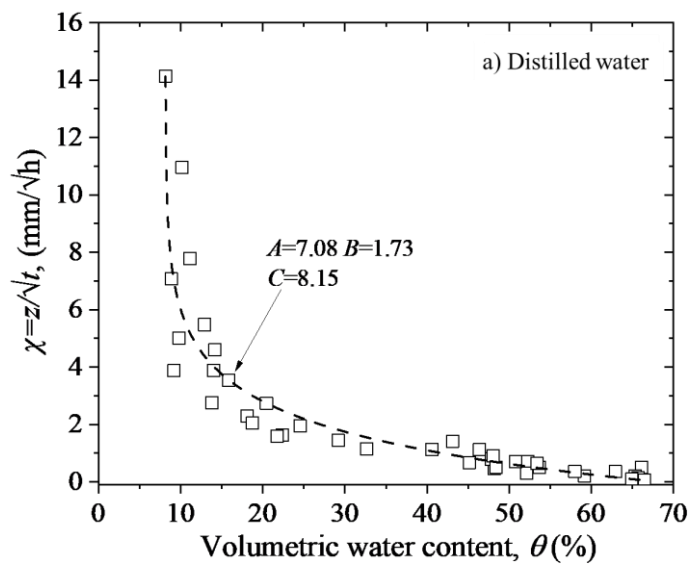
Figure 6-6 shows gravimetric water content changing with position saturated by NaCl solutions with different solution. It can be found from Fig. 6-6 that, gravimetric water content increases as distance from bottom of specimen grows, when the wetting duration is short. With the process of wetting duration, gravimetric water contents generally go towards stable values.





**Figure 6-6 Gravimetric water content changing with position saturated by NaCl solutions with different concentration**

Times needed for gravimetric water contents to reach relative stable values change with the concentration of solution. These times seem to decrease with increasing concentration, as: distilled water (~120h), 0.5 mol/l NaCl (24h), 1.0 mol/l NaCl (4h) and 2.0 mol/l NaCl (2h).



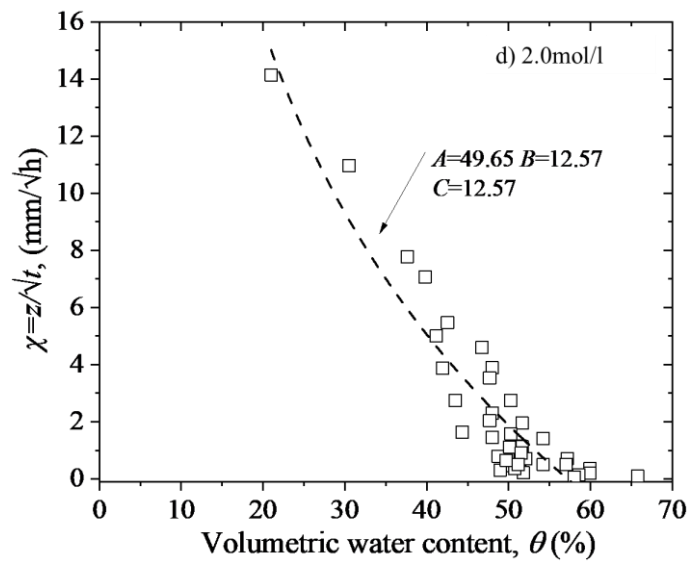
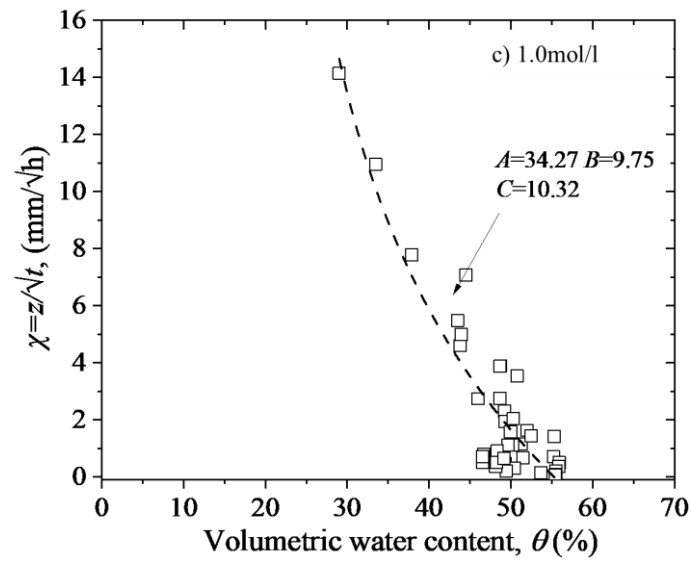
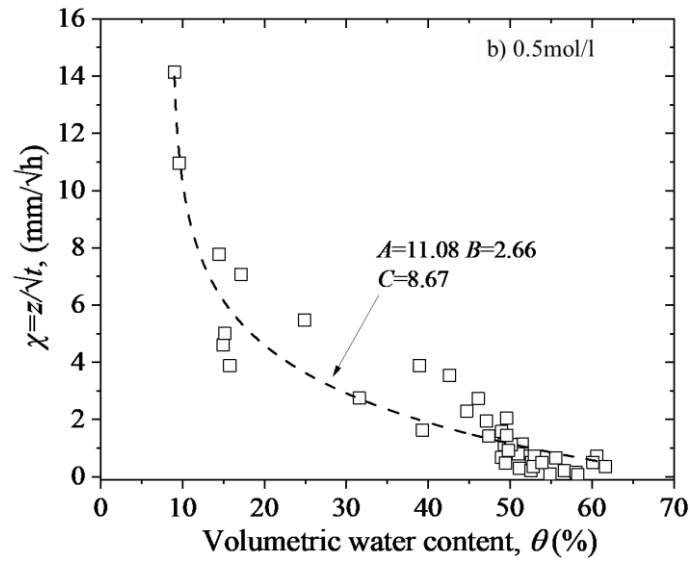
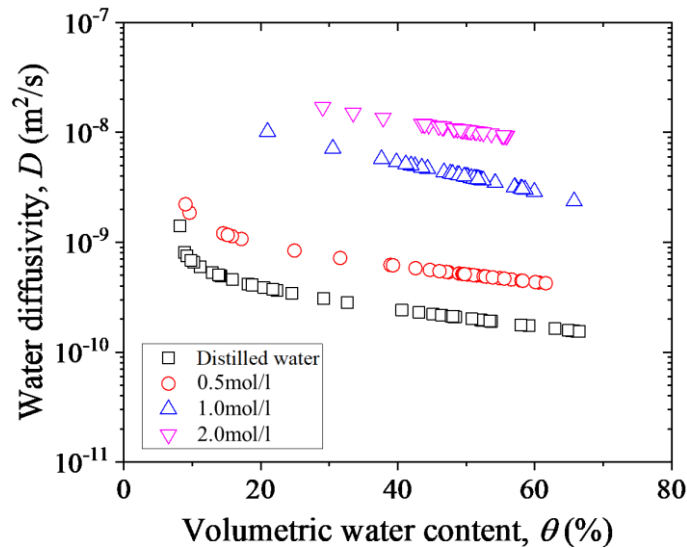


Figure 6-7 Relation between  $\theta$  and  $\chi$  of specimen saturated by NaCl solutions

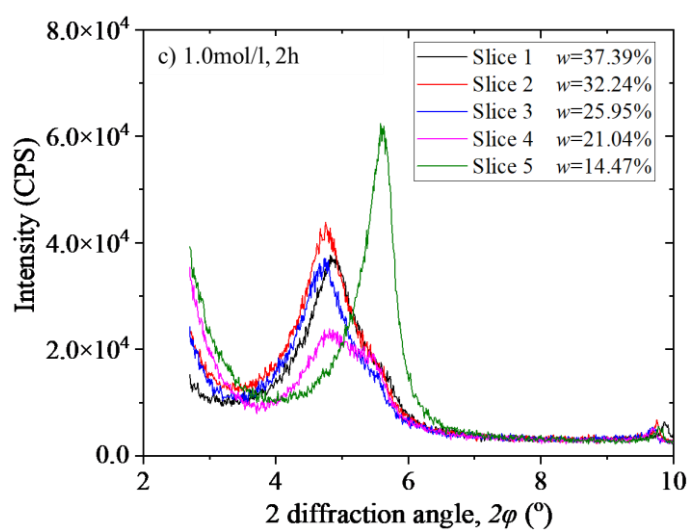
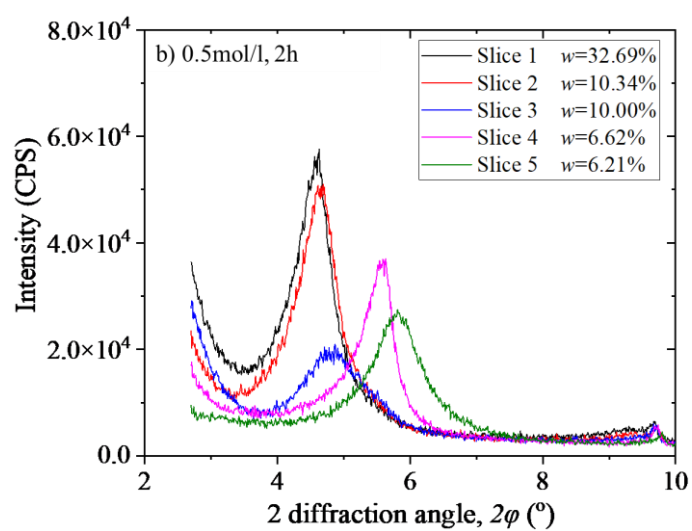
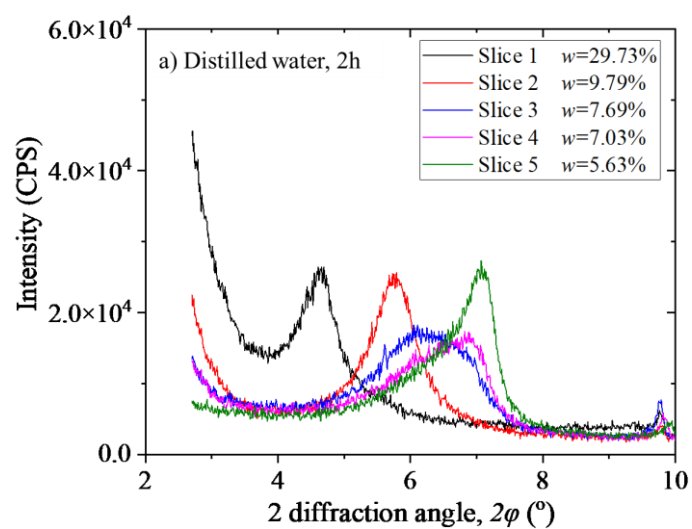
The determination of water diffusivity was followed as introduced in Chapter 4. Thus, it is necessary to check the relation between  $\chi$  and  $\theta$ . Relations between  $\chi$  and  $\theta$  for KV1 bentonite saturated by NaCl solution with different concentrations are presented in Fig. 6-7. As indicated in Fig. 6-7, for distilled water and 0.5 mol/l NaCl, the testing database preforms well with the fitting lines. However, in cases of 1.0 mol/l NaCl and 2.0 mol/l NaCl, the fitting lines just generally follow the fitting lines. This phenomenon can be contributed to the experimental device. As we can see from Fig. 6-2, the gap between outer ring and multi-ring may give an extra tunnel for the water to go into the specimen, thereby inducing the greater measured gravimetric water content.



**Figure 6-8 Water diffusivity changing with NaCl solution concentration**

Water diffusivity changing with NaCl solution concentration are revealed in Fig. 6-8. It is a generally truth as Fig. 6-8 that, water diffusivity decreases with the increase of volumetric water content, which is consistent with the former observations. Meanwhile, it is apparently from Fig. 6-8, when the volumetric water contents are the same, water diffusivity increases with rising concentration. This phenomenon may because of the increasing osmotic suction as concentration rises.

### 6.2.3 XRD results



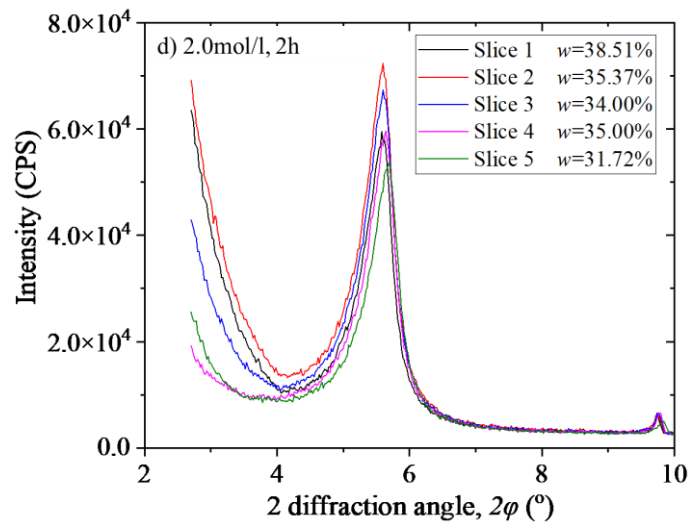
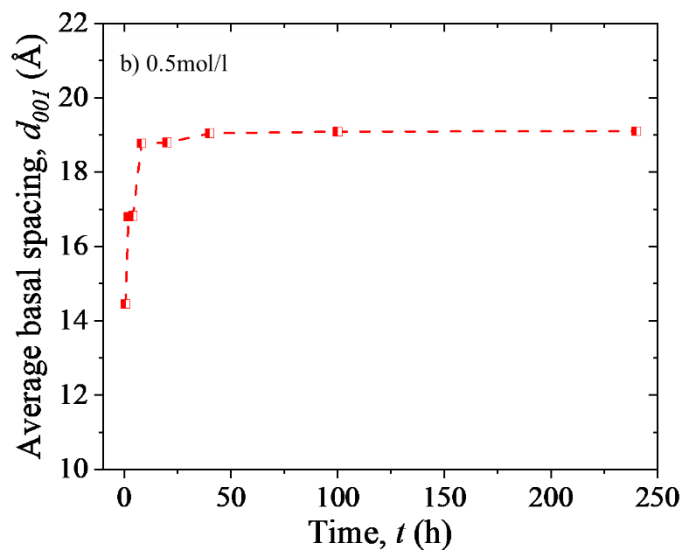
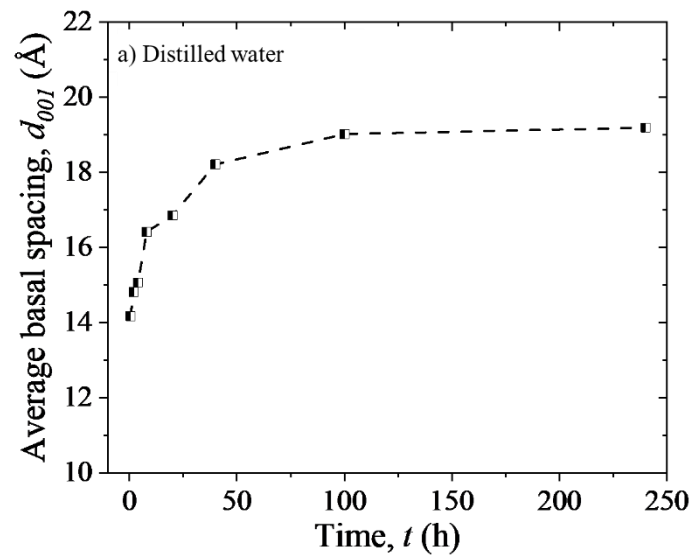
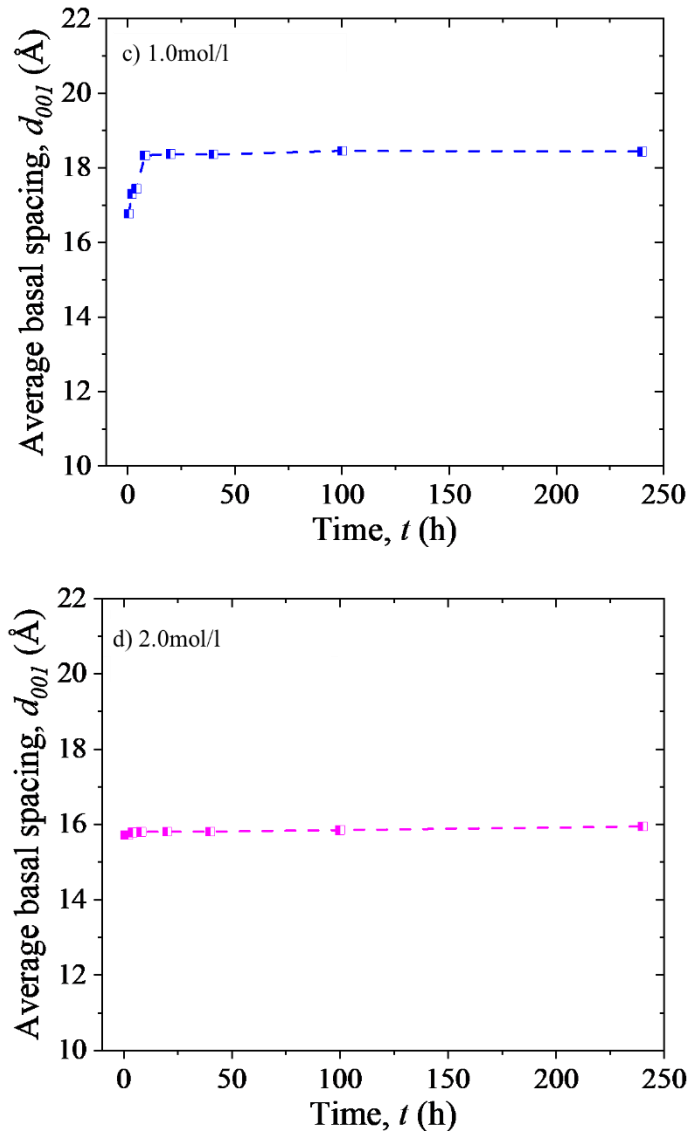


Figure 6-9 Some XRD profiles for KV1 saturated by NaCl solutions





**Figure 6-10 Average basal spacing for KV1 saturated by NaCl solutions**

XRD profiles for KV1 bentonite saturated by NaCl solutions when wetting duration is 2h are presented in Fig. 6-9. As we can see, as slice changes from No. 1-5, water content decreases. At the same time, it seems that, with the increase of concentration, the average water content of 5 slices rises. Regarding the peak angle, the peak angle moves to right as slice change from slice 1 to slice 5. Changing another word, the peak angel moves to left as water content increases.

Figure 6-10 reveals the average basal spacing of KV1 bentonite saturated by NaCl solutions. It can be seen that, in general, average basal spacing of slices increases

quickly in the beginning wetting durations. Then, basal spacing stays in relative stable value. Meanwhile, it might be concluded from Fig. 6-10, the increasing speed of basal spacing in the beginning wetting duration rises with the increase of concentration.

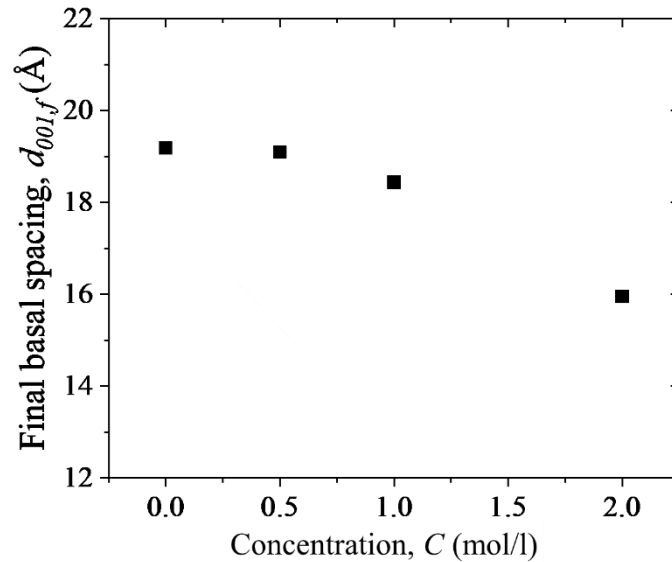


**Figure 6-11 Final basal spacing changing with NaCl concentration**

Figure 6-11 shows final basal spacing (when  $t=240h$ ) of KV1 bentonite changing with NaCl concentration. An easy conclusion can be found from Fig. 6-11 that, final basal spacing decreases with the increase of concentration.

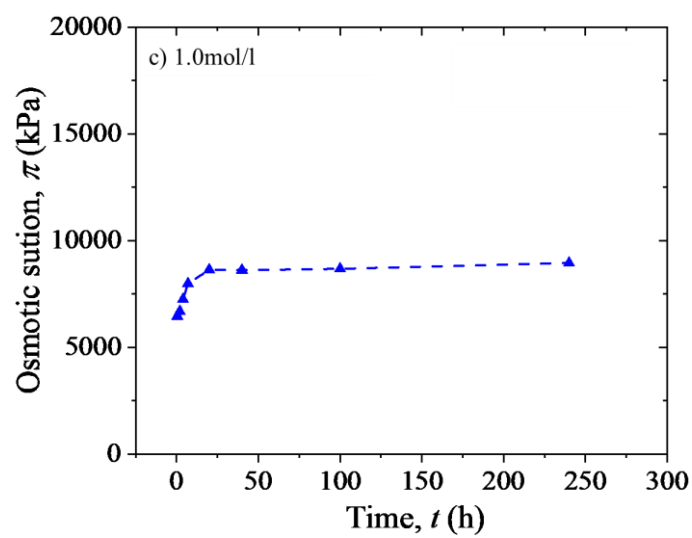
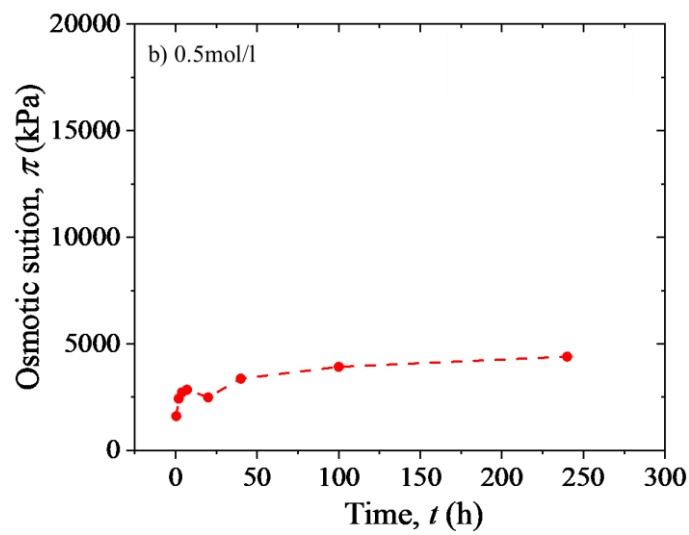
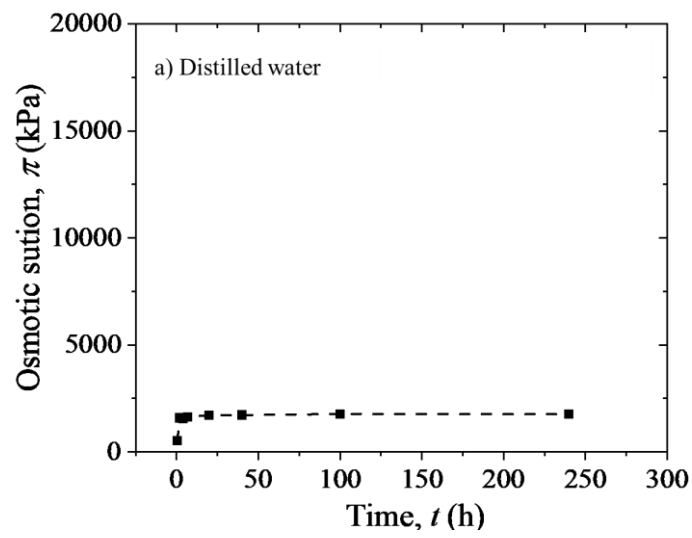
#### 6.2.4 Osmotic suction

The osmotic suction induced in the soil specimens were experimentally measured by the USAD (1954) method. This method relates the osmotic suctions to the electrical conductivities of soil water, as the following:

$$\pi = 31.92(EC_2^{1.074} - EC_1^{1.074}) \quad (6-1)$$

where  $\Delta\pi$  is the osmotic suction, kPa;  $EC_2$  is the electrical conductivity of soil water, mS/cm;  $EC_1=0.65$  mS/cm (Rao et al. 2006). Osmotic suction of soil waters at different wetting durations are presented in Fig. 6-12. As can be seen from Fig. 6-12, osmotic suction increases with the evolution of wetting time. Figure 6-13 indicates the final

osmotic suction ( $t=240\text{h}$ ) changing with concentration. It is apparent from Fig. 6-13 that, final osmotic suction increases with rising concentration.



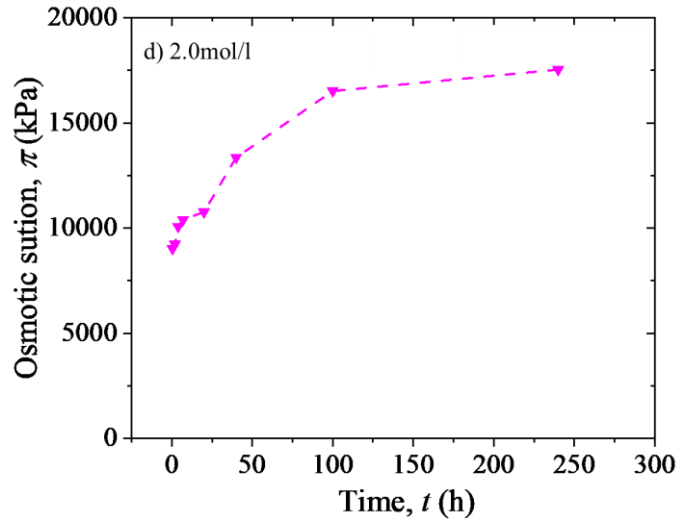


**Figure 6-12 Osmotic suction changing with time for specimen saturated by NaCl solutions**

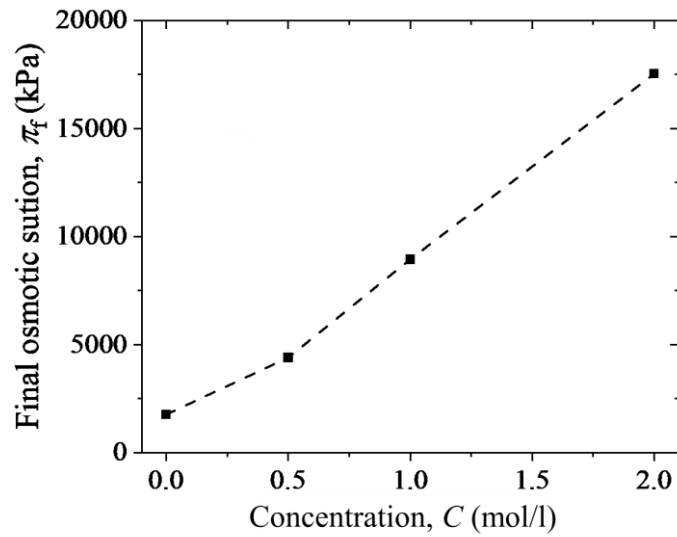
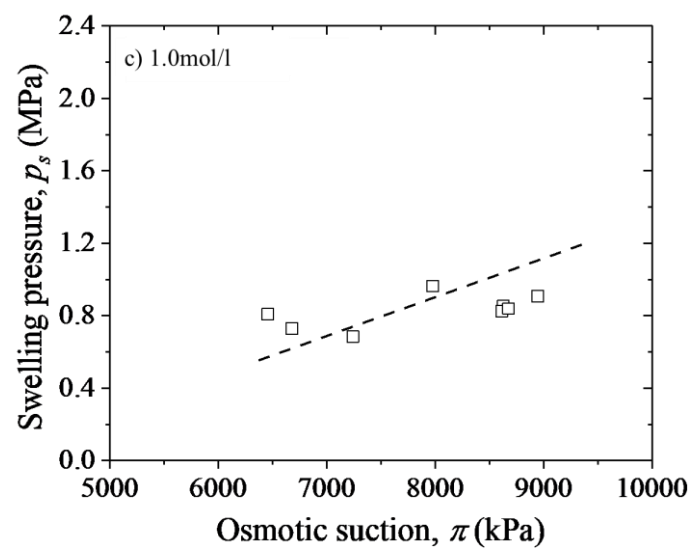
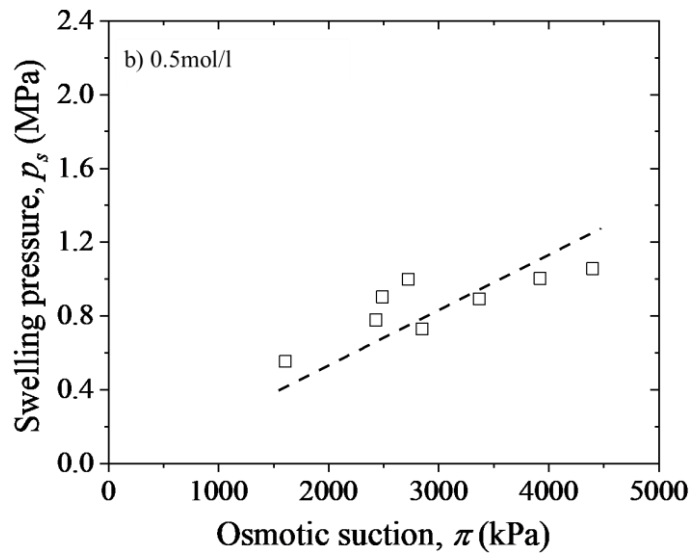
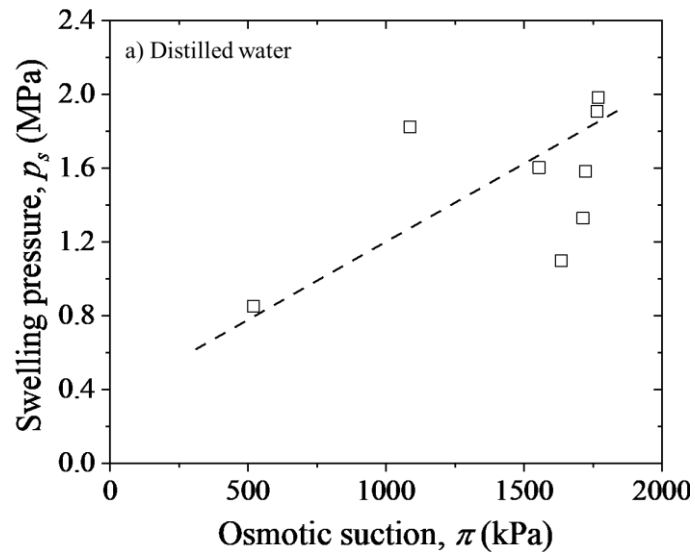


**Figure 6-13 Final osmotic suction changing with concentration**

### 6.3 Discussion

#### 6.3.1 Relation between osmotic suctions and swelling pressures

The relationship between swelling pressure and osmotic suction during saturation process is shown in Fig. 6-14. As can be seen from Fig. 6-14 that, swelling pressure increases with the increasing osmotic suction for specimen during hydration.



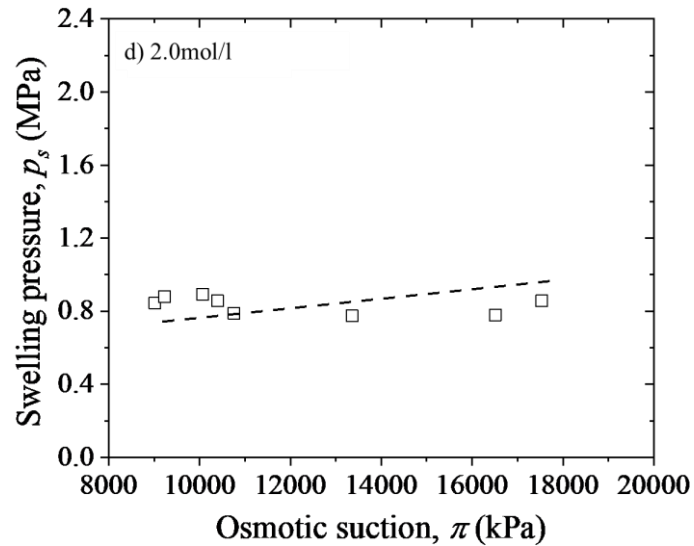


**Figure 6-14 Osmotic suction changing with swelling pressure during saturation**

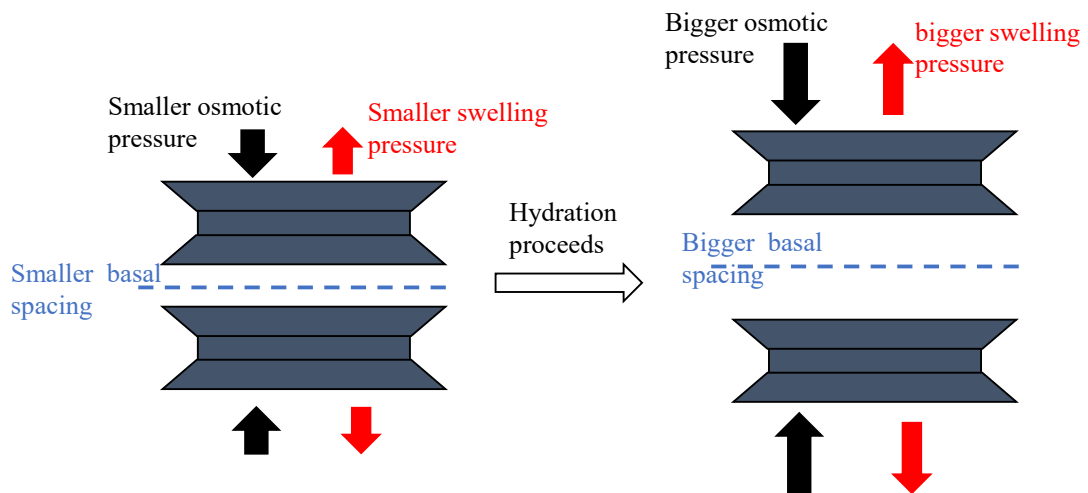


**Figure 6-15 Swelling pressure and osmotic pressure evolution during saturation**

During saturation process, the increase of swelling pressure induced by the rise of basal spacing (as introduced in Chapter 5) conquers the decrease of swelling pressure triggered by the increase of osmotic pressure (Fig. 6-15). Therefore, the swelling pressure exhibits an increasing curve.

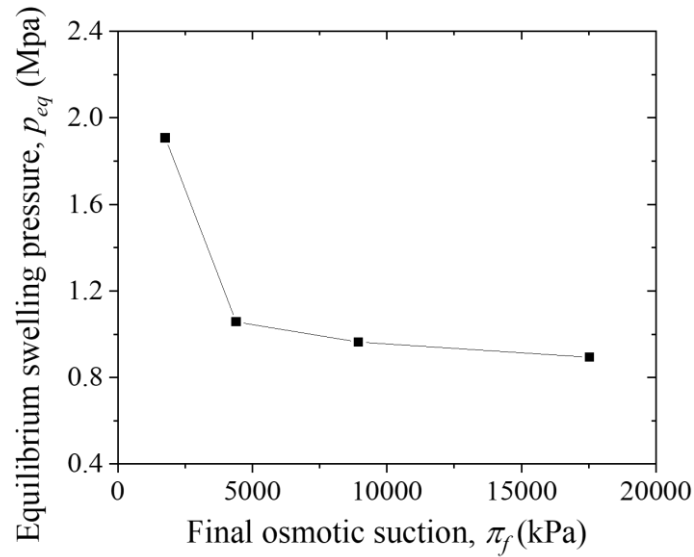


**Figure 6-16 Final osmotic suction changing with equilibrium swelling pressure**

Figure 6-16 indicates the relationship between equilibrium swelling pressure and final osmotic suction. As can be seen from Fig. 6-16, equilibrium swelling pressure decrease with the increasing osmotic suction, agrees with the conclusions by Rao and Thyagaraj. (2007) and Musso et al. (2013) for saturated specimen and disagrees with the phenomenon for unsaturated specimen as mentioned above. Osmotic suction would lead to the osmotic consolidation of compacted bentonite, thereby resulting in the drop of equilibrium swelling pressure (Castellanos et al. 2008).

## Conclusions

NaCl solutions with different concentrations were used as saturation liquids for researching the concentration effect on sodium type bentonite swelling pressure, water diffusivity and basal spacing during saturation process. The results can be concluded as:

1. Swelling pressure during saturation decreases with the increase of NaCl concentration;
2. Water diffusivity increases as the concentration rises.

## Reference

- ASTM. 1985. Standard test method for pore water extraction and determination of soluble salt content by refractometer, D 4542- 85. Philadelphia, PA: American Society for Testing and Materials.
- Castellanos, E., Villar, M.V., Romero, E., Lloret, A., and Gens, A., 2008. Chemical impact on the hydro-mechanical behaviour of high-density FEBEX bentonite. *Physics and Chemistry of the earth*, **33**: S516-S526.
- Lee, O.L., Lim, J.G., Kang, I.M., and Kwon, S., 2012. Swelling pressures of compacted Ca-bentonite. *Engineering Geology*, **129-130**: 20-26.
- Musso, G., Romero, E., and Della, V.G., 2013. Double-structure effects on the chemo-hydro-mechanical behaviour of a compacted active clay. *Géotechnique*, **63(3)**: 206–220.
- Rao, S.M., Thyagaraj, T., and Thomas, H.R., 2006. Swelling of compacted clay under osmotic gradients. *Géotechnique*, **55(10)**: 707–713.
- Rao, S.M., and Thyagaraj, T., 2007. Swell-compression behaviour of compacted clays under chemical gradients. *Canadian Geotechnical Journal*, **44**: 520-532.
- Sun, D.A., Zhang, L., Li, J., and Zhang, B.C. 2015. Evolution and prediction of the swelling pressures of GMZ bentonites saturated with saline solution. *Applied Clay Science*, **105-106**: 207–216.
- USDA. 1954. Diagenesis and improvement of saline and alkali soils, Agriculture Handbook No. 60. Madison, Wisconsin: United States Salinity Laboratory.
- Zhu, C. M., Ye, W. M., Chen, Y. G., Chen, B., and Cui, Y. J. 2013. Influence of salt solutions on the swelling pressure and hydraulic conductivity of compacted GMZ01 bentonite. *Engineering Geology*, **166**: 74–80.

# Chapter 7

## **THE EFFECT OF $\text{Na}^+$ CONCENTRATION ON MOVEMENT OF WATER AND SALTS IN BENTONITES WITH XRD**

## 7.1 Testing overview

This chapter used MX80 and KV1 bentonites. Meanwhile, the multi-ring (Fig. 3-6) was applied in a simple confined wetting device (Fig. 7-1). In each bentonite, twelve specimens were prepared for dismantling times of 1-3840 h. Specimen details are presented in Table 7-1.

After different wetting durations, water supply was terminated. Then, multi-ring and specimen were taken out and vertical deformation was constrained by a clip immediately (Fig. 7-2 (a)). Later, two-piece rings were removed one by one and specimen was carefully sliced from the tiny gap between mold rings into five slices using a thin saw ( $\sim 0.20$  mm thickness, Fig. 7-2 (a)). Afterwards, slices were sealed immediately using a Para film (Fig. 7-2 (a)). For achieving uniformly water distribution in slices under constrained condition, slices were sandwiched by two wooden boards, whose vertical deformation was restricted by bolts (Fig. 7-2 (b)), as soon as possible. Then, these combinations were placed at room temperature ( $20^{\circ}\text{C}$ ) for at least 48 h. Subsequently, slices were taken to XRD tests. A diffractometer, RINT-UltimaIII (Rigaku Corp., Japan), with Cu  $K\alpha$  source was employed and the X-ray scan range was  $2.7^{\circ}$ - $10^{\circ}$  with a scan speed of  $20^{\circ}/\text{min}$  under Bragg-Brentano geometry. A relative fast scanning speed was chosen in order to minimize the possible specimen rebound and water evaporation during scanning. Finally, water content of each slice was measured.

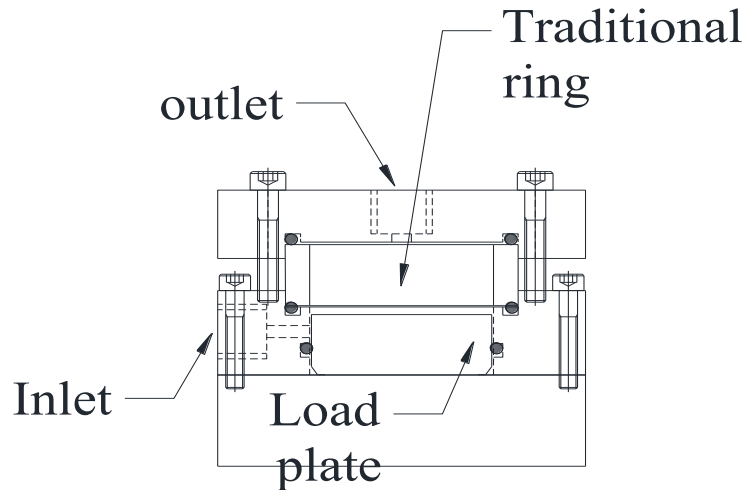


Figure 7-1 Scheme showing wetting device

Table 7-1 Specimens details

	Target dry density (g/cm <sup>3</sup> )	Concentration of NaCl (mol/l)	Initial gravimetric water content (%)	Dismantling time (h)
KV1	1.8	0.5, 1.0 and 2.0	8.27-8.46	1, 2, 4, 8, 24, 48, 120, 240, 480,
MX80	1.8	0.5, 1.0 and 2.0	8.92-8.99	960, 1920 and 3840

After oven dried and the measurement of water contents, slices were crushed and passed through a 0.25mm sieve. The method of making leaching liquid for Na<sup>+</sup> remained in soil was followed modified SL237-063-1999 as: ~1g (accurate to 1 mg) dried soil was put into 50ml telecentric tube, and 50ml distilled water was injected into telecentric tube. Hereafter, telecentric tubes were swayed in oscillator for 24h. Later, leachate and soil were distinguished by telecentric separator with a rotation speed of 5000r/min for 20min. Then, ~30ml clean leachate was carefully moved to another 50ml tube for obtaining Na<sup>+</sup> concentration. Measurement of Na<sup>+</sup> concentration in leachate was done by Rao et al. 2006 and Malusis et al. 2015 as: Na<sup>+</sup> concentration was calculated from the electrical conductivity ( $E_c$ ) of leachate. The concentration calculating equation was

followed by Malusis et al. 2015 and Sample-Lord et al, 2020 as:

$$c_b = 8.45 \times 10^{-5} \times E_c \quad (7-1)$$

where  $c_b$  represents the  $\text{Na}^+$  concentration in leachate (M or mol/L). Additionally,  $\text{Na}^+$  concentration in bentonite can be obtained by:

$$c_m = c_b \frac{1000}{m_s V_{l,w}} \quad (7-2)$$

where  $c_m$  is the  $\text{Na}^+$  concentration in bentonite specimen (M/g);  $V_{l,w}$  represents the volume of distilled water for making leachate (ml, ~50ml in this study); and  $m_s$  stands for the mass used for making leachate (g, ~1g in this study).

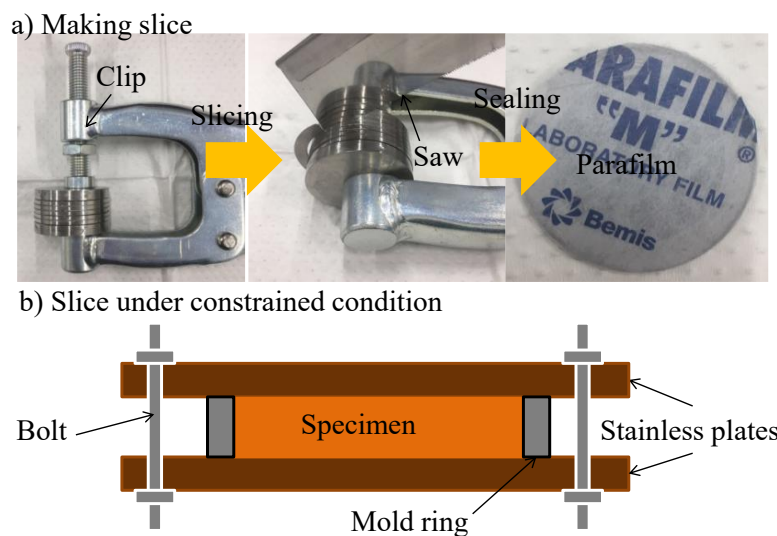


**Figure 7-2 Scheme showing making slices and XRD test**

## 7.2 Results

### 7.2.1 Movement of water

Gravimetric water contents of slices after different water absorption durations are presented in Fig. 7-3 and 7-4. It can be easily found from Fig. 7-3 and 7-4 that, gravimetric water content increases as the position close to the water supply ends in relative shorter saturation durations range. After ~ 480h, gravimetric water contents of slices in different positions at different durations tend to similar values.

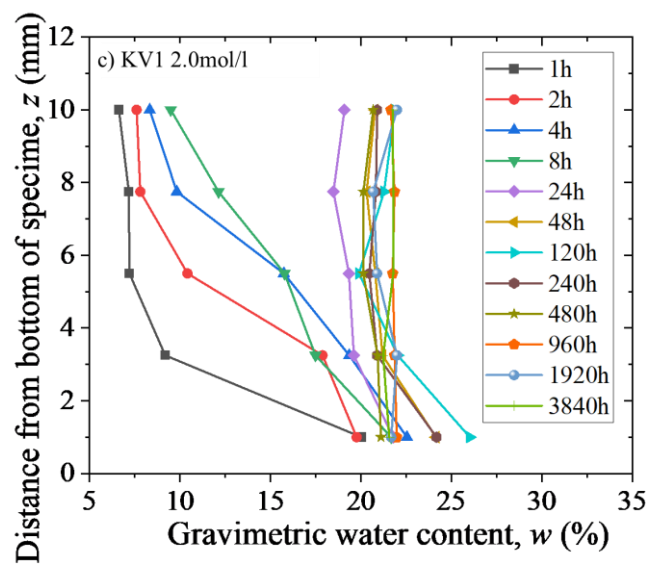
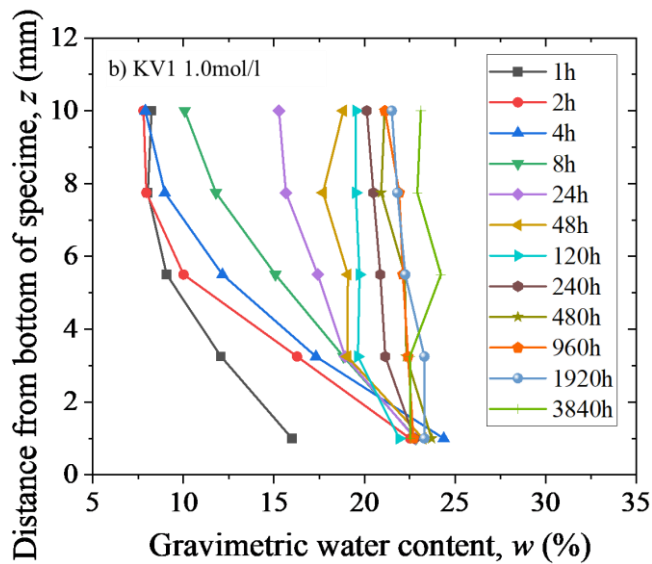
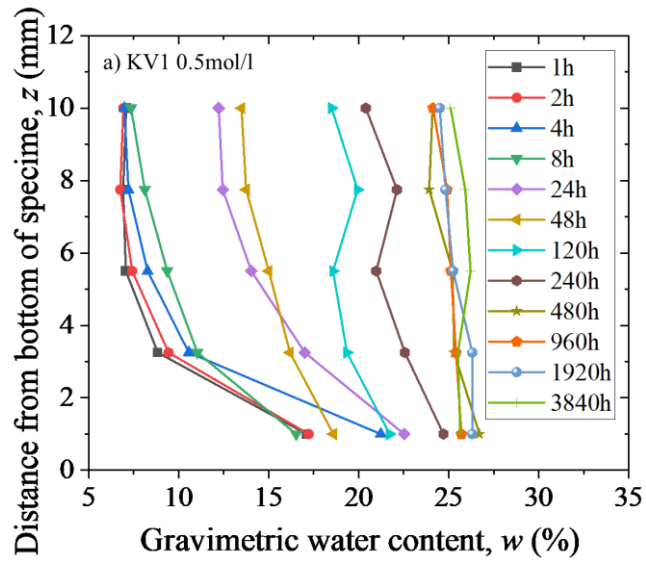


Figure 7-3 Gravimetric water contents of KV1 slices

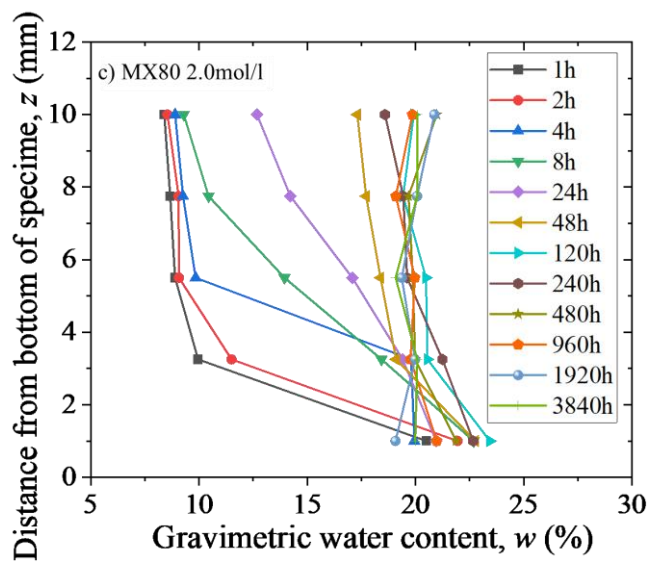
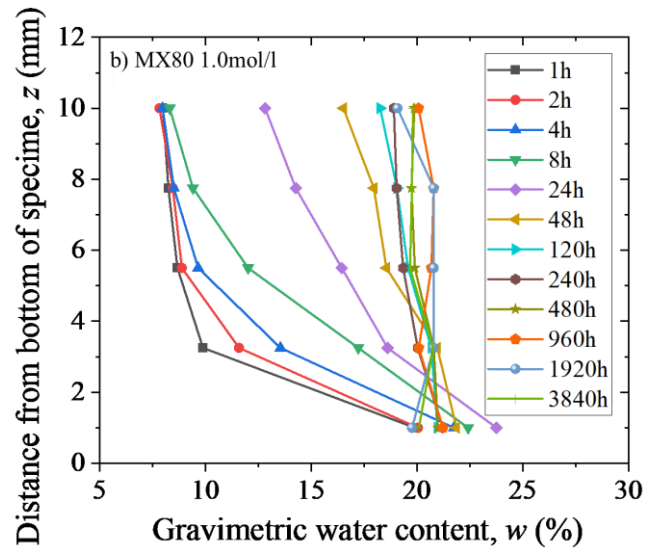
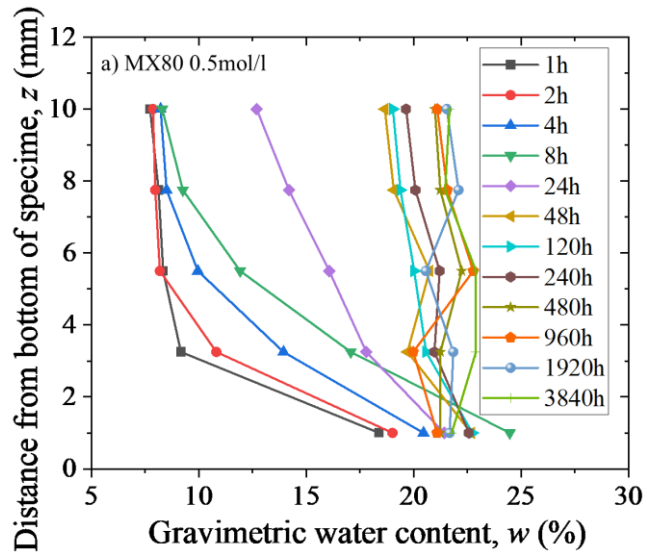


Figure 7-4 Gravimetric water contents of KV1 slices

Figure 7-5 and 7-6 indicates degree of saturation for bentonite specimen changing with wetting duration. By combining Figure 7-5 and 7-6, degree of saturation for different concentrations saturated bentonites are revealed in Fig. 7-7. As we can see from Fig. 7-7, for both KV1 and MX80, at the beginning of saturation, as the saturation liquid concentration increases, the degree of saturation becomes greater at the same saturation time. Meanwhile, Figure 7-7 shows that times for specimen reach saturated state (degree of saturation reaches and stays in relative stable value) varies with saturation liquid concentration. It can be easily concluded by Fig. 7-7, the time required to saturated state decreases with increasing concentration. This phenomenon may be due to the greater osmotic suction caused by the larger saturation liquid concentration. An interesting point can be indicted from Fig. 7-7 that, degree of saturation for different bentonites saturated by different concentration liquids all exceeds 100%. Similar phenomenon was reported by Komine (2018) and Wang et al. (2020). Wang et al. (2020) attributed degree of saturation  $> 100\%$  issue to the average water density in compacted bentonite  $> 1\text{g/cm}^3$ .

Additionally, it can be found from Fig. 7-7 that, the greater saturation liquid concentration induces smaller value of degree of saturation in saturated state. This may because of the issue for calculating degree of saturation. Generally used equation for obtaining degree of saturation can be given as:

$$S_r = \frac{wG_s}{e} \times 100\% \quad (7-3)$$

$$w = \frac{m_{wet} - m_{dry}}{m_{dry}} \times 100\% \quad (7-4)$$

where  $S_r$  is degree of saturation (%);  $e$  is the void ratio of specimen;  $G_s$  is the soil particle density;  $w$  is the gravimetric water content (%);  $m_{wet}$  is the wet mass for measuring dry density (g);  $m_{dry}$  is the oven dried mass for measuring dry density (g).

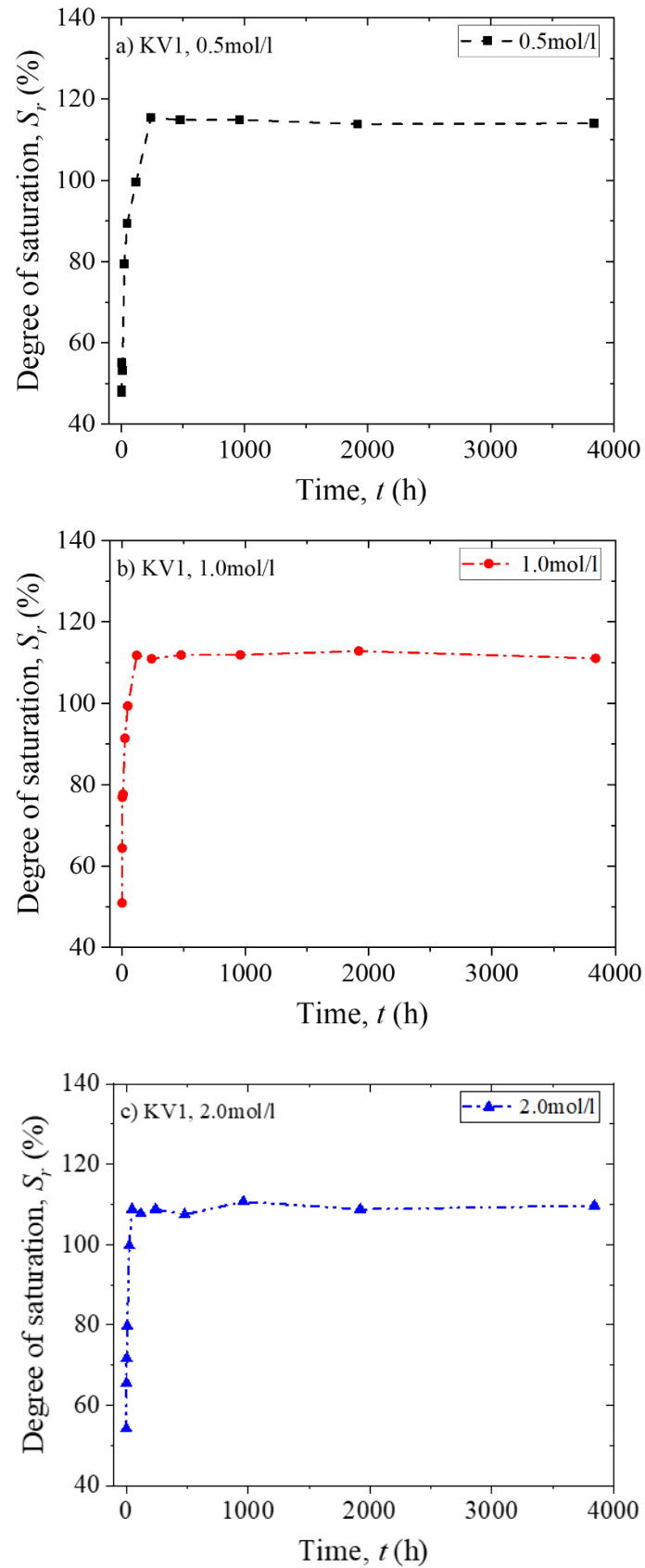


**Figure 7-5 Degree of saturation for KV1 specimen saturated by different NaCl solutions at different wetting durations**

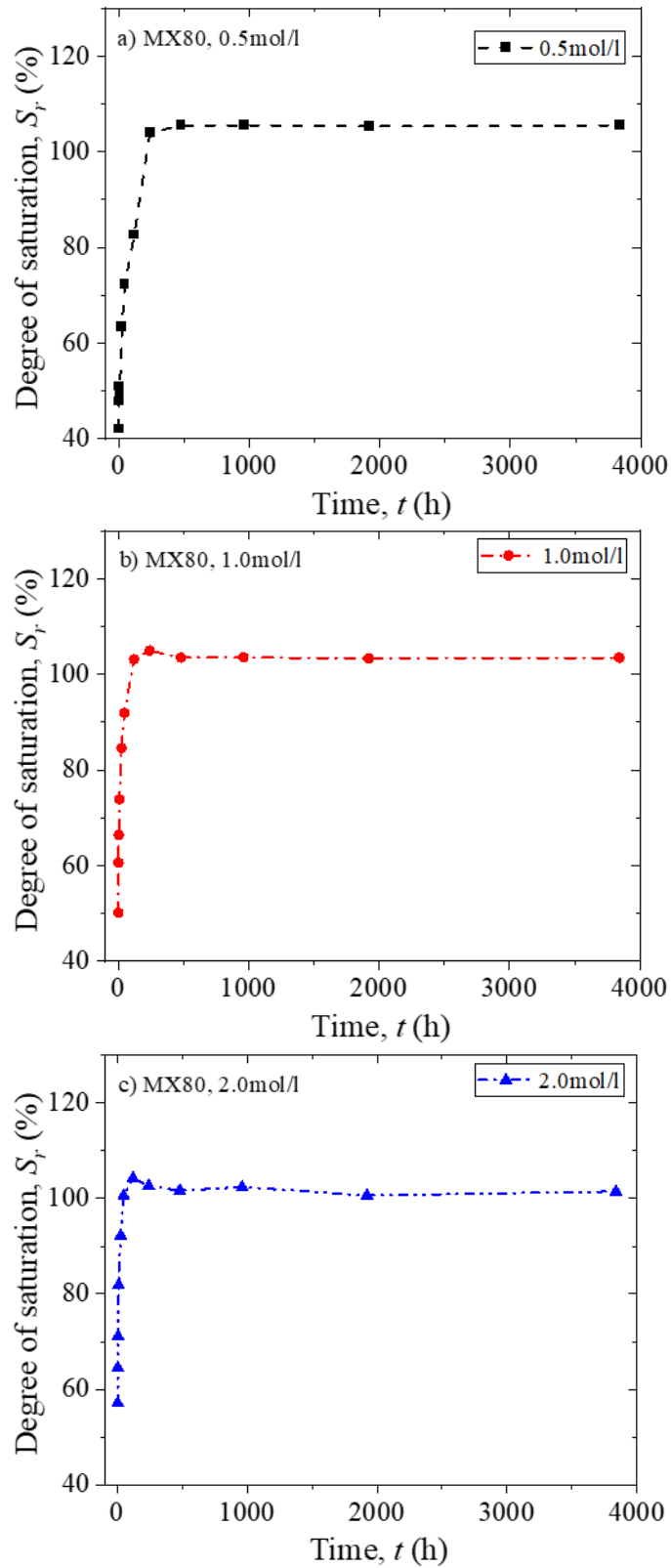


**Figure 7-6 Degree of saturation for MX80 specimen saturated by different NaCl solutions at different wetting durations**

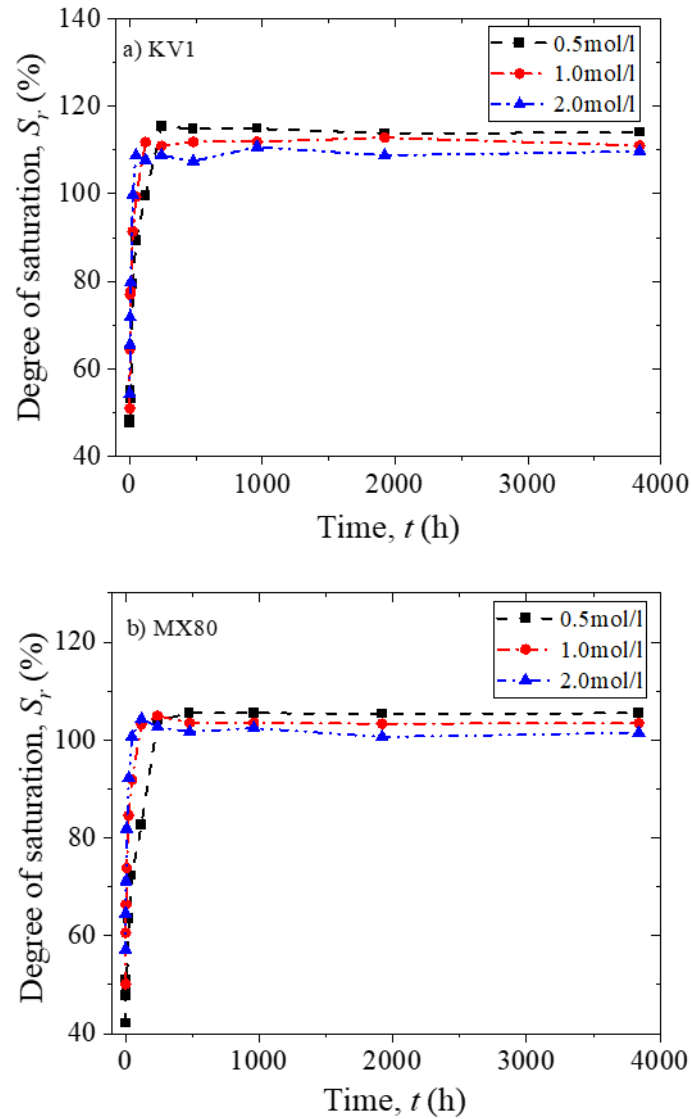


**Figure 7-7 Degree of saturation for different concentrations saturated bentonites**

In the saturated state, a higher concentration of saturation liquid would bring more solutes into specimen. After drying in the oven, these solutes still remain in the dried specimen, inducing a larger measurement value of  $m_{dry}$ . Larger  $m_{dry}$  value results in the smaller calculating value for  $w$ .  $e$  was assumed as the consistent for same dry density bentonite because no apparent deformation was observed during saturation. According to equation (7-3) and equation (7-4), same  $e$  and  $G_s$  with smaller  $w$ , leads to smaller  $S_r$ . The determination of water diffusivity was followed as introduced in Chapter 4. Thus, it is necessary to check the relation between  $\chi$  and  $\theta$ .

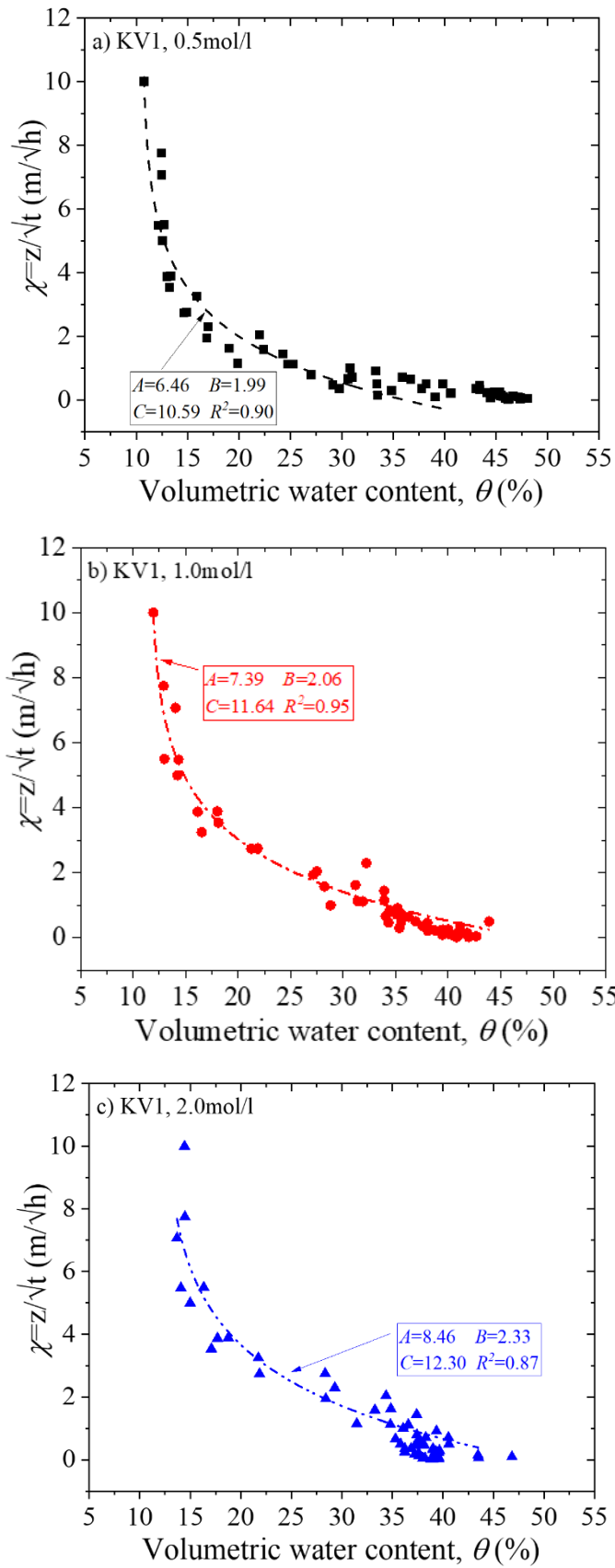


Figure 7-8 Relations between  $\chi$  and  $\theta$  for KV1 saturated by NaCl solutions

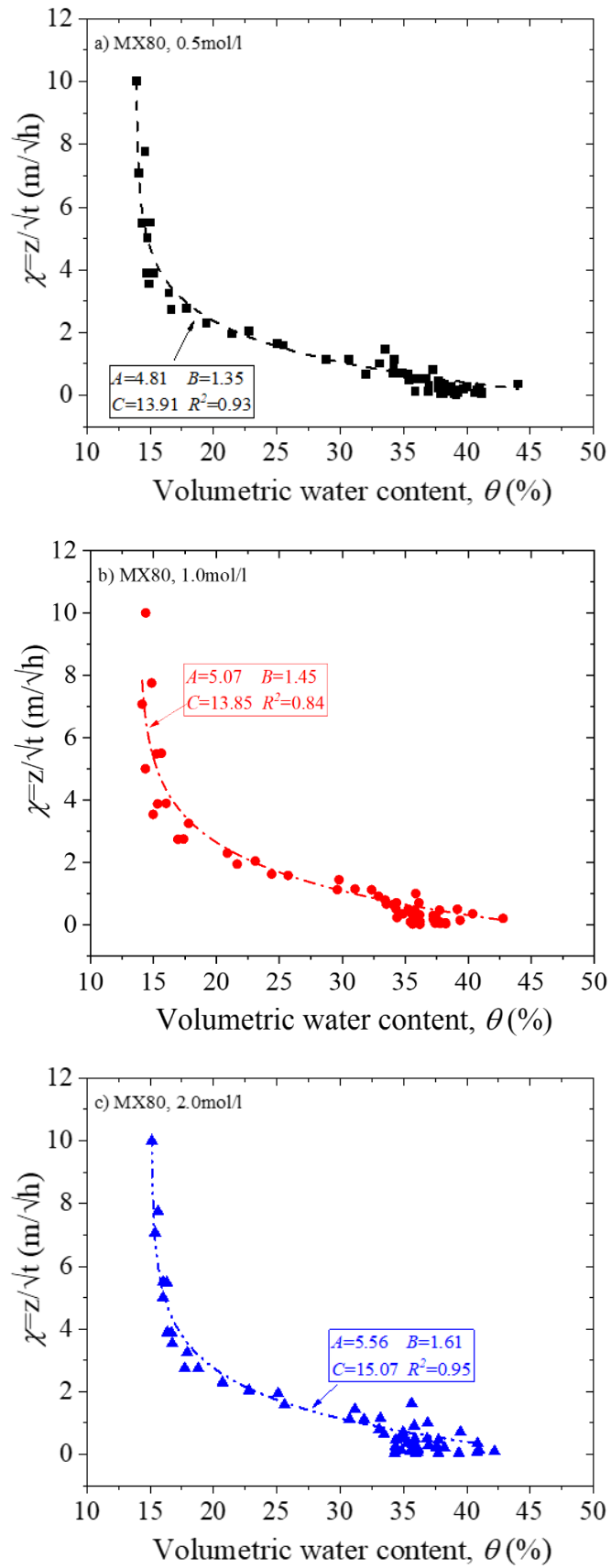
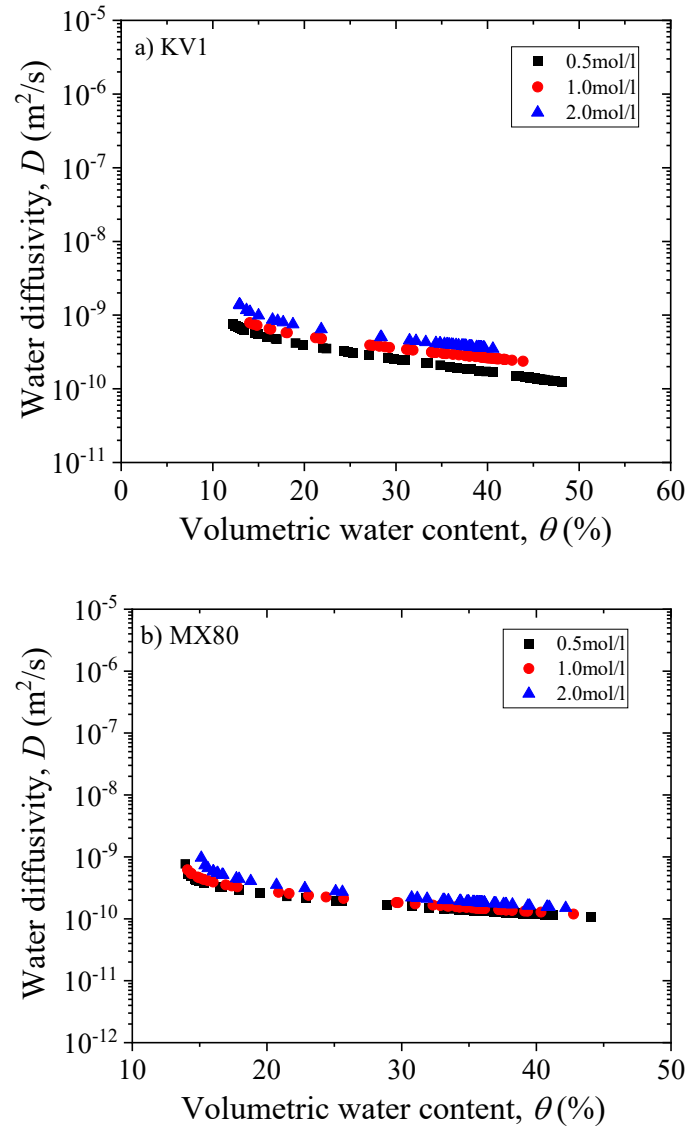


Figure 7-9 Relations between  $\chi$  and  $\theta$  for MX80 saturated by NaCl solutions

As indicated in Fig. 7-8 and 7-9, NaCl with different concentrations, the relations between  $\chi$  and  $\theta$  can agree with the fitting lines. Thus, the calculation can follow equation (4-5).



**Figure 7-10 Water diffusivity changing with volumetric water content for bentonites saturated by NaCl solutions**

Figure 7-10 depicts water diffusivity changes with the volumetric water content for NaCl saturated bentonites. A ready conclusion can be drawn from Fig. 7-10 that, for all bentonites, water diffusivity increases with rising saturation liquid concentration, which is consistent with the founding in chapter 6 for low dry densities ones.

### 7.2.2 Movement of Na<sup>+</sup>

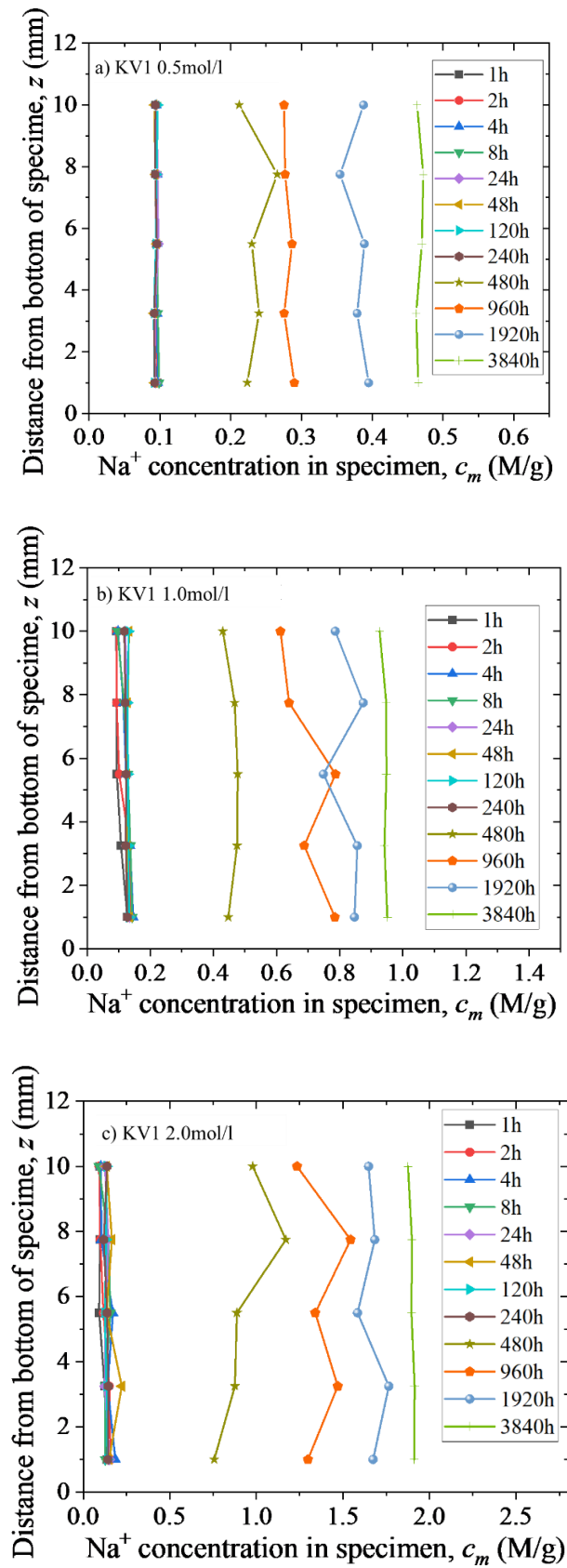


Figure 7-11 Na<sup>+</sup> concentrations of slices for KV1

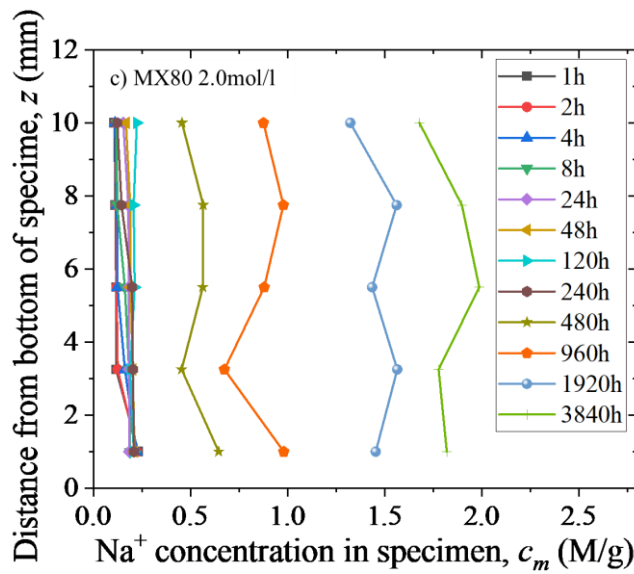
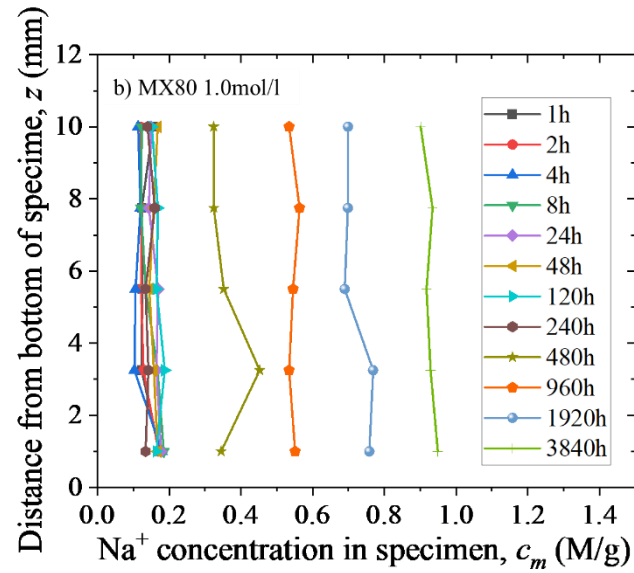
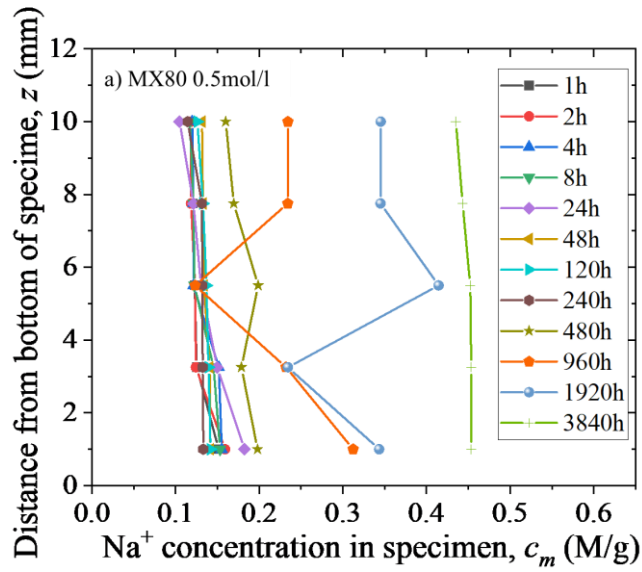
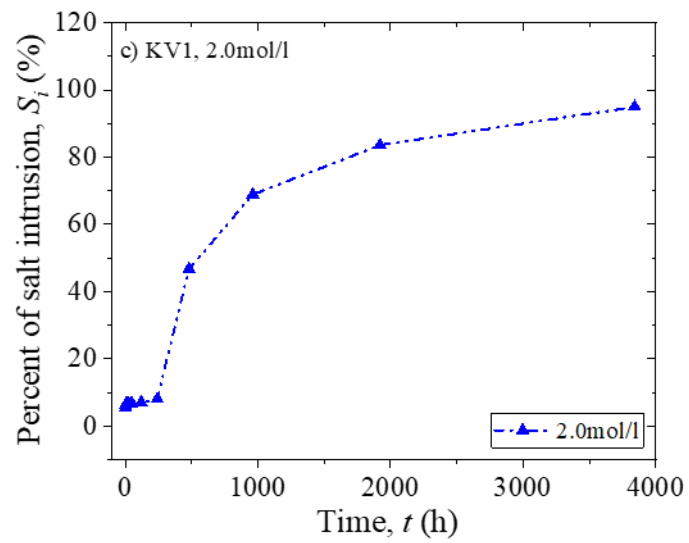
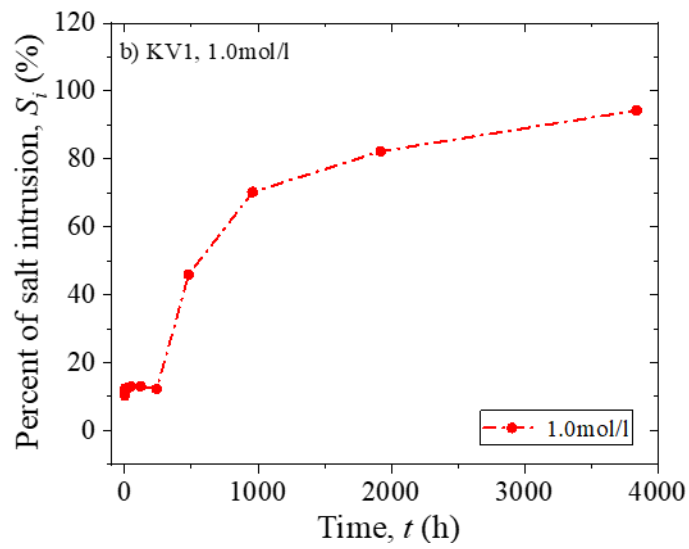
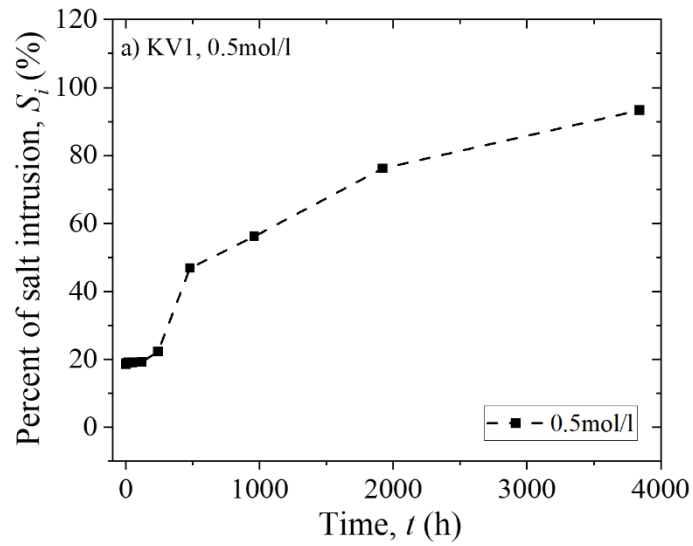
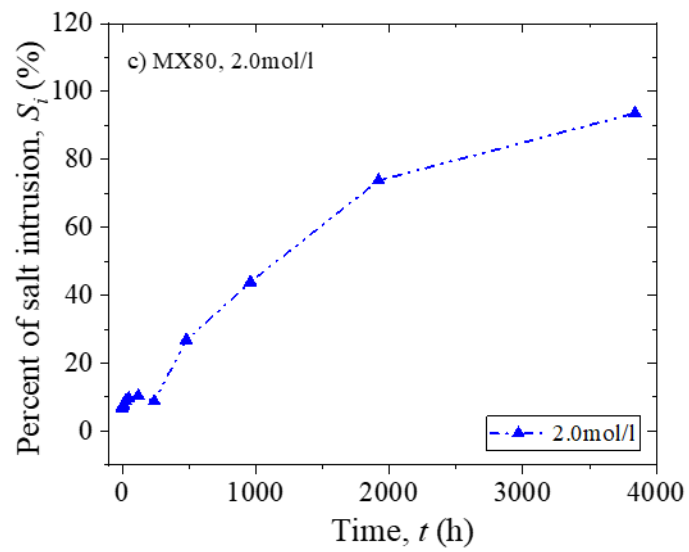
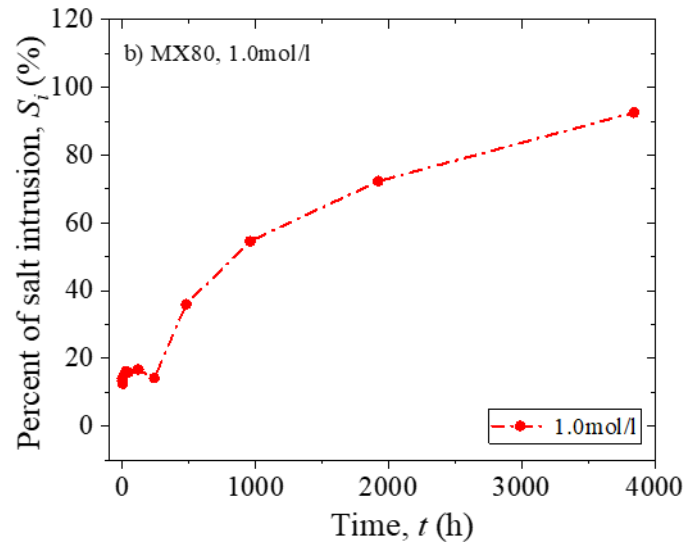
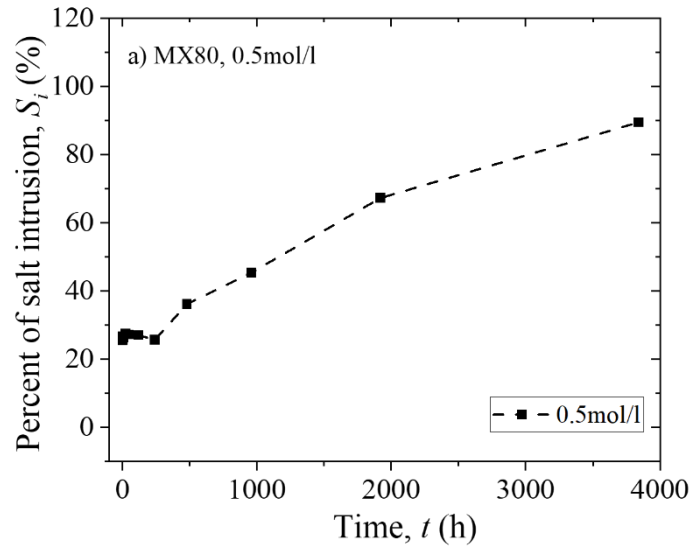


Figure 7-12  $\text{Na}^+$  concentrations of slices for MX80



**Figure 7-13 Percent of salt intrusion for KV1**



**Figure 7-14 Percent of salt intrusion for MX80**

Figure 7-11 and 7-12 present Na<sup>+</sup> concentrations in slices at different wetting durations for KV1 and MX80, respectively. It can be easily found from Fig. 7-11 and 7-12 that, in short wetting durations (approximately < 240h), Na<sup>+</sup> concentrations in slices increases as the position close to the water supply ends. After that, concentrations in five slices at each time point tend to be similar. But unlike the case of gravimetric water content in Fig. 7-3 and 7-4, after 240h, these values still raise with increasing wetting times.

Percentage of salt intrusion for specimen changing with time is indicated in Fig. 7-13 and 7-14. The percent of salt intrusion ( $S_i$ ) is defined as the Na<sup>+</sup> concentration in specimen to the Na<sup>+</sup> concentration of saturation liquid as:

$$S_i = \frac{c_m}{c} \times 100\% \quad (7-5)$$

where  $c$  is the Na<sup>+</sup> concentration of saturation liquid (mol/l). It is apparently from Fig. 7-13 and 7-14, percent of salt intrusion increases with increasing time. In the beginning 240h, the increase of percent of salt intrusion is very limited for KV1 and MX80 are very limited. After, 240h, the percent of salt intrusion much faster as the increasing wetting time than beginning 240h.

By combing Fig. 7-13 and 7-14, percent of salt intrusion changing with wetting duration for MX80 and KV1 are indicated in Fig. 7-15. It can be found from Fig. 7-15, in the shorter wetting times, percent of salt intrusion reduces with the rise of saturation liquid concentration. However, in the relative longer wetting durations range (approximately > 1920h), percent of salt intrusion rises with increasing saturation liquid concentration.

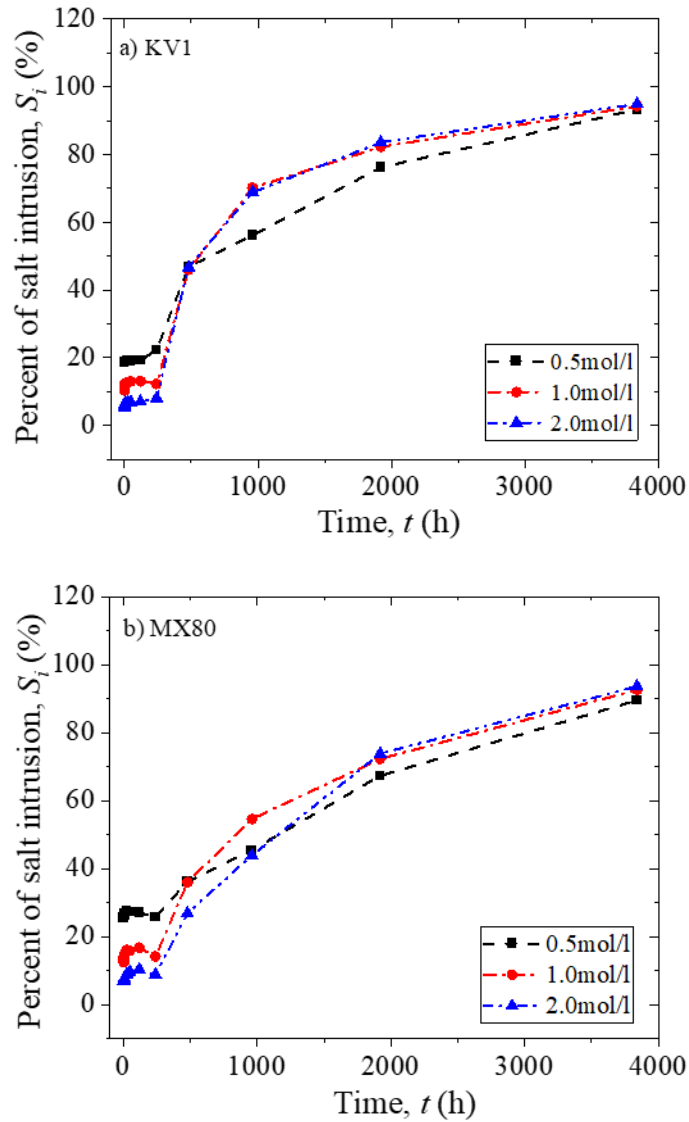


**Figure 7-15 Percent of salt intrusion for KV1 and MX80**

### 7.2.3 XRD results

By connecting average values of five slices with the same saturation periods by dash lines in Fig. 7-16, the overall trend of specimens with the same dry density is indicated. It can be readily inferred from Fig. 7-16 that basal spacings increase dramatically at the beginning of the wetting period. Then, basal spacings enter into stable state. Meanwhile, as we can easily found from Fig. 7-16, in the starting duration of wetting period (1-24h), higher concentration saturated specimens have bigger basal spacing in the same time point.

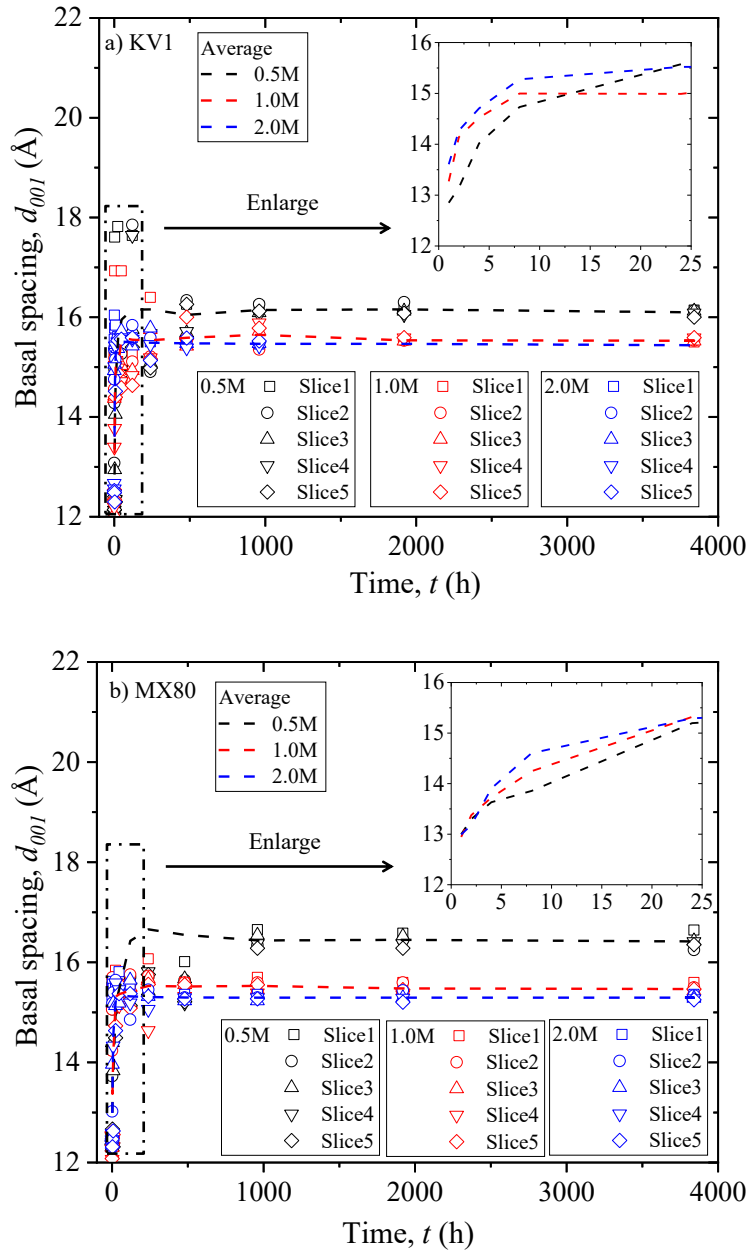


**Figure 7-16 Basal spacing changing with wetting duration for bentonites**

Figure 7-17 presents final basal spacings ( $d_{001,j}$ ) of specimens (average basal spacings of five slices, from 3840h). An easy conclusion can be summarized from Fig. 7-17 that, for all bentonites, final basal spacings reduce as  $\text{Na}^+$  concentrations rise. Similar phenomenon was reported by Lee et al. (2012). Meanwhile, as we can see from Fig. 7-17, final states of saturated specimens gradually move from  $2w$  to  $1w$  with increasing concentration.

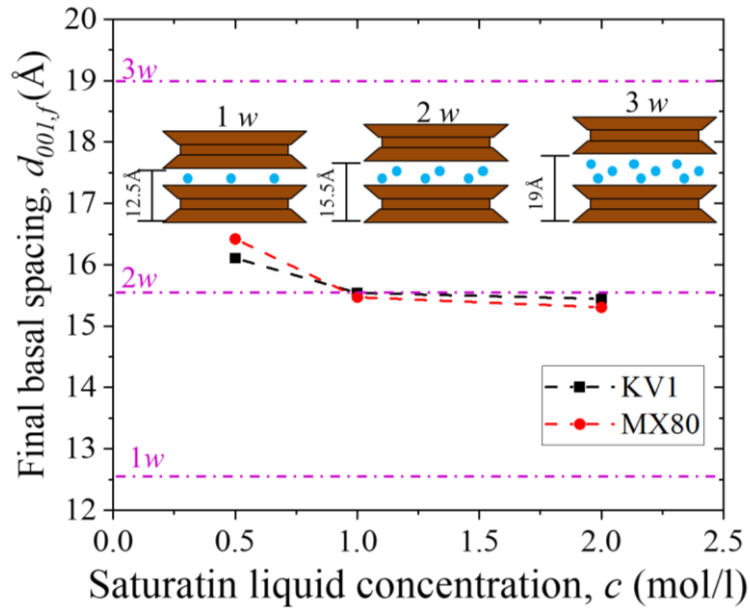


**Figure 7-17 Final basal spacing changing with saturation liquid concentration**

### 7.3 Discussion

#### 7.3.1 Mechanism for the movement of water and $\text{Na}^+$ in high dry density bentonite basing on pores distribution

The new dual pore system as introduced in Chapter 4 was used here to make sense the movement of water and salts in compacted bentonite, as: 1) micropore (inter-layer pore), and 2) macropore (inter-particle pore and inter-aggregate pore). As discussed in Chapter 4, the micropore has limited effect on the movement of water in compacted bentonite, which means the macropore is the main flowing path for the moveable waters. The cations movement mechanism is explained by different scholars, including an enrichment of cations in double diffusive layer (DDL) space, and an additional move pathway in the inter-layer space (Bourg et al. 2006; Appelo and Wersin 2007; Tachi et al. 2014). As the definition of pores in this study, it can be concluded that cations only move through micropore.

Figure 7-18 and 7-19 indicates basal spacing, degree of saturation and percent of salt solution changing with saturation durations. Meanwhile, Figure 7-18 and 7-19 was divided into saturation region and diffusion region. Additionally, there are several interesting phenomena found from Fig. 7-18 and 7-19. Firstly, it can be easily found that most of salt intrusion happened after specimen was saturated. Just a small portion of salt intrusion occurred in saturation process. This observation may indicate that the movement of water was carried out prior the movement of  $\text{Na}^+$ . Secondly, the developing curves for degree of saturation and basal spacing had similar shapes. This investigation may reveal that, the movement of water and the development of interlayer distance proceed simultaneously. Thirdly, in diffusion region, the basal spacings stayed in relative stable values. This may indicate that the intrusion of  $\text{Na}^+$  may had no effect on the development of basal spacing.

Basing on the above discussions, efforts were made to making sense the mechanisms for the movement of water and  $\text{Na}^+$  during saturation process. Figure 7-20 presents the mechanisms for the movement of water and  $\text{Na}^+$ . In initial state, montmorillonite aggregates, voids and non-swelling minerals exist together in the compacted bentonite (Fig. 7-20). During saturation process, after bentonite meets water, water move through macropores and some water is attracted into the micropore. Distance between montmorillonite layers increases with the increasing amount of immobile water between unit layers from swelling between layers, which induces the expanding of micropore volume. The void would gradually be occupied by the enlarging micropore volume. In this condition, salt movement is considered does not happen. After specimen saturated,  $\text{Na}^+$  would diffuse from macropore to micropore and move through micropore (Fig. 7-20).

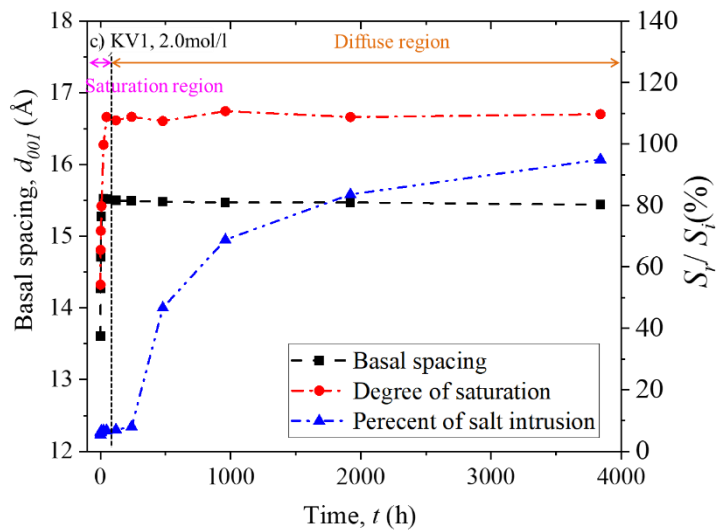
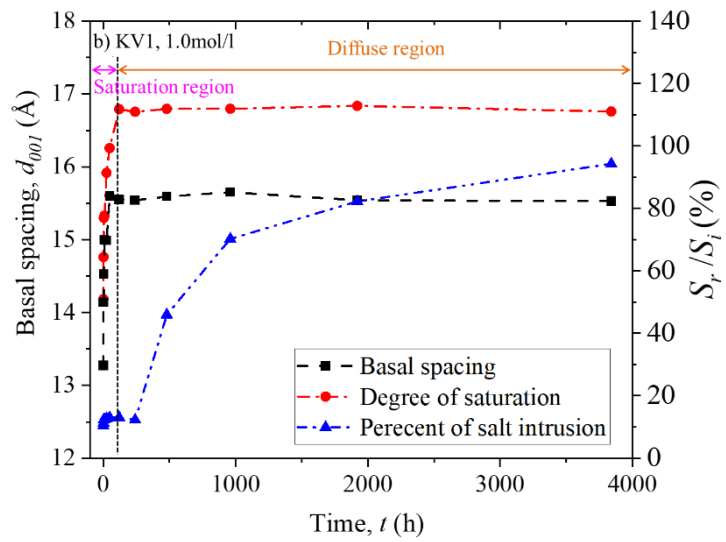
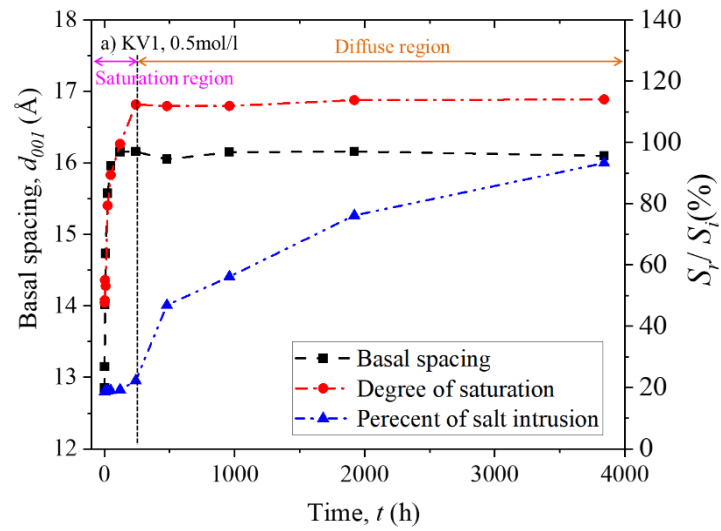
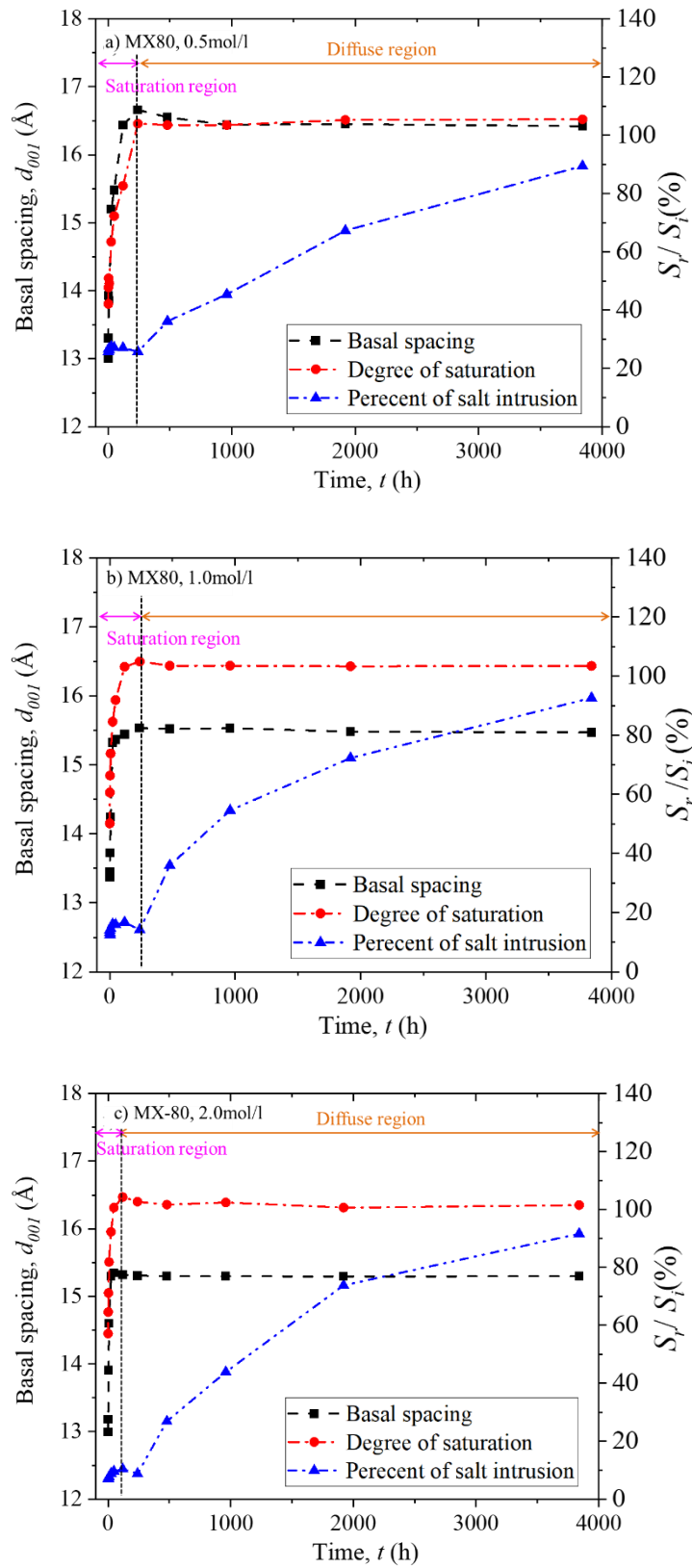


Figure 7-18 Basal spacing, degree of saturation and percent of salt intrusion for

KV1



**Figure 7-19 Basal spacing, degree of saturation and percent of salt intrusion for**

**MX80**

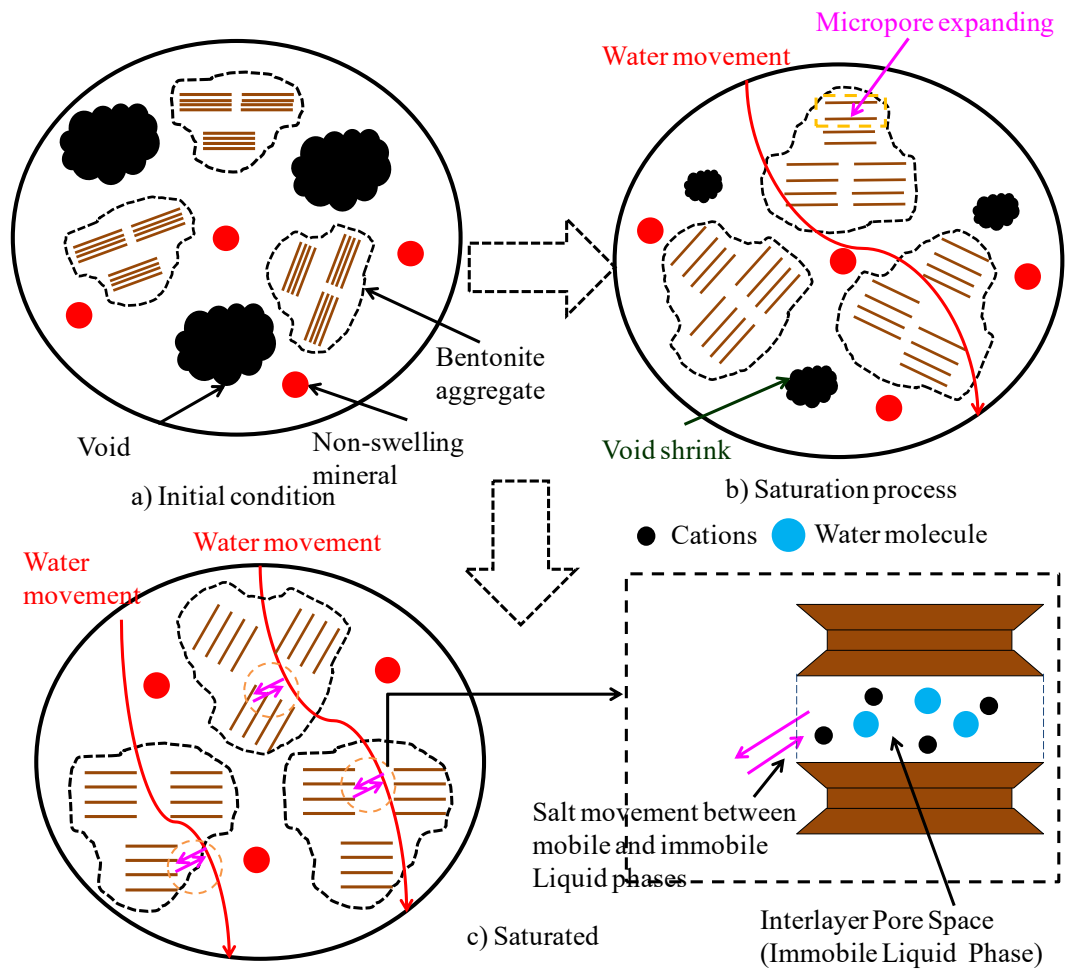


**Figure 7-20 Mechanisms for movements of water and salts in bentonite**

## Conclusion

A multi-ring mold was applied in wetting device to assess movement of water, movement of  $\text{Na}^+$  and development of basal spacing during saturation by infiltrating specimen with different concentrations NaCl solutions. Mechanisms for movement of water and  $\text{Na}^+$  under confined wetting were discussed by the dual pores system.

Conclusions include the followings.

1. Degree of saturation and basal spacing rise with saturation time initially, and then stayed in stable values. In the testing duration of this study, percent of salt intrusion increases along with saturation time. Movement of  $\text{Na}^+$  mainly happened after specimen was saturated.
2. Water diffusivity decreases with the increase of volumetric water content and increases with the rise of saturation liquid concentration.

## Reference

- Komine, H., Oyamada, T., Ozaki, T., and Iso, S., 2018. Discussion on water migration and swelling of compacted powder bentonites. *Journal of JSCE*, **74(1)**: 63–75. (in Japanese).
- Malusis, M.A., Kang, J. B., and Shackelford, C. D. 2015. Restricted salt diffusion in a geosynthetic clay liner. *Environmental Geotechnics*, **2(2)**: 68–77.
- Rao, S. M., Thyagaraj, T., and Thomas, H. R., 2006. Swelling of compacted clay under osmotic gradients. *Géotechnique*, **56(10)**: 707–713.
- SL237-063. 1999. Industry standards of the People’s Republic of China: Specification of soil test, SL237-1999. pp476-477, Ministry of Water Resources, China. (in Chinese)
- Sample-Load, K. M., Zhang, W. J., Tong, S., and Shackelford, C. D., 2020. Apparent salt diffusion coefficients for soil-bentonite backfills. *Canadian Geotechnical Journal*, **57**: 623-634.
- Takeuchi, S., Hara, K., and Nakano, M. 1995. Water retention curve, water diffusivity and water movement of compacted bentonite. *Soil and Foundations*, **35(3)**: 129–137. (in Japanese).
- Wang, H. L., Shirakawabe, T., Komine, H., Ito, D., Gotoh, T., Ichikawa, Y., and Chen, Q., 2020. Movement of water in compacted bentonite and its relation with swelling pressure. *Canadian Geotechnical Journal*, **57**: 921-932.

# Chapter 8

## **THE EFFECT OF SALT TYPES ON HYDROLOGICAL PROPERTIES AND SWELLING PRESSURE OF BENTONITES WITH XRD**

## 8.1 Testing overview

The testing methodology was the same as introduced in chapter 3. In each condition, 7 specimens were prepared for dismantling times of 2 h-240 h. The specimen details are presented in Table 8-1. The saturation liquids are distilled water, 0.5mol/l NaCl and 0.5mol/l CaCl<sub>2</sub>, respectively.

**Table 8-1 Specimen details**

Material	Dry density	Uncovered Time	Test type				
			Swelling pressure	XRD <sup>a</sup>	Moisture	XRD <sup>b</sup>	CEC, EXC
MX80		2, 4, 8, 24,					
KV1	1.4g/cm <sup>3</sup>	48, 120	√	√	√	×	×
KB		and 240h					
MX80							
KV1	1.4g/cm <sup>3</sup>	240h (×3) <sup>c</sup>	√	√	√	√	√
KB							

Note: <sup>a</sup>, scan range 2.7°-20°

<sup>b</sup>, scan range 4°-40°

<sup>c</sup>, specimens saturated for 240h was carried out for 3 times. The later 2 times just measured the swelling pressure

Besides the tests in Chapter 3, some extra tests were added in this chapter. After the detecting of moisture, slices from 240h wetted durations were left for the discovery of mineral composition, CEC (total cation exchange capacity) and EXC (amount of extractable cations). Firstly, slices were crushed and passed through a 0.25mm sieve. For removing the remained salts in specimens, the crushed powders were washed by

ultra-pure water (produced by Environmental safe center, Waseda University) for 6 times. The liquids left over from the last wash were sent for concentration tests to ensure that there is no salt in bentonites. Then, washed powders were air dried and brought to XRD tests again for achieving the mineral compositions. In this time, X-ray scan range was set from  $4^{\circ}$  to  $40^{\circ}$  with scan speed of  $10^{\circ}/\text{min}$ . Hereafter, powders were taken to CEC and EXC tests followed JGS 0261-2008 (all concentrations measurements mentioned above, including concentration for calculating CEC and EXC, were tested by ICP-OES in Environmental safe center, Waseda University) as introduced in Chapter 2.

## 8.2 Results

### 8.2.1 Swelling pressure

Figure 8-1, 8-2 and 8-3 presents swelling pressure evolution curves of three bentonites saturated by distilled water, 0.5mol/l NaCl and 0.5mol/l CaCl<sub>2</sub>, respectively. As mentioned in chapter 4, the development of swelling pressure can be divided into four regions: 1) initial quick increase region, 2) drop region, 3) re-increase region, and 4) long-term stable region. As we can see from Fig. 8-1, 8-2 and 8-3, swelling pressure evolution curves of MX80, KV1 and KB saturated by different liquids in this study agree with those reported in chapter 4. It is apparently from Fig. 8-1, 8-2 and 8-3 that, swelling pressures increase quickly for all three bentonites during the first approx. 5h. Swelling pressures subsequently drop at approx. 25 h. Later, another stable rising of swelling pressures occurs. Finally, swelling pressure remains a constant value for long time.

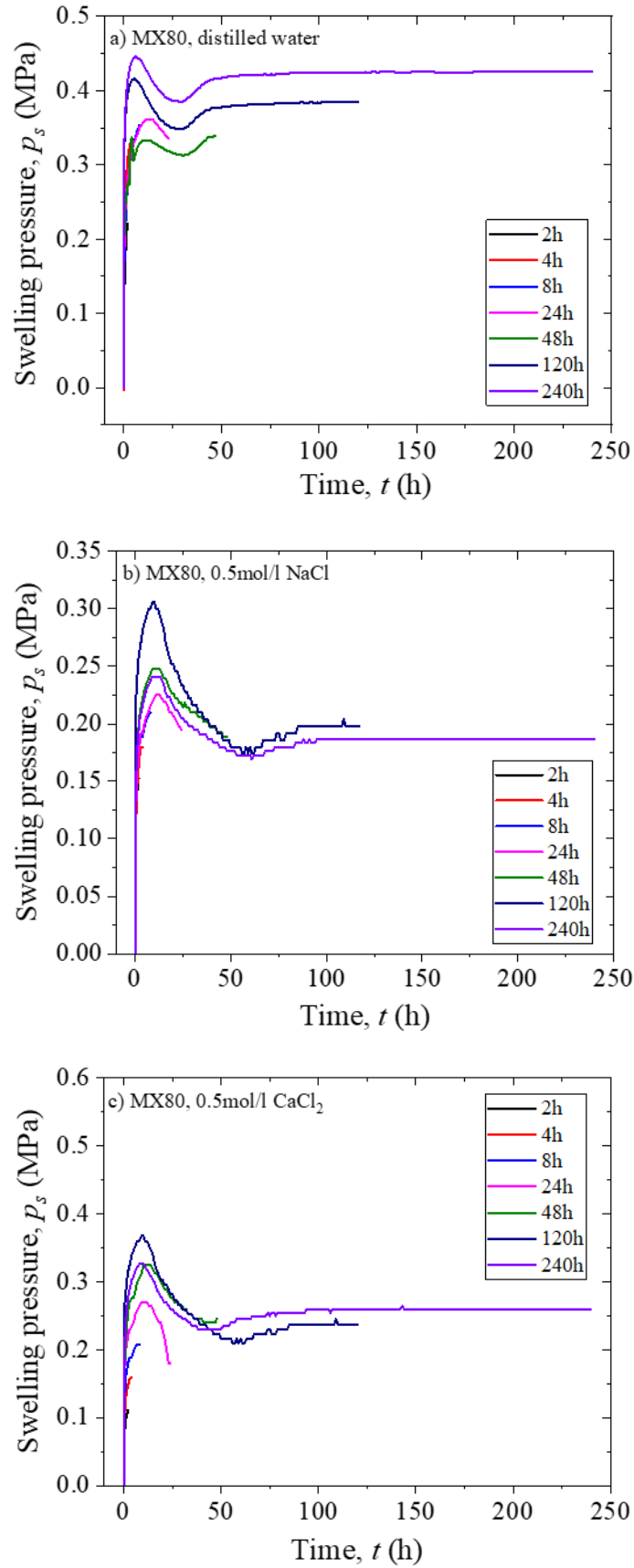


**Figure 8-1 Swelling pressure evolution curves of MX80 bentonite saturated by distilled water, 0.5mol/l NaCl and 0.5mol/l CaCl<sub>2</sub>.**

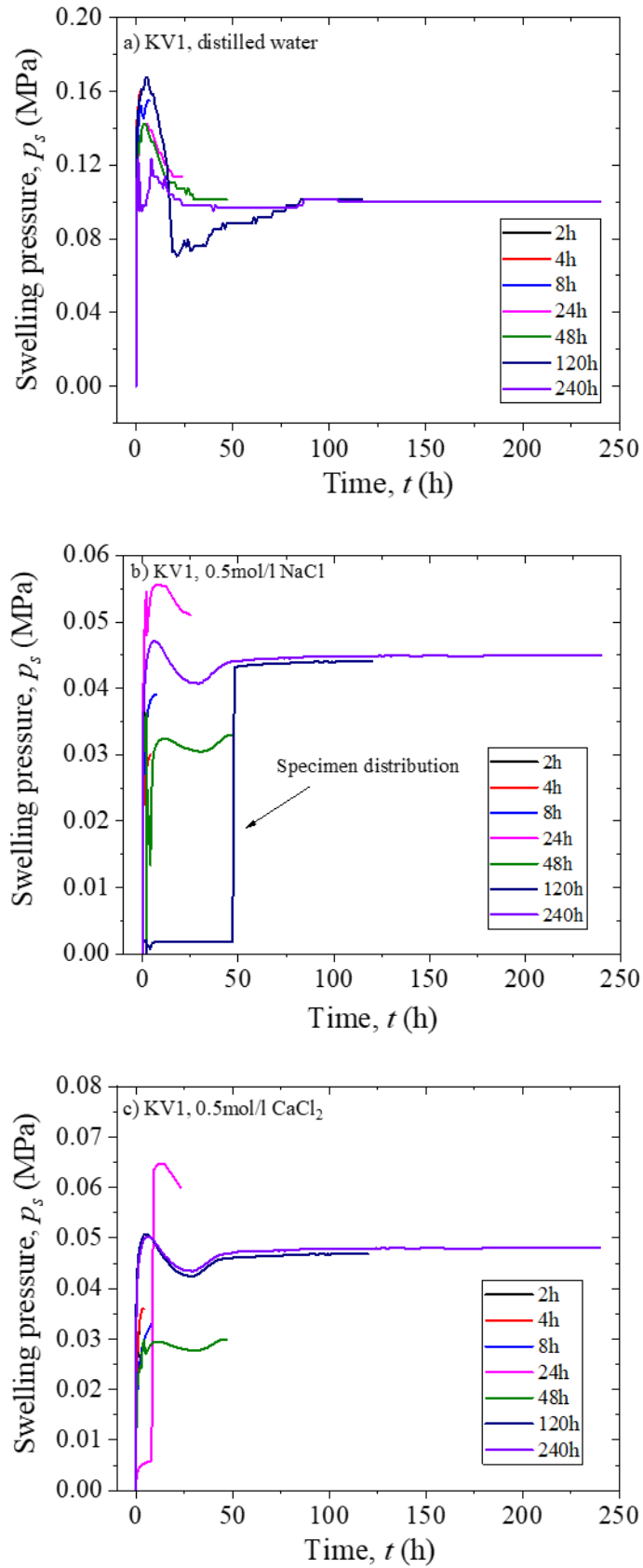


**Figure 8-2 Swelling pressure evolution curves of KV1 bentonite saturated by distilled water, 0.5mol/l NaCl and 0.5mol/l CaCl<sub>2</sub>.**

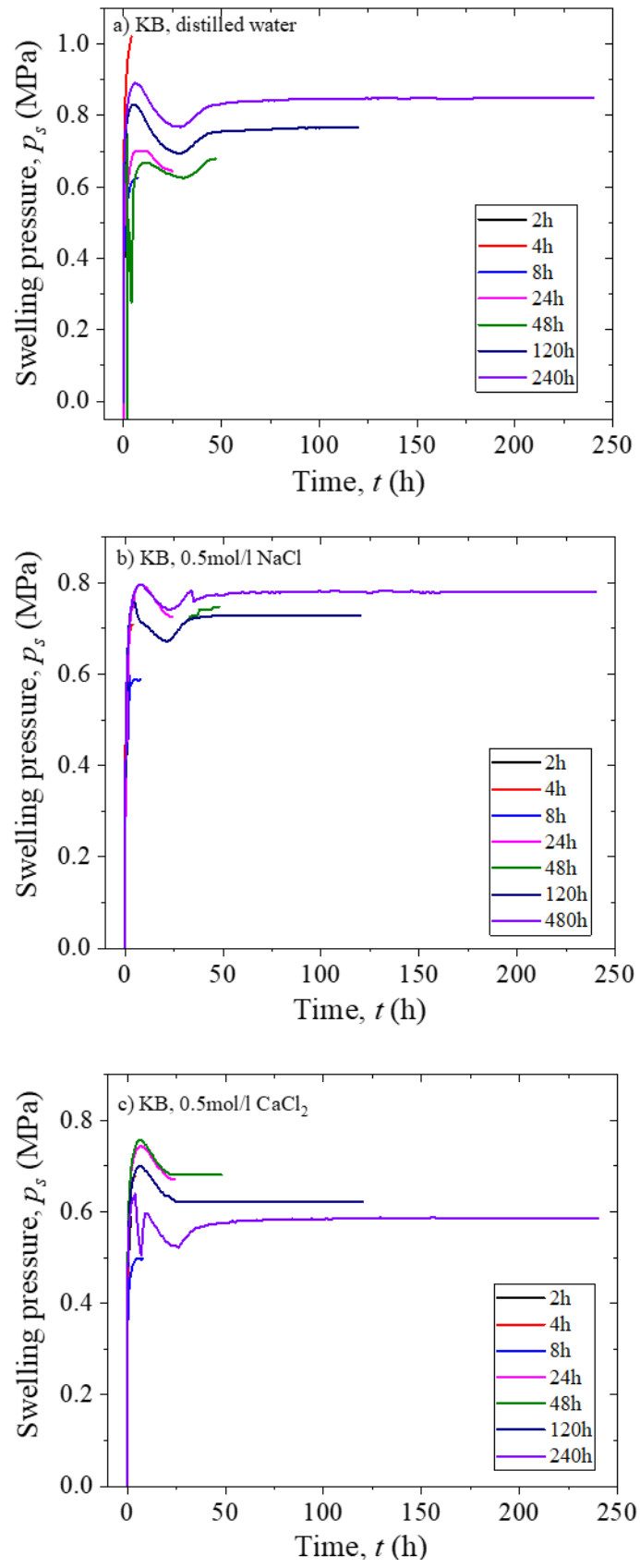


**Figure 8-3 Swelling pressure evolution curves of KB bentonite saturated by distilled water, 0.5mol/l NaCl and 0.5mol/l CaCl<sub>2</sub>.**

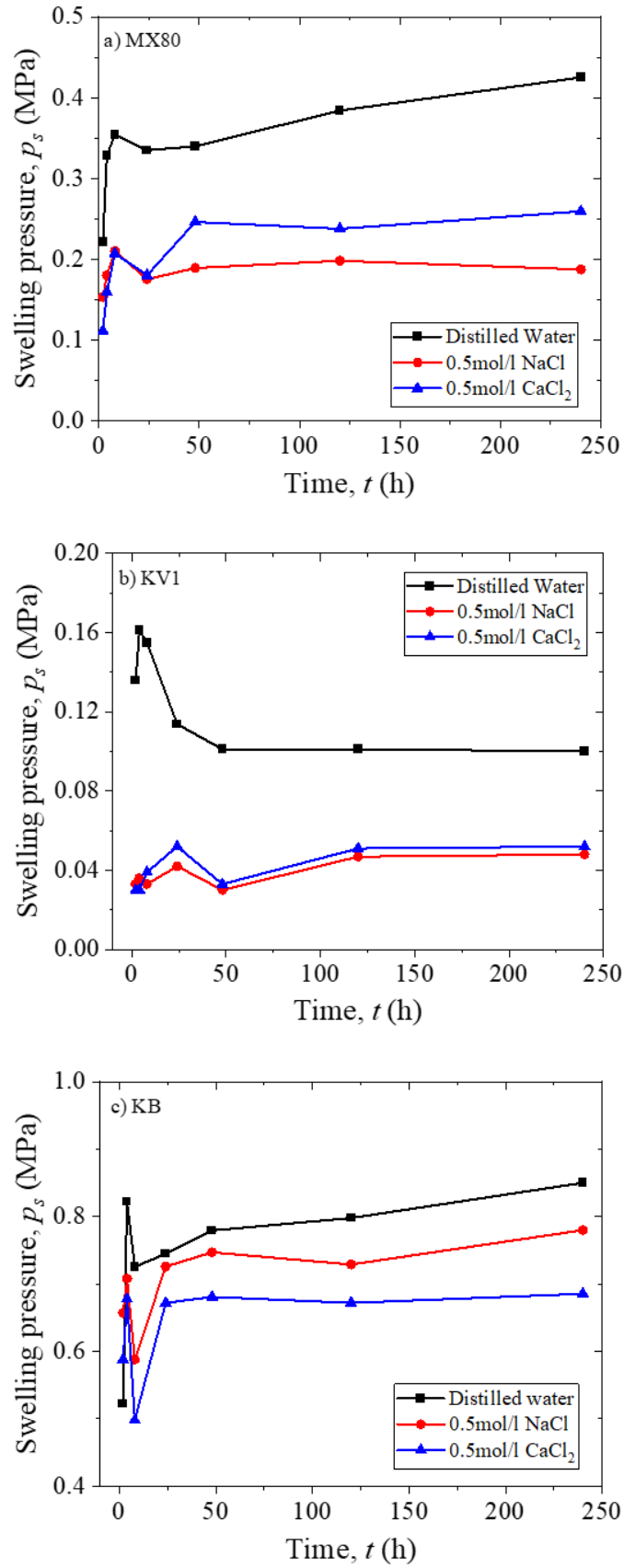


**Figure 8-4 Swelling pressures at different wetting durations of bentonites saturated by distilled water, 0.5mol/l NaCl and 0.5mol/l CaCl<sub>2</sub>.**

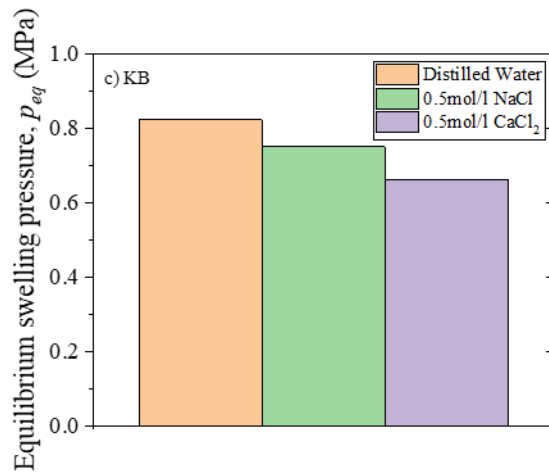
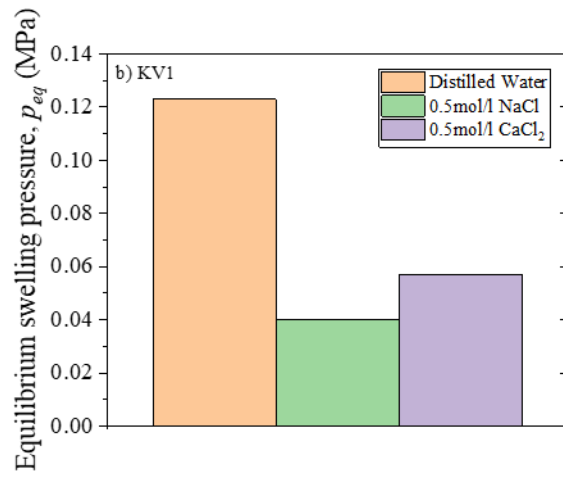
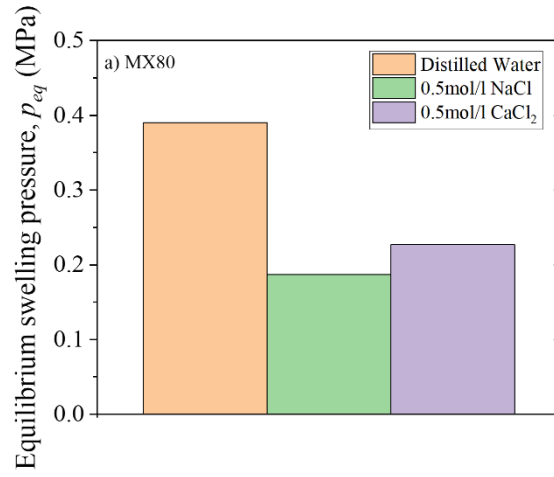


**Figure 8-5 Equilibrium swelling pressures of bentonites saturated by distilled water, 0.5mol/l NaCl and 0.5mol/l CaCl<sub>2</sub>.**

Figure 8-4 indicates swelling pressures at different wetting duration of MX80, KV1 and KB saturated by distilled water, 0.5mol/l NaCl and 0.5mol/l CaCl<sub>2</sub>, respectively. Figure 8-5 indicates equilibrium swelling pressures of compacted bentonites saturated by distilled water and salt solutions from 3 repeated tests. As we can see from Fig. 8-1, 8-2 and 8-3, swelling pressure evolution curves have somewhat dispersion. This phenomenon may be due to the fact that mold ring was changed to multi-ring mold. For 240h wetting tests, three repeated tests were adopted in order to observe the effect of saturation liquids on equilibrium swelling pressure accurately. As we can see from Fig. 8-5, for all three bentonites, equilibrium swelling pressures saturated by salt solutions are smaller than those saturated by distilled water. Massive investigators (e.g., Wang et al., 2014; Sun et al., 2015; Chen et al., 2018) saturated sodium type bentonites with different liquids, and showed consistent results with this study. However, some studies reported different results about calcium type bentonite. Lee et al. (2012) saturated Korean calcium type bentonite by NaCl solutions with different concentrations. There was an interesting founding reported by Lee et al. (2012) that equilibrium swelling pressures by 0.04mol/l NaCl were greater than distilled water.

Moreover, equilibrium swelling pressures of compacted bentonites saturated by NaCl and CaCl<sub>2</sub> are presented in Fig. 8-5. It is readily apparent from Fig. 8-5 that: 1) for sodium type bentonites (MX80 and KV1), equilibrium swelling pressures saturated by CaCl<sub>2</sub> are bigger than those saturated by NaCl. Zhu et al. (2013) and Chen et al. (2018) saturated sodium GMZ bentonite with NaCl and CaCl<sub>2</sub>, and reported the same conclusion. 2) for calcium type bentonite (KB), equilibrium swelling pressures saturated by CaCl<sub>2</sub> are smaller than those saturated by NaCl. NaCl and CaCl<sub>2</sub> may have totally different effect on the final swelling for different types of bentonites.

### 8.2.2 Water diffusivity

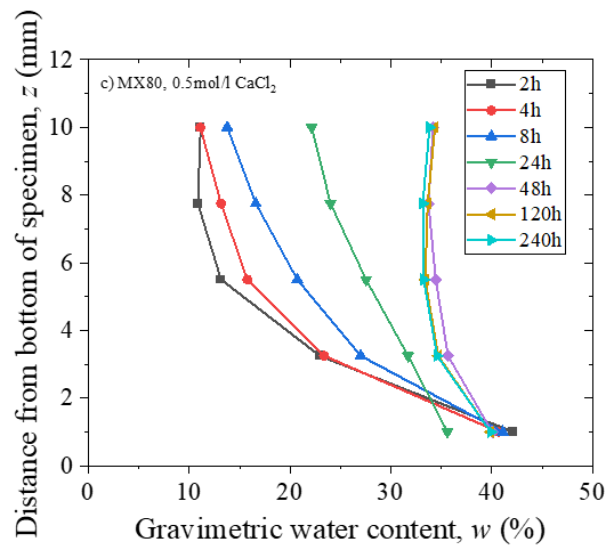
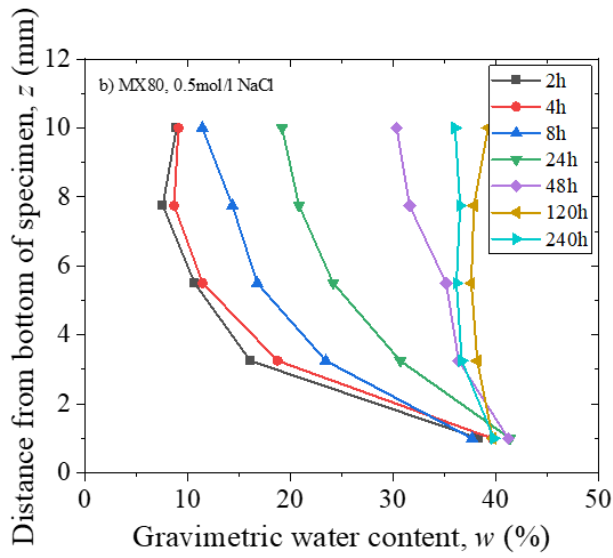
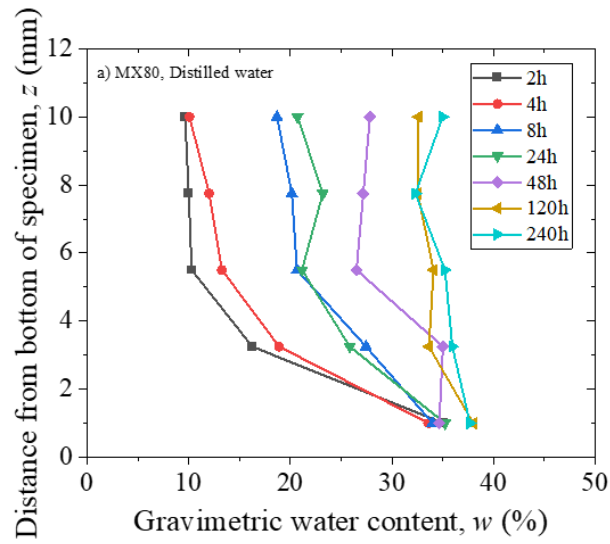


**Figure 8-6 Gravimetric water contents of MX80 saturated by distilled water, 0.5mol/l NaCl and 0.5mol/l CaCl<sub>2</sub>.**

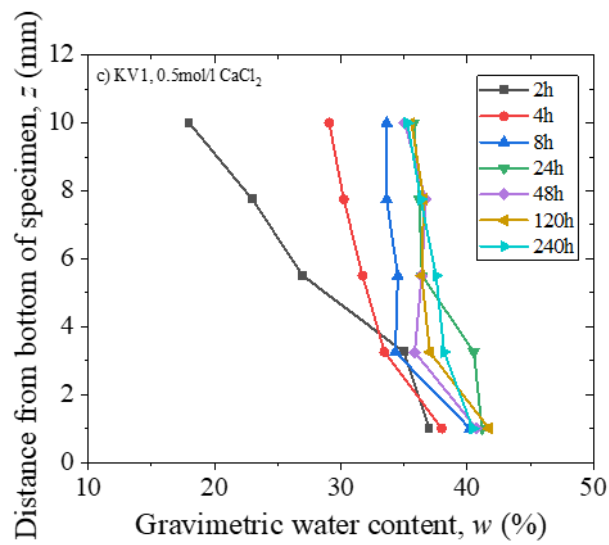
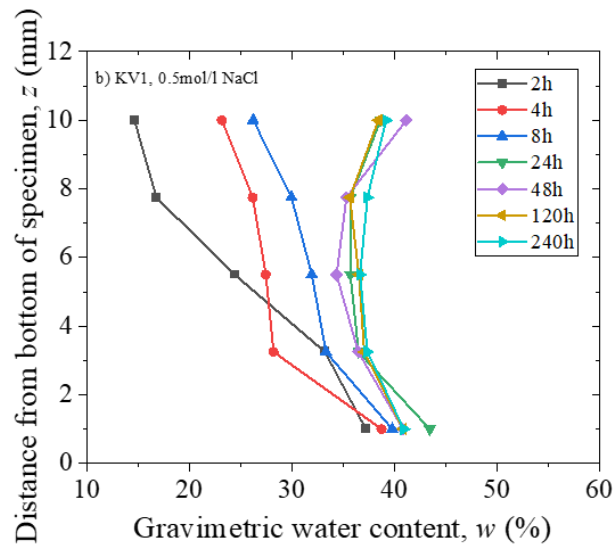
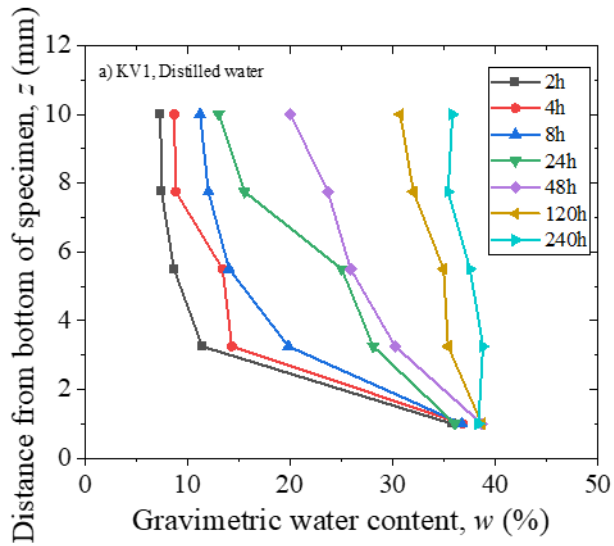


**Figure 8-7 Gravimetric water contents of KV1 saturated by distilled water, 0.5mol/l NaCl and 0.5mol/l  $\text{CaCl}_2$ .**

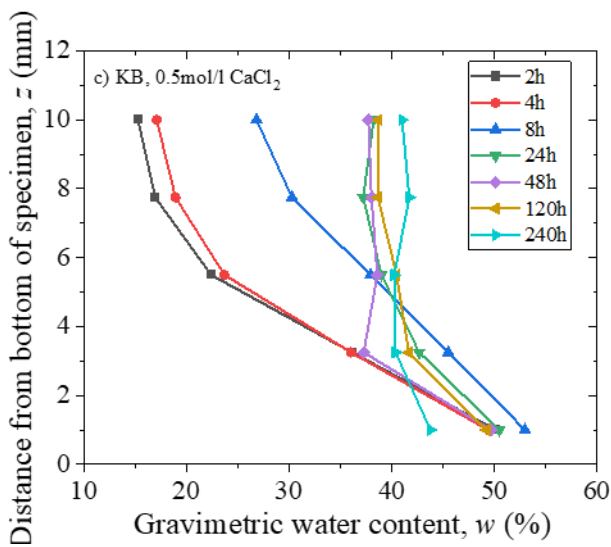
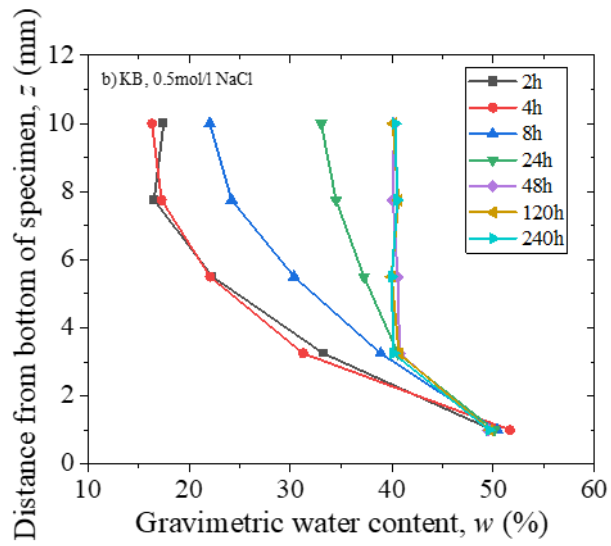
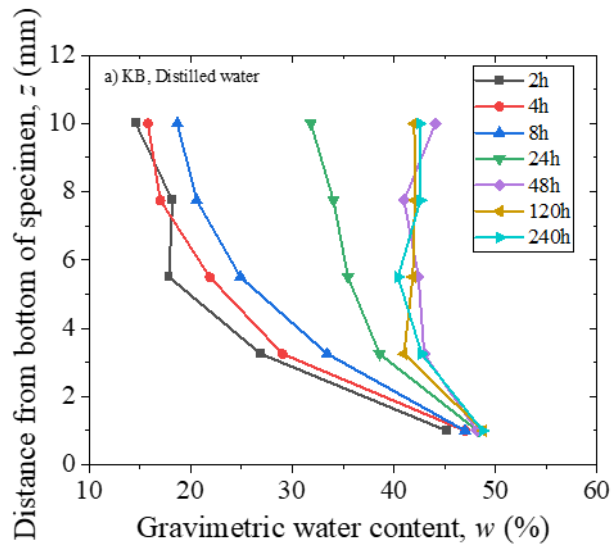


**Figure 8-8 Gravimetric water contents of KB saturated by distilled water, 0.5mol/l NaCl and 0.5mol/l CaCl<sub>2</sub>.**

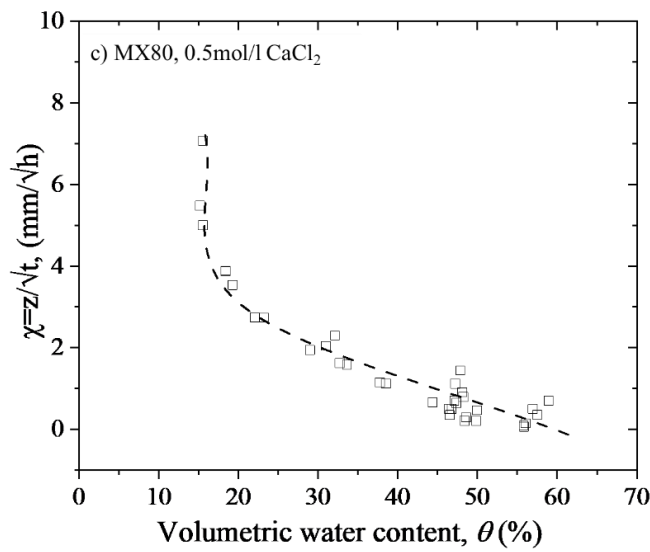
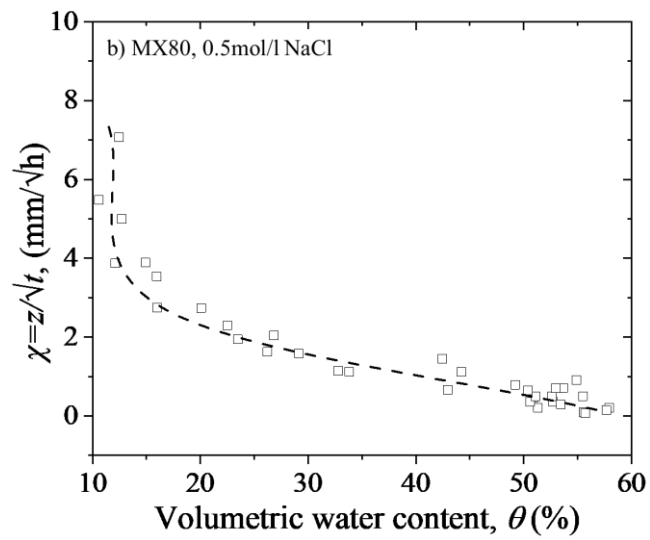
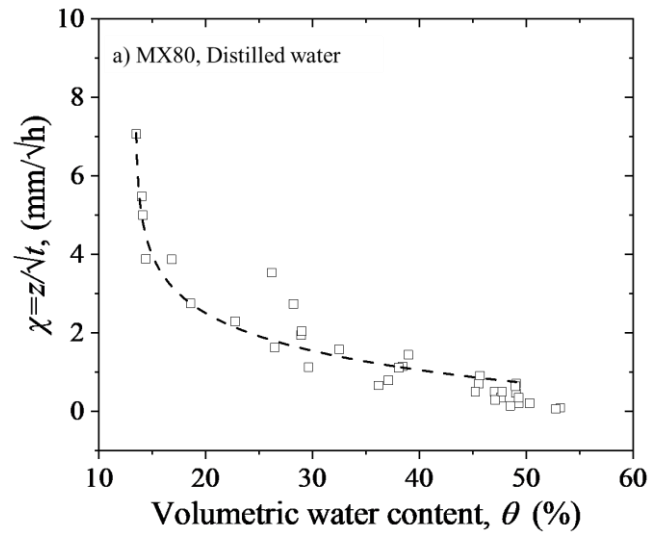


**Figure 8-9 Relation between  $\theta$  and  $\chi$  for MX80 saturated by distilled water, 0.5mol/l NaCl and 0.5mol/l CaCl<sub>2</sub>**

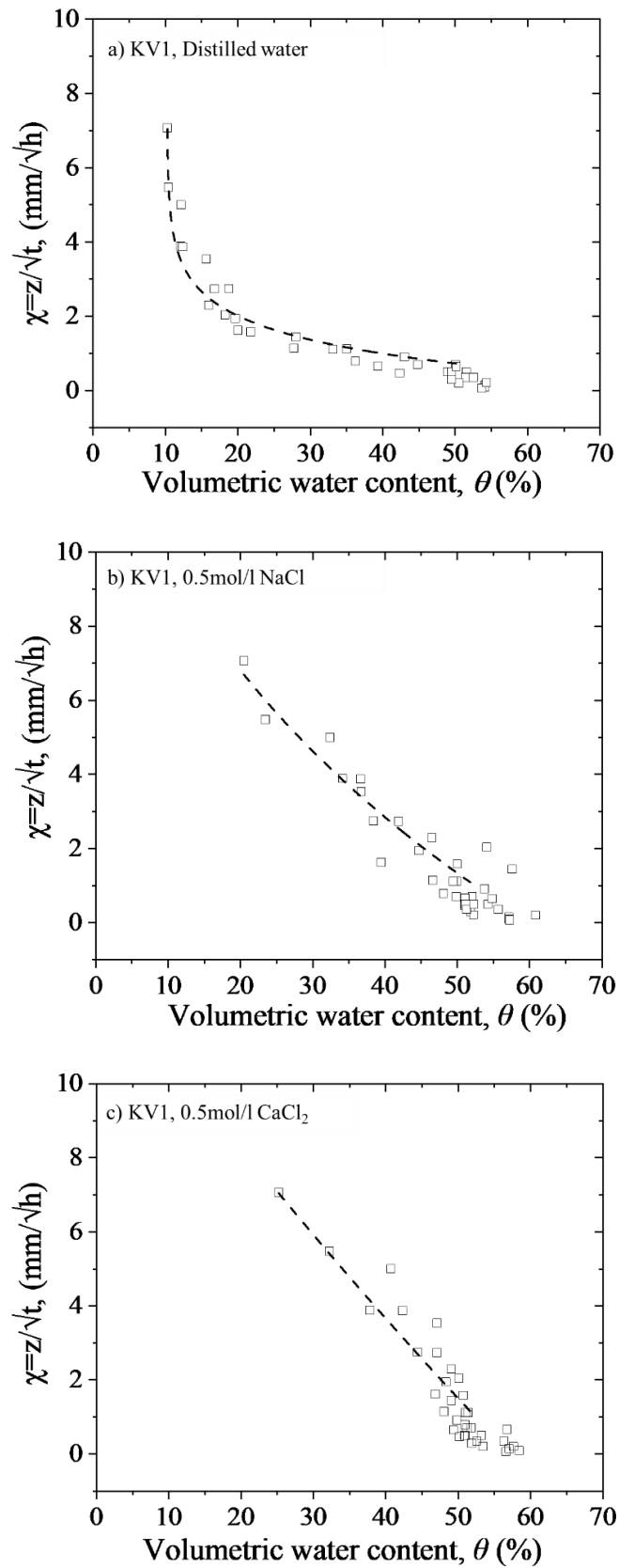


**Figure 8-10 Relation between  $\theta$  and  $\chi$  for KV1 saturated by distilled water, 0.5mol/l NaCl and 0.5mol/l CaCl<sub>2</sub>.**

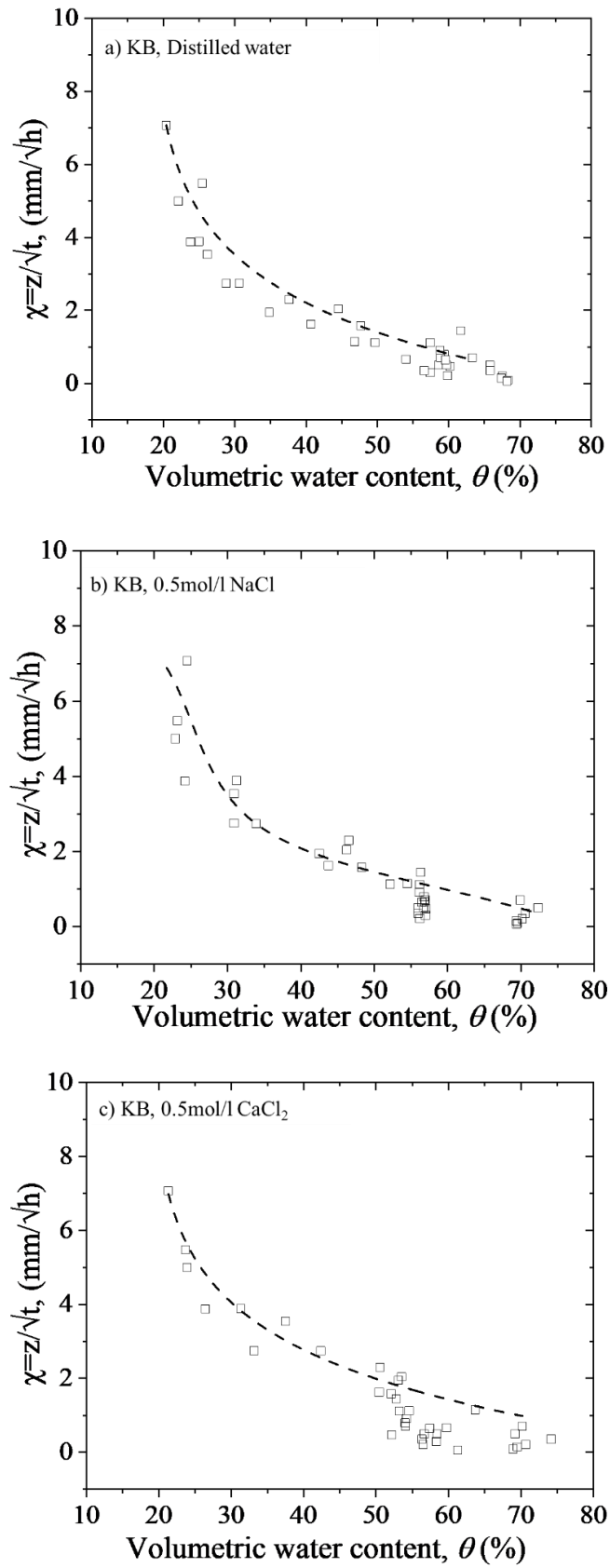


**Figure 8-11 Relation between  $\theta$  and  $\chi$  for KB saturated by distilled water, 0.5mol/l NaCl and 0.5mol/l CaCl<sub>2</sub>**

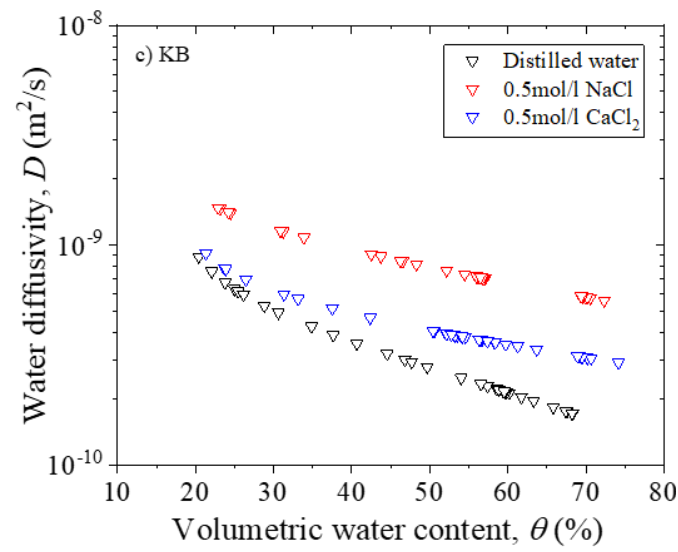
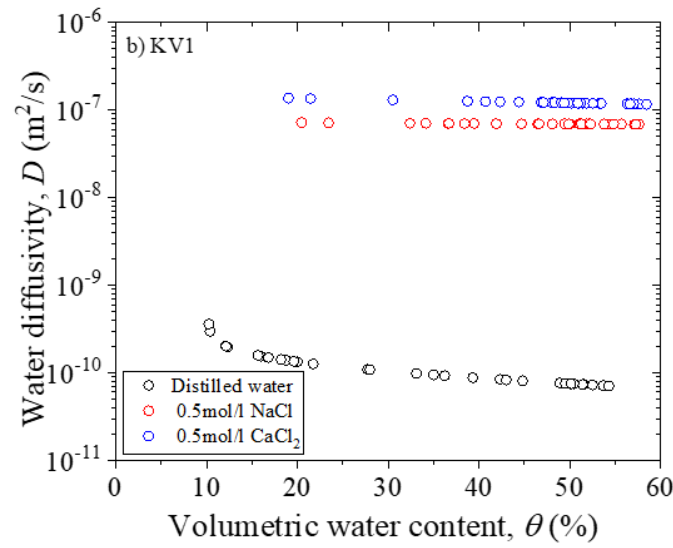
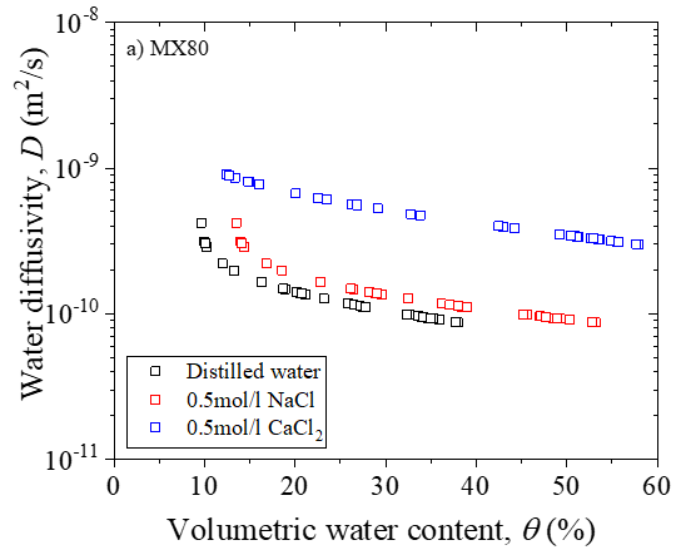


**Figure 8-12 Water diffusivity for bentonites saturated by distilled water, 0.5mol/l NaCl and 0.5mol/l  $\text{CaCl}_2$**

The distributions of gravimetric water contents in slices after water absorption are presented in Fig. 8-6, 8-7 and 8-8. It is a general truth from Fig. 8-6, 8-7 and 8-8 that, gravimetric water content increases as the position close to the water supply end and as time increases. Figure 8-9, 8-10 and 8-11 show relations between  $\theta$  and  $\chi$  for bentonites saturated by different solutions. As we can see from Fig. 8-9, 8-10 and 8-11, those relations can generally perform well with testing database. Thus, the calculation of water diffusivity can follow Wang et al. (2020) as introduced in Chapter 4.

Water diffusivity for bentonites saturated by different solutions is indicated in Fig. 8-12. It can be easily concluded from Fig. 8-12 that, water diffusivity decreases with volumetric water content. It may be clearly seen from Fig. 8-12, water diffusivity saturated by distilled water are smaller than those of salt solutions. Meanwhile, results about diffusivities of water saturated by different salt solutions are shown in Fig. 8-12. Easy conclusion can be made from Fig. 8-12 that, sodium bentonites (MX80 and KV1) saturated by  $\text{CaCl}_2$  has bigger diffusivities than  $\text{NaCl}$ . However, for calcium type bentonite (KB),  $\text{NaCl}$  saturated specimens have higher diffusivities.

### 8.2.3 XRD

Figure 8-13, 8-14 and 8-15 present the XRD profiles of MX80 saturated by different liquids at 8h, 48h and 240h, respectively. Figure 8-16, 8-17 and 8-18 reveal the XRD profiles of KV1 saturated by different liquids at 8h, 48h and 240h, respectively. Figure 8-19, 8-20 and 8-21 show the XRD profiles of KB saturated by different liquids at 8h, 48h and 240h, respectively. As we can see, when  $t=8\text{h}$ , water content of slice decreases with the increase of slice number. For the sodium bentonites (MX80 and KV1), the average water content of five slices saturated by  $\text{CaCl}_2$  seems bigger than those saturated by  $\text{NaCl}$ . And the average water content of 5 slices saturated by distilled may be smaller than salt solutions. In case of calcium bentonite, average water

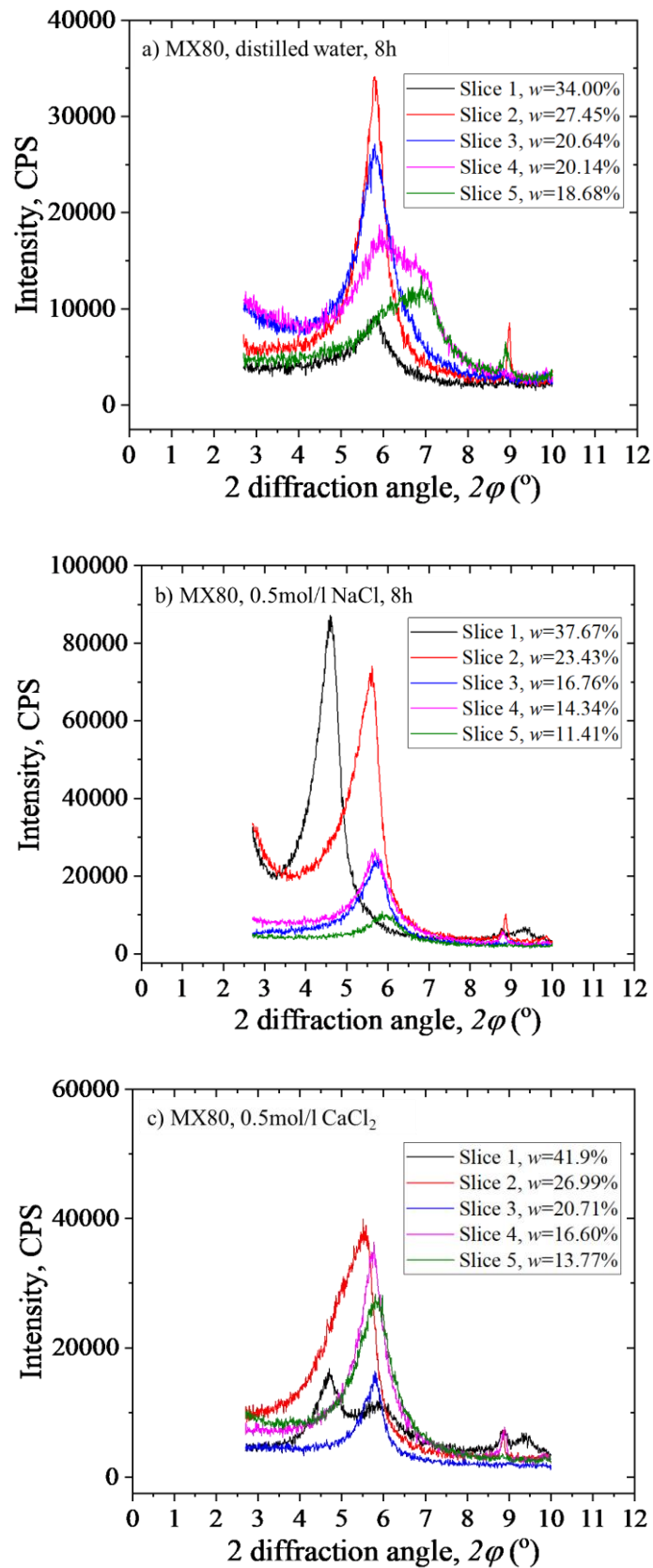


**Figure 8-13 XRD profiles for MX80 saturated by distilled water, 0.5mol/l NaCl and 0.5mol/l CaCl<sub>2</sub> at 8h**

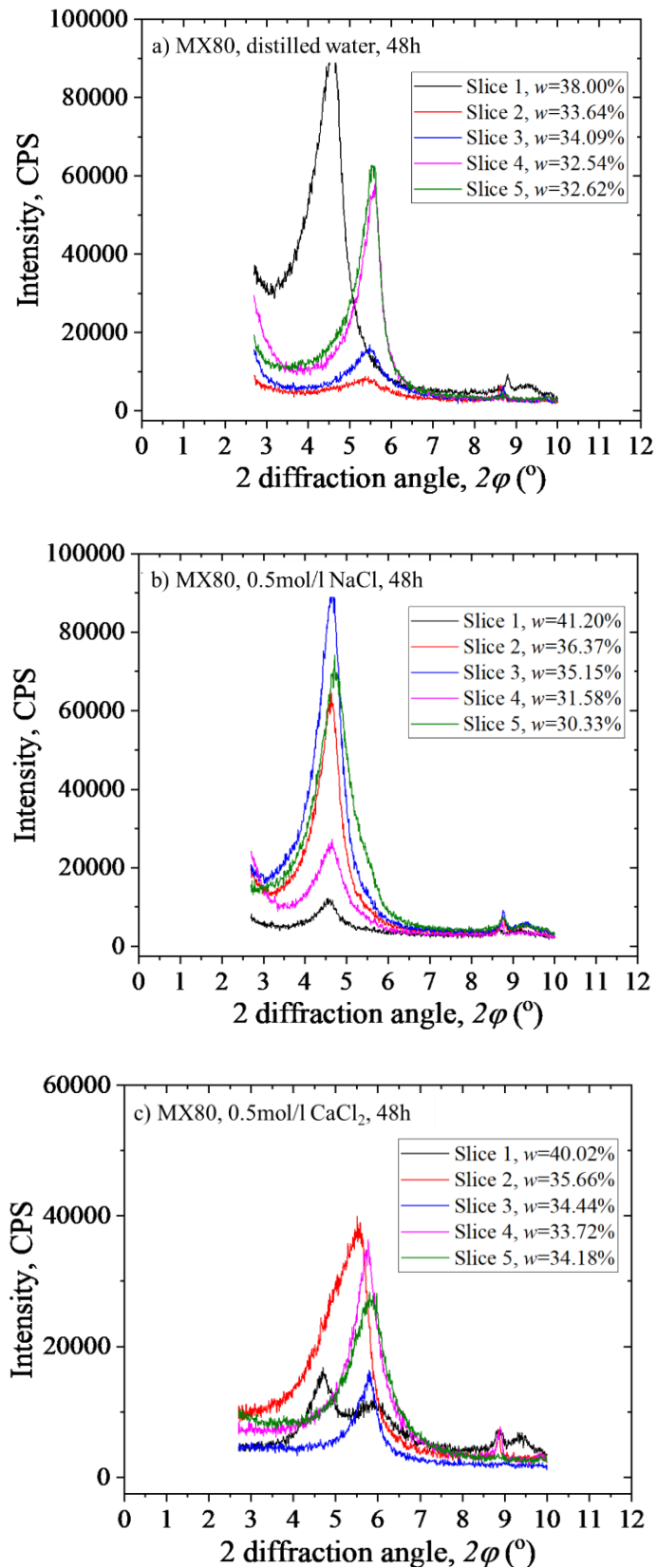


**Figure 8-14 XRD profiles for MX80 saturated by distilled water, 0.5mol/l NaCl and 0.5mol/l CaCl<sub>2</sub> at 48h**

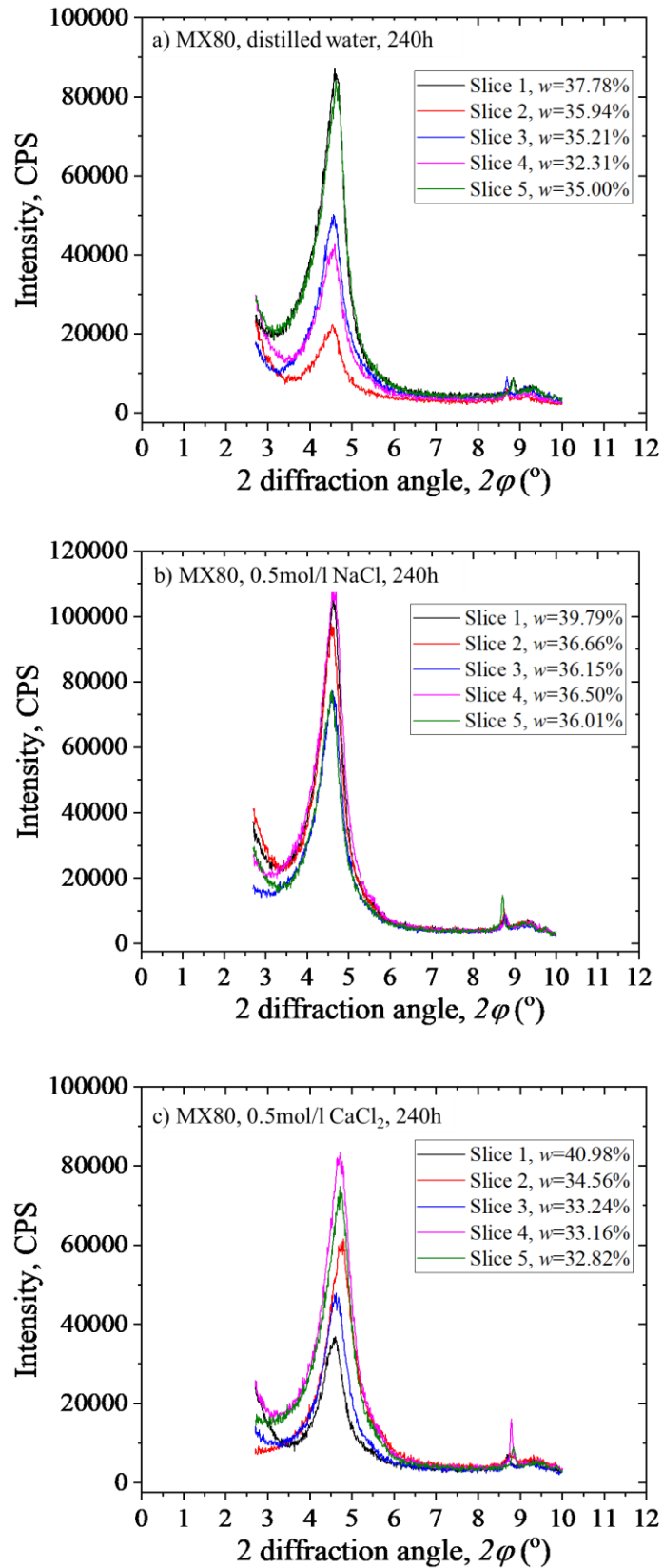


**Figure 8-15 XRD profiles for MX80 saturated by distilled water, 0.5mol/l NaCl and 0.5mol/l CaCl<sub>2</sub> at 240h**

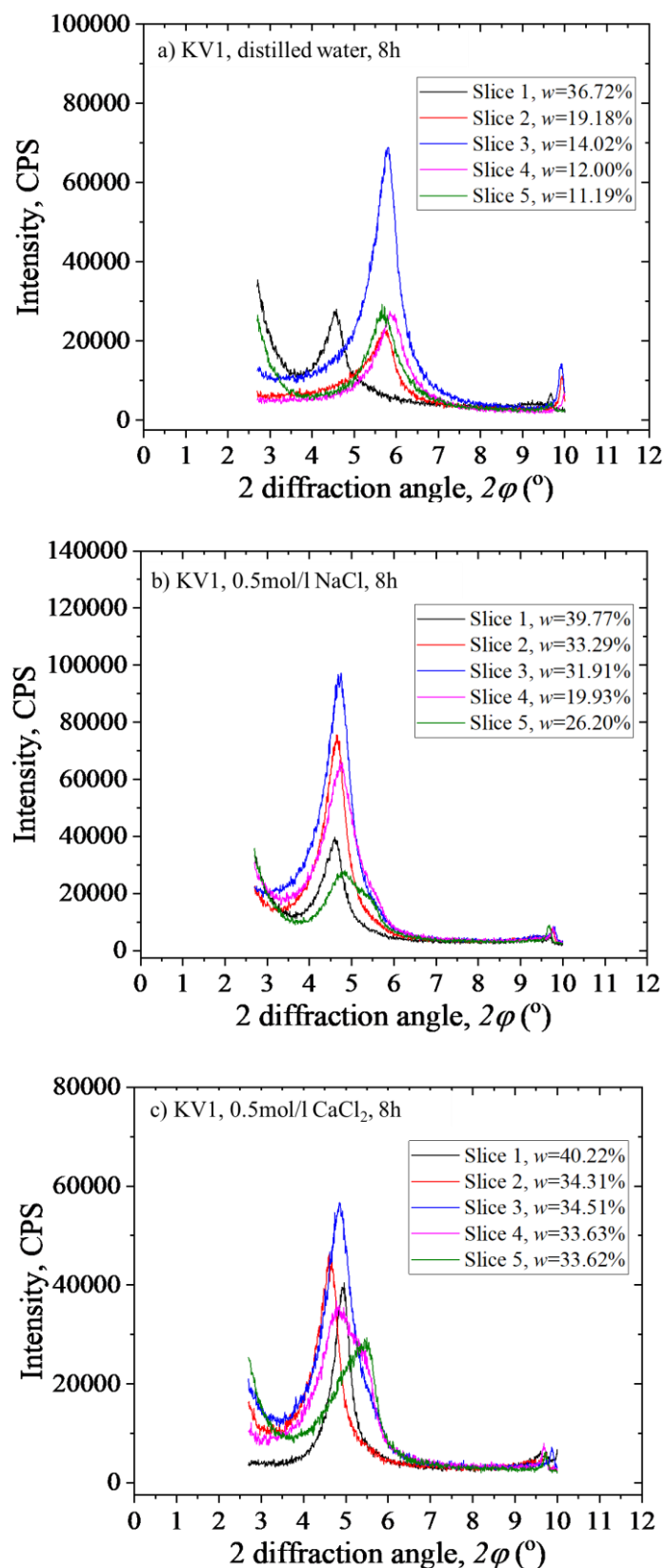


**Figure 8-16 XRD profiles for KV1 saturated by distilled water, 0.5mol/l NaCl and 0.5mol/l CaCl<sub>2</sub> at 8h**

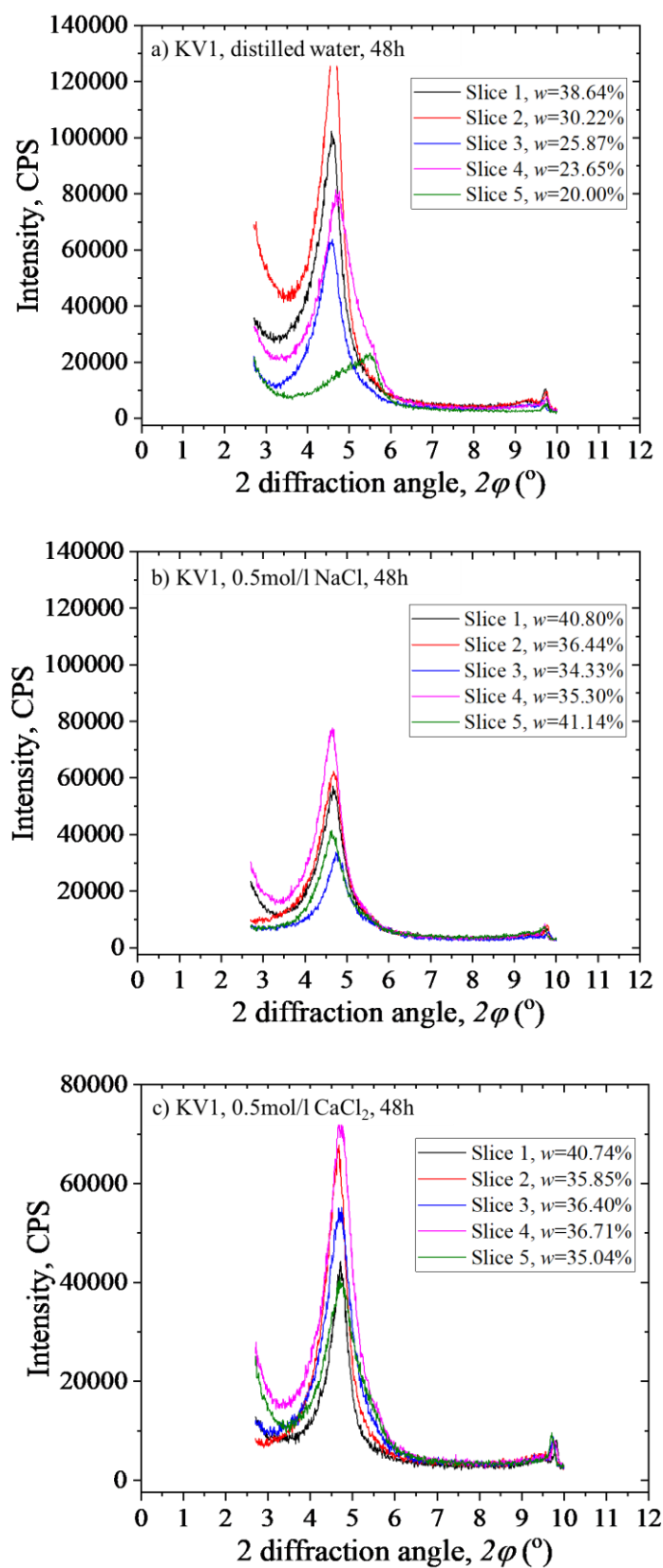


**Figure 8-17 XRD profiles for KV1 saturated by distilled water, 0.5mol/l NaCl and 0.5mol/l CaCl<sub>2</sub> at 48h**

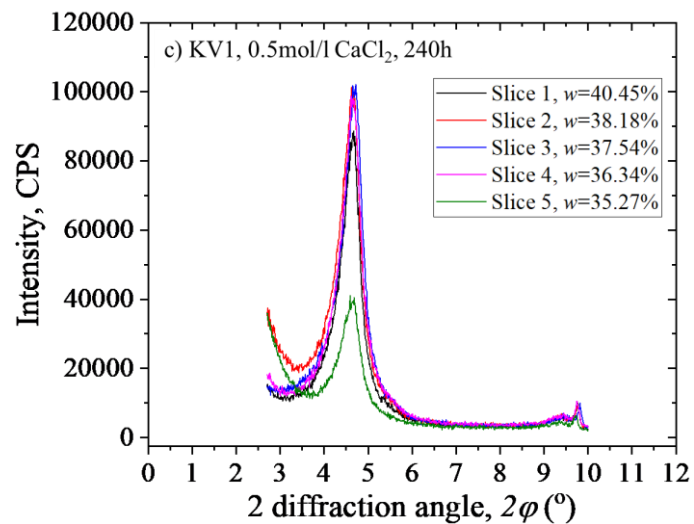
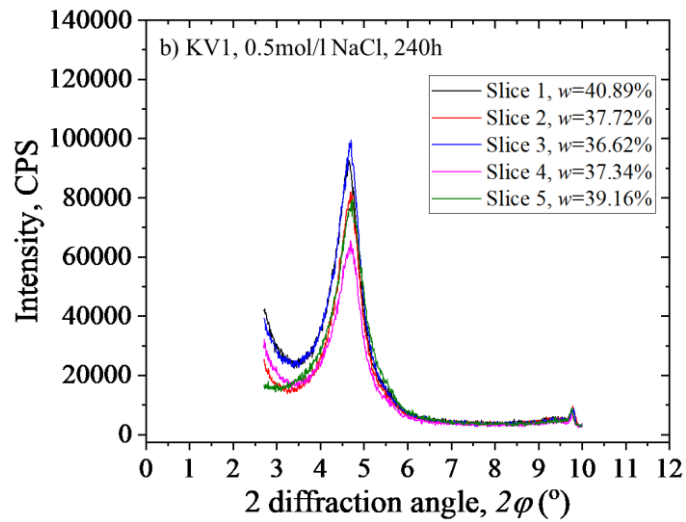
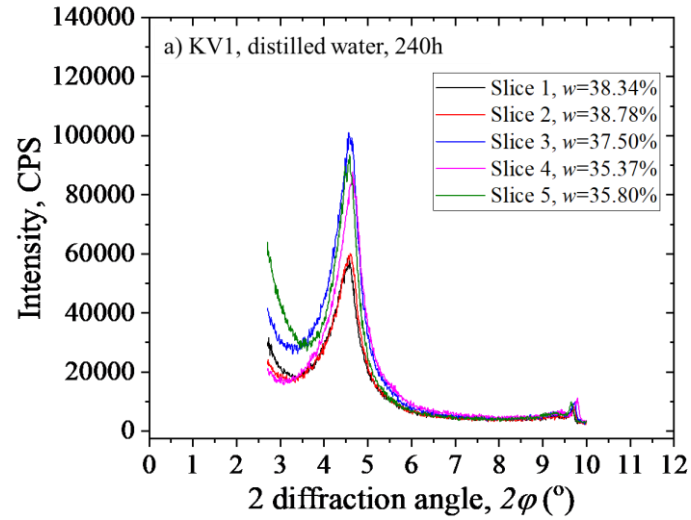


**Figure 8-18 XRD profiles for KV1 saturated by distilled water, 0.5mol/l NaCl and 0.5mol/l CaCl<sub>2</sub> at 240h**

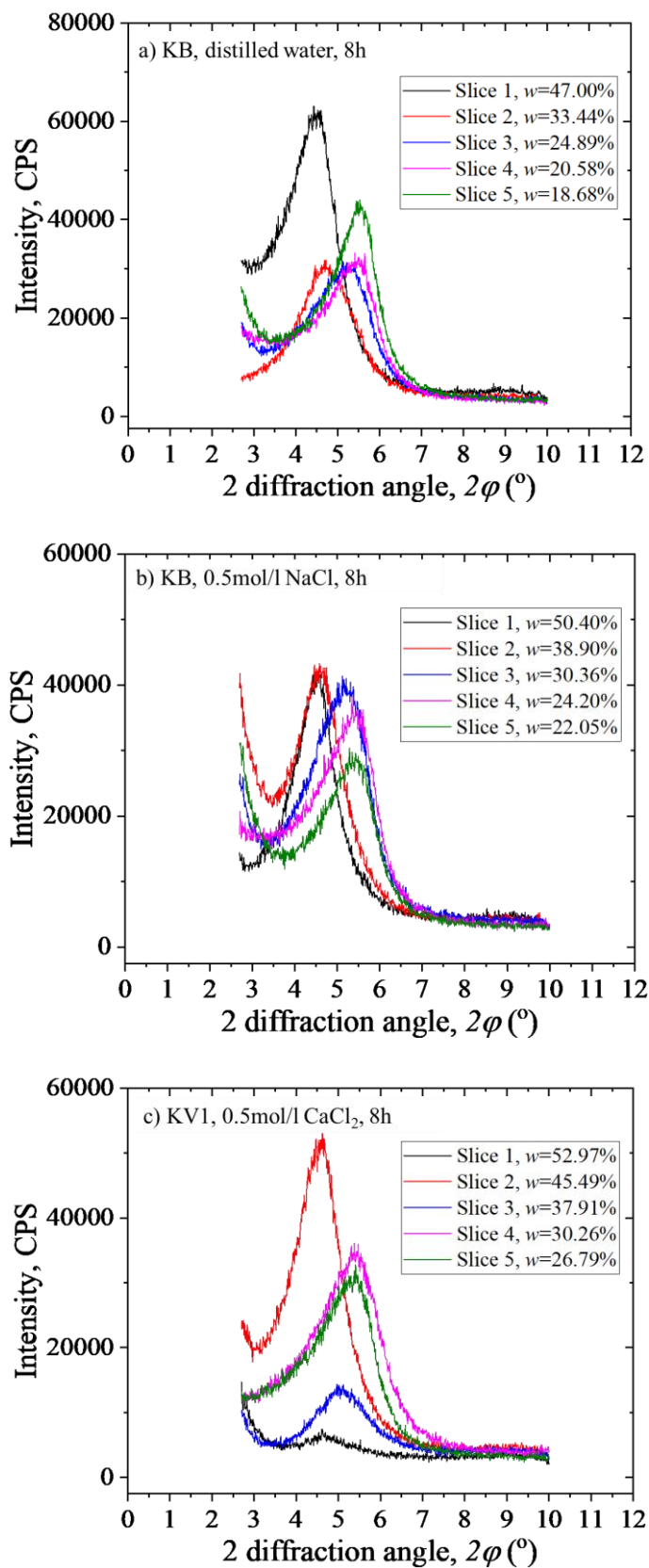


**Figure 8-19 XRD profiles for KB saturated by distilled water, 0.5mol/l NaCl and 0.5mol/l CaCl<sub>2</sub> at 8h**

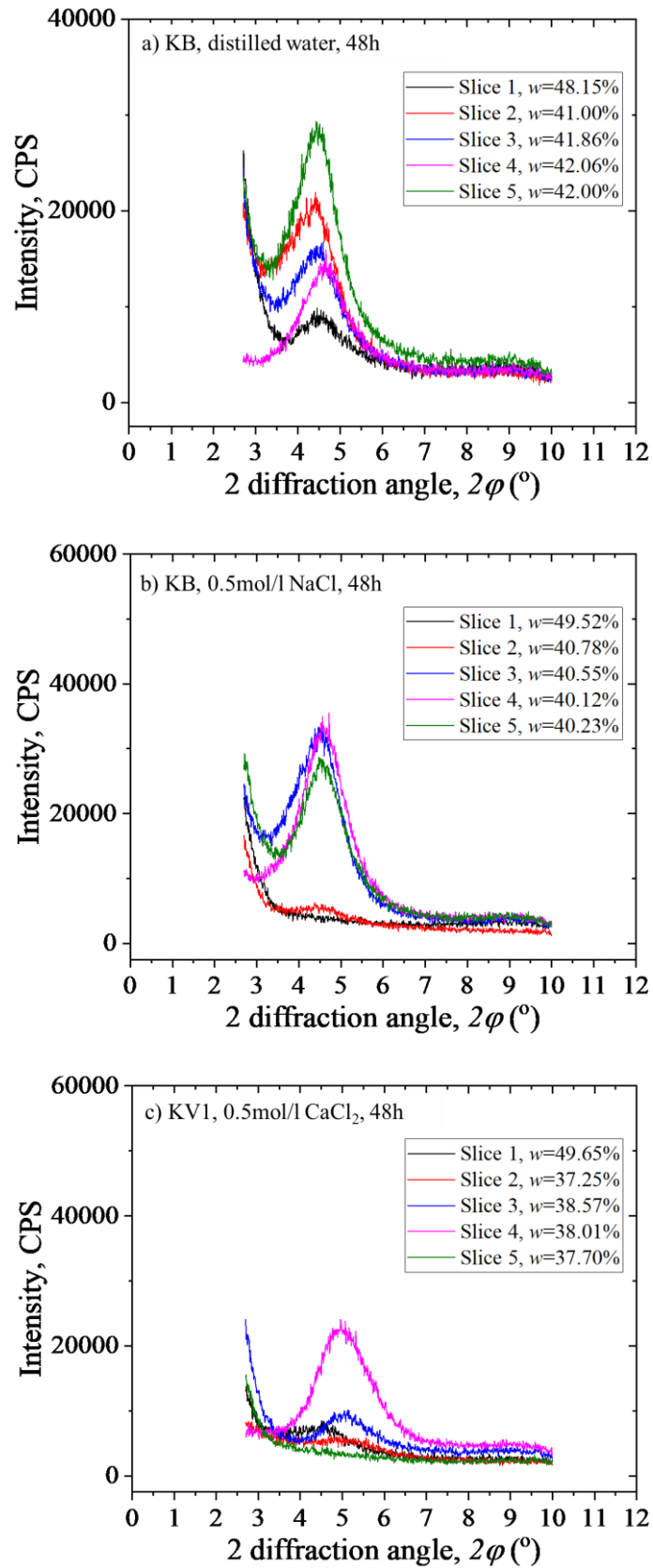


**Figure 8-20 XRD profiles for KB saturated by distilled water, 0.5mol/l NaCl and 0.5mol/l CaCl<sub>2</sub> at 48h**

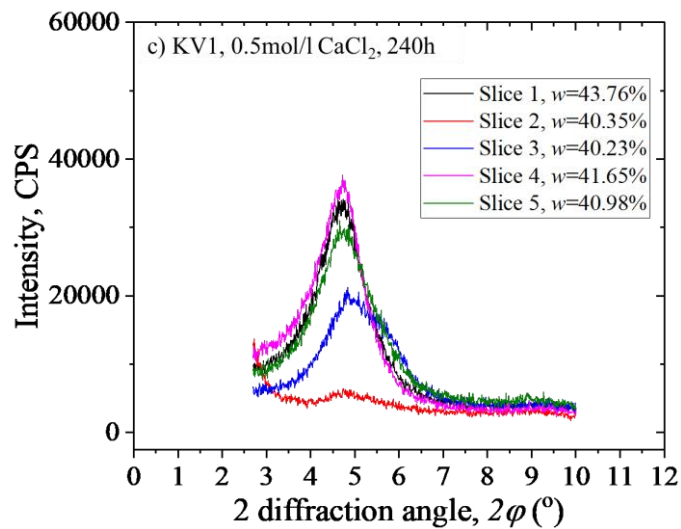
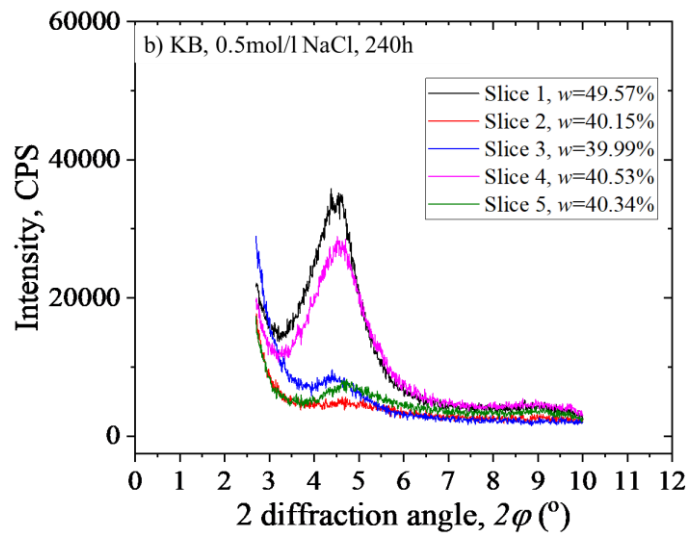
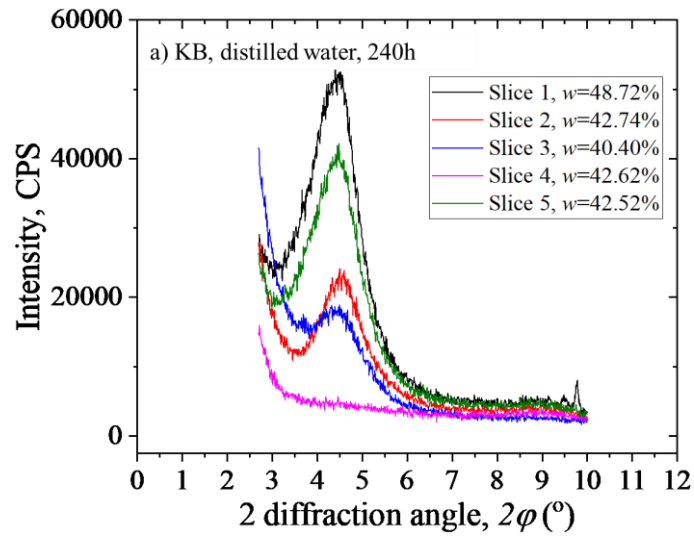
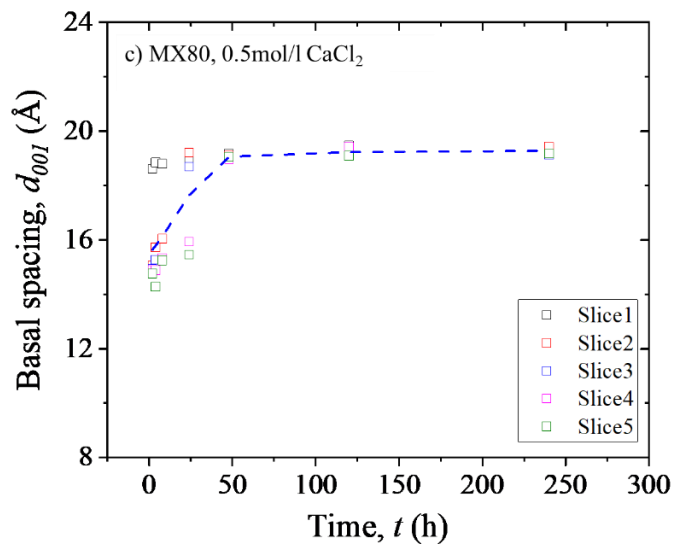
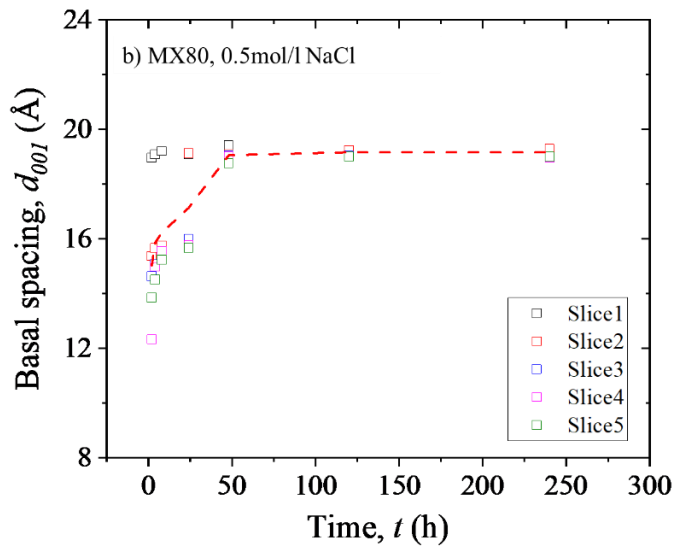
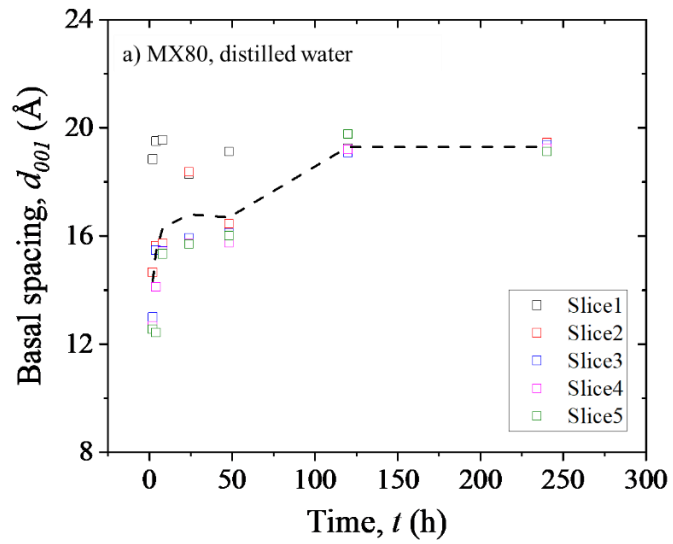
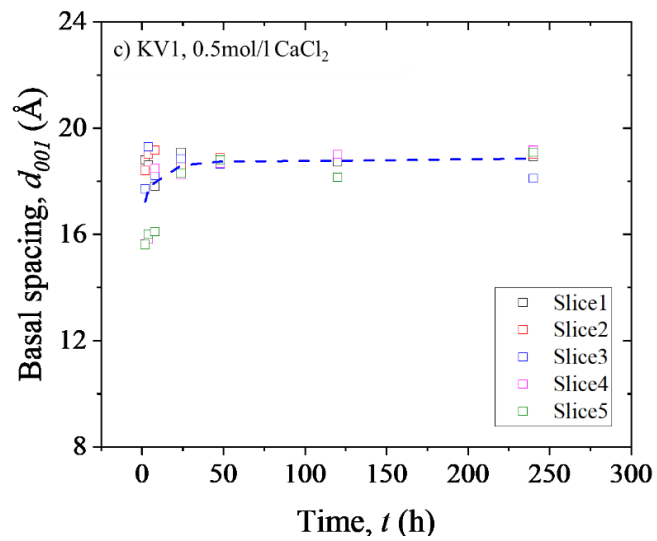
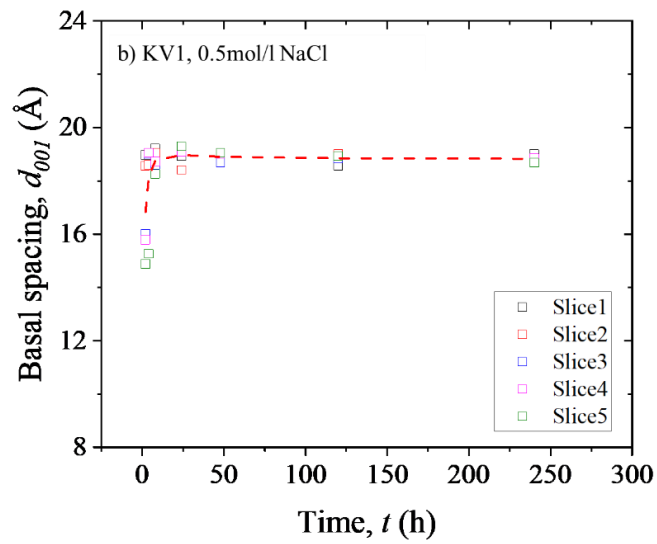
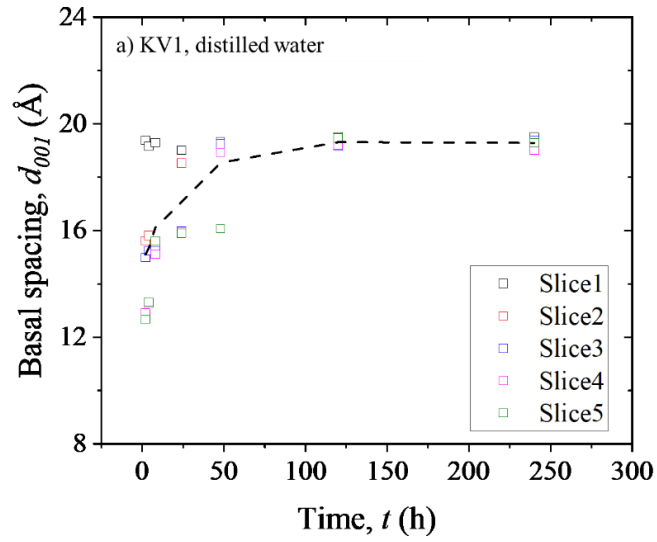


Figure 8-21 XRD profiles for KB saturated by distilled water, 0.5mol/l NaCl and 0.5mol/l CaCl<sub>2</sub> at 240h



**Figure 8-22 Basal spacing of MX80 saturated by distilled water, 0.5mol/l NaCl and 0.5mol/l CaCl<sub>2</sub>**



**Figure 8-23 Basal spacing of MX80 saturated by distilled water, 0.5mol/l NaCl and 0.5mol/l CaCl<sub>2</sub>**

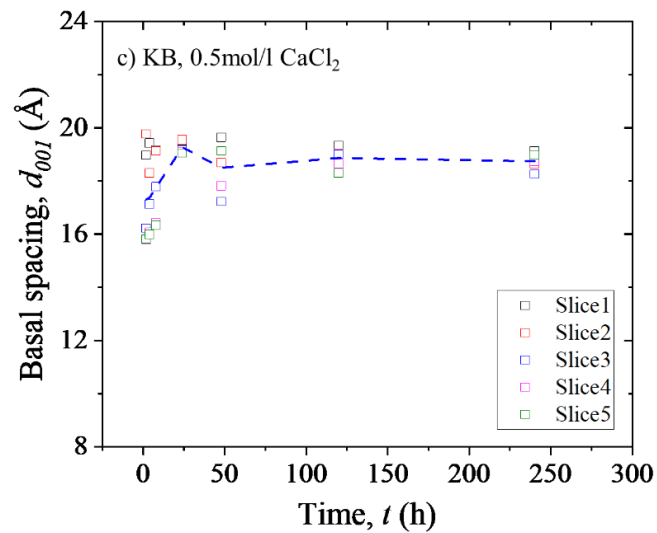
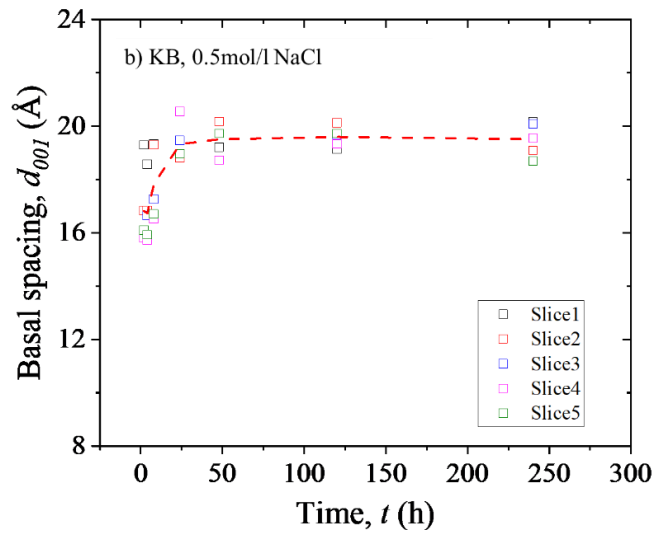
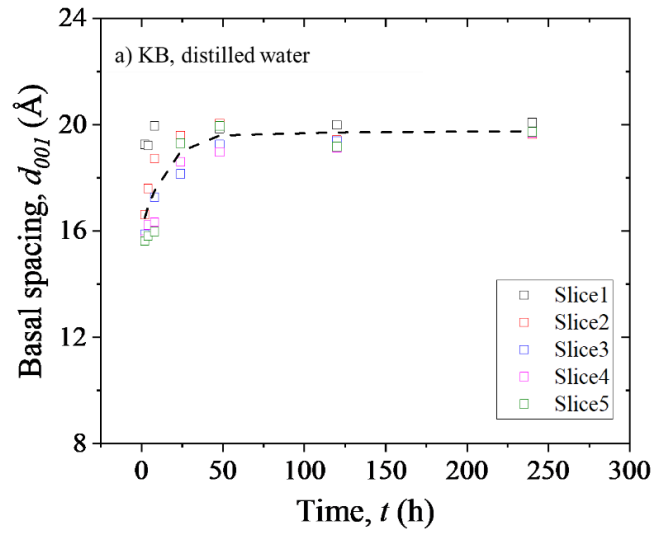
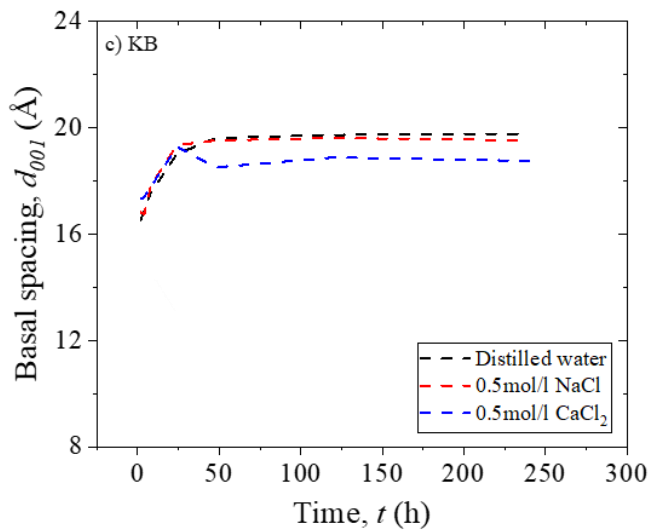
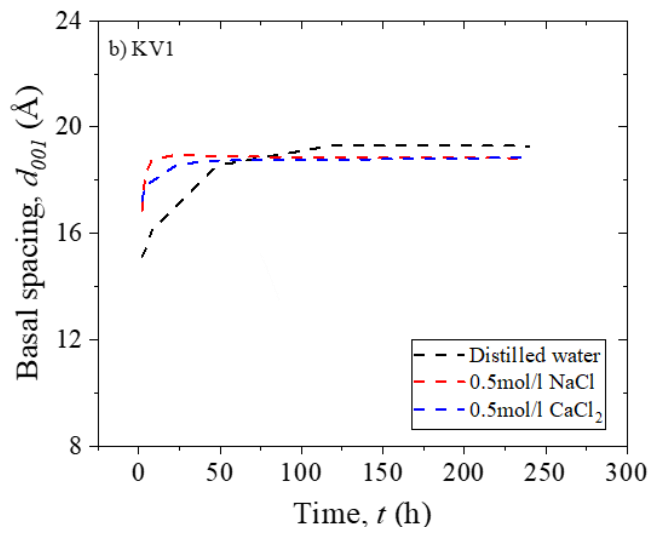
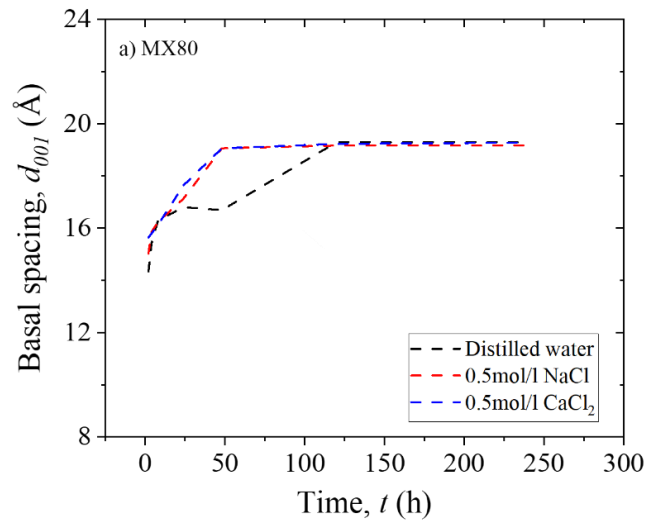
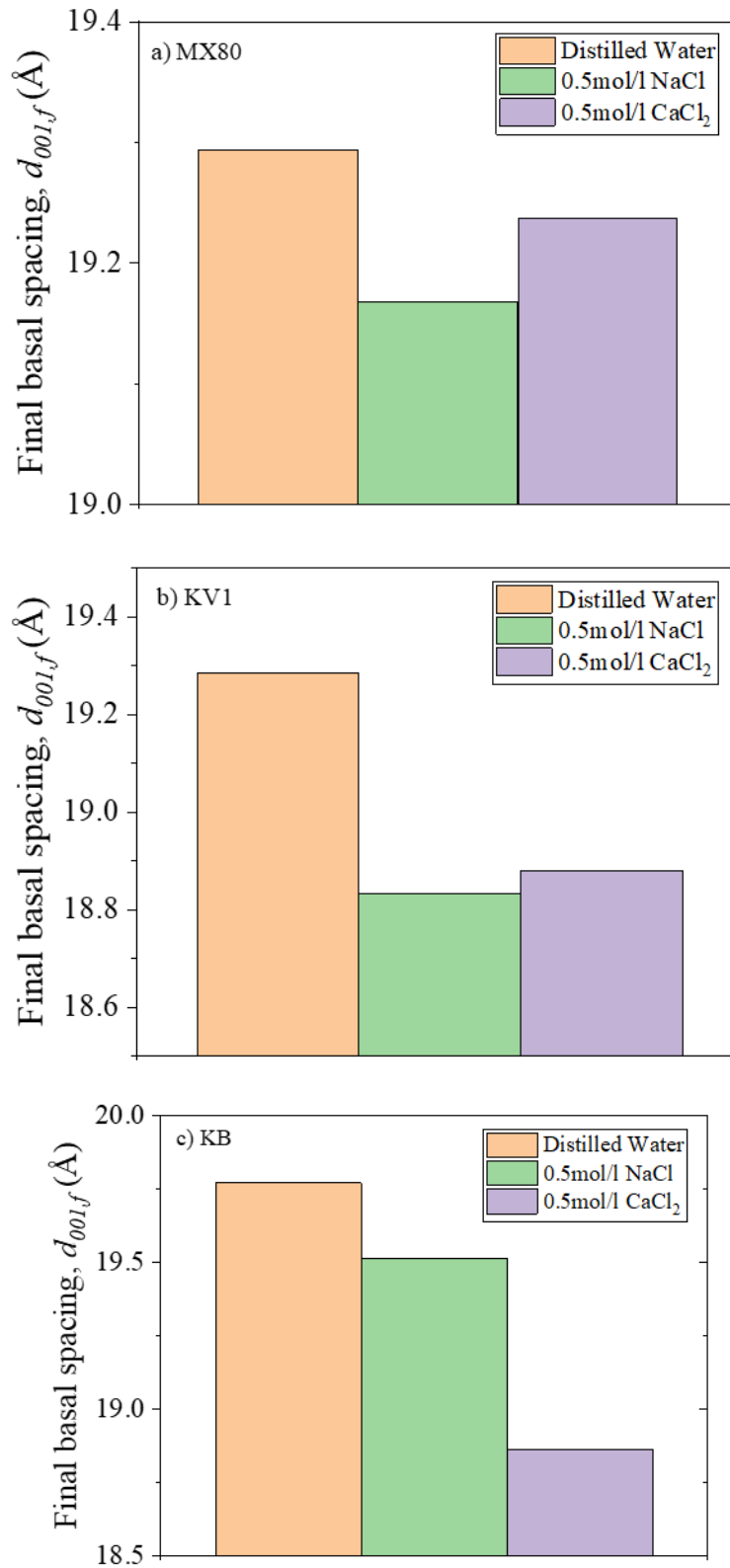


Figure 8-24 Basal spacing of KB saturated by distilled water, 0.5mol/l NaCl and 0.5mol/l CaCl<sub>2</sub>



**Figure 8-25 Basal spacing of bentonites saturated by distilled water, 0.5mol/l NaCl and 0.5mol/l CaCl<sub>2</sub>**



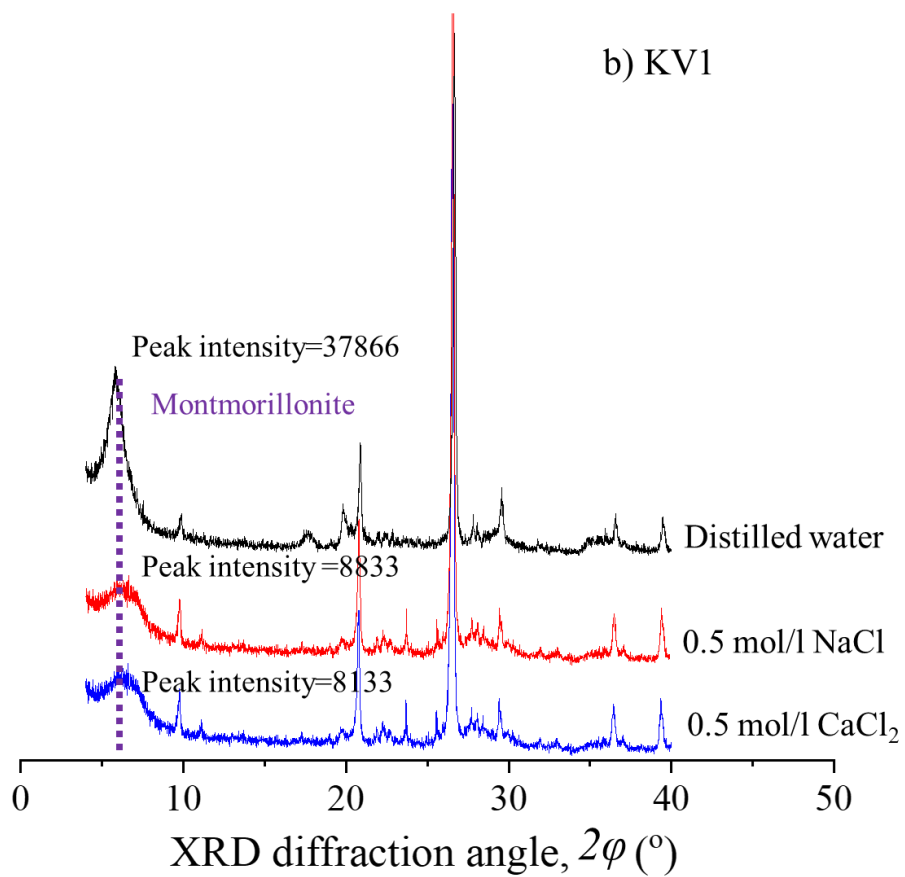
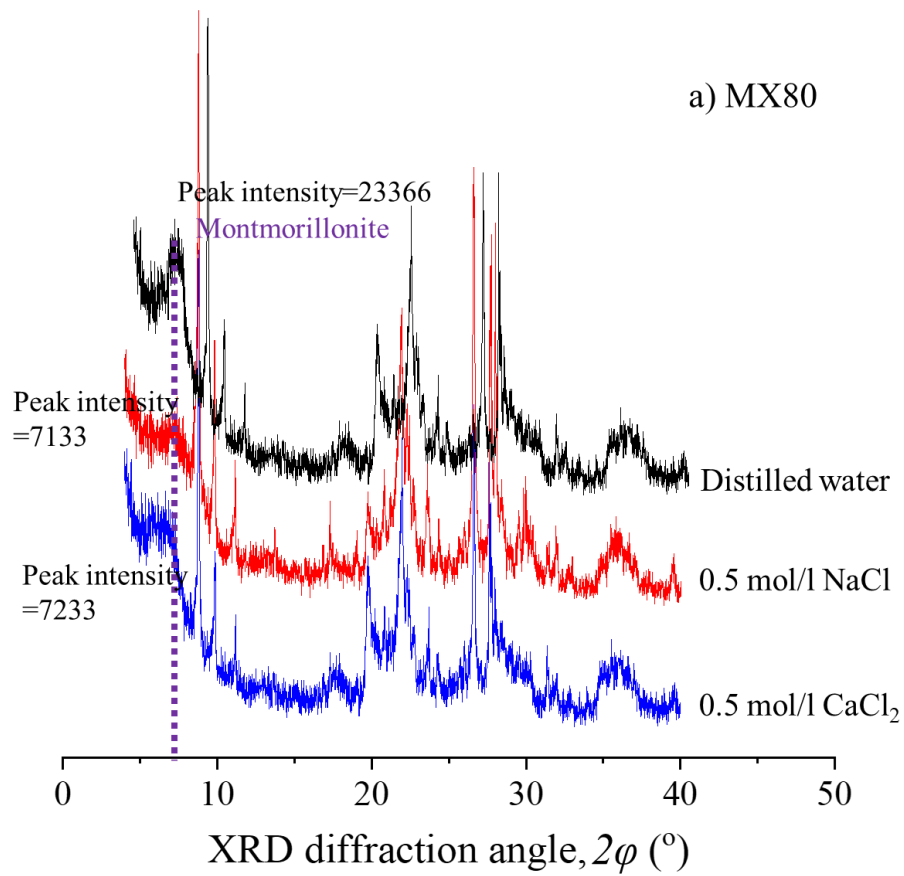
**Figure 8-26 Final basal spacing of bentonites saturated by distilled water, 0.5mol/l NaCl and 0.5mol/l  $\text{CaCl}_2$**

water contents of five slices saturated by NaCl are greater than ones saturated by CaCl<sub>2</sub> and distilled water. The peak positions of slices generally move right with the increase of slice number. When  $t=48$  and 240h, water contents of slices stay in relative stable values. The water content does not change greatly as the slice number changes. The peak angles of XRD profiles seems remain in similar values. However, about the intensity in XRD profile, no clear trend can be found from those XRD profiles.

Basal spacings of 5 slices and specimen (average basal spacing of five slices) saturated by different liquids during wetting is presented in Fig. 8-22, 8-23 and 8-24. Figure 8-22, 8-23 and 8-24 show that basal spacing increases with rising time drastically in the starting wetting period. Then, basal spacing enters into long term stable state. By combining Fig. 8-22, 8-23 and 8-24, Fig. 8-25 presents the basal spacing of bentonites saturated by different liquids. An interesting phenomenon might be found from Fig. 8-25, salt solutions may have higher basal spacing growing speed than distilled water in beginning duration. There is no clear trend for the effect on salt solution type on basal spacing growing speed in the beginning wetting durations.

Final basal spacings of compacted bentonites ( $t=240h$ ) saturated by different liquids are shown in Fig. 8-26 and their XRD profile are indicated in Fig. 8-15, 8-18 and 8-21. It can be easily found from Fig. 8-26 that, final basal spacings saturated by distilled water are bigger than those saturated by salt solutions (NaCl and CaCl<sub>2</sub>). Other interesting results could be achieved from Fig. 8-26 are: 1) for sodium bentonites (MX80 and KV1), final basal spacings saturated by CaCl<sub>2</sub> are greater than those by NaCl. 2) for calcium bentonite (KB), final basal spacing is larger when saturation liquid is NaCl.

#### 8.2.4 Mineral detection, CECs and EXCs



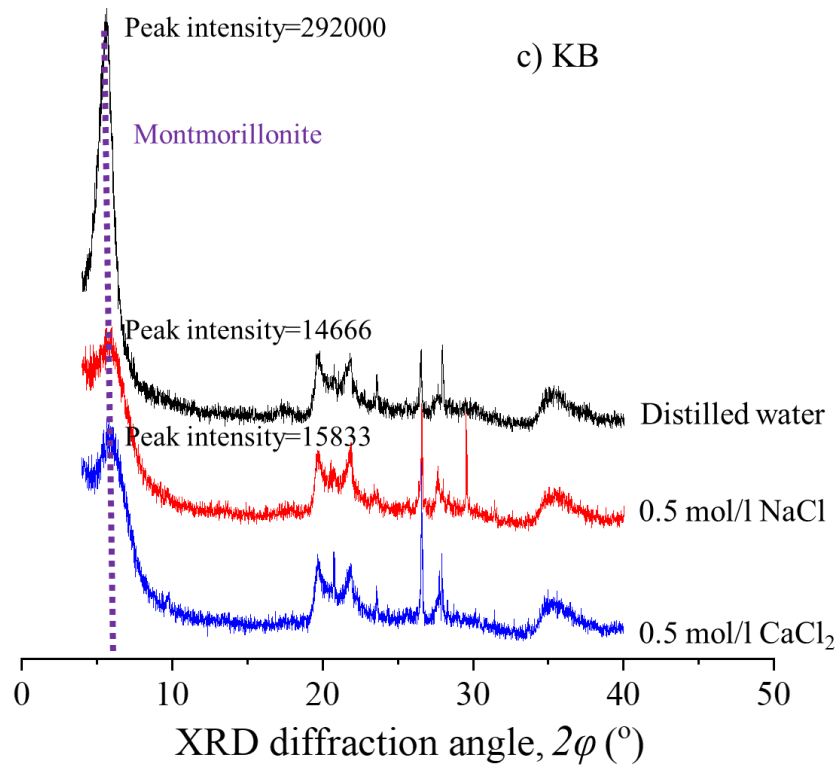


**Figure 8-27 Mineral detection of bentonites saturated by distilled water, 0.5mol/l NaCl and 0.5mol/l  $\text{CaCl}_2$**

Figure 8-27 presents the mineral detection of bentonites saturated by different liquids (uncovering at 240h) by XRD. As reported by tremendous scholars, the montmorillonite amount can be estimated by the intensity of the peak when the 2-diffraction angle at approximate.  $6^{\circ}$ . Even through there are some other peak positions can represent montmorillonite, the 2-diffraction angle at approximate.  $6^{\circ}$  was adopted as the determination of montmorillonite in this study.

It can be concluded from Fig. 8-27, distilled water saturated bentonite seems have more montmorillonite than salt solutions (0.5mol/l NaCl and 0.5mol/l  $\text{CaCl}_2$ ). However, the montmorillonite difference between NaCl and  $\text{CaCl}_2$  seems very small. Hence, this study assumes NaCl and  $\text{CaCl}_2$  have equal influence on the mineral composition of bentonites.

**Table 8-2 CECs and EXCs of different bentonites saturated by different liquids  
(meq/g).**

Material	MX80			KV1			KB		
	Liquids	DIW	NaCl	CaCl <sub>2</sub>	DIW	NaCl	CaCl <sub>2</sub>	DIW	NaCl
CEC	1.213	1.204	1.212	1.023	1.028	1.090	0.819	0.836	0.818
EXC <sub>Na<sup>+</sup></sub>	0.838	0.812	0.477	0.648	0.653	0.343	0.078	0.050	0.057
EXC <sub>Ca<sup>2+</sup></sub>	0.361	0.382	0.724	0.368	0.308	0.738	0.604	0.627	0.622
EXC <sub>K<sup>+</sup></sub>	0.003	0.004	0.003	0.002	0.004	0.004	0.002	0.003	0.002
EXC <sub>Mg<sup>2+</sup></sub>	0.011	0.006	0.008	0.002	0.003	0.003	0.135	0.156	0.133

It is generally recognized that cation exchange is a significant ingredient affecting the equilibrium swelling pressure. The cation exchange is greatly affected by the size of cation, valence and type (Abdullah et al., 1888; Mata, 2005). A typical order for cation exchanging capacity is:  $Na^+ < K^+ < Mg^{2+} < Ca^{2+}$  (Mitchell and Soga, 2005; Pusch, 2001). Hence, when sodium bentonites infiltrated with  $CaCl_2$ , sodium will be replaced by calcium, resulting in the transform from sodium bentonite to calcium bentonite (Zhu et al., 2013). In order to find whether sodium type bentonites undergo cation exchange when infiltrated with  $CaCl_2$ , CEC and EXC tests were performed. Table 8-2 expresses the CEC and EXC of different bentonites saturated by different liquids. In Table 8-2,  $EXC_{Ca^{2+}}$  of sodium type bentonites saturated by  $CaCl_2$  increases greatly than distilled water and NaCl, and same phenomenon was reported about sodium GMZ01 bentonite by Xiang et al. (2017). This phenomenon represents that, cation exchange might happen when sodium type bentonites saturated with  $CaCl_2$ . Meanwhile, as Table 8-2 indicates, there may be no cation exchange happens for KB infiltrated with NaCl and  $CaCl_2$ .

### 8.3 Discussion

### 8.3.1 The effect of solutions on water diffusivity

The movement of water is affected greatly by the pores distribution as discussed in chapter 4. As introduced in Chapter 4 and Chapter 5, the new macropore proposed in this study was assumed as the water flowing path in compacted bentonite. Ruan et al. (2022) associated micro porosity ( $n_{micro}$ , porosity of micro pore) and macro porosity ( $n_{macro}$ , porosity of macro pore) in bentonite with basal spacing by supposing that montmorillonite layers uniformly distributed in the compacted bentonite during saturation, as given:

$$n_{micro} \approx n_{nonmicro}C_m + n_{nonmicro}(1 - C_m) \quad (8-1)$$

$$n_{nonmicro} = \frac{d_{001} - \delta_s}{d_{001}} \quad (8-2)$$

$$n_{total} = 1 - \frac{\rho_d}{G_s} \quad (8-3)$$

$$n_{macro} = n_{total} - n_{micro} \quad (8-4)$$

where  $\rho_d$  is the dry density of the bentonite;  $G_s$  is the soil particle density of bentonite;  $\delta_s$  is the thickness of montmorillonite ( $\delta_s=9.6$  nm from Likos and Lu 2007).  $C_m$  is the montmorillonite content in bentonite;  $n_{total}$  is the total porosity;  $n_{nonmicro}$  is the montmorillonite microporosity;  $n_{micro}$  is non-montmorillonite microporosity (=0 from Ruan et al. 2022).

Macro porosity and water diffusivity changing with degree of saturation are indicated in Fig. 8-28. As Fig. 8-28 depicts, the effects of liquids on water diffusivity and macro porosity during saturation are consistent. This phenomenon shows that the water diffusivity might be controlled by macro pore. With the increase of macro pore, the water moving path was enlarged, thereby bringing larger water diffusivity.

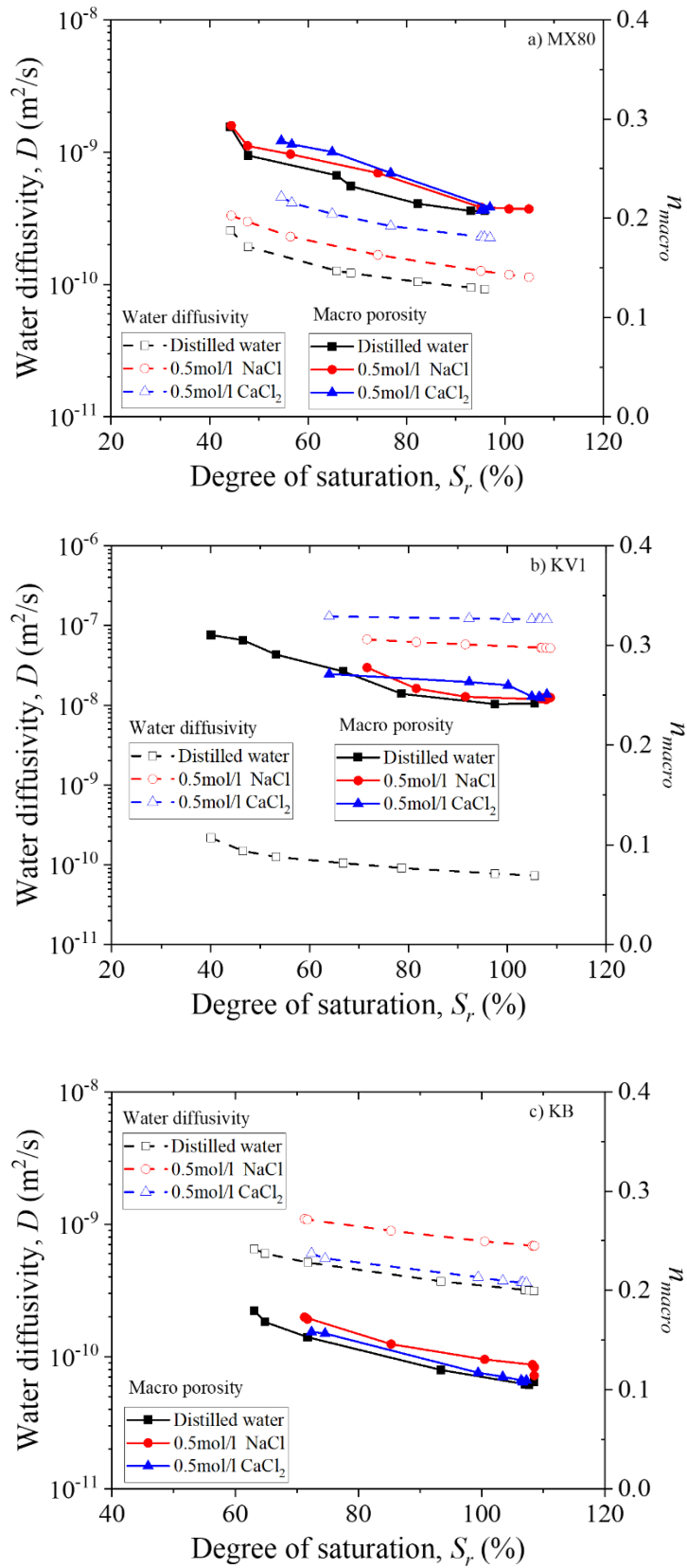


**Figure 8-28 Macro porosity and water diffusivity changing with degree of saturation**

### 8.3.2 Equilibrium swelling pressure of different type bentonites saturated by different salt solutions

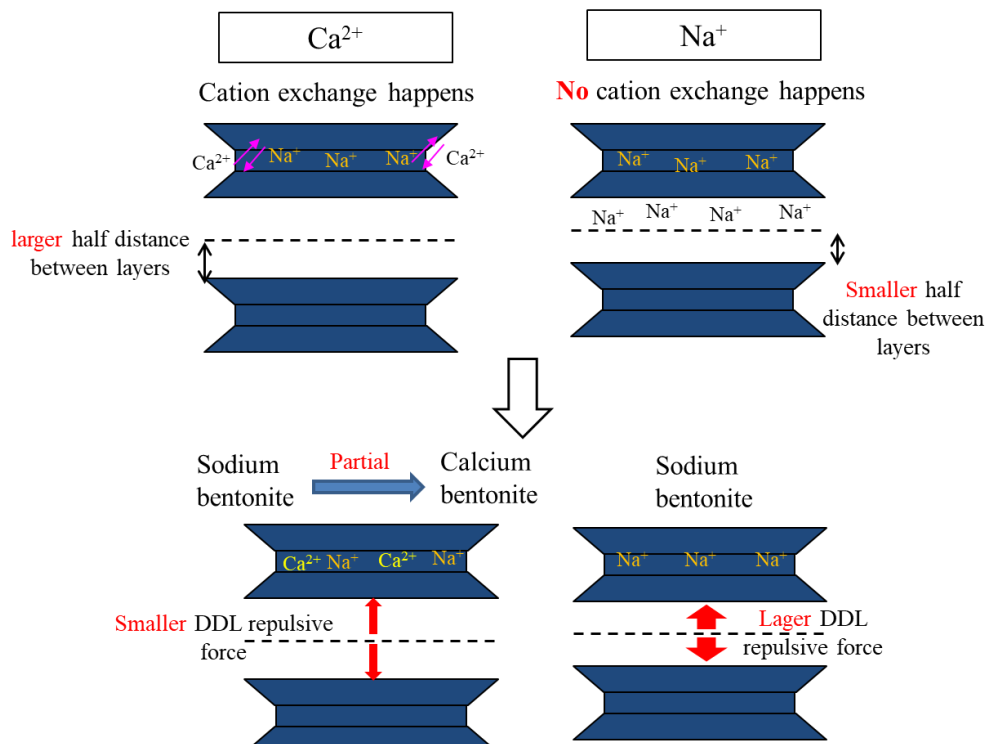


**Figure 8-29 Sodium type bentonite saturated by different salt solutions**

As interpreted above, salt solutions have inconsistent effect on swelling pressures of different cation type bentonite. A summary was conducted herein: 1) for sodium type bentonite (KV1 and MX80) in this study,  $\text{Ca}^{2+}$  solution saturated specimens have larger equilibrium swelling pressure than  $\text{Na}^+$  solution saturated ones; 2) for calcium type bentonite (KB),  $\text{Na}^+$  solution obtains larger equilibrium swelling than those from  $\text{Ca}^{2+}$ . Firstly, the effect of salt solutions on swelling pressure of sodium type bentonite. As indicated in Fig. 8-27, the  $\text{Na}^+$  and  $\text{Ca}^{2+}$  might have equal influence on the mineral composition of bentonites. The discussion in this section was considered from the aspect of basal spacing and cation exchange. In Table 8-2, it was reported that, when sodium bentonite saturated by  $\text{Ca}^{2+}$ , cation exchange may happen (Fig. 8-29), leading sodium type bentonite partially changes to calcium type bentonite. Some scholars considered that calcium type bentonite has larger swelling pressure than sodium type

bentonite (e.g., Jadda and Bag 2020). By applying a sodium type bentonite and another calcium type bentonite in swelling pressure tests, Jadda and Bag (2020) reported that calcium type bentonite has larger swelling pressure than sodium type bentonite during saturation. However, in Jadda and Bag (2020), in addition to the bentonite cation type, the specimens sent to swelling pressure tests still have certain difference in other conditions including montmorillonite content. Thus, it cannot be determined that the larger swelling pressure is only due to the bentonite cation type. Swelling pressure tests for different cation type bentonites of similar montmorillonite should be performed in the future. Additionally, the final basal spacing increased when saturation liquid changed from  $\text{Ca}^{2+}$  to  $\text{Na}^+$  (Fig. 8-26), which would result in smaller DDL repulsive force (Komine and Ogata 2004, Fig. 8-29). The increase of equilibrium swelling pressure from cation exchange conquers the decrease of equilibrium swelling pressure from increasing basal spacing, thereby giving larger equilibrium swelling pressure saturated by  $\text{Ca}^{2+}$ .

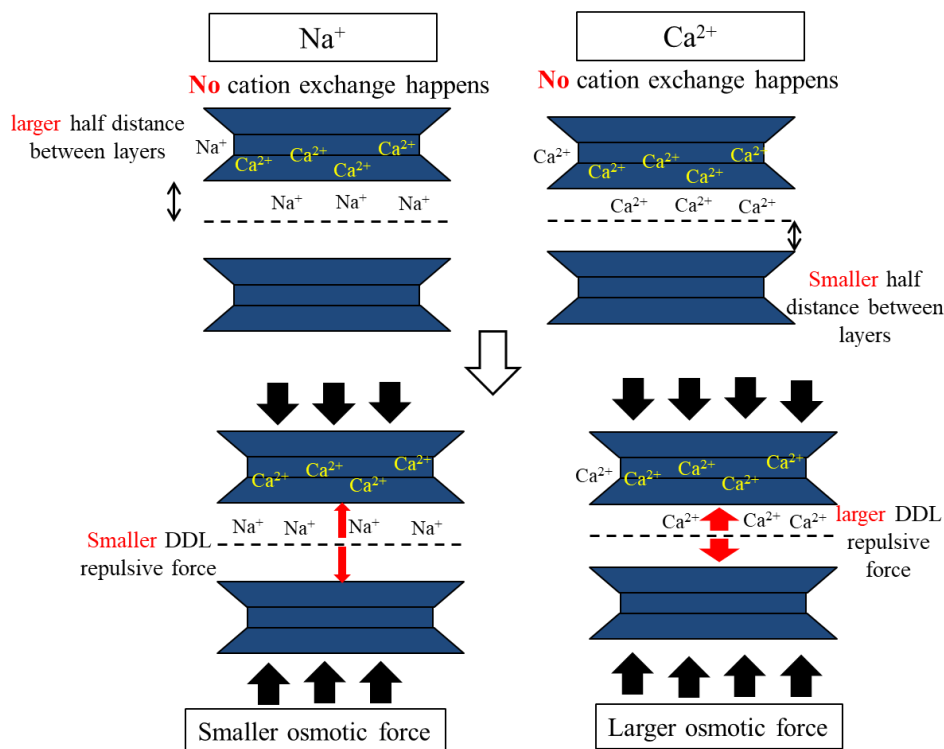


**Figure 8-30 Calcium type bentonite saturated by different salt solutions**

Secondly, the effect of salt solutions on calcium type bentonite. As interpreted and revealed in Table 8-2, when calcium bentonite saturated by  $\text{Na}^+$  and  $\text{Ca}^{2+}$ , cation exchange may does not happen (Fig. 8-30), thus the cation exchange on equilibrium swelling pressure for calcium type bentonite can be negligible. As indicated in Fig. 8-26, calcium bentonite from  $\text{Na}^+$  has larger final basal spacing than  $\text{Ca}^{2+}$ , giving smaller DDL repulsive force. However, the larger osmotic force from 0.5mol/l  $\text{CaCl}_2$  in bentonite (Castellanos et al. 2008) would give a negative effect on equilibrium swelling pressure, leading larger equilibrium swelling pressure for calcium bentonite saturated by 0.5mol/l  $\text{NaCl}$ .

## Conclusions

NaCl, CaCl<sub>2</sub> solutions and distilled water were used as the saturation liquids to observe the effect of liquid salt type on swelling pressure and water diffusivity of different cations bentonites. The testing findings can be concluded as:

1. For all three bentonites, distilled water saturated ones obtain bigger equilibrium swelling pressure than those saturated by NaCl and CaCl<sub>2</sub>. Larger equilibrium swelling pressure was achieved when sodium bentonites (MX80 and KV1) saturated by CaCl<sub>2</sub> than those saturated by NaCl. Equilibrium swelling pressure of KB increases when saturation liquid changed from CaCl<sub>2</sub> to NaCl.
2. No matter bentonite type, water diffusivities infiltrated by distilled water were lower than those infiltrated by NaCl and CaCl<sub>2</sub>. Sodium bentonites saturated by CaCl<sub>2</sub> has bigger water diffusivities than NaCl. For calcium type bentonite, NaCl saturated specimens have larger water diffusivities.
3. Final basal spacings saturated by distilled water are larger than those saturated by salt solutions. For sodium bentonites, final basal spacings saturated by CaCl<sub>2</sub> are greater than those by NaCl. Regarding calcium bentonite, final basal spacing is larger when saturation liquid is NaCl.

## References

- Abdullah, W.S., Alshibli, K.A., and Al-Zou'bi, M.S., 1988. Influence of pore water chemistry on the swelling behavior of compacted clays. *Applied Clay Science*, **15**: 447-462.
- Castellanos, E., Villar, M.V., Romero, E., Lloret, A., and Gens, A., Chemical impact on the hydro-mechanical behaviour of high-density FEBEX bentonite. *Physics and Chemistry of the Earth*, **33**: S516-S526.
- Chen, Y.G., Dong, X.X., Zhang, X.D., Ye, W.M., and Cui, Y.J., 2018. Cyclic thermal and saline effects on the swelling pressure of densely compacted Gaomiaozi bentonite. *Engineering Geology*, **255**: 37–47.
- Jadda, K., Bag, R. 2020. Variation of swelling pressure, consolidation characteristics and hydraulic conductivity of two Indian bentonites due to electrolyte concentration. *Engineering Geology*, 105637.
- Komine, H., and Ogata, N. 2004. Prediction swelling characteristics of bentonites. *Journal of Geotechnical and Geoenvironmental Engineering*, **130**(8): 818–829.
- Lee, O.L., Lim, J.G., Kang, I.M., Kwon, S., 2012. Swelling pressures of compacted Ca-bentonite. *Engineering Geology*, **128-130**: 20-26.
- Likos, W. J., and Lu, N., 2006. Pore-scale analysis of bulk volume change from crystalline interlayer swelling in Na<sup>+</sup>-and Ca<sup>2+</sup>-smectite. *Clays and Clay Minerals* 54(4), 515–528.
- Mata, C., Guimarães, L., do, N., Ledesma, A., Gens, A., and Olivella, S., 2005. A hydro-geochemical analysis of the saturation process with salt water of a bentonite crushed granite rock mixture in an engineered nuclear barrier. *Engineering Geology*, **81**: 227–245.

Pusch, R., and Yong, R. N., 2006. Microstructure of smectite clays and engineering performance. New York, NY, USA: Taylor and Francis.

Ruan, K.L., Komine, H., Ito, D., Miyoshi, K., and Gotoh, T., 2022. Hydraulic conductivity and X-ray diffraction tests of unsaturated bentonites with a multi-ring and their predictions by pores distributions. *Engineering Geology*, **306** (5): 106738.

Sun, D.A., Zhang, L., Li, J., and Zhang, B.C., 2015. Evaluation and prediction of the swelling pressures of GMZ bentonites saturated with saline solution. *Applied Clay Science*, **105**: 207-216.

Wang, H.L., Shirakawabe, T., Komine, H., Ito, D., Gotoh, T., Ichikawa, Y., and Chen, Q., 2020. Movement of water in compacted bentonite and its relation with swelling pressure. *Canadian Geotechnical Journal*, **57**(6): 821-832.

Xiang, G.S., Fang, Y., and Xu, Y.F., 2017. Swelling characteristics of GMZ bentonite affected by cation exchange reaction. *Journal of Zhejiang University (Engineering Science)*, 51(5): 831-836. (in Chinese).

Zhu, C.M., Ye, W.M., Chen, Y.G., Chen, B., and Cui, Y.J., 2013. Influence of salt solutions on the swelling pressure and hydraulic conductivity of compacted GMZ01 bentonite. *Engineering geology*, **166**: 74-80.

## Chapter 9

### **THE EFFECT OF TEMPERATURE ON HYDRAULIC PROPERTIES AND SWELLING PRESSURE OF BENTONITES**

## 9.1 Testing overview

This chapter used 3 bentonites, including MX80, KV1 and KB, to research the effect of temperature on swelling pressures and water diffusivity. This study measured the swelling pressure and water diffusivity separately instead of the multi-ring as introduced above. For swelling pressure test. The swelling apparatus used was introduced in Chapter3 as Fig. 3-2. Herein, in order to control the testing temperature, the swelling pressure device was placed into the oven with a water supply container (Fig. 9-1).

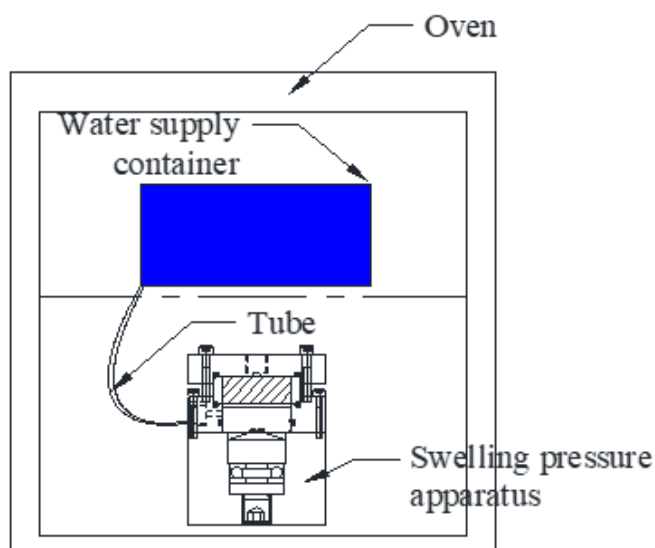


**Figure 9-1 Testing methodology for measuring swelling pressure at different temperatures**

**Table 9-1 Specimen details for swelling pressure tests**

	MX80	KV1	KB
Initial water content (%)	0		
Temperature (°C)	25, 50 and 80		
Dry density (g/cm <sup>3</sup> )	1.1–1.8	1.2–1.8	0.9–1.4

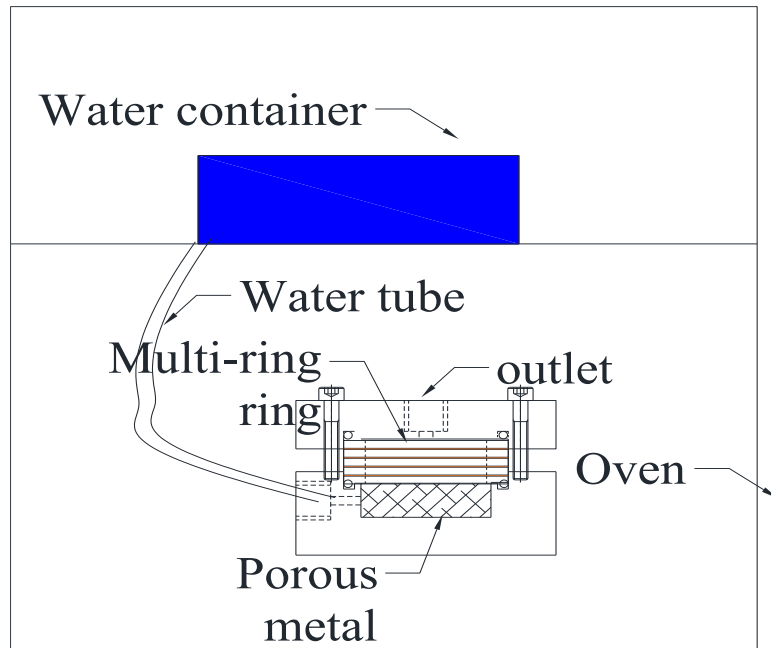


**Figure 9-2 Testing methodology for measuring water diffusivity at different temperatures**

**Table 9-2 Specimen details for water diffusivity tests**

	MX80	KV1	KB
Initial water content (%)	8.92-8.99	8.27-8.46	13.63-14.02
Temperature (°C)	30 and 50		
Dry density (g/cm <sup>3</sup> )	1.48, 1.61 and 1.75	1.48, 1.61 and 1.75	1.30 and 1.43

Regarding the water diffusivity tests at different temperatures. In this section, the multi-ring (Fig. 3-9) was applied in a traditional wetting apparatus (Fig. 7-1). In order to control experimental temperature, the wetting apparatus and water container were put together into the oven. For avoiding the evaporation of water during wetting tests, the part of multi-ring in contact of air was protected by plastic film. Specimen details for water diffusivity tests are presented in Table 9-2.

## 9.2 Results

### 9.2.1 Swelling pressures

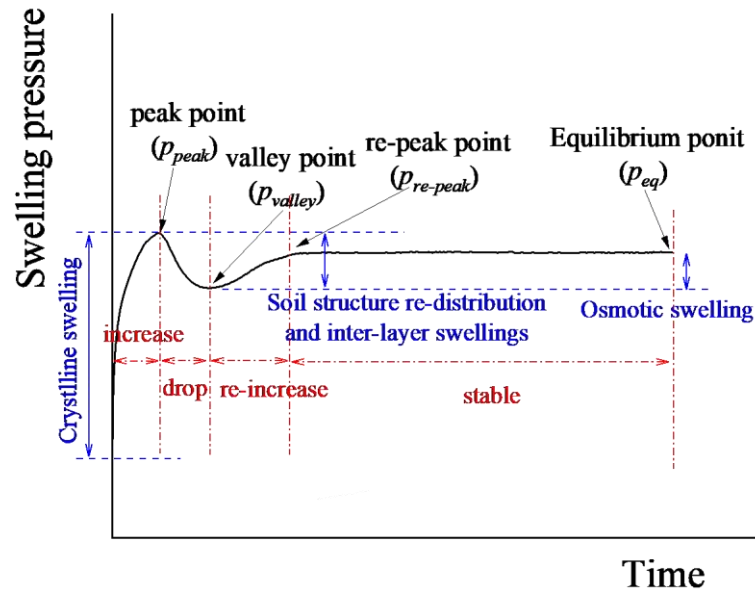


**Figure 9-3 Definitions of swelling pressures during saturation**

The generally reported swelling pressure curve of bentonite has been discussed a lot by scholars and the former chapters in this thesis. Normally, the swelling pressure evolution curve exhibits obvious peaks and valleys. The definitions of swelling pressures are indicated in Fig. 9-3, including peak swelling pressure, valley swelling pressure, re-peak swelling pressure and equilibrium swelling. From the literature review in Chapter 1, former studies focused on equilibrium swelling pressure instead of peak swelling pressure, valley swelling pressure and re-peak swelling pressure. Even though some scholars paid the attention on the dry density effect on swelling pressures during saturation (e.g., Wang et al. 2022; Wang et al. 2022). There is almost no research about the temperature effect on swelling pressures during saturation.

Figure 9-4, 9-5 and 9-6 show the swelling pressure evolution curves of MX80, KV1 and KB at different temperatures, respectively. As we can see from Fig. 9-4, 9-5 and 9-6, almost all swelling pressure evolution curves have clear peaks and valleys.

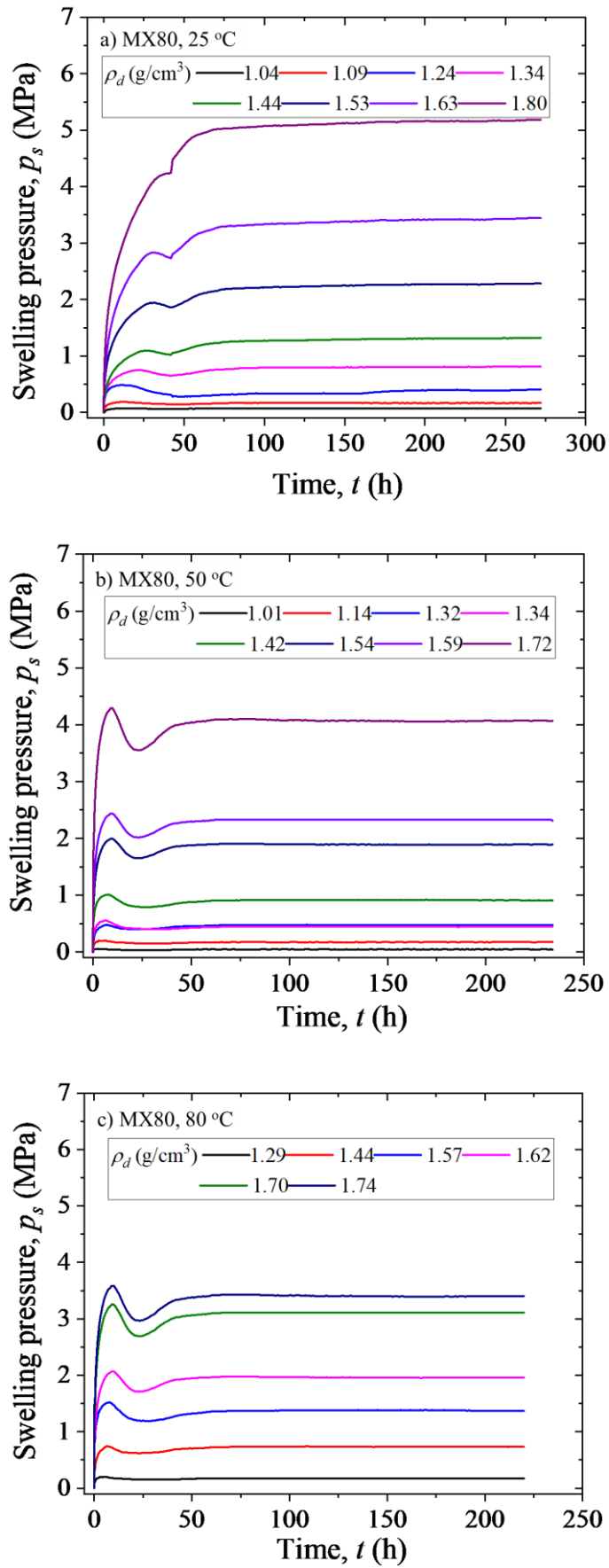


Figure 9-4 Swelling pressure evolution curves of MX80 at different temperatures

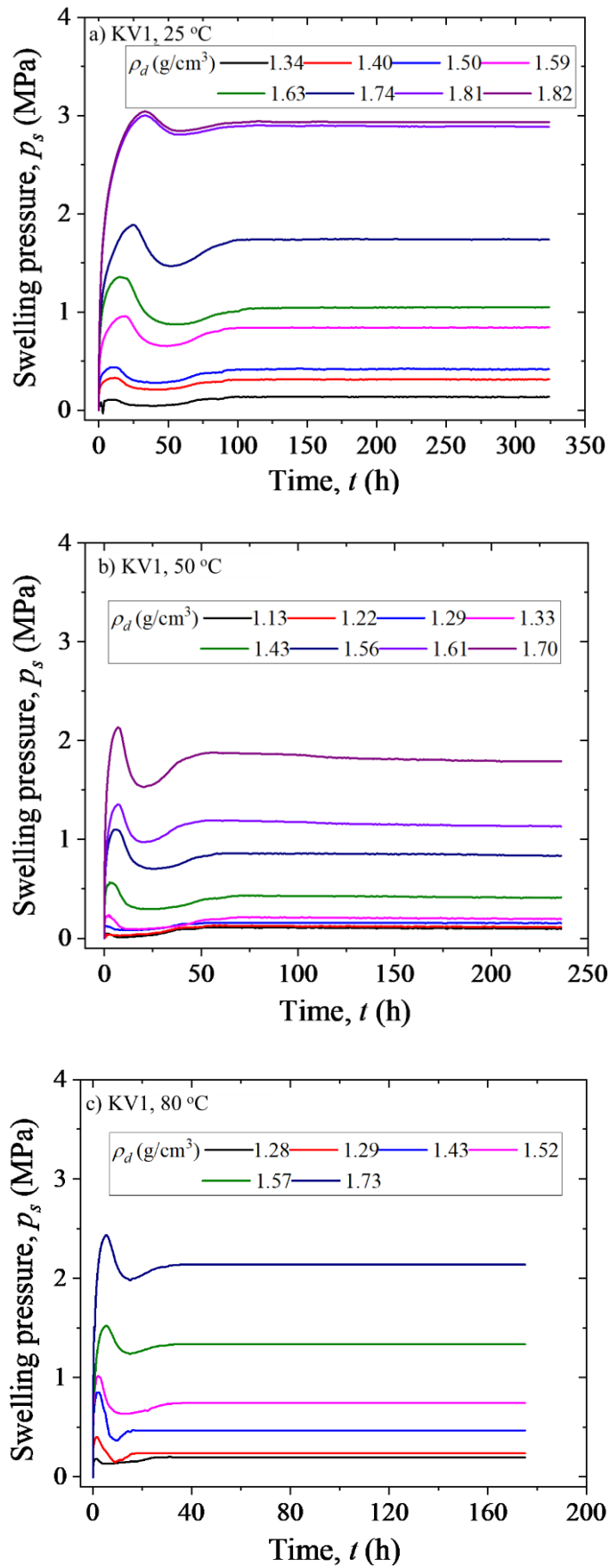


Figure 9-5 Swelling pressure evolution curves of KV1 at different temperatures

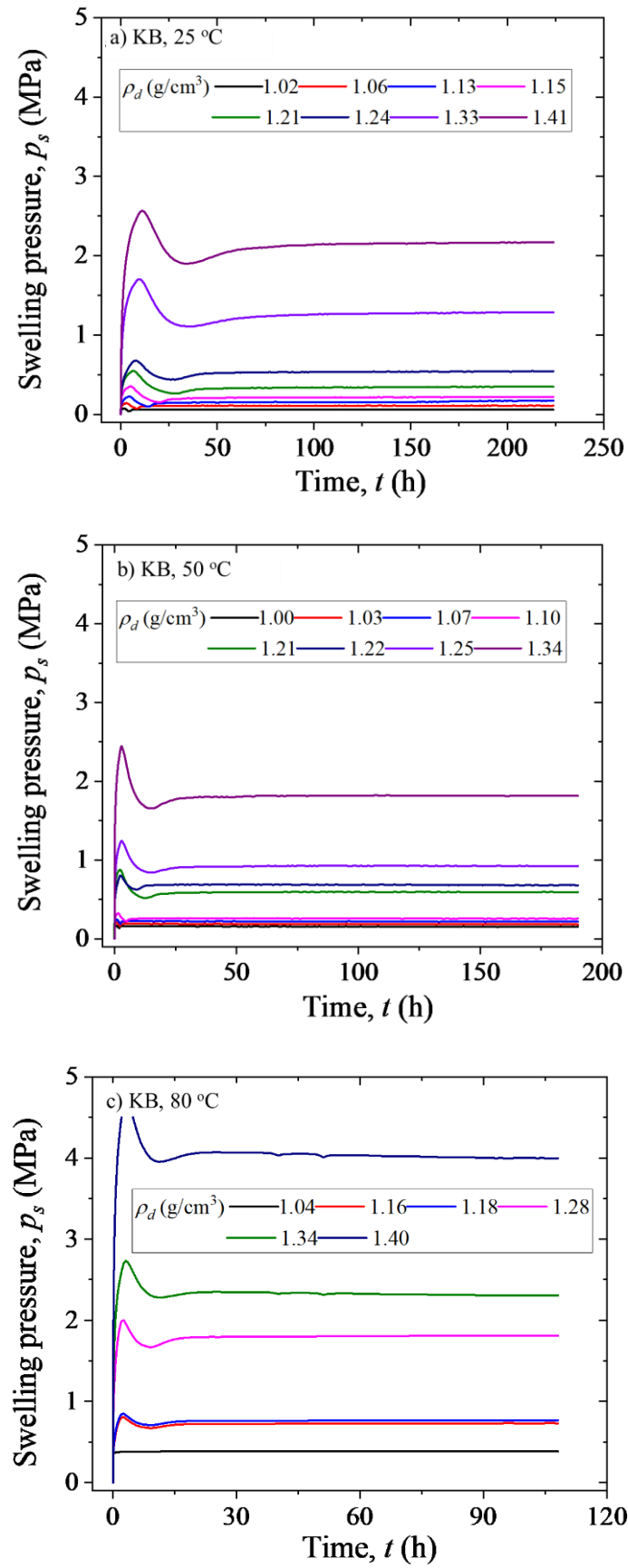


Figure 9-6 Swelling pressure evolution curves of KB at different temperatures

Other important information can be achieved from the swelling pressure evolution curve is the times for reaching peak, valley and re-peak point. An easy conclusion can be made from Fig. 9-4, 9-5 and 9-6 is that, for all three bentonites, times at peak, valley and re-peak points reduce as temperature rise. Figure 9-4 reveal the swelling pressure evolution curves of MX80 at different temperatures. It can be inferred from Fig. 9-4 that, for 25 °C, the times for peaks and re-peaks are, respectively, approx. 35 h and approx. 60 h. When the temperature for experiments is 50 °C, the times for swelling pressures to arrive peaks and re-peaks are, respectively, approx. 12.5 h and approx. 45 h. Then, after the temperature reaches 80 °C, those times change to approx. 9 h and to approx. 40 h. As might be apparent from Fig. 9-5, times for KV1 bentonite to arrive peak points are approx. 25 h, approx. 9 h, and approx. 5 h, respectively, at 25 °C, 50 °C, and 80 °C. From 25 °C to 50 °C to 80 °C, the times in the re-peak points decrease from approx. 90 h to approx. 50 h to approx. 30 h. The times for getting to peaks and re-peak points for KB are indicated in Fig. 9-6. Times in peak and re-peak points decrease gradually from approx. 9 h and approx. 45 h to approx. 5 h and approx. 25 h, then go to approx. 3 h and approx. 15 h, with rising temperatures.

Swelling pressures during saturation of MX80, KV1 and KB at different temperatures are presented in Fig. 9-7, 9-8 and 9-9, respectively. It is an apparent trend from Fig. 9-7 that, peak swelling pressure, valley swelling pressure and valley swelling pressure of MX80 reduce as the experimental temperature increases. However, opposite conclusion was made for KV1 as Fig. 9-8. A general truth from Fig. 9-8 is that, swelling pressures during saturation of KV1 increase with the rise of temperature. For KB, as Fig. 9-9 indicated swelling pressures during saturation increase with rising temperature, which is the same as KV1 and different with the finding for MX80.

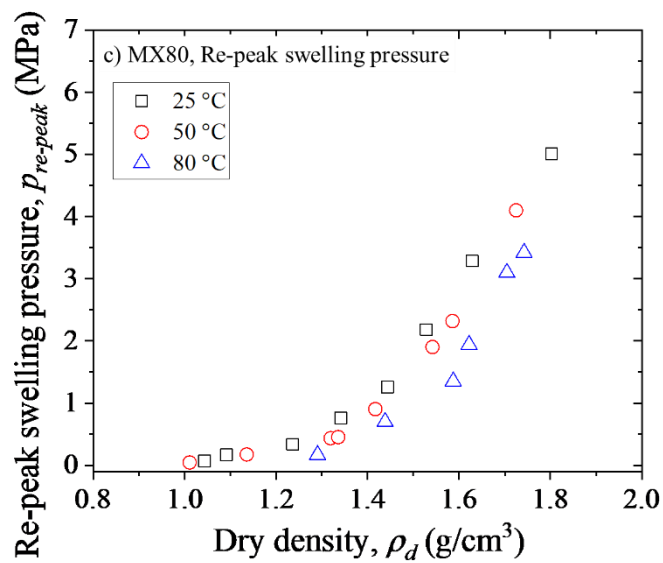
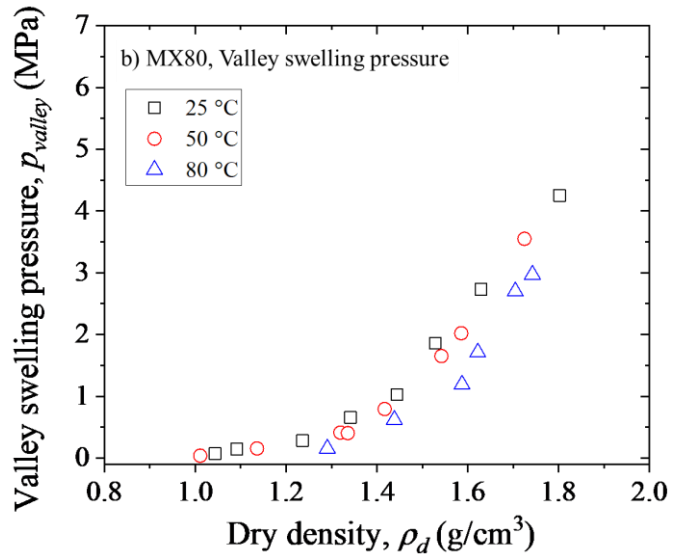
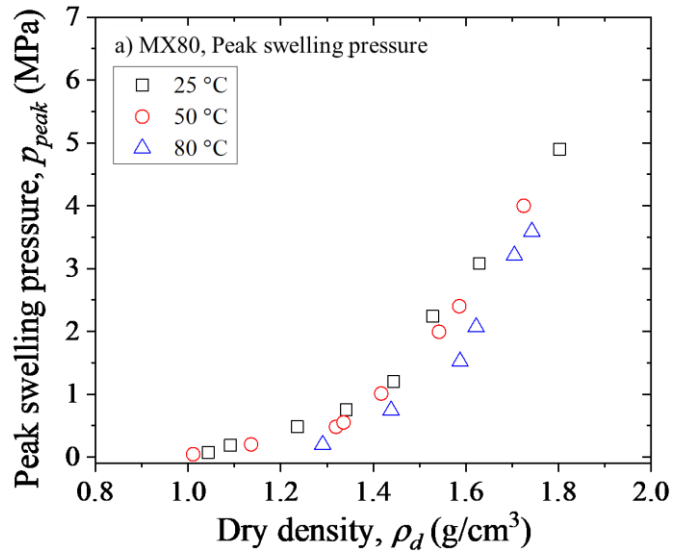


Figure 9-7 Swelling pressures during saturation of MX80

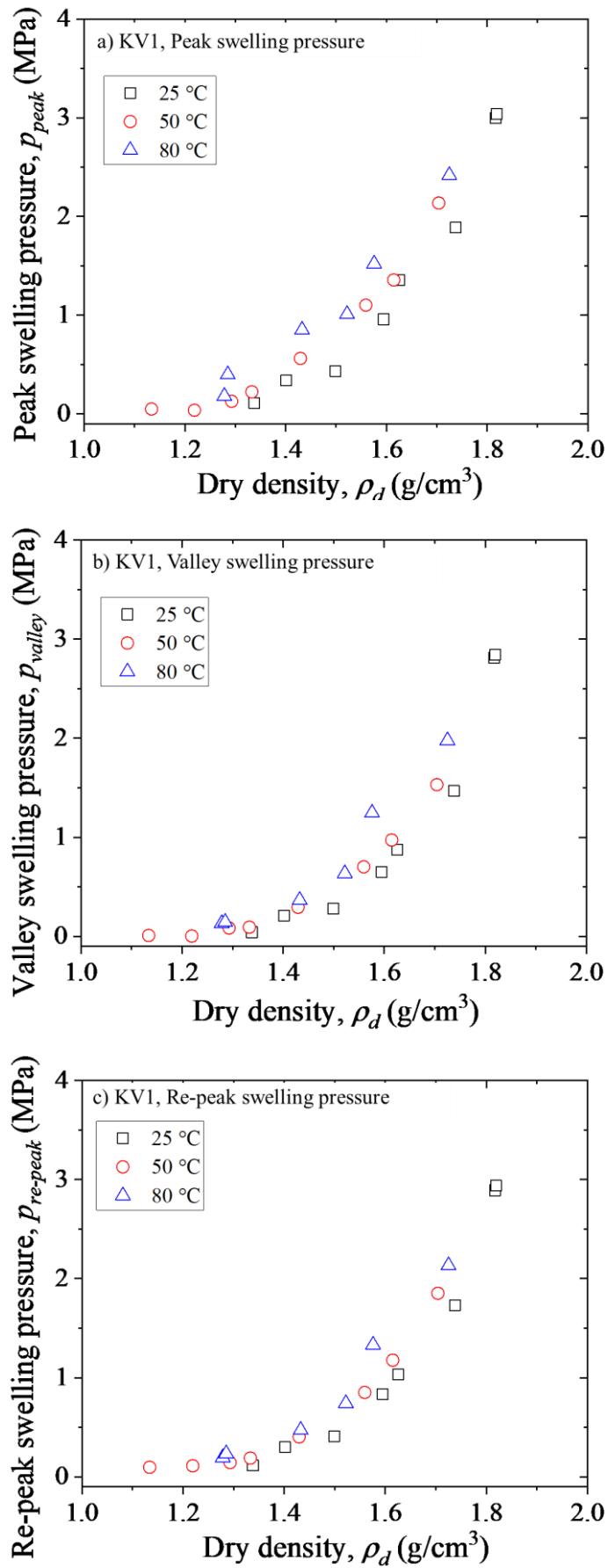


Figure 9-8 Swelling pressures during saturation of KV1

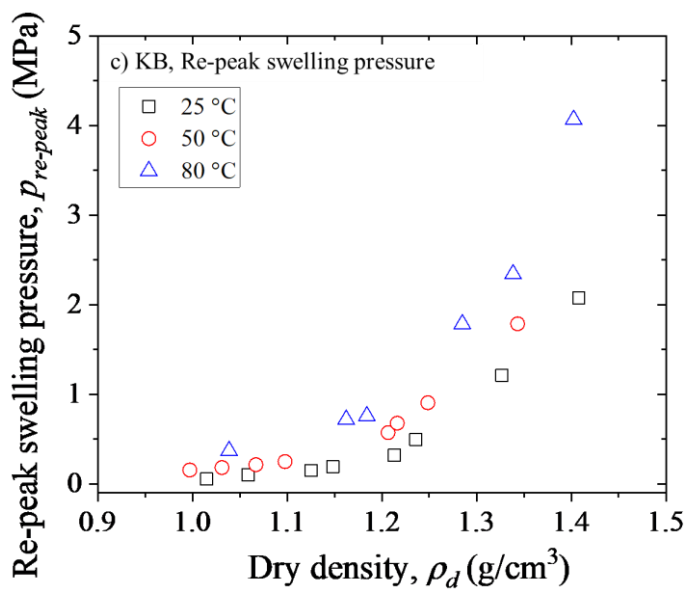
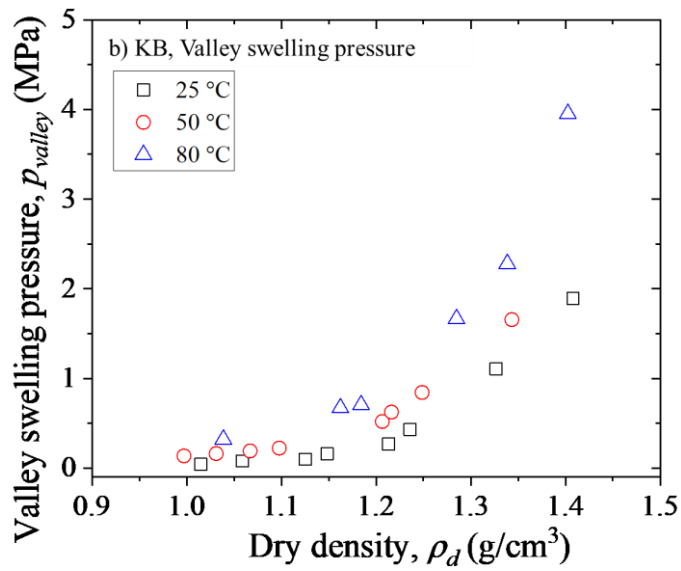
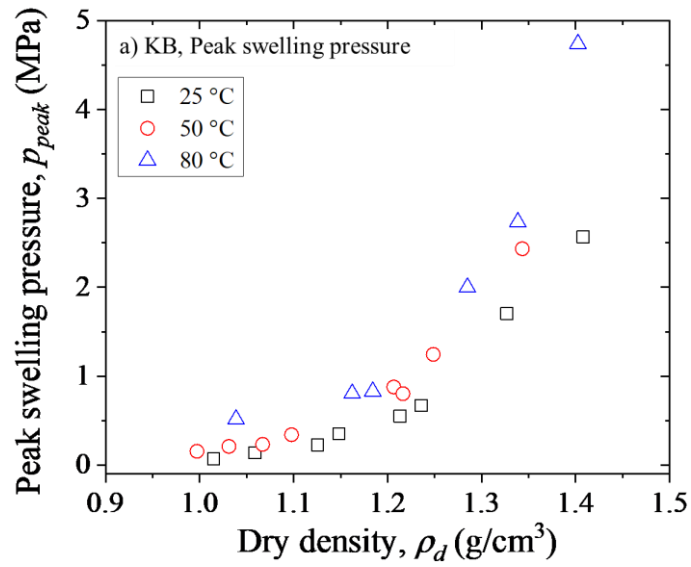


Figure 9-9 Swelling pressures during saturation of KB

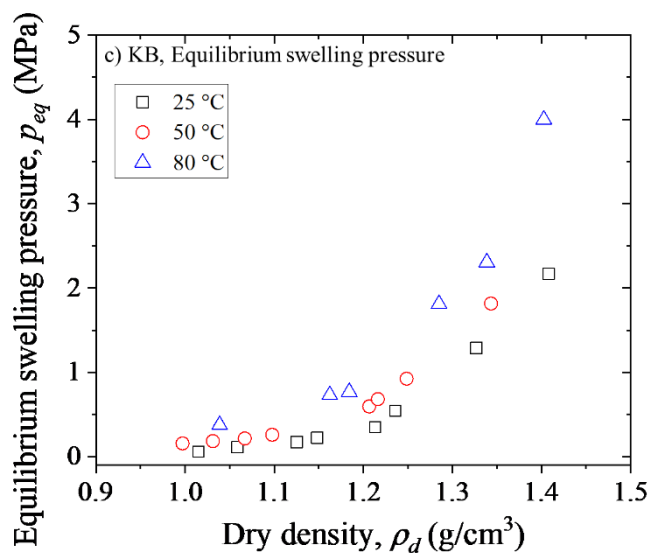
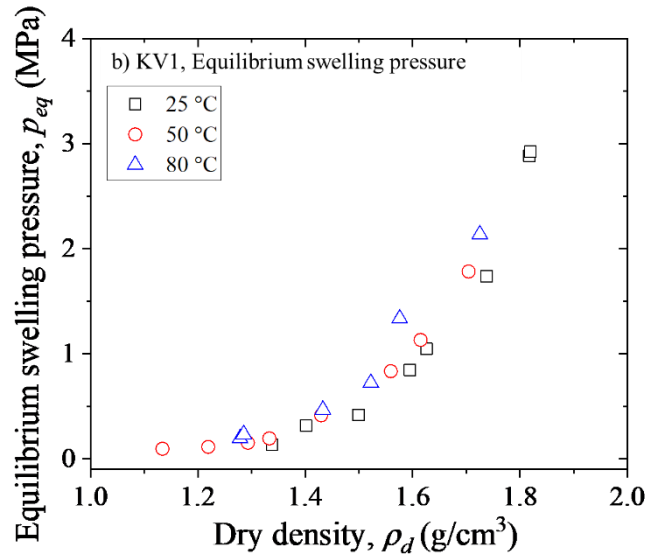
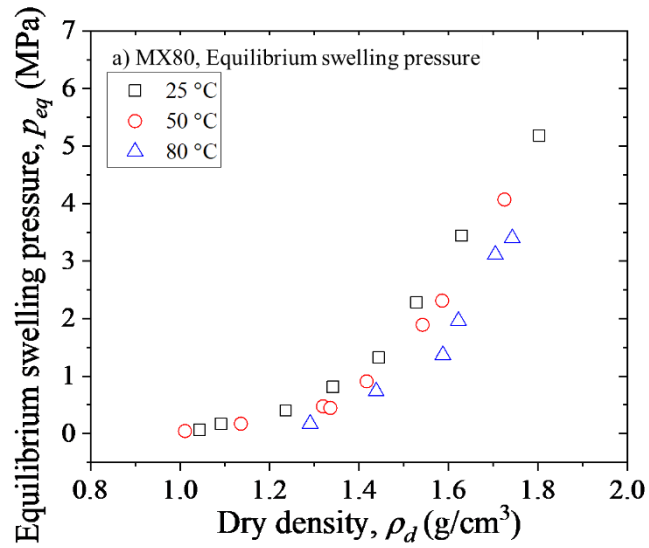


Figure 9-10 Equilibrium swelling pressures at different temperatures

As the literature survey in Table 9-3, the effect of temperature on equilibrium swelling pressures of bentonites was not consistent. Some studies informed that equilibrium swelling pressure decreases with the increase of temperature. But some investigations reported that temperature had a positive effect on equilibrium swelling pressure. In this chapter, the trend of temperature effect on equilibrium swelling pressure is also not consistent. Figure 9-10 indicates the equilibrium swelling pressure of three bentonites in this study at different temperatures. It can be easily found from Fig. 9-10 (a), equilibrium swelling pressure of MX80 decreases as increasing experimental temperature. The conclusion agrees with the research from Pusch et al. (1990), Bag (209), Tripathy et al. (2015). However, for KV1 and KB as revealed in Fig. 9-10 (b) and (c), equilibrium swelling pressure rises with the growth of temperature. Same founding was informed for KV1 by Kodama et al. (2004) and by Kanazawa et al. (2020).

**Table 9-3 Temperature effect on equilibrium swelling pressure of bentonites from Literatures**

Bentonite	<sup>1</sup> KV1	<sup>2</sup> MX80	<sup>3</sup> FEBEX	<sup>4</sup> GMZ01	<sup>5</sup> Bikaner	<sup>6</sup> B
Type	Na	Na	Ca-Mg	Na	Ca	Na
Temperature (°C)	20–90	20–90	20–80	20–80	25–90	25–95
Dry density (g/cm <sup>3</sup> )	1.6 and 1.8	1.2–2.0	1.5–1.8	1.7	1.6	1.6
Effect	Increase	Decrease	Decrease	Decrease	Increase	Decrease

**Notes:** Increase, increase with rising temperature; Decrease, decrease with rising temperature.

<sup>1</sup> Kodama et al. 2004, Kanazawa et al. 2020; <sup>2</sup> Pusch et al. 1990, Bag 2011, Tripathy et al. 2015;

<sup>2</sup> Villar and Lloret 2004, Villar et al. 2010; <sup>4</sup> Chen et al. 2018, Chen et al. 2019;

<sup>5</sup> Bag and Rabbani 2017; <sup>6</sup> Jadda and Bag 2020.

## 9.2.2 Water diffusivity

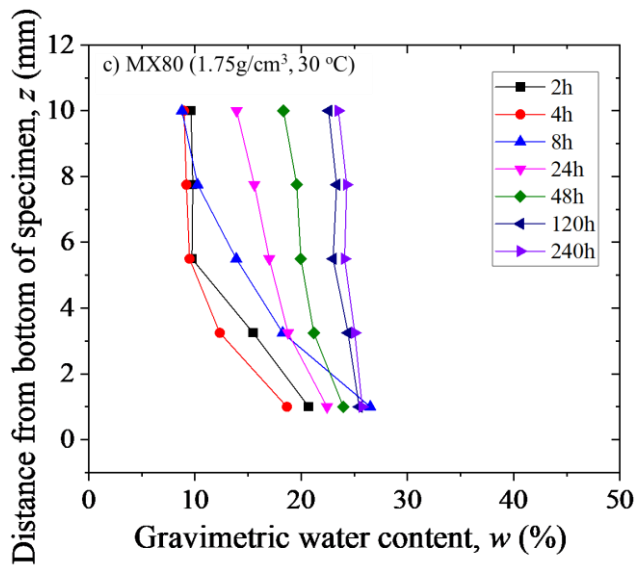
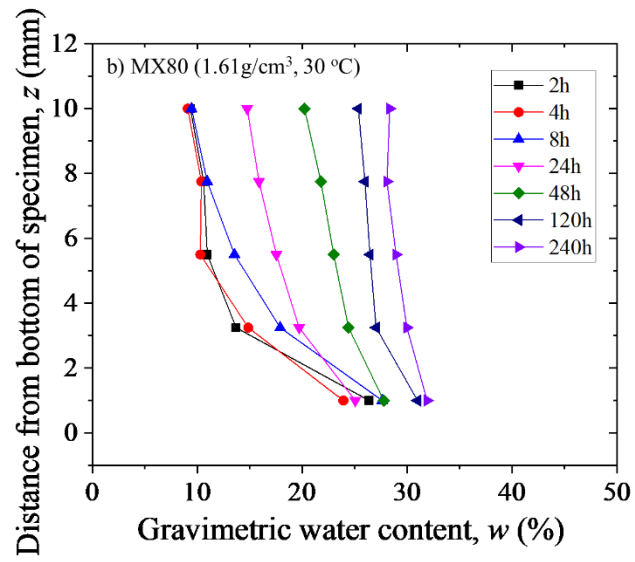
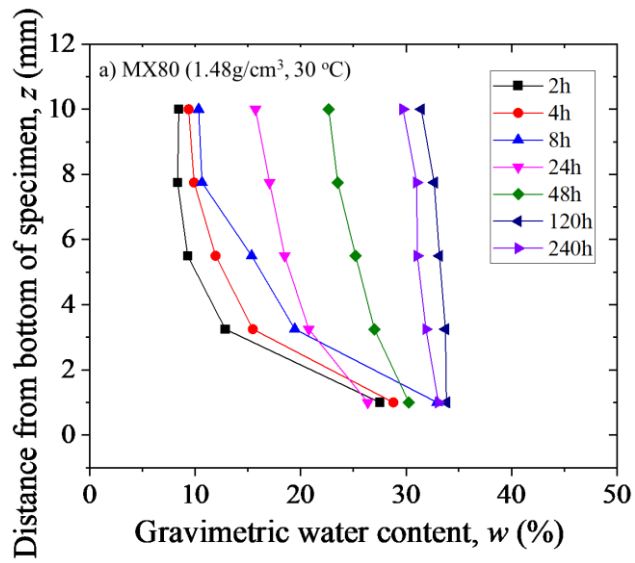


Figure 9-11 Water contents of different dry densities MX80 slices at 30°C

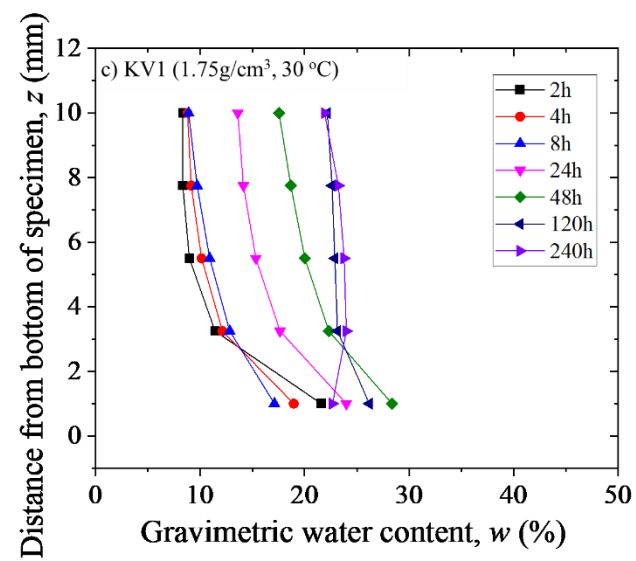
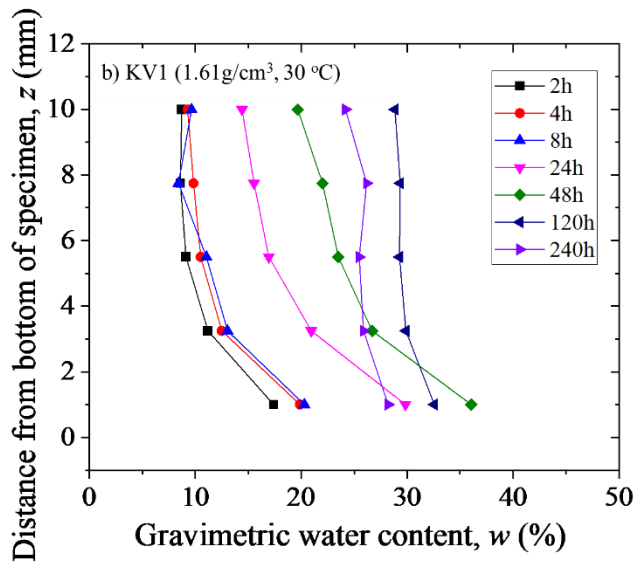
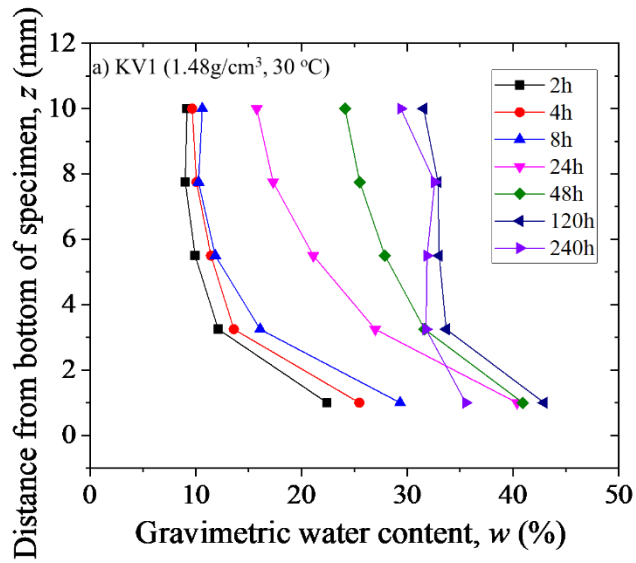
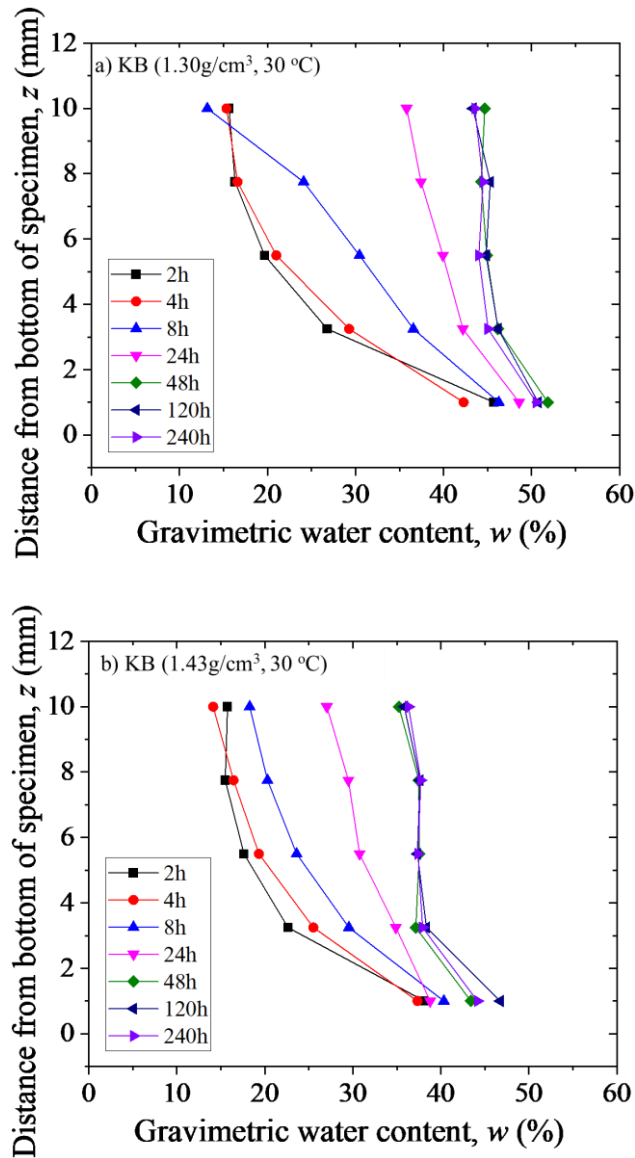


Figure 9-12 Water contents of different dry densities KV1 slices at 30°C



**Figure 9-13 Water contents of different dry densities KB slices at 30°C**

Water contents of slices of different dry densities MX80, KV1 and KB at 30°C are revealed in Fig. 9-11, 9-12 and 9-13, respectively. It is clearly from Fig. 9-11, 9-12 and 9-13, water contents of slices generally decrease with the increase of distance from the bottom of specimen, in the beginning wetting durations. Then, as the hydrations proceeds, the water contents values do not change a lot, indicating the specimen get into the saturated state. Another interesting founding can be seen from Fig. 9-11, 9-12 and 9-13 that, the maximum water contents of bentonites seem decrease with the increase of dry density.

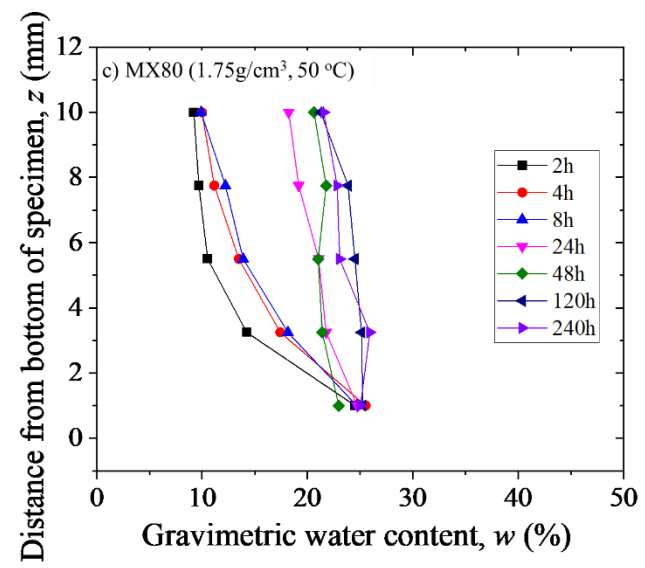
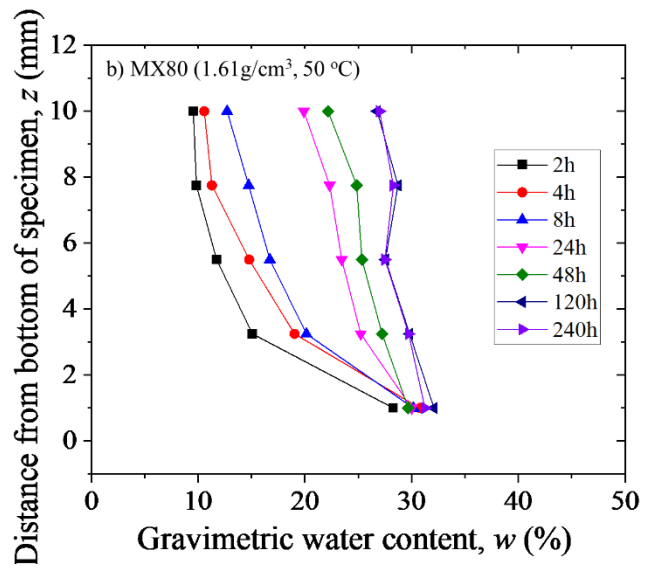
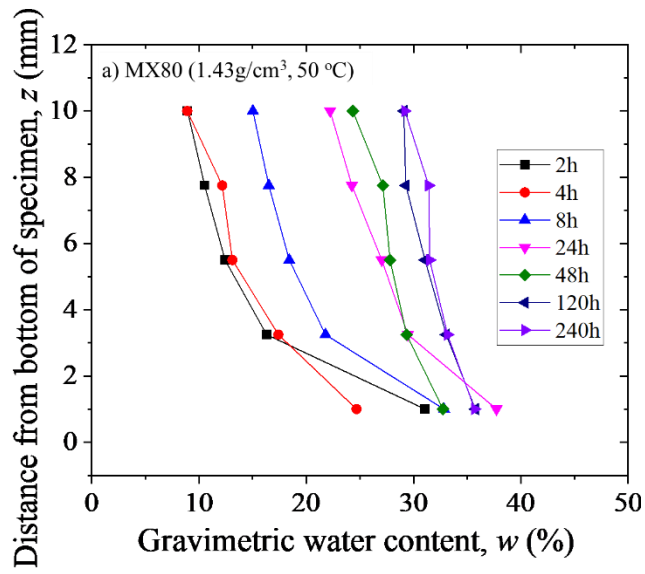


Figure 9-14 Water contents of different dry densities MX80 slices at 50°C

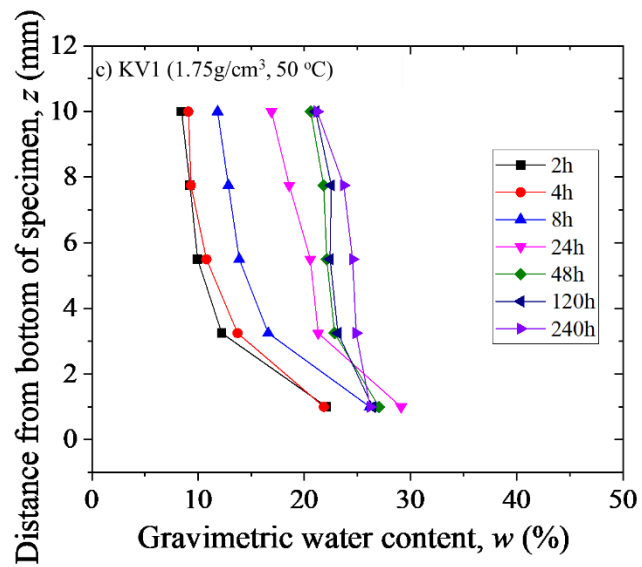
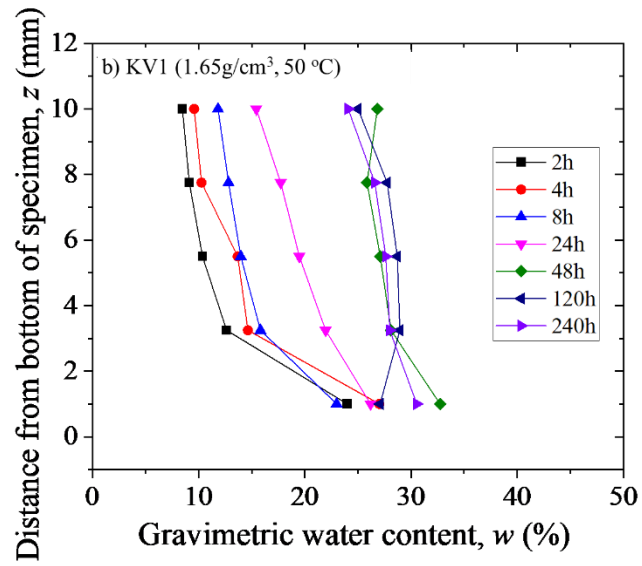
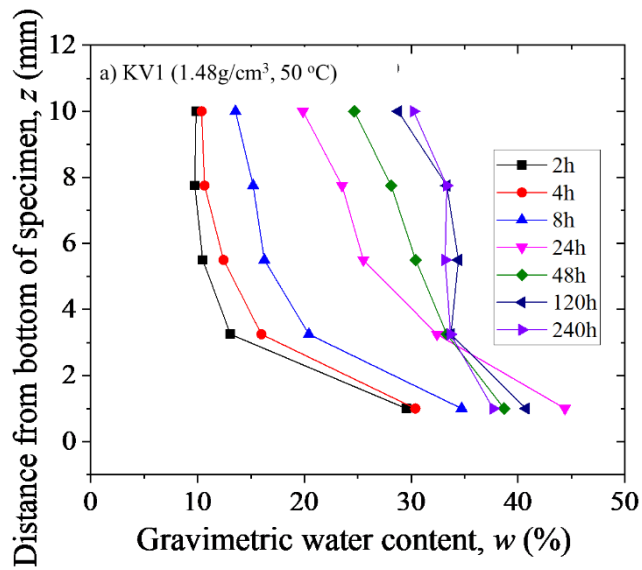
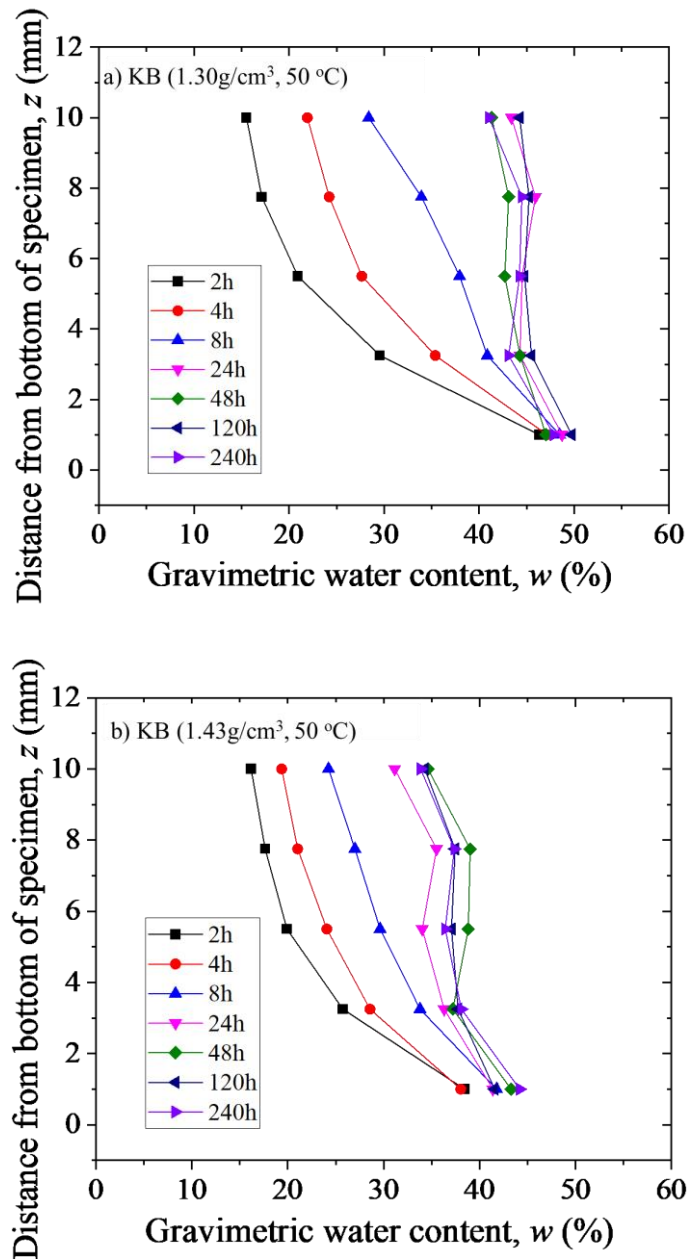


Figure 9-15 Water contents of different dry densities KV1 slices at 50°C



**Figure 9-16 Water contents of different dry densities KB slices at 50°C**

Figure 9-14, 9-15 and 9-16 show water contents of slices of different dry densities MX80, KV1 and KB at 50°C, respectively. Same phenomenon can be found for 50°C condition to the 30°C condition that, water contents of slices generally decrease with the increase of distance from the bottom of specimen. And the maximum water contents of bentonites seem decrease with the increase of dry density.

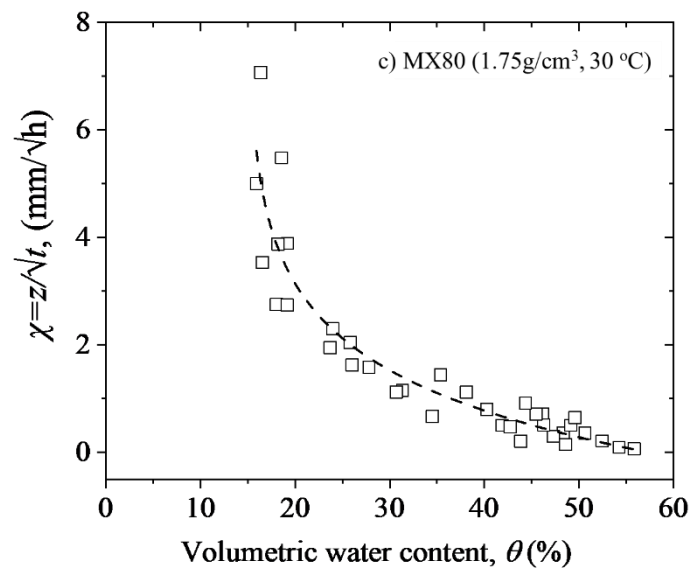
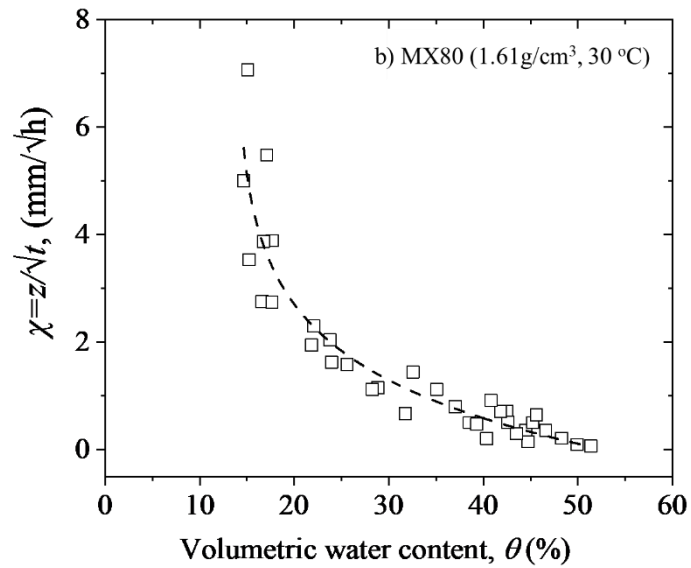
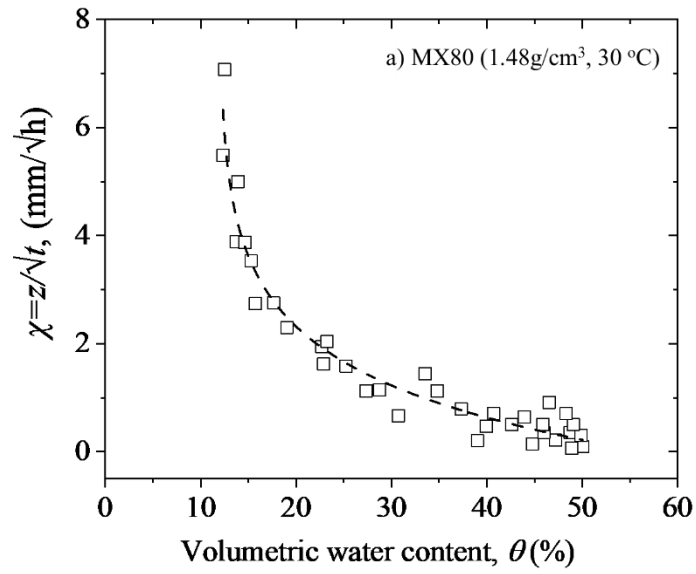


Figure 9-17 Relations between  $\theta$  and  $\chi$  for different dry densities MX80 at 30°C

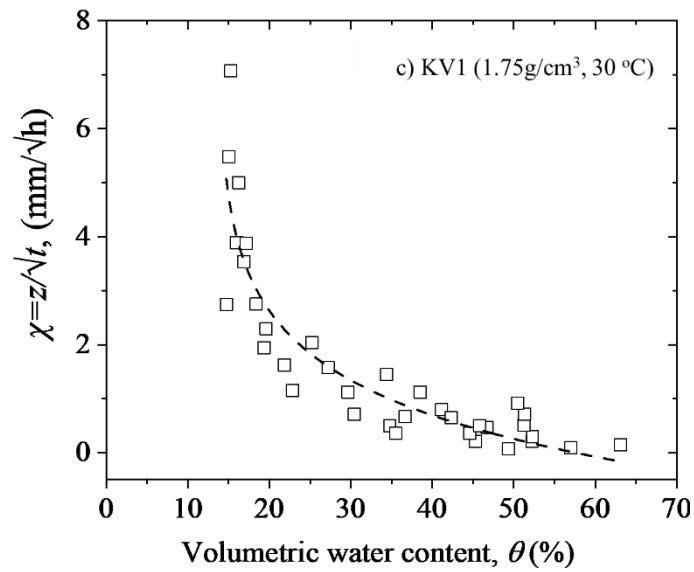
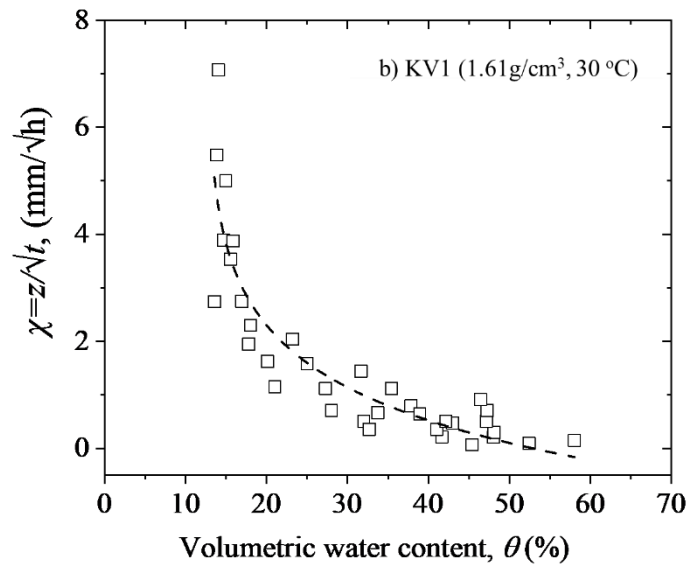
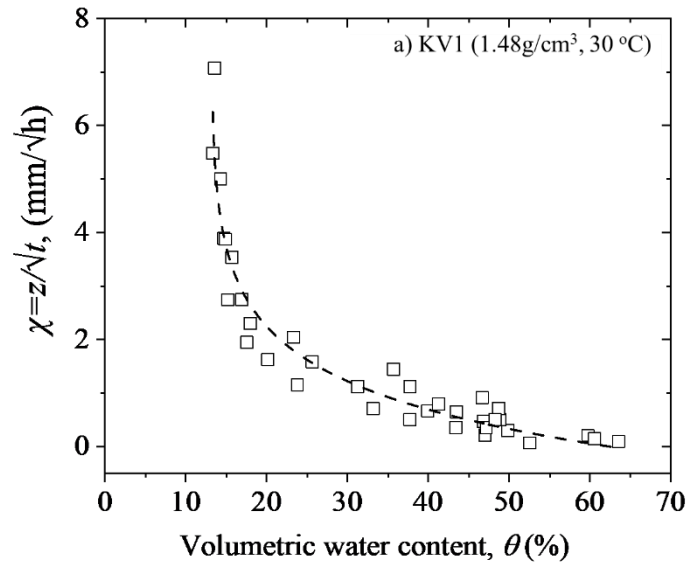


Figure 9-18 Relations between  $\theta$  and  $\chi$  for different dry densities KV1 at 30°C

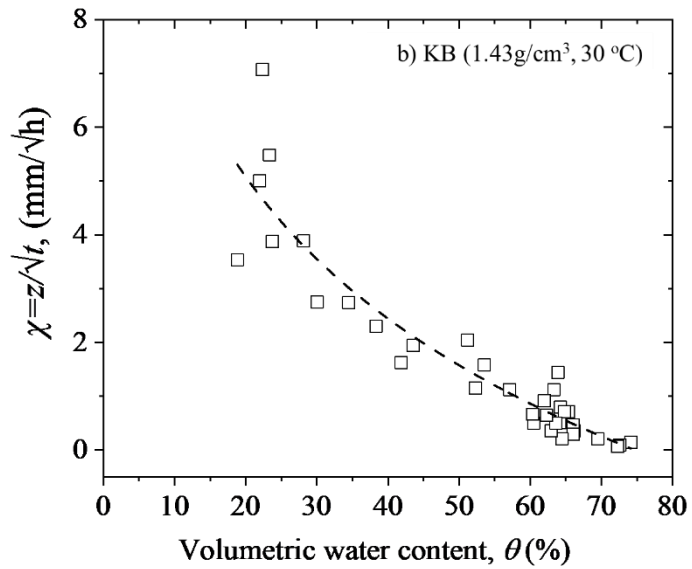
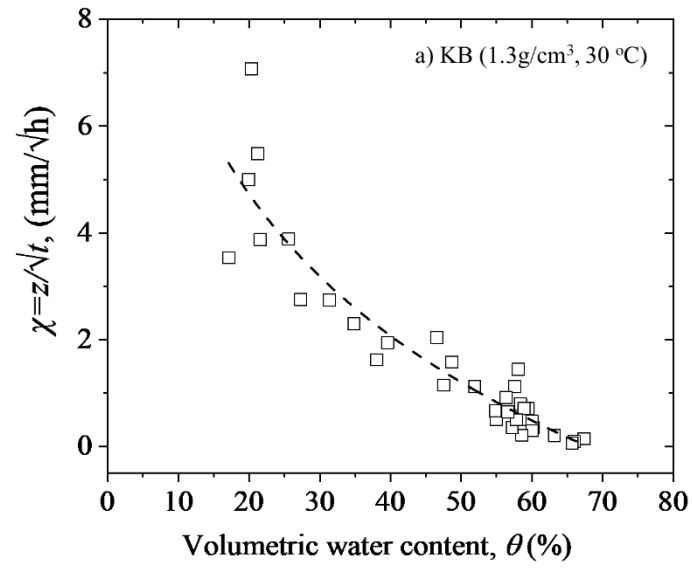


Figure 9-19 Relations between  $\theta$  and  $\chi$  for different dry densities KB at 30°C

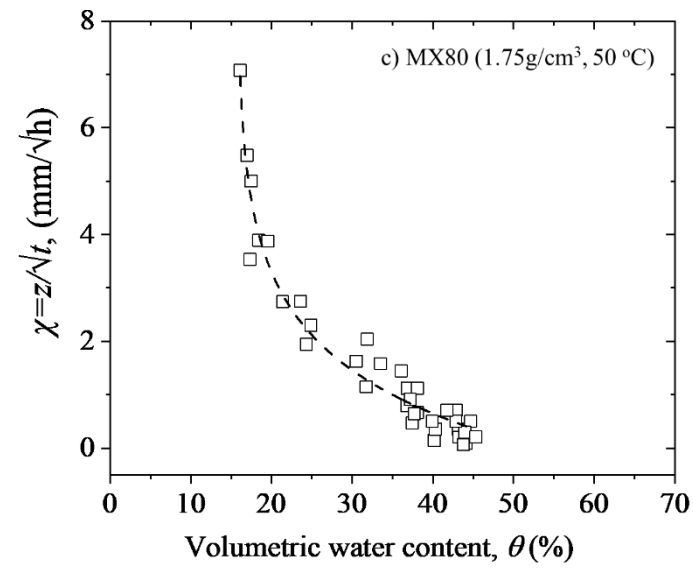
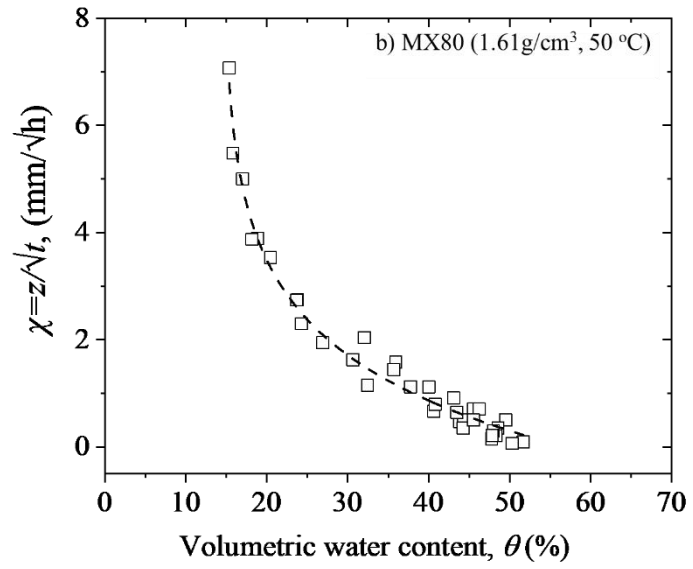
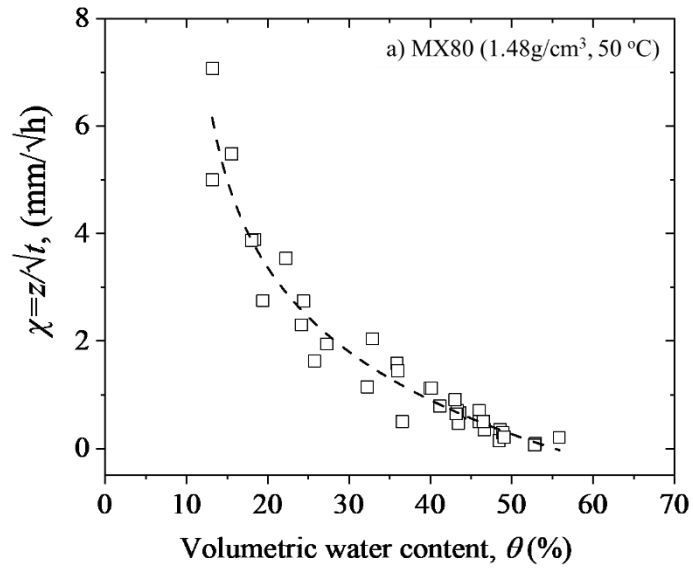


Figure 9-20 Relations between  $\theta$  and  $\chi$  for different dry densities MX80 at 50°C

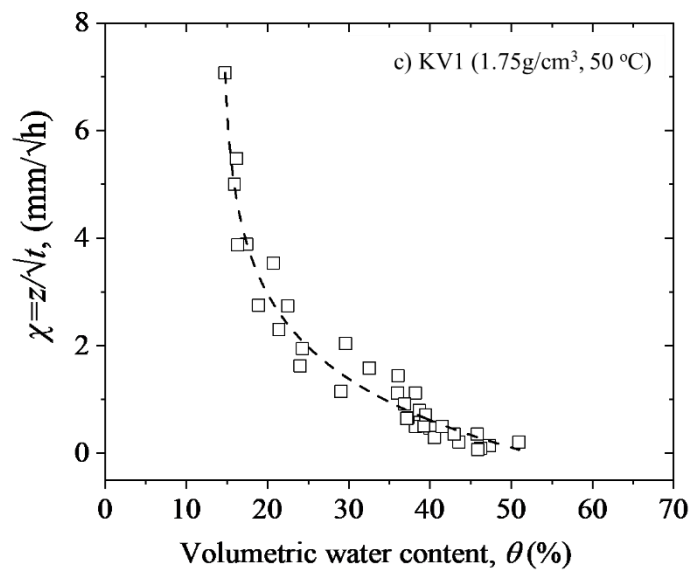
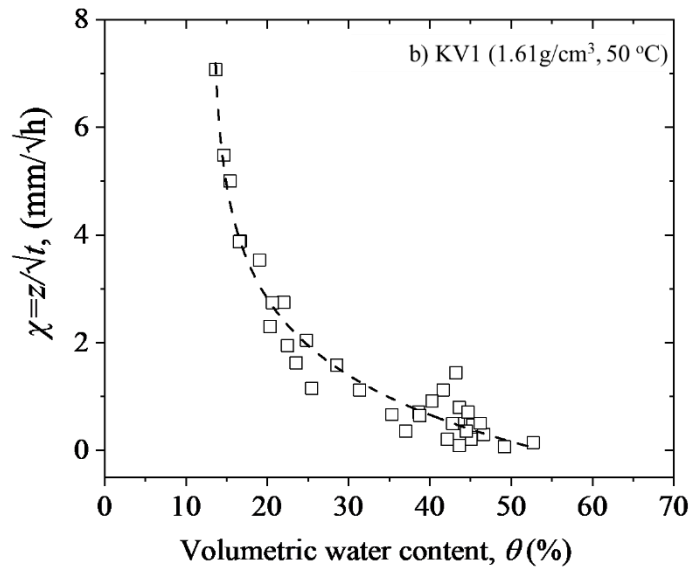
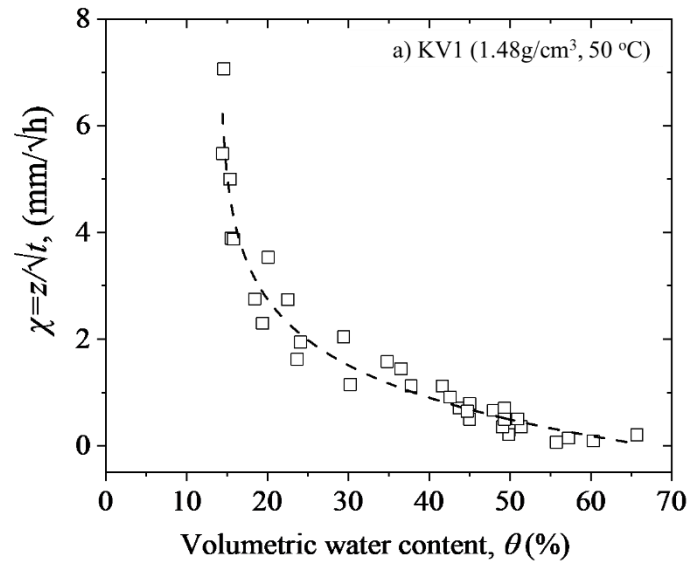
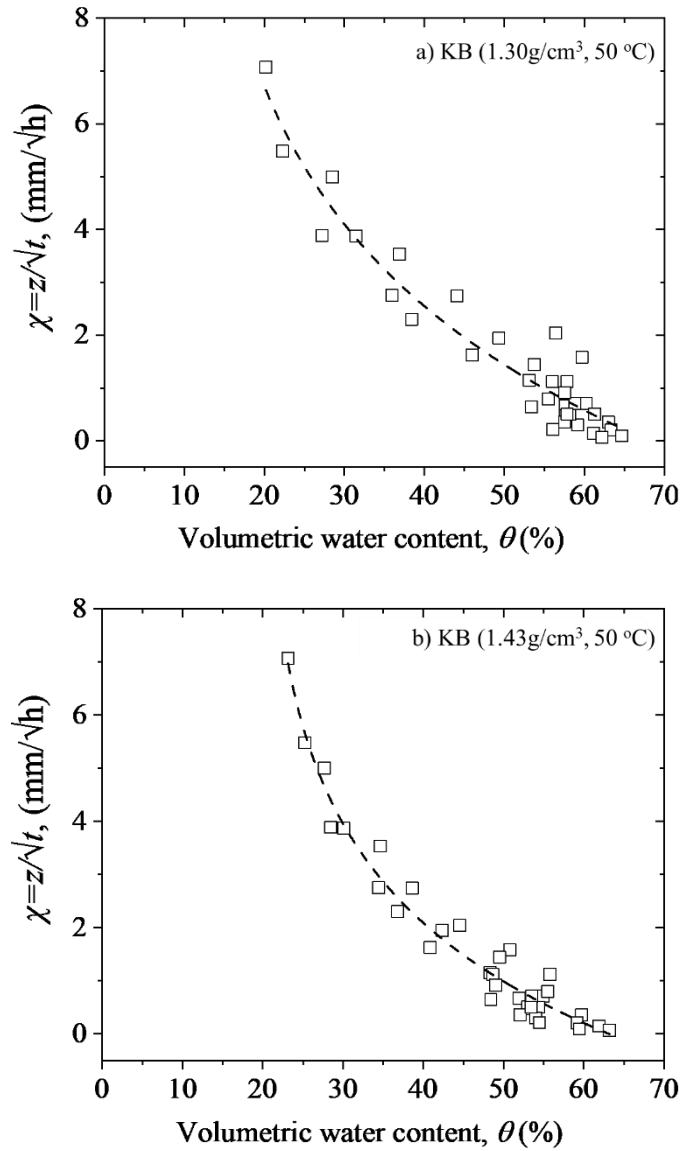


Figure 9-21 Relations between  $\theta$  and  $\chi$  for different dry densities KV1 at 50°C



**Figure 9-22 Relations between  $\theta$  and  $\chi$  for different dry densities KB at 50°C**

Relations between  $\theta$  and  $\chi$  for different dry densities MX80, KV1 and KB at 30°C are presented in Fig. 9-17, 9-18 and 9-19, respectively. Figure 9-20, 9-21 and 9-22 show relations between  $\theta$  and  $\chi$  for different dry densities MX80, KV1 and KB at 50°C, respectively. It is apparent from these figures that, the database generally can follow equation (4-4). Therefore, the calculation for water diffusivity at different temperatures can use equation (4-5).

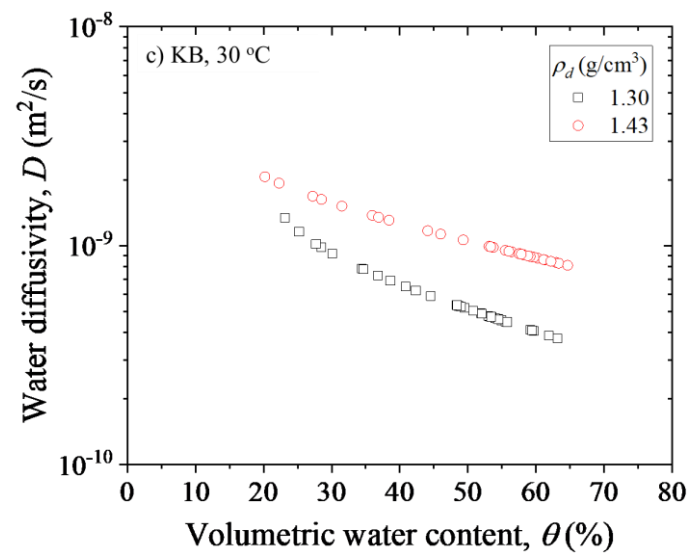
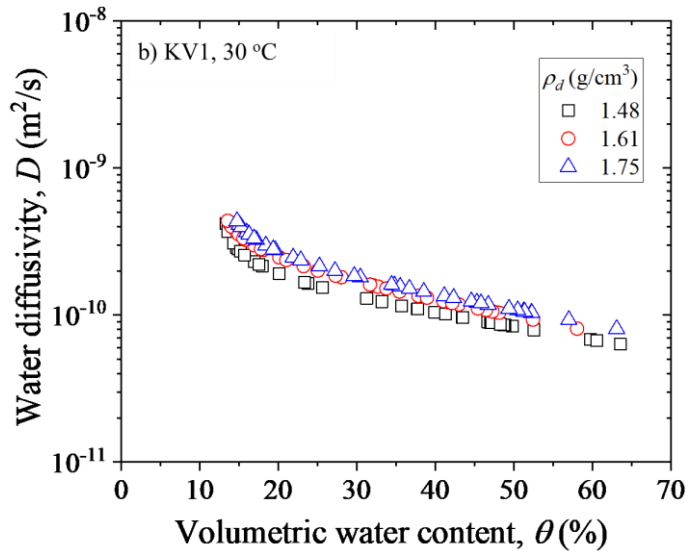
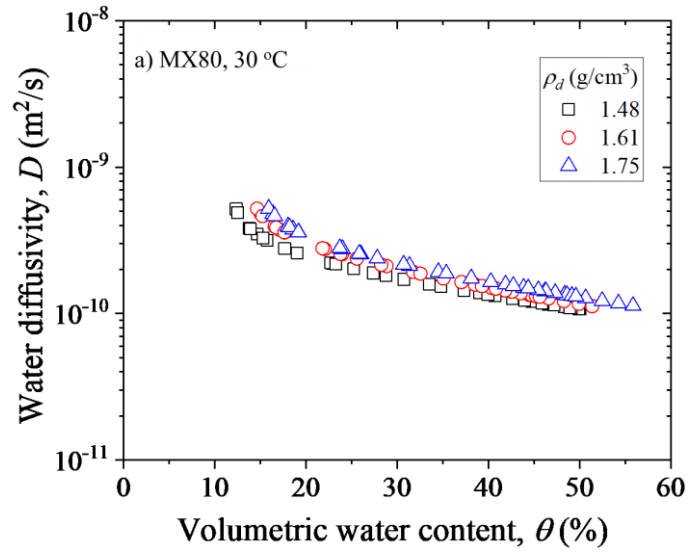


Figure 9-23 Water diffusivities of different dry densities bentonites at 30°C

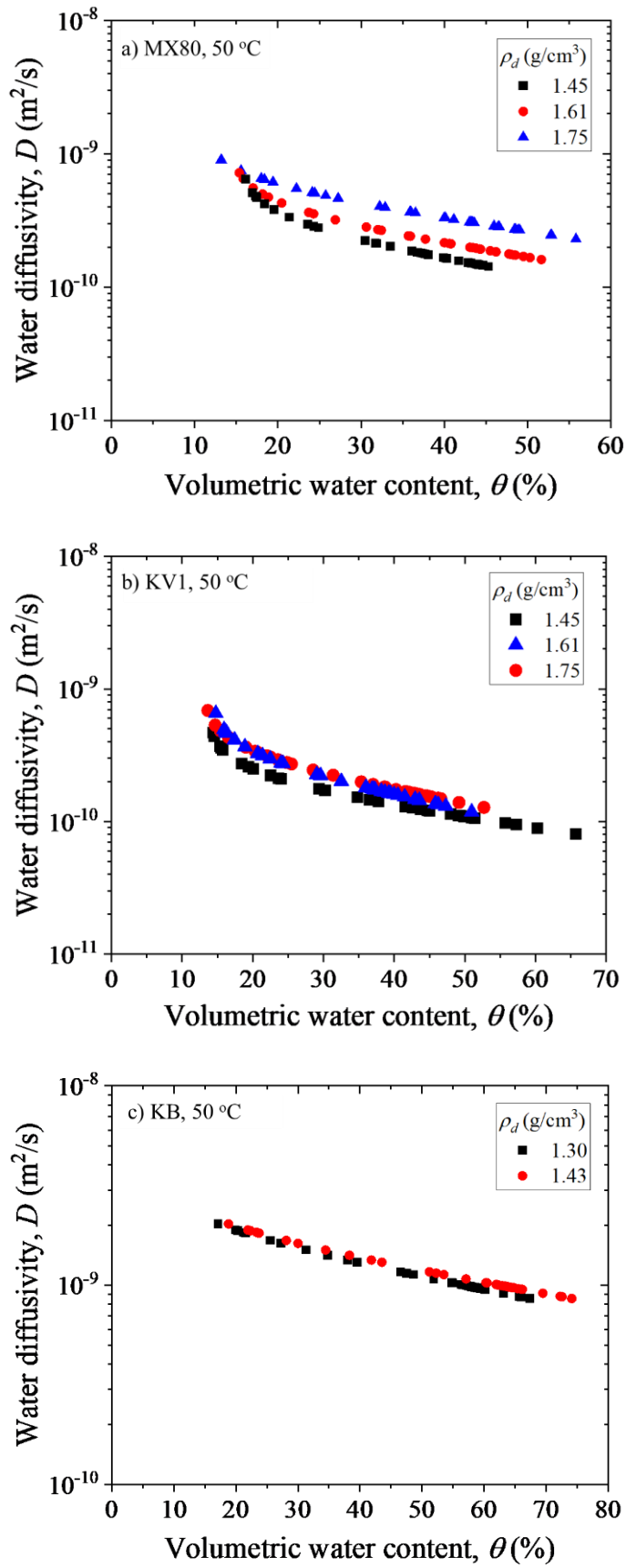


Figure 9-24 Water diffusivities of different dry densities bentonites at  $50^\circ\text{C}$

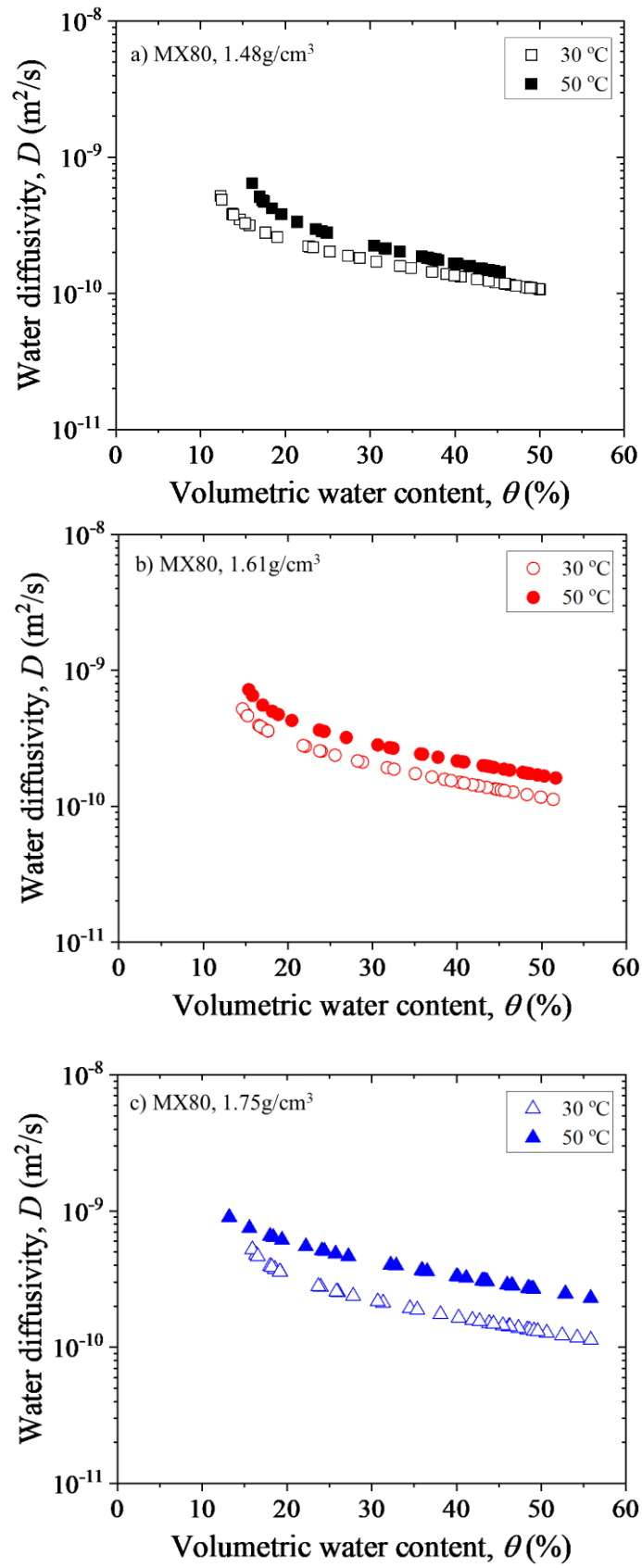


Figure 9-25 Water diffusivities of MX80 at different temperatures

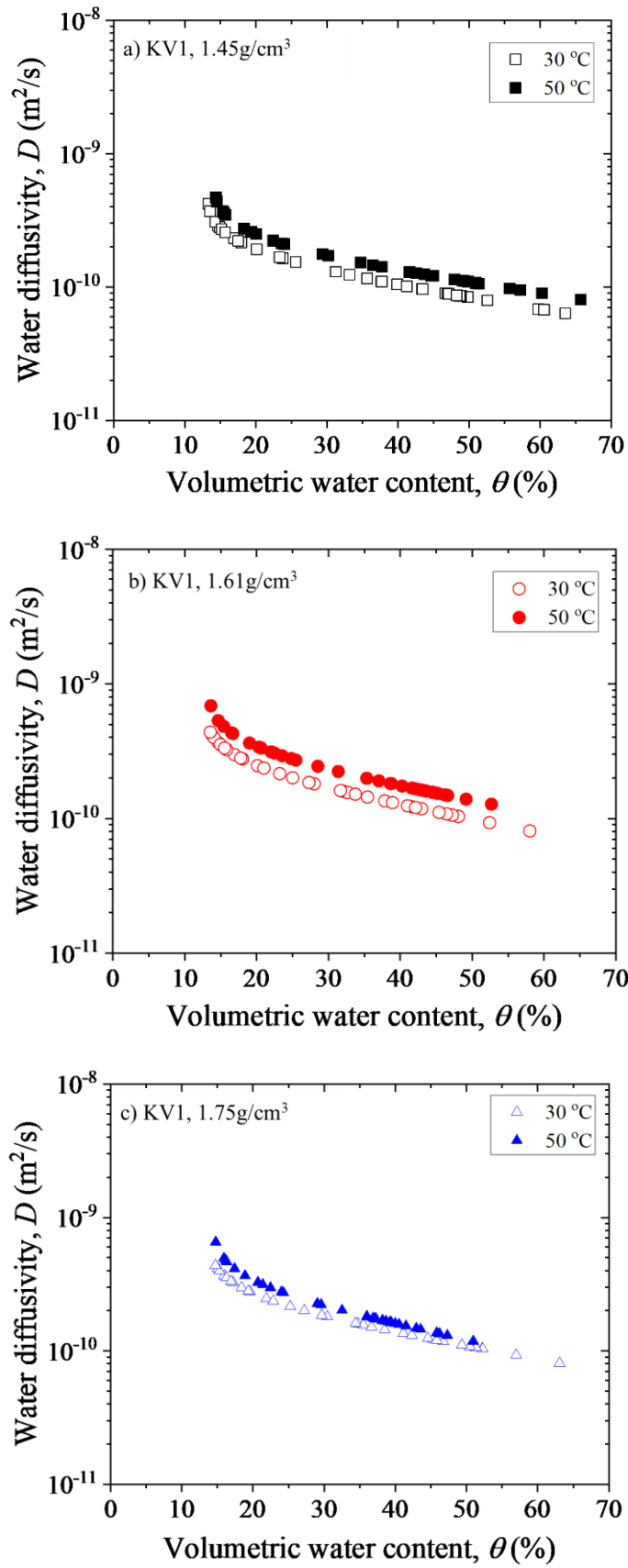
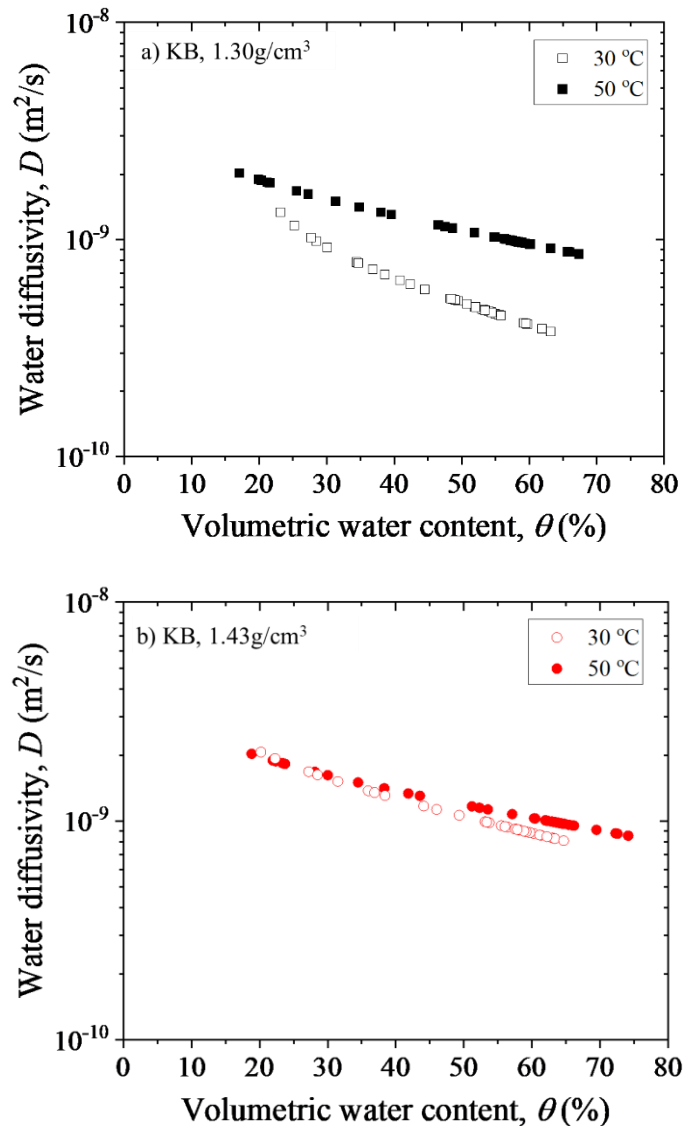


Figure 9-26 Water diffusivities of KV1 at different temperatures



**Figure 9-27 Water diffusivities of KB at different temperatures**

Figure 9-23 and 9-24 show water diffusivities of different dry densities bentonite at 30 °C and 50 °C, respectively. It is apparent from Fig. 9-23 and 9-24 that, no matter the testing temperature, water diffusivity decreases with the increase of volumetric water content, which is consistent as the conclusions above. Meanwhile, when the volumetric water contents are the same, water diffusivity rises as the dry densities increases. Same phenomenon was reported in chapter 5.

Water diffusivity at different temperatures of MX80, KV1 and KB are presented in Fig. 9-25, 9-26 and 9-27, respectively. It is a general truth from Fig. 9-25, 9-26 and 9-27,

for all three bentonites, when the volumetric water contents are same, water diffusivity rises with increasing testing temperature. Figure 9-28 reveals the water diffusivities of KV1 at different temperatures from Takeuchi et al. (1995) and this study. As clearly from Fig. 9-28, same phenomenon can be found from Takeuchi et al. (1995) that: water diffusivity grows as the temperature rises.

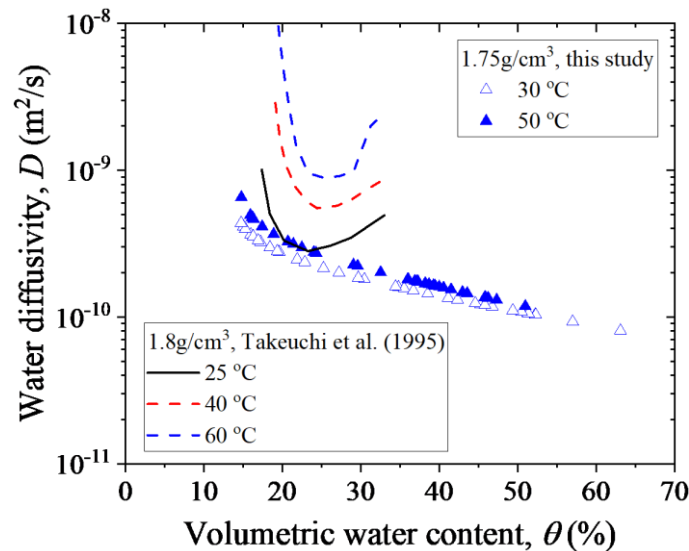


**Figure 9-28 Water diffusivities of KV1 at different temperatures from literatures and this study**

### 9.3 Discussion

#### 9.3.1 Equilibrium swelling pressure at different temperatures for bentonite with different grain sizes

The effects of temperature on montmorillonite fabric units can be summarized as the following (Villar and Lloret 2004; Chen et al. 2019): 1) change of adsorbed water in inter-layer space (basal spacing); 2) change of distance between particles; and 3) free water volume change. For adsorbed water, increasing temperature can be expected to encourage adsorbed water in inter-layer spaces to flow out (Fig. 9-29, Romero et al.

2001; Villar and Lloret 2004; Villar et al. 2010; Chen et al. 2018; Chen et al. 2019), leading to smaller basal spacing (Fig. 9-29). Swelling between layers decreases with increasing basal spacing (Chen et al. 2019). Regarding the distance between particles, in the case of high temperature situation, the distance between particles becomes larger. The outflow of adsorbed inter-layer water might cause single particle volume reduction, which gives more space between two particles (Fig. 9-29). Greater distance between particles lead to decreasing swelling between particles. Aside from that, with increased temperature, free water volume can be expected to expand. In the confined condition, for higher temperature specimens, insufficient space exists for free water to expand arbitrarily, thereby giving grains greater back stress. Thermal expansion is reported negligible for adsorbed water and can be ignored (Baldi et al. 1988; Chen et al. 2019).

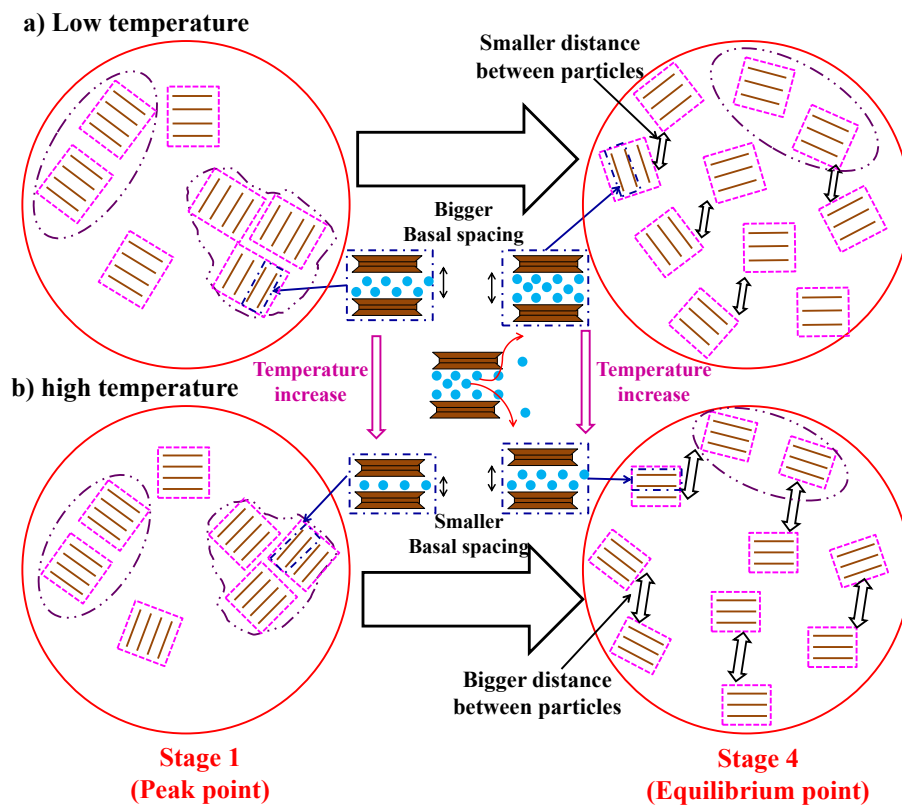


**Figure 9-29 Schematic showing montmorillonite fabric units at different temperatures**

Figure 9-30 presents the movement of water in powder and particle bentonites. The

grains of powder bentonites are much smaller than those of particle bentonites (Fig. 2-4). For particle bentonites, much larger voids are left in compacted specimens (Fig. 9-30) comparing to powder bentonite. For powder bentonite compacted specimen, because of the smaller void, most of the water would enter the intra-grain space directly. Consequently, free water volume change effects at different temperatures of powder bentonites might be negligible. In the case of particle bentonite compacted specimens, water would pass synchronously into intra-grain spaces and larger inter-grain pores (Fig. 9-30). Therefore, the effects of free water volume changes need to be examined.

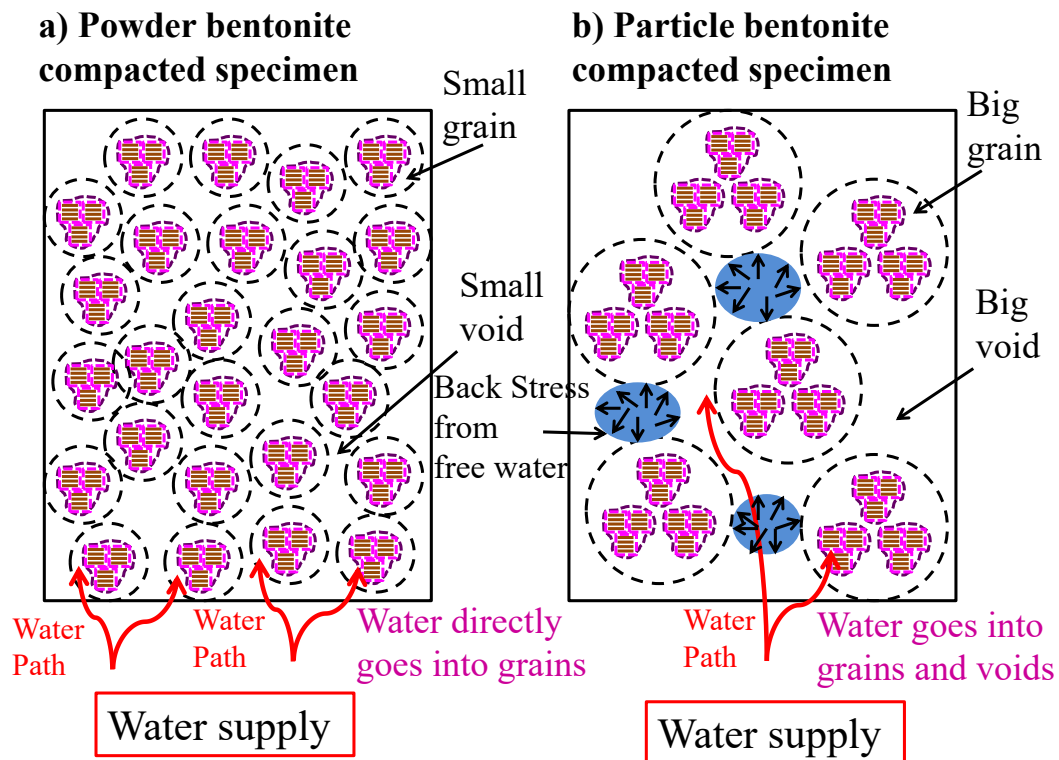


**Figure 9-30 Schematic showing movement of water in powder and particle bentonites**

From this study, as might be inferred from Fig. 9-10, all powder bentonites have larger values of equilibrium swelling pressure at higher temperatures. However, data of Table 9-3 show that not all powder bentonites exhibit the same phenomenon. For GMZ powder bentonite (Chen et al. 2018; Chen et al. 2019) and B powder bentonite from

India (Jadda and Bag 2020), equilibrium swelling pressure is smaller at higher temperatures. Therefore, regarding powder bentonites, the effects of temperature on equilibrium swelling pressure are not consistent. Figure 9-29 reveals fabric units changes at the equilibrium point of powder bentonite at different temperatures. In high-temperature conditions, the larger swelling between layers from smaller basal spacing competes with smaller swelling between particles from larger distance between particles, which leads to inconsistent effects of temperature on equilibrium swelling pressure for powder bentonites.

Secondly, regarding particle bentonite (MX80). Results of this study show that equilibrium swelling pressure values of all granular bentonites decrease concomitantly with increasing temperature, as presented in Fig. 9-10. Other particle bentonites (MX80 by Pusch et al. 1990, Bag 2011, Tripathy et al. 2015; FEBEX by Villar and Lloret 2004, Villar et al. 2010) exhibit the same phenomenon as those shown by results of this study. It might be assumed that, for all particle bentonites, higher temperatures lead to smaller equilibrium swelling pressure. This finding can be attributed to the free water expansion as increasing temperature. Unlike powder bentonites, free water among grains makes great contributions to the detection of swelling pressure at different temperatures for particle bentonite. With the increase of temperature, greater back stress caused by the expansion of free water can be expected to give greater back stress to the grains. These back stresses may adversely affect the measurement of equilibrium swelling.

### 9.3.2 Water diffusivity at different temperatures

As introduced above, basal spacing decreases as the temperature rises, thus the micropore would become smaller with the increasing temperature. The decreasing micropore would give larger macropore (Fig. 9-31) outside the inter-layer space. Meanwhile, as interpreted in Chapter 4, the macropore in this study was assumed as the

water flowing path. With the increase of temperature, larger water diffusivity would be induced by the bigger macropore.

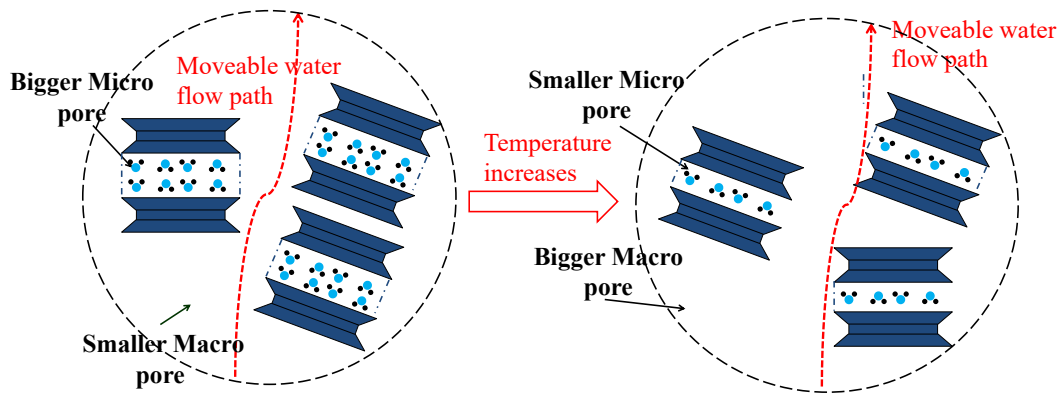


**Figure 9-31 Schematic showing micropore and macropore at different temperatures**

## Conclusion

Swelling pressure tests and confined wetting tests were conducted in oven with different temperatures to investigate the temperature on swelling pressures and water diffusivity, respectively. The results from the experiments can be concluded as:

1. Swelling pressures during saturation (peak, valley and re-peak swelling pressures) and equilibrium swelling pressure of MX80 decrease as temperature rises;
2. For KV1 and KB, swelling pressures during saturation and equilibrium swelling pressure increases with the growth of temperature.
3. Water diffusivity of bentonites increase with the increase of temperature and rises as the growth of dry density.

## Reference

- Bag, R. 2010. Coupled thermo-hydro-mechanical-Chemical behaviour of MX80 bentonite in geotechnical applications. Doctor thesis, Cardiff University.
- Baldi, G., Hueckel, T., and Pellegrini, R. 1988. Thermal volume changes of the mineral–water system in low porosity clay soils. *Canadian Geotechnical Journal*, **25**(4): 807–825.
- Chen, Y.G., Dong, X.X., Zhang, X.D., Ye, W.M., and Cui, Y.J. 2018. Combined thermal and saline effects on the swelling pressure of densely compacted GMZ bentonite. *Applied Clay Science*, 166: 318–326.
- Chen, Y.G., Dong, X.X., Zhang, X.D., Ye, W.M., and Cui, Y.J. 2019. Cyclic thermal and saline effects on the swelling pressure of densely compacted Gaomiaozhi bentonite. *Engineering Geology*, 255: 37–47.
- Jadda, T., and Bag, R. 2020. Effect of initial compacted pressure and elevated temperature on swelling pressure of two Indian bentonites. *Environmental Earth Science*, 79: 197.
- Kanazawa, S., Kobayashi, S., Ichikawa, N., Yanai, M., and Ishiyama, K. 2020. The swelling behaviour of bentonite buffer material considering the effect of temperature. *International Journal of Geomate*, 19(74): 216–221.
- Komada, J., Adachi, K., Tanabe, R., Suzuki, E., and Yamamoto, S. 2004. Swelling characteristics of bentonite–silica mixture under high temperature. *Journal of JSCE*, 764: 319–328. (in Japanese)
- Pusch, R., Karnland, O., and Hokmark, H. 1990. GMM – a general microstructural model for qualitative and quantitative studies on smectite clays. SKB Technical Report 90-43.
- Romero, E., Gens, A., Lloret, A., 2001. Laboratory testing of unsaturated soils under

simultaneous suction and temperature control. Proc. 15th Int. Conf. on Soil Mechanics and Geotechnical Engineering, Istanbul 1, 619 – 622. Tripathy, S., Bag, R., and Thomas, H.R., 2015. Enhanced isothermal effect on swelling pressure of compacted MX80 bentonite. *Engineering Geology for Society and Territory*, 6: 537–539.

Villar, M.V., and Lloret, A. 2004. Influence of temperature on the hydro-mechanical behaviour of a compacted bentonite. *Applied Clay Science*, 26: 337–350.

Villar, M.V., Rgomez, E.R., and Lloret, A. 2010. Experimental investigation into temperature effect on Hydro mechanical behaviors of bentonite. *Journal of Rock Mechanics and Geotechnical Engineering*, 2(1): 71–78.

Wang, H.L., Komine, H., and Gotoh, T. 2021. A swelling pressure cell for X-ray diffraction test. *Géotechnique*. <https://doi.org/10.1680/jgeot.20.00005>

Wang, H.L., Ruan, K.L., Harasaki, S., and Komine, H. 2022. Effects of specimen thickness on apparent swelling pressure evaluation of compacted bentonite. *Soil and Foundations*, 62: 101099.

# Chapter 10

## **THE EFFECTS OF INITIAL WATER CONTENT AND SPECIMEN PREPARATION METHOD ON SWELLING PRESSURES OF BENTONITE WITH XRD**

## 10.1 Testing overview

In this chapter, the effect of initial water content of bentonite on swelling pressures, including swelling pressure developing pattern and equilibrium swelling pressure, were studied by swelling pressure tests. With different specimen producing methods, the specimen preparation method effect on swelling pressures were researched as well. Herein, only KV1 bentonite was used. The swelling pressure apparatus was the same as introduced in chapter 3. In this chapter, an integral ring (Height: 10mm; Inner diameter: 28mm) was used instead of the multi-ring used in former chapters.

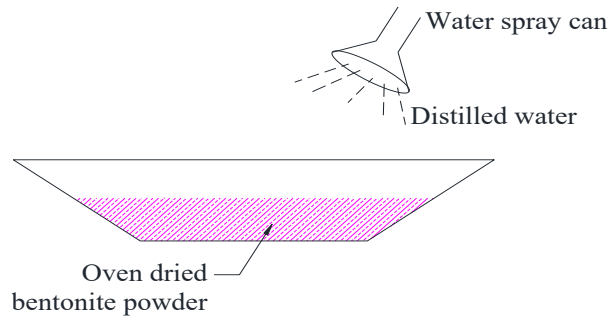


**Figure 10-1 Schematic of making bentonite powders with different water contents by water spray method**

**Table 10-1 Specimens details by water spray method for swelling pressure and XRD tests**

Test type	Swelling pressure	XRD
Height (mm) × Diameter (mm)	10 × 28	2 × 28
Dry density, $\rho_d$ (g/cm <sup>3</sup> )	1.2–2.0	
Initial water content, $w_i$ (%)	0–22.51	

There were two methods adopting to the study the specimen preparation method on swelling pressures of KV1 in this chapter. Firstly, spray water to the oven dried powder samples (Water spray method). The water contents of powder bentonites were achieved

as described followings: 1) KV1 bentonite powders were dried in the oven at 110 °C for approximate. 24 h; 2) bentonite powders were taken out from the oven; 3) by using a water spray can, the distilled water was sprayed immediately to the oven-dried powders (Fig. 10-1); 4) distilled water was mixed with bentonite powders as evenly as possible by using a spoon; 5) wetted bentonite powders were sieved through a 0.25 mm sieve; 6) sieved bentonite powders were sealed in polyethylene bags and were placed at 25°C for at least 120 h for obtaining samples with uniformly distributed water; 7) bentonite powder with different water contents were putted into the integral ring and compressed in static compacted device. The specimen details for swelling pressure tests by water spray method are indicated in Table 10-1.

Secondly, control the relative humidity of bentonite powder (Humidity control method). The testing details were listed as followings as: saturated salt solutions and natural air-dried bentonite powders were put together in sealed boxes for 5 months (Fig. 10-2). The relative humidity and powder bentonite water contents are presented in Table 10-2. After that, bentonite powders with different water contents were putted into the integral ring and compressed in static compaction device. The specimen details for swelling pressure tests by humidity control method are revealed in Table 10-3.

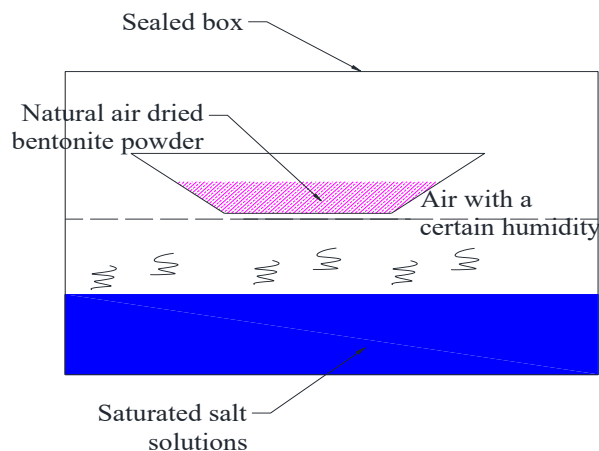


**Figure 10-2 Schematic of making bentonite powders with different water contents by humidity control method**

**Table 10-2 Relative humidity and water contents of powder bentonites from saturated salt solutions**

Salt solution	Relative humidity, RH (%)	Water content of bentonite, $w$ (%)
LiCl	11.34	3.53
MgCl <sub>2</sub>	33.28	6.15
NaNO <sub>2</sub>	66.32	9.17
NaCl	75.47	11.16
NH <sub>4</sub> H <sub>2</sub> PO <sub>4</sub>	93.02	14.18
K <sub>2</sub> SO <sub>4</sub>	97.27	15.93

**Table 10-3 Specimens from humidity control method for swelling pressure and XRD tests**

Test type	Swelling pressure	XRD
Height (mm) × Diameter (mm)	10 × 28	2 × 28
Dry density, $\rho_d$ (g/cm <sup>3</sup> )	1.2–2.0	
Initial water content, $w_i$ (%)	3.53–15.93	

Besides swelling pressure tests, XRD tests were conducted in this study as well for making sense the initial water content and specimen preparation method effects on bentonite microstructure. Herein, in this section, a 2mm ring was used for wetting tests with a simple wetting apparatus as presented in Fig. 10-3. Details for specimens prepared by different producing methods with this easily wetting apparatus are revealed in Table 10-1 and Table 10-3. The compacted 2mm height specimen was made as the same introduced above by using a static compaction device.

For every specimen, XRD tests were conducted before and after wetting. Firstly, specimens with different water contents were used for XRD tests. Then, specimens were wetted in a confined condition with the simple wetting apparatus (Fig. 10-3) by immersion of them directly into distilled water. Wetting durations of approximately 48 h were adopted for this study to ensure that the specimen was saturated. Later, the 2 mm ring and specimens were taken from the distilled water and were sealed immediately using Para film (Fig. 10-4). Each specimen covered by Para film was cured under a constrained condition at 25°C for at least 48 h to achieve uniform water distribution. Subsequently, these saturated specimens were subjected to XRD tests again.

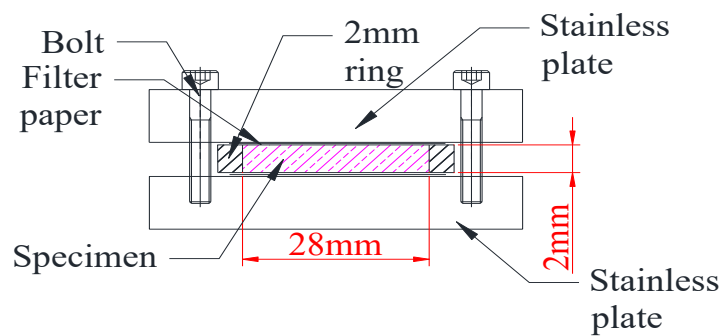


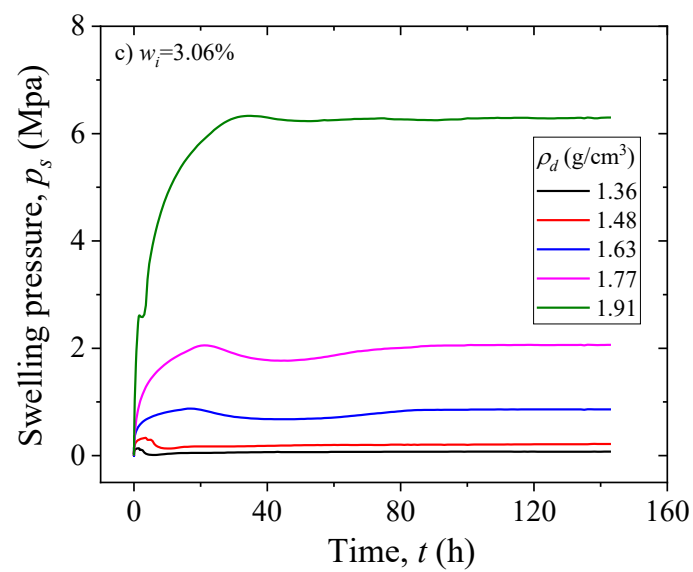
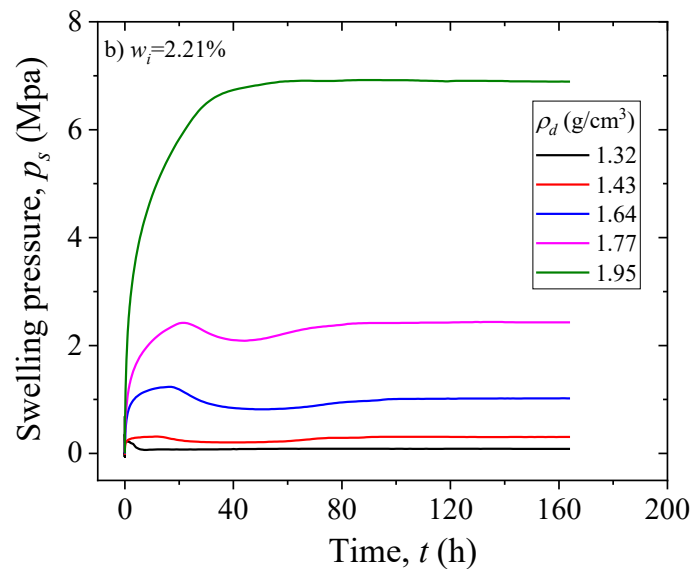
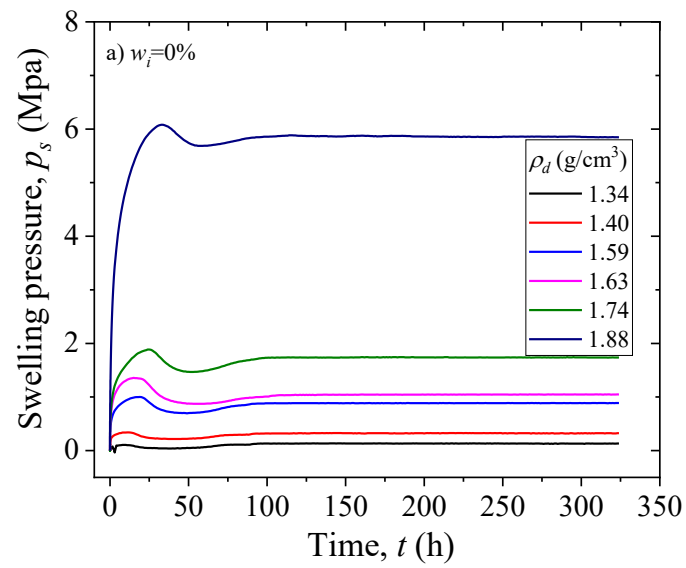
**Figure 10-3 A simple wetting apparatus with 2mm ring**

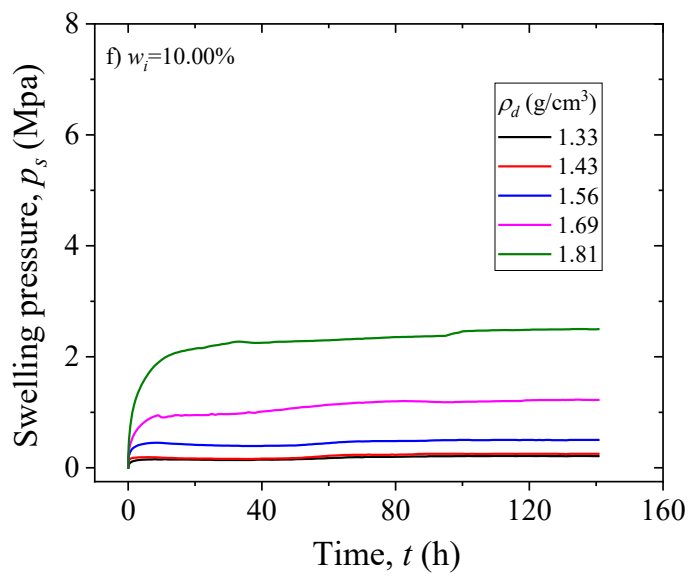
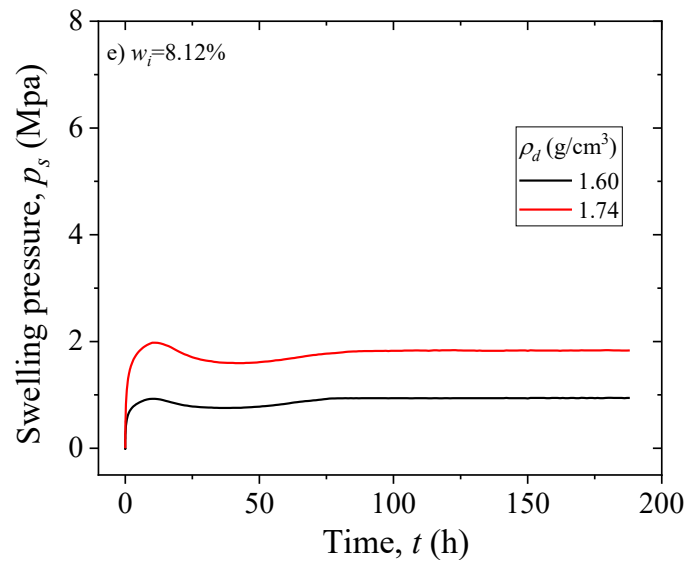
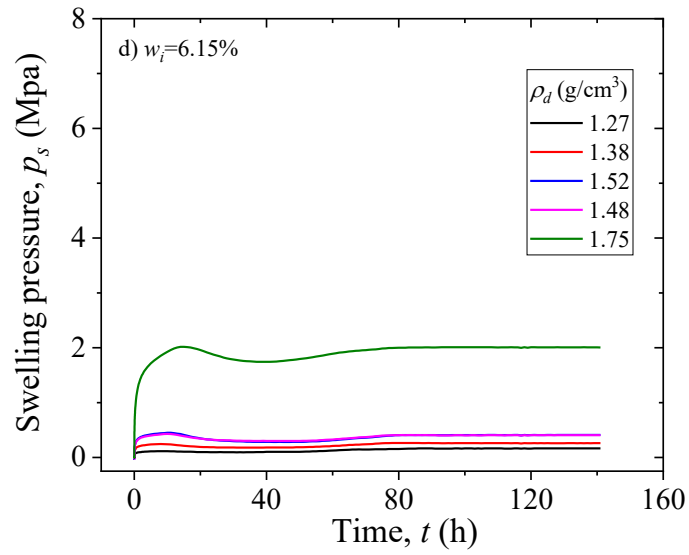


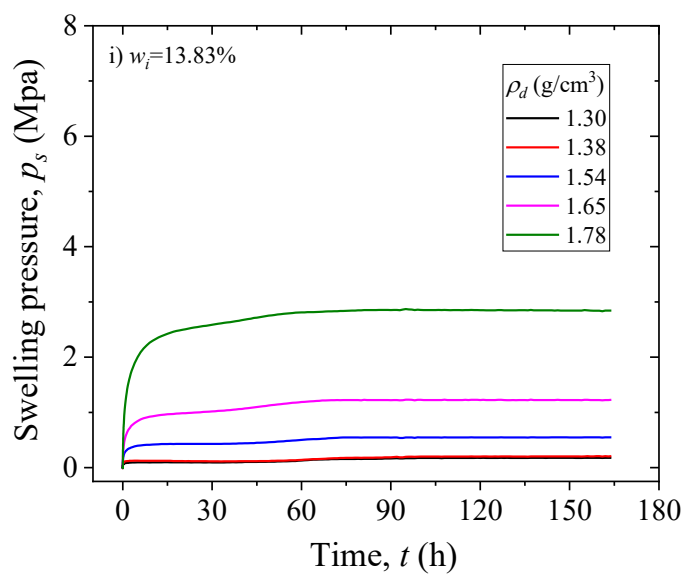
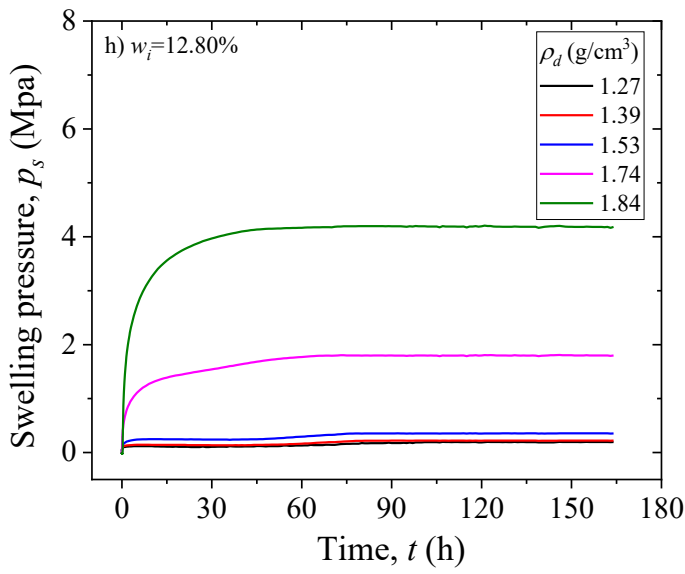
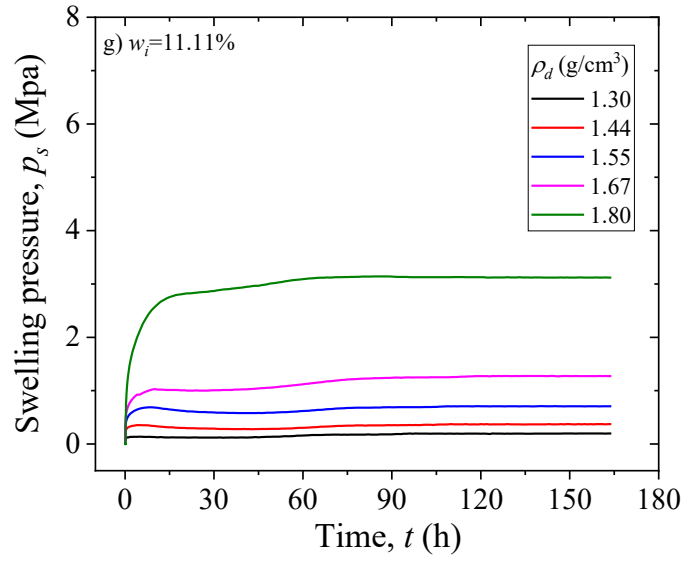
**Figure 10-4 2mm specimen for XRD tests and specimen sealed by parafilm**

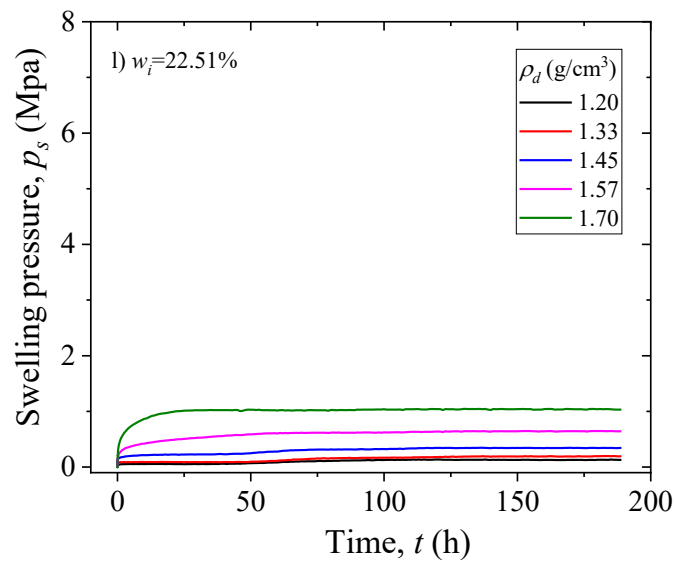
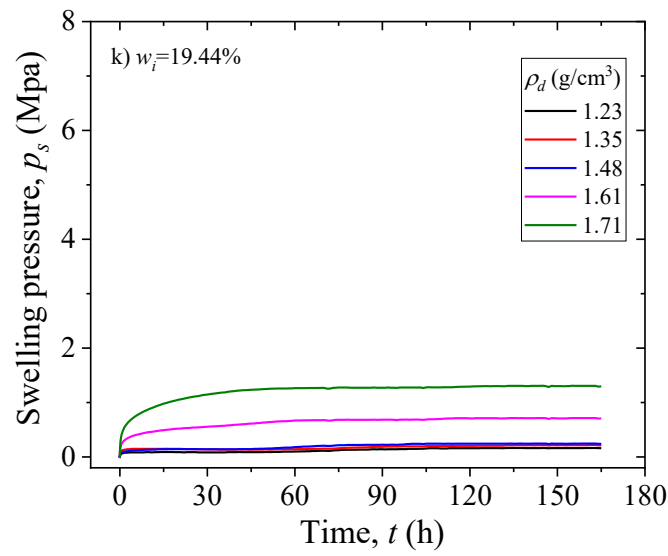
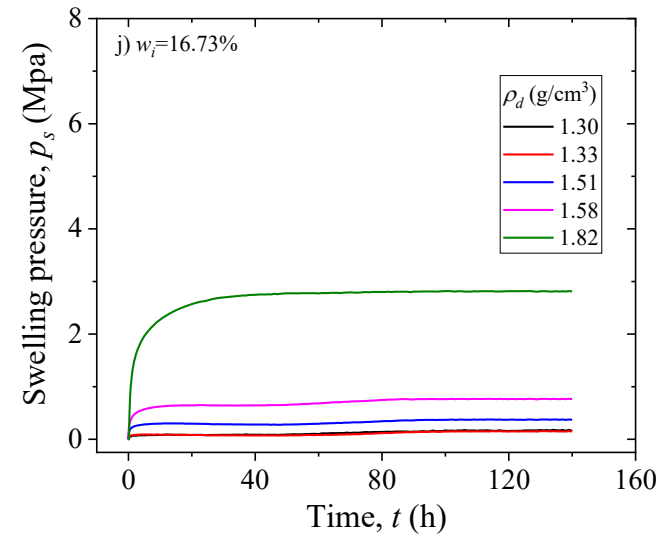
## 10.2 Results

### 10.2.1 Swelling pressures and XRD results from water spray method

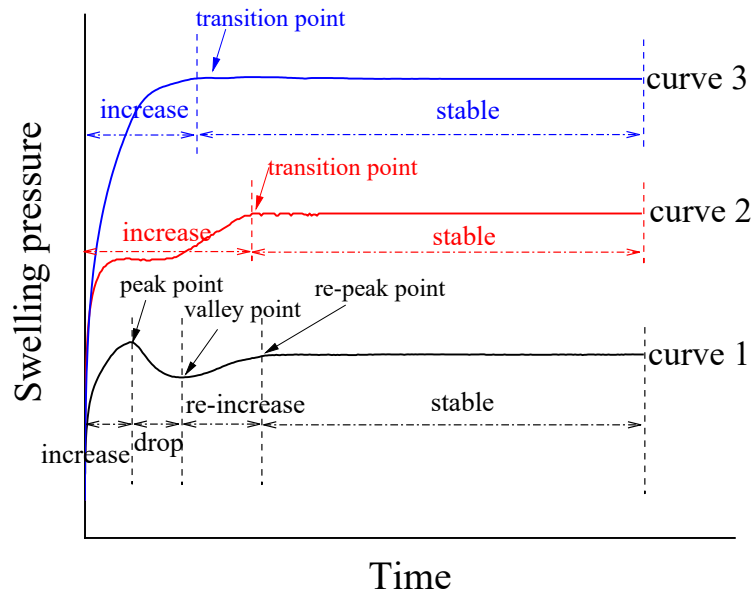








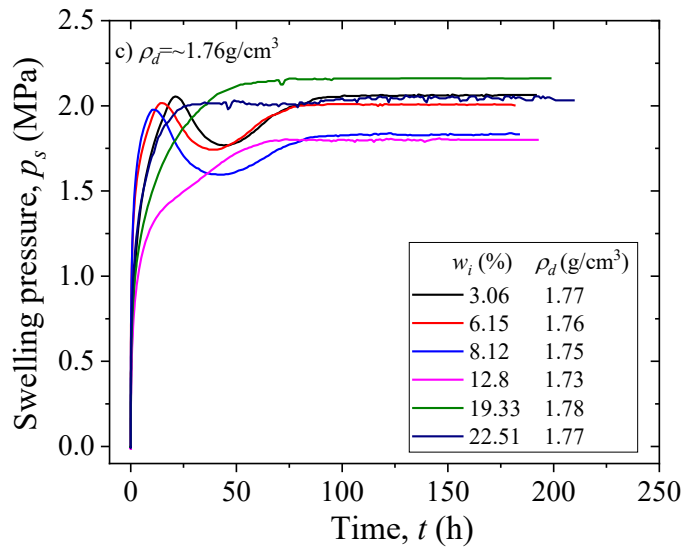
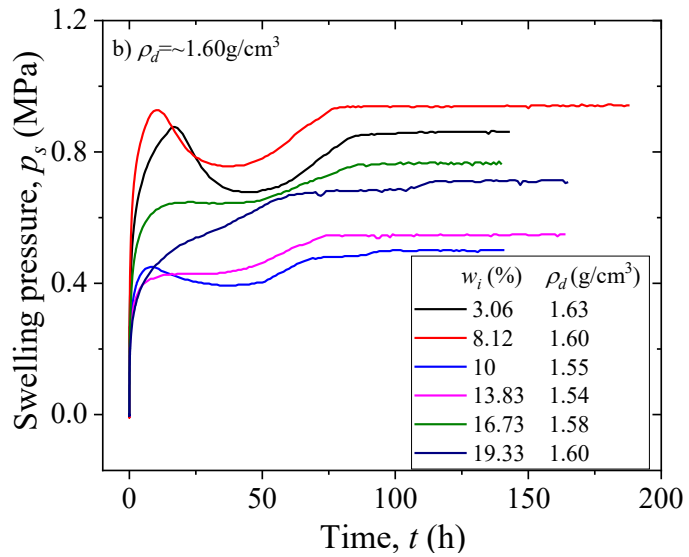
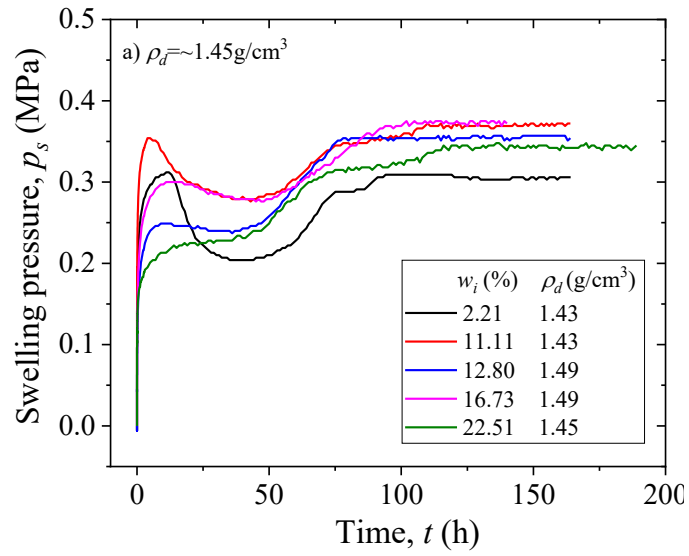
**Figure 10-5 Swelling pressure evolution curves of specimens with different initial water contents by water spray method**

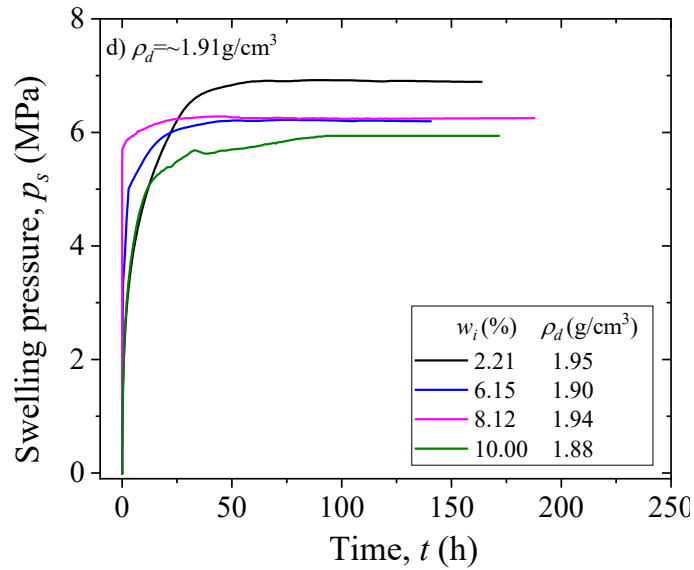


**Figure 10-6 Traditional swelling pressure evolution curves**

Swelling pressure curves of KV1 with different initial water contents by water spray are presented in Fig. 10-5. Tremendous scholars reported swelling pressure evolution curves patterns of bentonites as revealed in Fig. 10-6 as: (1) a curve with obvious peak and Valley (Curve 1); and (2) a curve with continuous rise in the initial wetting duration (Curve 2 and Curve 3). Pattern Curve 1 is often reported for low and middle dry densities compacted bentonites. Patterns Curve 2 and Curve 3 are generally revealed for high dry densities compacted bentonites by some scholars.

As can be seen from Fig. 10-5, for low initial water content specimens ( $w_i=0\%-10\%$ ), with the increase of dry density, swelling pressure developing pattern changes from Curve1 to Curve 2 and Curve 3. Changing another word, as dry density rises, swelling pressure evolution curve varies from a curve with peak and valley to a curve with steady rise in the beginning wetting duration. The same observation was informed by Chen et al. (2018) and Chen et al. (2019). Regarding high initial water content specimens ( $w_i=10.00\%-22.51\%$ ), swelling pressure curves all show the pattern as Curve 2 and Curve 3, which were not affected by the dry density.

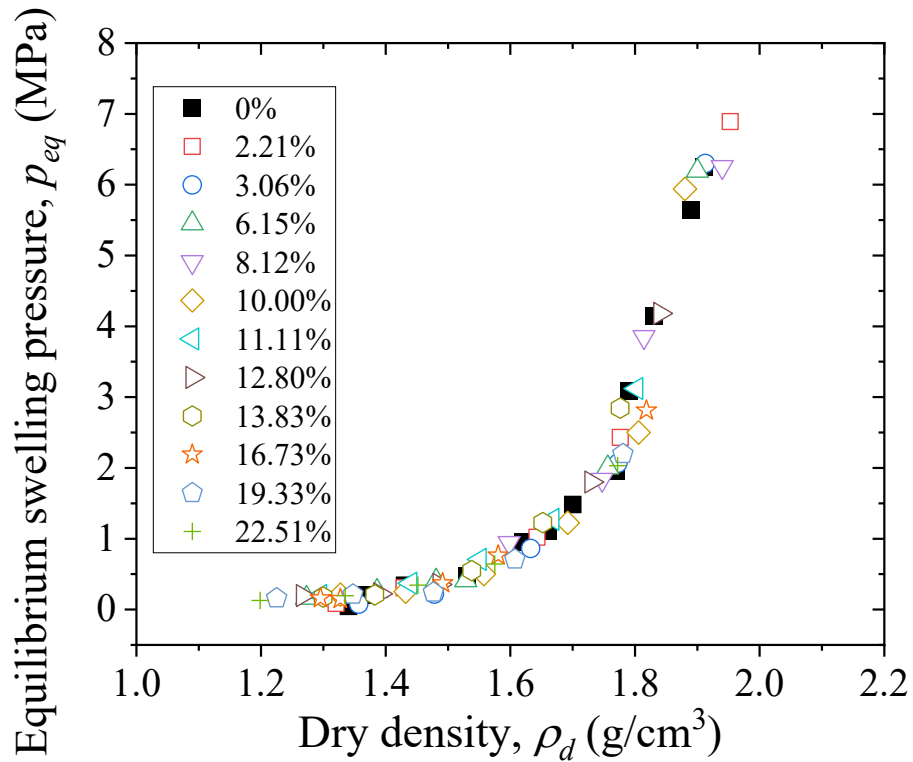




**Figure 10-7 Some swelling pressure evolution curves of specimens by water spray method at similar dry densities**

By combining some similar dry densities specimens in Fig. 10-5, Fig. 10-7 shows some swelling pressure evolution curves of specimens with different initial water contents. As Fig. 10-7 (a) (b) and (c) shown, in case of low dry density and middle dry density ( $\rho_d$ =approximate. 1.45, 1.60 and 1.76  $\text{g/cm}^3$ ) specimens, swelling pressure evolution curve changes from Curve 1 to Curve 2 and Curve 3 as initial water content rises. However, for high dry density specimens ( $\rho_d$ =approximate. 1.91  $\text{g/cm}^3$ ), the swelling pressure evolution curves all exhibit the pattern as Curve 1.

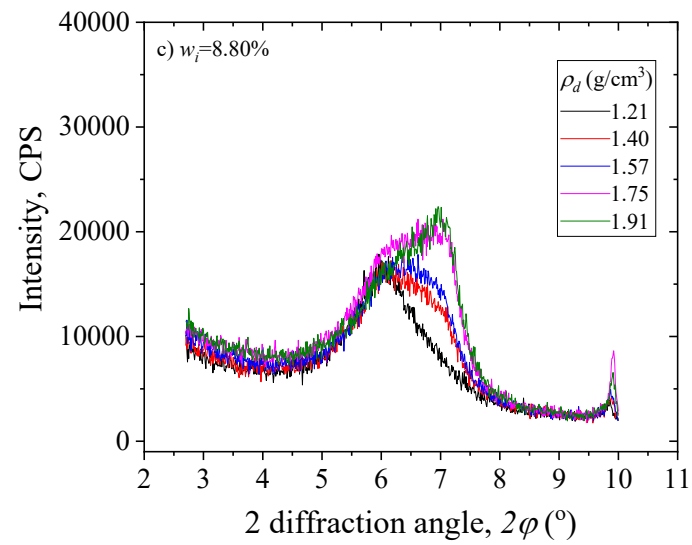
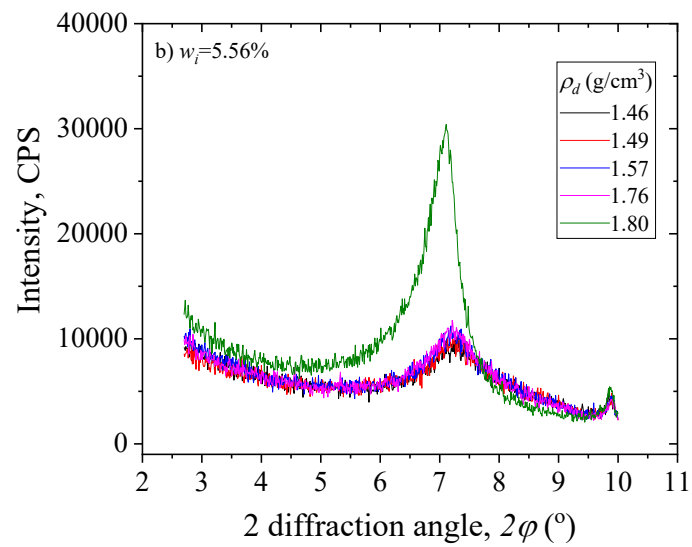
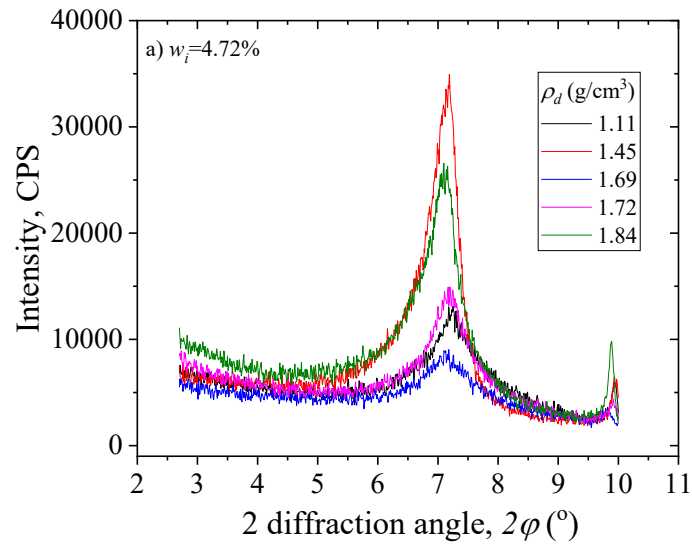
Figure 10-8 reveals the equilibrium swelling pressures of KV1 bentonite with different initial water contents by water spray method. It is general truth from Fig. 10-8 that, equilibrium swelling pressure rises with the increase of dry density. Additionally, an easy phenomenon can be found from Fig. 10-8 that, initial water content may have no apparent effect on the equilibrium swelling pressure of KV1 bentonite when the specimens were made by water spray method. The same conclusion was reported by the testing investigation from Komine and Ogata (1994), Wang et al. (2022) for KV1 bentonite, Villar and Lloret (2008) for FEBEX bentonite.

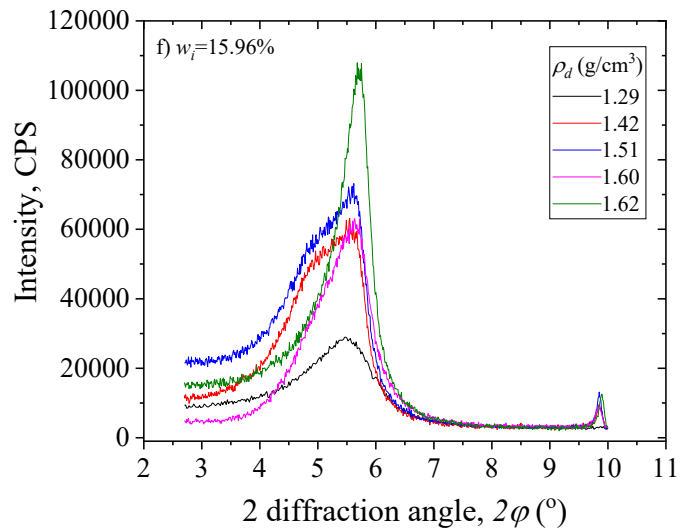
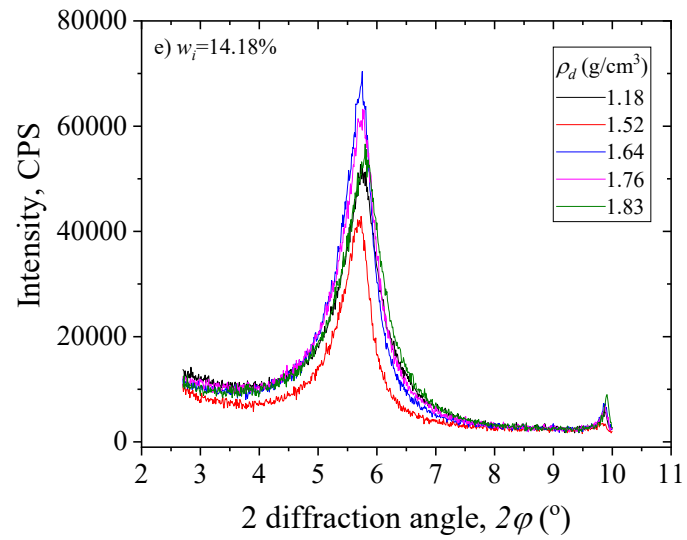
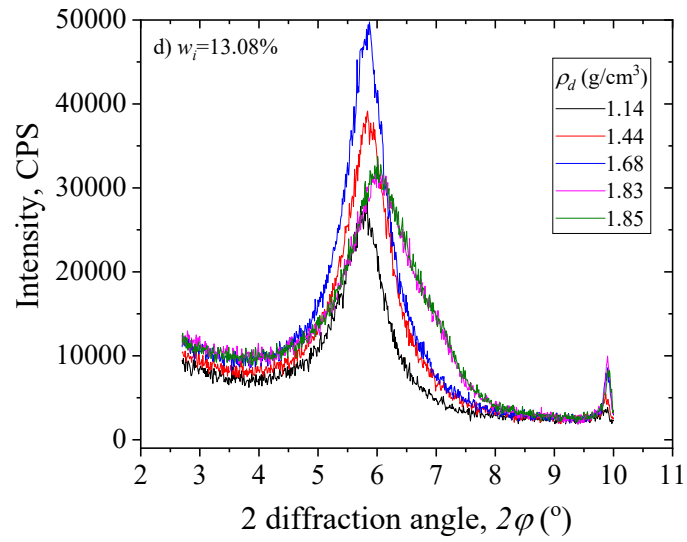


**Figure 10-8 Equilibrium swelling pressure of specimen with different initial water contents by water spray method**

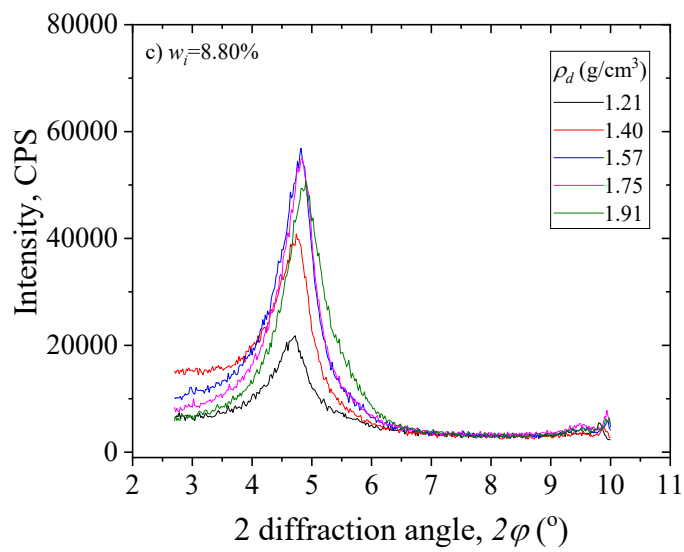
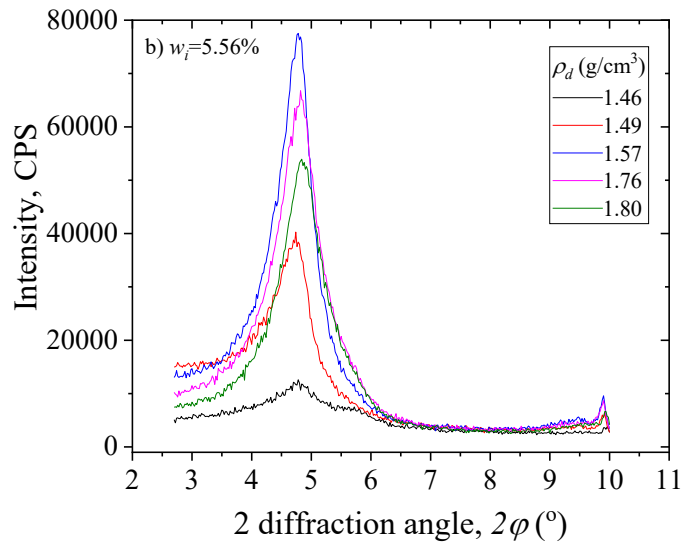
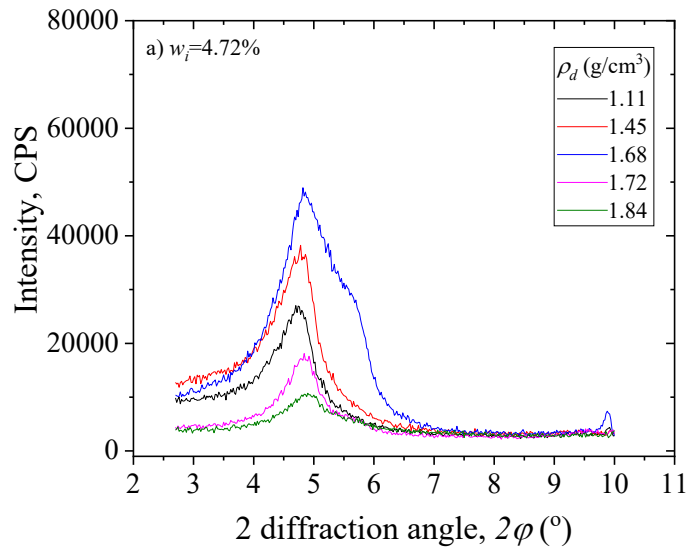
XRD profiles of specimens before wetting by water spray method are presented in 10-9. It can be seen from 10-9 (a) and (b), for low initial water contents ( $w_i=4.72$  and  $5.56\%$ ) specimens, the peak angle seems does not being affected greatly by the variation of dry density. Figure 10-9 (c) (d) (e) and (f) show the XRD profiles of high initial water contents specimens before wetting. It seems from Fig. 10-9 (c) (d) (e) and (f) that, peak angle moves to right with rising dry density.

Figure 10-10 shows XRD profiles of specimens after wetting by water spray method. Regarding the peak angle, comparing to the specimen before wetting, the peak angle generally moves from  $\sim 6^\circ\sim 8^\circ$  to  $\sim 4^\circ\sim 6^\circ$ . From Fig. 10-10, the peaks of saturated specimens were found slowly moves to right with the increase of dry density. Meanwhile, from Fig. 10-9 and 10-10, no matter unsaturated or saturated specimen, there is no clear trend for the dry density effect on the peak intensity.





**Figure 10-9 XRD profiles of specimens with different initial water contents before wetting by water spray method**



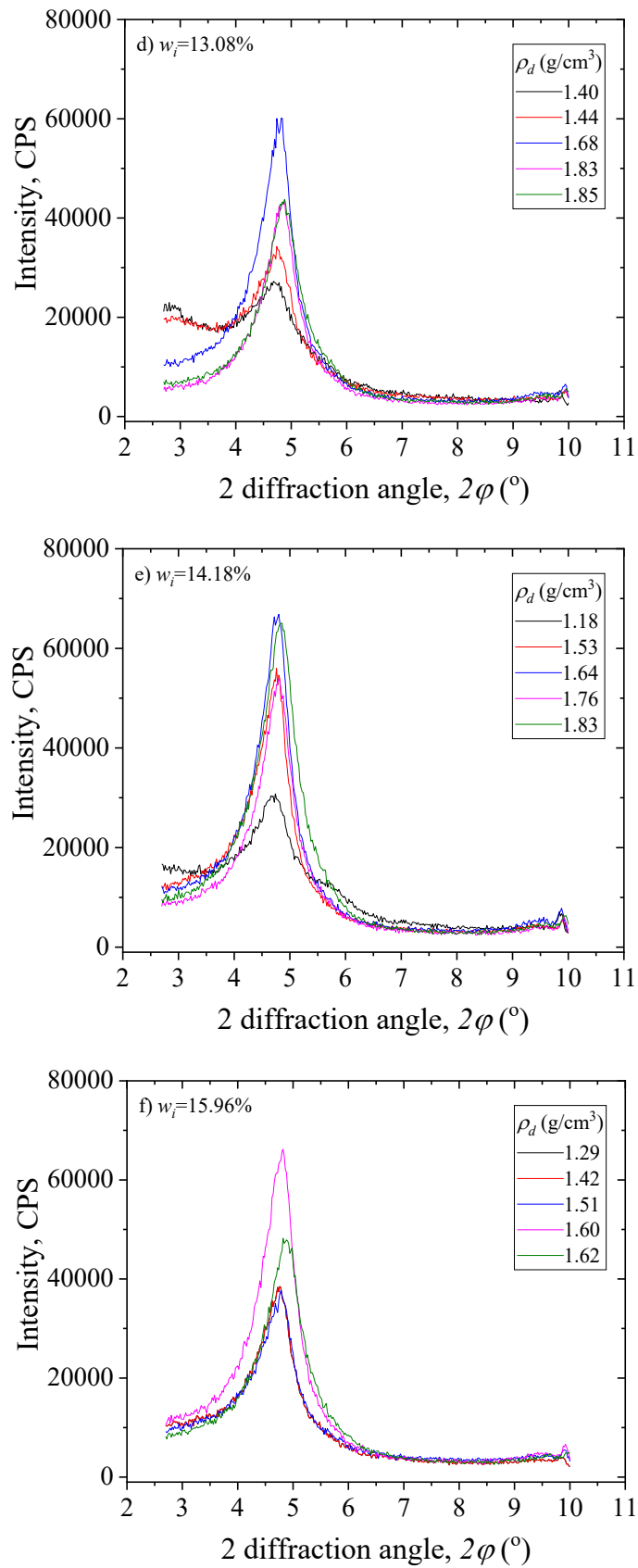


**Figure 10-10 XRD profiles of specimens with different initial water contents after wetting by water spray method**

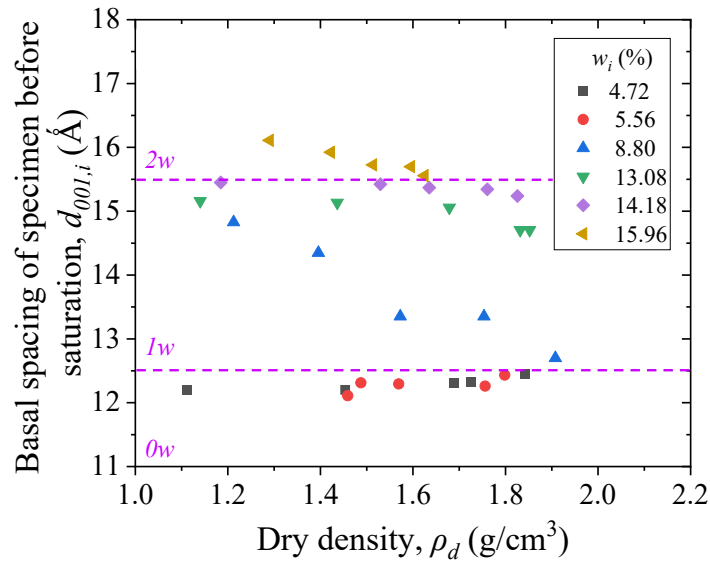


**Figure 10-11 Basal spacing of specimens before wetting with different initial water contents by water spray method**

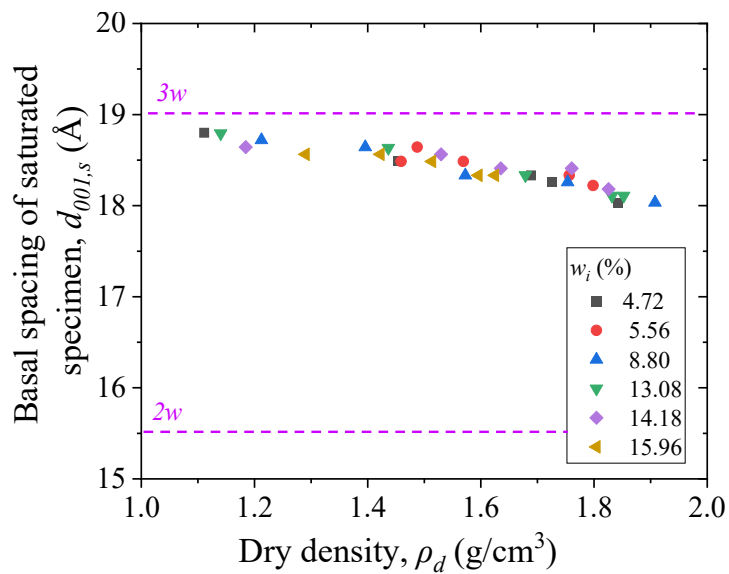


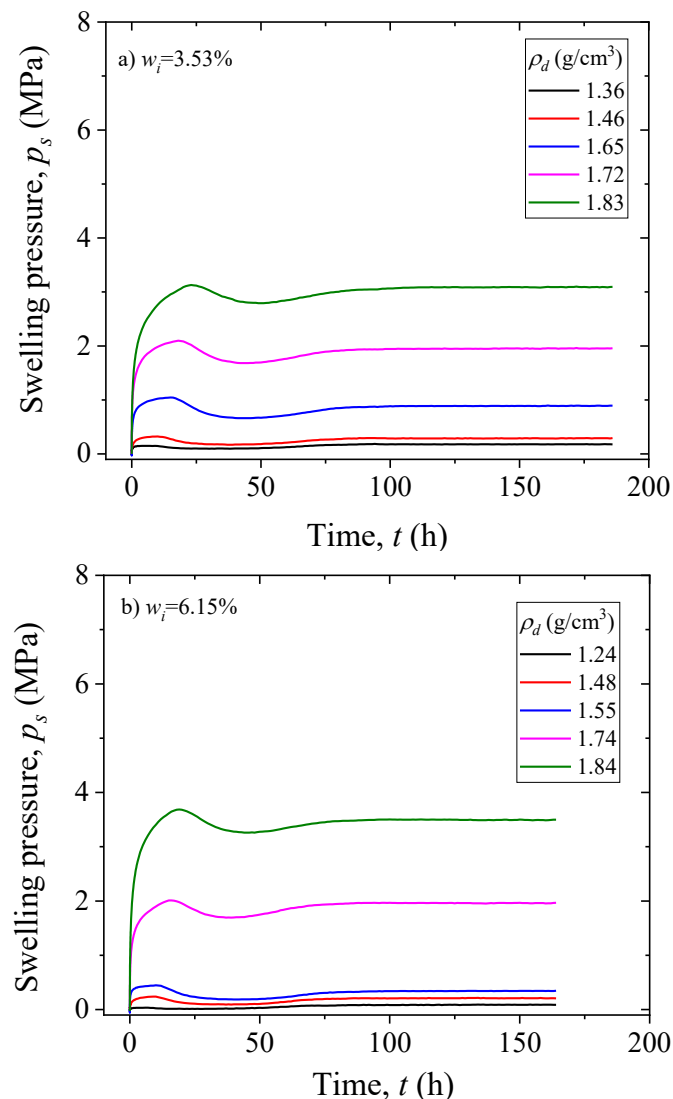
**Figure 10-12 Basal spacing of specimens after wetting with different initial water contents by water spray method**

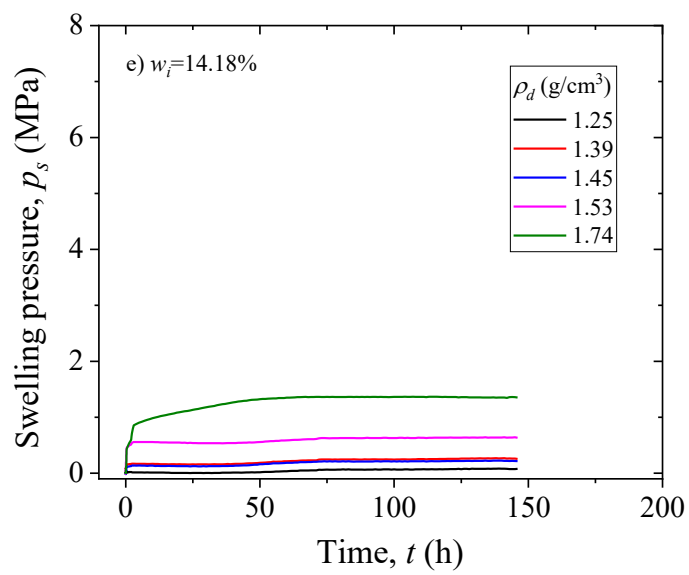
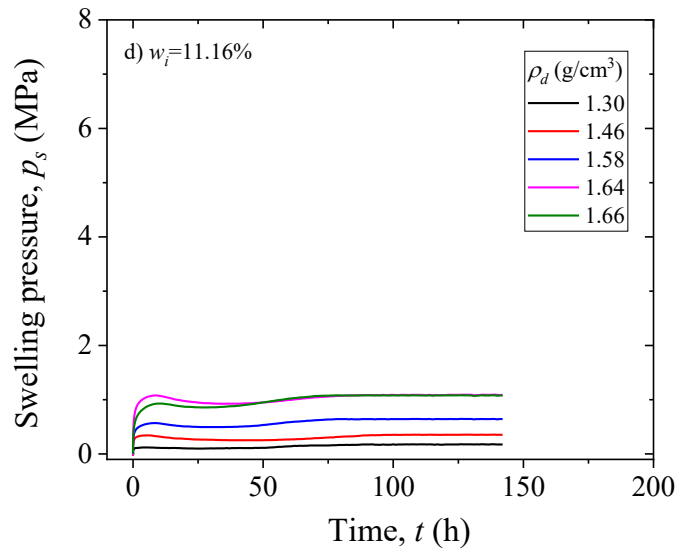
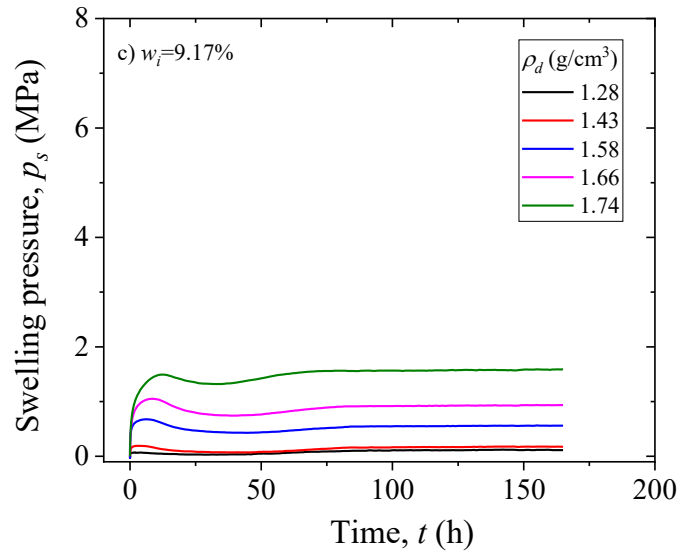
Basal spacings of specimens before wetting with different initial water contents produced by water spray method is revealed in Fig. 10-11. When initial water contents are 4.72% and 5.56%, the effect of dry density on the basal spacing is very small. Then, for the initial water contents are 8.8%, 13.08%, 14.18% and 15.96%. The basal spacing reduces with the increasing of dry density. Meanwhile, it is an apparent trend from Fig.

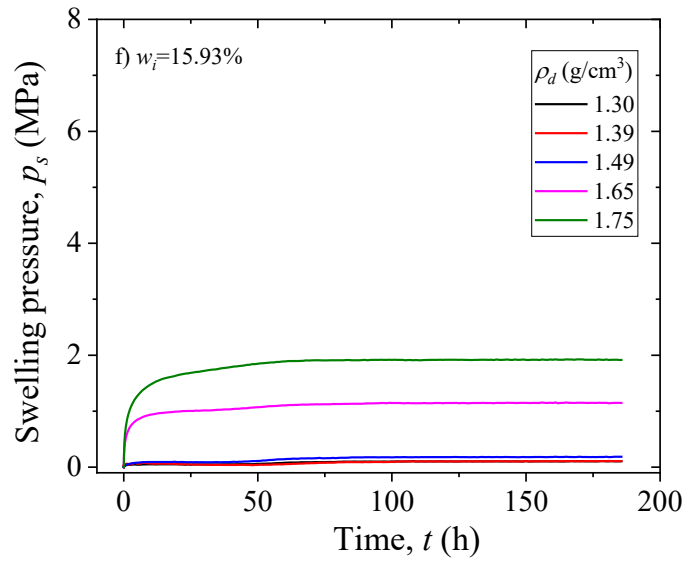
10-11 that, basal spacing rises with the increase of initial water content, when they have same dry density. The water molecule states in inter-layer pore of specimens stay from  $0w$  to  $2w$  state with rising initial water content.

Basal spacings of saturated specimens after wetting with different initial water contents by water spray method is shown in Fig. 10-12. It can be easily concluded from Fig. 10-12, with the increase of dry density, basal spacing of saturated specimen decreases. The water molecule states in inter-layer pore of specimens all stay in  $2w$  state with the variation of dry density. Meanwhile, it seems that there is no effect of initial water content on basal spacing of saturated specimen.

### 10.2.2 Swelling pressures and XRD results from humidity control method

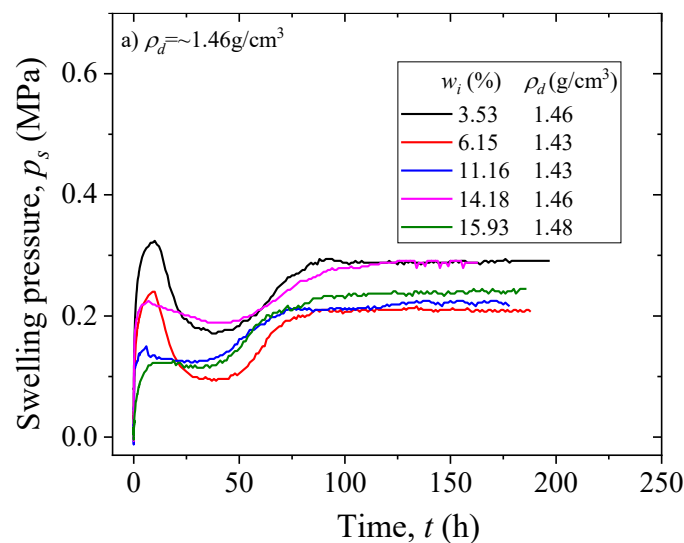


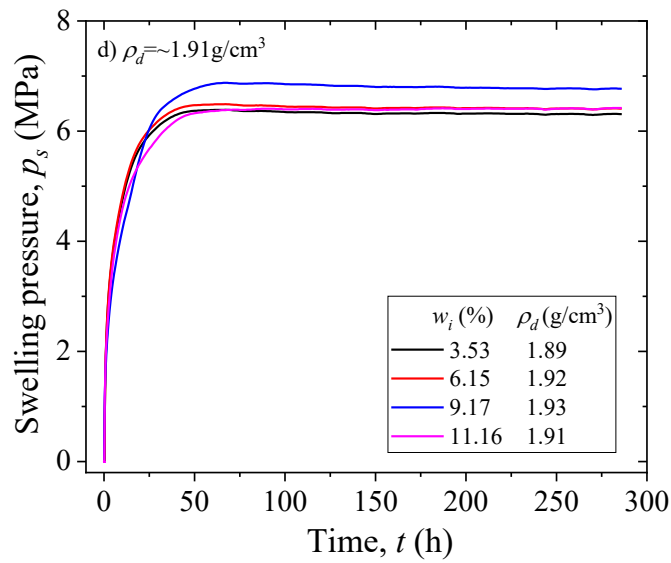
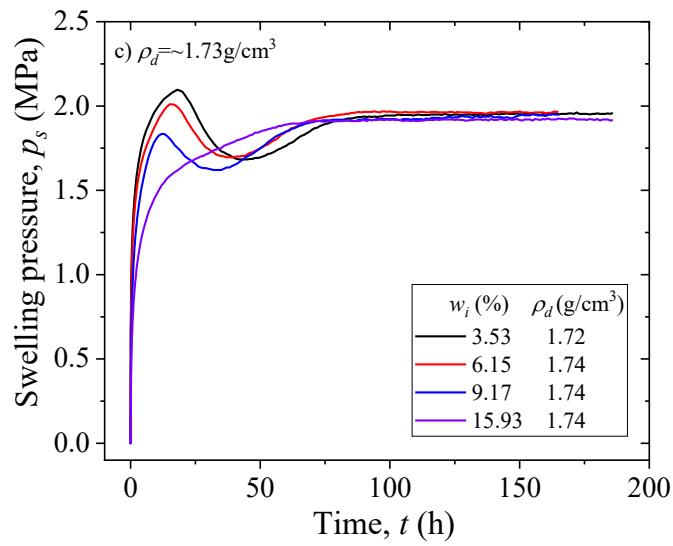
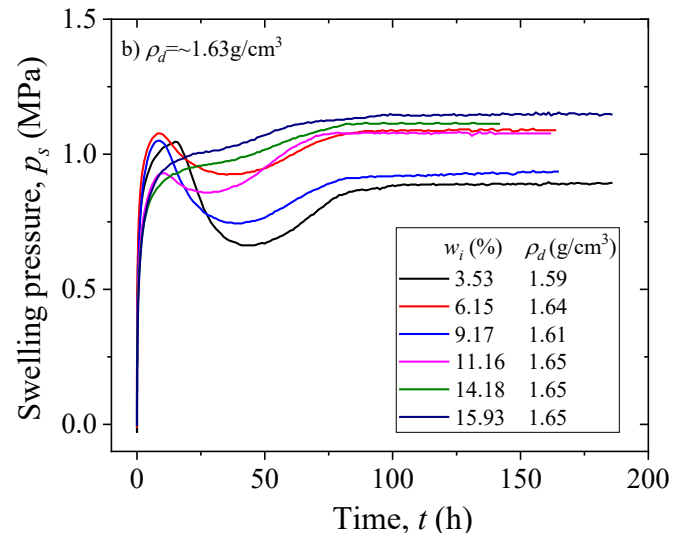




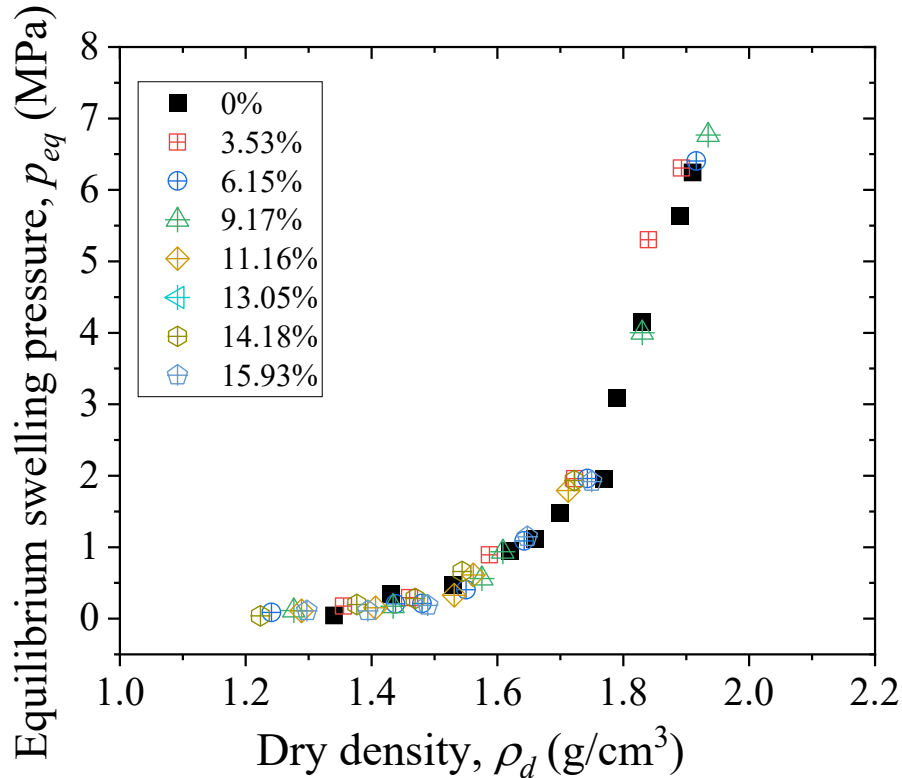
**Figure 10-13 Swelling pressure evolution curves of specimens with different initial water contents by humidity control method**

Figure 10-13 shows swelling pressure evolution curves of specimens with different water contents by humidity control method. By connecting same similar dry densities conditions, some swelling pressure evolution curves for specimens with different initial water contents are presented in Fig. 10-14. It can be seen from Fig. 10-14 (a), (b) and (c), when  $\rho_d \approx 1.46, 1.63$  and  $1.73 \text{ g/cm}^3$ , with the increase of initial water content, swelling pattern changes from Curve 1 to Curve 2 and Curve 3. When  $\rho_d \approx 1.91 \text{ g/cm}^3$ , all swelling pressure curves exhibit the pattern similar with Curve 3.





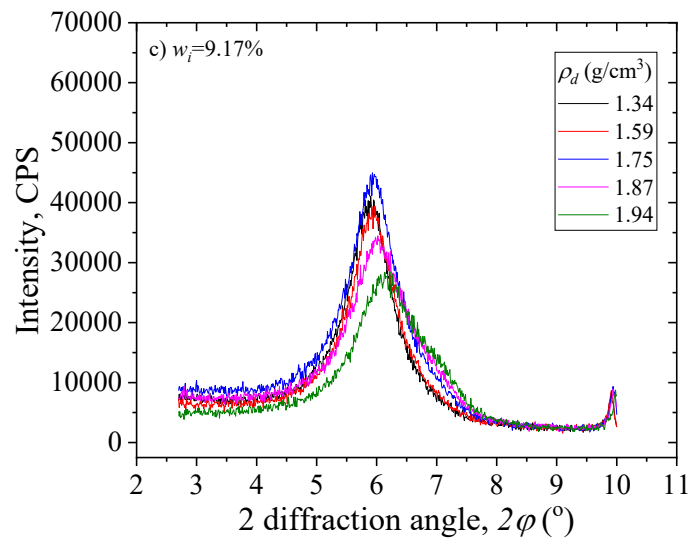
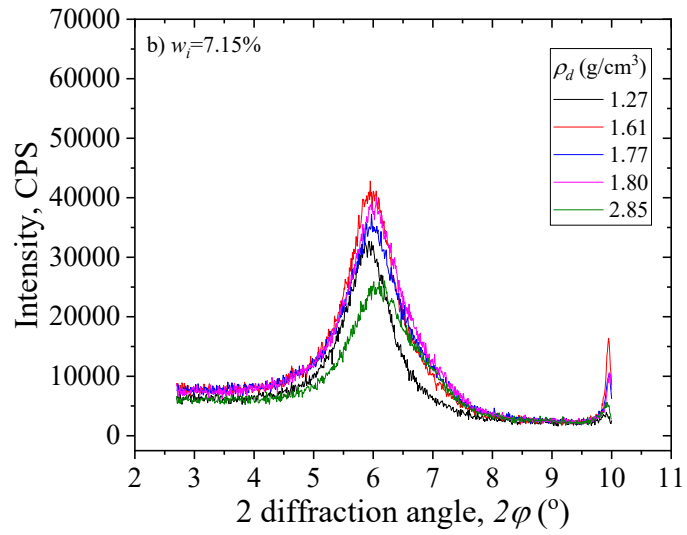
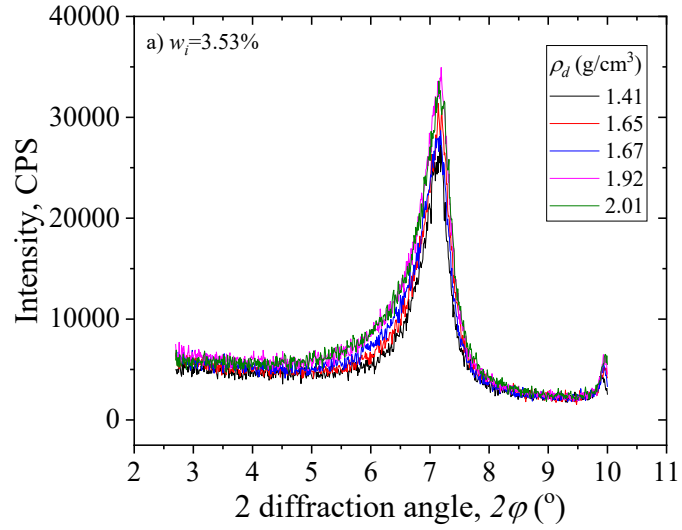
**Figure 10-14 Some swelling pressure evolution curves of specimens by humidity control method at similar dry densities**

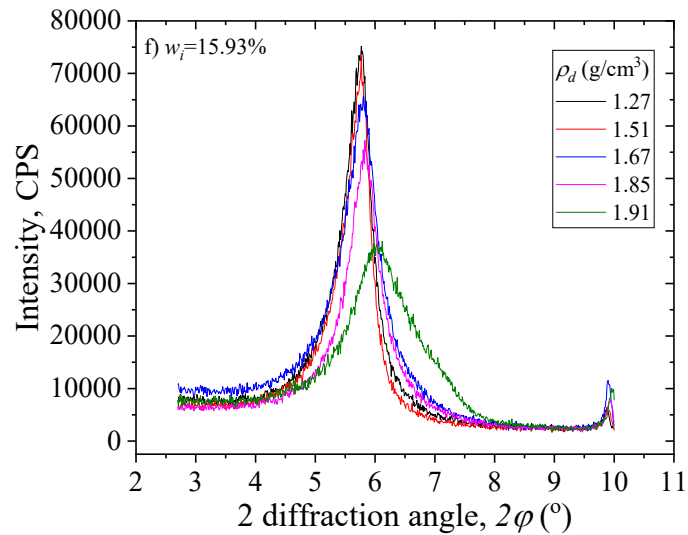
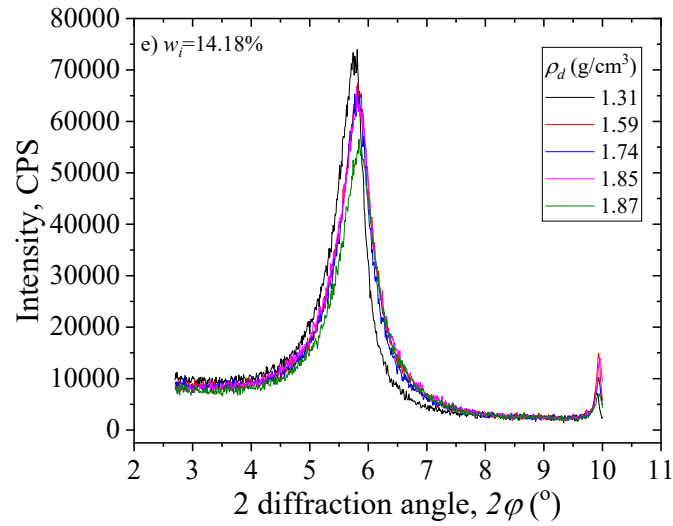
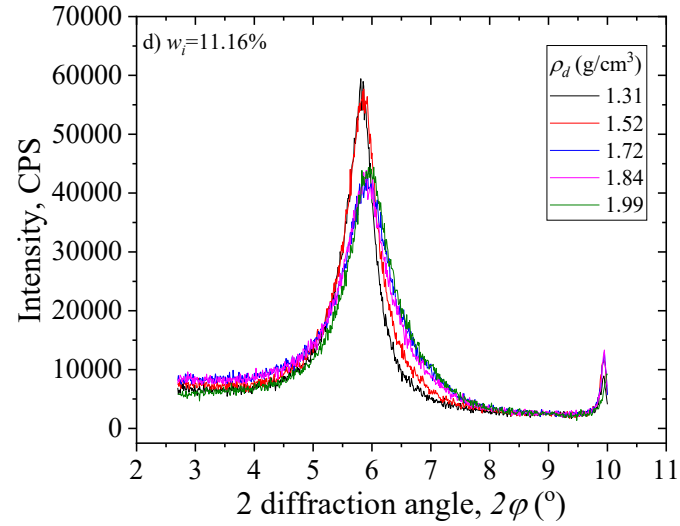


**Figure 10-15 Equilibrium swelling pressure of specimen with different initial water contents by humidity control method**

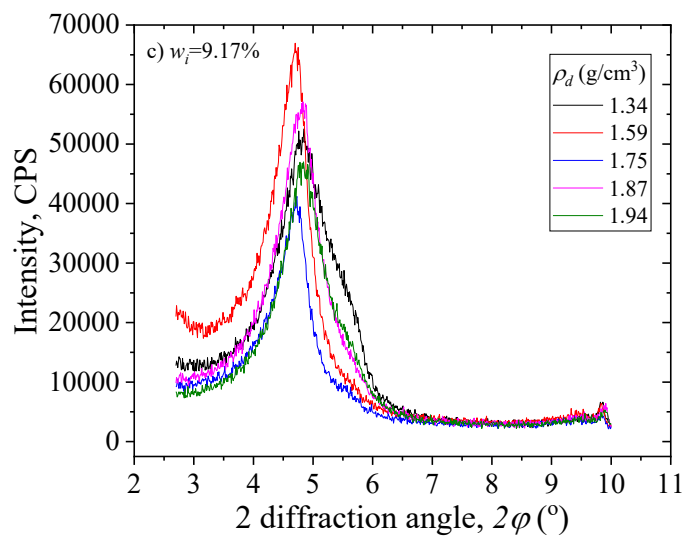
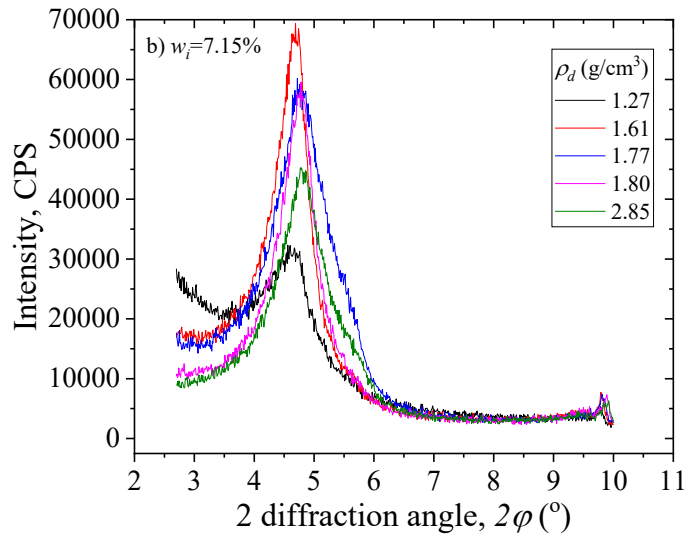
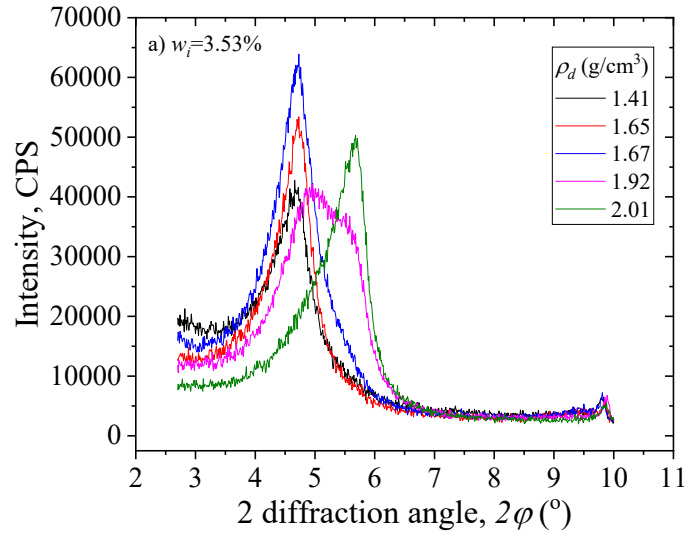
Figure 10-15 indicates the equilibrium swelling pressures of KV1 bentonite with different initial water contents by humidity control method. It can be seen from Fig. 10-15 that, equilibrium swelling pressure increases as dry density grows. At the same time, it is apparent from Fig. 10-15 that, there is no initial water content effect on the equilibrium swelling pressure of KV1 bentonite, which agrees with the founding for water spray method.

From Fig. 10-8 and Fig. 10-15, the effect of specimen preparation method on equilibrium swelling pressure of KV1 bentonite can be discovered. As can be seen from Fig. 10-8 and Fig. 10-15, the changing lines of dry density and equilibrium swelling pressure is similar with the equilibrium swelling pressures when  $w_i=0\%$ . Therefore, it can be concluded that, specimen preparation method has no effect on the equilibrium swelling pressure of KV1 bentonite.





**Figure 10-16 XRD profiles of specimens before wetting with different initial water contents by humidity control method**



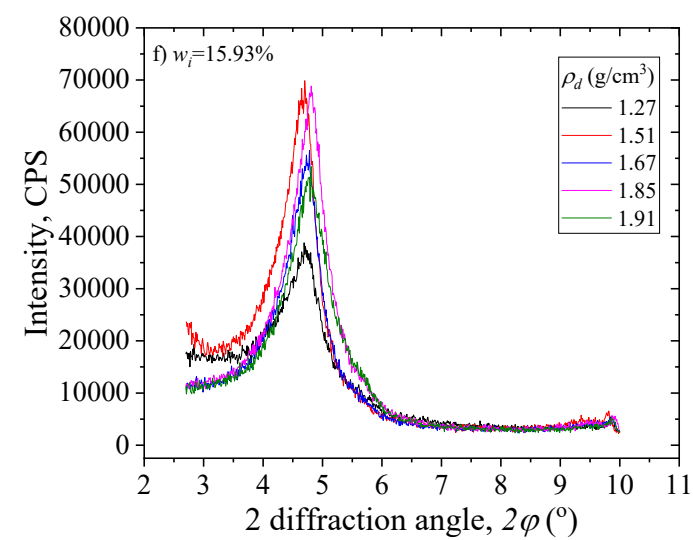
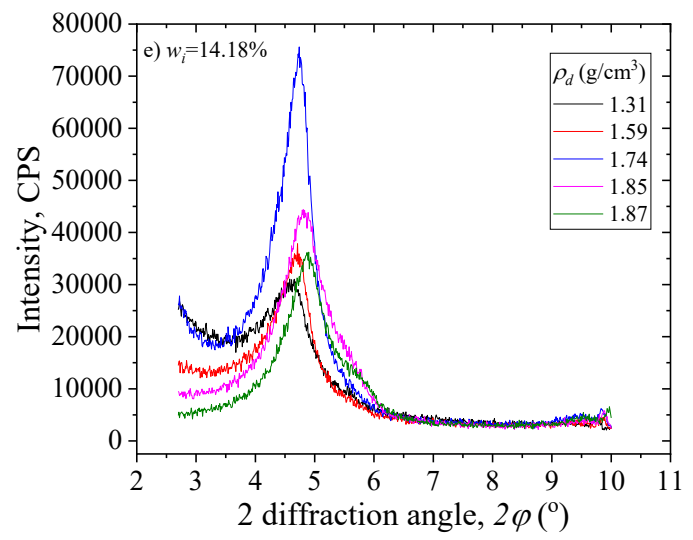
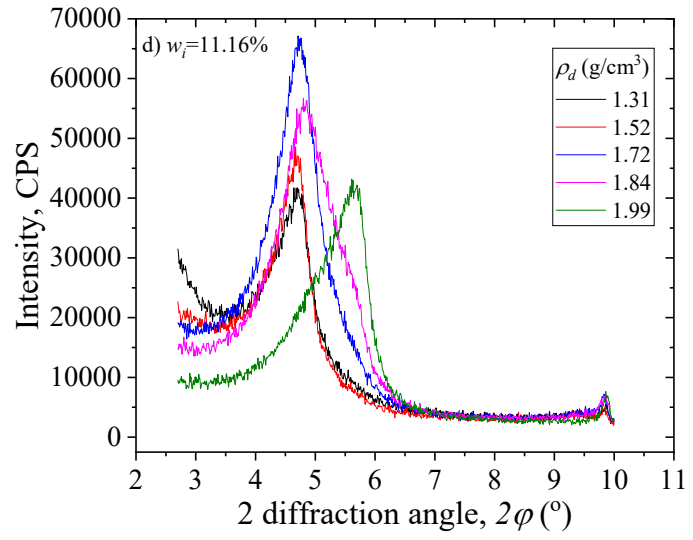


**Figure 10-17 XRD profiles of specimens after wetting with different initial water contents by humidity control method**

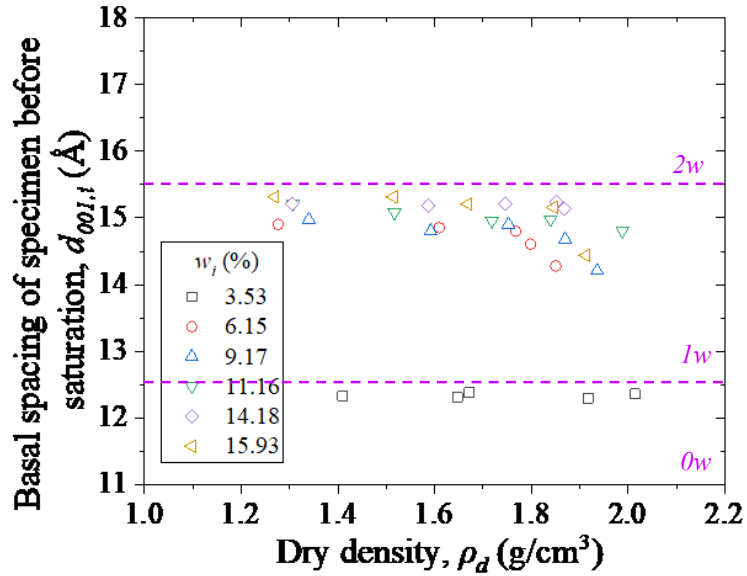


**Figure 10-18 Basal spacing of specimens before wetting with different initial water contents by humidity control method**

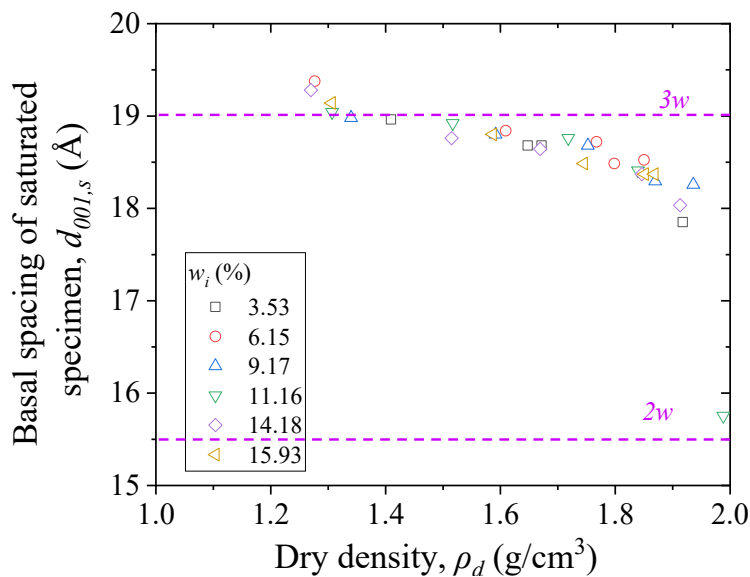


**Figure 10-19 Basal spacing of specimens after wetting with different initial water contents by humidity control method**

Figure 10-16 and 10-17 show XRD profiles of specimens with different initial water contents by humidity control method before and after wetting. As we can see from Fig. 10-16, for specimens before wetting, when  $w_i=3.53\%$ , the peak angle seems stay in relative stable values. When  $w_i=6.15, 9.17, 11.16, 14.18$  and  $15.93\%$ , the peak position

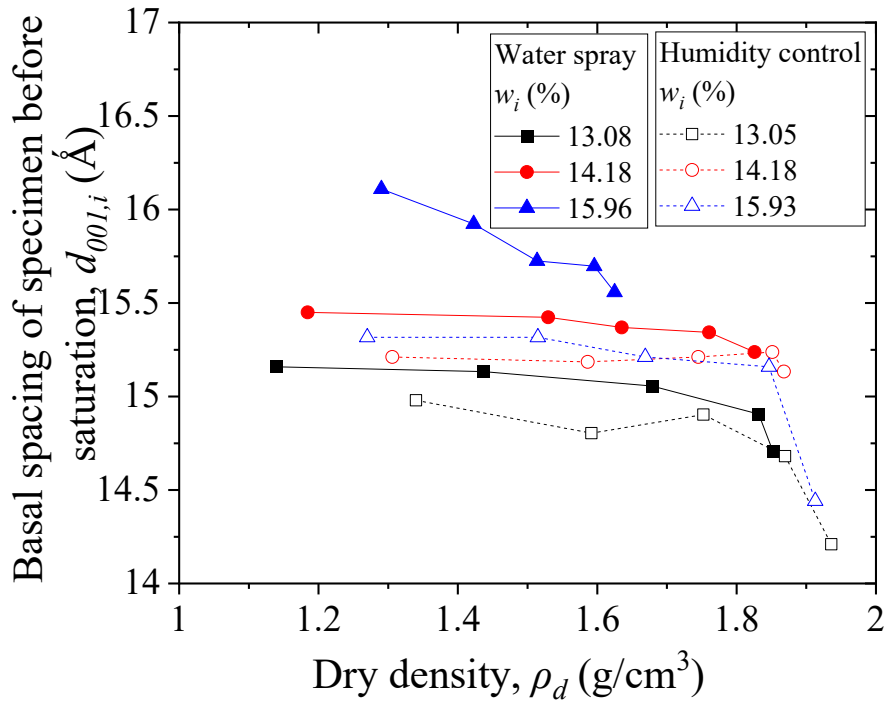
slowly moves to right as dry density increases. Regarding the XRD profiles of specimens after wetting, the peak moves to right with the increase of dry density.

Figure 10-18 and 1-19 show basal spacings of specimens with different initial water contents by humidity control method before wetting and after wetting, respectively. It can be concluded from Fig. 10-18 that, for specimens before wetting, when  $w_i=3.53\%$ , basal spacing was not affected by the dry density. With the rise of initial water content, basal spacing reduces with the increasing of dry density. Additionally, at similar dry densities, increase of initial water content induces bigger basal spacing. Additionally, the water molecule states in inter-layer pore of specimens stay from  $0w$  to  $1w$  as initial water content increases. Basal spacing of saturated specimen with different initial water contents by humidity control method is revealed in Fig. 10-19. It is a general truth from Fig. 10-19, with the increase of dry density, basal spacing decreases. This founding is the same as the results from water spray method. The water molecule states in inter-layer pore of specimens all stay in  $2w - 3w$  state with the change of dry density. At the same time, in Fig.10-19, one can inferred that, the basal spacing of saturated specimen is not affected by the initial water content.

### 10.3 Discussion

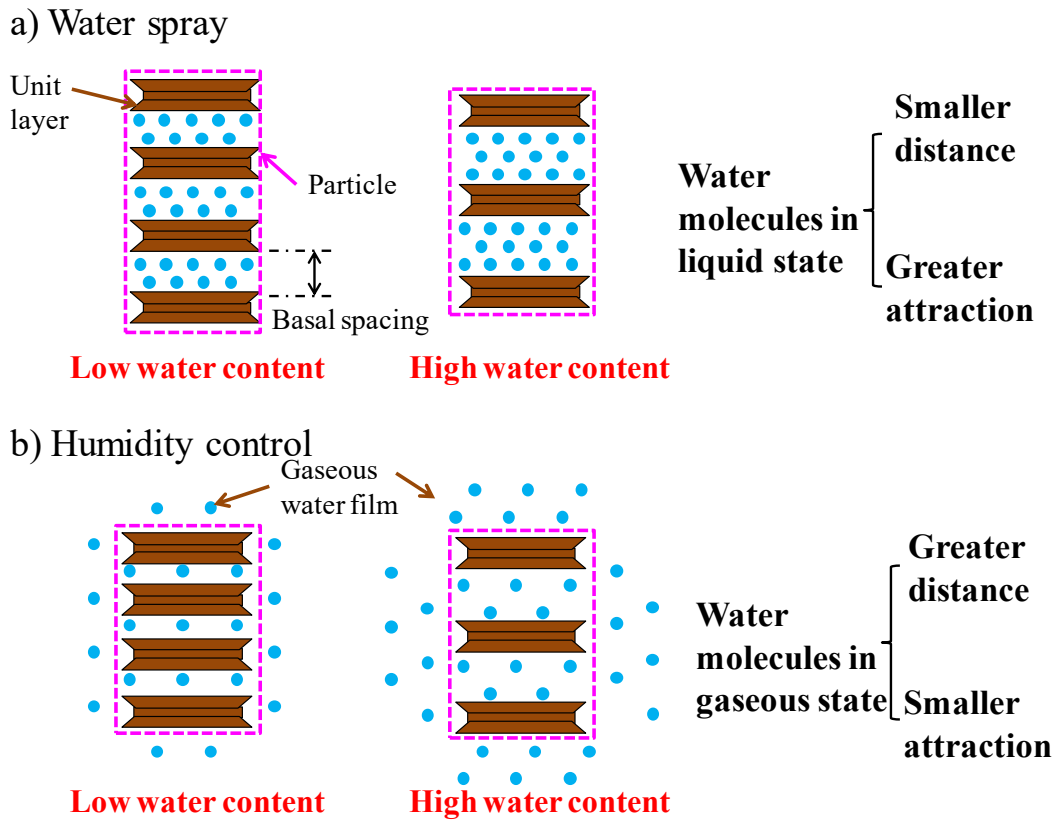
#### 10.3.1 Effects of specimen preparation method and initial water content on basal spacing of specimens in initial and saturated states

Figure 10-20 shows some basal spacings of specimens before wetting produced by different specimen preparation methods. As Fig. 10-20 illustrates, for specimens before wetting, water spray method has larger basal spacing than the humidity control method when their initial water contents are similar.



**Figure 10-20 Basal spacing of specimens at similar initial water contents before wetting by different methods.**

This phenomenon can be inferred from the liquid types that produce powders with different water contents. Water spray method uses liquid water to wet powders. The water molecules in a liquid state are separated by smaller mutual distances and have greater attraction (Linus 1988). Therefore, it is easier for water molecules in a liquid state to enter spaces between interlayers (Fig. 10-21). By contrast, water molecules in a gaseous state have greater mutual distance separating them and smaller mutual attraction, which raise the difficulty for water molecules to enter interlayer interstices. Because a larger amount of gaseous water molecules cannot enter the interstices, they adsorb on the particle surface to form a “gaseous water film” (Fig. 10-21). Given similar initial water contents, more water molecules would occupy the interstices when using a water spray method for preparation, thereby leading to larger initial basal spacing.



**Figure 10-21 Schematic showing specimen preparation effects on the microstructure of the initial specimen.**

Herein, Figure 10-12 and 10-19 are combined together in Fig. 10-22 for making sense the specimen preparation method effect on basal spacing after wetting. As indicated in Fig.10-22, for specimens after wetting, humidity control method leads to larger basal spacing than the water spray method because a “gaseous water film” exists among particles of the initial specimen by humidity control method, which causes the larger initial distance among particles (Fig. 10-23). As described in some reports of the relevant literature (Suzuki et al. 2005; Liu 2013), swelling pressure among particles decreases concomitantly with increasing distance among particles. Consequently, during saturation processes, smaller back stress from swelling among particles for humidity-controlled specimens give smaller obstacle to the swelling between layers, leading to the fully development of swelling between layers and larger basal spacing in saturated state (Fig. 10-23).

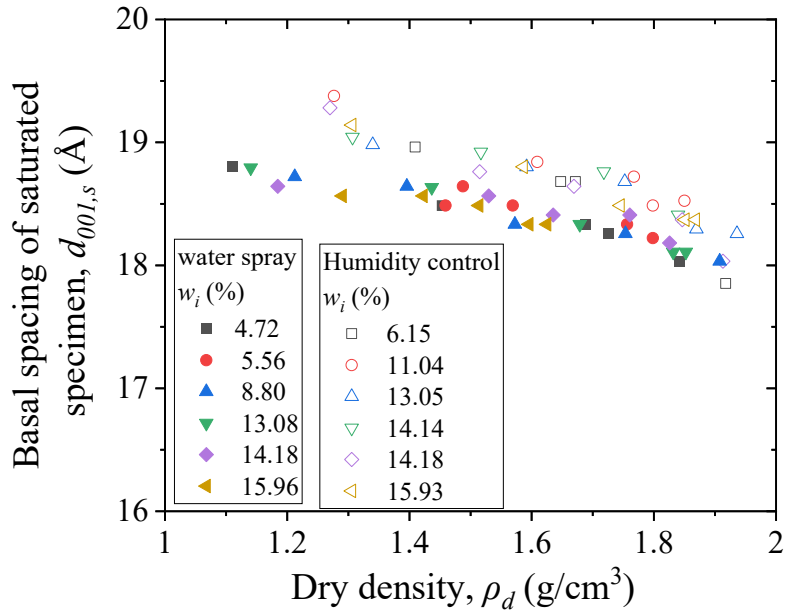


Fig. 10-22 Basal spacing of saturated specimen by different methods.

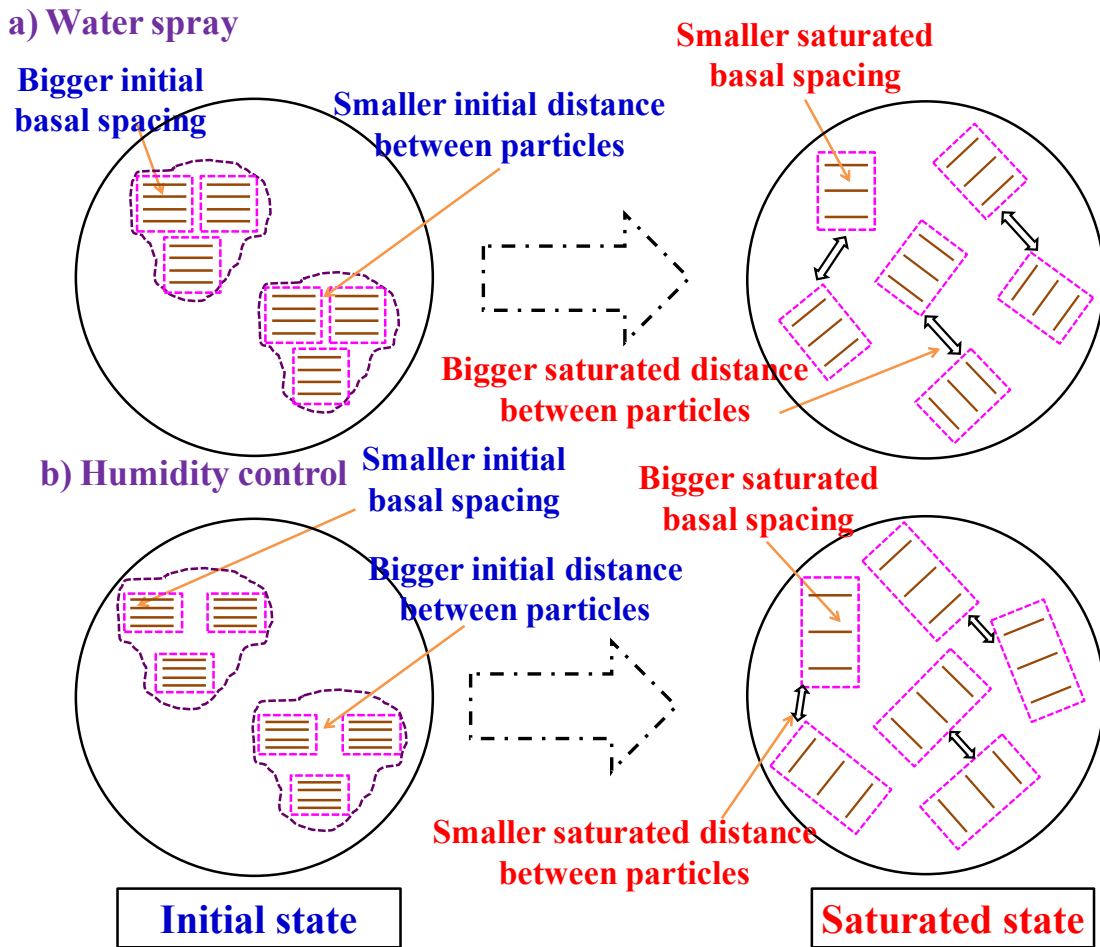
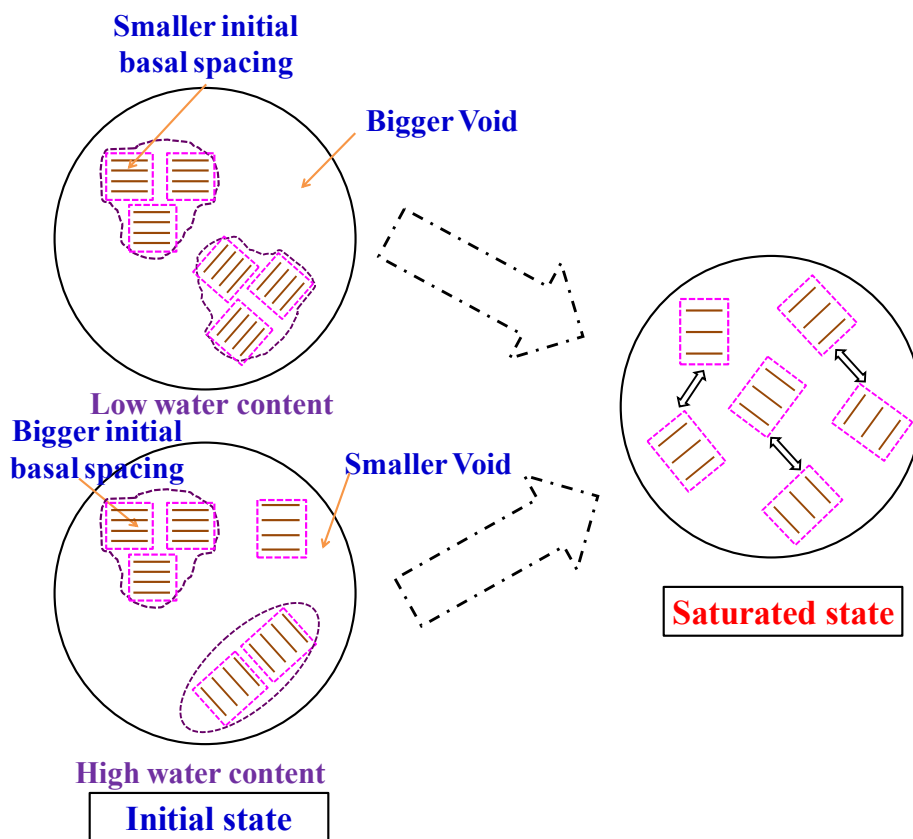


Figure 10-23 Schematic showing specimen preparation effects on the microstructures of initial and saturated states.

Additionally, Figure 10-12 and 10-19 reveal that initial water content has no effect on the basal spacing of a saturated specimen. One can examine the initial specimens used for the water spray method as an example for explanation, as presented in Fig. 10-24. This figure shows that a smaller initial basal spacing from low water content specimen would leave a larger void outside the interlayer space for swelling between layers. However, larger initial basal spacing from a high water content specimen can not leave a sufficiently large void outside the interlayer space for swelling between layers. These phenomena might contribute to the possibility of two initial water content specimens reaching a similar state in saturated state (Fig. 10-24).



**Figure 10-24 Schematic showing effects of initial water contents on microstructures of initial and saturated states.**

10.3.2 Effects of specimen preparation and initial water contents on equilibrium swelling pressure

From Fig. 10-8 and 10-15, one can infer that the specimen preparation method has no effect on the equilibrium swelling pressure. Larger basal spacing and distance among particles leads to less swelling pressure among layers and particles (e.g. Liu 2013). As Fig. 10-23 shows, in a saturated state, application of the water spray method leads to smaller basal spacing and larger distance among particles. The humidity control method leads to larger basal spacing and smaller distance among particles. The mutual compensation of the two swellings results in the similarity equilibrium swelling pressure produced by the two specimen preparation methods.

As Fig. 10-8 and 10-15 shows, the equilibrium swelling pressure is unaffected by the initial water content. According to the discussion above, specimens with different initial water contents might reach a similar state in a saturated state (Fig. 10-24), which leads to similar equilibrium swelling pressures.

## Conclusion

Compacted bentonite with different water contents were achieved by spraying water and controlling the relative humidity of bentonite powder. Effects of initial water content and specimen preparation method on swelling pressures, including swelling pressure pattern and equilibrium swelling pressures, were researched. Another individual set of X-ray diffraction test was conducted to make sense the effects of initial water content and specimen preparation method on microstructure of bentonite. The results can be summarized as:

1. With the increase of initial water content, swelling pressure developing pattern changes from a curve with apparent peaks and valleys to a curve with quick continuous increase in initial stage;
2. There is no apparent effect from initial water content to equilibrium swelling pressure of bentonite. Specimen preparation method has no effect on equilibrium swelling pressure;
3. The initial water content just affect the basal spacing of specimen before saturation and have no influence on basal spacing of saturated specimen. The specimen preparation affects both basal spacings of specimens before and after wetting.

## Reference

- Chen, Y.G., Dong, X.X., Zhang, X.D., Ye, W.M., and Cui, Y.J. 2018. Combined thermal and saline effects on the swelling pressure of densely compacted GMZ bentonite. *Applied Clay Science*, 166: 318–326.
- Chen, Y.G., Dong, X.X., Zhang, X.D., Ye, W.M., and Cui, Y.J. 2019. Cyclic thermal and saline effects on the swelling pressure of densely compacted Gaomiaozhi bentonite. *Engineering Geology*, 255: 37–47.
- Komine, H., and Ogata, N. 1996. Prediction for swelling characteristics of compacted bentonite. *Canadian Geotechnical Journal*, 33(1): 10–22.
- Linus, P. 1988. *General Chemistry Third edition*. Dover Publication. New York, USA.
- Liu, L.C. 2013. Prediction of swelling pressures of different types of bentonite in dilute solutions. *Colloid Surface A: Physicochemical and Engineering Aspects*, 434: 303–318.
- Rao, S.M., and Ravi, K. 2015. Influence of initial degree of saturation on swelling pressures of compacted Barmer bentonite specimens. *Annals of Nuclear Energy*, **80**: 303–310.
- Suzuki, S., Prayongphan, S., Ichikawa, Y., and Chae, B.G. 2005. In situ observations of the swelling of bentonite aggregates in NaCl solution. *Applied Clay Science*, **29** (2): 89–98.
- Villar, M.V., and Lloret, A. 2008. Influence of dry density and water content on the swelling of a compacted bentonite. *Applied Clay Science*, **39**: 38–49.
- Wang, H.L., Ito, D., Shirakawabe, T., Ruan, K., and Komine, H., 2022. On swelling behaviours of a bentonite under different water contents. *Géotechnique*. Ahead of Print. <https://doi.org/10.1680/jgeot.21.00312>

# Chapter 11

## **APPLICATION IN PRACTICAL FIELD AND CONCLUSIONS**

## 11. 1 Overview

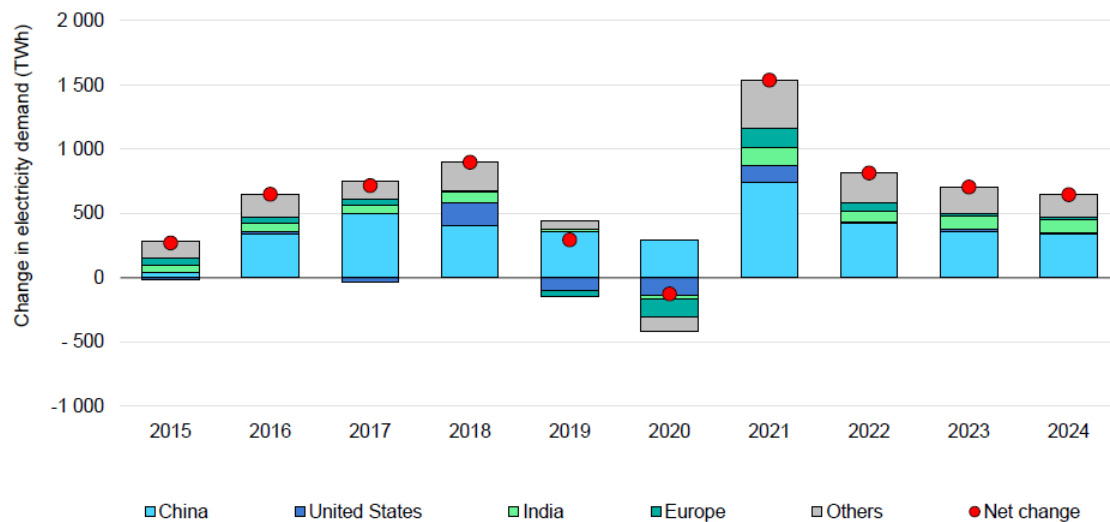


**Figure 11-1 Global change in electricity demand (IEA 2022)**

The responsibility of civil engineer and geotechnical engineer is not only to build a better society, but also help the world to be a better place. As Figure 11-1 shows, the demand of electricity all over the world is increasing very quickly in recent years for progressing the industrialization. However, electricity generation methods in nowadays brought massive damage to the earth and environment. For example, temperature increased quickly in recent years because of the over emit of CO<sub>2</sub> from coal electricity, thereby inducing the fluent occurrence of natural disasters. It is an emergent issue to find a way that can provide human beings enough energy without damaging the environment of the earth.

In recent years, nuclear power has been paid more and more attention. However, it is a very hard issue to handle the high-level radioactive waste from nuclear power industry. Deep geological disposal method, which tried to seal nuclide water in deeply underground, had been selected by Japanese government to deal with high level radioactive waste (JNC 1999; NUMO 2022). Figure 11-2 reveals the timeline for Japanese Geological Disposal program from NUMO (2022). The technical feasibility

research was conducted in 1992 and 2000. From approximate. 2005- approximate. 2030 is the R&D programs of supporting organizations. The disposal site would be determined in approximate. 2030. And, the operation of repository would be carried out in approximate. 2040. Therefore, the application study of bentonites for Japanese deep geological disposal project in needed to be finished in recent years. As mentioned above in Chapter 1, a multi-barrier system would be applied in the Japanese deep geological project. And bentonite was selected as the buffer material, which is a very important part in multi-barrier system, for avoiding the leakage of nuclide waste. Thus, it is an urgent issue to comprehensive study the properties of bentonites.

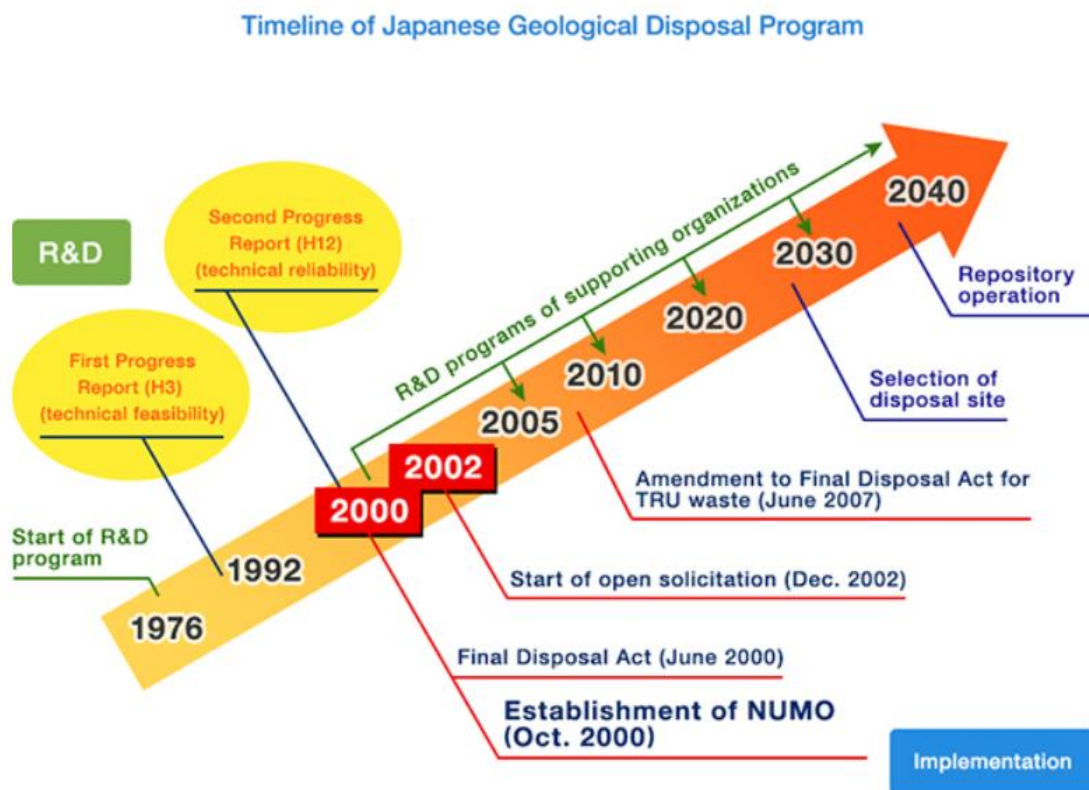


**Figure 11-2 Timeline for Japanese Geological Disposal Program (from NUMO 2022)**

As introduced in Chapter 1, in Japanese deep geological project, the multi-barrier system would be constructed in more than 300 m underground (Fig. 11-3). In such a

deep position, the underground environments are very complicated and unforeseen. The underground environments effects on bentonites properties are needed to be taken into consideration in order to make sure the long-term stability of the multi-barrier system.

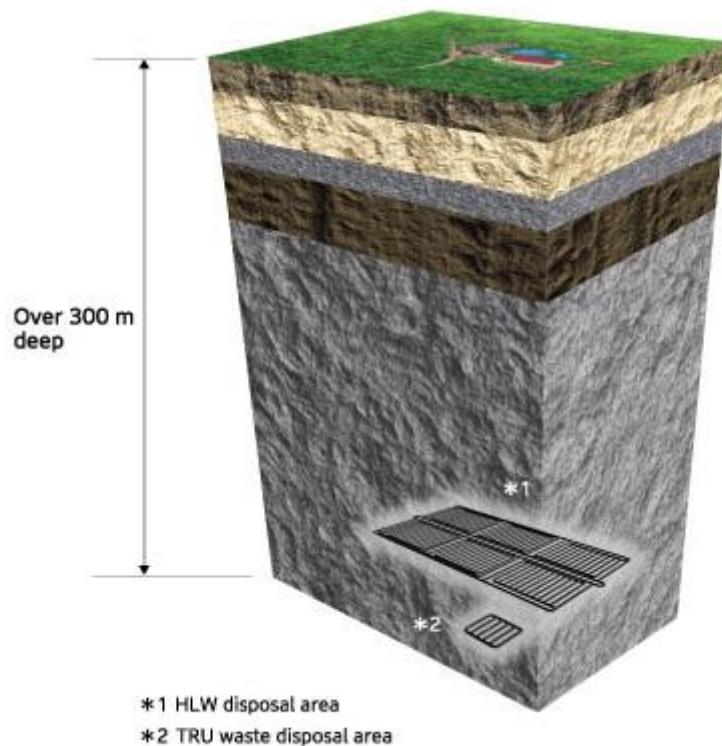


**Figure 11-3 Visual impression of a repository (from NUMO 2022)**

Self-healing capacity of bentonite is a very crucial characteristic of bentonite. As shown in Fig. 11-4, there would be some cracks or pores (Fig. 11-4) existing in the multi-barrier system after the construction of the multi-barrier. These cracks and pores would have a negative effect on the long-term characteristics of the deep geological project. After bentonite meets water, the volume of bentonite would expand and fill possible cracks in multi-barrier system, which is designated a self-healing capacity. In geotechnical engineering, the self-healing capacity was normally evaluated by swelling rate and swelling pressure (Komine and Ogata 1994). In this study, swelling pressure was adopted as the evaluation parameter to assess self-healing capacity of the bentonite.

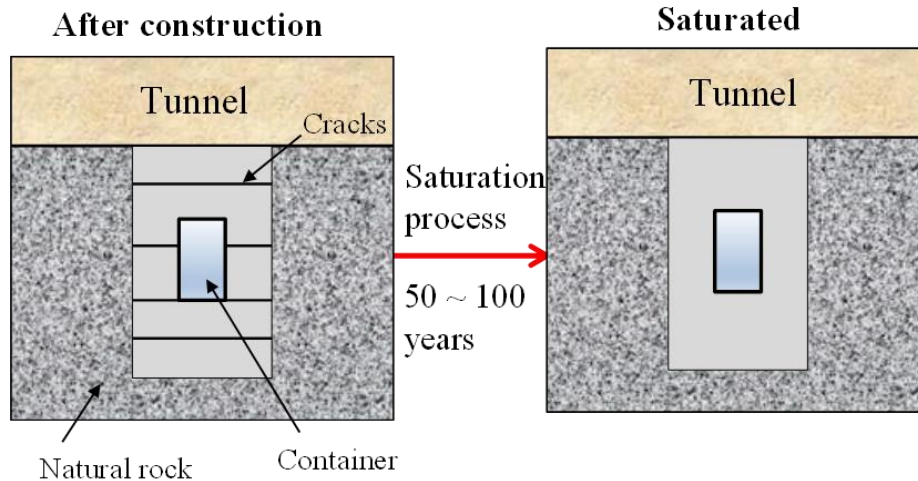


**Figure 11-4 Multi-barrier system after construction and in saturated state**

The hydraulic properties of bentonite are very significant for avoiding the leakage of nuclide waste. Comparing to other soils, the saturated hydraulic conductivities of bentonites are much lower than non-swelling soils (Komine 2008), which can effectively prevent the nuclide water going out. Besides hydraulic conductivity, the water diffusivity was adopted as an important parameter to assess the movement of water in bentonite (Wang et al. 2020). Additionally, as introduced in Chapter 4, the hydraulic conductivity can be obtained combining soil water retention curve and water diffusivity. In this research, the hydraulic properties, including water diffusivity and hydraulic conductivity, were studied carefully.

Usually, scholars all over the world paid most of the attention to the properties of bentonite in saturated state. The reason that they focused on the saturated state properties may be that in traditional soil mechanics or geotechnical engineering, the saturated state is the weakest state. However, the properties for bentonites in unsaturated state are also very important. As reported by massive studies (Komine et al. 2009; Wang et al. 2020) and technical reports (SKB 2011; Posiva 2012), thousands or even millions of years are needed for nuclide waste to decay fully. During that such a long period, hundreds of years saturation process would be included (Fig. 11-4). In this

such a long wetting duration, the underground environments may vary greatly. Therefore, the swelling pressure and hydraulic properties changes of bentonite in this special process should be taken into consideration.

## **11. 2 The choice of dry density**

A sufficiently large swelling pressure and a sufficiently small hydraulic conductivity of bentonite need to be provided not only in the saturated state but also in the unsaturated state. As reported by massive scholars, the dry density of bentonite affects the equilibrium swelling pressure (e.g., Komine and Ogata 1994; Komine and Ogata 1996) and saturated hydraulic conductivity greatly (e.g., Komine 2008). The results from those testing observations indicated that, equilibrium swelling pressure increased with the rise of dry density and saturated hydraulic conductivity decreased as the growth of dry density as mentioned in Chapter 1. However, there is still a lack of swelling pressure and hydraulic conductivity for bentonite during saturation. In this study, new swelling apparatus and new multi-ring as introduced in Chapter 3 were used to obtain swelling pressure and hydraulic conductivity of bentonites during saturation. New method for calculating the hydraulic conductivity of the bentonite during saturation was followed as Chapter 4. The effect of dry density on swelling pressure during saturation of MX80 bentonite is shown in Fig. 11-5 from Chapter 5 and the dry density effect of hydraulic conductivity during saturation of KB bentonite is revealed in Fig. 11-6 from Chapter 5. As can be found from Fig. 11-5 and concluded in Chapter 5, the swelling pressure during saturation increase with the increasing dry density. Meanwhile, an easily conclusion can be made from Chapter 6 that, hydraulic conductivity during saturation decreases as the dry density rises. Larger swelling pressure and lower hydraulic

conductivity give better resistance to nuclide waste seepage. Thus, a larger dry density of bentonite was recommended for the buffer material in deep geological disposal.

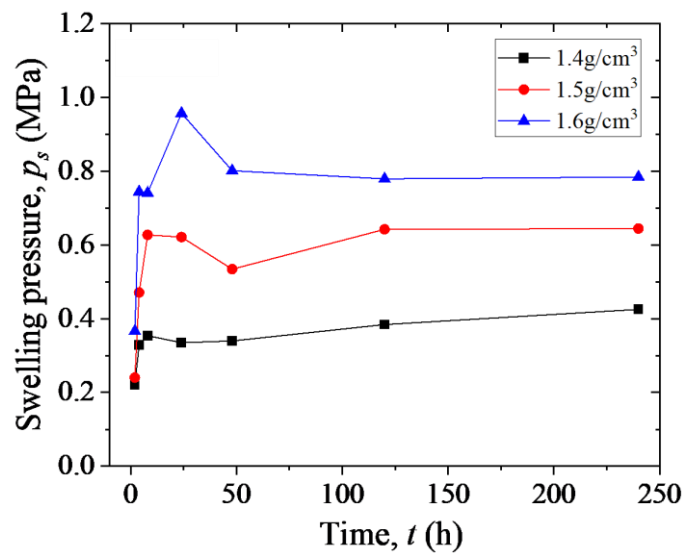


**Figure 11-5 Swelling pressure changing with wetting duration for MX80 bentonite at different dry densities**

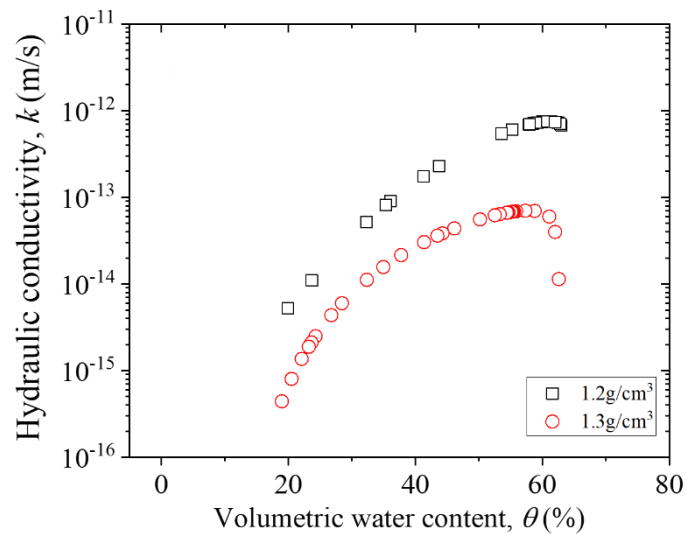


**Figure 11-6 Hydraulic conductivity changing with volumetric water content for KB bentonite at different dry densities**

### 11. 3 The choice of bentonite cation type

Different locations were chosen by different countries to cite deep geological disposal project. The ions compositions of the liquid intrude into the buffer material were

different due to the project location. Japanese deep geological had been decided to cite in coastal area (JNC 1999; Komine 2009; NUMO 2022, Fig. 11-7) because of the feasibility of transportation. As well known, Japan is an island country. The transportation by ship is much easier and economic than by trains and roads. Now, in Japan, two countries in Hokkaido are discussing by the government to site the deep geological program (Fig. 11-7, NUMO 2022). These two countries are both beside the sea. However, siting the deep geological project in coastal area has some disadvantages. During the decay of nuclide waste, the seawater may intrude into the deep geological project, especially the multi-barrier system, including buffer material and waster container. It is necessary to study the effect of seawater on the hydraulic properties and swelling pressure of bentonites for ensuring the long-term reliability of multi-barrier system.



**Figure 11-7 The location in discussion for Japanese Deep Geological project  
(modified from NUMO 2022)**

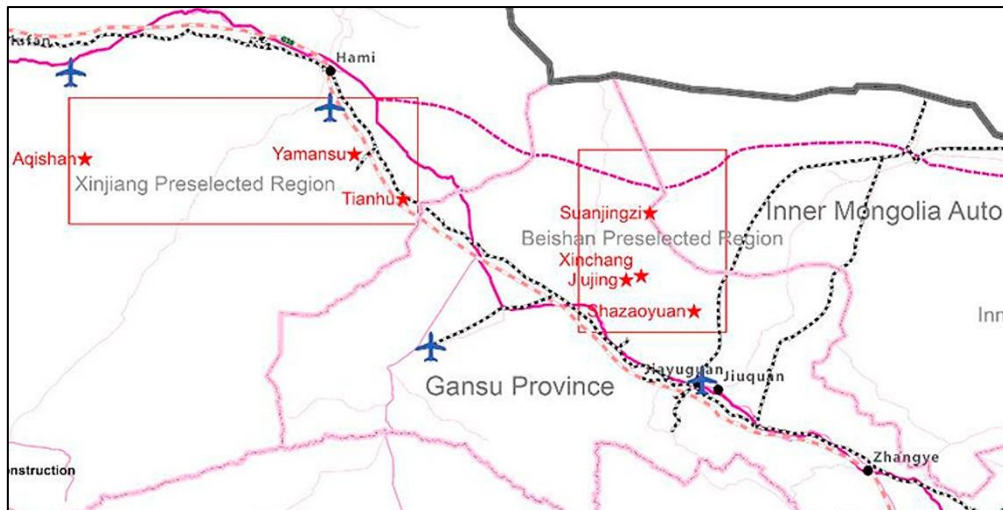


**Figure 11-8 The location in discussion for Chinese Deep Geological project (Wang et al. 2018)**

After comprehensive geological, hydrogeological and geophysical investigations based on surface mapping and drilling of deep boreholes have been conducted in parallel at several candidate sites, providing a sound basis for comparison. Two sites (Xinchang and Shazaoyuan areas) in Beishan region in Gansu Province (Wang et al. 2018) were recommended to the deep geological project in China. Considering that the Xinchang area has better rock quality, the Chinese deep geological disposal project is determined to be constructed in Xinchang (Wang et al. 2018). Among the long-term operation period of deep geological disposal project, the ground water in Beishan area would intrude into the buffer material. Thus, it is very important to investigate the Beishan area ground water effect on hydraulic properties and swelling pressure of bentonite to ensure the safety of deep geological disposal project.

**Table 11-1 Ions and concentration of seawater in Japanese coastal area (Komine et al. 2009)**

Ion concentration	Na <sup>+</sup>	Ca <sup>2+</sup>	K <sup>+</sup>	Mg <sup>2+</sup>
mol/m <sup>3</sup>	454.4	6.2	9.0	50.0

**Table 11-2 Ions and concentration of groundwater in Beishan area (Sun et al. 2019)**

Ion concentration	Na <sup>+</sup>	Ca <sup>2+</sup>	K <sup>+</sup>	Mg <sup>2+</sup>
mol/m <sup>3</sup>	62.96	8.09	3.14	10

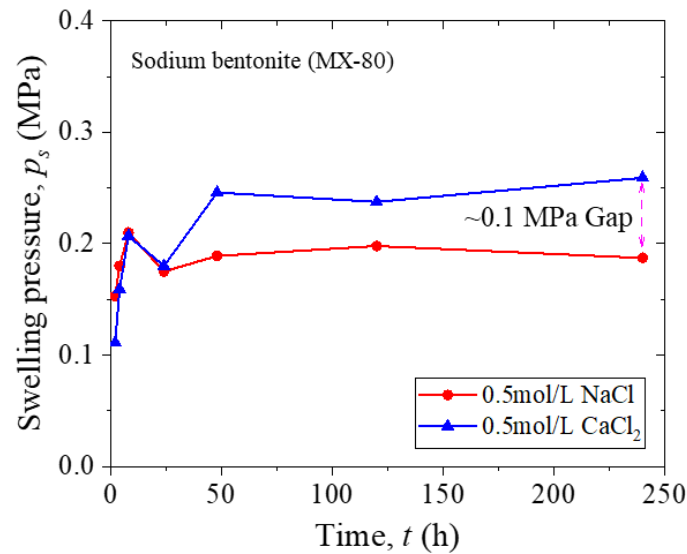


**Figure 11-9 Swelling pressure during saturation of sodium type bentonite saturated by Ca<sup>2+</sup> and Na<sup>+</sup> ions**

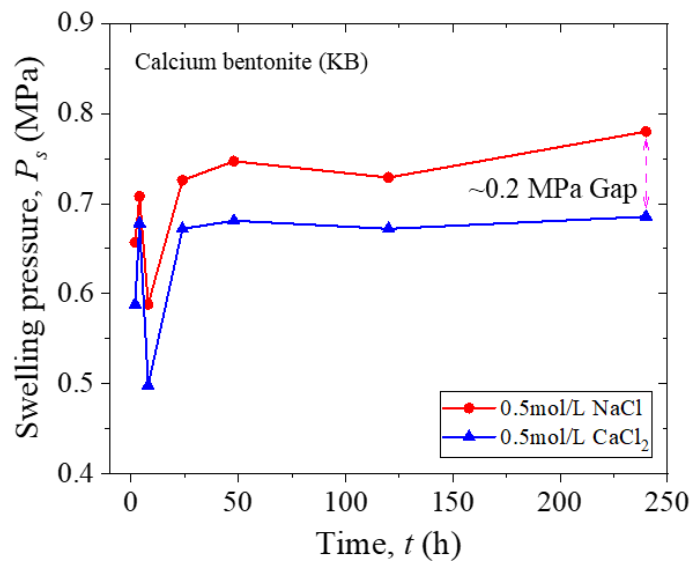


**Figure 11-10 Swelling pressure during saturation of calcium type bentonite saturated by Ca<sup>2+</sup> and Na<sup>+</sup> ions**

Table 11-1 shows the ions compositions and concentrations of seawater in Japanese coastal area. Table 11-2 indicates the ions compositions and concentration of groundwater in Beishan area. As we can see from Table 11-1 and Table 11-2, the ions difference between two countries conditions is very big. The ions composition has great effect on the properties of bentonites. It is necessary to investigate the ions compositions of groundwater and select the suitable bentonite for the deep geological disposal projects in different countries.

In Chapter 8,  $\text{Ca}^{2+}$  and  $\text{Na}^+$  were used as the saturation liquid solutes to observe the swelling pressure of bentonites. As presented in Fig. 11-9, for sodium type bentonite,  $\text{Ca}^{2+}$  saturated specimens have larger swelling pressures during saturation than  $\text{Na}^+$  saturated ones. Additionally, in Fig. 11-10, in case of calcium type bentonite,  $\text{Na}^+$  obtained larger swelling pressure during saturation than  $\text{Ca}^{2+}$ . Through the investigation of groundwater quality, it is determined which cation dominates the composition of groundwater, further suitable bentonite can be selected as buffer material.

#### **11. 4 The choice of bentonite grain size**

Additionally, during the decay period of nuclide waste, a great amount of heat is expected emitting (Fig. 11-11). Thus, the temperature in the buffer material is much higher than that of room. Figure 11-12 presents the temperature inside and outside the buffer material among the operation of deep geological disposal project. As Fig. 11-12 indicates, the temperature would increase to approximate. 100 °C with the proceeding time in the beginning 100 years. After that, the temperature will decline to approximate. 60 °C. It can be easily found that in Fig. 11-12, temperature changes greatly during the

operation of deep geological project. The effect of temperature on the properties of bentonite is needed to be studied.

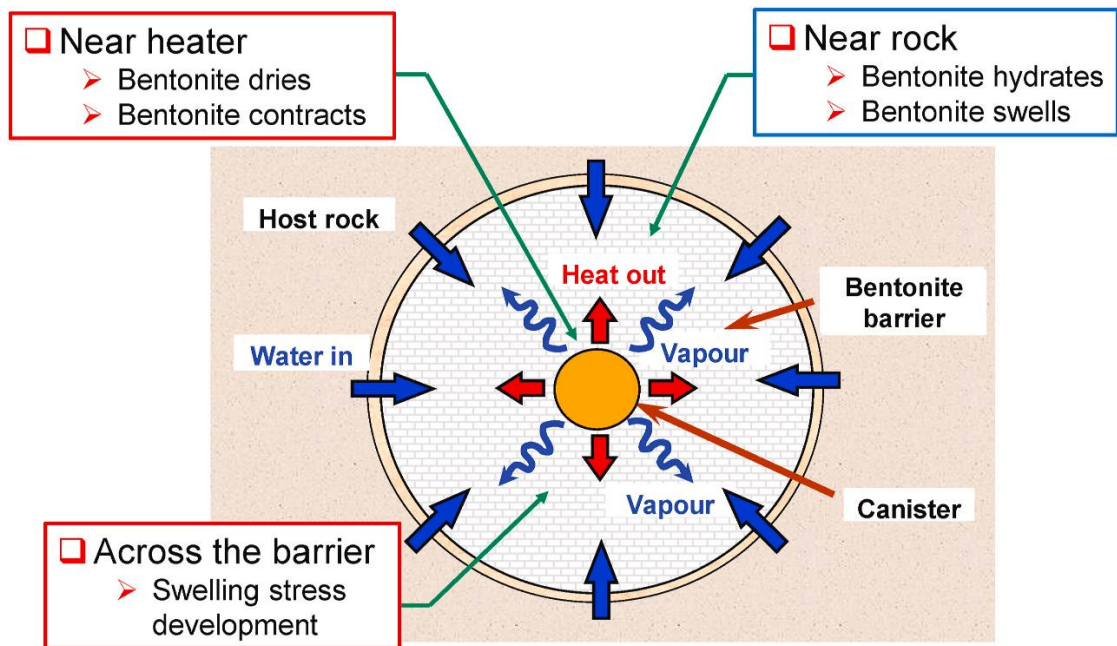


Figure 11-11 The emission of heat in deep geological disposal project (Gens et al.

2021)

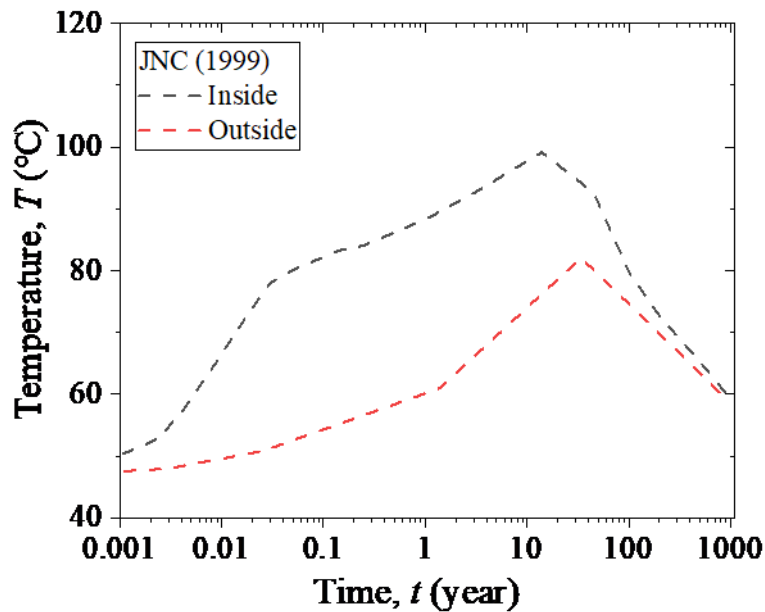
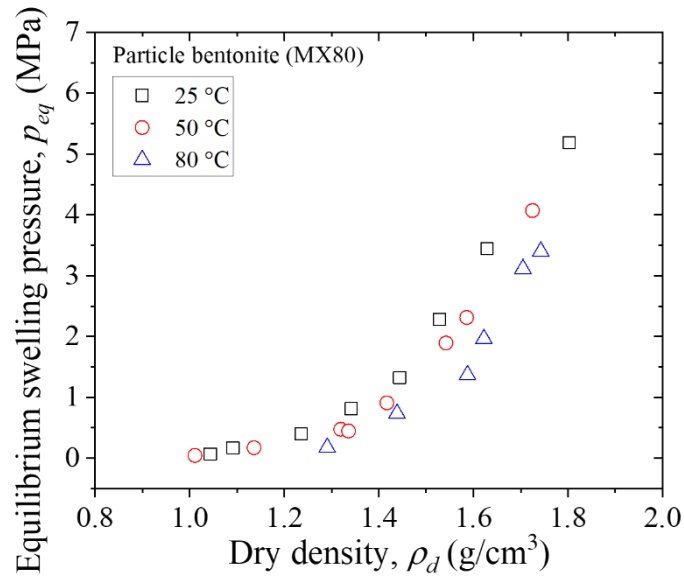


Figure 11-12 Temperature in and outside buffer material during HLW decay

(JNC 1999)

In this thesis, the effect of temperature on swelling pressures during saturation was carefully researched in Chapter 9. As introduced in Chapter 9, particle and powder bentonites have inconsistent effect on equilibrium swelling pressure. For particle



**Figure 11-13 Equilibrium swelling pressure of particle bentonite (MX80) at different temperatures**

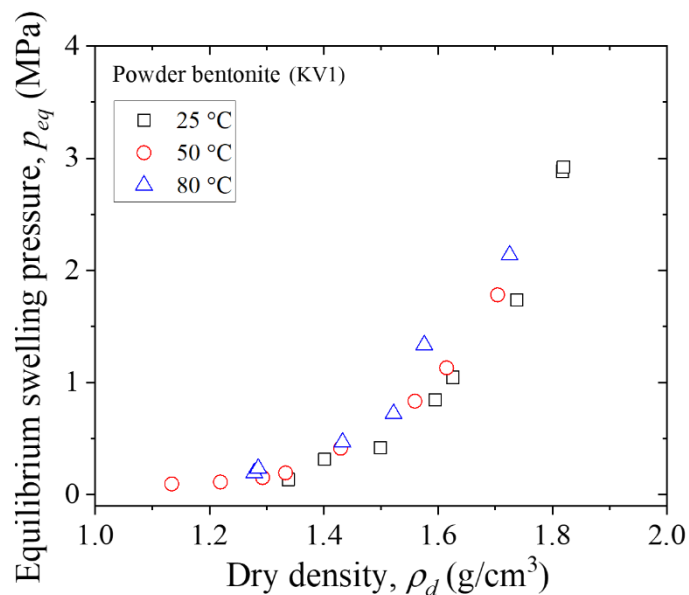


**Figure 11-14 Equilibrium swelling pressure of powder bentonite (KV1) at different temperatures**

bentonite, equilibrium swelling pressure decreases with the rise of temperature as indicated in Fig. 11-13. In case of powder bentonite, as shown in Fig. 11-14, equilibrium swelling pressure increases as the temperature increases. This discovery gives designers a reference for what grain size bentonite to choose for deep geological disposal project by the conditions in different countries.

### 11.5 The choice of Initial water content and specimen preparation method

As introduced before, larger dry density compacted bentonite was recommended to the deep geological disposal project for providing big enough swelling pressure and low enough hydraulic conductivity. If bentonite can be compressed in optimize water content, the maximum dry density can be achieved. Thus, it is necessary to study whether the initial water content has significantly influence on swelling pressure. The results from Chapter 10 for the initial water content effect on equilibrium swelling

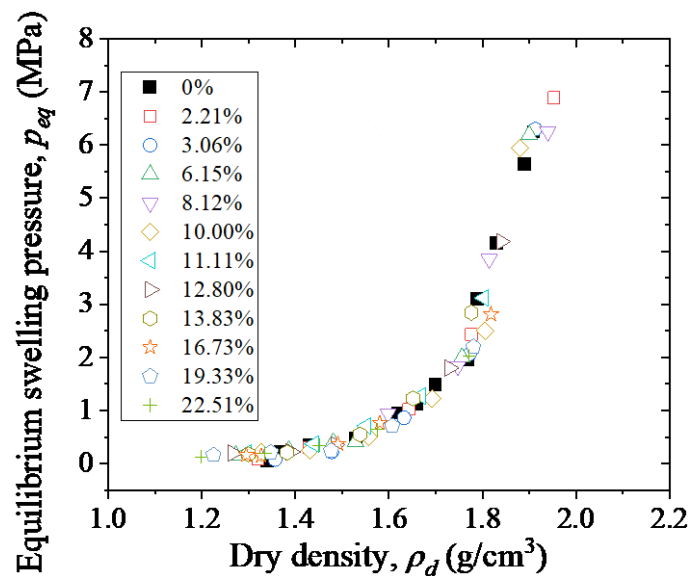
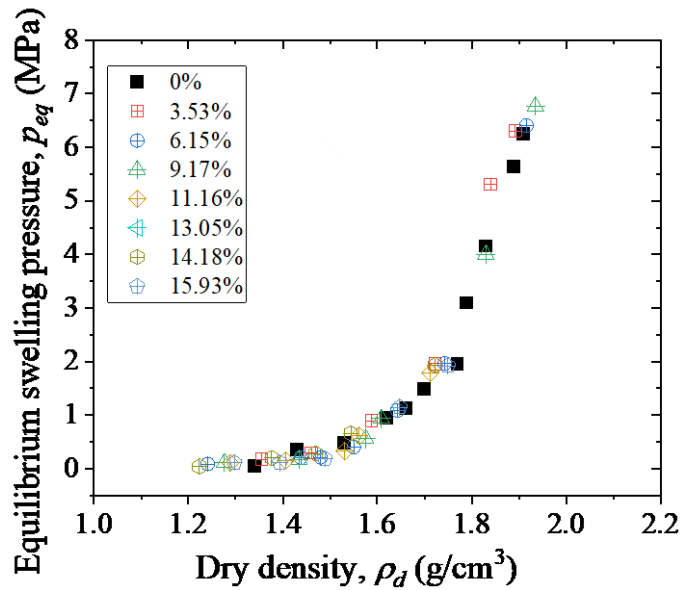


Figure 11-15 Equilibrium swelling pressure from different initial water content

KV1 specimen by water spray method



**Figure 11-16 Equilibrium swelling pressure from different initial water content**

#### **KV1 specimen by humidity control method**

pressure for KV1 bentonite is revealed in Fig. 11-15 and Fig. 11-16. It can be easily concluded from Fig. 11-15 and Fig. 11-16 that, initial water content has very limit effect on equilibrium swelling pressure. Thus, it is recommended that bentonite sample can be compressed in optimize water content for obtaining maximum dry density.

Additionally, a convenient method needs to be found to obtain samples of target water content. In geotechnical engineering, two methods, including water spray and humidity control method (as introduce in Chapter 10), were normally adopted to achieve soils with different water content. The results from Chapter 10, which is also presented in Fig. 11-15 and Fig. 11-16, indicated that the specimen preparation method does not have apparent effect on equilibrium swelling pressure. The water spray method is more convenient and more timesaving than humidity control method. Therefore, the water spray method is recommended during the construction on site.

## 11. 6 Future plan

In this study, the hydraulic conductivity was just researched for different dry densities bentonites. The reasons that other effects were ignored is the fact that the soil water retention curve for compacted bentonite saturated by salt solutions and soil water retention curve for compacted bentonite at different temperatures were lacked. It is pretty hard to obtain precise soil water retention curves of bentonite saturated by salt solutions because it is hard to achieve a uniformly distribution of salts in bentonite during saturation. For achieving suction of bentonites at different temperature, the existing technology still has certain shortcomings. For example, by using Whatman 42 filter paper method to measure the suction of bentonite at different temperatures, it is impossible to make sure the loss of water content of filter paper is controllable during the process between the filter paper is taken out at different temperatures and the weight of filter paper mass. More efforts should be made to progressing the technology for measuring the suction of bentonite saturated by salt solutions and at different temperatures.

In this thesis, only  $\text{Na}^+$  and  $\text{Ca}^{2+}$  ions were used as saturation solutes. However, the compositions of the liquid intrude into the buffer material is very complicated as introduce above. Thus, it is not enough to just take the  $\text{Na}^+$  and  $\text{Ca}^{2+}$  ions into consideration. In the future, more saturation liquid ions, for example  $\text{K}^+$  and  $\text{Mg}^{2+}$  would like to be focused.

## Reference

Gens, A., Alcoverro, J., Blaheta, R., Hasal, M., Michalec, Z., Takayama, Y., Lee, C., Lee, J., Kim, G., Kuo, W., and Lin, C., 2021. HM and THM interactions in bentonite engineered barriers for nuclear waste disposal. *International Journal of Rock Mechanics and Mining Science*, 137: 104572.

IEA 2022. Electricity Market Report-January 2022, International Energy Agency. <https://www.iea.org/reports/electricity-market-report-january-2022> (Accessed 7 Feb. 2022).

JNC 1999. Technical reliability of the geological disposal for high-level radioactive waste in Japan - geological disposal research and development Second compiled – General report. Japan Nuclear Cycle Development Institute, JNC TN1400 99-020. (in Japanese) <https://www.jaea.go.jp/04/tisou/houkokusyo/dai2jitoimatome.html> (Accessed 8 Feb. 2022)

Komine, H., and Ogata, N. 1994. Experimental study of swelling characteristics of compacted bentonite. *Canadian Geotechnical Journal*, **31**(4): 478–490.

Komine, H., and Ogata, N. 1996. Prediction for swelling characteristics of compacted bentonite. *Canadian Geotechnical Journal*, **33**(1): 11–22.

Komine, H., 2008. Theoretical equations on hydraulic conductivities of bentonite-based buffer and backfill for underground disposal of radioactive wastes. *Journal of Geotechnical and Geoenvironmental Engineering*, **134**(4): 497–508.

Komine, H., Yasuhara, K., and Murakami, S. 2009. Swelling characteristics of bentonites in artificial seawater. *Canadian Geotechnical Journal*, **46**(2): 177-189.

NUMO 2022. The Nuclear Waste Management Organization of Japan. <https://www.numo.or.jp/en/jigyuu/geological.html> (Accessed 8 Feb. 2022).

Posiva 2012. Safety Case for the Disposal of Spent Nuclear Fuel at Olkiluoto- Synthesi

s2012. Posiva Oy, December 2012.

SKB 2011. Long-term safety for the final repository for spent nuclear fuel at Forsmark

-Main report of the SR-Site project, Volume 1, TR-11-01.

Wang, H.L., Shirakawabe, T., Komine, H., Ito, D., Gotoh, T., Ichikawa, Y., and Chen,

Q. 2020. Movement of water in compacted bentonite and its relationship with swelling pressure. *Canadian Geotechnical Journal*, **57**: 921–932.

## **References**

References were attached in each chapter.

## Acknowledgement

The results of this study were obtained during the 3 years doctoral course in Komine lab, Waseda University.

I would like to take this opportunity to express my deepest gratitude to my distinguished and respectable supervisor, Prof. Komine Hideo, who has given me invaluable guidance and constant support and encouragement through the whole process of the doctoral course. My motivations to explore the mechanisms behind the experiments come from the encouragement from Prof. Komine, who allows me to conduct research from my own curiosity and enthusiasm. Prof. Komine also taught me the importance of independent thinking as a researcher, which makes me constantly reflect on myself in the research.

I wish to extend my sincere gratitude to Prof. Akagi Hirokazu, Prof. Yamazaki Atsushi, Prof. Akiyama Mitsuyoshi and Prof. Wang Hailong for their valuable comments and suggestions along with this study.

I also own my appreciation to Prof. Wang Hailong who has given me a lot of inspirations, insightful advice and instructions. What I learned from the discussions with Prof. Wang is not only the scientific method, but also the strict requirement to be a researcher, which would become a ladder for me to improve in the future.

I would also like to thank Dr. Ito Daichi for his continuous help and support during these years study in Waseda University. I want to thank the graduated and current students in Komine Lab, Waseda University. When I first came to Japan, it was their enthusiasm and help that made me quickly integrate in the life in Japan. The gratitude also extends to Mr. Sun Danxi and Mr. Cai Guodong for their accompaniment in the normal life.

My thanks also go to Mr. Gotoh Takahiro and Mr. Miyoshi Kentaro for their help and guidance for the X-ray diffraction tests in Materials Characterization Central Laboratory, Waseda University. I also want to express my gratitude to Mr. Takahashi Ryota for his guidance for the ICP-OES tests in Environmental Safety Center, Waseda University.

Finally, I feel indebted to my parents, my family members for their continuous understandings and incredible love in my life.

RUAN Kunlin

December 2022 in 58-203, Waseda University

## Figure list

Figure 1-1 Global change in electricity demand (IEA 2022).....	2
Figure 1-2 Global change in electricity generation (IEA 2022) .....	3
Figure 1-3 Regional evaluation of CO2 intensity (IEA 2022).....	3
Figure 1-4 Disposal methods for high level radioactive waste (WNA 2022).....	4
Figure 1-5 Deep geological disposal method in Japan (modified from NUMO 2022) .	6
Figure 1-6 Host rock, buffer material and over packer.....	6
Figure 1-7 Mineral structure of montmorillonite (Mitchell and Soga 2005).....	8
Figure 1-8 Microstructure of montmorillonite (Ruan et al. 2022).....	9
Figure 1-9 Instantaneous profile method by cutting evenly height slices (Modified from Cho 2022).....	10
Figure 1-10 Water diffusivity changing with degree of saturation by using different equations .....	11
Figure 1-11 Water diffusivity by reading the reduction of the water in tube.....	12
Figure 1-12 Effect of dry density on water diffusivity by instantaneous profile method .....	13
Figure 1-13 Effect of dry density on water diffusivity by reading water reduction in water tube.....	13
Figure 1-14 Effect of temperature on water diffusivity by instantaneous profile method .....	14
Figure 1-15 Saturated hydraulic conductivity changing with the dry density of some bentonites .....	15
Figure 1-16 Hydraulic conductivity test device for bentonite by adding air pressure (from Ito 2022).....	16
Figure 1-17 Hydraulic conductivity for bentonite by compression apparatus (from Butsuda 2006) .....	16
Figure 1-18 An apparatus for measuring hydraulic conductivity of unsaturated bentonite (from Cui et al. 2008).....	18
Figure 1-19 Hydraulic conductivity changing with suction for MX-80 bentonite .....	18
Figure 1-20 Traditional swelling pressure evolution curve and definition of swelling pressures.....	19
Figure 1-21 Peak, valley and re-peak swelling pressures changing with dry density from 5mm thickness specimen (Wang et al. 2022).....	20
Figure 1-22 Equilibrium swelling pressure of some bentonites changing with dry density from literatures .....	21

Figure 1-23 XRD profile of Kunigel-V1 bentonite used in this study .....	23
Figure 1-24 Schematic showing state of water molecule arrangement between montmorillonite layers ( <i>L</i> ) .....	24
Figure 1-25 Basal spacing of saturated specimen changing with dry density for MX-80 bentonite from literatures .....	25
Figure 1-26 Relation between water content, basal spacing and interlayer water molecule state.....	25
1-27 Research flow .....	27
Figure 2-1 Outlooking of bentonites.....	40
Figure 2-2 Sieve and hydrometer for grainsize distribution test.....	41
Figure 2-3 Grain size distributions of bentonites.....	42
Figure 2-4 Soil particle density testing details.....	42
Figure 2-5 Liquid and plastic limits testing details.....	44
Figure 2-6 Montmorillonite content testing details .....	46
Figure 2-7 CEC testing details .....	46
Figure 3-1 Equilibrium swelling pressures from literatures: a) KV1 and b) FBBEX .52	
Figure 3-2 New swelling pressures apparatus .....	53
Figure 3-3 Schematic diagram of specimen after swelling pressure test.....	55
Figure 3-4 Schematic diagram of swelling apparatus.....	56
Figure 3-5 Water flow histories conducted on new apparatus and traditional apparatus .....	56
Fig. 3-7 Swelling pressure evolution curve of KV1 bentonite by different traditional apparatus .....	58
Figure 3-8 Some swelling pressure evolution curves of bentonites by the new apparatus .....	59
Figure 3-9 Schematic of Multi-ring .....	60
Figure 3-10 Schematic of Mold ring and Two-piece ring.....	60
Figure 3-11 Schematic of making compacted specimen.....	61
Figure 3-13 Schematic for making slices from multi-ring.....	62
Figure 3-14 Schematic for XRD test .....	62
Figure 3-15 XRD apparatus .....	63
Figure 4-1 Swelling pressure evolution curves of bentonites .....	68
Figure 4-2 Swelling pressures of bentonites at different wetting durations .....	69
Figure 4-3 Gravimetric water content of slice changing with distance from bottom of bentonites .....	70
Figure 4-4 Relation between $\theta$ and $\chi$ of bentonites.....	72
Figure 4-5 Water diffusivity changing with volumetric water content of bentonites ..	73

Figure 4-6 Water diffusivity changing with degree of saturation for bentonites .....	74
Figure 4-7 Water diffusivity changing with degree of saturation for KV1 from literatures and this study .....	74
Figure 4-8 Schematic for showing the SWRC test .....	75
Figure 4-9 Total suction changing with volumetric water content and their fitting by VG equation.....	76
Figure 4-10 Hydraulic conductivity changing with volumetric water content .....	77
Figure 4-11 XRD profiles of slices in vertical direction for MX80.....	79
Figure 4-12 XRD profiles of slices in vertical direction for KV1 .....	80
Figure 4-13 XRD profiles of slices in vertical direction for KB .....	81
Figure 4-14 XRD profiles and <i>L</i> state of slices changing with wetting duration for MX80 .....	82
Figure 4-15 XRD profiles and <i>L</i> state of slices changing with wetting duration for KV1 .....	83
Figure 4-16 XRD profiles and <i>L</i> state of slices changing with wetting duration for KB .....	84
Figure 4-17 Basal spacings of bentonites changing with saturation time.....	86
Figure 4-18 Basal spacing changing with volumetric water content.....	87
Figure 4-19 Basal spacing changing with degree of saturation .....	88
Figure 4-20 Water flow path in Kaolinite and Illite.....	90
Figure 4-21 Water flow path in montmorillonite .....	91
Figure 4-22 Fabric units of bentonite and their evolution during saturation .....	91
Figure 5-1 Swelling pressure evolution curves of MX80 at different dry densities ....	98
Figure 5-2 Swelling pressure evolution curves of KV1 at different dry densities.....	99
Figure 5-3 Swelling pressure evolution curves of KB at different dry densities.....	100
Figure 5-4 Swelling pressures at different wetting durations of different dry densities bentonites .....	101
Figure 5-5 Equilibrium swelling pressure from literatures and this study.....	103
Figure 5-6 Swelling pressure apparatus with multi-ring.....	103
Figure 5-7 Gravimetric water content of slices for MX80 at different dry densities. ....	104
Figure 5-8 Gravimetric water content of slices for KV1 at different dry densities ...	105
Figure 5-9 Gravimetric water content of slices for KB at different dry densities .....	106
Figure 5-10 Relation between $\theta$ and $\chi$ of MX80 at different dry densities.....	107
Figure 5-11 Relation between $\theta$ and $\chi$ of KV1 at different dry densities.....	108
Figure 5-12 Relation between $\theta$ and $\chi$ of KB at different dry densities.....	109
Figure 5-13 Water diffusivity changing with degree of saturation for bentonites at different dry densities.....	110

Figure 5-14 Water diffusivity changing with volumetric water content of KV1 bentonite from Takeuchi et al. (1995) and this study.....	111
Figure 5-15 Volumetric water content changing with total suction for different dry densities bentonites .....	112
Figure 5-16 Hydraulic conductivities changing with volumetric water content for bentonites at different dry densities .....	113
Figure 5-17 XRD profiles of different dry densities MX80 at 4h .....	114
Figure 5-18 XRD profiles of different dry densities MX80 at 24h .....	115
Figure 5-19 XRD profiles of different dry densities MX80 at 240h .....	116
Figure 5-20 XRD profiles of different dry densities KV1 at 4h .....	117
Figure 5-21 XRD profiles of different dry densities KV1 at 24h .....	118
Figure 5-22 XRD profiles of different dry densities KV1 at 24h .....	119
Figure 5-23 XRD profiles of different dry densities KB at 4h .....	120
Figure 5-24 XRD profiles of different dry densities KB at 24h .....	121
Figure 5-25 XRD profiles of different dry densities KB at 240h .....	122
Figure 5-26 Basal spacing changing with time of MX80 bentonite at different dry densities.....	123
Figure 5-27 Basal spacing changing with time of KV1 bentonite at different dry densities.....	124
Figure 5-28 Basal spacing changing with time of KB bentonite at different dry densities .....	125
Figure 5-29 Final basal spacing changing with dry density of bentonites.....	126
Figure 5-30 Final basal spacing of MX80 from literatures and this study .....	127
Figure 5-31 Final basal spacing of KV1 from literatures and this study .....	127
Figure 5-32 Basal spacing changing with swelling pressure of different dry densities MX80 .....	128
Figure 5-33 Basal spacing changing with swelling pressure of different dry densities KV1.....	129
Figure 5-34 Basal spacing changing with swelling pressure of different dry densities KB.....	130
Figure 5-35 Schematic showing montmorillonite fabric units evolution during saturation.....	131
Figure 5-36 Final Basal spacing changing with equilibrium swelling pressure of bentonites .....	132
Figure 5-37 Final basal spacing changing with equilibrium swelling pressure form Villar et al. (2012).....	132
Figure 5-38 Micropore and Macropore for bentonite at different dry densities .....	133

Figure 6-1 Traditional swelling pressure apparatus .....	138
Figure 6-2 Multi-ring mold applied in traditional swelling pressure apparatus .....	139
Figure 6-3 Swelling pressure evolution curves for KV1 bentonite saturated by different concentrations NaCl solutions .....	140
Figure 6-4 Swelling pressure changing with wetting duration saturated by different concentration NaCl solutions .....	141
Figure 6-5 Equilibrium swelling pressure changing with concentration of NaCl solution .....	142
Figure 6-6 Gravimetric water content changing with position saturated by NaCl solutions with different concentration.....	144
Figure 6-7 Relation between $\theta$ and $\chi$ of specimen saturated by NaCl solutions.....	145
Figure 6-8 Water diffusivity changing with NaCl solution concentration.....	146
Figure 6-9 Some XRD profiles for KV1 saturated by NaCl solutions .....	148
Figure 6-10 Average basal spacing for KV1 saturated by NaCl solutions.....	149
Figure 6-11 Final basal spacing changing with NaCl concentration .....	150
Figure 6-12 Osmotic suction changing with time for specimen saturated by NaCl solutions .....	152
Figure 6-13 Final osmotic suction changing with concentration.....	152
Figure 6-14 Osmotic suction changing with swelling pressure during saturation.....	154
Figure 6-15 Swelling pressure and osmotic pressure evolution during saturation ....	154
Figure 6-16 Final osmotic suction changing with equilibrium swelling pressure.....	155
Figure 7-1 Scheme showing wetting device .....	160
Figure 7-2 Scheme showing making slices and XRD test.....	161
Figure 7-3 Gravimetric water contents of KV1 slices .....	162
Figure 7-4 Gravimetric water contents of KV1 slices .....	163
Figure 7-5 Degree of saturation for KV1 specimen saturated by different NaCl solutions at different wetting durations .....	165
Figure 7-6 Degree of saturation for MX80 specimen saturated by different NaCl solutions at different wetting durations.....	166
Figure 7-7 Degree of saturation for different concentrations saturated bentonites....	167
Figure 7-8 Relations between $\chi$ and $\theta$ for KV1 saturated by NaCl solutions .....	168
Figure 7-9 Relations between $\chi$ and $\theta$ for MX80 saturated by NaCl solutions .....	169
Figure 7-10 Water diffusivity changing with volumetric water content for bentonites saturated by NaCl solutions .....	170
Figure 7-11 Na <sup>+</sup> concentrations of slices for KV1 .....	171
Figure 7-12 Na <sup>+</sup> concentrations of slices for MX80.....	172
Figure 7-13 Percent of salt intrusion for KV1 .....	173

Figure 7-14 Percent of salt intrusion for MX80.....	174
Figure 7-15 Percent of salt intrusion for KV1 and MX80 .....	176
Figure 7-16 Basal spacing changing with wetting duration for bentonites .....	177
Figure 7-17 Final basal spacing changing with saturation liquid concentration .....	178
Figure 7-18 Basal spacing, degree of saturation and percent of salt intrusion for KV1 .....	180
Figure 7-19 Basal spacing, degree of saturation and percent of salt intrusion for MX80 .....	181
Figure 7-20 Mechanisms for movements of water and salts in bentonite .....	182
Figure 8-1 Swelling pressure evolution curves of MX80 bentonite saturated by distilled water, 0.5mol/l NaCl and 0.5mol/l CaCl <sub>2</sub> . .....	188
Figure 8-2 Swelling pressure evolution curves of KV1 bentonite saturated by distilled water, 0.5mol/l NaCl and 0.5mol/l CaCl <sub>2</sub> . .....	189
Figure 8-3 Swelling pressure evolution curves of KB bentonite saturated by distilled water, 0.5mol/l NaCl and 0.5mol/l CaCl <sub>2</sub> . .....	190
Figure 8-4 Swelling pressures at different wetting durations of bentonites saturated by distilled water, 0.5mol/l NaCl and 0.5mol/l CaCl <sub>2</sub> . .....	191
Figure 8-5 Equilibrium swelling pressures of bentonites saturated by distilled water, 0.5mol/l NaCl and 0.5mol/l CaCl <sub>2</sub> . .....	192
Figure 8-6 Gravimetric water contents of MX80 saturated by distilled water, 0.5mol/l NaCl and 0.5mol/l CaCl <sub>2</sub> . .....	194
Figure 8-7 Gravimetric water contents of KV1 saturated by distilled water, 0.5mol/l NaCl and 0.5mol/l CaCl <sub>2</sub> . .....	195
Figure 8-8 Gravimetric water contents of KB saturated by distilled water, 0.5mol/l NaCl and 0.5mol/l CaCl <sub>2</sub> . .....	196
Figure 8-9 Relation between $\theta$ and $\chi$ for MX80 saturated by distilled water, 0.5mol/l NaCl and 0.5mol/l CaCl <sub>2</sub> .....	197
Figure 8-10 Relation between $\theta$ and $\chi$ for KV1 saturated by distilled water, 0.5mol/l NaCl and 0.5mol/l CaCl <sub>2</sub> . .....	198
Figure 8-11 Relation between $\theta$ and $\chi$ for KB saturated by distilled water, 0.5mol/l NaCl and 0.5mol/l CaCl <sub>2</sub> . .....	199
Figure 8-12 Water diffusivity for bentonites saturated by distilled water, 0.5mol/l NaCl and 0.5mol/l CaCl <sub>2</sub> . .....	200
Figure 8-13 XRD profiles for MX80 saturated by distilled water, 0.5mol/l NaCl and 0.5mol/l CaCl <sub>2</sub> at 8h .....	202
Figure 8-14 XRD profiles for MX80 saturated by distilled water, 0.5mol/l NaCl and 0.5mol/l CaCl <sub>2</sub> at 48h .....	203

Figure 8-15 XRD profiles for MX80 saturated by distilled water, 0.5mol/l NaCl and 0.5mol/l CaCl <sub>2</sub> at 240h .....	204
Figure 8-16 XRD profiles for KV1 saturated by distilled water, 0.5mol/l NaCl and 0.5mol/l CaCl <sub>2</sub> at 8h .....	205
Figure 8-17 XRD profiles for KV1 saturated by distilled water, 0.5mol/l NaCl and 0.5mol/l CaCl <sub>2</sub> at 48h .....	206
Figure 8-18 XRD profiles for KV1 saturated by distilled water, 0.5mol/l NaCl and 0.5mol/l CaCl <sub>2</sub> at 240h .....	207
Figure 8-19 XRD profiles for KB saturated by distilled water, 0.5mol/l NaCl and 0.5mol/l CaCl <sub>2</sub> at 8h .....	208
Figure 8-20 XRD profiles for KB saturated by distilled water, 0.5mol/l NaCl and 0.5mol/l CaCl <sub>2</sub> at 48h .....	209
Figure 8-21 XRD profiles for KB saturated by distilled water, 0.5mol/l NaCl and 0.5mol/l CaCl <sub>2</sub> at 240h .....	210
Figure 8-22 Basal spacing of MX80 saturated by distilled water, 0.5mol/l NaCl and 0.5mol/l CaCl <sub>2</sub> .....	211
Figure 8-23 Basal spacing of MX80 saturated by distilled water, 0.5mol/l NaCl and 0.5mol/l CaCl <sub>2</sub> .....	212
Figure 8-24 Basal spacing of KB saturated by distilled water, 0.5mol/l NaCl and 0.5mol/l CaCl <sub>2</sub> .....	213
Figure 8-25 Basal spacing of bentonites saturated by distilled water, 0.5mol/l NaCl and 0.5mol/l CaCl <sub>2</sub> .....	214
Figure 8-26 Final basal spacing of bentonites saturated by distilled water, 0.5mol/l NaCl and 0.5mol/l CaCl <sub>2</sub> .....	215
Figure 8-27 Mineral detection of bentonites saturated by distilled water, 0.5mol/l NaCl and 0.5mol/l CaCl <sub>2</sub> .....	218
Figure 8-28 Macro void ratio and water diffusivity changing with degree of saturation .....	221
Figure 8-29 Sodium type bentonite saturated by different salt solutions .....	222
Figure 8-30 Calcium type bentonite saturated by different salt solutions .....	223
Figure 9-1 Testing methodology for measuring swelling pressure at different temperatures.....	229
Figure 9-2 Testing methodology for measuring water diffusivity at different temperatures.....	230
Figure 9-3 Definitions of swelling pressures during saturation.....	231
Figure 9-4 Swelling pressure evolution curves of MX80 at different temperatures..	232
Figure 9-5 Swelling pressure evolution curves of KV1 at different temperatures ....	233

Figure 9-6 Swelling pressure evolution curves of KB at different temperatures.....	234
Figure 9-7 Swelling pressures during saturation of MX80.....	236
Figure 9-8 Swelling pressures during saturation of KV1 .....	237
Figure 9-9 Swelling pressures during saturation of KB.....	238
Figure 9-10 Equilibrium swelling pressures at different temperatures.....	239
Figure 9-11 Water contents of different dry densities MX80 slices at 30°C.....	241
Figure 9-12 Water contents of different dry densities KV1 slices at 30°C .....	242
Figure 9-13 Water contents of different dry densities KB slices at 30°C .....	243
Figure 9-14 Water contents of different dry densities MX80 slices at 50°C .....	244
Figure 9-15 Water contents of different dry densities KV1 slices at 50°C .....	245
Figure 9-16 Water contents of different dry densities KB slices at 50°C .....	246
Figure 9-17 Relations between $\theta$ and $\chi$ for different dry densities MX80 at 30°C....	247
Figure 9-18 Relations between $\theta$ and $\chi$ for different dry densities KV1 at 30°C .....	248
Figure 9-19 Relations between $\theta$ and $\chi$ for different dry densities KB at 30°C.....	249
Figure 9-20 Relations between $\theta$ and $\chi$ for different dry densities MX80 at 50°C....	250
Figure 9-21 Relations between $\theta$ and $\chi$ for different dry densities KV1 at 50°C .....	251
Figure 9-22 Relations between $\theta$ and $\chi$ for different dry densities KB at 50°C.....	252
Figure 9-23 Water diffusivities of different dry densities bentonites at 30°C.....	253
Figure 9-24 Water diffusivities of different dry densities bentonites at 50°C.....	254
Figure 9-25 Water diffusivities of MX80 at different temperatures .....	255
Figure 9-26 Water diffusivities of KV1 at different temperatures .....	256
Figure 9-27 Water diffusivities of KB at different temperatures .....	257
Figure 9-28 Water diffusivities of KV1 at different temperatures from literatures and this study .....	258
Figure 9-29 Schematic showing montmorillonite fabric units at different temperatures .....	259
Figure 9-30 Schematic showing movement of water in powder and particle bentonites .....	260
Figure 9-31 Schematic showing micropore and macropore at different temperatures .....	262
Figure 10-1 Schematic of making bentonite powders with different water contents by water spray method.....	267
Figure 10-2 Schematic of making bentonite powders with different water contents by humidity control method.....	268
Figure 10-3 A simple wetting apparatus with 2mm ring.....	270
Figure 10-4 2mm specimen for XRD tests and specimen sealed by parafilm.....	270
Figure 10-5 Swelling pressure evolution curves of specimens with different initial water	

contents by water spray method.....	274
Figure 10-6 Traditional swelling pressure evolution curves.....	275
Figure 10-7 Some swelling pressure evolution curves of specimens by water spray method at similar dry densities .....	277
Figure 10-8 Equilibrium swelling pressure of specimen with different initial water contents by water spray method.....	278
Figure 10-9 XRD profiles of specimens with different initial water contents before wetting by water spray method .....	280
Figure 10-10 XRD profiles of specimens with different initial water contents after wetting by water spray method .....	282
Figure 10-11 Basal spacing of specimens before wetting with different initial water contents by water spray method.....	283
Figure 10-12 Basal spacing of specimens after wetting with different initial water contents by water spray method.....	283
Figure 10-13 Swelling pressure evolution curves of specimens with different initial water contents by humidity control method.....	286
Figure 10-15 Equilibrium swelling pressure of specimen with different initial water contents by humidity control method .....	288
Figure 10-16 XRD profiles of specimens before wetting with different initial water contents by humidity control method .....	290
Figure 10-17 XRD profiles of specimens after wetting with different initial water contents by humidity control method .....	292
Figure 10-18 Basal spacing of specimens before wetting with different initial water contents by humidity control method .....	293
Figure 10-19 Basal spacing of specimens after wetting with different initial water contents by humidity control method .....	293
Figure 10-20 Basal spacing of specimens at similar initial water contents before wetting by different methods. ....	295
Figure 10-21 Schematic showing specimen preparation effects on the microstructure of the initial specimen. ....	296
Fig. 10-22 Basal spacing of saturated specimen by different methods.....	297
Figure 10-23 Schematic showing specimen preparation effects on the microstructures of initial and saturated states.....	297
Figure 10-24 Schematic showing effects of initial water contents on microstructures of initial and saturated states. ....	298
Figure 11-1 Global change in electricity demand (IEA 2022).....	303
Figure 11-2 Timeline for Japanese Geological Disposal Program (from NUMO 2022)	

.....	304
Figure 11-3 Visual impression of a repository (from NUMO 2022) .....	305
Figure 11-4 Multi-barrier system after construction and in saturated state .....	306
Figure 11-5 Swelling pressure changing with wetting duration for MX80 bentonite at different dry densities.....	308
Figure 11-6 Hydraulic conductivity changing with volumetric water content for KB bentonite at different dry densities.....	308
Figure 11-7 The location in discussion for Japanese Deep Geological project (modified from NUMO 2022) .....	309
Figure 11-8 The location in discussion for Chinese Deep Geological project (Wang et al. 2018) .....	310
Figure 11-9 Swelling pressure during saturation of sodium type bentonite saturated by $\text{Ca}^{2+}$ and $\text{Na}^{+}$ ions.....	311
Figure 11-10 Swelling pressure during saturation of calcium type bentonite saturated by $\text{Ca}^{2+}$ and $\text{Na}^{+}$ ions.....	311
Figure 11-11 The emission of heat in deep geological disposal project (Gens et al. 2021) .....	313
Figure 11-12 Temperature in and outside buffer material during HLW decay (JNC 1999) .....	313
Figure 11-13 Equilibrium swelling pressure of particle bentonite (MX80) at different temperatures.....	314
Figure 11-14 Equilibrium swelling pressure of powder bentonite (KV1) at different temperatures.....	314
Figure 11-15 Equilibrium swelling pressure from different initial water content KV1 specimen by water spray method.....	315
Figure 11-16 Equilibrium swelling pressure from different initial water content KV1 specimen by humidity control method.....	316

## Table list

Table 1-1 Details for deep geological disposal world widely (from Chen 2022) .....	5
Table 1-2 Bentonites selected by different countries as buffer material .....	7
Table 1-3 Temperature effect on equilibrium swelling pressure of bentonites from Literatures .....	22
Table 2-1 Soil particle densities of bentonites .....	43
Table 2-2 Liquid and plastic limits of bentonites.....	45
Table 2-3 Montmorillonite contents of bentonites.....	46
Table 2-4 CECs and EXCs of bentonites .....	47
Table 3-1 Physical parameters values of materials in literature survey .....	51
Table 4-1 Specimen details .....	67
Table 4-2 Fitting parameters values of SWRCs by Van Genuchten model .....	76
Table 5-1 Specimen details .....	97
Table 6-1 Specimen details .....	139
Table 7-1 Specimens details.....	160
Table 8-1 Specimen details .....	186
Table 8-2 CECs and EXCs of different bentonites saturated by different liquids (meq/g). .....	219
Table 9-1 Specimen details for swelling pressure tests.....	229
Table 9-2 Specimen details for water diffusivity tests.....	230
Table 9-3 Temperature effect on equilibrium swelling pressure of bentonites from Literatures .....	240
Table 10-1 Specimens details by water spray method for swelling pressure and XRD tests .....	267
Table 10-2 Relative humidity and powder bentonite water contents from saturated salt solutions .....	269
Table 10-3 Specimens from humidity control method for swelling pressure and XRD tests .....	269
Table 11-1 Ions and concentration of seawater in Japanese coastal area (Komine et al. 2009) .....	310
Table 11-2 Ions and concentration of groundwater in Beishan area (Sun et al. 2019) .....	311

## List of research achievements for application of Doctor of Engineering, Waseda University

Full Name : 阮 坤林

seal or signature

Date Submitted(yyyy/mm/dd): 2022/12/2

種類別 (By Type)	題名、発表・発行掲載誌名、 (theme, journal name, date & year of publication, name of authors inc. yourself)
Paper	<p><u>Kunlin Ruan</u>, Hideo Komine, Hailong WANG, Daichi Ito. 2022. "Experimental study of initial water content and specimen preparation method effects on Kunigel-V1 bentonite swelling pressures", Canadian Geotechnical Journal In press, <a href="https://doi.org/10.1139/cgj-2021-0532">https://doi.org/10.1139/cgj-2021-0532</a></p> <p><u>Kunlin Ruan</u>, Hailong WANG, Hideo Komine, Daichi Ito. 2022. "Experimental study for temperature effect on swelling pressures during saturation of bentonites", Soils and Foundations, 62(6): 101245.</p> <p><u>Kunlin Ruan</u>, Hideo Komine, Hailong WANG, Daichi Ito, Takahiro Gotoh. 2022. "Microstructural changes and swelling pressure of low dry density compacted bentonites during saturation combining X-ray diffraction", Canadian Geotechnical Journal. In press, <a href="https://doi.org/10.1139/cgj-2020-0342">https://doi.org/10.1139/cgj-2020-0342</a></p> <p><u>Kunlin Ruan</u>, Hideo Komine, Daichi Ito, Kentaro Miyoshi, Takahiro Gotoh. 2022. "Hydraulic Conductivity and X-ray Diffraction Tests of Unsaturated Bentonites with a Multi-ring and Their Predictions by Pores Distributions", Engineering Geology, 306: 106738</p> <p><u>Kunlin Ruan</u>, Xianlei Fu. 2022 "A Modified Kozeny-Carman Equation for Predicting Saturated Hydraulic Conductivity of Compacted Bentonite in Confined Condition", Journal of Rock Mechanics and Geotechnical Engineering, 14 (3): 984-993.</p> <p>Hailong WANG, <u>Kunlin Ruan</u>, Satoru Harasaki, Hideo Komine. 2021. "Effects of specimen thickness on apparent swelling pressure evolution of compacted bentonite ", Soils and Foundations, 61(1): 101099.</p> <p>Hailong WANG, Daichi Ito, Takumi Shirakawabe, <u>Kunlin Ruan</u>, Hideo Komine. 2022. "On swelling behaviors of a bentonite under different water contents ", Geotechnique, Ahead of Print. <a href="https://doi.org/10.1680/jgeot.21.00312">https://doi.org/10.1680/jgeot.21.00312</a></p>
Conferences	<p><u>Kunlin Ruan</u>, Dean Sun, Xianlei Fu, Hailong Wang, Hideo Komine, Daichi Ito. 2021/10. "Reversibility of micro and macrostructure in compacted bentonite under chemo-mechanical couplings". 3rd International Symposium on Coupled Phenomena in Environmental Geotechnics. Kyoto university, Kyoto, JAPAN.</p> <p><u>Kunlin Ruan</u>, Dean Sun, Hailong Wang, Hideo Komine, Daichi Ito. 2020. "Effects of Calcium Carbonate on hydro-mechanical properties of Bentonite". The 55th annual meeting of the Japan national conference on geotechnical engineering. Kyoto, JAPAN. [22-1-3-05]</p> <p><u>Kunlin Ruan</u>, Daichi Ito, Hideo Komine, Hailong Wang. 2021. "Tests for pores of Kunigel-V1 compacted bentonite during saturation". The 56th annual meeting of the Japan national conference on geotechnical engineering. Yamagata, JAPAN. [13-4-4-02]</p> <p><u>Kunlin Ruan</u>, Daichi Ito, Hideo Komine, Hailong Wang. 2021. "Swelling pressure and water diffusivity of sodium bentonite saturated by different solutions under confined wetting". 76 th Annual Meeting of the Japan Society of Civil Engineers. Kanagawa, JAPAN. [CS2-38]</p>
Research fund	<p><u>Kunlin Ruan</u>. "Effects of ions on swelling pressures of compacted bentonites combining X-ray diffraction" , 2021-2022, B2R101231001, W-Spring, Japan Science and Technology Agency (JST).</p>